MULTISCALE PERFORMANCE OF CEMENT-BASED COMPOSITES WITH CARBON NANOFIBERS

By

Catherine Stephens

Dissertation

Submitted to the Faculty of the

Graduate School of Vanderbilt University

in partial fulfillment of the requirements

for the degree of

DOCTOR OF PHILOSOPHY

in

Civil Engineering

May, 2013

Nashville, Tennessee

Approved:

Professor Florence Sanchez

Professor Prodyot K. Basu

Professor David S. Kosson

Professor Sankaran Mahadevan

Doctor Paul G. Allison

To my husband, family, and the

people who have encouraged me along the way

ACKNOWLEDGEMENTS

Firstly, I would like to thank my advisor, Dr. Florence Sanchez for her encouragement and patience during my PhD journey. Her work ethic and dedication is admirable. I would also like to thank my committee members, Dr. David S. Kosson, Dr. Prodyot K. Basu, Dr. Sankaran Mahadevan, and Dr. Paul G. Allison for their time and valuable suggestions.

This dissertation would not have been possible without the financial support from the Department of Civil and Environmental Engineering at Vanderbilt University, the National Science Foundation under NSF CAREER CMMI 0547024, and the SMART Scholarship Program funded by the Office of Secretary of Defense-Test and Evaluation, Defense–Wide/PE0601120D8Z National Defense Education Program/BA-1, Basic Research, Grant Number N00244-09-1-0081.

I am especially thankful for the people that have met at Vanderbilt University and the Army Corps of Engineers Engineer Research and Development Center (ERDC) in Vicksburg, Mississippi, including too many to name, for their many conversations, suggestions, and collaboration. I especially want to recognize Lesa Brown, Dr. David Delapp, and Dr. Rossane Delapp for their advice and help with my experimental program at Vanderbilt, and Dr. Paul Allison, Bill Heard, and Dr. Robert Moser at ERDC for their friendship and mentorship throughout this process.

Lastly, I am infinitely thankful for my understanding and patient husband, Justin. I am also very thankful for the many years of support from my parents, Greg and Susan. Also, to my brother, Jacob, my family, and my friends thank you for encouraging me and challenging me to be myself.

TABLE OF CONTENTS

Appendix

LIST OF TABLES

LIST OF FIGURES

NOMENCLATURE

Abbreviation/Symbol	**Description**
α	Degree of hydration
β	Dimensionless correction factor for nanoindenter tip
γ	Volume fraction of unhydrated cement
ν	Poisson's ratio
ν_i	Poisson's ratio of nanoindenter
ρ_c	Specific gravity of cement
A_c	Area of contact
AE	Air entraining admixture
AFM	Atomic force microscopy
C_2S	Dicalcium silicate ($2CaO \cdot SiO_2$)
C_3A	Tricalcium aluminate ($3CaO \cdot Al_2O_3$)
C_3S	Tricalcium silicate ($3CaO \cdot SiO_2$)
C_4AF	Tetracalcium aluminoferrite ($4CaO \cdot Al_2O_3 \cdot Fe_2O_3$)
$CaSO_4 \cdot 1/2H_2O$	Calcium sulfate hemihydrate
CFs	Carbon microfibers
CH	Calcium hydroxide
CNFs	Carbon nanofibers
CNTs	Carbon nanotubes
C-S-H	Calcium silicate hydrate
E	Elastic modulus
E_{eff}	Effective elastic modulus
E_i	Elastic modulus of nanoindenter
EDS	Energy dispersive X-ray spectroscopy
ERDC	Army Corps of Engineers Engineer Research and Development Center (Vicksburg, Mississippi)
FRC	Fiber reinforced concrete
H	Hardness
HNO_3	Nitric acid
HRWR	High-range water reducer
ITZ	Interfacial transition zone
KOH	Potassium hydroxide
MWCNTs	Multi-walled carbon nanotubes
NaOH	Sodium hydroxide
N-HRWR	Sulfonated naphthalene condensate high-range water reducer
P-HRWR	Polycarboxylate-based high-range water reducer
PC paste	Portland cement paste
P_{max}	Maximum nanoindentation force
S	Measured nanoindentation unloading stiffness
SEM	Scanning electron microscope/microscopy
SF paste	Portland cement and silica fume paste

SWCNTs	Single-walled carbon nanotubes
TEM	Transmittance electron microscopy
w/b	Water-to-binder
w/c	Water-to-cement
wt%	Percent weight by weight of cement
XRF	X-ray fluorescence

<u>Nomenclature for Suspensions (Chapter 3)</u>

Name	**Description**
AE/CNF	"*As received*" CNFs in water dispersed by AE
N-HRWR/CNF	"*As received*" CNFs in water dispersed by N-HRWR
P-HRWR/CNF	"*As received*" CNFs in water dispersed by P-HRWR
P-HRWR/T-CNF	CNFs surface treated with HNO_3 in water dispersed with P-HRWR
PW/CNF	"*As received*" CNFs in simulated cement pore water
PW/AE/CNF	"*As received*" CNFs in simulated cement pore water dispersed by AE
PW/N-HRWR/CNF	"*As received*" CNFs in simulated cement pore water dispersed by N-HRWR
PW/P-HRWR/CNF	"*As received*" CNFs in simulated cement pore water dispersed by P-HRWR
W/CNF	"*As received*" CNFs in water
W/T-CNF	CNFs surface treated with HNO_3 in water

<u>Nomenclature for Composites (Dispersion Method – Chapters 3 and 5)</u>

Name	**Description**
PC-AE/CNF	PC paste (w/c=0.28) with 0.2 wt% "as received" CNFs dispersed with AE
PC-AE/Control	PC paste (w/c=0.28) control (no fibers) with AE
PC-N-HRWR/CNF	PC paste (w/c=0.28) with 0.2 wt% "as received" CNFs dispersed with N-HRWR
PC-N-HRWR/Control	PC paste (w/c=0.28) control (no fibers) with N-HRWR
PC-P-HRWR/CNF	PC paste (w/c=0.28) with 0.2 wt% "as received" CNFs dispersed with P-HRWR
PC-P-HRWR/Control	PC paste (w/c=0.28) control (no fibers) with P-HRWR
PC-P-HRWR/T-CNF	PC paste (w/c=0.28) with 0.2 wt% CNFs surface treated with HNO_3 dispersed with P-HRWR
PC-W/CNF	PC paste (w/c=0.28) with 0.2 wt% "as received" CNFs and no dispersing agent
PC-W/Control	PC paste (w/c=0.28) control (no fibers) with no dispersing agent
PC-W/T-CNF	PC paste (w/c=0.28) with 0.2 wt% CNFs surface treated with HNO_3 and no dispersing agent

Nomenclature for Composites (CNF Loading – Chapters 3 and 5)

Name	Description
PC-0%	PC paste (w/c=0.28) control (no fibers) with P-HRWR
PC-0.02%	PC paste (w/c=0.28) with 0.02 wt% "as received" CNFs dispersed with P-HRWR
PC-0.08%	PC paste (w/c=0.28) with 0.08 wt% "as received" CNFs dispersed with P-HRWR
PC-0.2%	PC paste (w/c=0.28) with 0.2 wt% "as received" CNFs dispersed with P-HRWR
PC-0.5%	PC paste (w/c=0.28) with 0.5 wt% "as received" CNFs dispersed with P-HRWR
PC-1%	PC paste (w/c=0.28) with 1 wt% "as received" CNFs dispersed with P-HRWR
SF-0%	SF paste (w/c=0.28) control (no fibers) with P-HRWR
SF-0.02%	SF paste (w/c=0.28) with 0.02 wt% "as received" CNFs dispersed with P-HRWR
SF-0.08%	SF paste (w/c=0.28) with 0.08 wt% "as received" CNFs dispersed with P-HRWR
SF-0.2%	SF paste (w/c=0.28) with 0.2 wt% "as received" CNFs dispersed with P-HRWR
SF-0.5%	SF paste (w/c=0.28) with 0.5 wt% "as received" CNFs dispersed with P-HRWR
SF-1%	SF paste (w/c=0.28) with 1 wt% "as received" CNFs dispersed with P-HRWR

Nomenclature for Composites (Hybrid Composites – Chapters 4 and 6)

Name	Description
PC	PC paste (w/c=0.315) control (no fibers) with P-HRWR
PC-CF	PC paste (w/c=0.315) with 0.5 wt% CFs and P-HRWR
PC-CF-CNF	PC paste (w/c=0.315) with 0.5 wt% "as received" CNFs, 0.5% CFs, and dispersed with P-HRWR
PC-CNF	PC paste (w/c=0.315) with 0.5 wt% "as received" CNFs dispersed with P-HRWR

CHAPTER 1

INTRODUCTION

1.1. Overview

According to the American Society of Civil Engineers, the United States' infrastructure is outdated and needs trillions of dollars in investment [1]. The National Academy of Engineering also recognizes restoring and improving urban infrastructure as one of the Grand Challenges for Engineering which are awaiting engineering solutions in the 21st century [2]. An important aspect of improving infrastructure is improving and advancing construction materials.

Portland cement concrete is the most used construction material for civil infrastructure in the world [3]. Research has led to advanced cement-based composites for civil infrastructure that have properties such as the ability to stay clean while removing pollutants from the air [4, 5], transmit light through the material [6], or sense damage [7, 8]. The use of short, randomly distributed, discontinuous fibers in cement-based composites has led to increases in strength, toughness, impact and fatigue resistance, and durability as well as a decrease in plastic shrinkage cracking [3, 9-11]. Additionally short, randomly distributed, discontinuous fibers have been shown to provide multifunctional capabilities to cement-based composites such as strain, temperature, and damage sensing and thermal conductivity [12-30].

More recently, the use of hybrid discontinuous fiber reinforcement consisting of the combination of multiple fiber types and/or sizes that are randomly distributed within the material has been found to improve the mechanical properties beyond the sum of the improvements from each individual fiber size/type alone [31]. However, current hybrid fiber reinforced cement-based composites mostly use only macroscale and microscale discontinuous fibers. Because cracking and flaws in cement-based composites exist from the nanoscale to the macroscale, the use of discontinuous fiber reinforcements implemented from the nanoscale to the macroscale could allow for novel, advanced cement-based composites with tailored properties and improved mechanical performance and durability.

Recent advances in nanotechnology have allowed for large-scale commercial production and characterization capabilities of carbon nanotubes (CNTs) and carbon nanofibers (CNFs) [32]. CNTs/CNFs have properties such as large surface areas, high aspect ratios, good chemical resistance, electrical conductivity, and thermal conductivity, and extraordinary strength, which make them excellent candidates for nanoscale reinforcement in cement-based composites [32-35]. However, CNTs and CNFs have a strong van der Waals self-attraction and high hydrophobicity, which cause the CNTs/CNFs to form bundles that create microscale agglomerates in the composite [35]. Most research efforts to date have been placed on dispersing CNTs/CNFs in cement-based composites [13-16, 26, 35-65] and the effect of CNTs/CNFs on the composite mechanical properties [15-19, 36, 37, 39-47, 50, 52, 55-58, 64, 66, 67]. Despite these efforts, the dispersion state of CNTs/CNFs in cement-based materials is still not well understood and remains a major and on-going challenge. Additionally, results to date on the mechanical properties have been mixed with some studies showing significant improvements (up to 47% increase for the flexural strength [57] and over 100% increase for the tensile strength [19, 29]) even for small addition of CNTs/CNFs such as 0.05% by weight of cement (wt%), while others have reported border line improvements to no improvement and in some cases deterioration of the composite mechanical properties [15-19, 29, 36, 37, 39-47, 50, 52, 55-58, 64, 66, 67].

1.2. Objectives and Approach

The objective of the research included in this dissertation was to investigate the inclusion of CNFs in cement paste for use as nanoreinforcement. In particular, this research focused on: (i) the dispersion and distribution of CNFs in cement pastes, (ii) the effect of CNFs on the micro- and macromechanical properties of the composite material, and (iii) the hybrid effect of CNFs and carbon microfibers (CFs) on the microstructure and multiscale mechanical properties of portland cement pastes. There are four specific objectives addressed in this dissertation including:

1. Determining the effect of dispersion methods and CNF loading on: (i) CNF disaggregation and dispersion in solutions and (ii) subsequent dispersion and distribution in cement pastes.
2. Investigating the micromechanical properties of hydrated cement pastes containing CNFs, including the effect of CNFs on the overall distribution of micromechanical properties at the local level and on representative major cement phases (i.e., C-S-H and CH) and the micromechanical response at the local level in and around CNF agglomerates.
3. Determining the effect of CNFs on the macromechanical properties of cement pastes, including strength, modulus, and toughness in compression, splitting tension, and flexure.
4. Evaluating the hybrid effect of CNFs and CFs on the microstructure and multiscale mechanical properties of cement pastes.

An integrated multiscale experimental approach was used to better understand the capabilities of CNFs as nanoreinforcement. Cement-based composites were investigated using both traditional and state-of-the-art experimental methods for mechanical, physical, and chemical characterization. Studies were conducted at both the micro- and macroscale levels to better understand the processing-microstructure-dispersion and dispersion-property relationships for these materials. State of the art experimental characterizations, including variable pressure scanning electron microscopy (SEM) equipped with energy-dispersive X-ray spectroscopy (EDS), nanoindentation, optical microscopy, and traditional mechanical testing (i.e., three-point bending, splitting tension, and uniaxial compression) were integrated to convey the key aspects of CNF addition and dispersion in cement-based composites and the effects of CNFs on the mechanical properties (i.e., strengths, elastic moduli, and toughness values) of the composites.

1.3. Structure of the Dissertation

This dissertation is organized in seven chapters. Chapter 1 provides an overview of the dissertation, the overall and specific research objectives, and the structure of the dissertation. Chapter 2 contains a review of the literature pertaining to this dissertation. An overview of fiber reinforced cement-based composites, the use of CNTs/CNFs as nanoreinforcement in cement-based composites, and the micromechanical properties and mineralogy/microstructure of cement-based composites is given. Chapter 3 discusses the dispersion of CNFs. The dispersion of CNFs in solution and in cement-based composites is investigated including the migration of CNFs during cement curing. Chapter 4 discusses the micromechanical properties of cement-based composites containing CNFs. The overall distribution of micromechanical properties at the local level (i.e., cement-based composite constituents), the distribution of micromechanical properties of the cement hydration phases, and the micromechanical responses obtained in and around CNF agglomerates are determined. Chapter 5 discusses the macromechanical properties of cement-based composites containing CNFs. The effects of the CNF dispersion method and CNF loading on the macromechanical properties are determined. Also, the effect of CNFs on the macromechanical properties of cement-based composites with the addition of silica fume is examined. Chapter 6 discusses the use of CNFs with CFs as a multiscale hybridization of fiber reinforcement for cement-based composites. The hybrid effect of CNFs and CFs on the microstructure and CNF dispersion and distribution, the micromechanical properties, and the macromechanical properties of cement-based composites is determined. Lastly, Chapter 7 summarizes the results of this research and includes recommendations for future work.

CHAPTER 2

LITERATURE REVIEW

2.1. Overview

This chapter provides a review of the literature. An overview of fiber reinforced cement-based composites including their properties, multifunctional capabilities, and ability to be tailored to specific needs and the use of hybrid fiber reinforcement is given. Also discussed, is the use of CNTs/CNFs as nanoreinforcement in cement-based composites including CNT/CNF properties and dispersion and the mechanical properties of cement-based composites containing CNTs/CNFs. Lastly, the micromechanical properties of individual cement phases and unhydrated cement particles determined by nanoindentation and the micromechanical, mineralogical, and microstructural differences seen in cement-based composites with fiber reinforcement including nanoscale fiber reinforcement are summarized.

2.2. Fiber Reinforced Cement-Based Composites

The use of relatively short, randomly distributed, discontinuous fibers including steel, polymeric, carbon, and glass in cement-based composites, known as fiber reinforced concrete (FRC), is of high interest because of the fibers' ability to improve post cracking load bearing capability by controlling the growth of cracks [3]. The mechanism of the fiber reinforcement is to transfer stresses across flaws and cracks (Figure 2.1), which can improve the strength, toughness, impact resistance, fatigue strength, and durability and reduce plastic shrinkage cracking of cement-based composites [3, 9-11, 68].

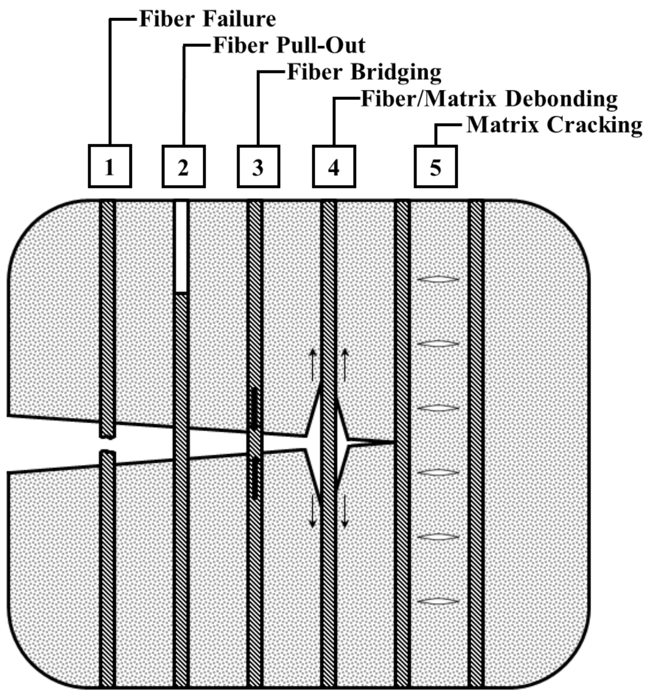

Figure 2.1. Mechanisms of fiber reinforcement modified from [68].

In addition to mechanical and durability improvements, randomly distributed, discontinuous fibers can give cement-based composites multifunctional capabilities. FRC containing carbon fibers has been shown to have self-sensing capabilities because of a determinable relationship that exists with the material's electrical resistivity and strain known as piezoresistivity [12-26]. In addition to strain sensing, the piezoresistive behavior of carbon FRC has also been shown to be useful for damage sensing, traffic monitoring, weighing in motion, and corrosion monitoring of rebar [23-25, 27, 28]. Carbon FRC has also been shown to be effective for protection from electromagnetic radiation such as radio waves produced by cell phones, which is important for sensitive electronic devices [18, 19, 29]. Furthermore, steel FRC has been shown to be effective for melting snow on roadways because of the material's thermal conductivity [30].

The characteristics of FRC including its mechanical performance, durability, or multifunctional capabilities can be affected by many variables including but not limited to the fiber type, fiber size, fiber distribution, and mix composition [9]. The many variables that influence the characteristics of FRC can make designing and reproducing composites challenging, but those same variables allow FRCs to be tailored for specific applications [9]. For example, steel fibers have been used in highway and airport runway overlay pavements to reduce the thickness of the slab and cracking [3]. In addition, FRCs have been tailored for airport runway pavements to be resistant to temperatures greater than 1500°C for the high temperature exhaust blasts [69].

More recently, using fibers in combination, called fiber hybridization, has become of interest [10, 31]. Hybrid fiber reinforcement can include multiple fiber types or multiple fiber sizes to improve multiple constitutive responses, control multiple size cracks, or provide multiple functions such as one fiber type/size for early age response and another for long-term mechanical properties [31]. The use of hybrid fiber reinforcement also has the potential to improve cement-based composites more than the use of fiber reinforcement of a single type/size by "synergy." Synergy refers to each fiber type/size improving the composites with the combination of the fiber types/sizes being more beneficial than the sum of the improvements from each fiber type/size alone [10, 31]. The work by Yao et al. [70] shows an example of synergy as the flexural behavior of a cement-based composite containing carbon and steel microfibers allowed for a flexural strength of over 12 MPa after the initial cracking of the matrix while the strength of the composite with only CFs at a similar deflection was less than 2 MPa and only steel fibers was *ca.* 5 MPa.

Several other instances of hybrid fiber reinforcement in cement-based composites have shown material improvements [71-77]. Cement-based composites containing three sizes of steel fibers from the micro- to macroscale were found to have a tensile strength of more than 20 MPa (typical cement-based composites have a tensile strength of *ca.* 7-11% of the compressive strength, i.e., *ca.* 2-4 MPa [3]) in addition to improved fatigue behavior, ductility, strain capacity, and durability compared to traditional FRC [78-83]. Impact resistance has also been shown to be improved by the use of hybrid fiber reinforcement [84]. However, one study has shown decreased flexural toughness with steel and glass and steel and polyester hybrid microfiber reinforcements, compared to steel microfibers alone in cement-based composites [85]. More recently, cement-based composites containing microscale polyvinyl alcohol fibers and nanoscale CNFs together were shown to have increased flexural strength, modulus of elasticity, and toughness as compared to cement-based composites with no fibers or polyvinyl alcohol fibers or CNFs alone [49].

2.3. CNTs/CNFs as Nanoreinforcement in Cement-Based Composites

2.3.1. CNT/CNF Properties

The unique properties of CNTs and CNFs (also known as cup-stacked CNTs) such as high aspect ratios, strength to density ratios, thermal and electrical conductivities, and corrosion resistivity allow them to be excellent candidates for nanoscale material reinforcement [33-35]. CNTs and CNFs are both graphitic [34] and can be produced commercially using chemical vapor deposition [86]. CNTs are different from CNFs in that they are smaller in size [86, 87], are closed at both ends, and are available in two varieties: single-walled carbon nanotubes

(SWCNTs) and multi-walled carbon nanotubes (MWCNTs) [88]. The mechanical and electrochemical properties decrease from SWCNT to MWCNT to CNF, but the cost also decreases in the same order [86, 87]. SWCNTs have diameters of 0.3-2 nm and lengths of 200+ nm, MWCNTs have diameters of 10-50 nm and lengths of 1-50 μm [86], and CNFs have diameters of 50 to 200 nm and lengths up to a few hundred microns [87]. While SWCNTs and MWCNTs are closed continuous hollow tubes, CNFs are open at both ends and consist of multiple concentric tubes so that step-like edges exist at the termination of each tube (Figure 2.2) [86, 87]. The smooth graphitic structure of the CNTs does not allow for proper adhesion between the CNTs and the material matrix [55]. In contrast, the step-like edges of the CNFs are advantages for bonding with the material matrix [42].

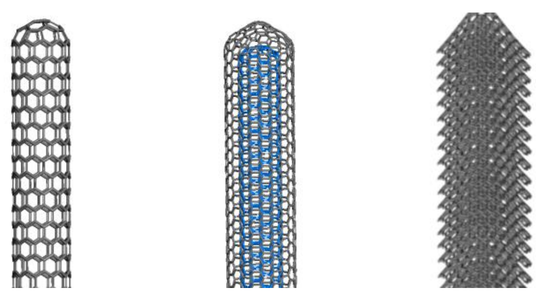

SWCNT MWCNT CNF

Figure 2.2. Comparison of CNTs and CNFs.

2.3.2. CNT/CNF dispersion

CNTs and CNFs both possess a strong van der Waals self-attraction and high hydrophobicity that cause them to agglomerate and form bundles, hindering their dispersion [13-19, 26, 32, 35-45, 47, 50, 53-60, 64, 66, 89-91]. A large amount of research has gone into dispersing CNTs and CNFs, especially in the area of polymer science [32, 90, 91]. Methods used to disperse CNTs/CNFs include covalent, non-covalent, and mechanical methods [90]. Covalent methods involve using acid treatment to functionalize the surface of the CNTs/CNFs [90]. Non-covalent methods involve using a surfactant to wrap the CNTs/CNFs [90]. Mechanical methods include various methods of mixing and agitation such as high shear mixing and ultrasonication [90].

Each type of method, covalent, non-covalent, and mechanical, has been used both, individually and in combination, to aid in the dispersion of CNTs/CNFs in cement-based composites. Covalent methods that have been used to aid in dispersing CNTs/CNFs include mainly surface treatment with nitric acid (HNO_3) and/or sulfuric acid [15, 16, 36-42]. The many non-covalent methods that have been used to date to aid in the dispersion of CNTs/CNFs in cement-based composites include: cetylrimenthyl ammonium bromide [58], gum Arabic [36, 43], lignosulfonate salt [44], modified acrylic polymer high-range water reducer (HRWR) [40], polyacrylic acid polymer HRWR [36, 45], polycarboxylate-based HRWR (P-HRWR) [37, 38, 46-52], sodium deoxycholate [43], sodium dodecyl benzene sulfonate [43], sodium dodecyl sulfate [16], and solvents such as acetone, ethanol, and isopropanol [35, 41, 53, 54]. The most predominant mechanical method used is ultrasonication [13-15, 26, 35-38, 40, 41, 43, 45, 47, 50, 54-60]. Additional methods that have been used for dispersing CNTs/CNFs in cement-based composites with various levels of success include direct synthesis of the nanofilaments on the cement particles and silica fume particles [61-63] and adding silica fume to the cement mix [42, 50, 64].

A major issue with dispersing CNTs/CNFs in cement-based composites is that the method used to disperse the CNTs/CNFs must be compatible with the cement hydration process [65]. For example, lignosulfonate salts are known to slow the hydration reaction as they are often used as set retarding admixtures [3]. Solvents such as isopropanol and acetone also have a negative effect on the cement hydration process as they are commonly used to stop the hydration reaction of cement for experimental purposes [92].

Another difficulty with the dispersion of CNTs/CNFs is that quantifying the dispersion in a material is challenging [90]. Optical microscopy can be used to visualize CNTs/CNFs in materials but mostly to see agglomerates on the microscale [90]. Methods such as light scattering, fluorescence, small angle neutron scattering, and Raman spectroscopy can also be used to evaluate dispersions of CNTs/CNFs [90, 93-96] but are not appropriate for dispersions of CNTs/CNFs in cement-based composites. SEM, transmittance electron microscopy (TEM), and atomic force microscopy (AFM) are techniques that have been shown to be useful for examining the dispersion of CNTs/CNFs in cement-based composites, though challenges exist with each one of these methods such as viewing too small of a sample size or a non-representative sample or requiring pretreatment that affects the sample [90].

2.3.3. Mechanical Properties of CNT/CNF Reinforced Cement-Based Composites

Several authors have presented strength values of cement-based composites containing CNTs/CNFs [15-19, 36, 37, 39-47, 50, 52, 55-58, 64, 66, 67]. The studies vary by composite mix design, CNT/CNF loading rates, and dispersion method, and the results to date have been conflicting. CNT/CNF loadings have ranged from 0.006 wt% to 5 wt%, but most results have been reported on CNT/CNF loadings up to 1 wt% [15-19, 36, 37, 39-47, 50, 52, 55-58, 64, 66, 67]. Compressive strengths have been shown to increase by up to 70% when CNTs are used in cement-based foam concrete [44] while decreases of 6 times lower than the control specimens have been seen in cement mortars containing CNTs [40]. Similarly, compressive strengths have been shown to increase by up to 43% when CNFs were added to concrete [17] but decrease by up to 30% when CNFs were added to cement pastes [18, 19]. Flexural strengths were shown to increase by up to 47% when cement-based composites contained CNTs [57], but no change in the flexural strength [45] and a decrease in flexural strength of up to 2.5 times that of the control [40, 52] were also seen in different instances. No change in flexural strength was reported for CNFs in cement-based composites [67]. Tensile strengths for cement-based composites containing CNFs have ranged from no significant change to over a 100% increase in strength [18, 19, 41, 42, 46, 64].

Additional mechanical properties of cement-based composites with CNTs/CNFs have been reported in the literature, but are not as prevalent as the strength values. Like the strength values, conflicting results have been presented for the Young's modulus and compressive modulus of cement-based composites containing CNTs/CNFs [18, 19, 47, 50, 66]. However, composites with CNTs/CNFs have shown an increased failure strain and deformation ability [17-19, 39]. CNTs have also been reported to increase the toughness of cement-based composites [57], and CNFs have been shown to improve the structural integrity of cement-based composites [41, 64].

2.4. Micromechanical Properties and Mineralogy/Microstructure of Cement-Based Composites

Although the macroscale properties, especially macromechanical properties, of cement-based composites are important for civil infrastructure applications, cement-based materials have a multiscale structure, and consideration of this structure is important for tailoring multiscale fiber reinforced cement-based composites. Nanoindentation paired with SEM/EDS, optical microscopy, or statistical methods has been used to determine the micromechanical properties of cement phases and unhydrated cement particles in cement-based materials (Table 2.1) [97-111].

Nanoindentation has revealed that the main building block of cement-based composites, calcium-silicate-hydrate (C-S-H), exists as a low stiffness and high stiffness form [100, 101, 103]. The technique has also shown the high stiffness form of C-S-H to be resultant of the presence of calcium hydroxide (CH), another major phase of cement-based materials, between the C-S-H layers [108].

Table 2.1. Elastic modulus and hardness of cement phases as reported in the literature from nanoindentation.

	Modulus (GPa)	**Hardness (GPa)**	**Reference**
Unhydrated cement particles	122.2 ± 7.85	6.67 ± 1.23	Mondal, Shah, and Marks [104]
	141.1 ± 34.8	9.12 ± 0.90	Sorelli, et al. [107]
Tricalcium silicate, $3CaO \cdot SiO_2$	135 ± 7	8.7 ± 0.5	Velez, et al. [99]
(C_3S)	135 ± 7	8.7 ± 1	Acker [97, 98]
Dicalcium silicate, $2CaO \cdot SiO_2$	130 ± 20	8 ± 1.0	Velez, et al. [99]
(C_2S)	130 ± 20	8 ± 2	Acker [97, 98]
Tricalcium aluminate,	145 ± 10	10.8 ± 0.7	Velez, et al. [99]
$3CaO \cdot Al_2O_3$ (C_3A)	145 ± 10	10.8 ± 1.5	Acker [97, 98]
Tetracalcium aluminoferrite,	125 ± 25	9.5 ± 1.4	Velez, et al. [99]
$4CaO \cdot Al_2O_3 \cdot Fe_2O_3$ (C_4AF)	125 ± 25	9.5 ± 3	Acker [97, 98]
Alite	125 ± 7	9.2 ± 0.5	Velez, et al. [99]
Belite	127 ± 10	8.8 ± 1.0	Velez, et al. [99]
Calcium hydroxide, CH	40.3 ± 4.2	1.31 ± 0.23	Constantinides and Ulm [103]
	36 ± 3	1.35 ± 0.5	Acker [97, 98]
	38 ± 5		Constantinides and Ulm [100]
Calcium silicate hydrate, C-S-H			
High stiffness	29.1 ± 4.0	0.83 ± 0.18	Constantinides and Ulm [103]
	31 ± 4	0.9 ± 0.3	Acker [97, 98]
	29.4 ± 2.4		Constantinides and Ulm [100]
	38.0 ± 5.6	1.43 ± 0.29	Mondal, Shah, and Marks [104]
	31.4 ± 2.1	1.27 ± 0.18	Zhu, et al. [105]
	31.0 ± 4.0		Jennings, et al. [106]
	29.8 ± 2.3		Jennings, et al. [106]
	28.5 ± 2.6		Jennings, et al. [106]
	29.1 ± 5.3		Jennings, et al. [106]
	34.2 ± 5.0	1.36 ± 0.35	Sorelli, et al. [107]
Low stiffness	18.2 ± 4.2	0.45 ± 0.14	Constantinides and Ulm [103]
	20 ± 2	0.8 ± 0.2	Acker [97, 98]
	21.7 ± 2.2		Constantinides and Ulm[100]
	22.89 ± 0.76	0.93 ± 0.11	Mondal, Shah, and Marks [104]
	23.4 ± 3.4	0.73 ± 0.15	Zhu, et al. [105]
	18.1 ± 4.0		Jennings, et al. [106]
	17.8 ± 4.3		Jennings, et al. [106]
	18.0 ± 3.1		Jennings, et al. [106]
	18.3 ± 3.8		Jennings, et al. [106]
	19.7 ± 2.5	0.55 ± 0.03	Sorelli, et al. [107]

The micromechanical properties summarized in Table 2.1 were determined from many different cement-based composites including plain cement pastes with a water-to-cement (w/c) ratio of 0.5 [103] and ultra-high performance concretes with a w/c ratio below 0.2 [97]. Additionally, values were obtained from cement-based composites that had been heat treated during curing or had included alternative binders such as silica fume [106, 110]. The consistency in the micromechanical properties presented to date show that the values are intrinsic to the individual phases and, therefore, do not change from one cement-based composite to another [100, 106].

The micromechanical properties of the interfacial transition zone (ITZ) around inclusions including aggregates and steel microfibers have also been investigated [109-111]. Findings suggest that the ITZ can be tailored by changes in the w/c ratio and the addition of alternative binders such as silica fume [109]. In the cases where the ITZ was weaker than the bulk matrix, an increase in porosity was to blame [110, 111].

Recently, the micromechanical properties of cement-based composites containing CNTs have been reported [47, 66, 112-114]. An increased probability of high stiffness C-S-H at the expense of low stiffness C-S-H has been reported when CNTs were used as nanoreinforcement [47, 112, 113]. However, two separate studies have shown that changes in the micromechanical properties of CNT reinforced cement-based composites are dependent on the method of dispersion used [66, 114].

Besides the micromechanical properties, the mineralogy and microstructure of cement-based composites have been shown to be affected by the presence of fibers. When macroscale fibers with diameters ranging from 0.1 to 1.0 mm have been used, ITZ of up to 100 μm wide with high porosity and large CH crystal deposits have been reported [115]. The ITZ is thought to be caused by the combination of bleeding of the hydration water and wall effects, which lead to the presence of water-filled space at the fiber-matrix interface and the development of less hydration products around the fibers [115]. In contrast, in the presence of microscale fibers, the ITZ has been shown to be significantly reduced. Because the size of the microfibers is similar to that of the cement grains, the wall effect around microscale fibers is reduced allowing the microstructure of the ITZ to be similar to that of the bulk cement matrix [115, 116]. Additionally, the use of microscale metal fibers including steel, brass, and brass-coated steel fibers have shown to act as a preferential nucleation site for CH and C-S-H [117]. Furthermore, the interface between CFs and a cement-based matrix has been reported to be influenced by the presence of silica fume causing a change in failure mode from fiber pull-out to fiber fracture [118]. Smaller scale fibers, including CNTs and CNFs, have been shown to reduce the formation of CH and affect its crystallinity and size [37, 60], reduce the amount of tobermorite or change the C-S-H phase when functional groups are present [39, 40], and increase the degree of hydration by acting as nucleation sites [67]. Conversely, one study has indicated that CNTs had no chemical interaction with cement or fly ash and, therefore, no effect on the degree of hydration of cement/fly ash composites [56].

2.5. Conclusions

Literature pertaining to this dissertation was reviewed, and the following conclusions were made:

- Research to date on hybrid fiber reinforcement of cement-based composites has mostly included microscale and macroscale fibers. Because cement-based composites contain flaws and cracks on the nanoscale, the addition of nanoscale fibers has great potential for further improving the properties of FRC and more research in this area is needed.

- The state of dispersion of CNTs/CNFs in cement-based composites is still not well understood. The literature mostly considers the dispersion state of CNTs/CNFs in aqueous solution prior to mixing with cement, and to date the connection between the dispersion state in solution and in the hydrated cement-based composites has not been made. As the overall dispersion state affects the efficiency of the CNTs/CNFs as nanoreinforcement in cement-based composites, this area needs to be further investigated.
- Most research to date on the mechanical properties of cement-based composites with nanoreinforcement has concentrated mainly on CNTs, and the results have been mixed. Research on the use of CNFs is still scarce, and the effects of CNFs on the mechanical properties of cement-based composites are still not well understood. Additionally, little is known concerning the effect of the state of CNF dispersion on the composite mechanical properties.
- Nanoindentation offers a unique opportunity to access the micromechanical signature of the elementary building blocks that constitute cement-based composites. While several studies have investigated the micromechanical properties of pure hydrated and unhydrated cement phases, fewer studies have been conducted to investigate the effect of inclusions. The addition of CNFs and any subsequent formation of microscale CNF agglomerates are expected to have a significant impact on the microscale properties of cement-based composites. Yet, the effect of CNFs and CNF microscale agglomerates on the micromechanical properties of cement-based composites has not been investigated.

CHAPTER 3

DISPERSION OF CNFS IN CEMENT-BASED COMPOSITES

3.1. Overview

CNFs have the potential to be excellent nanoscale reinforcement of cement-based composites due to their excellent properties including high aspect ratios and extraordinary strength (i.e., aspect ratios of about 1000:1 [87] and strengths of over 2.5 GPa [119]). However, CNFs are hydrophobic and possess a strong van der Waals self-attraction that causes them to form agglomerates. The objective of this chapter is to determine the effect of dispersion methods and CNF loading on: (i) CNF disaggregation and dispersion in solutions and (ii) subsequent dispersion and distribution in cement pastes.

The effect of dispersion methods, including covalent, non-covalent, and mechanical methods, and CNF loading on the CNF disaggregation and dispersion in solutions and the subsequent dispersion and distribution in cement pastes was determined using a multiscale experimental approach involving both qualitative and quantitative analysis. The dispersion of CNFs was examined in portland cement pastes and in two (2) types of solutions: (i) an aqueous solution typically as the mix water to make cement-based composites ("*mix water*" solution) and (ii) a solution that simulated the pore solution found in cement-based composites during the hydration process ("*cement pore water*" solution). Visual inspection was used to qualitatively evaluate the dispersion of the CNFs in the solutions and cement pastes on the macroscale, while optical microscopy was used on the microscale. In addition, SEM was used for qualitative evaluation on the microscale for the cement pastes. Quantitative analysis of the dispersion of

CNFs in the solutions and cement pastes was completed using image analysis of micrographs. In addition, a study to determine the effect of w/c ratio on potential CNF migration in cement pastes was performed.

3.2. Experimental Detail

3.2.1. Materials

Commercially available, vapor grown, Pyrograf®-III PR-19-XT-LHT CNFs (Applied Sciences, INC., Cedarville, OH, USA) were used for the study. As per the manufacturer, the CNFs ranged from 70-200 nm in diameter and 50,000 to 200,000 nm in length and had a density of 1.95 g/cm^3 and a surface area of 20-30 m^2/g. The CNFs were used "*as received*" or after surface treatment with HNO_3. Surface treatment with HNO_3 consisted of the immersion and ultrasonication of the CNFs in 67-70% Trace Metal Grade HNO_3 (Fisher Chemical, Waltham, MA, USA) using a liquid to solid ratio of 28.5 mL/g for approximately three (3) hours [42, 120]. The resulting suspension was repeatedly washed in Milli-Q water and filtered using a vacuum filtration system and GHPolypro membrane filters (Pall Corporation, Ann Arbor, Michigan, USA) with 0.45 µm pores until the pH of the wash water was neutral. The filtered CNFs were dried in an oven at 105°C for 24 hours.

Three non-covalent dispersing agents, known to have minimal negative effects on cement hydration reactions [3], were evaluated: a sulfonated naphthalene condensate HRWR (N-HRWR)–*Rheobuild® 1000* (BASF, Ludwigshafen, Germany), a P-HRWR–*Glenium® 7500* (BASF, Ludwigshafen, Germany), and an air-entraining admixture (AE)–*MicroAir®* (BASF, Ludwigshafen, Germany). HRWRs are frequently used in concrete technology to improve the workability of fresh cement-based composites [3]. The N-HRWR works through electrostatic repulsion (i.e., providing particles with a highly negative surface charge by adsorption onto the particle surface so that the particles repel each other) [3]. The P-HRWR works through a dual mechanism: electrostatic repulsion and steric stabilization [3]. Steric stabilization is a mechanism in which the long molecules of the polymer wrap around the particles and inhibit them from approaching each other within the distance that the van der Waals forces are dominant [121]. Sterically stabilized dispersions are not significantly affected by the presence of electrolytes compared to electrostatically stabilized dispersions that are readily disrupted by electrolyte presence [121]. AEs are common practice in concrete technology to increase freeze-thaw and scaling resistances [3]. The AE used for the study is a modified resin acid compound-based anionic surfactant that lowers the surface tension of water allowing for easier dispersion of particles in aqueous solution [3].

The cement pastes were made with type I Portland cement (Holcim (US) Inc., Waltham, MA, USA). The cement composition as determined by X-ray fluorescence (XRF) performed by Lafarge North America Terminal Office (Nashville, TN, USA) and the Bogue equations [122] is given in Table 3.1. The specific surface area of the cement, determined by Lafarge using the Blaine air permeability test, was 423 m^2/kg.

Table 3.1. Composition of the portland cement used as determined by XRF and the Bogue equations (Lafarge North America Terminal Office, Nashville, TN, USA).

Oxide	Percent Mass (%)	Mineral	Percent Mass (%)
SiO_2	20.27	C_3S	57.93
Al_2O_3	5.03	C_2S	14.39
Fe_2O_3	3.86	C_3A	6.8
CaO	63.86	C_4AF	11.75
MgO	1.23		
SO_3	3.03		
Na_2O	0.111		
K_2O	0.471		
Mn_2O_3	0.034		
TiO_2	0.289		
P_2O_5	0.192		
SrO	0.087		

3.2.2. Preparation of CNF Suspensions

3.2.2.1. CNF Suspensions in "Mix Water" Solution

A total of six (6) aqueous suspensions were prepared with 7.2 g/L of CNFs in various Milli-Q water-dispersing agent solutions. The dispersing agent–water weight ratio used was 3.6%. All ratios for the suspensions were selected based on the mix water requirements to make a cement-based composite with 0.2 wt% CNFs (based on values found in the literature [35, 64, 113]), a w/c ratio of 0.28 (based on the study included in Section 3.3.3), and 1 wt% of dispersing agent (based on the manufacture's recommendations). All suspensions were ultrasonicated in a bath sonicator (Aquasonic model 250D, VWR, West Chester, Pennsylvania, USA) for 30 minutes to aid in the disaggregation of the CNFs.

The following suspensions were prepared: (i) "*as received*" CNFs in water [W/CNF], (ii) surface treated CNFs in water [W/T-CNF], (iii) "*as received*" CNFs in water–N-HRWR solution [N-HRWR/CNF], (iv) "*as received*" CNFs in water–AE solution [AE/CNF], (v) surface treated

CNFs in water–P-HRWR solution [P-HRWR/T-CNF], and (vi) "*as received*" CNFs in water–P-HRWR solution [P-HRWR/CNF].

3.2.2.2. CNF Suspensions in "Cement Pore Water" Solution

A total of four (4) suspensions were prepared in "*cement pore water*" solution. The "*cement pore water*" solution simulated the pore water of cement paste at an age of two (2) hours with a composition as reported in [123]. The solution was made with Milli-Q water and 20.2 g/L potassium hydroxide (KOH), 1.16 g/L sodium hydroxide (NaOH), and 21.34 g/L calcium sulfate hemihydrate ($CaSO_4{\cdot}½H_2O$), resulting in a measured pH of ~13.3 and conductivity of ~43.9 mS/cm and a calculated ionic strength of 0.977 mol/L. The solution was stirred with a magnetic stirrer for 1 hour and ultrasonicated for 30 minutes in a bath sonicator (Aquasonic model 250D, VWR, West Chester, Pennsylvania, USA) before addition to the CNFs and dispersing agents. A dispersing agent–Milli-Q water weight ratio of 3.6% and 7.2 g/L of CNFs were used similar to the suspensions made with the "*mix water*" solution. After the "*cement pore water*" solution was added to the CNFs and dispersing agents, the suspensions were ultrasonicated for 30 minutes in the bath sonicator.

The following suspensions were prepared: (i) "*as received*" CNFs in "*cement pore water*" solution with no dispersing agent [PW/CNF], (ii) "*as received*" CNFs in "*cement pore water*"–N-HRWR solution [PW/N-HRWR/CNF], (iii) "*as received*" CNFs in "*cement pore water*"–AE solution [PW/AE/CNF], and (iv) "*as received*" CNFs in "*cement pore water*"–P-HRWR solution [PW/P-HRWR/CNF].

3.2.3. Preparation of CNF/Cement-Based Composites

3.2.3.1. Preliminary Study for Determining W/C Ratio

A preliminary study was performed to determine the w/c ratio to be used for the cement pastes in the study of CNF dispersion to limit excessive bleeding or segregation and in turn potential migration of CNFs. Six (6) cement-based composites were made each with a different w/c ratio. The w/c ratios evaluated were 0.25, 0.28, 0.30, 0.43, and 0.50. CNFs were used at a loading of 0.2 wt% and were dispersed using 1 wt% of P-HRWR. The Milli-Q water, P-HRWR, and CNF suspensions were ultrasonicated in a bath sonicator (Aquasonic model 250D, VWR, West Chester, Pennsylvania, USA) for 30 minutes before mixing with the cement for 6 minutes using a variable-speed stand mixer (KitchenAid Artisan 5-quart, Whirlpool Corporation, Benton Charter Township, Michigan, USA). After mixing, the cement pastes were poured into 5.08 cm × 10.16 cm (2 in. × 4 in.) cylindrical molds and compacted by hand. The cylinders were observed during the first two (2) hours of curing and then cured at room temperature in 100% relative humidity for seven days before comparison. The molds were removed carefully by hand to ensure minimal disruption of the top surface of the specimens.

3.2.3.2. CNF/Cement-Based Composites

Cement pastes were prepared using the different "*mix water*" solutions discussed in Section 3.2.2.1 including: PC-W/CNF made with the W/CNF suspension, PC-W/T-CNF made with the W/T-CNF suspension, PC-N-HRWR/CNF made with the N-HRWR/CNF suspension, PC-AE/CNF made with the AE/CNF suspension, PC-P-HRWR/CNF (also referred to as PC-0.2%) made with the P-HRWR/CNF suspension, and PC-P-HRWR/T-CNF made with P-

HRWR/T-CNF suspension. Additionally cement pastes with 0.02, 0.08, 0.5, and 1 wt% loading of “*as received*” CNFs were prepared using only P-HRWR as the CNF dispersing agent (PC-0.02%, PC-0.08%, PC-0.5%, and PC-1%). In addition, four (4) control composites containing no CNFs were made with the “*mix water*” solutions discussed in Section 3.2.2.1 including: PC-W/Control made with water and no dispersing agent, PC-N-HRWR/Control made with water and N-HRWR, PC-AE/Control made with water and AE, and PC-P-HRWR/Control (also referred to as PC-0%) made with water and P-HRWR. A w/c ratio of 0.28 was used for all composites to limit CNF migration in the cement pastes and prevent dispersion issues due to excessive bleeding or segregation. This w/c ratio was determined from the study discussed in Section 3.2.3.1 and Section 3.3.3. The dispersive agents were all used at 1 wt%, the same ratio as in Section 3.2.2.1, which was chosen based on the manufacturer’s recommendations.

To make the composites, the water, dispersing agent, and CNFs were first ultrasonicated in a bath sonicator (Aquasonic model 250D, VWR, West Chester, Pennsylvania, USA) for 30 minutes to disaggregate the CNFs. Then the water, dispersing agent, and CNF suspension were added to the cement and blended for 6 minutes in a variable-speed stand mixer (KitchenAid Artisan 5-quart, Whirlpool Corporation, Benton Charter Township, Michigan, USA). The cement-based composites were made into 5 cm × 10.16 cm (2 in.× 4 in.) cylinders and 2.54 cm × 2.54 cm × 68.58 cm (1 in.× 1 in.× 27 in.) beams for mechanical testing. The cylinders and beams were compacted by hand to avoid reagglomeration of the CNFs that could occur during vibration. Samples were cured at room temperature in 100% relative humidity for 7 and 28 days prior to testing.

Representative cross-sections of each composite were cut for image mapping and analysis using a precision saw with oil to ensure further hydration of the cement-based composites did not occur due to the specimen preparation procedure. The cross-sections were furthermore polished to at least 35 μm particle size using silicon carbide paper in an alcohol and ethylene/polypropylene glycol solution. Additionally, fracture surfaces of each composite were dried in acetone to stop the hydration reaction at the curing ages of 7 and 28 days for SEM observations. Before SEM observation, the fracture surfaces were sputter-coated with gold using a Cressington Sputter Coater 108 (Cressington Scientific Instruments Ltd., Watford, Hertfordshire, England) with a deposition time of 100 seconds and mounted on an aluminum stub using copper tape.

3.2.4. Characterization

3.2.4.1. Visual Inspection

CNF suspensions. Visual inspection of the CNF suspensions made with the "*mix water*" and "*cement pore water*" solutions was used to collect comparative data on the effectiveness of the dispersion methods to disaggregate and disperse CNFs in solution. The CNF suspensions were observed for a minimum of fifteen (15) days.

CNF migration in CNF/cement-based composites. The top surfaces of the cement-based composites with varying w/c ratios were visually examined for the presence of excessive CNFs due to CNF migration during curing. In addition, the composites were compared side-by-side to determine any physical differences in the composites or their top surfaces.

3.2.4.2. Optical Microscopy

CNF suspensions. Suspensions of CNFs in the "*mix water*" and "*cement pore water*" solutions were evaluated using an Zeiss Axiovert 200M motorized inverted microscope (Carl Zeiss MicroImaging, Inc., Thornwood, New York, USA) with Achroplan40x/0.60 Corr objective and a W-PL 10X/23 eyepiece. Drops of the suspensions were placed on a glass slide and covered with a cover glass for microscopic examination. Interference of moving particles due to Brownian motion was alleviated by allowing sufficient time for the particles to settle (i.e., 5-10 minutes) and by recording several images of each drop taken at different locations. For each suspension, a minimum of fifteen (15) representative drops was examined and ten (10) representative micrographs were collected for each drop. Images were taken at 400X magnification.

Quantitative data was obtained by analyzing the digital micrographs of the CNF suspensions obtained using ImageJ (National Institute of Health, Bethesda, Maryland, USA), a Java-based open source digital image processing software. A minimum of 150 images were analyzed for each CNF suspension. A similar cumulative area of the projected CNF particle system was used for all suspensions, resulting in an investigated total area of *ca*. 1.2 mm^2 per suspension type. A binary image was created from each micrograph by applying a threshold to the image that was set manually to an appropriate limit. The threshold limit was chosen so that all CNFs present in the image were captured and that background pixels were not converted to black and therefore interfering with the analysis. After conversion to a binary image, the images were cropped such that all images covered the same area and the interference from the reduced illumination around the edge of the images was eliminated. The state of CNF dispersion in each “*mix water*” solution was then evaluated by plotting the number of CNF particles per mm^2 areal coverage versus the area of the projected CNF particles of each area class. The CNF suspensions in “*cement pore water*” solution were evaluated by plotting the cumulative area of CNF particles versus the maximum Feret's diameter of each CNF particle.

CNF/cement-based composites. Several cross-sections from each composite were evaluated qualitatively for dispersion and distribution of CNF agglomerates using optical microscopy with 30X magnification such that a representative cross-section could be chosen for quantitative analysis. Image mapping of each specimen’s representative cross-section (total surface area of 6.45 cm^2) consisting of 1350 images, each 27.6 × 20.6 pixels, was completed using the image mapping system of a New Wave UP-213 Laser Ablation System (Electro Scientific Industries, Inc., Portland, Oregon, USA). A combination of thresholding techniques and visual inspection was used to create a binary image showing only agglomerates of CNFs in the cement pastes. ImageJ software was used to determine the size and shape properties of the CNF agglomerates, and histograms were used to evaluate the dispersion quantitatively. Only CNF agglomerates larger than 0.007 mm^2 in size were evaluated because of limitations in the analysis due to the capabilities of the optical microscope.

3.2.4.3. SEM

The microstructure and morphology of fracture surfaces of the cement-based composites was evaluated using a Hitachi S4200 high resolution SEM (Hitachi Ltd., Chiyoda, Tokyo, Japan) equipped with a cold field emission electron gun and digital imaging. An accelerating voltage of 20 kV and a working distance of 15 mm were used.

3.3. Results and Discussion

*3.3.1. Disaggregation and Dispersion of CNFs in "*Mix Water*" Solutions*

Visual inspection of the macroscale dispersion showed the CNF suspensions made with the "*mix water*" solutions to be uniformly dispersed when a dispersing agent was used (AE/CNF, N-HRWR/CNF, P-HRWR/CNF, and P-HRWR/T-CNF). When a dispersing agent was not used (W/CNF and W/T-CNF), the CNFs either stayed mostly at the liquid air interface or precipitated out of the suspension (Figure 3.1). Although the disaggregation and dispersing ability of the dispersing agents (AE, N-HRWR, and P-HRWR) was better than surface treatment with HNO_3 alone, the surface treatment did improve the dispersion of the CNFs compared to the W/CNF suspension. Surface treating the CNFs with HNO_3 reduced the hydrophobicity of the CNFs allowing more of the CNFs to enter into the solution instead of staying at the liquid-air interface [124]. However, the W/T-CNF suspension showed overall a poor dispersion quality with large size agglomerates and poor content uniformity. While the AE/CNF, N-HRWR/CNF, P-HRWR/CNF, and P-HRWR/T-CNF solutions showed good macroscopic dispersion, the dispersion quality of each solution could not be distinguished from the others from sole visual inspection, except for the presence of a thin film of CNF agglomerates observed at the surface of the N-HRWR assisted dispersion and a layer of foam with CNF agglomerates at the surface of the AE assisted dispersion.

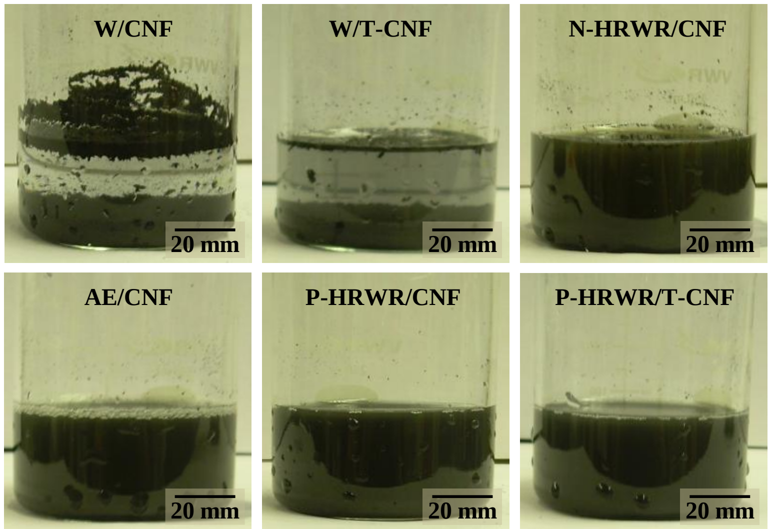

Figure 3.1. Visual comparison of aqueous suspensions containing CNFs. From top left to bottom right: "*as received*" CNFs in Milli-Q water, surface treated CNFs in water, N-HRWR assisted dispersion of "*as received*" CNFs, AE assisted dispersion of "*as received*" CNFs, P-HRWR assisted dispersion of "*as received*" CNFs, and P-HRWR assisted dispersion of surface treated CNFs.

Differences in the CNF dispersion state when the dispersing agents were used was revealed from optical microscopy investigations (Figure 3.2). The largest number of CNF particles per mm^2 in the smallest size area class (0-100 μm^2) was seen for the P-HRWR assisted dispersions, indicating a greater ability of the P-HRWR dispersing agent to break up a larger number of bigger particles into smaller particles than N-HRWR and AE. Surface treatment with HNO_3 further improved the CNF dispersion in the water–P-HRWR solution as evidenced by the greater number of particles per mm^2 in the smallest size area class (less than 100 μm^2) compared to that with the "*as received*" CNFs. The N-HRWR assisted dispersion showed the highest frequency of relatively large size agglomerates (>500 μm^2) and the lowest number of particles per mm^2 in the smallest size area class (0-100 μm^2), indicating that N-HRWR was not as effective in the disaggregation of large agglomerates as the other dispersing agents. The AE assisted dispersion decreased the CNF aggregative tendency in water but not as well as the P-

HRWR assisted dispersion. For all CNF suspensions, the number of particles in the smallest size area class (0-100 μm^2) was at least one order of magnitude greater compared to the other size area classes. The largest agglomerate size was seen for the AE and N-HRWR assisted dispersions (~25,000 μm^2) and was twice as the maximum size seen for the P-HRWR assisted dispersions.

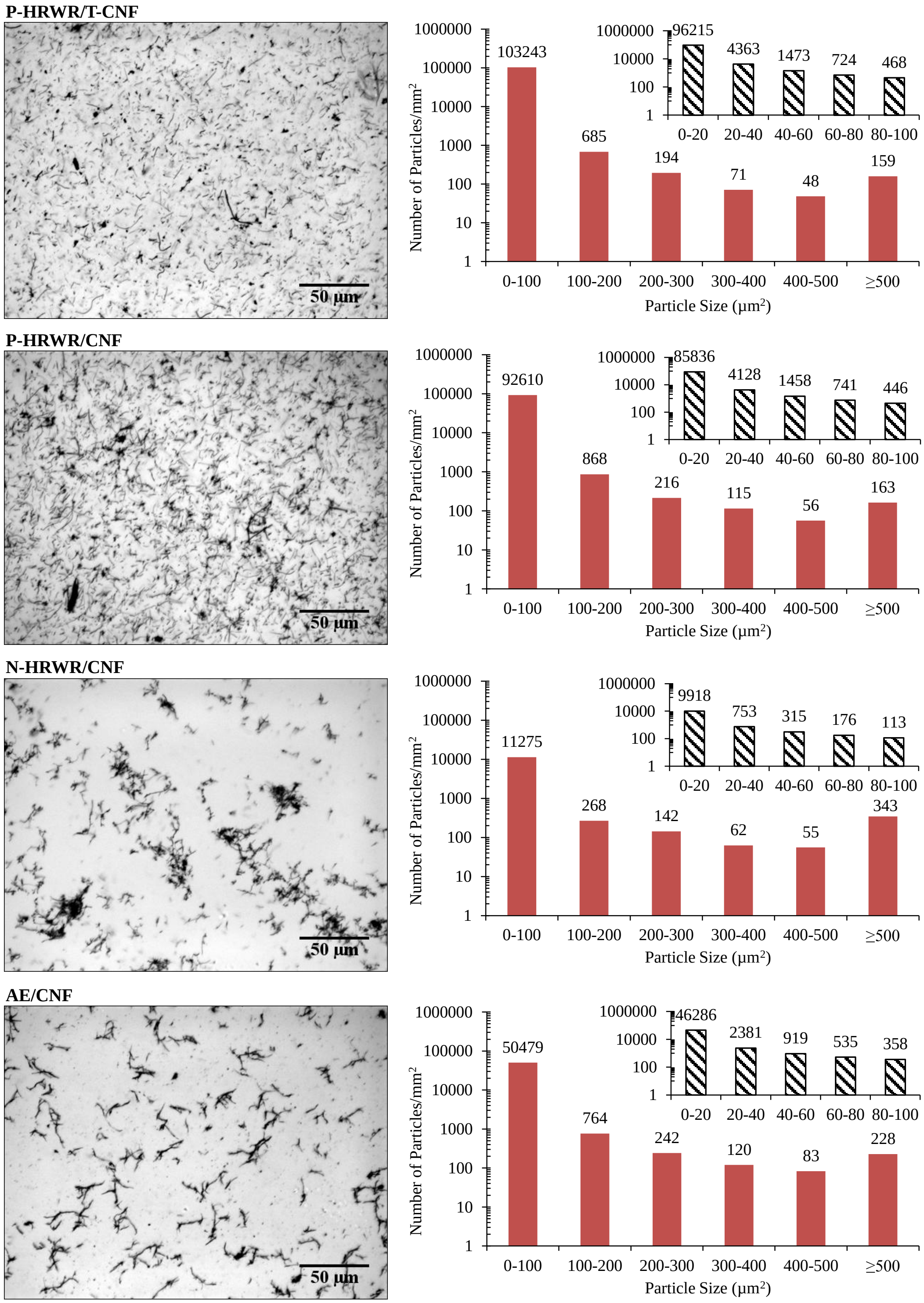

Figure 3.2. Optical micrographs (400X) and histograms of the number of CNF particles per mm² areal coverage versus the area of the projected CNF particles of each area class showing the state of CNF dispersion in "*mix water*" solutions (raw data is included in Appendix A). From top to bottom: P-HRWR assisted dispersion of surface treated CNFs, P-HRWR assisted dispersion of "*as received*" CNFs, N-HRWR assisted dispersion of "*as received*" CNFs, and AE assisted dispersion of "*as received*" CNFs.

*3.3.2. Disaggregation and Dispersion of CNFs in "*Cement Pore Water*" Solutions*

Visual inspection showed all "*cement pore water*" CNF suspensions containing dispersing agents to be uniformly dispersed at the macroscale level immediately after ultrasonication (Figure 3.3). The "*cement pore water*" CNF suspension with no dispersing agent showed, however, a large layer of unwetted CNFs at the liquid-air interface. Thirty (30) minutes after ultrasonication, settling of the CNFs had occurred for all suspensions, independent of the dispersing agent used. The settling was least noticeable in the suspension that contained P-HRWR with a large number of CNFs that were still suspended in the solution. Three (3) hours of resting after ultrasonication allowed the majority of the CNFs to fall out of the suspension when no dispersing agent, AE, or N-HRWR was used. (Note: the brown color of the solution that contained N-HRWR was resultant from the N-HRWR not the CNFs.) The suspension that contained P-HRWR still had enough CNFs suspended in the solution to make visibility of CNF settling difficult, but closer examination showed that the majority of the CNFs had settled out of the suspension. In contrast, the settling of the CNFs was not observed when the "*mix water*" solutions were used, even after 15 days indicating that the instability of the "*cement pore water*" suspensions was the result of the highly alkaline environment and increased ionic strength (pH ≈ 13.3 and conductivity ≈ 44 mS/cm) of the simulated cement pore solution [121, 125]. The ions present in the "*cement pore water*" solution have been shown to increase the surface tension of aqueous solutions [126]. Therefore, it was believed that the decreased surface tension allowed by the AE was negated by the increases caused by the ions which negatively affected the dispersing ability of the AE. Additionally, the electrostatic boundary layer around the CNFs from the P-HRWR and N-HRWR is reduced by the increased amount of electrolytes present in the solution allowing the CNFs to come into contact or within the distance in which the van der Waals forces are dominant [121]. Thus, microscale CNF agglomerates were formed, and settling of the agglomerates occurred. In contrast, the steric hindrance of the P-HRWR was minimally affected by the increased amount of electrolytes allowing some CNFs to stay suspended.

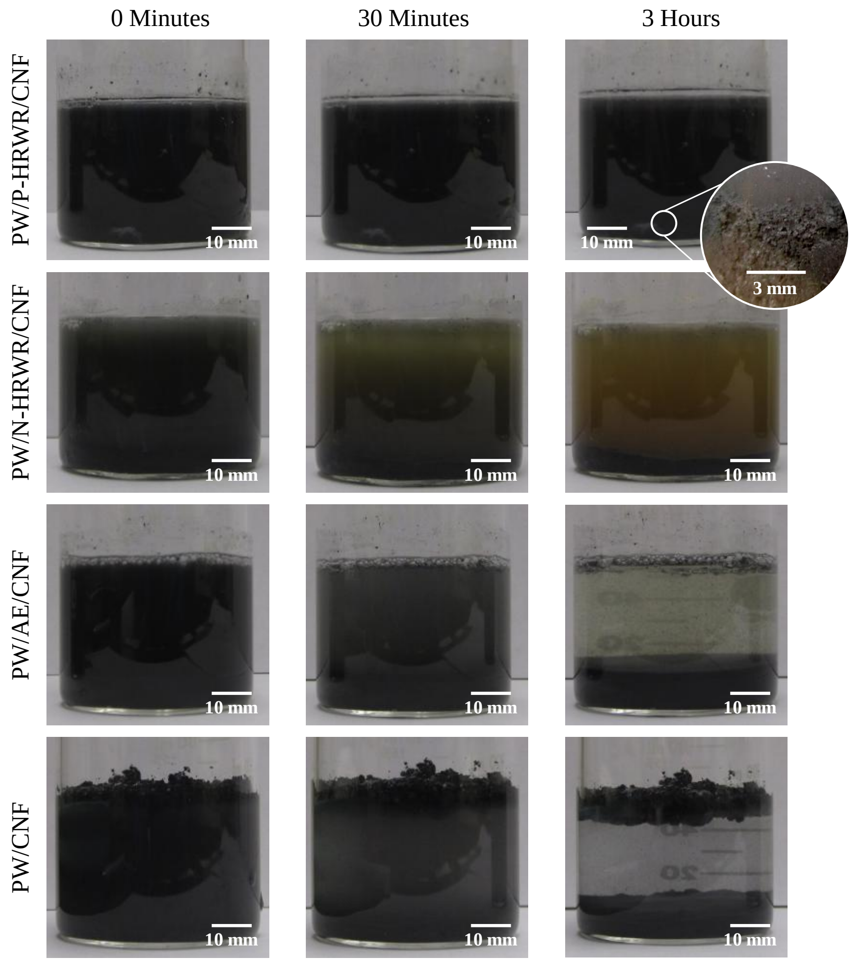

Figure 3.3. Visual comparison of suspensions containing CNFs in a solution made to simulate the pore solution of cement paste during the early hours of curing. From left to right: immediately after ultrasonication, 30 minutes after ultrasonication, and 3 hours after ultrasonication. From top to bottom: "*as received*" CNFs with P-HRWR in "*cement pore water*" solution, "*as received*" CNFs with N-HRWR in "*cement pore water*" solution, "*as received*" CNFs with AE in "*cement pore water*" solution, and "*as received*" CNFs with no dispersing agent in "*cement pore water*" solution.

Further examination of the suspensions made with the "*cement pore water*" solution (PW/P-HRWR/CNF) using optical microscopy showed a decreased dispersion of the CNFs when compared to the "*mix water*" (P-HRWR/CNF) (Figure 3.4). CNFs were found in larger agglomerates in the PW/P-HRWR/CNF suspension than the P-HRWR/CNF suspension. In addition, overall there were less CNFs in the micrographs of the PW/P-HRWR/CNF suspension due to the sedimentation of the CNFs that was occurring. By plotting the cumulative area of CNFs as a function of the maximum Feret's diameter of each CNF particle, it can be noticed that a greater percentage of the area of CNFs are made up of particles with a larger diameter when the "*cement pore water*" solution was used than when the "*mix water*" solution was used (Figure 3.5).

a) b)

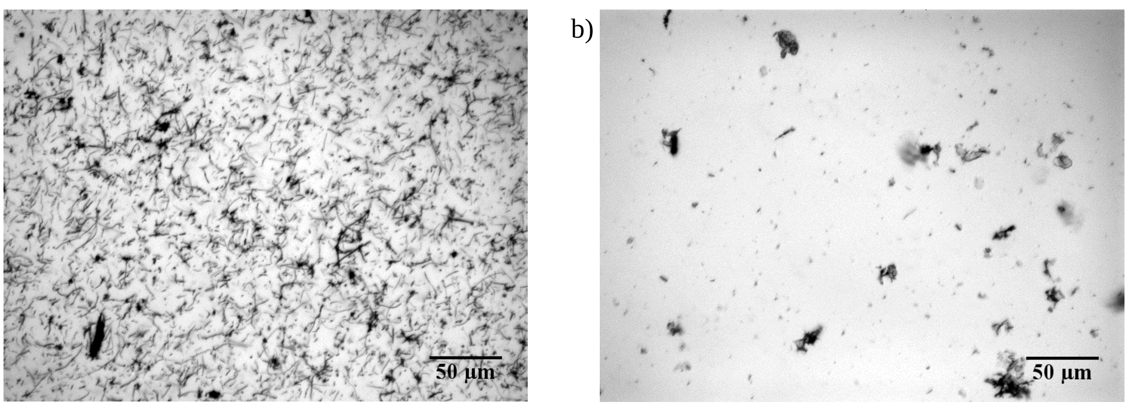

Figure 3.4. Optical micrographs (400X) showing the dispersion of CNFs in a) aqueous solution ("*mix water*", P-HRWR/CNF) and b) simulated pore solution immediately after ultrasonication ("*cement pore water*", PW/P-HRWR/CNF).

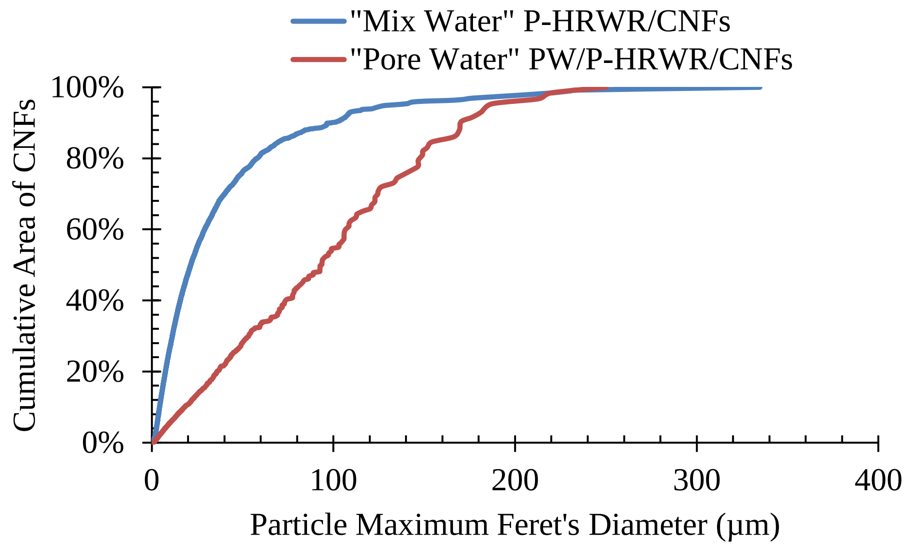

Figure 3.5. Cumulative area of CNFs and the maximum Feret's diameter of each CNF particle comparing P-HRWR/CNF (“*mix water*”) and PW/P-HRWR/CNF (“*cement pore water*”).

3.3.3. CNF Migration with Bleed Water and W/C Ratio

Cylinders with w/c ratios ranging from 0.25 to 0.50 were compared to determine the effect of the w/c ratio on the CNF dispersion in cement pastes (Figure 3.6). The amount of CNFs present at the upper surface of the specimens and the color of each cylinder clearly varied as a function of the w/c ratio. All cylinders with a w/c ratio greater than or equal to 0.33 had a visible porous layer of CNFs intermixed with cement paste at the upper surface of the specimens. The layer became more friable and softer to the touch as the w/c ratio increased. The porous layer was resultant of the CNFs migrating with the bleed water during curing. A closer look at the porous layer showed a high amount of CNFs intermixed with cement phases (Figure 3.7). The results of this study were used to determine the w/c ratio used in all subsequent studies.

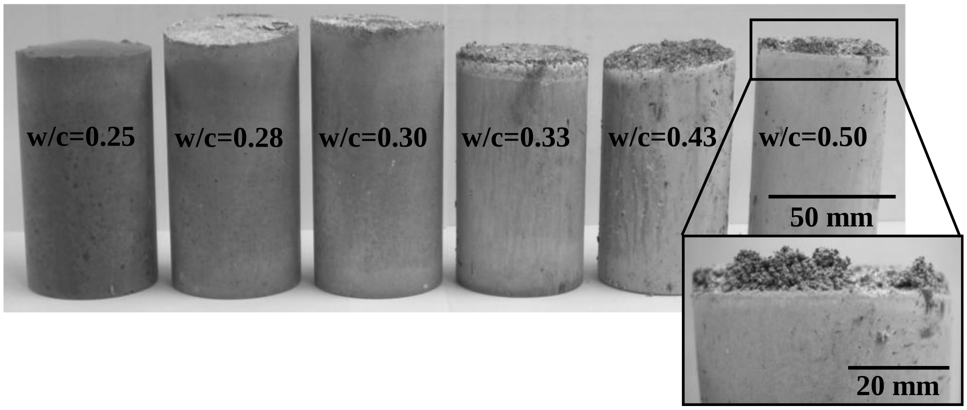

Figure 3.6. Visual comparison of CNF migration in cement paste specimens with varying w/c ratios.

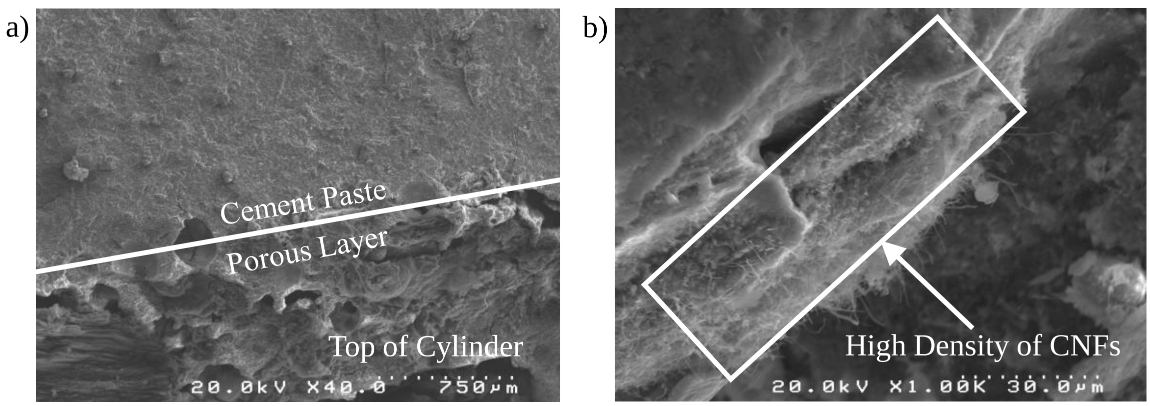

Figure 3.7. SEM images of the porous layer caused by CNF migration during curing showing: a) clear separation between the porous layer and cement paste and b) the high density of CNFs present in the porous layer.

3.3.4. Dispersion and Distribution of CNFs in Cement-Based Composites

The dispersion state of the CNFs in the cement-based composites was evaluated on the micro- and macroscale. The state of CNF dispersion was dependent upon the scale of evaluation and was not homogenous throughout the specimens. Independent of the dispersion method used, the CNFs were not uniformly distributed in the cement-based composites with both individual and agglomerated CNFs being present. Furthermore, the distribution of individual CNFs (also independent of the dispersion method used) was not uniform within the composites with the presence of CNF-rich and CNF-poor regions (Figure 3.8). The large size and clumping of cement grains have been reported to be responsible for the non-uniform dispersion of the CNFs by creating zones absent of CNFs even after hydration has progressed [52]. Additionally, the instability of CNF suspensions reported in Section 3.3.2 in a highly alkaline environment similar to what would be found in cement-based composites and the CNF migration with the bleed water during curing as discussed in Section 3.3.3 were expected to increase the probability of reagglomeration of CNFs during cement mixing and curing.

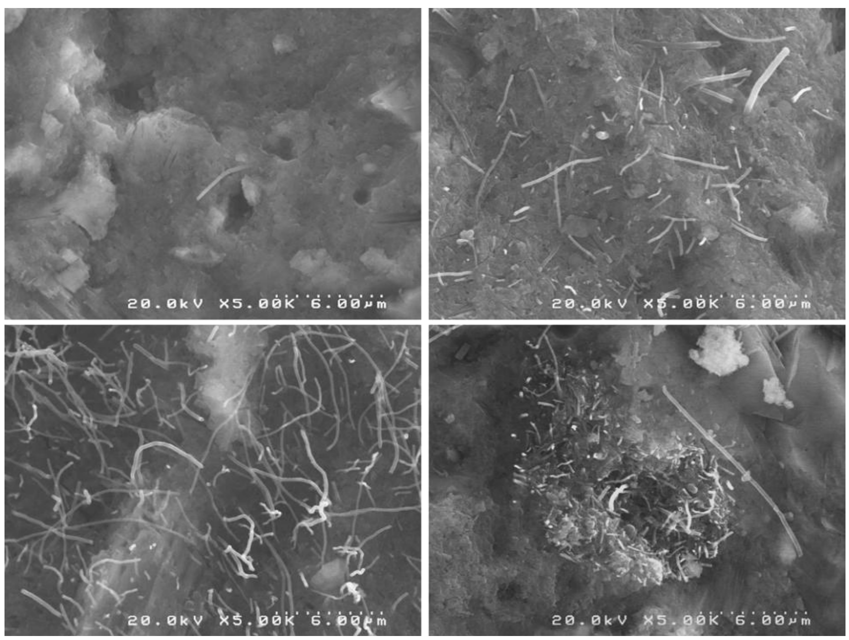

Figure 3.8. SEM images showing the varying distribution of CNFs in cement-based composites taken from a single, representative fracture surface using the same magnification (composite with 1 wt% CNFs dispersed with P-HRWR).

The microscale CNF agglomerates were seen regardless of the initial degree of CNF dispersion in solution and became more prominent with increasing CNF loading (Figure 3.9 and Figure 3.10). (Note: CNF agglomerates less than 0.007 mm^2 in size were not included in Figure 3.9 and Figure 3.10 due to limitations of the micrograph analysis method.) Larger size agglomerates (as much as an order of magnitude greater) than what was observed in the CNF suspensions were seen in all composites, indicating secondary agglomeration of formerly dispersed CNFs after cement mixing. For the composites prepared with the P-HRWR, N-HRWR, and AE assisted dispersions, more than 40% of the CNF agglomerates observed at the surface of the composite cross-sections had a size area greater than the maximum size observed in the "*mix water*" suspensions. Secondary agglomeration occurred independent of the CNF loading and dispersing agent used. The high pH (i.e., 13.5-13.8 [127]) and ionic strength (i.e., 0.3-0.7 mol/L [127]) occurring during cement mixing was thought to have caused the reagglomeration of the CNFs because of the instability of the electrostatic boundary layer in the presence of electrolytes for the P-HRWR and N-HRWR assisted dispersions [121] and the increase in the surface tension caused by the electrolytes [126] as was seen in the "*cement pore water*" study discussed in Section 3.3.2. Though electrosteric stabilized dispersions, as is found with the P-HRWR, are less sensitive to the presence of the electrolytes, the reagglomeration observed in the composite prepared with the P-HRWR assisted dispersion was believed to be the result of the complex interplay between electrostatic and steric effects and a potential decrease in the thickness of the sterically-stabilizing "hairy" layer on exposure to the cement solution and mechanical mixing [128]. Consequently, the steric hindrance imposed by the P-HRWR solution on CNFs became practically nonexistent. Surface treatment with HNO_3 did not prevent secondary agglomeration.

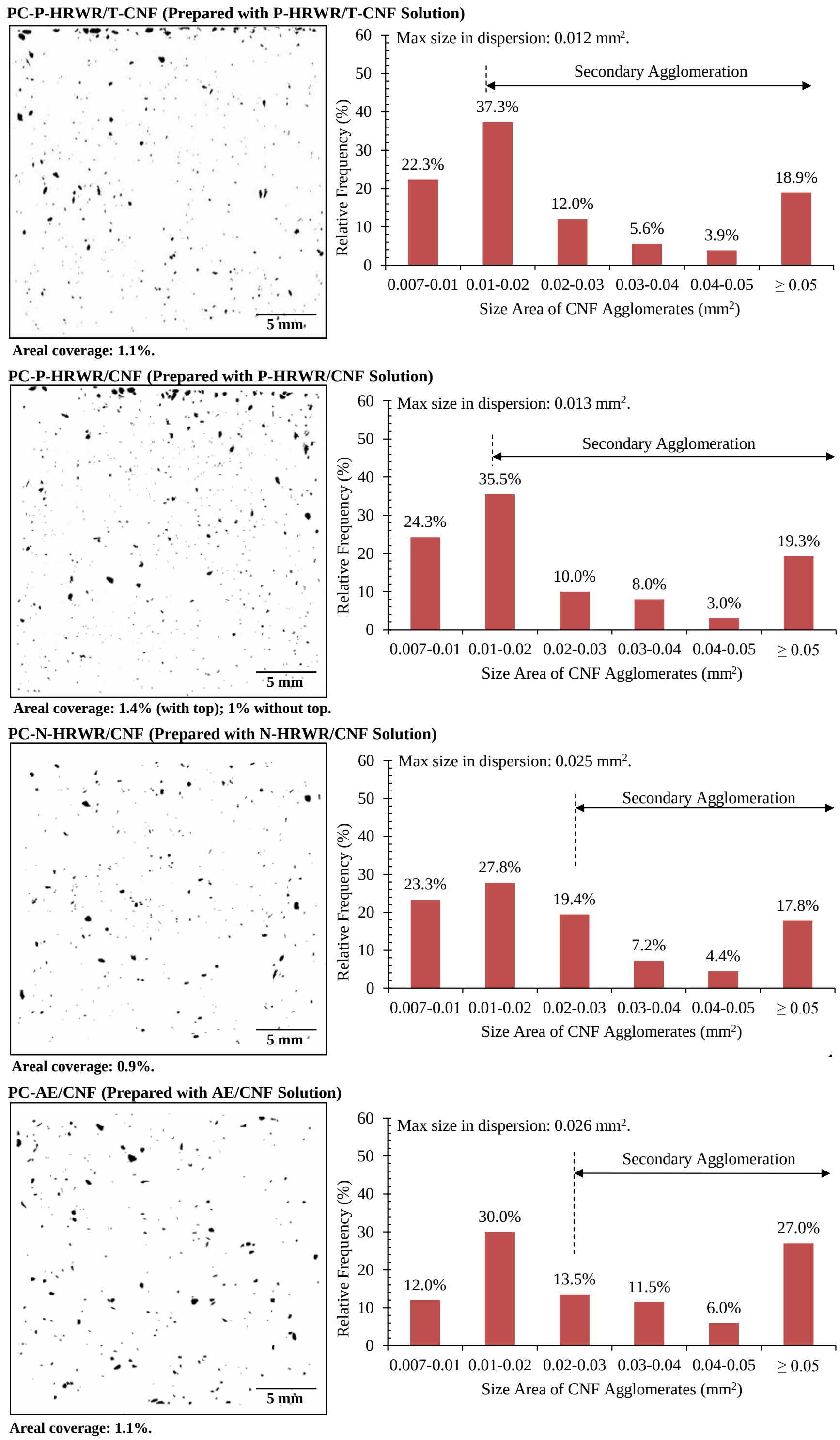

Figure 3.9. Binary images of cement-based composite cross-sections containing 0.2 wt% CNFs dispersed by various methods and distributions of CNF agglomerate sizes larger than 0.007 mm^2 in the cross-section showing secondary agglomeration (raw data included in Appendix B). [From top to bottom: P-HRWR assisted dispersion of surface treated CNFs, P-HRWR assisted dispersion of "*as received*" CNFs, N-HRWR assisted dispersion of "*as received*" CNFs, and AE assisted dispersion of "*as received*" CNFs].

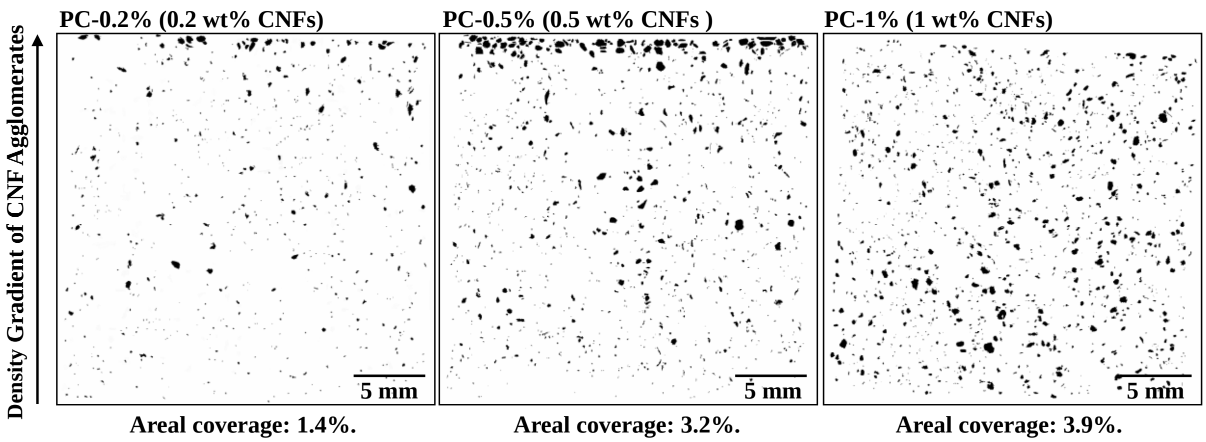

Figure 3.10. Binary images of the surface of cross-sections of CNF/cement-based composites prepared with the P-HRWR assisted dispersion showing CNF agglomerates of size area greater than 0.007 mm^2 with a density gradient of CNF agglomerates seen for 0.2 wt% and 0.5 wt% CNF loadings.

Composites prepared with the AE and N-HRWR assisted dispersions exhibited a greater relative frequency of large size agglomerates than that prepared with the P-HRWR assisted dispersion, as evidenced from the distribution of maximum Feret's diameters (Figure 3.11). For the composites prepared with the AE and N-HRWR assisted dispersions, as much as 79% and 64%, respectively, of the CNF agglomerates observed at the surface of the representative composite cross-sections had a maximum Feret's diameter greater than 200 μm versus 58% for the composite prepared with the P-HRWR assisted dispersion and 56% for that prepared with surface treated CNFs suspended in water–P-HRWR solution. In comparison, the composites prepared with the W/CNF and W/T-CNF suspensions showed 62% and 76%, respectively, of the CNF agglomerates with a maximum Feret's diameter greater than 200 μm. Surface treatment alone favored large scale agglomeration of the CNFs in the cement-based composite. However, when used in combination with the P-HRWR dispersing agent, surface treatment did not affect the relative frequency of large size CNF agglomerates.

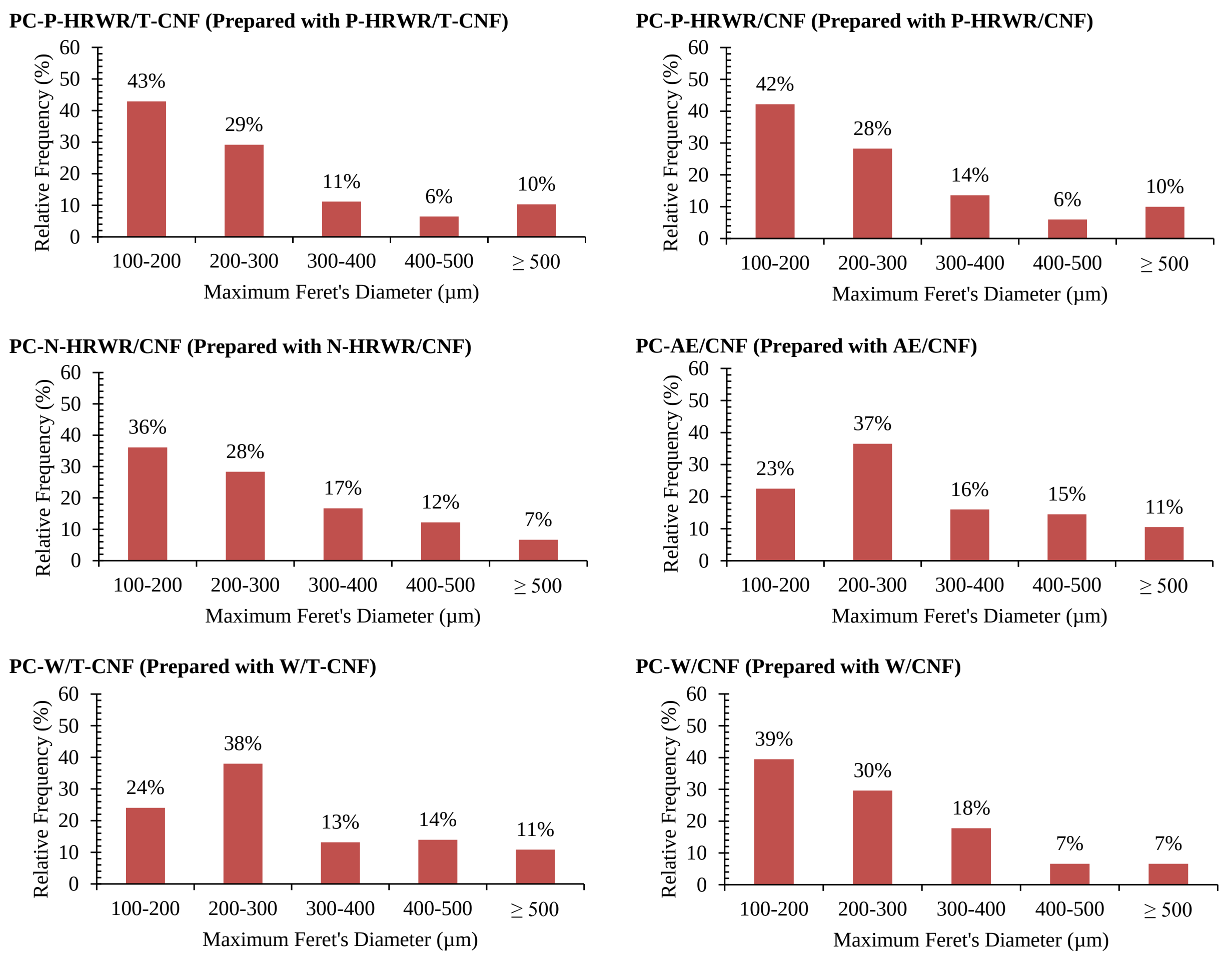

Figure 3.11. Relative frequency histograms of maximum Feret's diameter of CNF agglomerates observed at the surface of the CNF/cement-based composite cross-sections (composites with 0.2 wt% CNF loading, raw data included in Appendix B).

These results clearly showed that the dispersion state of the CNFs in solution is not indicative of the final dispersion state in the hydrated cement paste. The final state of dispersion of the CNFs within the cement paste was the result of a competition between: (i) the tendency of CNFs to migrate towards each other or existing agglomerates due to Brownian motion and van der Waals interactions during cement mixing, (ii) the influence of the high ionic strength of the cement paste medium on altering the surface properties of the CNFs, resulting in greater propensity for loss of individual CNFs and rebundling, and (iii) the effect of mechanical mixing, further increasing the probability of CNF agglomerates or individual CNFs to come in contact with each other. CNF agglomerate size was a balance of agglomerate growth and destruction.

Interestingly, the composites prepared with the P-HRWR assisted dispersion showed a density gradient of CNF agglomerates, with a higher density of CNF agglomerates at the top surface (as cured) of the specimens and a lower density at the bottom surface (Figure 3.10). Furthermore, smaller size CNF agglomerates were seen at the bottom than at the top surface of the specimens. Migration of the CNFs within the cement paste occurred with the bleed water during the initial stage of curing before hardening. This migration resulted additionally in a porous layer containing a large amount of CNF agglomerates observed at the upper surface of the specimens. The CNF agglomerates tended to locate themselves to minimize their surface tension, concentrating at the top surface of the specimens (i.e., air-liquid interface) during curing. The density gradient and layer of CNF agglomerates were predominant at CNF loadings less than or equal to 0.5 wt% but not present for a loading of 1 wt%, most likely as a result of changes in paste rheology resulting in a lower water movement during curing. Migration of the CNFs within the cement paste was not observed for the other composites, including the composites prepared with N-HRWR and AE assisted dispersions and that prepared with CNFs in water likely due to the reduced workability of the fresh pastes compared to the fresh pastes containing P-HRWR (Figure 3.12). In addition, it can be seen in Figure 3.12 that surface treatment of the CNFs with HNO_3 had minimal effect on the migration of the CNFs. The mechanism of CNF migration in the paste was related to the cement paste rheology which was affected by the CNF loading and type of dispersing agent used with a lower workability observed for the composites prepared with 1 wt% CNF loading, N-HRWR and AE assisted dispersions, and that prepared with no dispersing agents, resulting in a lower water movement during curing.

For all cases, including that where a density gradient was observed, the distribution of the CNF agglomerates showed no difference at the edge of the composites compared to the center, indicating that edge and mold effects had no impact on the CNF agglomerate distribution.

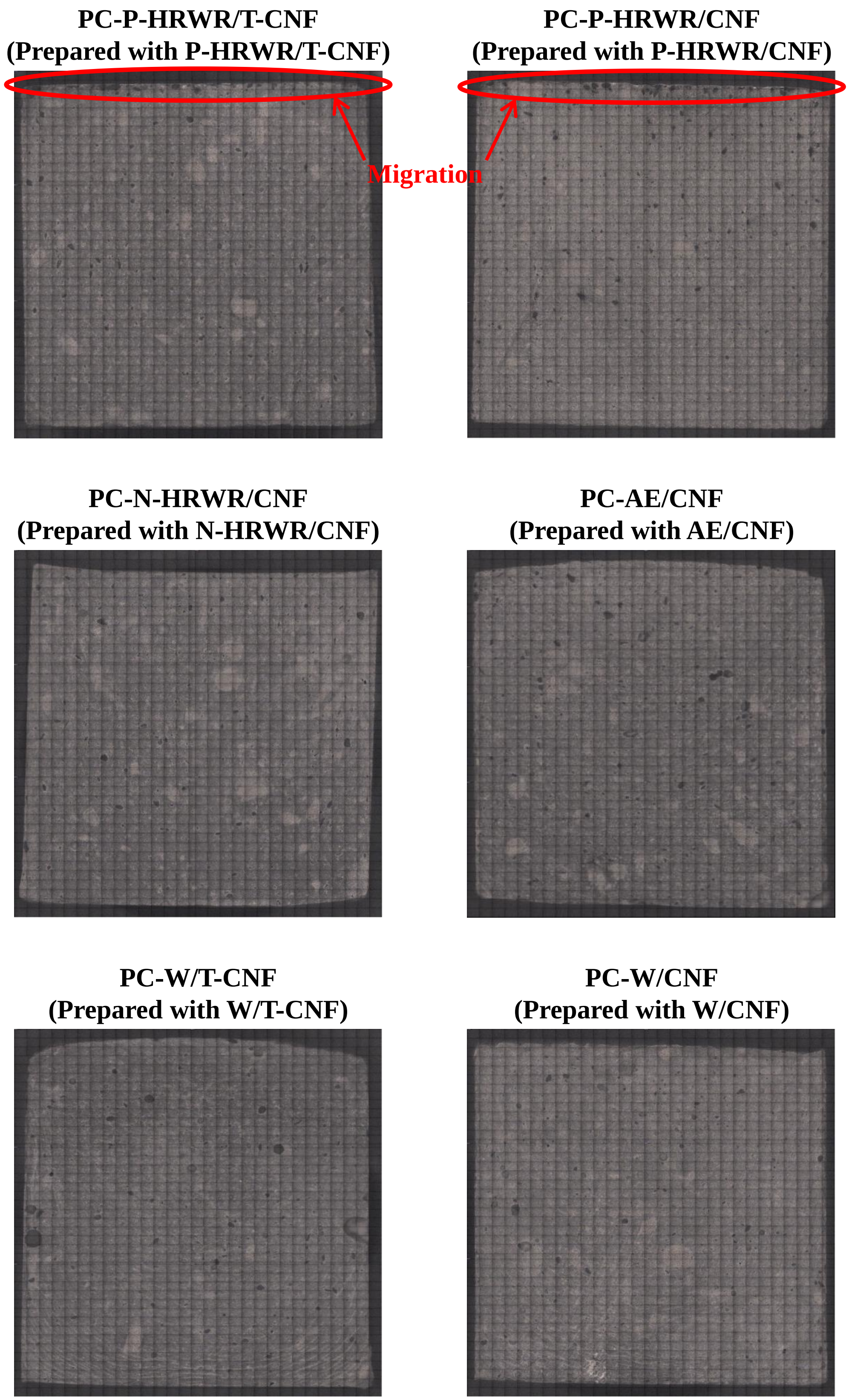

Figure 3.12. Images of cement-based composites showing evidence of CNF migration only in the composites with P-HRWR.

Additional details of the structure of the microscale agglomerates and the curved morphology of the CNFs can be seen in Figure 3.13 from secondary SEM image of the 0.08 wt% CNF loading. The presence of the agglomerate in and around a void in Figure 3.13 showed that the edge of the agglomerate was well integrated with the cement matrix surrounding it. However, the microscale agglomerates were not found fully infiltrated by the cement phases. Closer examination showed the agglomerates consist of a loosely packed structure of a disordered network of entangled fibers and bundles.

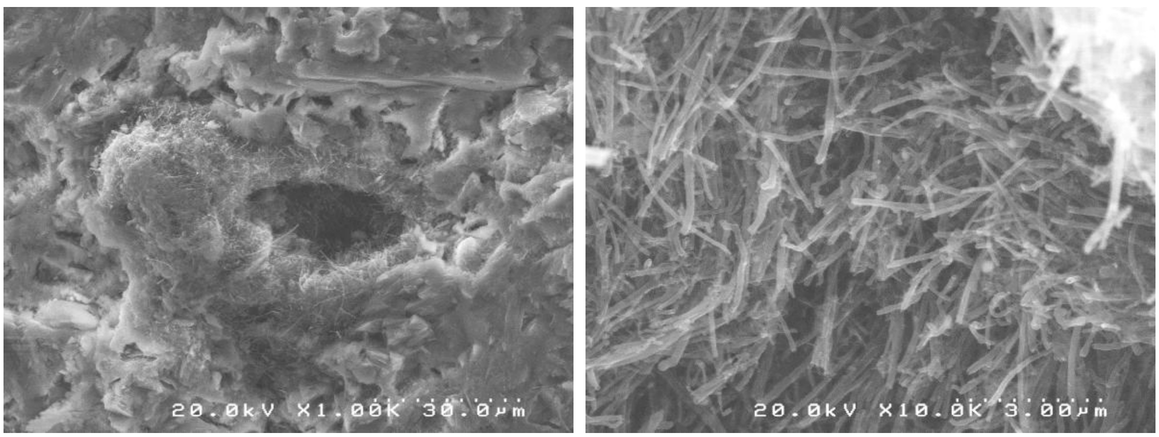

Figure 3.13. SEM images showing the disordered structure of the microscale agglomerates (cement-based composites prepared with the P-HRWR assisted dispersion and 0.08 wt% CNF loading).

3.4. Conclusions

The dispersion of CNFs was investigated including their disaggregation and dispersion in a "*mix water*" solution and a "*cement pore water*" solution, and their subsequent dispersion and distribution in cement pastes. Three (3) different dispersing agents (P-HRWR, N-HRWR, and AE) and surface treatment with HNO_3 were investigated. The following conclusions were drawn:

- In "*mix water*" solutions, the dispersive ability of the three dispersing agents was not distinguishable at the macroscale level, but at the microscale level the P-HRWR improved the disaggregation of the CNFs the most.
- Surface treatment with HNO_3 further improved the dispersion of the CNFs in the "*mix water*" solution containing P-HRWR. However, surface treatment with HNO_3 alone was not as efficient at dispersing CNFs in "*mix water*" solutions as the dispersing agents.
- In "*cement pore water*" solutions, the use of dispersing agents in combination with ultrasonication showed the ability to disaggregate the CNFs, but the suspension was not stable with sedimentation occurring even for the solution containing P-HRWR.
- CNF migration with the bleed water occurred in cement pastes during the curing process resulting in a porous layer containing a high density of CNFs on the top-surface of the specimens. The porous layer was found to be dependent on the w/c ratio.
- At the microscale, the dispersion of CNFs in cement pastes was not uniform with the presence of individual and agglomerated CNFs. In addition, the distribution of the individual CNFs was not uniform within the cement pastes leading to CNF-rich and CNF-poor regions.
- Regardless of the dispersion method used, the CNFs reagglomerated during the mixing and/or curing process. However, cement-based composites made with P-HRWR showed

the fewest number of agglomerates larger than 200 μm in diameter.

- The final state of dispersion of the CNFs within the cement paste was the result of a competition between: (i) the tendency of CNFs to migrate towards each other or existing agglomerates due to Brownian motion and van der Waals interactions during cement mixing, (ii) the influence of the high pH and ionic strength of the cement paste medium on altering the surface properties of the CNFs, resulting in greater propensity for loss of individual CNFs and rebundling, and (iii) the effect of mechanical mixing, further increasing the probability of CNF agglomerates or individual CNFs to come in contact with each other.

CHAPTER 4

MICROMECHANICAL PROPERTIES OF CEMENT-BASED COMPOSITES WITH CNFS

4.1. Overview

The potential of CNFs as cement reinforcement is indicated by their high strength and aspect ratio (i.e., strengths of over 2.5 GPa [119] and aspect ratios of about 1000:1 [87]). Because it is now widely accepted that the macromechanical properties of cement-based materials originate from the mechanics of the material at lower scales (i.e., micro- and nanoscales) [129], the effects of CNFs on the micromechanical properties of that underlying structure are of interest. The objective of this chapter is to investigate the micromechanical properties of hydrated cement pastes containing CNFs, including the effect of CNFs on the overall distribution of micromechanical properties at the local level and on representative major cement phases (i.e., C-S-H and CH) and the micromechanical response at the local level in and around CNF agglomerates.

Nanoindentation studies combined with SEM/EDS analyses of hydrated cement pastes with and without CNFs were performed to determine the effect of CNFs on the micromechanical properties, including modulus of elasticity and hardness, of representative major cement phases (i.e., C-S-H and CH). In addition, nanoindentation studies of the area in and around CNF agglomerates were performed to determine the effect of CNF agglomerates on the micromechanical properties of cement-based composites at the local level.

4.2. Experimental Detail

4.2.1. Materials

The materials discussed in Section 3.2.1 were used in this study including "*as received*" CNFs, P-HRWR (*Glenium® 7500*), and type I portland cement. In addition, EpoFix epoxy (Struers, Cleveland, Ohio, USA) was used to support the cement specimens during polishing and testing.

4.2.2. Preparation of CNF/Cement-Based Composites

Three composites were examined, including a PC paste with no CNFs (PC), a PC paste with 0.5 wt% CNFs (PC-CNF), and a PC paste with 1 wt% CNFs (PC-1%). PC and PC-CNF had a w/c ratio of 0.315 while PC-1% had a w/c ratio of 0.28. All composites contained 1 wt% of P-HRWR as a dispersing agent for the CNFs and were made in the same manner as in Section 3.2.3.2 using a bath sonicator to disaggregate the CNFs in the water and P-HRWR solution and a stand mixer to blend the CNF suspension with the cement.

After mixing the cement-based composites were made into 2.54 cm × 2.54 cm × 68.58 cm (1 in. × 1 in. × 27 in.) beams, cured for 28 days in 100% humidity, and tested by standard macromechanical testing. After macromechanical testing, the beams were cured in a controlled laboratory environment at approximately 21ºC (70ºF) and 30% relative humidity for approximately one year before specimens, 1.27 cm × 1.27 cm × 2.54 cm (0.5 in. × 0.5 in. × 1 in.) in size, were cut from the beams using a precision saw with an oil lubricant so as to not cause further hydration of the cement. Specimens were then mounted in 3.175 cm (1.25 in.) diameter disks of EpoFix epoxy such that the cement-based composites did not become impregnated with the epoxy.

Before nanoindentation, the specimens mounted in epoxy were polished in a four step process recommended by experts at Buehler (Lake Bluff, Illinois, USA). The polishing process began with a grinding step with 240 grit silicon carbide paper followed by polishing with 9 μm and 3 μm diamond pastes and 50 nm alumina powder suspension on specialized polishing pads. Specimens were ultrasonicated in a bath sonicator for 10 minutes after each polishing step to reduce contamination between steps, and optical microscopy was used during the polishing process after each step to ensure a proper polish (Figure 4.1). All polishing and cleaning between polishing steps was completed in an alcohol and ethylene glycol solution to prevent further hydration of the cement-based composite. The polishing process used was similar to that found in the literature for nanoindentation of cement-based composites and exceeded the lowest particle size used in those studies [100, 103, 108, 110, 130]. An example of an acceptable and unacceptable final polish can be seen in Figure 4.2.

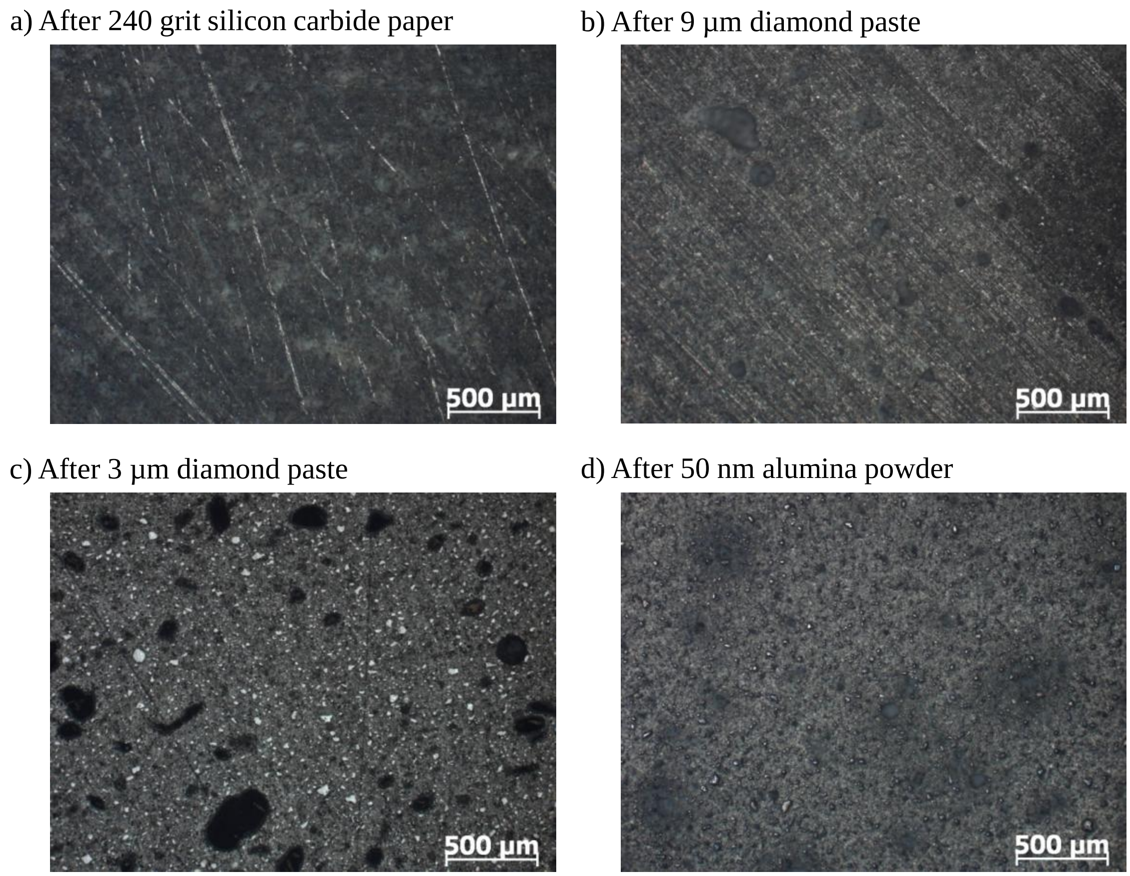

Figure 4.1. Micrographs of various cement-based composites showing the different steps of the Buehler recommended polishing process used to prepare cement-based composite specimens for nanoindentation. a) Polish after 240 grit silicon carbide paper, b) polish after 9 μm diamond paste, c) polish after 3 μm diamond paste, and d) polish after 50 nm alumina powder.

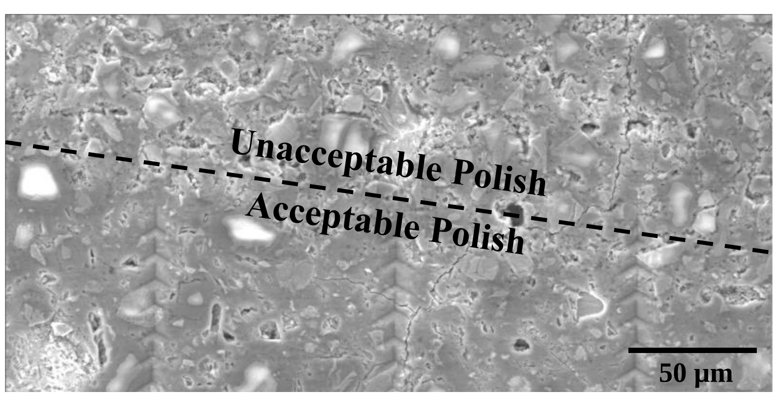

Figure 4.2. SEM image showing areas of a cement-based composite considered to have an acceptable and unacceptable polish for nanoindentation.

4.2.3. Characterization

4.2.3.1. Nanoindentation

Nanoindentation was completed at the Army Corps of Engineers Engineer Research and Development Center (ERDC, Vicksburg, Mississippi) using an Agilent Nanoindenter G200 Testing System (Agilent Technologies, Santa Clara, California, USA) (Figure 4.3). The Agilent Nanoindenter G200 Testing System has a displacement resolution of less than 0.01 nm, up to 1000 times magnification for viewing specimens, and an accuracy of 1 μm for indentation positioning. Indentation was completed with a Berkovich tip made of diamond, which was calibrated using a second-order area function and a fused silica sample with known mechanical properties. A maximum force of 2 mN was applied with a targeted strain rate of 0.050 s^{-1}. The maximum load was selected as 2 mN because it was in between the 0.5 mN suggested by [103] in order to have indentation depths of less than 300 nm to capture the individual response of C-S-H and the 4 mN suggested by [108] to have indentation depths greater than 200 nm needed because of the surface roughness of polished cement-based composites. The maximum load was held for 15 seconds before a 10 second unloading period was completed. All indentation curves were evaluated before further analysis (Figure 4.4). Abnormal curves were discarded because they represented contact issues, cracking during testing, or the response of multiple constituents of the composite and interfered with the calculation of the micromechanical properties [103, 131]. Curves that were accepted after evaluation are referred to as "*valid*" curves, and curves that were discarded for irregularities are referred to as "*invalid*".

The elastic modulus (E) and hardness values (H) were calculated from the unloading portion of the force versus displacement (i.e., indentation depth) curve (Figure 4.4) using the

Oliver and Pharr method [132] in which the area of contact (A_C) is estimated and the following relationships are used:

$$E = \frac{(1-\nu)^2}{\frac{1}{E_{eff}} - \frac{(1-\nu_i)^2}{E_i}} \qquad \text{Equation 4.1}$$

where ν is the Poisson's ratio of the cement-based composite (assumed to be 0.3), ν_i is the Poisson's ratio of the indenter, E_i is the elastic modulus of the indenter, and E_{eff} is the effective elastic modulus defined by:

$$E_{eff} = \frac{\sqrt{\pi}}{2}\frac{S}{\beta\sqrt{A_C}} \qquad \text{Equation 4.2}$$

where S is the measured unloading stiffness and β is a dimensionless correction factor (i.e., 1.034 for Berkovich indenter) and

$$H = \frac{P_{max}}{A_C} \qquad \text{Equation 4.3}$$

where P_{mas} is the maximum indentation force (Figure 4.4a). The theory of contact mechanics behind nanoindentation and its validity for cement-based materials are discussed elsewhere [101, 103, 108, 110, 130, 133-136].

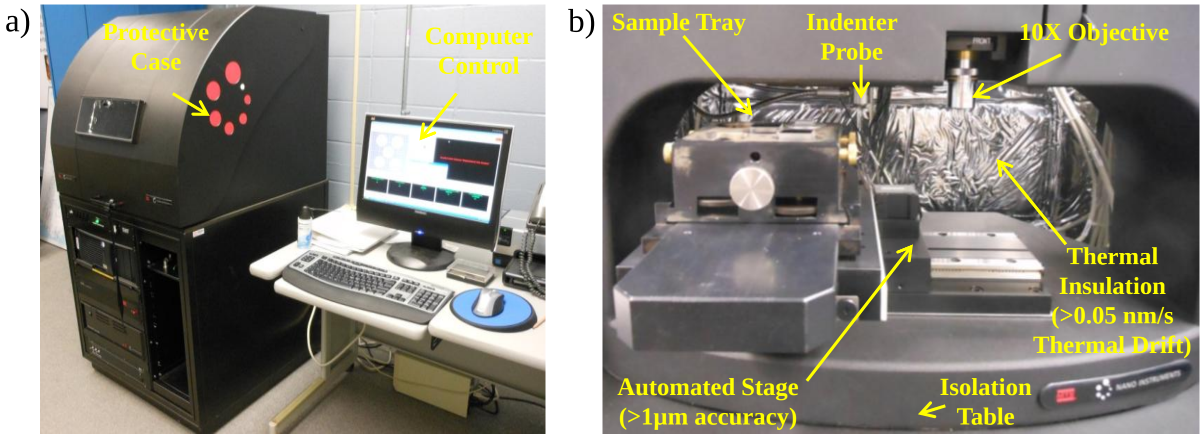

Figure 4.3. Agilent Nanoindenter G200 Testing System at ERDC (Vicksburg, Mississippi). a) Full system including protective casing and computer control and b) isolation table, thermal insulation, sample tray, automated stage, indenter probe, and optical microscope objective (interchangeable 10X or 40X).

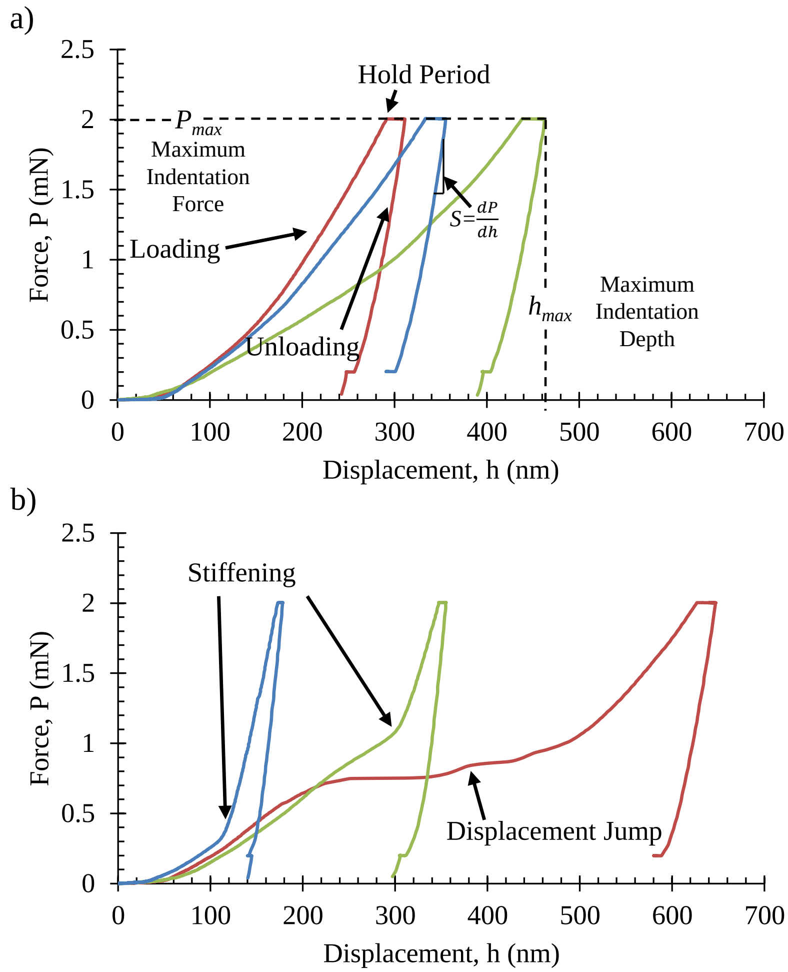

Figure 4.4. Example of force versus displacement curves from nanoindentation of a cement-based composite. a) "*Valid*" curves showing P_{max}, h_{max}, and S and the loading, hold period, and unloading portions of the curve and b) "*invalid*" curves showing a sudden stiffening or jump in displacement from damage during testing.

Three (3) grids of 20 indents spaced 10 µm apart in the X-direction and 10 indents spaced 10 µm apart in the Y-direction were used for PC and PC-CNF while two (2) grids of the same number of indents and spacing were used for PC-1%. Two (2) representative cross-sections from different specimens of each composite were used for PC (PC A and PC B) and PC-CNF (PC-CNF A and PC-CNF B) with one grid on PC A and PC-CNF B and two on PC B and PC-CNF A in order to ensure that the results were similar across specimens of the same composite. The location of the nanoindentation grids were selected at random in order to reduce bias, but the areas used were examined before testing with SEM in order to ensure that the polishing in the area was acceptable for nanoindentation, that there were not abnormalities in the cement paste within the area, and that the area was representative of the cement-based composite. Only one (1) cross-section was used for PC-1%, and the two grids were located across one or more CNF agglomerates. Fiducial indents were placed at the beginning, middle, and end of each row of indents for every grid using a force of 100 mN so that the indentation grid could be located with the SEM and the precise location of the indents could be found for further SEM/EDS analysis.

The modulus and hardness values obtained from nanoindentation were plotted in a contour plot with respect to the indent grid location. All indent locations that resulted in an indentation error or an "*invalid*" force versus displacement curve was plotted as having a modulus and hardness value of zero (0). The modulus and hardness values for the area between indents were then interpolated. Additionally, the modulus and hardness values were plotted as histograms with the bin sizes selected based on recommendations from [137]. In addition to the histograms, empirical distributions scaled to correspond with the histograms were used for visualization of the data. Because the SEM/EDS data was available for each individual indent (similar to [108, 131]) analysis of the data was not reliant on statistical methods to determine the cement phases as in [103], and the histograms were decomposed into the phases determined from the SEM/EDS studies.

4.2.3.2. SEM/EDS

An FEI Quanta FEG 650 SEM (FEI Company, Hillsboro, Oregon, USA) equipped with Schottky field emission, high vacuum, low vacuum and ESEM capabilities, digital imaging, and an Oxford X-Max Silicon Drift Detector with a 20 mm^2 active area (Oxford Instruments, Abingdon, Oxfordshire, England) was used to obtain secondary and backscattered electron images and semi-quantitative chemical data. A pressure of 130 Pa, a voltage of 15 kV, a working distance of 10 mm, and a spot size of 5 was used to collect all SEM images and EDS data. A voltage of 15 kV was used for EDS to allow for sufficient energy to meet the required K shell characteristic ionization energy of the typical elements found in cement-based materials (i.e., iron) [138], while maintaining the interaction volume of EDS (i.e., less than 2 µm [108]) similar to that of nanoindentation (i.e., less than 1.5 µm [108]). EDS was completed using point analysis at the locations of each indent with five (5) iterations and a livetime of 20 seconds. Calibrations were made with calcium carbonate, silicon dioxide, albite, magnesium oxide, aluminum oxide, gallium phosphide, iron sulphide, MAD-10 feldspar, wollastonite, manganese, and iron, and the XPP scheme, a Phi-Rho-Z method, was used for matrix corrections as analyzed by INCA Energy Software (Oxford Instruments, Abingdon, Oxfordshire, England) [139].

The backscatter and secondary SEM images were used to classify the location of the indents as flaw/hydrate combination, flaw/hydrate/unhydrated cement combination, flaw/unhydrated cement combination, hydrate, hydrate/unhydrated cement combination, or unhydrated cement (Figure 4.5). Gray scale analysis was completed on the backscatter image to assign false color such that the unhydrated cement, hydrates, and flaws were all identified (Figure 4.5c). Secondary images allowed the points of the fiducial indents to be located and assisted in placement of markers where each indent was located (the markers are exaggerated in size for viewing, Figure 4.5d). When the false color and accurate indentation locations were combined together, the locations of the indents could be easily classified. In addition, for PC-1% the secondary SEM image was used to determine the location of the CNF agglomerates in relationship to the indent locations (Figure 4.6). Indents were classified as being: (i) within the CNF agglomerate (which mostly consisted of a void with a tangled mass of CNFs and a few hydrates present), (ii) on the edge of the agglomerate (where many CNFs were still present but were mostly anchored in hydrated cement), or (iii) outside of the CNF agglomerate.

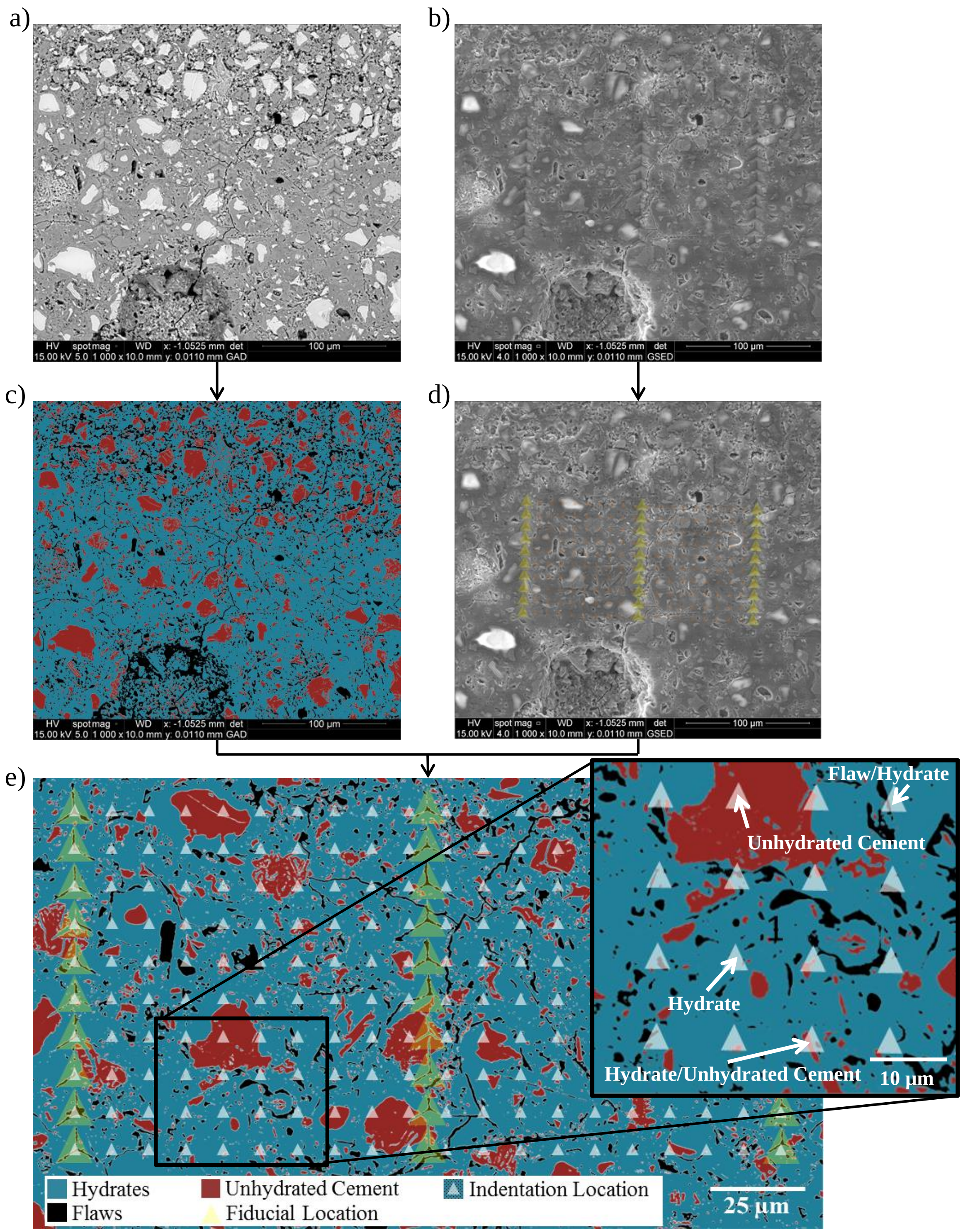

Figure 4.5. SEM images showing the location of a nanoindentation grid (PC-CNF A Grid 2) and the process to determine the constituents on which each indent is located. a) Backscatter SEM image, b) secondary SEM image, c) backscatter SEM image with false color, d) secondary SEM image with enlarged markers showing the nanoindentation and fiducial grid, and e) nanoindentation and fiducial grid with markers enlarged transferred to false color image and enlargement of part of nanoindentation grid with indents labeled.

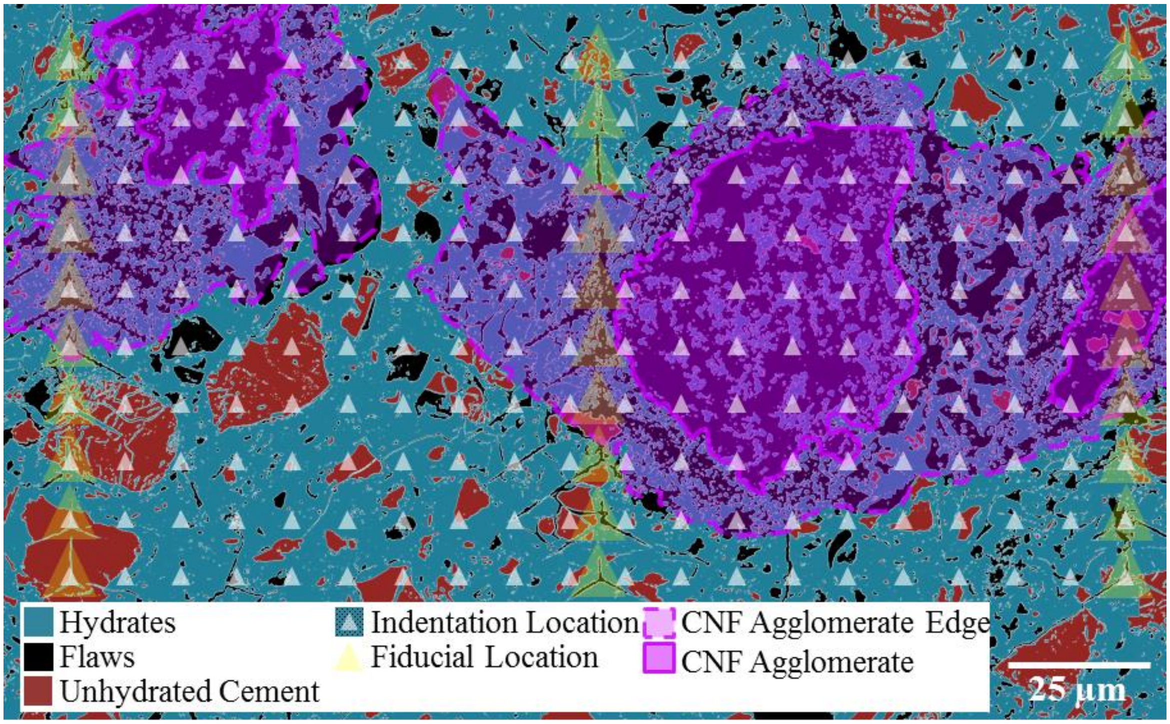

Figure 4.6. Backscatter SEM image of PC-1% Grid 1 with false color showing the location of indents with respect to constituents (flaws, hydrates, and unhydrated cement) and with respect to CNF agglomerates (raw images included in Appendix C).

EDS data was used to determine the cement hydration product(s) present at indents that were located solely within the hydrated portion of the paste. The hydration products were identified as: (i) C-S-H, (ii) CH, (iii) a combination of C-S-H and CH mostly comprised of C-S-H, (iv) a combination of C-S-H and CH mostly comprised of CH, and (v) Al-rich phases. Although EDS could be used to further study the unhydrated cement particles, the number of indents located on unhydrated cement particles was not sufficient to further separate the data set.

Identification of the hydrated phases was determined by comparing the Si/Ca ratios with the Al/Ca ratios with respect to the molecular weights (Figure 4.7). Typically, the atomic Si/Ca ratios obtained from EDS are plotted compared to the atomic Al/Ca ratios as in Figure 4.7a with the intersecting lines representing theoretical atomic ratios of calcium, aluminum, and silicon for C-S-H, CH, monosulfoaluminate, and ettringite [140]. The Si/Ca ratio for C-S-H is typically taken as 0.5-0.667, while the Al/Ca ratio is typically taken as 0.06 [140]. Because each indent located on hydrated cement phases needed to be classified, ranges of Si/Ca ratios and Al/Ca ratios were set for each cement phase (Figure 4.7b) allowing for a variation of 0.1 in the ratio to account for the mixture of phases. The ranges were chosen as follows:

- If the Si/Ca ratio was greater than or equal to 0.4 and the Al/Ca ratio was less than or equal to 0.16, then the hydrate was considered to be C-S-H. A variance of -0.1 from the lowest Si/Ca ratio (i.e., 0.5) and +0.1 from the highest Al/Ca ratio (i.e. 0.06) typically considered to be C-S-H was allowed for minor impurity of the C-S-H phase.
- If both the Si/Ca and Al/Ca ratios were less than or equal to 0.1, the hydrate was considered to be CH. Though pure CH has no Al and Si, a variance of +0.1 was allowed in the Si/Ca and Al/Ca ratios to account for some minor impurity of the CH phase.
- If the Si/Ca ratio was between 0.1 and 0.4 and the Al/Ca ratio was less than or equal to the values interpolated between those considered to be CH and C-S-H, then the hydrate was considered to be a mixture between C-S-H and CH. The range of Si/Ca ratios in this classification was further divided in half with the lower values of Si/Ca ratios being considered mostly CH and the higher values being considered mostly C-S-H.
- All other hydrates were considered to be Al-rich.

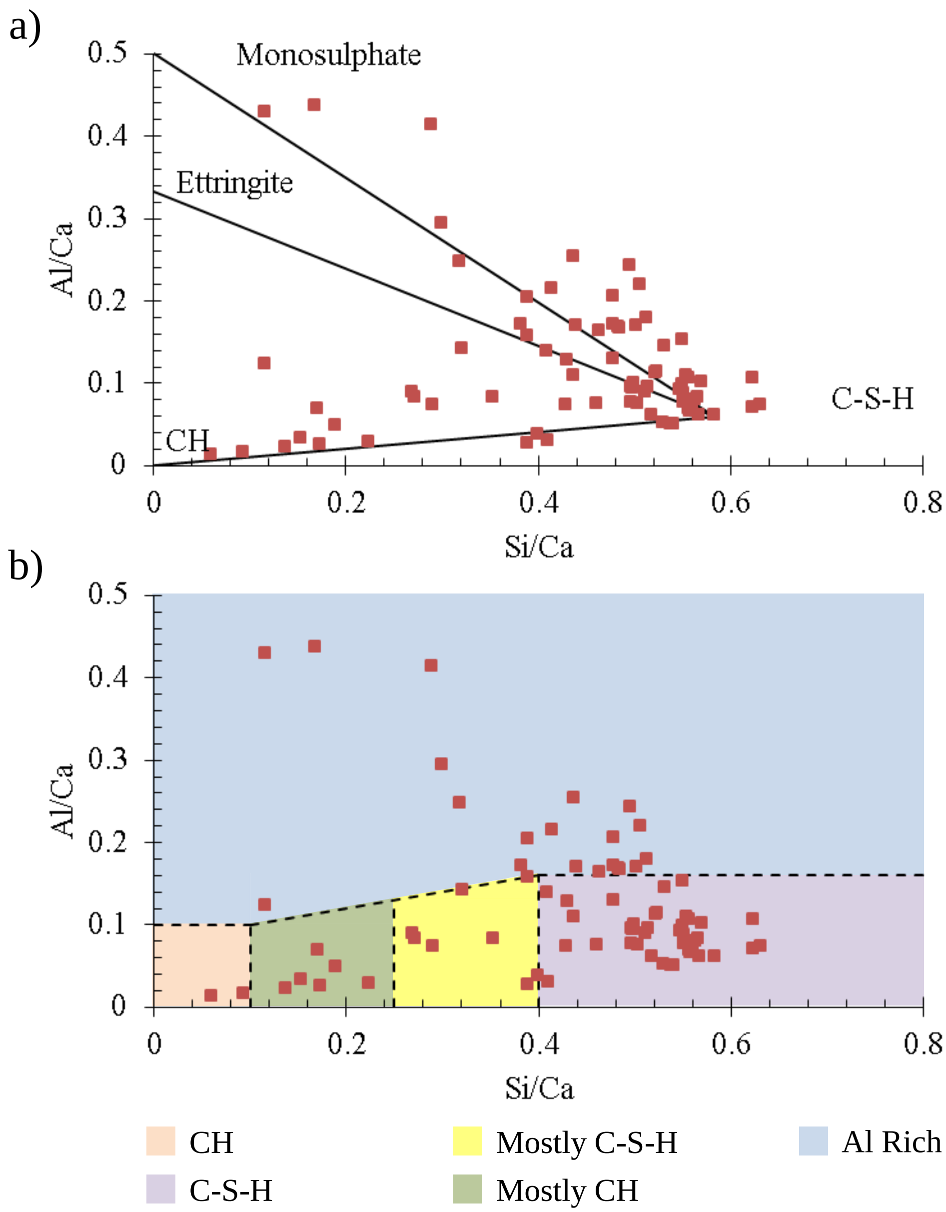

Figure 4.7. Example of EDS results that were spatially correlated with nanoindentation data (PC B Grid 1) as determined by SEM to be cement hydrates (raw data included in Appendix C). a) Typical Al/Ca ratio versus Si/Ca ratio plot with theoretical values for C-S-H, CH, ettringite, and monosulfoaluminate and b) Al/Ca versus Si/Ca plot showing classifications of the ratio ranges used to correlate with nanoindentation data.

4.3. Results and Discussion

4.3.1. Effects of CNFs on the Distribution of Micromechanical Properties at the Local Level

The effects of CNFs on the micromechanical properties of cement pastes at the local level were investigated. The modulus and hardness of plain PC paste (PC) and PC paste with 0.5 wt% CNFs (PC-CNF) were compared.

4.3.1.1. Indent Locations and Indentation Depths

Indentation locations. Of the 600 indents analyzed for both PC and PC-CNF, over 35%, equivalent to over 200 indents, were located solely on cement hydration products as determined by backscatter SEM image analysis (Figure 4.8), while *ca.* 1-2% and *ca.* 7-8% of indents were located solely on flaws and unhydrated cement particles, respectively. The rest of the indents were located on combinations of multiple cement paste constituents (i.e., cement hydrates, unhydrated cement particles, and flaws) or were discarded due to indenter error or "*invalid*" force versus displacement curves. Although PC-CNF had more indent locations that were indentation errors or force versus displacement curves that were considered "*invalid*" compared to PC (i.e., *ca.* 28% versus *ca.* 14%), this was not thought to be caused by the presence of CNFs because one indentation grid (PC-CNF B Grid 1) was responsible for the majority (126 out of 165) of the indentation errors/"*invalid*" curves. The polish quality of PC-CNF B Grid 1 was equivalent to the other specimens (see secondary SEM images, APPENDIX C), the porosity or presence of flaws was not out of the ordinary compared to the other specimens (see backscatter SEM images, APPENDIX C), and only three (3) indents were classified as indentation errors, the large majority (i.e., 123 indents) being "*invalid*" curves. Because no issues could be found with the specimen quality or testing procedure, the large number of indents considered indentation errors/"*invalid*" curves was thought to be caused by an increased number of indents on multiple cement paste constituents, (i.e., hydrates, unhydrated cement particles, and flaws). Composites have been shown to have a multiphase response when the interaction volume of the indent includes multiple material constituents [108, 131, 133, 141].

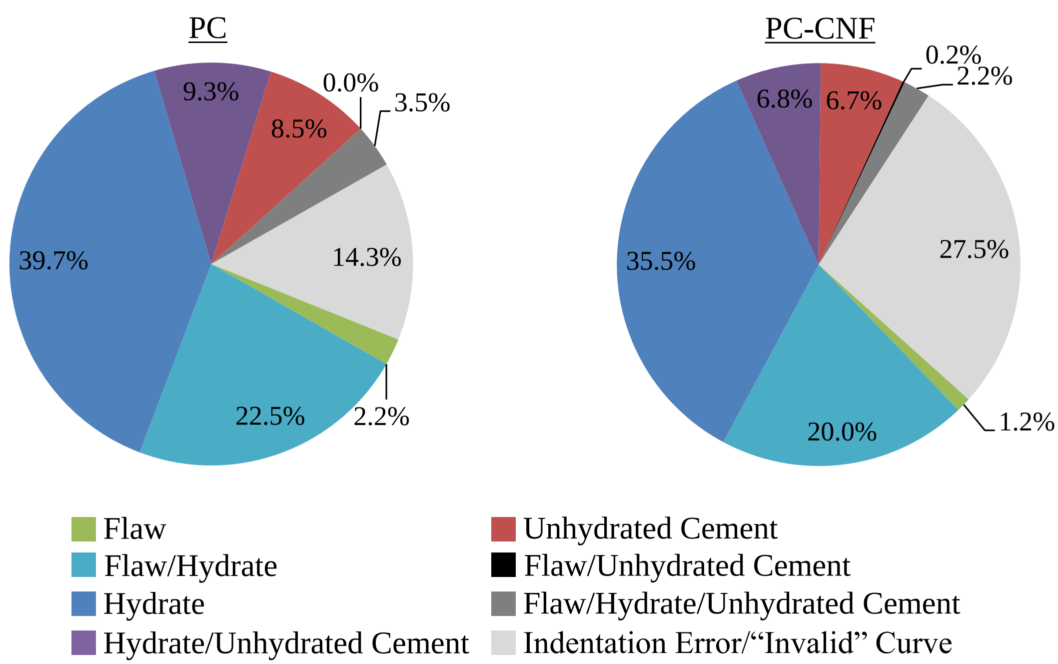

Figure 4.8. Pie charts showing the percentage distribution of indents located on various cement paste constituents (i.e., hydrates, unhydrated cement particles, and flaws), combinations of cement paste constituents, and indentation errors/invalid curves as analyzed by nanoindentation combined with SEM (raw data included in Appendix C). a) PC composite and b) PC-CNF composite.

Further treatment of the indentation data was performed to compare the results to the Power's model of hydration [142]. Indents corresponding to indentation errors/"*invalid*" curves were removed from the percentage distribution calculations, and indents that were located on a combination of multiple cement paste constituents were assumed to be composed of either 1/2 or

1/3 of each constituent for a combination of two or three constituents. *Ca.* 70%, *ca.*15%, and *ca.* 15% of indents were thus located on hydrates, unhydrated cement particles, and flaws, respectively (Figure 4.9). Using the Power's model [142], the degree of hydration (α) was calculated as:

$$\alpha = 1 - \gamma(\rho_c \cdot {}^{w}/_{c} + 1) \qquad \text{Equation 4.4}$$

where, γ is the volume fraction of unhydrated cement (i.e., 16.7% and 15.0% for PC and PC-CNF respectively), ${}^{w}/_{c}$ is the w/c ratio (i.e., 0.315), and ρ_c is the specific gravity of cement, which was assumed to be 3.15 [108]. The theoretical degree of hydration calculated using the Power's model was 0.667 and 0.701 for PC and PC-CNF, respectively. The experimental degree of hydration (i.e., 0.662 and 0.685 for PC and PC-CNF, respectively) obtained from SEM analysis (Figure 4.9), was thus in good agreement with the Power's model.

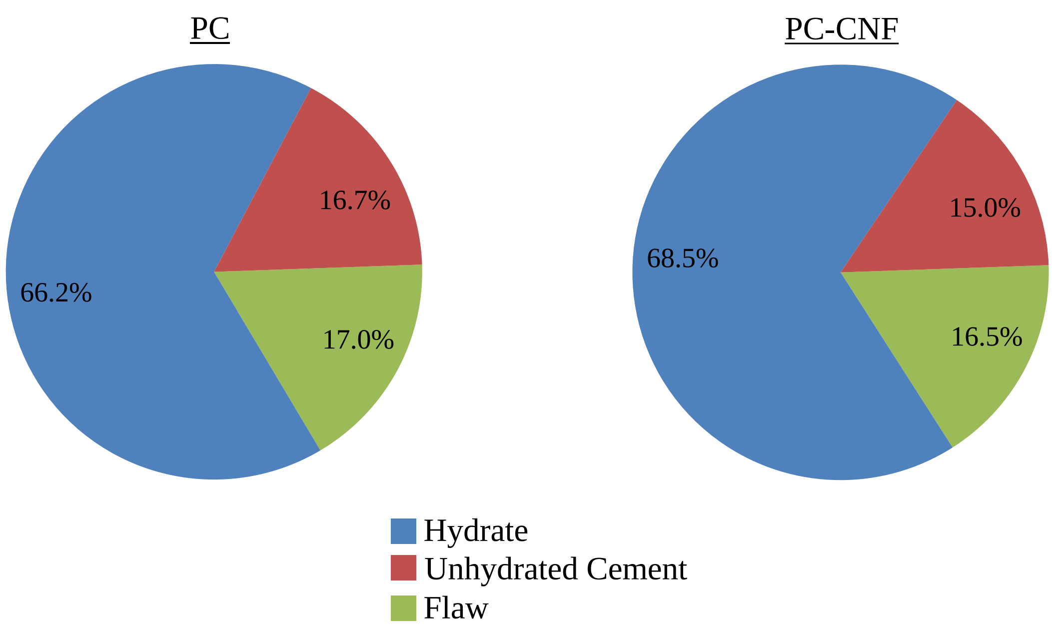

Figure 4.9. Pie charts showing the percentage distribution of indents located on hydrates, unhydrated cement particles, and flaws as analyzed by nanoindentation combined with SEM (raw data included in Appendix C). a) PC composite and b) PC-CNF composite.

Indentation depths. The nanoindentation testing that was performed at a maximum load of 2 mN, resulted in indentation depths (i.e., contact depths measured by the nanoindenter) ranging from *ca.* 55 nm to *ca.* 790 nm. The indentation depths mostly satisfied the requirements needed of an indentation depth of at least about 200 nm in order to be acceptable because of the surface roughness of polished cement specimens [108] with the majority of indents with an indentation depth of less than 200 nm being located on unhydrated cement particles or a mixture between unhydrated cement and hydration products.

4.3.1.2. Micromechanical Properties

Contour plots that spatially correlate the indent locations to the modulus and hardness data clearly showed the highest modulus and hardness values (i.e., greater than 60 GPa and 2 GPa, respectively) to correlate to unhydrated cement particles, as visually determined with backscatter SEM, while the lowest modulus and hardness values (i.e., less than 15 GPa and 0.25 GPa, respectively) corresponded to the highly porous areas of the cement-based composites (Figure 4.10-4.15). These modulus and hardness values were in agreement with the values found in the literature (Table 2.1) [97-100, 103-107].

.

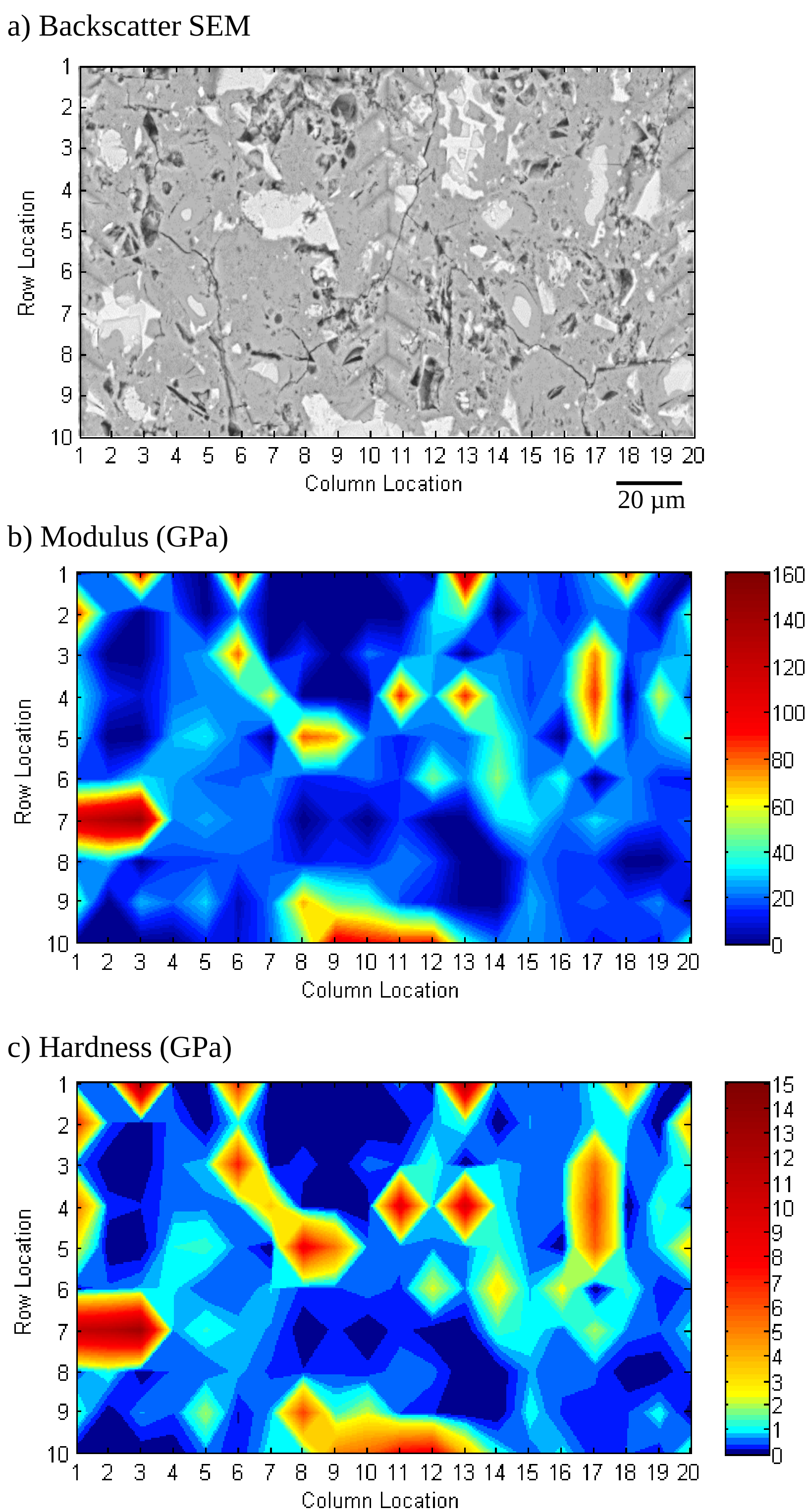

Figure 4.10. Spatial correlation of micromechanical properties of PC A Grid 1. Indents are located in a grid of 200 with 10 rows and 20 columns. a) Backscatter SEM image, b) contour plot of elastic modulus with linear interpolation between indents, c) contour plots of hardness with linear interpolation between indents.

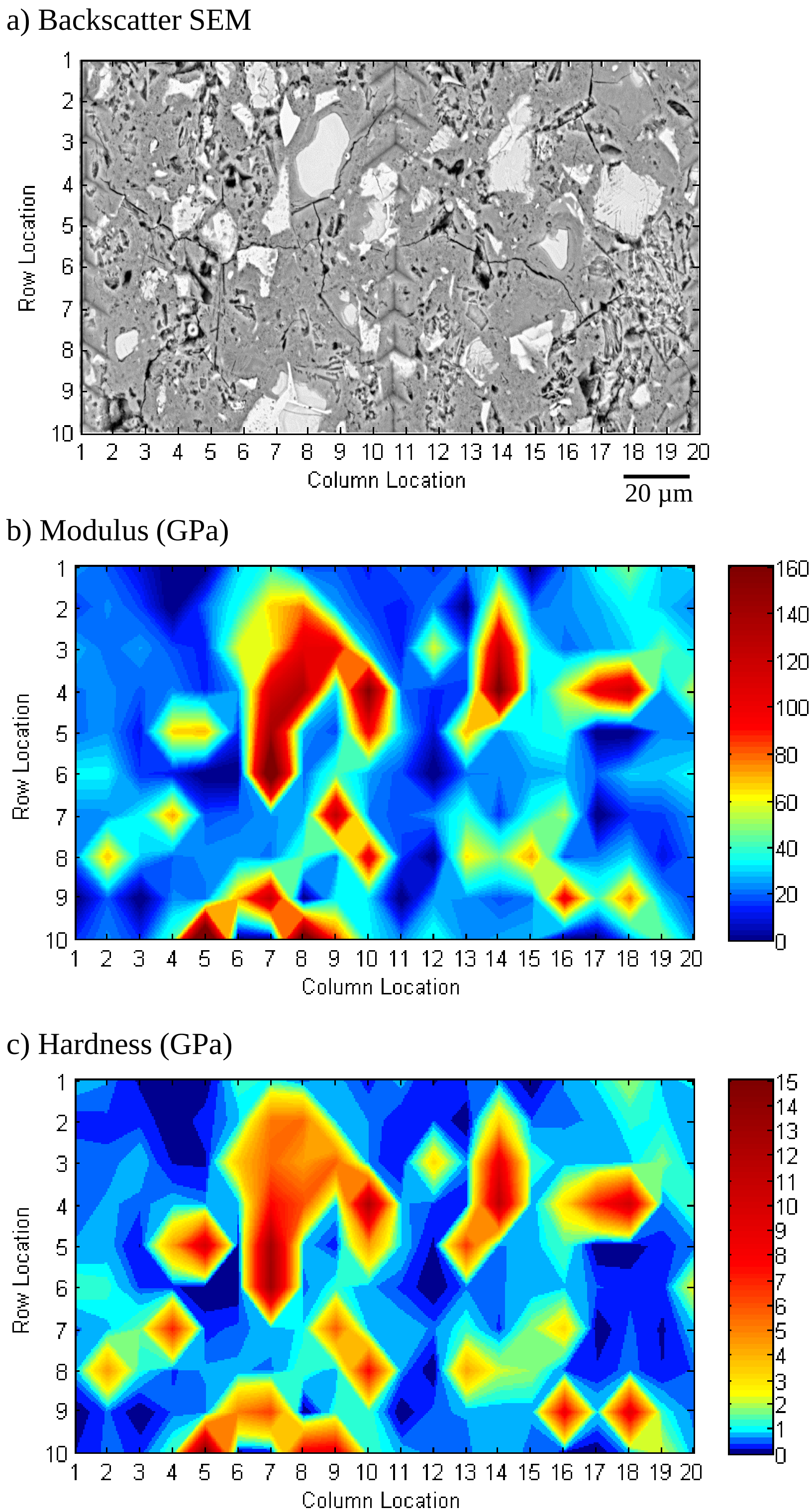

Figure 4.11. Spatial correlation of micromechanical properties of PC B Grid 1 (raw data included in Appendix C). Indents are located in a grid of 200 with 10 rows and 20 columns. a) Backscatter SEM image, b) contour plot of elastic modulus with linear interpolation between indents, c) contour plots of hardness with linear interpolation between indents.

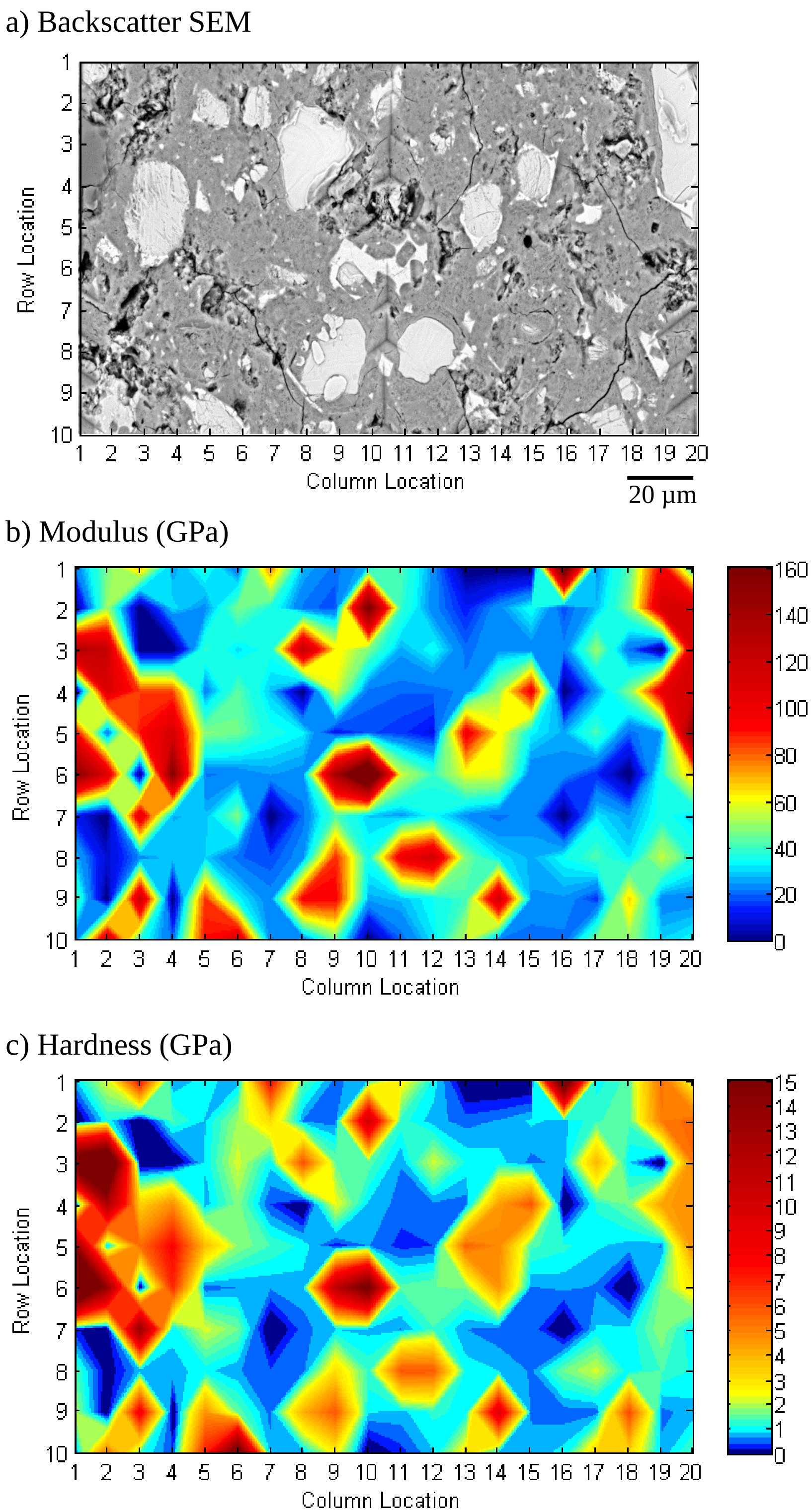

Figure 4.12. Spatial correlation of micromechanical properties of PC B Grid 2 (raw data included in Appendix C). Indents are located in a grid of 200 with 10 rows and 20 columns. a) Backscatter SEM image, b) contour plot of elastic modulus with linear interpolation between indents, c) contour plots of hardness with linear interpolation between indents.

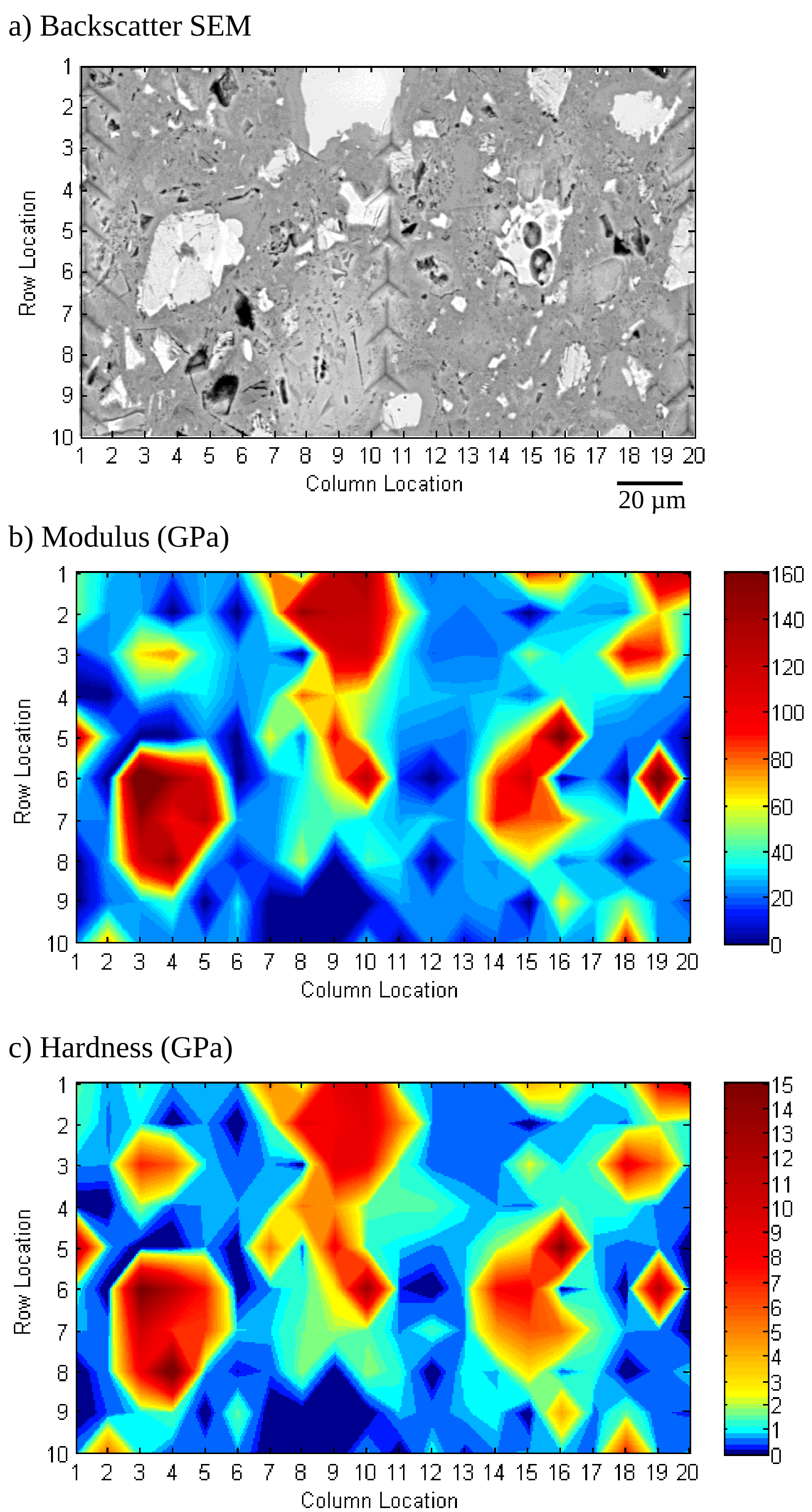

Figure 4.13. Spatial correlation of micromechanical properties of PC-CNF A Grid 1 (raw data included in Appendix C). Indents are located in a grid of 200 with 10 rows and 20 columns. a) Backscatter SEM image, b) contour plot of elastic modulus with linear interpolation between indents, c) contour plots of hardness with linear interpolation between indents.

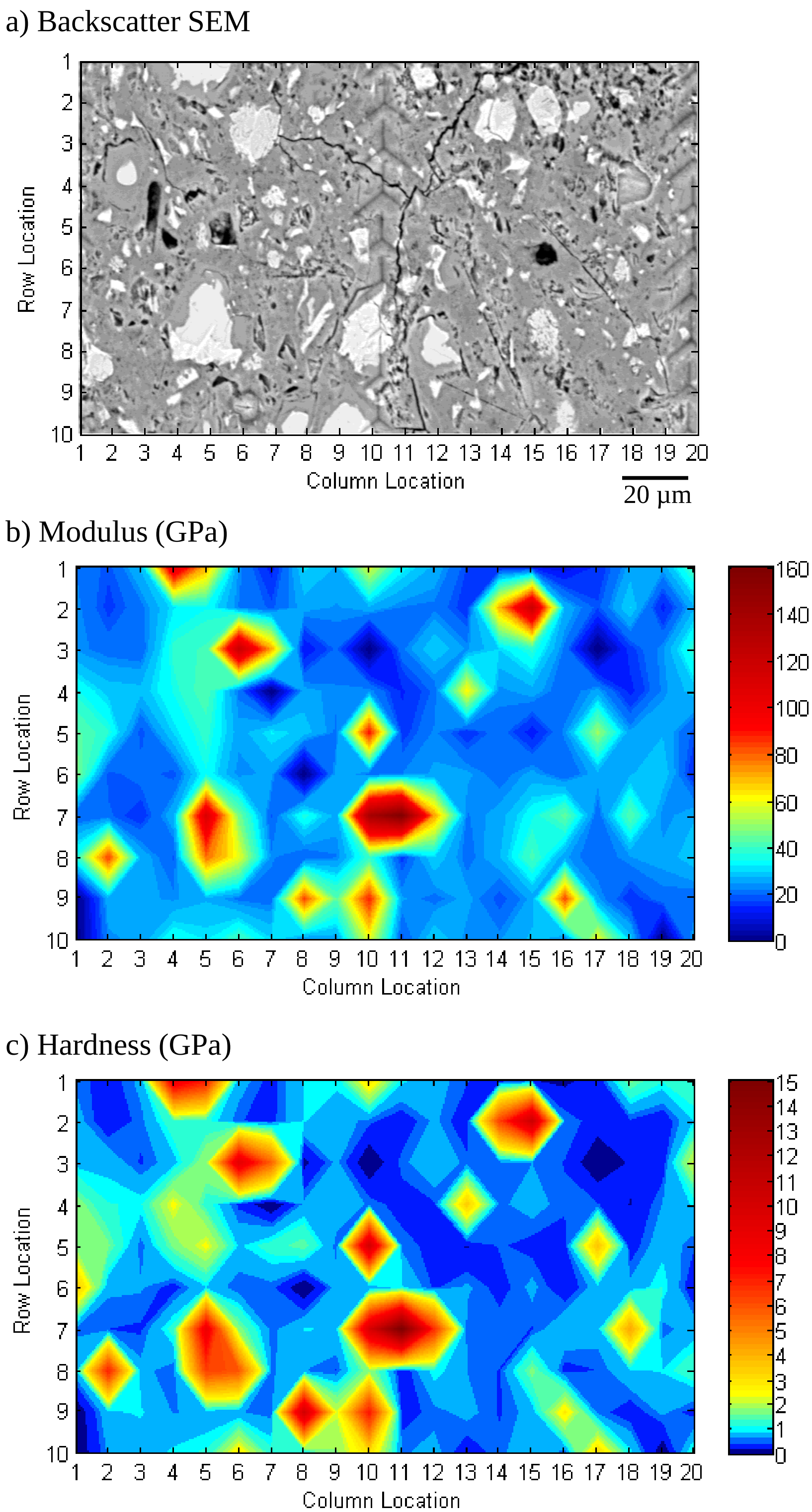

Figure 4.14. Spatial correlation of micromechanical properties of PC-CNF A Grid 2 (raw data included in Appendix C). Indents are located in a grid of 200 with 10 rows and 20 columns. a) Backscatter SEM image, b) contour plot of elastic modulus with linear interpolation between indents, c) contour plots of hardness with linear interpolation between indents.

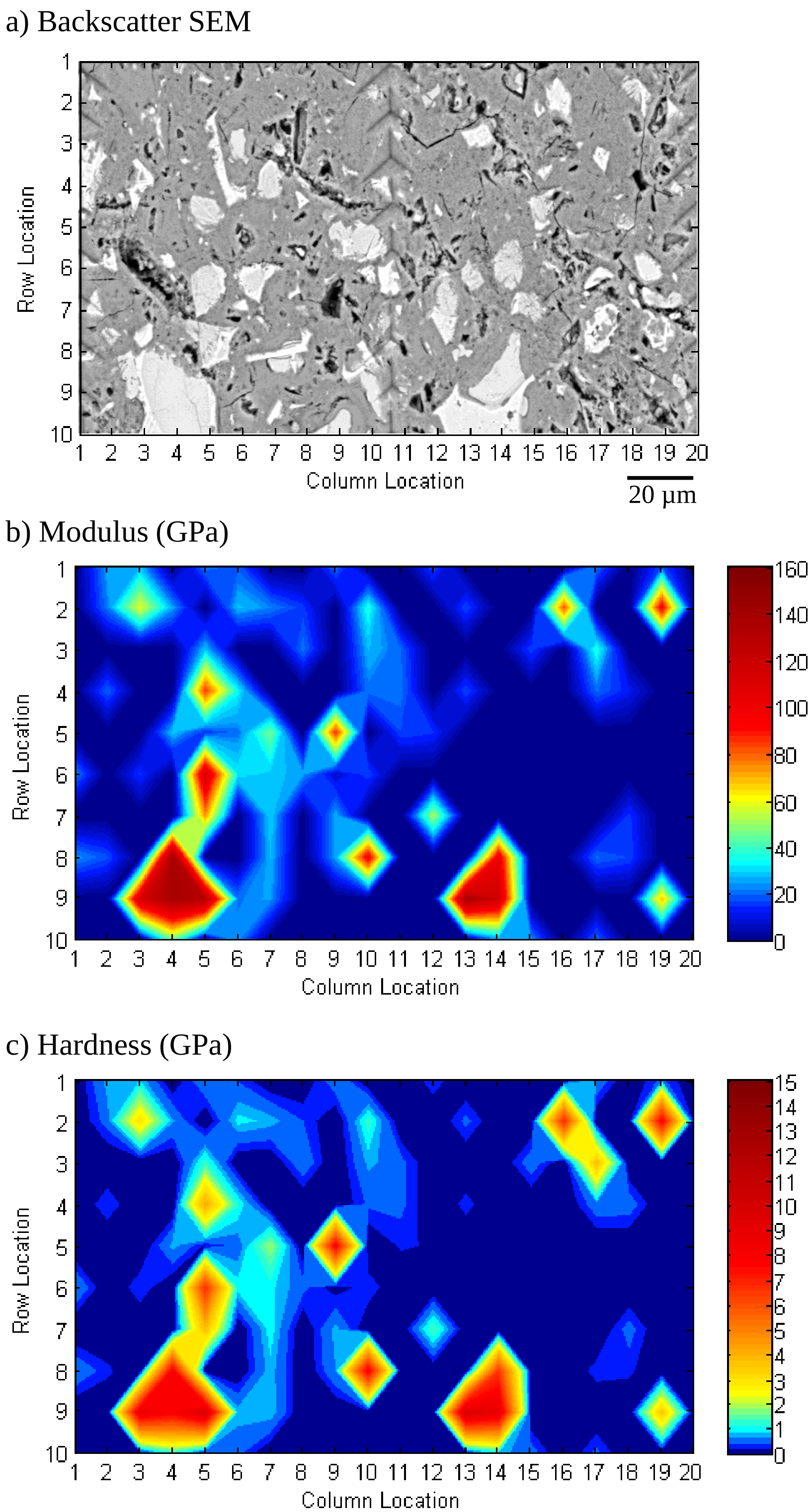

Figure 4.15. Spatial correlation of micromechanical properties of PC-CNF B Grid 1 (raw data included in Appendix C). Indents are located in a grid of 200 with 10 rows and 20 columns. a) Backscatter SEM image, b) contour plot of elastic modulus with linear interpolation between indents, c) contour plots of hardness with linear interpolation between indents.

Nanoindentation of PC and PC-CNF resulted in elastic moduli ranging from *ca.*8 GPa to *ca.* 210 GPa and hardness values ranging from *ca.* 0.1 GPa to *ca.* 17 GPa. The relative frequency histogram of the elastic moduli for PC and PC-CNF is shown in Figure 4.16 for modulus values less than 160 GPa (only 3 indents resulted in an elastic modulus of over 160 GPa). The relative frequency histogram of the hardness values is shown in **Error! Reference source not found.** for hardness values less than 10 GPa (only 10 indents resulted in a hardness of over 10 GPa). In general, the modulus and hardness histograms showed one main peak ranging from 8-40 GPa and 0-1.6 GPa, respectively. In addition to the main peak, an intermediate shoulder could be seen in the range of modulus and hardness values slightly higher than the main peak, i.e., 40-48 GPa and 1.6-2.0 GPa, respectively. Lastly, minor peaks were seen at modulus values beyond 80 GPa and hardness values beyond 4 GPa. Decomposition of the histograms showed the major cement constituents that were indented as determined by spatial correlation of the micromechanical properties and backscatter SEM image analysis. The decomposition of the histogram showed the majority of the main peak and intermediate shoulder to be mostly composed of cement hydrates and the minor peaks to mostly be composed of unhydrated cement in agreement with the literature [97-99, 103, 104, 107, 108] The main peak was found to correspond to the values typically associated with C-S-H in the literature [103, 108]. However, evidence of two distinct phases of C-S-H as reported in the literature (i.e., high stiffness C-S-H and low stiffness C-S-H [103]) could not be seen solely from examination of Figure 4.16 and **Error! Reference source not found.**. The values within the range of the intermediate shoulder have been associated with CH [103]. The values corresponding to the minor peaks were found to be mostly unhydrated cement, which was also in agreement with the literature [97-99, 104, 107].

.

a)

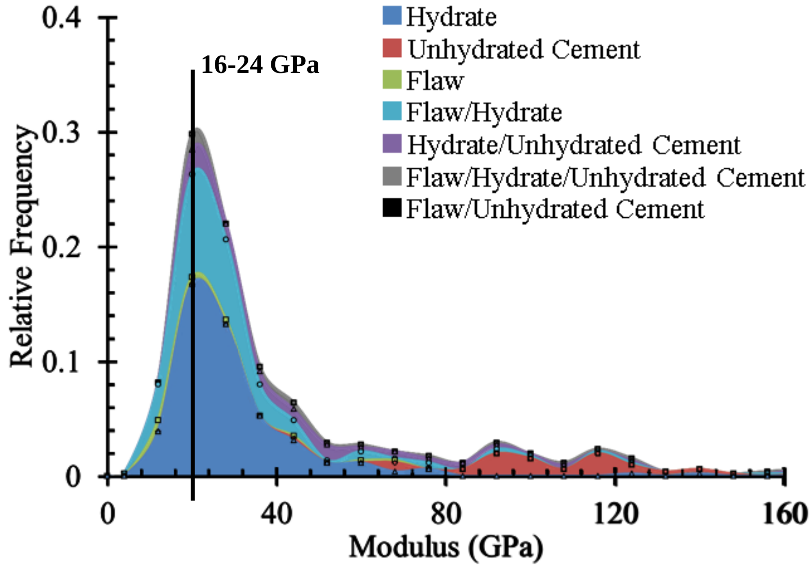

b)

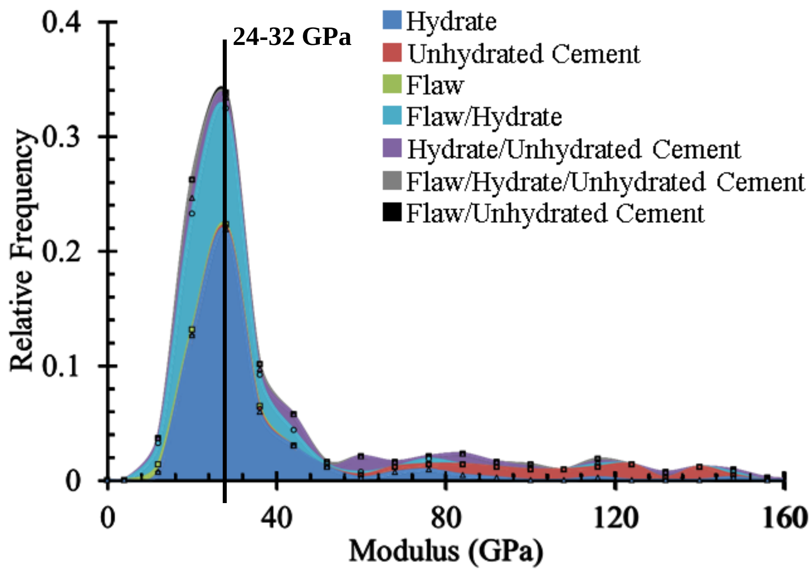

Figure 4.16. Histograms of the modulus values obtained by nanoindentation with scaled empirical distributions decomposed into hydrates, unhydrated cement, and flaws for cement-based composites (raw data included in Appendix C). a) PC and b) PC-CNF.

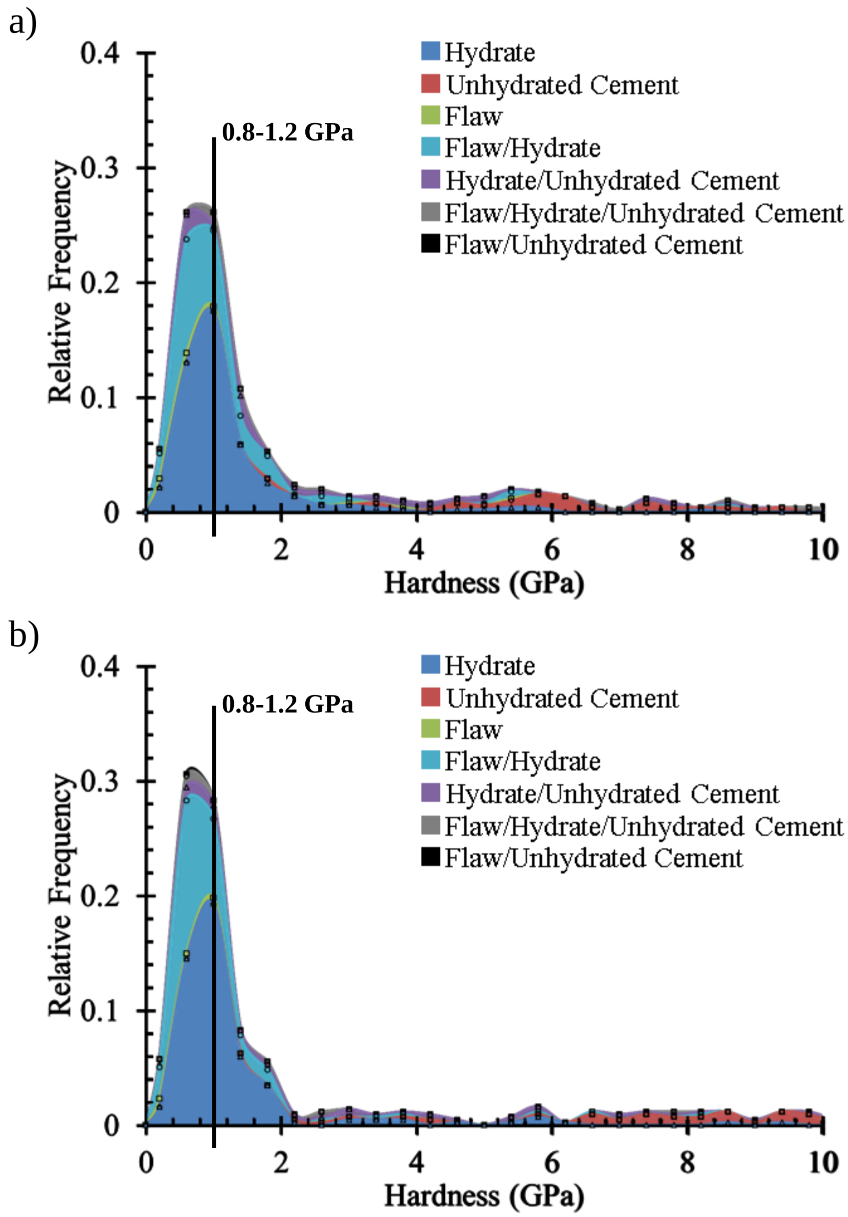

Figure 4.17. Histograms of the hardness values obtained by nanoindentation with scaled empirical distributions decomposed into hydrates, unhydrated cement, and flaws for cement-based composites (raw data included in Appendix C). a) PC and b) PC-CNF.

Elastic modulus. The addition of CNFs resulted in a clear shift in the main peak of the elastic modulus histograms from the 16-24 GPa range for PC to 24-32 GPa range for PC-CNF (Figure 4.16). This observed shift was almost entirely the result of the majority of the hydrates having a higher elastic modulus when CNFs were present in the cement paste. A similar shift has been reported by Shah, Konsta-Gdoutous, and Metaxa [47, 112, 113, 143-145] for CNTs in cement pastes (i.e., shift from 15-20 GPa to 20-25 GPa). Shah et al. [112] attributed the shift in elastic modulus to the ability of the CNTs to create more high stiffness C-S-H.

In addition to the shift in the main peak of the histogram of the elastic modulus, a reduction in the relative frequency of the modulus values less than 16 GPa, corresponding to a highly porous region dominated by capillary pores [103], was seen with the addition of CNFs. A similar reduction in the relative frequency of the modulus values less than 16 GPa has been reported for cement pastes with CNTs and was attributed to a decrease in the nanoporosity of the cement paste as a result of CNTs acting as filler [112].

Differences in the elastic modulus of the unhydrated cement particles were also seen between PC and PC-CNF with two clear peaks centered in the 88-96 GPa and 112-120 GPa ranges seen for PC but no clear peak observed for PC-CNF with data mostly evenly distributed between 80 and 144 GPa. The differences were attributed to the small data set of unhydrated particles indented (i.e., 51 values for PC and 40 values for PC-CNF) and the multiple phases that were captured in the data set (i.e., C_3S, C_2S, C_4AF, etc.).

Hardness. Overall, similar shapes of the histograms of the total hardness were observed for PC and PC-CNF (Figure 4.17). The main peak in the histogram was shifted from being equally distributed in the 0.4-0.8 GPa and 0.8-1.2 GPa ranges to having a higher relative frequency in the 0.4-0.8 GPa range with the addition of CNFs. From the decomposition of the histogram it could be seen that the shift was due to “valid” curves that were located on flaw/hydrate combination and was therefore not considered significant because of the effect of the flaws on the hardness values. Additionally, the portion of the histogram representing only cement hydrates was nearly identical for PC and PC-CNF except for the second peak within the hydrate phase, centered in the 1.6-2.0 GPa range, which was more pronounced with the addition of CNFs. The range of 1.6-2.0 GPa was higher than the published range for CH (i.e. 1.31 ± 0.23 GPa). Similarly to the modulus values, differences could be seen in the portion of the histogram of hardness values associated with unhydrated cement particles (i.e., hardness values greater than 4 GPa) that were also attributed to the small sample size of unhydrated particles indented and the multiple phases with different hardness values that were included with the unhydrated cement particle data.

4.3.2. Effects of CNFs on the Micromechanical Properties of Individual Cement Hydrates

The micromechanical properties of specific individual cement hydrate phases were extracted by coupling the nanoindentation results with phase identification results from SEM-EDS, and only that data is included in this section. The modulus and hardness values corresponding to the cement hydrate phases was mostly less than 60 GPa and 4 GPa, respectively (only 13 modulus values were greater than 60 GPa and only 11 hardness values were greater than 4 GPa). The cement hydrate phases considered include: (i) C-S-H, (ii) CH, (iii) a combination of C-S-H and CH that is mostly C-S-H, (iv) a combination of C-S-H and CH that is mostly CH, and (v) Al-rich phases.

4.3.2.1. Indent Locations and Indentation Depths

Indent locations. The percentages of representative major cement hydration products indented are summarized in Figure 4.18. For both PC and PC-CNF, over 20% of indents were located on Al-Rich phases while over 50% of indents were located on C-S-H and less than 3%

were located on CH. Compared to the typical phase distribution reported in the literature for a portland cement matrix (i.e., 50% C-S-H, 20-25% CH, 10-15% Al-rich phases, and additional minor phases [3]), PC and PC-CNF were found to have more C-S-H (i.e., *ca.* 11% and 2%, respectively) and Al-rich phases (i.e., *ca.* 11% and 8%, respectively) and less CH (i.e., *ca.* 19% and 17%, respectively). PC-CNF compared to PC had 115% more CH and 14% less Al-rich phases.

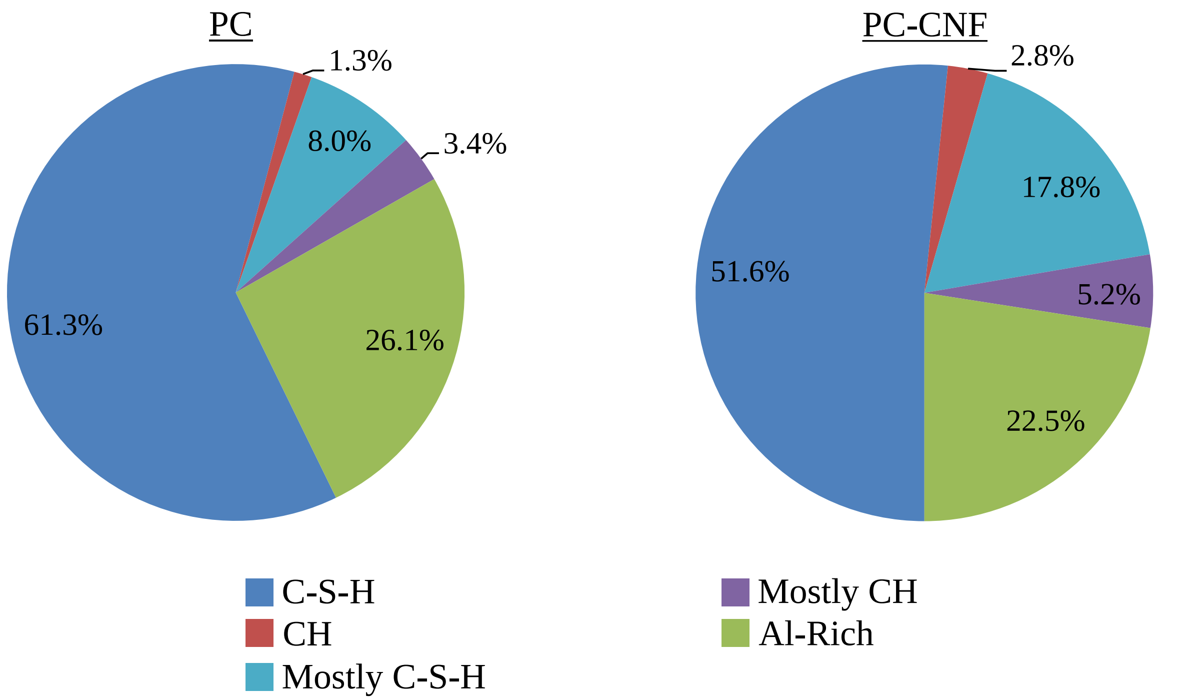

Figure 4.18. Pie charts showing the percentages of indents located on various cement hydration products including C-S-H, CH, a combination of C-S-H and CH but mostly C-S-H, a combination of C-S-H and CH but mostly CH, and Al-rich phases as analyzed by nanoindentation combined with SEM/EDS on cement-based composites including PC and PC-CNF (raw data included in Appendix C).

Indentation depths. The hydration products had indentation depths ranging from *ca.* 57 nm to *ca.* 620 nm (i.e., contact depths measured by the nanoindenter), and were mostly larger than the 200 nm required because of the surface roughness of polished cement [108]. Many of the depths for indents that were considered to be solely located on C-S-H were larger than 300 nm, which is considered then too large to characterize C-S-H using statistical methods [103]. However, because EDS analysis was coupled with the nanoindentation data, the experimentally obtained micromechanical properties could be directly associated with the individual phases and no statistical treatment of the data was needed. The range of indentation depths for PC and PC-CNF was, therefore, considered acceptable for characterization of the individual cement phases.

4.3.2.2. Micromechanical Properties

The modulus and hardness values of the cement hydrates for PC and PC-CNF are summarized in Figure 4.19 and **Error! Reference source not found.**. As discussed in Section 4.3.1, the major peak in the histogram of the hydration products (Figure 4.16, Figure 4.17, Figure 4.19, and **Error! Reference source not found.**) shifted to increased modulus values when CNFs were added to the cement paste. With the refined bin sizes allowed by the number of data points compared to the reduced range of the data, the shift occurred from the 20-25 GPa range to the 25-30 GPa range. The decomposition of the modulus histogram into the major cement hydration products showed the shift to be from the response of the indents located solely on C-S-H.

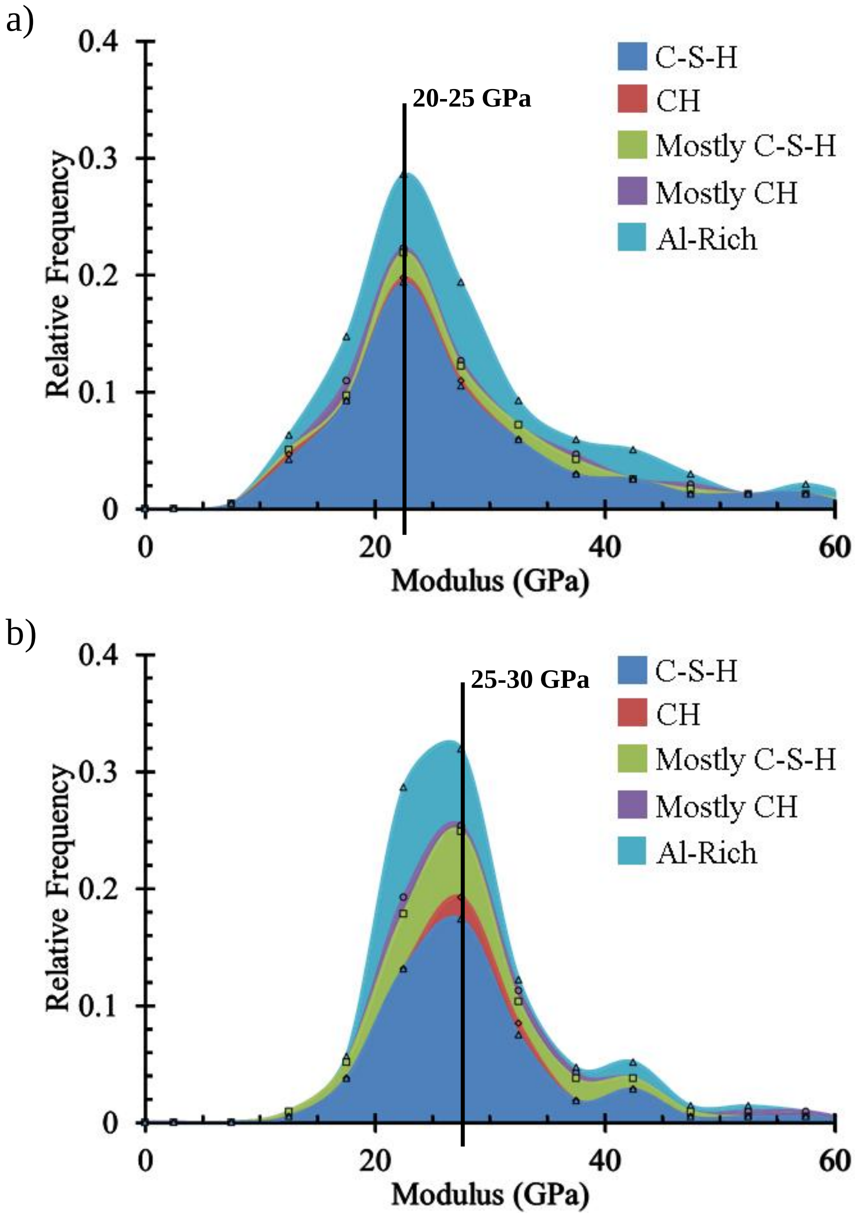

Figure 4.19. Histograms of the modulus values of the cement hydration products with scaled empirical distributions decomposed into the cement hydration phases of C-S-H, CH, a combination of C-S-H and CH but mostly C-S-H, a combination of C-S-H and CH but mostly CH, and Al-rich phases for cement-based composites (raw data included in Appendix C). a) PC and b) PC-CNF.

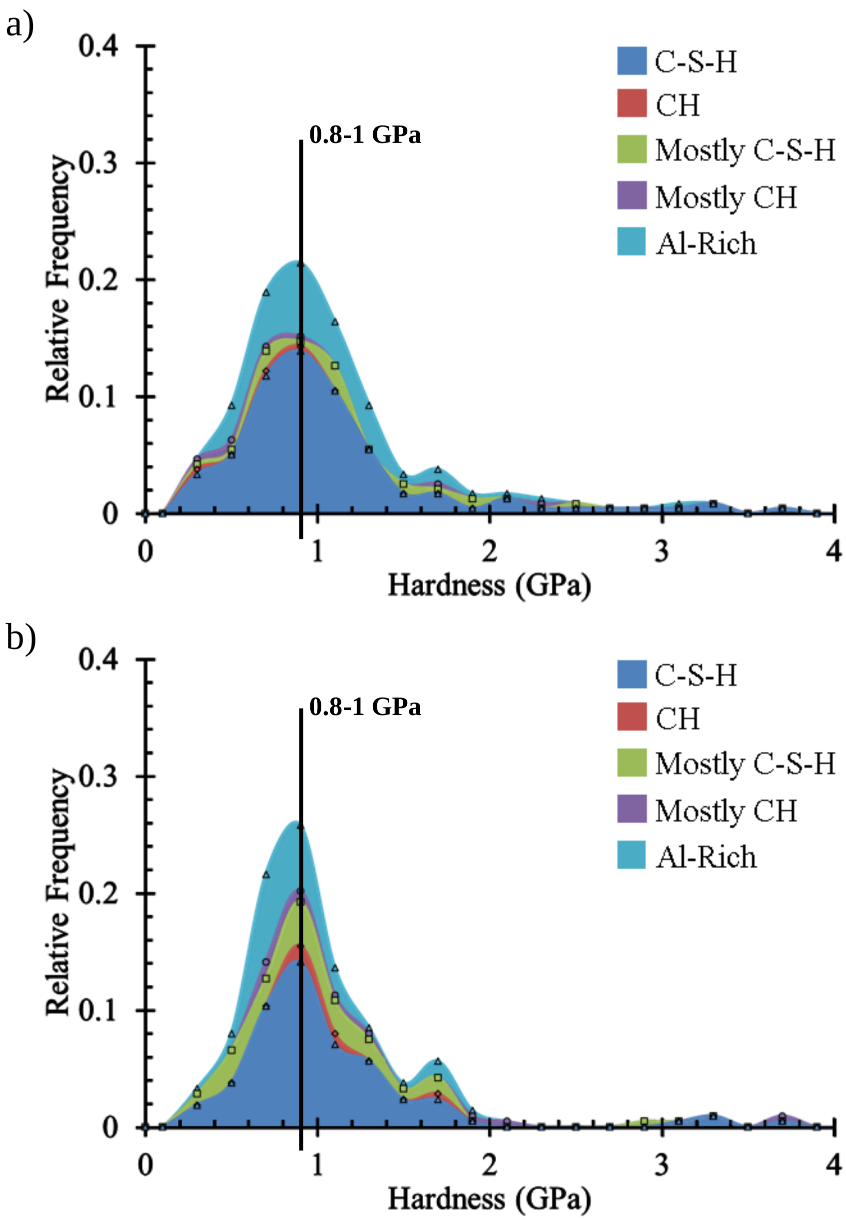

Figure 4.20. Histograms of the hardness values of the cement hydration products with scaled empirical distributions decomposed into the cement hydration phases of C-S-H, CH, a combination of C-S-H and CH but mostly C-S-H, a combination of C-S-H and CH but mostly CH, and Al-rich phases for cement-based composites (raw data included in Appendix C). a) PC and b) PC-CNF.

If Gaussian distributions are assumed, the histograms of the modulus and hardness values from indents located solely on C-S-H visually appeared to support the theory that there was more than one C-S-H phase. The mean, standard deviation, and weight of the Gaussian distributions within the total distribution were determined using an expectation maximization algorithm [146]. The modulus and hardness histograms for the C-S-H phase of PC and PC-CNF were best matched when three (3) Gaussian distributions were assumed as opposed to two (2). The use of four (4) Gaussian distributions was also examined, but it was determined that there was no benefit to using four (4) distributions as opposed to three (3) distributions. Figure 4.21 shows the distributions of modulus and hardness values as estimated by: (i) the Gaussian mixture model (i.e., summation of the estimated Gaussian distributions, red dash-dot line) with the Gaussian components (blue dashed lines) determined by the expectation maximization algorithm and (ii) for reference, a normal kernel function [147] with a bandwidth chosen such that the shape of the density estimate matched the shape of the histograms from Figure 4.19 and **Error! Reference source not found.** for the C-S-H phase (black solid line). The modulus and hardness values of each estimated Gaussian component and its weight are summarized in Table 4.1. The modulus and hardness values reported in Table 4.1 corresponded well to that found in the literature (Table 2.1). As can be seen from both the modulus and hardness values, the percentage of low stiffness C-S-H was decreased by 6% with the addition of CNFs compared to the control composite as determined by the Gaussian mixture model from the modulus values, suggesting the preferential formation of high stiffness C-S-H over low stiffness as reported in [47, 112, 113, 144, 145] with the addition of CNTs.

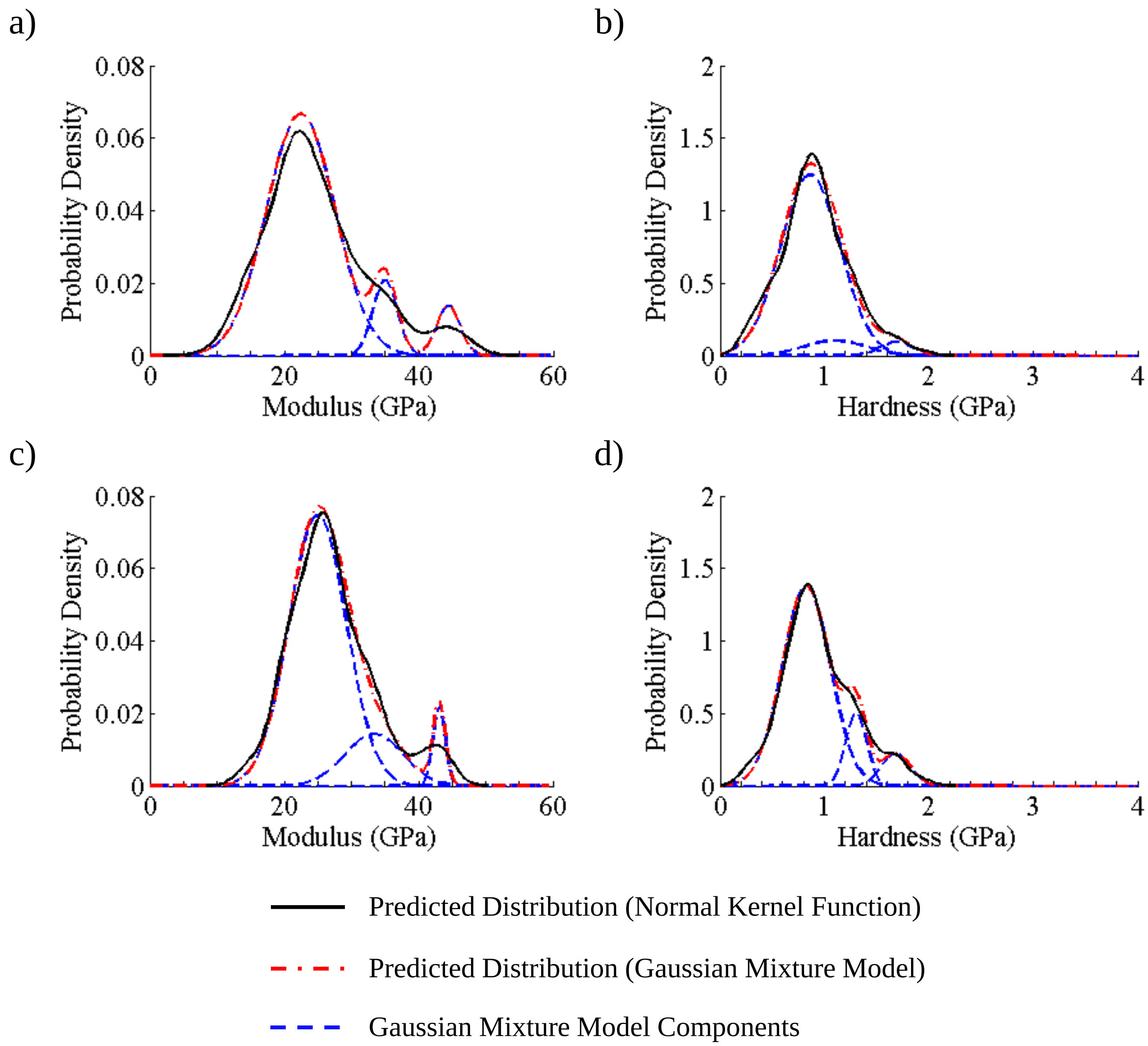

Figure 4.21. Micromechanical property distributions of the C-S-H phase in cement-based composites as predicted by a Gaussian mixture model and kernel density estimation and the Gaussian components of the Gaussian mixture model (raw data included in Appendix C). a) PC modulus values, b) PC hardness values, c) PC-CNF modulus values, and d) PC-CNF hardness values.

Table 4.1. Summary of mean modulus and hardness values of the C-S-H phases in PC and PC-CNF and their weights assuming three Gaussian distributions (raw data included in Appendix C).

		Modulus (GPa)	**Hardness (GPa)**
PC	Ultra-High Stiffness	44.4 ± 1.7 (6.0%)	1.7± 0.2 (3.7%)
	High Stiffness	35.0 ± 1.8 (9.4%)	1.1 ± 0.3 (7.6%)
	Low Stiffness	22.4 ± 5.1 (84.7%)	0.9 ± 0.3 (88.7%)
PC-CNF	Ultra-High Stiffness	43.1 ± 0.9 (5.0%)	1.7 ± 0.1 (7.7%)
	High Stiffness	33.4 ± 4.3 (15.4%)	1.3 ± 0.1 (12.7%)
	Low Stiffness	25.0 ± 4.2 (79.6%)	0.8 ± 0.2 (79.6%)

() Indicates % weight of phase in total distribution.

The modulus and hardness values were compared to both the Si/Ca and Al/Ca ratios to determine if the Si/Ca and Al/Ca ratios of the C-S-H had an impact on the modulus and hardness values, but no correlation could be determined (Figure 4.22). The packing density of the C-S-H phase was, therefore, thought to be responsible for the changes seen in the percentages of the low and high stiffness C-S-H as was suggested in [103].

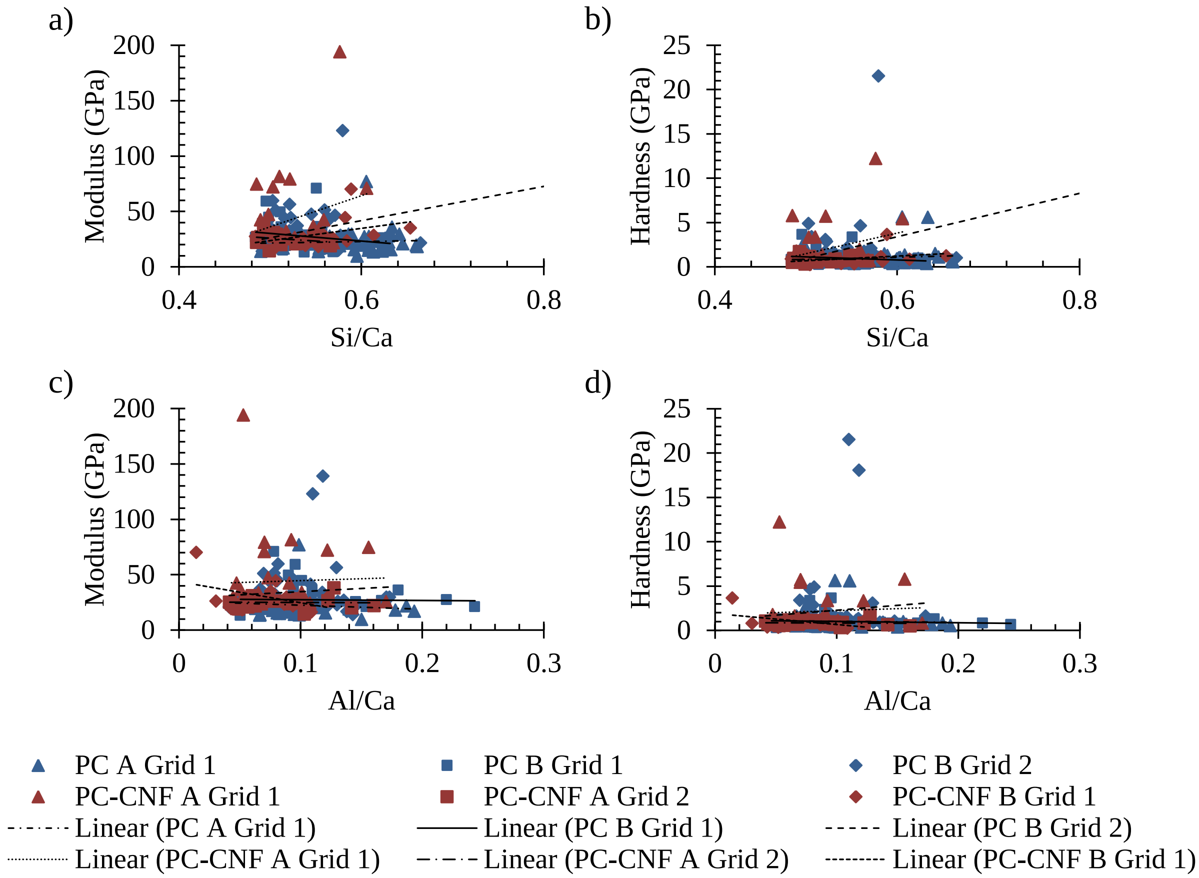

Figure 4.22. Micromechanical properties of the C-S-H phase in cement-based composites compared to the chemistry at the indent location (raw data included in Appendix C). a) Modulus values versus Si/Ca ratios, b) hardness values versus Si/Ca ratios, c) modulus values versus Al/Ca ratios, and d) hardness values versus Al/Ca ratios.

The modulus values found for CH and mostly CH, ranged from 12 to 193 GPa with only 36% of indents on CH having a modulus greater than 33 GPa, compared to 38 ± 5 GPa [100] and 40.3 ± 4.2 GPa [103] which have been reported in the literature. Instead, the majority of values found in the 32-48 GPa bin of the histogram, which is typically associated with CH, were found to be from indents located on Al-rich phases and the multiphase C-S-H/CH combination that was mostly C-S-H as determined with nanoindentation coupled with SEM/EDS. C-S-H and CH have been reported in the literature to form nanocomposites that result in higher local mechanical properties than the individual C-S-H and CH phases [108]. The low sampling of indents on CH could also be responsible for the discrepancy with the published values.

4.3.3. Micromechanical Properties located in and around CNF Agglomerates

The micromechanical properties at the local level of cement-based composites in and around CNF agglomerates were investigated using 1 wt% CNF loading.

4.3.3.1. Indent Locations

The locations of indents from nanoindentation with respect to a CNF agglomerate were examined for PC-1% when the nanoindentation grid was purposefully located in the vicinity of one or more CNF agglomerates (Figure 4.23). Approximately 55% of the indents examined were outside of the CNF agglomerates entirely, while *ca.* 45% of the indents were located inside of the CNF agglomerates. Of the indents located inside of an agglomerate, *ca.* 60% of the indents were classified as a part of the inner agglomerate (i.e., mostly entangled CNFs with little to no hydrates present), while *ca.* 40% of the indents were classified as a part of the outer agglomerate (i.e., mostly individual CNFs embedded in the cement hydration products on the outer edge of a agglomerate).

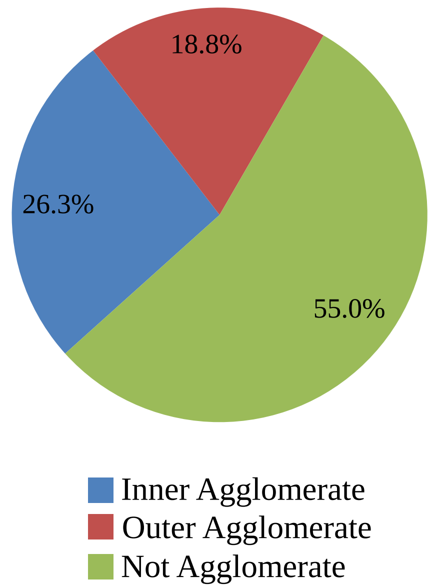

Figure 4.23. Pie charts showing the percentages of indents located with respect to a CNF agglomerate (i.e., inner agglomerate, outer agglomerate, or not agglomerate) as analyzed by nanoindentation combined with SEM/EDS on PC-1% (raw data included in Appendix C).

4.3.3.2. Micromechanical Properties

Contour mapping of the modulus and hardness values compared to backscatter SEM images showed the CNF agglomerates to clearly be associated with the low modulus and hardness values, i.e., less than 15 GPa and less than 0.5 GPa, respectively (Figure 4.24 and Figure 4.25). While a few high modulus and hardness values were also found inside of the CNF agglomerates (Figure 4.25), the secondary SEM image of PC-1% Grid 2 (Appendix C) showed that their location did not meet the contact requirements for nanoindentation and therefore those high modulus and hardness values were not considered valid.

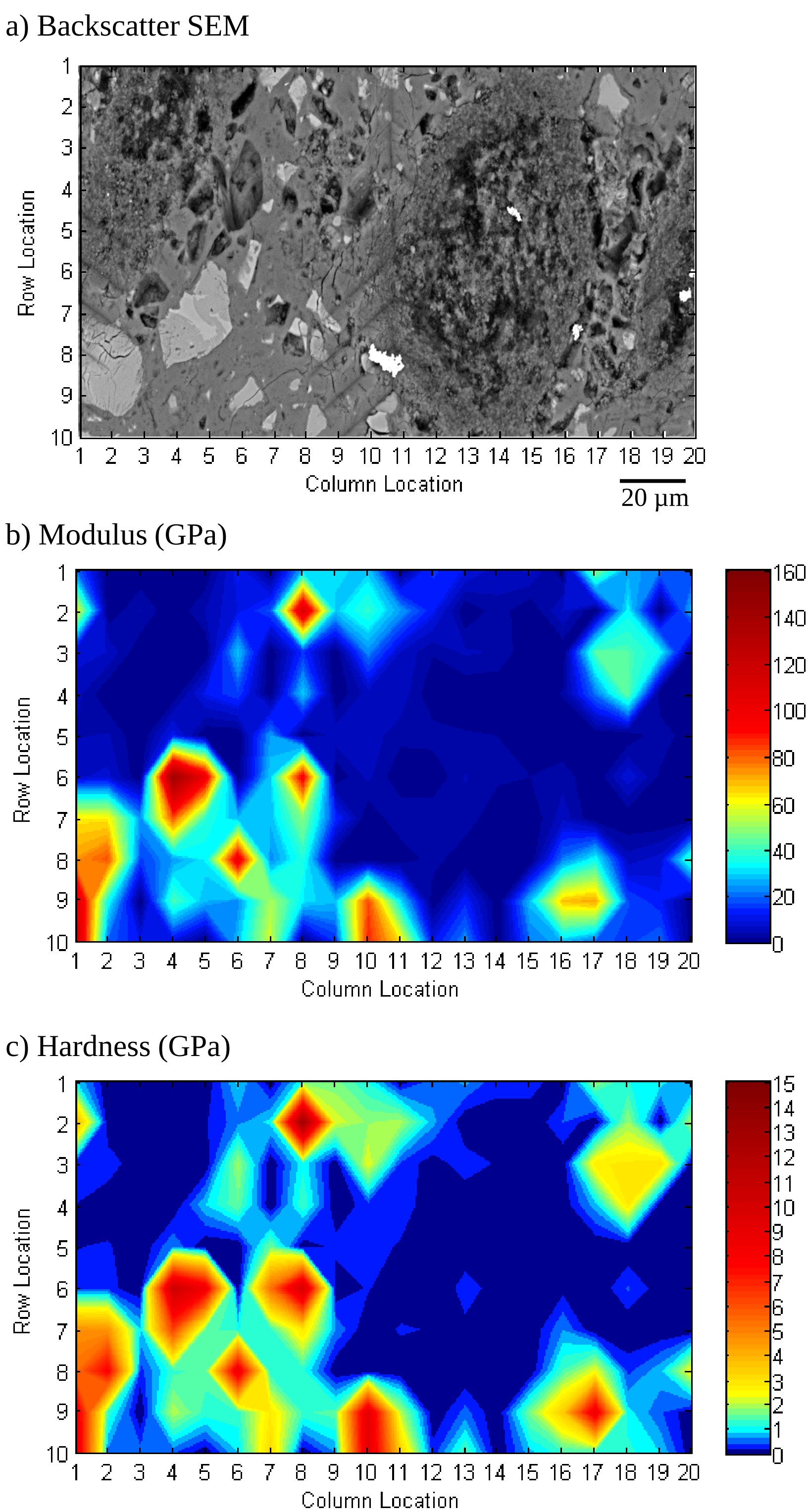

Figure 4.24. Spatial correlation of micromechanical properties of PC-1% Grid 1 (raw data included in Appendix C). Indents are located in a grid of 200 with 10 rows and 20 columns. a) Backscatter SEM image, b) contour plot of elastic modulus with linear interpolation between indents, c) contour plots of hardness with linear interpolation between indents.

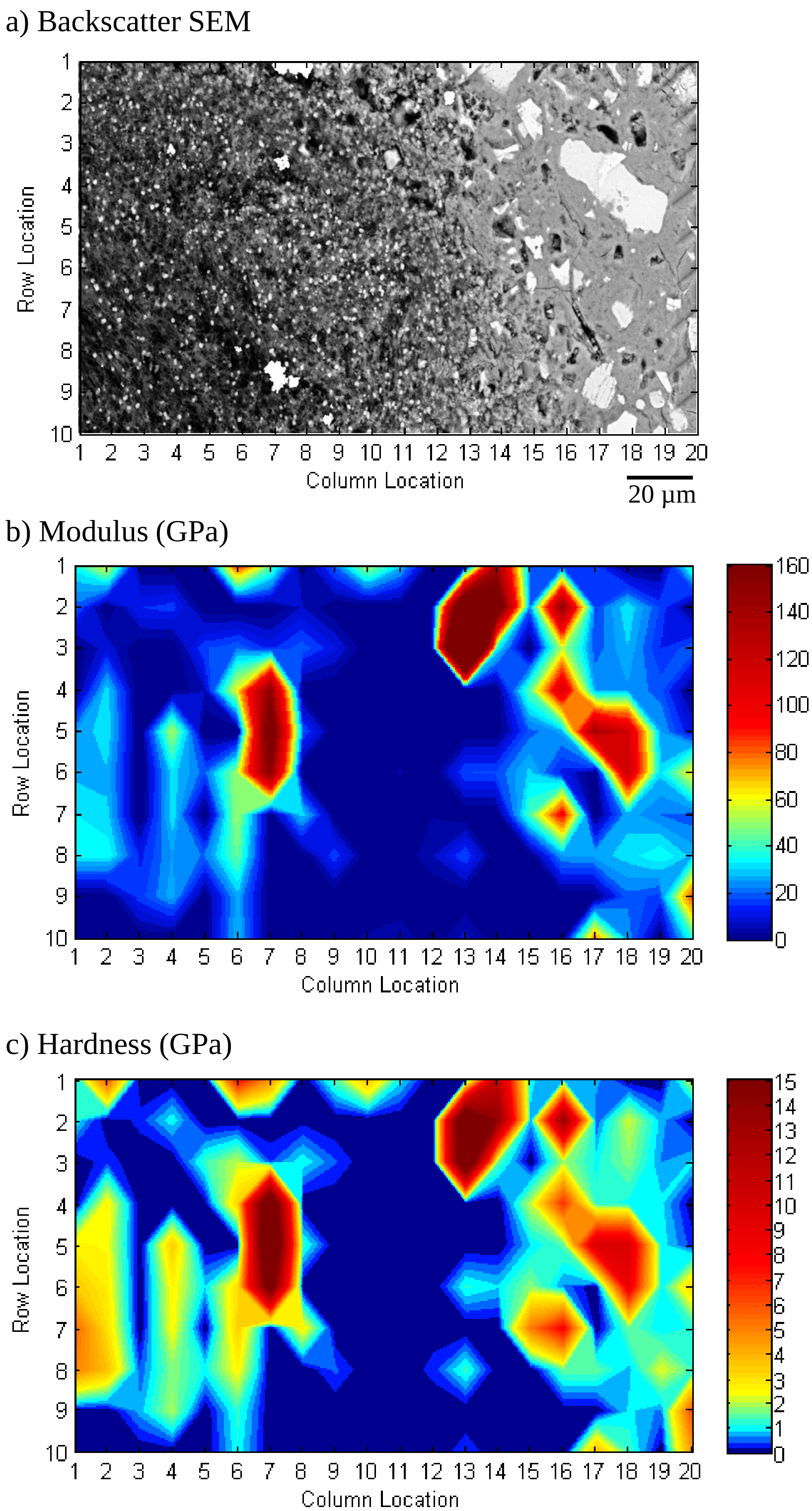

Figure 4.25. Spatial correlation of micromechanical properties of PC-1% Grid 2 (raw data included in Appendix C). Indents are located in a grid of 200 with 10 rows and 20 columns. a) Backscatter SEM image, b) contour plot of elastic modulus with linear interpolation between indents, c) contour plots of hardness with linear interpolation between indents.

Histograms decomposed by indent location with respect to the CNF agglomerates showed the elastic modulus and hardness to decrease when the indent was located on the inner or outer agglomerate (Figure 4.26). Although modulus and hardness values greater than 16 GPa and 1.2 GPa, respectively, were seen for indent locations inside of the agglomerates, those values were associated with the indent locations that were found to not meet the contact requirements of nanoindentation by the coupling of a contour map of the modulus values with a secondary SEM image. The high concentration of CNFs on the edge of the agglomerates where the CNFs were imbedded in the cement paste also caused a decrease in the micromechanical properties. The large number of indentation test results showing a decrease in the micromechanical properties supported the theory that the CNF agglomerates acted as flaws within the cement paste. Additionally, the majority of the data from the outer agglomerate having reduced micromechanical properties suggested that there was no reinforcing effect around the edge of the CNF agglomerates from the large quantity of CNFs embedded in the cement paste.

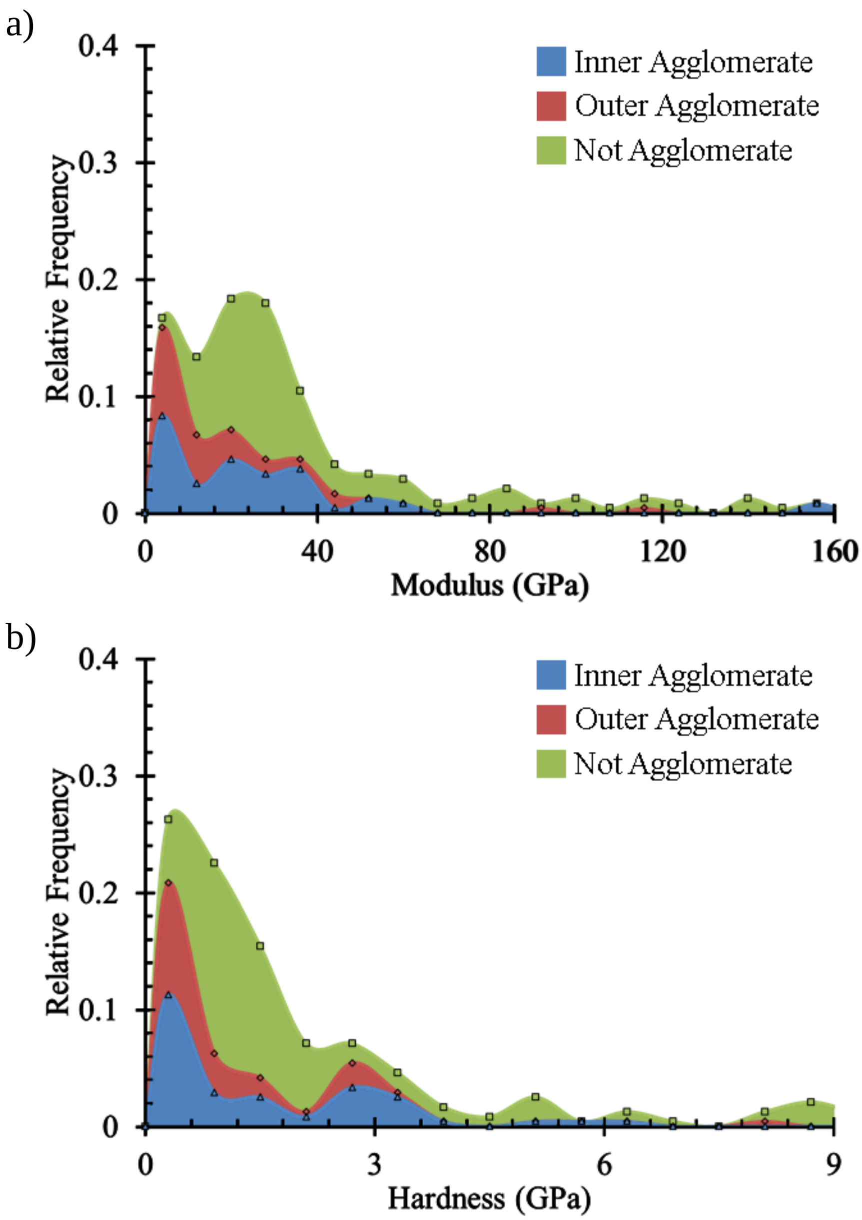

Figure 4.26. Histograms of the micromechanical properties of the cement hydration products indented on PC-1% with scaled empirical distributions decomposed into the cement hydration phases of C-S-H, CH, a combination of C-S-H and CH but mostly C-S-H, a combination of C-S-H and CH but mostly CH, and Al-rich phases (raw data included in Appendix C). a) Modulus and b) hardness.

4.4. Conclusions

The micromechanical properties of cement-based composites containing CNFs were determined, including the properties of the major cement hydration products and in and around CNF agglomerates. The following conclusions were made:

- CNFs caused a shift in the histograms of modulus values obtained from nanoindentation coupled with SEM/EDS towards higher modulus values for the C-S-H phase. The CNFs were found to cause the preferential formation of high stiffness C-S-H at the expense of low stiffness C-S-H with a 6% decrease in the percentage of low stiffness C-S-H present as determined by the Gaussian mixture model of the modulus values which was thought to be related to the packing density of the C-S-H.
- CNF agglomerates showed significantly lower modulus and hardness values than the rest of the cement paste, indicating that the CNF agglomerates acted as flaws. Additionally the edge of CNF agglomerates also had lower micromechanical properties indicating that there was no reinforcing effect around the edge of the CNF agglomerates.

CHAPTER 5

MACROMECHANICAL PROPERTIES OF CEMENT-BASED COMPOSITES WITH CNFS

5.1. Overview

CNFs have the potential to improve the macromechanical properties of cement-based materials as they have ultimate tensile strengths at least 5 times greater than steel [119] and their small size and large aspect ratio (i.e., diameters of 50-200 nm, lengths of 50-200 μm, aspect ratios of about 1000:1 [87]) make them excellent candidates to slow the growth of cracks at the nanoscale. The objective of this chapter is to determine the effect of CNFs on the macromechanical properties of cement-based composites, including ultimate strength, modulus, and toughness during compression, splitting tension, and flexure.

Traditional macromechanical testing including uniaxial compression, splitting tension, and three-point bending were performed using modified versions of ASTM standards. In addition, SEM observations were used to obtain a further understanding of the macromechanical testing results. The macromechanical properties were determined with respect to the CNF dispersion state and loading. Composites with and without 10 wt% of silica fume (SF and PC pastes, respectively) were considered. Load and displacement data captured for each specimen during testing were used to plot the stress versus strain curves and determine the ultimate strength, modulus, toughness, and strain capacity. The relationships between CNF dispersion state, CNF loading, and macromechanical properties were investigated.

5.2. Experimental Detail

5.2.1. Materials

The materials discussed in Section 3.2.1 were used in this study including the CNFs with and without surface treatment with HNO_3, the dispersing agents (*Rheobuild® 1000*, *Glenium® 7500*, and *MicroAir®*), and the type I portland cement. In addition, dry, undensified silica fume (Norchem, Inc., Hauppauge, NY, USA) was used as an alternative binder. As per the manufacturer, the silica fume was the by-product from the production of silicon metal and had a bulk density of 192-320 kg/m^3. Also as per the manufacturer, the composition of the silica fume was ~95% silicon dioxide, and ~99% of its particles were retained on a 45 μm sieve.

5.2.2. Preparation of Cement-Based Composites

5.2.2.1. PC Paste Composites

PC paste composites were prepared as discussed in Section 3.2.3.2 and included: (i) PC pastes prepared using various dispersing agents and a CNF loading of 0.2% (PC-W/Control, PC-W/CNF, PC-W/T-CNF, PC-AE/Control, PC-AE/CNF, PC-N-HRWR/Control, PC-N-HRWR/CNF, PC-P-HRWR/Control, PC-P-HRWR/CNF, and PC-P-HRWR/T-CNF) and (ii) PC pastes prepared using the P-HRWR dispersing agent and various CNF loadings (PC-0%, PC-0.02%, PC-0.08%, PC-0.2%, PC-0.5%, and PC-1%). (Note: The PC-P-HRWR/Control and PC-0% are the same composites and the PC-P-HRWR/CNF and PC-0.2% are the same composites.) Cylinders for compressive testing were shaved to remove any edges that would cause seating issues during testing. The 2.54 cm × 2.54 cm × 68.58 cm (1 in.× 1 in.× 27 in.) beams were cut into six (6) 2.54 cm × 2.54 cm × 11.43 cm (1 in.× 1 in.× 4.5 in.) beams for flexural testing. After flexural testing, the longer half of the tested beam was shaved to approximately 5.08 cm (2 in.) in length to allow for the majority of the damage zone from flexural testing to be discarded for compressive testing. After all macromechanical testing was complete, fracture surfaces of each composite were prepared as described in Section 3.2.3.2 for SEM observations.

5.2.2.2. SF Paste Composites

SF paste composites were prepared using 10 wt% of silica fume and 0, 0.02, 0.08, 0.2, 0.5, and 1 wt% CNFs loadings (SF-0%, SF-0.02%, SF-0.08%, SF-0.2%, SF-0.5%, and SF-1%). A water-to-binder (cement + silica fume, w/b) ratio of 0.28 (or w/c ratio of 0.308) was used. The CNFs were first dispersed in water using an equivalent of 1% of P-HRWR by weight of binder and ultrasonication to prepare the CNF suspension as discussed in Section 3.2.2.1. The cement and silica fume were blended for three (3) minutes in a variable-speed stand mixer (KitchenAid Artisan 5-quart, Whirlpool Corporation, Benton Charter Township, Michigan, USA) before the CNF suspension was added. The mixture was then blended for six (6) minutes and poured into cylinders and beams as described in Section 3.2.3.2. The specimens were further prepared for macromechanical testing as described in Section 3.2.3.2.

5.2.3. Characterization

5.2.3.1. Macromechanical Testing

The mechanical performance of the composites was evaluated at 7 and 28 days by uniaxial compressive, splitting tensile, and three-point bending tests. The tests were performed using a Tinius Olsen Super L 60 K (300 kN) universal testing machine (Tinius Olsen, Inc., Horsham, PA, USA). In all cases, testing was discontinued when the load had decreased to 75% of the maximum. A minimum of five (5) specimens per composite was tested for each test setup. For all tests, force and displacement data were recorded. The obtained mechanical properties were analyzed statistically to determine the median, 1st quartile, 3rd quartile, maximum, and minimum values as well as any outliers in the data set. Data points were considered outliers if they were outside of the 1st and 3rd quartile by 1.5 times the interquartile range. Data sets were analyzed using the Welch's t-test at 90% and 95% confidence to determine if the data sets were statistically different. Percent difference calculations were based on the median values of data sets as opposed to averages because of the robustness of the median and the small size of the data sets used.

Compressive testing. The compressive testing was completed on cylindrical specimens following a modification of ASTM C39. The test setup is shown in Figure 5.1. The cylinders were tested in displacement-controlled mode with a displacement rate of 0.3 mm/min. The load and displacement data from the testing on cylindrical specimens was used to determine the compressive strength, modulus, strain capacity at failure, and toughness. The displacement was measured as the crosshead displacement. The strength was taken as the ultimate strength, i.e. the maximum strength value during testing. The modulus was determined by using a linear fit to determine the slope of the portion of the stress versus strain plot before major cracking events occurred, and it was taken as the slope of the line when the R^2-value of the linear fit was 0.999. The strain capacity at failure was determined as the strain just before a strength loss greater than 20% in which the change in strain was less than 20%. The compressive toughness was estimated using the trapezoidal method for estimating the area under the curve. Compression on beam specimens was used to show the structural integrity after testing by visual inspection. The structural integrity was compared as a function of CNF loading.

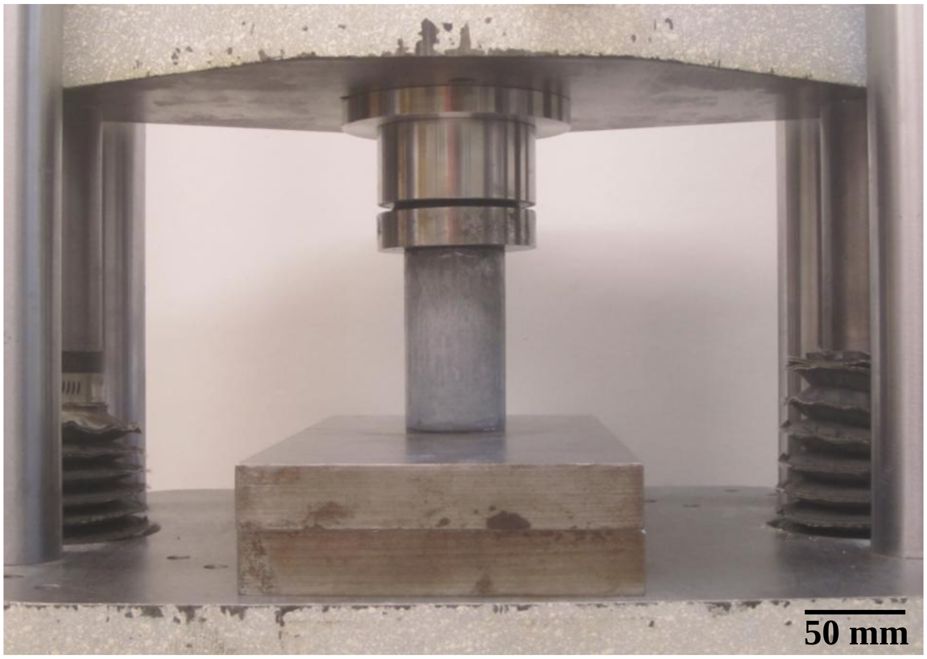

Figure 5.1. Compressive test setup for testing cylinder specimens of cement-based composites. The cylinder has a diameter of 50.8 mm (2 in.) and height of 101.6 mm (4 in.).

Splitting tensile testing. Splitting tensile testing was completed on cylindrical specimens following a modification of ASTM C496. The test setup is shown in Figure 5.2. The cylinders were tested in load-controlled mode with a loading rate of 51.2 kN/min. The load and displacement data was used to determine the splitting tensile strength. The splitting tensile strength was defined as the maximum splitting tensile strength, and the displacement was determined by the crosshead displacement.

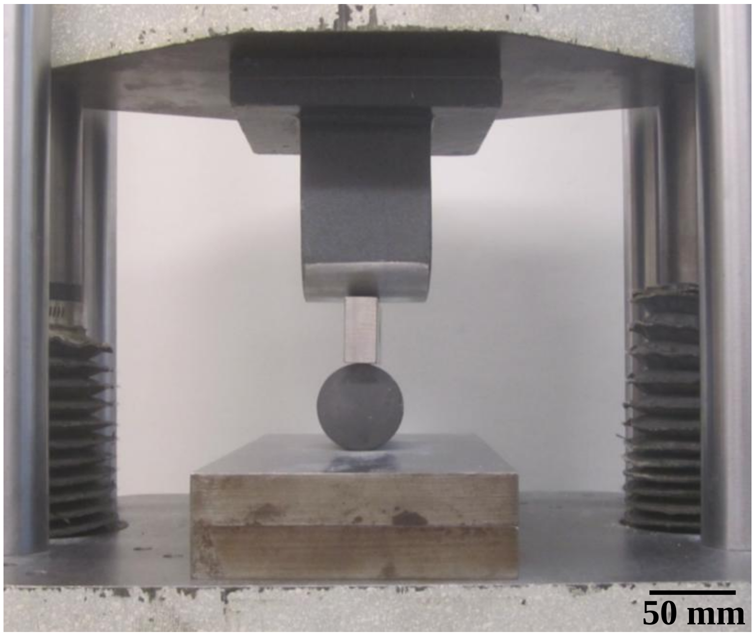

Figure 5.2. Splitting tensile test setup for testing cylinder specimens of cement-based composites. The cylinder has a diameter of 50.8 mm (2 in.) and height of 101.6 mm (4 in.).

Flexural testing. Flexural testing was performed on beam specimens by three-point bending using a modification of ASTM C293. The test setup is shown in Figure 5.3. The span between supports was 76.2 mm (3 in). The beams were tested in displacement-controlled mode with a displacement rate of 0.1 mm/min, and the values of applied displacement and resulting load were recorded until the beam fractured. The load and displacement data was used to determine the ultimate strength, flexural modulus, strain capacity at failure, and flexural toughness. The displacement data was recorded as the crosshead displacement. The ultimate flexural strength was determined from the peak load. The modulus was determined as the slope of the line from a linear fit with a R^2-value of 0.995. The strain capacity at failure was determined as the strain at the peak load. The toughness was estimated using the trapezoidal method for estimating the area under the stress versus strain curve. A few sets of flexural specimens (i.e., SF-0.5% and SF-1% at 7 days and SF-0% and SF-0.08% at 28 days) suffered a crushing effect during testing due to a rough edge of the specimens' top surface, which affected the strain capacity and toughness results of these specimens. For the data sets that were affected by the crushing effect, the strain capacity and toughness values were estimated using the ultimate stress and flexural modulus values.

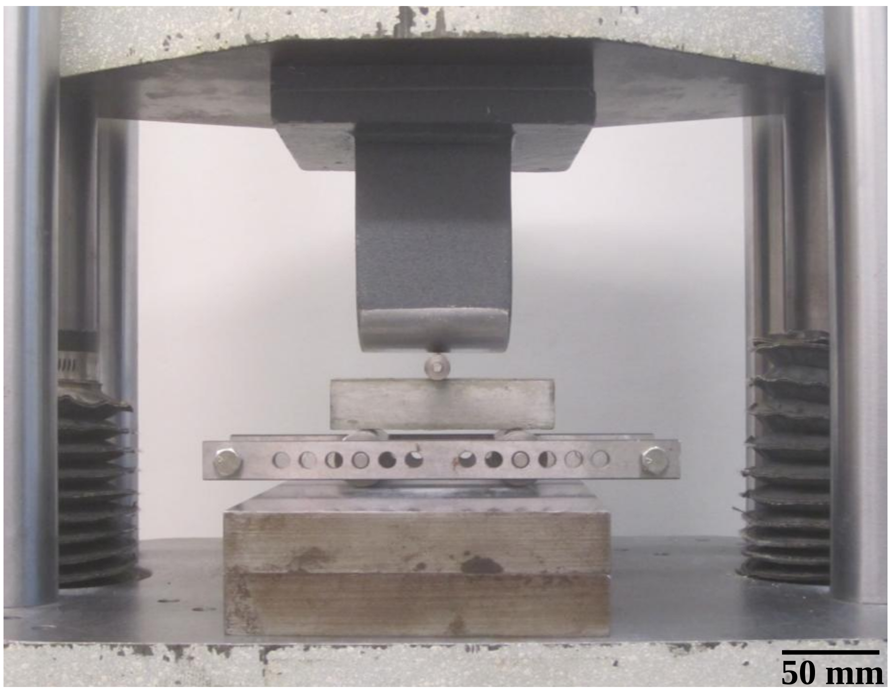

Figure 5.3. Three-point bending setup for testing beam specimens of cement-based composites. The beam has a height and width of 25.4 mm (1 in.) and length of 114.3 mm (4.5 in.).

5.2.3.2. Microstructural Analysis

The microstructure and morphology of the composites was evaluated using a Hitachi S4200 high resolution SEM (Hitachi Ltd., Chiyoda, Tokyo, Japan) equipped with a cold field emission electron gun and digital imaging. Fracture surfaces of the 7-day-cured PC paste composites were kept in acetone for at least 7 days to stop further hydration prior to being sputter coated with gold and mounted on an aluminum stub using copper tape. For imaging, an accelerating voltage of 10-20 kV and a working distance of 15 mm were employed.

5.3. Results and Discussion

5.3.1. Influence of CNF Dispersion on the Flexural Strength of PC Paste Composites

A strong coupling existed between the flexural response of the composites, the state of dispersion of the CNFs, and the interfacial interaction between the CNFs and the cement paste (Figure 5.4). Only the composites containing CNFs dispersed with the assistance of P-HRWR showed improvement in the 7-day flexural strength (Welch's t-test, Table 5.1). All of the other composites (i.e., PC-W/CNF, PC-W/T-CNF, PC-N-HRWR/CNF, and PC-AE/CNF) showed no statistically significant changes at the 95% confidence level in the 7-day flexural strength with respect to their control (Table 5.1).

The increase in the median flexural strength of the PC-P-HRWR/CNF and PC-P-HRWR/T-CNF composites compared to the reference composite prepared without CNFs was modest with only about an11% and 22% increase, respectively (Table 5.1). The greater improvement in flexural strength obtained when surface treatment with HNO_3 was used in combination with the P-HRWR assisted dispersion was believed to be resultant from an improved interfacial bond between the CNFs and the cement matrix, since both composites showed similar relative frequency of large size CNF agglomerates (i.e., 58% and 56% with a maximum Feret's diameter > 200 μm for the P-HRWR/CNF and P-HRWR/T-CNF composites, respectively). The improved bond was believed to be due to chemical interactions between the cement matrix and functional groups (i.e., most likely hydroxyl and carboxyl) present at the surface of the CNFs [36, 148].

The presence of CNF agglomerates resulting from non-dispersed primary agglomerates or secondary agglomerates formed during cement mixing/curing clearly hindered the ability of the CNFs to act as nanoreinforcement. The composite reinforcement was dominated by the collective behavior of the CNF agglomerates rather than the strength of the individual CNFs. The CNF agglomerates acted as flaws within the cement matrix (see Chapter 4), causing non-uniform stress distributions and high stresses near the agglomerates, which weakened the composites. This behavior was exacerbated when a significant number of larger size agglomerates was present in the paste (i.e., more than 60% with a maximum Feret's diameter greater than 200 µm), as in the PC-W/CNF, PC-W/T-CNF, PC-N-HRWR/CNF, and PC-AE/CNF composites (see Chapter 3), causing the mechanical behavior of the agglomerates to completely outweigh the potential benefit of the individual CNFs.

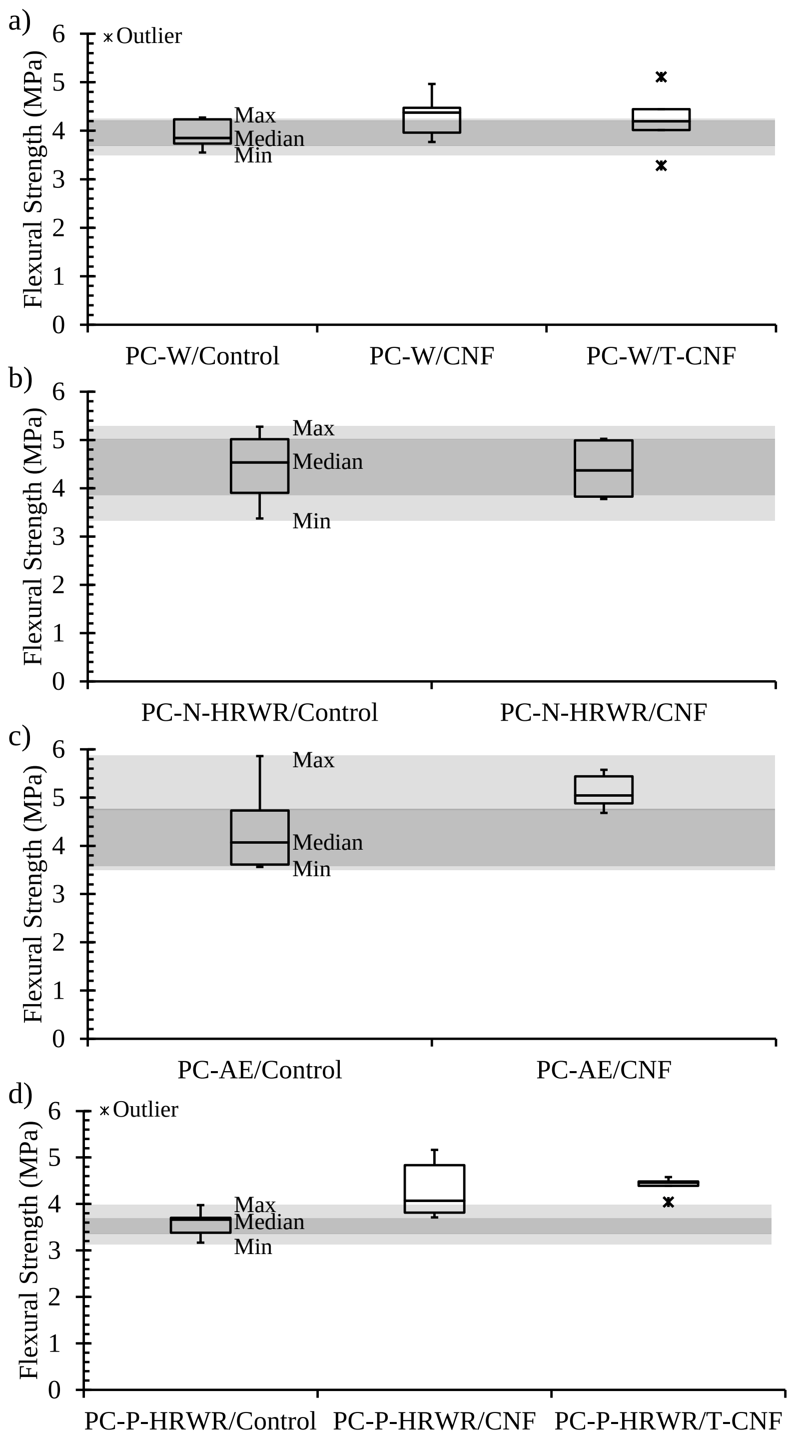

Figure 5.4. 7-day flexural strengths of PC paste composites with 0.2 wt% CNFs as a function of CNF dispersion method (raw data included in Appendix D). a) Cement pastes made with no dispersing agent, b) cement pastes made with N-HRWR, c) cement pastes made with AE, and d) cement pastes made with P-HRWR.

Table 5.1. P-values (Welch's t-test) and conclusions at the 90% and 95% confidence levels for the 7-day flexural strength of PC paste composites with 0.2 wt% CNFs as a function of CNF dispersion method compared to the corresponding control composite (raw data included in Appendix D).

	P-value (compared to corresponding control composites)	**Summary at the 90% and 95% confidence levels**
PC-W/CNF	0.083 (13.7%)	Increase in 7-day ultimate strength.
PC-W/T-CNF	0.312	
PC-N-HRWR/CNF	0.910	
PC-AE/CNF	0.077 (24.1%)	Increase in 7-day ultimate strength.
PC-P-HRWR/CNF	0.039 (11.1%)	Increase in 7-day ultimate strength.
PC-P-HRWR/T-CNF	2.6×10^{-4} (21.7%)	Increase in 7-day ultimate strength.

() Indicates % difference compared to the control.

Indicates P-value less than or equal to 0.100 (significance at the 90% confidence level).

Indicates P-value less than or equal to 0.050 (significance at the 95% confidence level).

5.3.2. Effect of CNF Loading on the Mechanical Properties of PC Paste Composites

5.3.2.1. Compressive Properties

The compressive properties of the PC paste composites were mostly controlled by the cement matrix and not the fiber reinforcement. The addition of CNFs showed, in general, no statistically significant effect at the 95% confidence level (Welch's t-test) in the composite compressive strength for CNF loadings up to 0.5 wt% (Figure 5.5a, Figure 5.6a, and Table 5.2). Similarly, in most cases, no statistically significant differences with the control were seen at the 95% confidence level (Welch's t-test) for the compressive modulus, strain, and toughness of the composites up to 0.5 wt% CNF loading (Figure 5.5, Figure 5.6, and Table 5.2). When statistical differences were noted with respect to the control, they were mainly the result of the inherent variable nature of the material and not due to the effect of the addition of CNFs (e.g., the 0.02 wt% CNF loading showed statistical differences with the control but not with the other composites).

The negative effects of the presence of CNF agglomerates on the compressive properties were seen for 1 wt% CNF loading with *ca*. 20% decrease at the 95% confidence level (Welch's t-test, Table 5.2) in the 7-day median compressive strength and *ca*. 15% decrease at the 95% confidence level (Welch's t-test, Table 5.2) in the 28-day median compressive modulus. The CNF agglomerates acted as randomly distributed defects in the cement matrix creating weak zones in the composite. During compression, the CNF agglomerates acted as voids, affecting the compressive properties similar to porosity (i.e., decreasing compressive properties with increasing porosity [3]). A decrease in the compressive strength was seen when a significant number of larger size CNF agglomerates was present in the cement matrix as was the case for the 1 wt% CNF loading (i.e., 3.9% of the cross-sectional area composed of CNF agglomerates of size area greater than 0.007 mm^2 compared to 1.4% and 3.2% for the 0.2 wt% and 0.5 wt% CNF loading, respectively).

Though the addition of CNFs had limited effect on the composite compressive properties, the presence of CNFs noticeably improved the structural integrity of the composites after compressive testing (Figure 5.7). It was believed that the network created by the CNFs inside of the agglomerates may have limited the propagation of cracks, allowing the cement matrix to hold together even after multiple cracking events and thus to remain quasi-intact after testing.

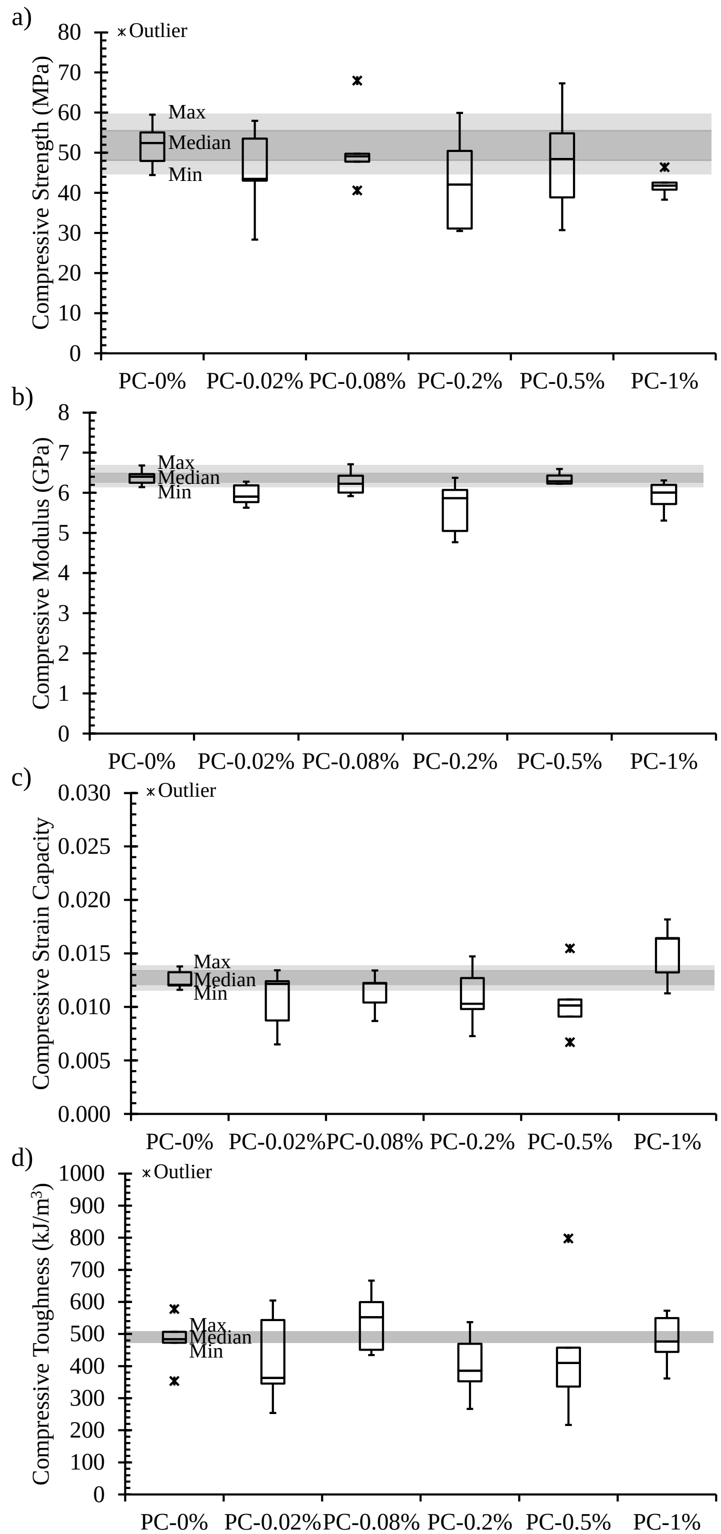

Figure 5.5. 7-day compressive properties of PC paste composites as a function of CNF loading (0-1 wt% CNFs dispersed by P-HRWR, raw data included in Appendix D). a) Ultimate strength, b) modulus, c) strain capacity at failure, and d) toughness.

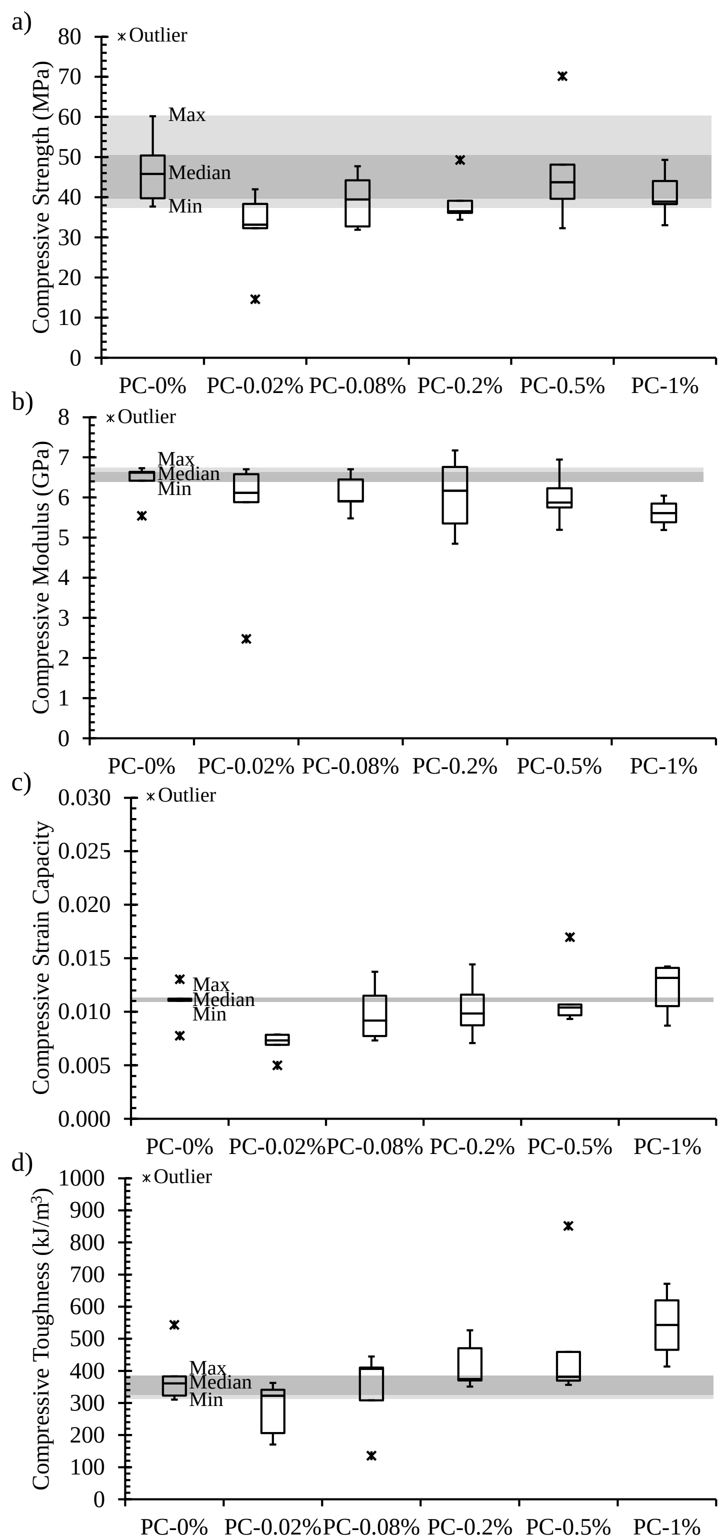

Figure 5.6. 28-day compressive properties of PC paste composites as a function of CNF loading (0-1 wt% CNFs dispersed by P-HRWR, raw data included in Appendix D). a) Ultimate strength, b) modulus, c) strain capacity at failure, and d) toughness.

Table 5.2. P-values (Welch's t-test) and conclusions at the 90% and 95% confidence levels for the compressive properties of PC paste composites as a function of CNF loading (0.02-1 wt% CNFs dispersed by P-HRWR) compared to the control (raw data included in Appendix D).

	P-value (compared to PC-0%)								**Summary at the 90% and 95% confidence levels**
	Strength		Modulus		Strain Capacity		Toughness		
	7 days	28 days	7 days	28 days	7 days	28 days	7 days	28 days	
PC-0.02%	0.295	0.046 (-27.6%)	0.023 (-7.8%)	0.354	0.226	0.007 (-34.5%)	0.475	0.107	Decrease in 28-day ultimate strength, 7-day modulus, and 28-day strain capacity at failure.
PC-0.08%	0.878	0.179	0.472	0.354	0.261	0.542	0.312	0.558	
PC-0.2%	0.200	0.156	0.066 (-8.4%)	0.520	0.294	0.750	0.235	0.541	Decrease in 7-day modulus.
PC-0.5%	0.597	0.997	0.769	0.312	0.218	0.740	0.747	0.373	
PC-1%	0.016 (-20.2%)	0.256	0.055 (-6.2%)	0.028 (-15.2%)	0.111	0.375	0.972	0.058 (50.5%)	Increase in 28-day strain capacity at failure. Decrease in 7-day ultimate strength and 7- and 28-day modulus.

() Indicates % difference compared to PC-0%.

Indicates P-value less than or equal to 0.100 (significance at the 90% confidence level).

Indicates P-value less than or equal to 0.050 (significance at the 95% confidence level).

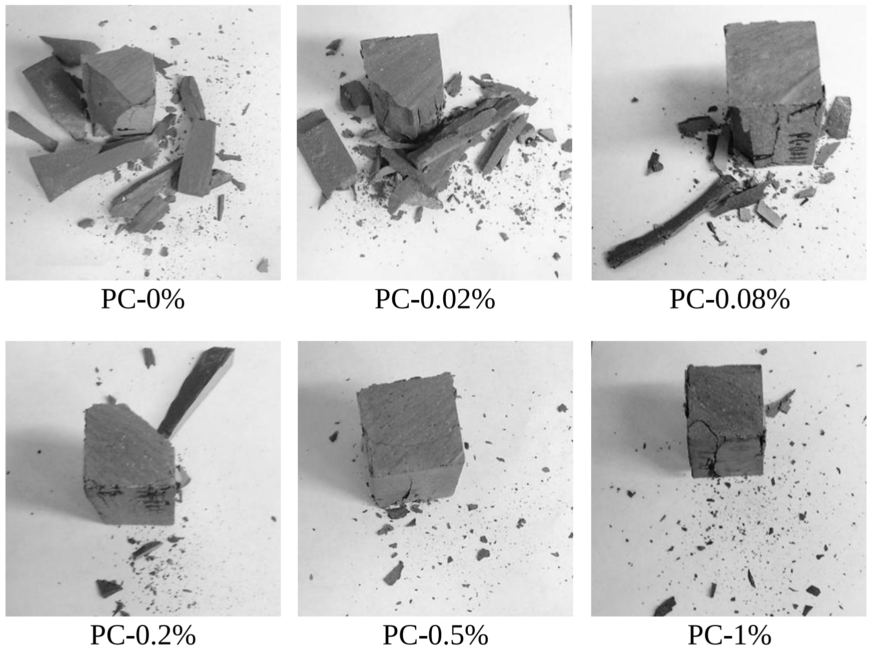

Figure 5.7. Structural integrity of PC paste composites after 28-day compressive testing as a function of CNF loading (0-1 wt% CNFs dispersed by P-HRWR).

5.3.2.2. Splitting Tensile Strength

The addition of CNFs improved the 7-day splitting tensile strength of the PC paste composites but was not statistically conclusive for the splitting tensile strength at 28 days due to the high variability within each data set (i.e., standard deviations greater than 1 MPa) (Figure 5.8 and Figure 5.9). The median 7-day splitting tensile strengths of the PC-0.08%, PC-0.2%, and PC-0.5% were about 35%, 70%, and 18% higher, respectively, than in the control composite without CNFs. No statistically significant differences from the control composite were, however, noted in the 7-day splitting tensile strength at the 95% confidence level (Welch's T-test) for CNF loadings of 0.02 wt% and 1 wt% (Table 5.3). The inherent variability of the cement matrix in combination with air voids, poorly distributed CNFs, and the existence of randomly distributed large size CNF agglomerates within the cement pastes were believed to have dominated the splitting tensile properties of the composites.

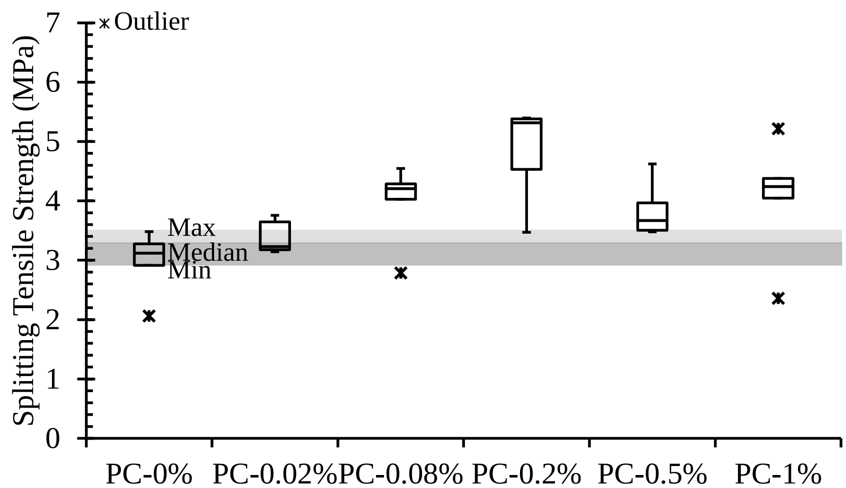

Figure 5.8. 7-day splitting tensile strength of PC paste composites as a function of CNF loading (0-1 wt% CNFs dispersed by P-HRWR, raw data included in Appendix D).

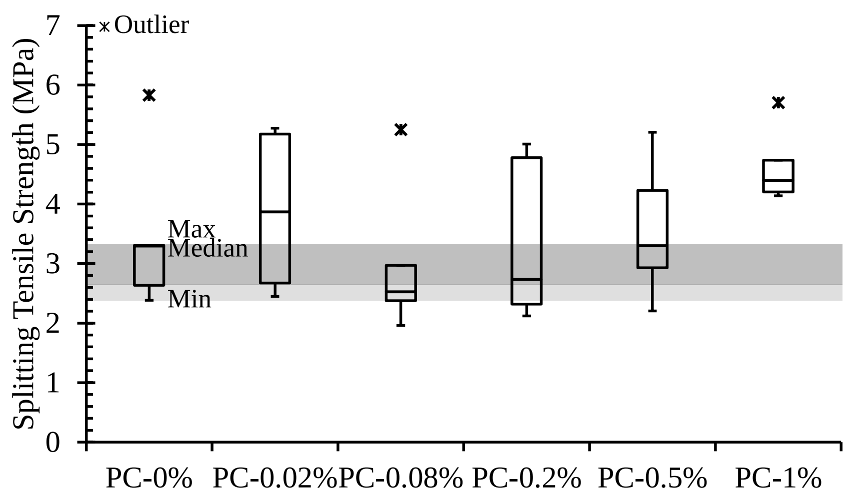

Figure 5.9. 28-day splitting tensile strength of PC paste composites as a function of CNF loading (0-1 wt% CNFs dispersed by P-HRWR, raw data included in Appendix D).

Table 5.3. P-values (Welch's t-test) and conclusions at the 90% and 95% confidence levels for the splitting tensile strength of PC paste composites as a function of CNF loading (0.02-1 wt% CNFs dispersed by P-HRWR) compared to the control (raw data included in Appendix D).

	P-value (compared to PC-0%)		**Summary at the 90% and 95% confidence levels**
	Strength		
	7 days	28 days	
PC-0.02%	0.181	0.653	
PC-0.08%	0.036 (35.0%)	0.592	Increase in 7-day ultimate strength.
PC-0.2%	0.005 (70.5%)	0.913	Increase in 7-day ultimate strength.
PC-0.5%	0.027 (17.6%)	0.919	Increase in 7-day ultimate strength.
PC-1%	0.086 (36.0%)	0.144	Increase in 7-day ultimate strength.

() Indicates % difference compared to PC-0%.

Indicates P-value less than or equal to 0.100 (significance at the 90% confidence level).

Indicates P-value less than or equal to 0.050 (significance at the 95% confidence level).

5.3.2.3. Flexural Properties

Overall, the addition of CNFs improved the flexural properties of the PC paste composites with additional improvements seen with increasing CNF loading. In general, the CNFs increased the 7-day flexural strength, modulus, and toughness but not the strain capacity. In contrast, at 28 days, the strain capacity and flexural strength were increased but not the modulus for most cases (Figure 5.10 and Figure 5.11). These results showed that CNFs can improve the flexural properties of PC paste composites even when poorly distributed and agglomerated. The weak zones formed in the cement pastes by the CNFs contained in agglomerates or otherwise poorly distributed were thought to be partially counterbalanced by the presence of an effective fraction of CNFs.

Ultimate flexural strength. In general, an increasing trend in 7- and 28-day flexural strengths was observed with increasing CNF loading (Figure 5.10a and Figure 5.11a). While the increase in the 7-day flexural strength was only marginal for CNF loadings at and below 0.2 wt% (i.e., *ca*.11% increase in the median flexural strength for 0.2 wt% CNFs at the 95% confidence level, Welch's t-test), the addition of 0.5 wt% and 1 wt% CNFs resulted in *ca.* 35% and *ca.* 66% increase in the median peak stress at the 95% confidence level (Welch's t-test, Table 5.4), respectively. Further improvement in the flexural strength was seen at 28 days for the 0.02 wt% and 0.08wt% CNF loading (i.e., *ca.* 27% and *ca.* 31% increase in the median flexural strength over the control, respectively) but not for the other loadings.

Flexural modulus. The addition of CNFs had a limited effect on the composite flexural modulus (i.e., stiffness) (Figure 5.10b and Figure 5.11b). Though at 7 days, as much as 30% increase in the median flexural modulus was noted with the addition of 0.02 wt%, 0.2 wt%, and 0.5 wt% CNFs, at 28 days, similar or lower flexural modulus values than the control were seen for most CNF loadings at the 95% confidence level (Welch's t-test, Table 5.4).

Strain capacity at failure. At 7 days, no significant effect on the strain capacity at the 95% confidence level was observed with CNF addition; however, at 28 days, the flexural strain capacity increased beyond that of the control at the 95% confidence level for 0.08 wt% and 0.2 wt% CNFs and the 90% confidence for 0.5 wt% and 1 wt% CNFs with a maximum increase of *ca.* 92% based on the median value seen at 0.2 wt% CNF loading (Welch's t-test, Table 5.4).

Flexural toughness. The flexural toughness showed overall the same general increasing trend as the ultimate flexural strength (Figure 5.10 and Figure 5.11) upon CNF addition. At 7 days, the median flexural toughness was increased by as much as 41% and 124% upon addition of 0.5 wt% and 1 wt% CNFs, respectively but showed not statistical differences compared to the control at the 95% confidence level (Welch's t-test, Table 5.4) at lower CNF loadings (i.e., 0.02 wt%, 0.08 wt%, and 0.2 wt%). At 28 days, the median flexural toughness was increased by as much as 55%, 99%, and 122% at the 95% confidence level (Welch's t-test, Table 5.4) upon addition of 0.08 wt%, 0.2 wt%, and 1 wt% CNFs, respectively. The increasing trend in toughness with increasing CNF addition was the result of the combined increase in ultimate strength and strain capacity and not of a strain-hardening behavior.

The general increasing trend in 7 and 28-day flexural strength and toughness seen with increasing CNF loadings in spite of a greater proportion of CNF agglomerates (i.e., 1.4%, 3.2%, and 3.9% areal coverage for 0.2 wt%, 0.5 wt%, and 1 wt% CNFs) was indicative of the presence of a greater effective fraction of CNFs in the paste with increased CNF addition.

A closer inspection of the fracture surface (taken from compressive specimens after testing) of the composites revealed that the mechanism of CNF reinforcement was dominantly CNF pull-out. Upon failure most of the individual CNFs were pulled out from the other wall of the cement matrix rather than broken apart with no evidence of cement phases covering the surface of the protruding CNFs. Holes and groves left by fiber pull-out and CNFs pulled out from a microcrack can be seen in Figure 5.12. While some evidence of fiber breakage was observed, it was believed that the breakage most likely occurred during ultrasonication of the

CNFs and/or mixing of the cement pastes [149, 150]. The tensile stresses created during the mechanical testing slid the CNFs from the cement matrix without evidence of cement phases on the CNF surface, indicating that the interfacial interaction between the CNFs and the cement matrix was weaker than the cement matrix itself. As a result, the full potential reinforcing ability of the individual CNFs was not realized. The weak bond between CNFs and the cement matrix has been reported by others [35, 39].

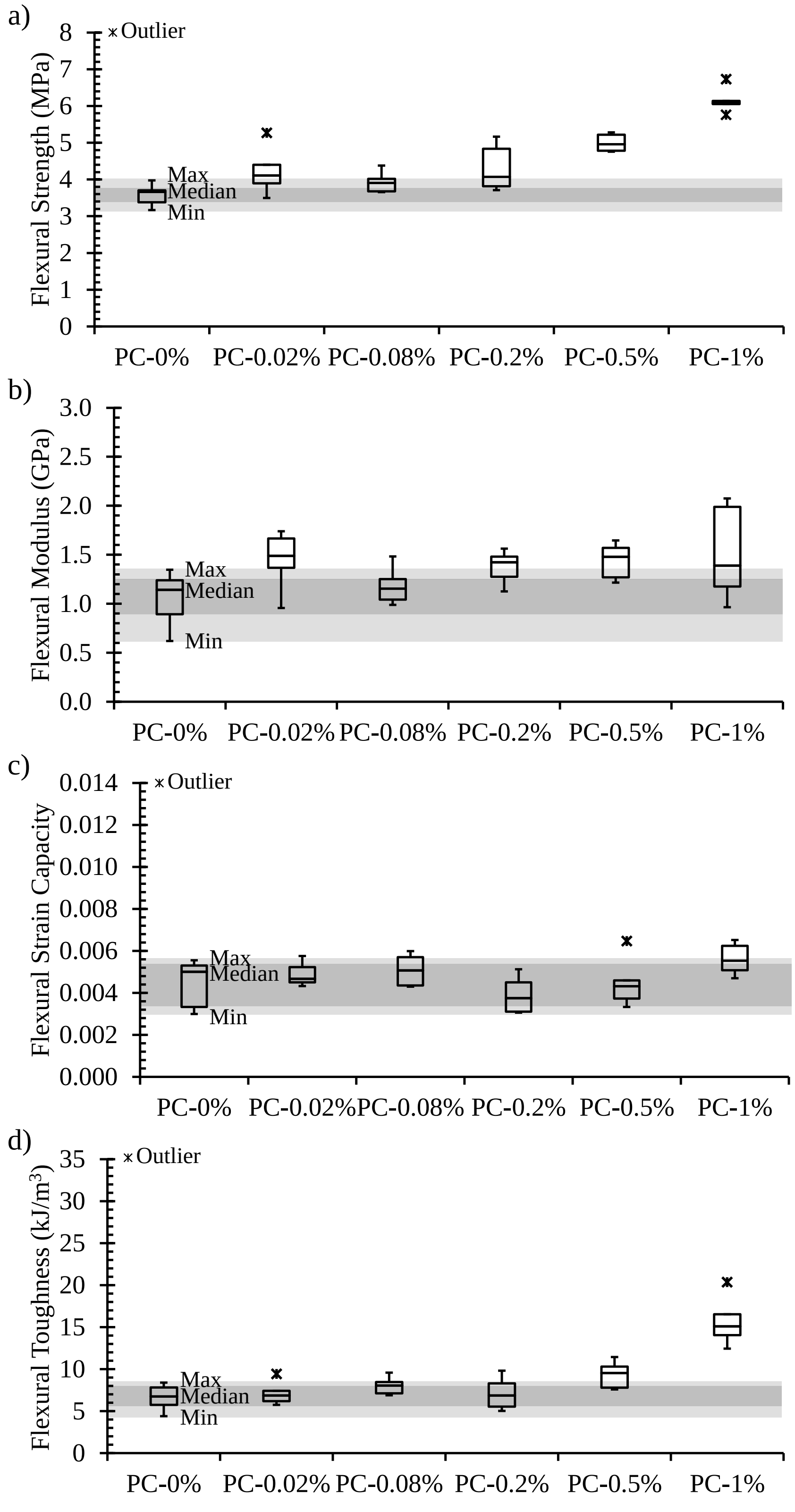

Figure 5.10. 7-day flexural properties of PC paste composites as a function of CNF loading (0-1 wt% CNFs dispersed by P-HRWR, raw data included in Appendix D). a) Ultimate strength, b) modulus, c) strain capacity at failure, and d) toughness.

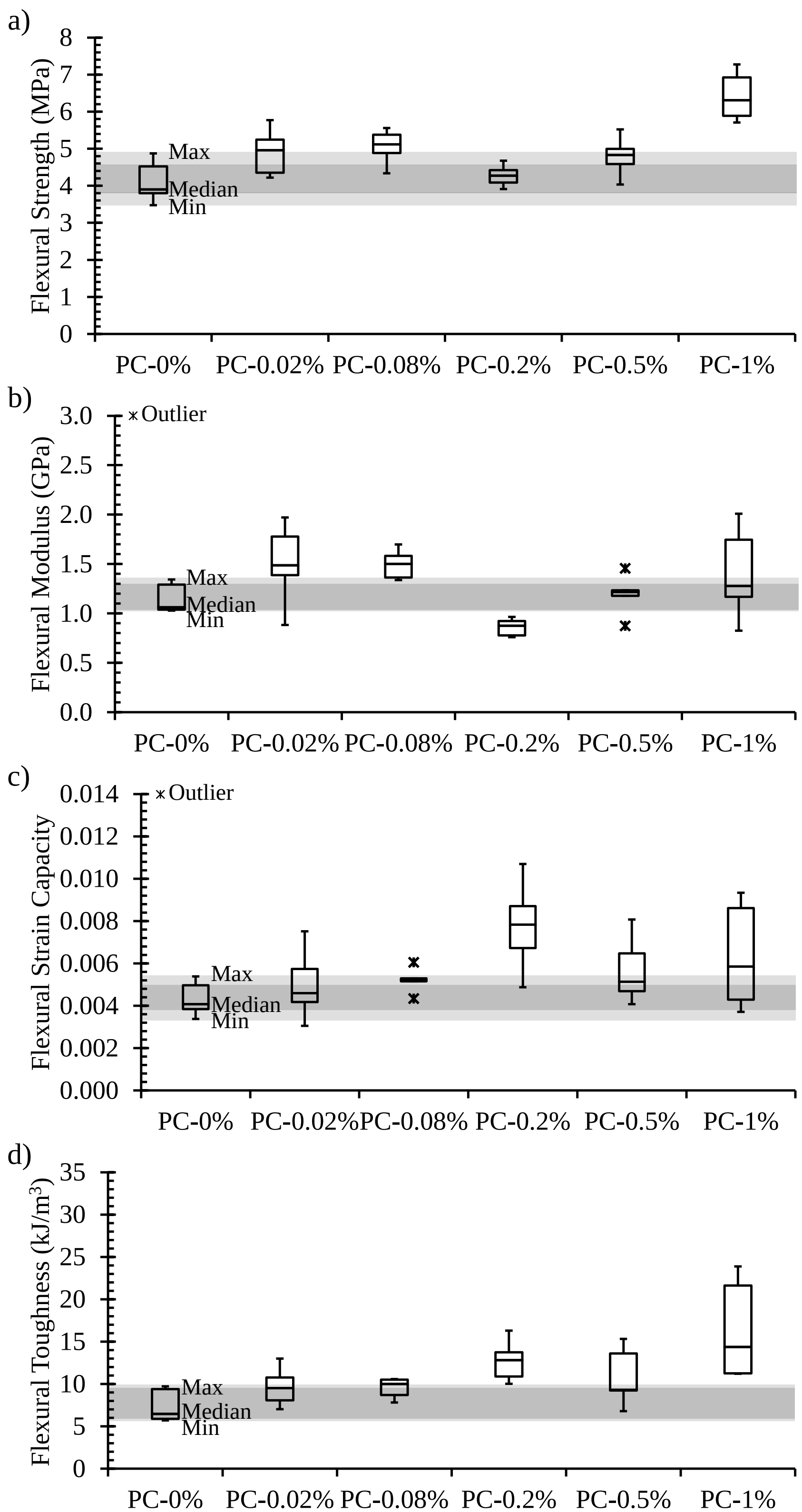

Figure 5.11. 28-day flexural properties of PC paste composites as a function of CNF loading (0-1 wt% CNFs dispersed by P-HRWR, raw data included in Appendix D). a) Ultimate strength, b) modulus, c) strain capacity at failure, and d) toughness.

Table 5.4. P-values (Welch's t-test) and conclusions at the 90% and 95% confidence levels for the flexural properties of PC paste composites as a function of CNF loading (0.02-1 wt% CNFs dispersed by P-HRWR) compared to the control (raw data included in Appendix D).

	P-value (compared to PC-0%)								**Summary at the 90% and 95% confidence levels**
	Strength		Modulus		Strain Capacity		Toughness		
	7 days	28 days	7 days	28 days	7 days	28 days	7 days	28 days	
PC-0.02%	0.057 (12.1%)	0.025 (27.1%)	0.034 (30.4%)	0.067 (39.9%)	0.531	0.377	0.589	0.070 (47.3%)	Increase in 7- and 28-day ultimate strength, 7- and 28-day modulus, and 28-day toughness.
PC-0.08%	0.061 (6.7%)	0.005 (31.2%)	0.406	0.001 (41.2%)	0.336	0.036 (28.3%)	0.084 (19.5%)	0.026 (54.9%)	Increase in 7- and 28-day ultimate strength, 28-day modulus, 28-day strain capacity at failure, and 7- and 28-day toughness.
PC-0.2%	0.039 (11.1%)	0.438	0.038 (24.6%)	0.003 (-17.8%)	0.277	0.006 (92.1%)	0.657	0.001 (98.5%)	Increase in 7-day ultimate strength, 7- and 28-day modulus, 28-day strain capacity at failure, and 28-day toughness.
PC-0.5%	3.7×10^{-6} (35.4%)	0.033 (23.9%)	0.019 (29.5%)	0.560	0.912	0.088 (26.0%)	0.009 (41.3%)	0.058 (44.0%)	Increase in 7- and 28-day ultimate strength, 7-day modulus, 28-day strain capacity at failure, and 7- and 28-day toughness.
PC-1%	5.2×10^{-8} (65.9%)	4.8×10^{-5} (61.7%)	0.079 (21.6%)	0.231	0.079 (10.7%)	0.092 (43.6%)	1.2×10^{-4} (124%)	0.011 (122%)	Increase in 7- and 28-day ultimate strength, 7-day modulus, 7- and 28-day strain capacity at failure, and 7- and 28-day toughness.

() Indicates % difference compared to PC-0%.

Indicates P-value less than or equal to 0.100 (significance at the 90% confidence level).

Indicates P-value less than or equal to 0.050 (significance at the 95% confidence level).

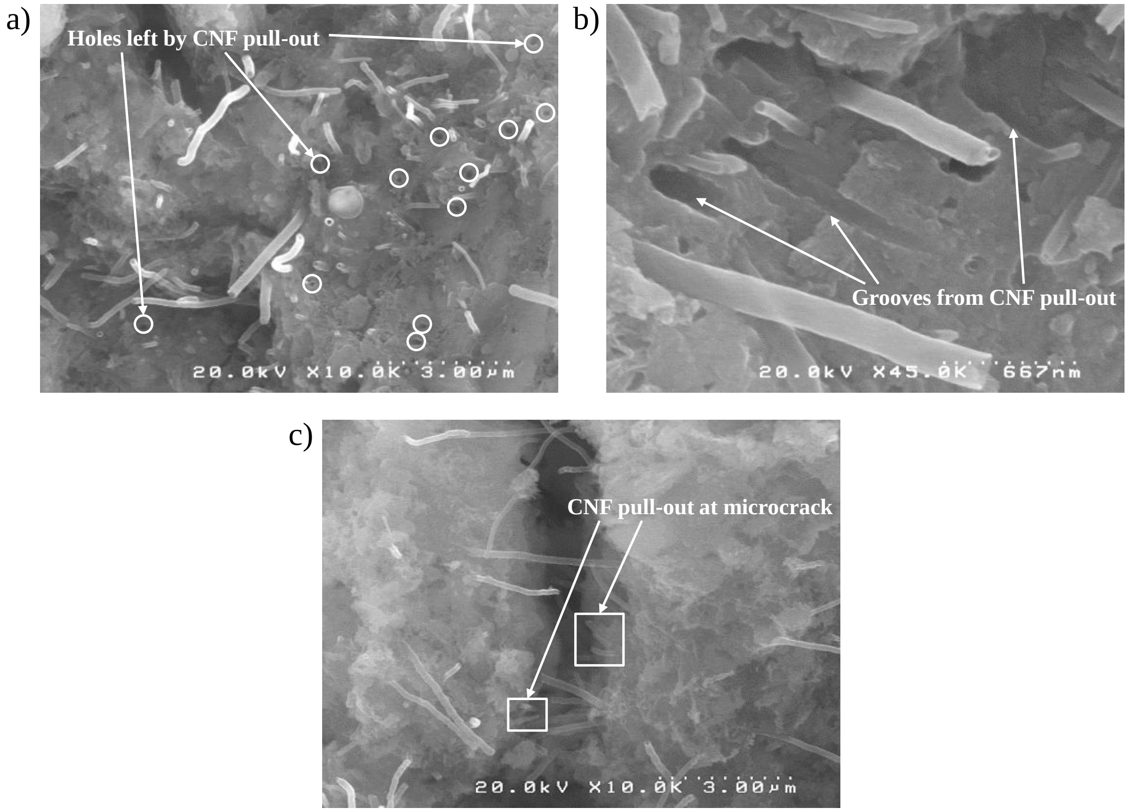

Figure 5.12. SEM images showing evidence of fiber pull-out on fracture surfaces of PC-0.5% (7 days) after compressive testing. a) Holes left by CNF pull-out (white circles), b) grooves from CNF pull-out, and c) CNFs pulled out from a microcrack.

5.3.3. Effect of CNF Addition on the Mechanical Properties of SF Paste Composites

5.3.3.1. Compressive Properties

In general, the compressive properties of SF paste composites were not affected by the addition of CNFs (Figure 5.13 and Figure 5.14). Like the PC paste composites, the compressive properties of the SF paste composites were mostly controlled by the cement matrix and not the fiber reinforcement. The addition of CNFs showed, in general, no statistically significant effect at the 95% confidence level for compressive strength, modulus, strain capacity, and toughness for all CNF loadings (Welch’s t-test, Table 5.5) including the 1 wt% CNF loading that had shown a negative effect on the compressive properties of the PC paste composites. The 1 wt% loading of CNFs was thought to have less of an impact on the SF pastes because silica fume particles have been shown to help in the disaggregation of CNF agglomerates [64] and silica fume has been shown to improve the interfacial bond between fibers and a cement-based matrix [151]. When statistical differences were noted with respect to the control (Welch's t-test, Table 5.5), they were mainly the result of the inherent variable nature of the material and not due to the effect of the addition of CNFs (e.g., the 0.2 wt% showing a difference at the 95% confidence level but higher and lower loadings showing no statistical difference).

Though the compressive properties of the SF paste composites were minimally affected by the addition of CNFs, the structural integrity of the composites was noticeably improved with increasing CNF loading. Similarly to the PC paste composites, it was believed that the CNF network inside the SF paste matrix may have limited the propagation of cracks, allowing the composite to remain relatively intact even after failure (Figure 5.15).

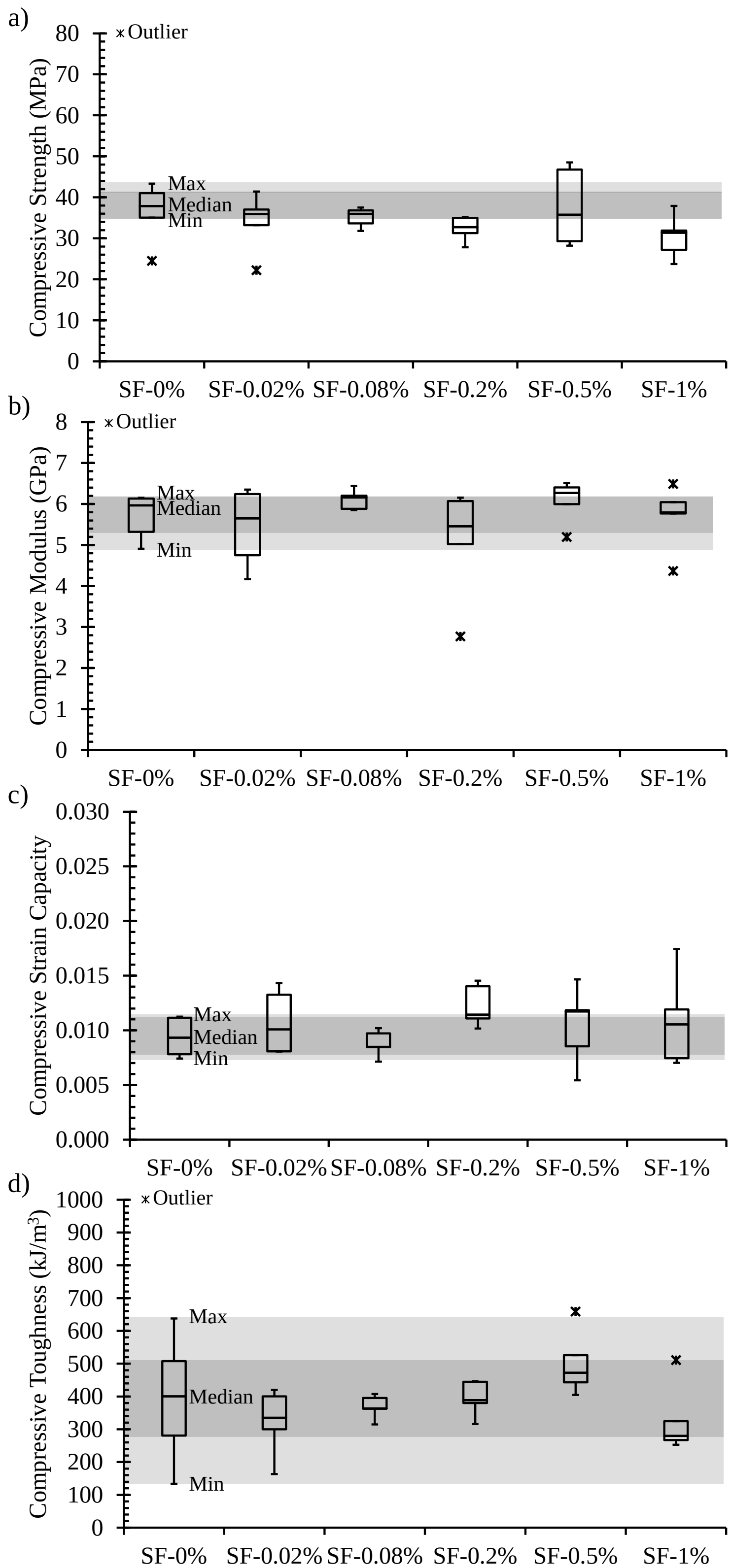

Figure 5.13. 7-day compressive properties of SF paste composites as a function of CNF loading (0-1 wt% CNFs dispersed by P-HRWR, raw data included in Appendix D). a) Ultimate strength, b) modulus, c) strain capacity at failure, and d) toughness.

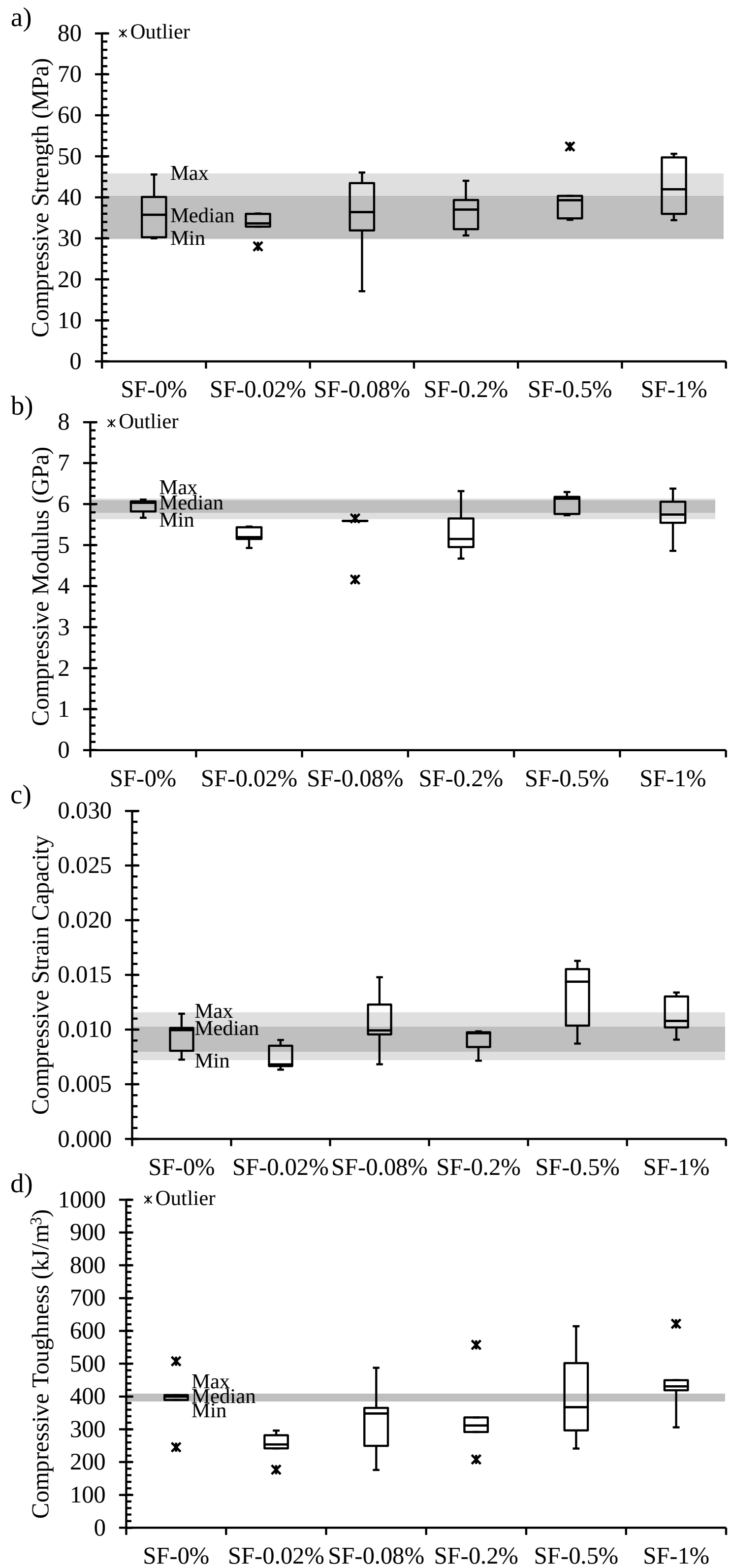

Figure 5.14. 28-day compressive properties of SF paste composites as a function of CNF loading (0-1 wt% CNFs dispersed by P-HRWR, raw data included in Appendix D). a) Ultimate strength, b) modulus, c) strain capacity at failure, and d) toughness.

Table 5.5. P-values (Welch's t-test) and conclusions at the 90% and 95% confidence levels for the compressive properties of SF paste composites as a function of CNF loading (0.02-1 wt% CNFs dispersed by P-HRWR) compared to the control (raw data included in Appendix D).

	P-value (compared to SF-0%)								**Summary at the 90% and 95% confidence levels**
	Strength		Modulus		Strain Capacity		Toughness		
	7 days	28 days	7 days	28 days	7 days	28 days	7 days	28 days	
SF-0.02%	0.615	0.396	0.609	0.001 (-13.9%)	0.402	0.080 (-31.6%)	0.514	0.026 (-36.5%)	Decrease in 28-day modulus, 28-day strain capacity at failure, and 28-day toughness.
SF-0.08%	0.741	0.828	0.185	0.098 (-7.3%)	0.565	0.429	0.806	0.373	Decrease in 28-day modulus.
SF-0.2%	0.309	0.935	0.405	0.112	0.042 (22.6%)	0.673	0.974	0.521	Increase in 7-day strain capacity at failure.
SF-0.5%	0.809	0.396	0.301	0.604	0.576	0.070 (44.5%)	0.309	0.858	Increase in 28-day strain capacity at failure.
SF-1%	0.185	0.204	0.993	0.228	0.500	0.126	0.537	0.419	

() Indicates % difference compared to SF-0%.

Indicates P-value less than or equal to 0.100 (significance at the 90% confidence level).

Indicates P-value less than or equal to 0.050 (significance at the 95% confidence level).

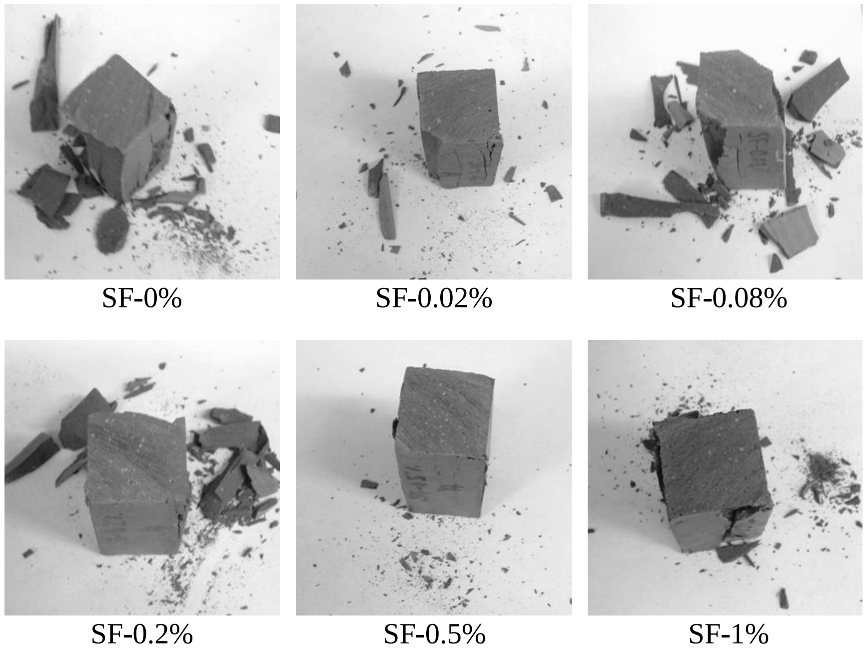

Figure 5.15. Structural integrity of SF paste composites after 28-day compressive testing as a function of CNF loading (0-1 wt% CNFs dispersed by P-HRWR).

5.3.3.2. Splitting Tensile Strength

The addition of CNFs had, in general no effect on 28-day splitting tensile strength of SF paste composites, but a decrease was seen for 0.08 and 0.2 wt% CNFs at 7 days (Figure 5.16 and Figure 5.17). The decrease in splitting tensile strength for SF-0.08% and SF-0.2% based on the median values compared to the control at the 95% confidence level was 26.5% and 23.5%, respectively (Welch's t-test, Table 5.6). Similar to the PC paste composites, high variability in the splitting tensile strength of the SF paste composites was seen at all CNF loadings. The variability was, however, slightly less for the SF paste composites than that seen for the PC paste composites (i.e., standard deviations less than 1 MPa for the SF paste composites instead of greater than 1 MPa for the PC paste composites).

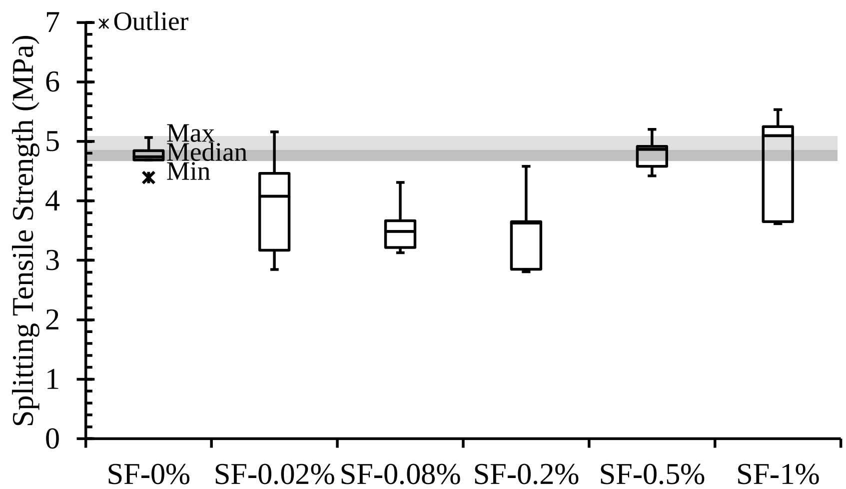

Figure 5.16. 7-day splitting tensile strength of SF paste composites as a function of CNF loading (0-1 wt% CNFs dispersed by P-HRWR, raw data included in Appendix D).

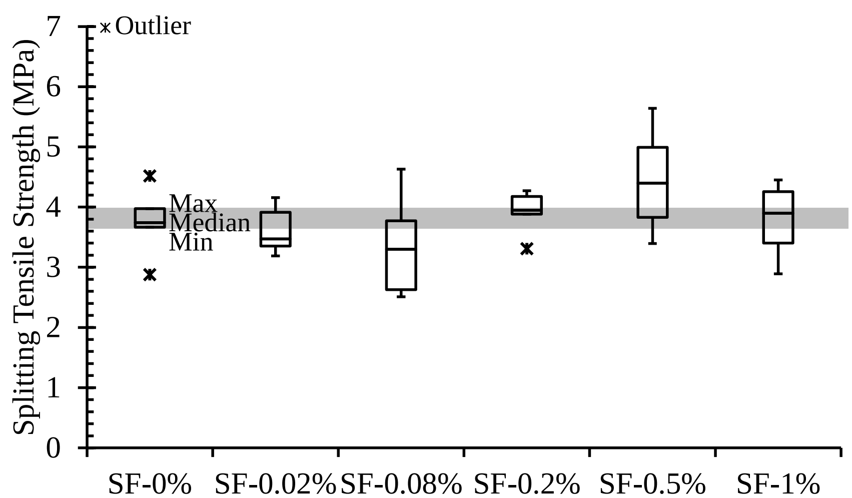

Figure 5.17. 28-day splitting tensile strength of SF paste composites as a function of CNF loading (0-1 wt% CNFs dispersed by P-HRWR, raw data included in Appendix D).

Table 5.6. P-values (Welch's t-test) and conclusions at the 90% and 95% confidence levels for the splitting tensile strength of SF paste composites as a function of CNF loading (0.02-1 wt% CNFs dispersed by P-HRWR) compared to the control (raw data included in Appendix D).

	P-value (compared to SF-0%)		**Summary at the 90% and 95% confidence levels**
	7 days	28 days	
SF-0.02%	0.131	0.677	
SF-0.08%	0.002 (-26.5%)	0.438	Decrease in 7-day ultimate strength.
SF-0.2%	0.016 (-23.5%)	0.621	Decrease in 7-day ultimate strength.
SF-0.5%	0.780	0.191	
SF-1%	0.796	0.952	

() Indicates % difference compared to SF-0%.

Indicates P-value less than or equal to 0.100 (significance at the 90% confidence level).

Indicates P-value less than or equal to 0.050 (significance at the 95% confidence level).

5.3.3.3. Flexural Properties

The flexural properties of the SF paste composites were, in general, impacted by the CNF loadings at 28 days but not at 7 days. At 7 days, only the 1 wt% CNF loading showed an effect on the flexural modulus, strain capacity, and toughness (Figure 5.18). In general, the 28-day flexural strength and modulus of the SF paste composites were increased with CNF addition while the 28-day strain capacity was decreased for all CNF loadings (Figure 5.19). Silica fume caused the strength gained by the addition of CNFs to be delayed from 7 to 28 days and allowed for an increase in the 28-day flexural modulus with CNF addition compared to the PC paste composites.

Ultimate flexural strength. The 7-day flexural strength of the SF paste composites was not affected by the inclusion of CNFs while the 28-day flexural strength was generally improved with increasing CNF loadings up to 1 wt% (Figure 5.18a and Figure 5.19a). The 28-day median ultimate flexural strength was increased by 21%, 18%, 48%, and 43% for CNF loadings of 0.02 wt%, 0.08 wt%, 0.5 wt%, and 1 wt%, respectively, at the 95% confidence level, but the 0.2 wt% CNF loading was not statistically different from the control at the 95% confidence level (Welch's t-test, Table 5.7).

Flexural modulus. The addition of CNFs in the SF paste composites had a substantial impact on the flexural modulus especially at 28 days (Figure 5.18b and Figure 5.19b). At 7 days, the flexural modulus of SF-0.08% and SF-0.2% increased by *ca.* 30% at the 90% and 95% confidence level, respectively, but the flexural modulus of SF-1% decreased by 59% at the 95% confidence level (Welch's t-test, Table 5.7). At 28 days, the flexural modulus of all SF pastes with CNF addition except SF-0.08% was improved by at least 100% at the 95% confidence level (Welch's t-test, Table 5.7).

Strain capacity at failure. At 7 days, only SF-1% showed a statistically significant difference in the flexural strain capacity with an increase of *ca.* 66% at the 95% confidence level compared to the control (Welch's t-test, Table 5.7). In contrast, at 28 days, SF-0.02%, SF-0.2%, and SF-0.5% showed a statistically significant difference in the flexural strain capacity with decreases of up to 46% at the 95% confidence level (Welch's t-test, Table 5.7).

Flexural toughness. The flexural toughness of SF paste was improved at 7 days by over 100% at the 95% confidence level (Welch's t-test, Table 5.7) when 1 wt% CNFs were added to the composite. However, at 28 days, the addition of 0.02 and 0.2 wt% CNFs resulted in a decrease in the flexural toughness by over 40% at the 95% confidence level (Welch's t-test, Table 5.7). As with the PC paste composites, no strain hardening behavior was seen with the addition of CNFs. The flexural toughness was thus directly related to the other flexural properties: at 7 days, the increase in toughness seen for SF-1% was due to a decreased modulus and increased strain capacity while at 28 days, the decrease seen for SF-0.02% and SF-0.2% was due to an increased modulus and decreased strain capacity.

The lack of impact at 7 days with the addition of CNFs in the SF pastes and the changes seen compared to the PC pastes in the effect of the CNFs on the modulus, strain capacity, and toughness from 7 to 28 days was thought to be due to the delayed pozzolanic reaction that occurs with silica fume [3, 152]. By 28 days, the pozzolanic reaction of the silica fume had most likely progressed enough for the CNFs to improve the flexural strength in the SF pastes similarly to the PC pastes. Additionally, the 28-day flexural strength of SF-0.5% was improved more so than PC-0.5%. It was believed that the greater improvement in flexural strength seen for SF-0.5% compared to PC-0.5% was the result of a greater effective fraction of CNFs because secondary agglomeration due to CNF migration in the bleed water was reduced by the decreased workability of SF pastes compared to the PC pastes (Figure 5.20). In addition, the improvements in strength for SF-0.5% compared to PC-0.5% could have resulted from an improved interfacial bond between the CNFs and the SF matrix. The use of silica fume has been shown to improve the interfacial bond between the cement matrix and CFs with diameters of 10 μm and 46 μm [151].

The improvements in the flexural modulus and reductions in the flexural strain capacity were also believed to be most likely due to an improved bond between the CNFs and the cement/silica fume matrix. Because of the silica fume refining the porous layer typically found at the fiber/matrix interface [151], it was thought that the CNFs had an increased ability to reduce the expansion of nanocracks compared to in PC pastes. The reduction in the expansion of nanocracking allowed the specimens to hold higher loads with less deformation, therefore increasing the flexural modulus. The strain capacity was, thus, reduced because as the composite reached higher strengths (which were not possible without the reduction of nanocracking), the flaws in the cement matrix larger than the CNFs in length expanded and caused the failure of the material at lower strains.

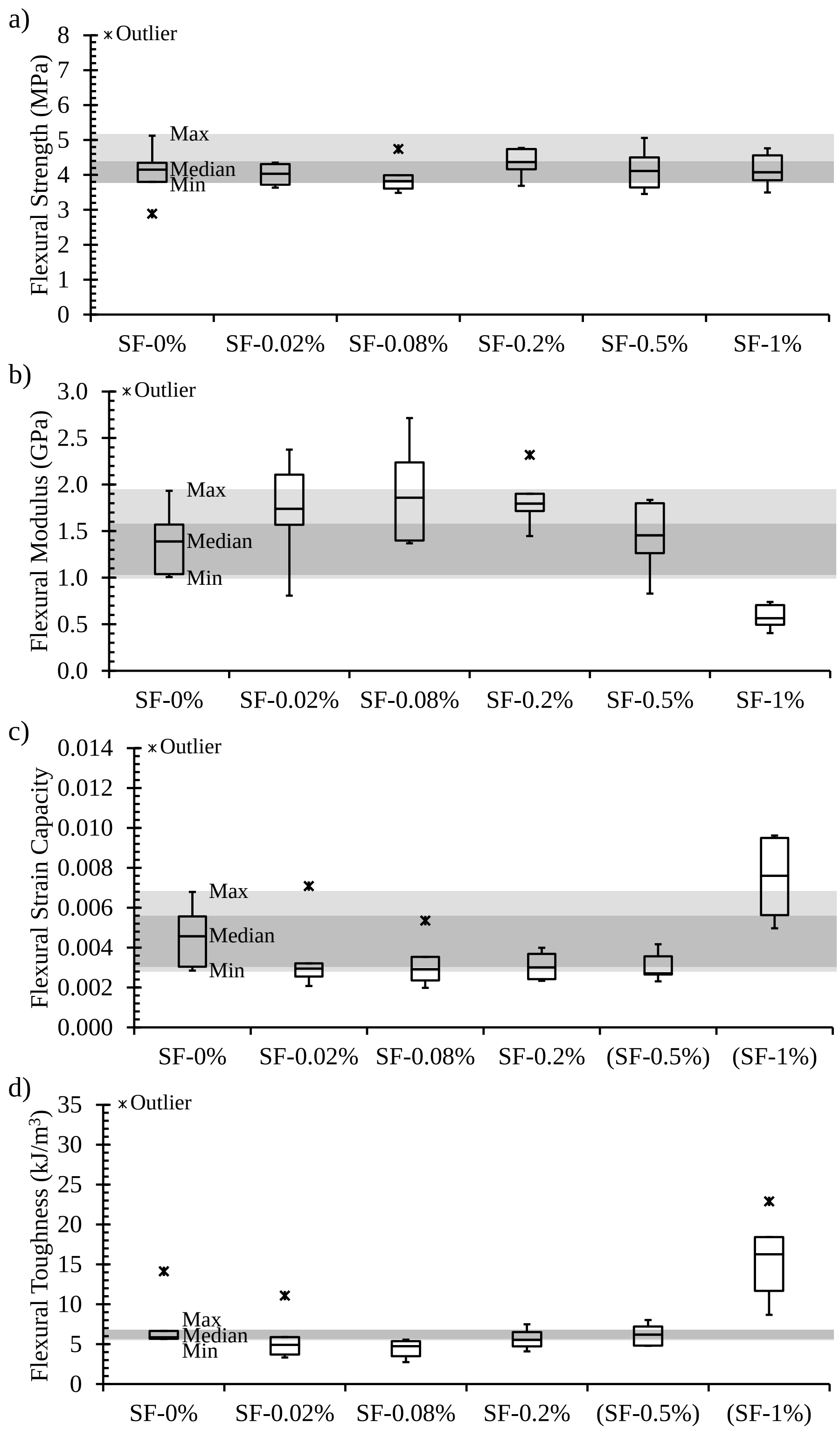

() Indicates values were approximated based on ultimate flexural strength and flexural modulus.

Figure 5.18. 7-day flexural properties of SF paste composites as a function of CNF loading (0-1 wt% CNFs dispersed by P-HRWR, raw data included in Appendix D). a) Ultimate strength, b) modulus, c) strain capacity at failure, and d) toughness.

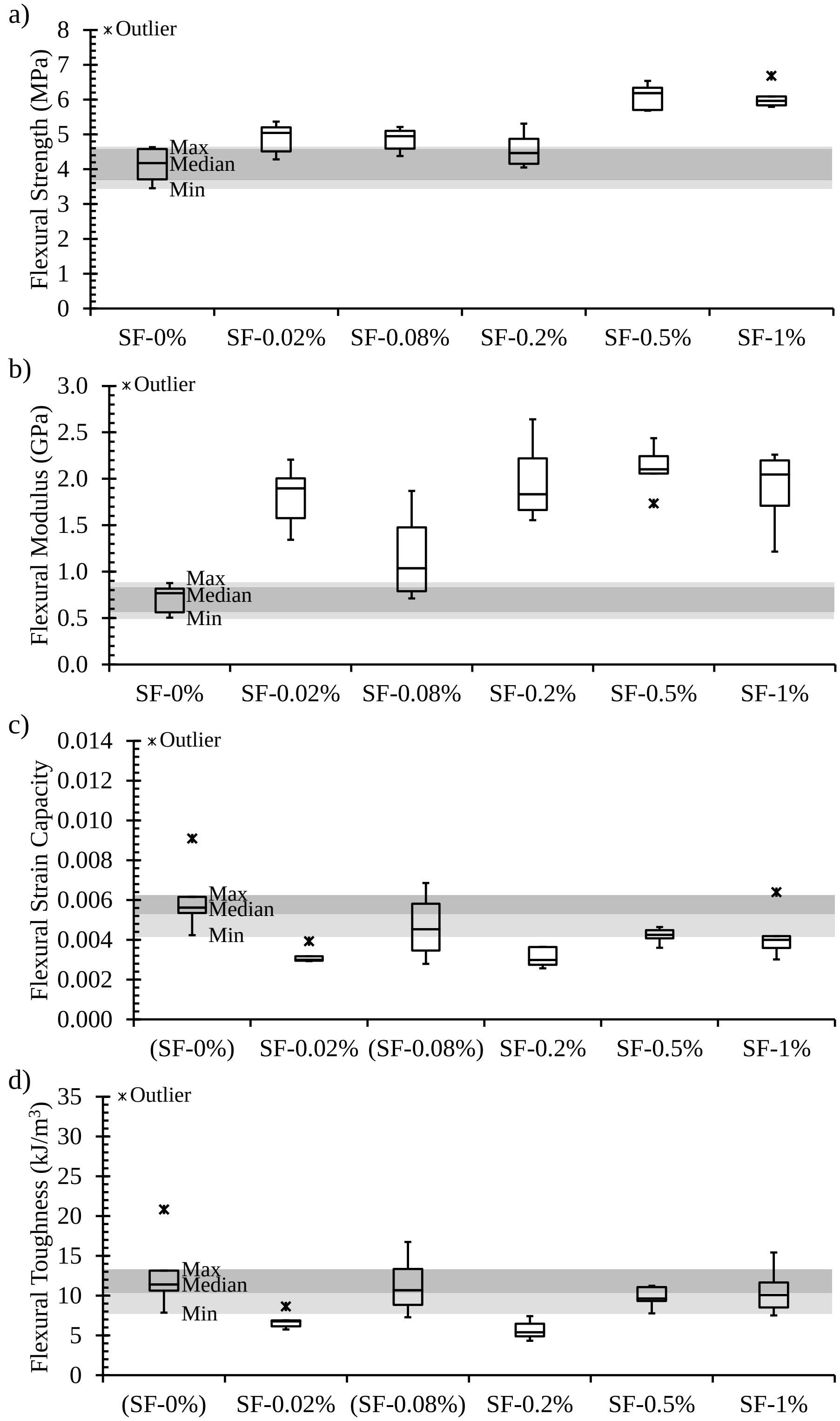

() Indicates values were approximated based on ultimate flexural strength and flexural modulus.

Figure 5.19. 28-day flexural properties of SF paste composites as a function of CNF loading (0-1 wt% CNFs dispersed by P-HRWR, raw data included in Appendix D). a) Ultimate strength, b) modulus, c) strain capacity at failure, and d) toughness.

Table 5.7. P-values (Welch's t-test) and conclusions at the 90% and 95% confidence levels for the flexural properties of SF paste composites as a function of CNF loading (0.02-1 wt% CNFs dispersed by P-HRWR) compared to the control (raw data included in Appendix D).

	P-value (compared to SF-0%)								**Summary at the 90% and 95% confidence levels**
	Strength		Modulus		Strain Capacity		Toughness		
	7 days	28 days	7 days	28 days	7 days	28 days	7 days	28 days	
SF-0.02%	0.851	0.013 (20.7%)	0.234	1.0×10^{-4} (147.4%)	0.297	0.007 (-46.8%)	0.375	0.024 (-40.7%)	Increase in 28-day ultimate strength and 28-day modulus. Decrease in 28-day strain capacity at failure and 28-day toughness.
SF-0.08%	0.653	0.011 (18.4%)	0.076 (33.8%)	0.060 (35.1%)	0.127	0.168	0.095 (-18.7%)	0.588	Increase in 28-day ultimate strength and 7- and 28-day modulus. Decrease in 7-day toughness.
SF-0.2%	0.449	0.144	0.038 (29.4%)	3.3×10^{-4} (139.1%)	0.078 (-34.2%)	0.006 (-46.8%)	0.301	0.011 (-52.7%)	Increase in 7- and 28-day modulus. Decrease in 7- and 28-day strain capacity at failure and 28-day toughness.
SF-0.5%	0.860	1.4×10^{-5} (48.0%)	0.809	9.5×10^{-7} (174.2%)	0.070 (-40.8)	0.043 (-24.3%)	0.484	0.193	Increase in 28-day ultimate strength and 28-day modulus. Decrease in 7- and 28-day strain capacity at failure.
SF-1%	0.869	1.8×10^{-5} (42.6%)	0.002 (-59.4%)	3.1×10^{-4} (166.9%)	0.019 (66.3%)	0.054 (-28.8%)	0.009 (177.8%)	0.376	Increase in 28-day ultimate strength, 28-day modulus, 7-day strain capacity at failure, and 7-day toughness. Decrease in 7-day modulus and 28-day strain capacity at failure.

() Indicates % difference compared to SF-0%.

Indicates P-value less than or equal to 0.100 (significance at the 90% confidence level).

Indicates P-value less than or equal to 0.050 (significance at the 95% confidence level).

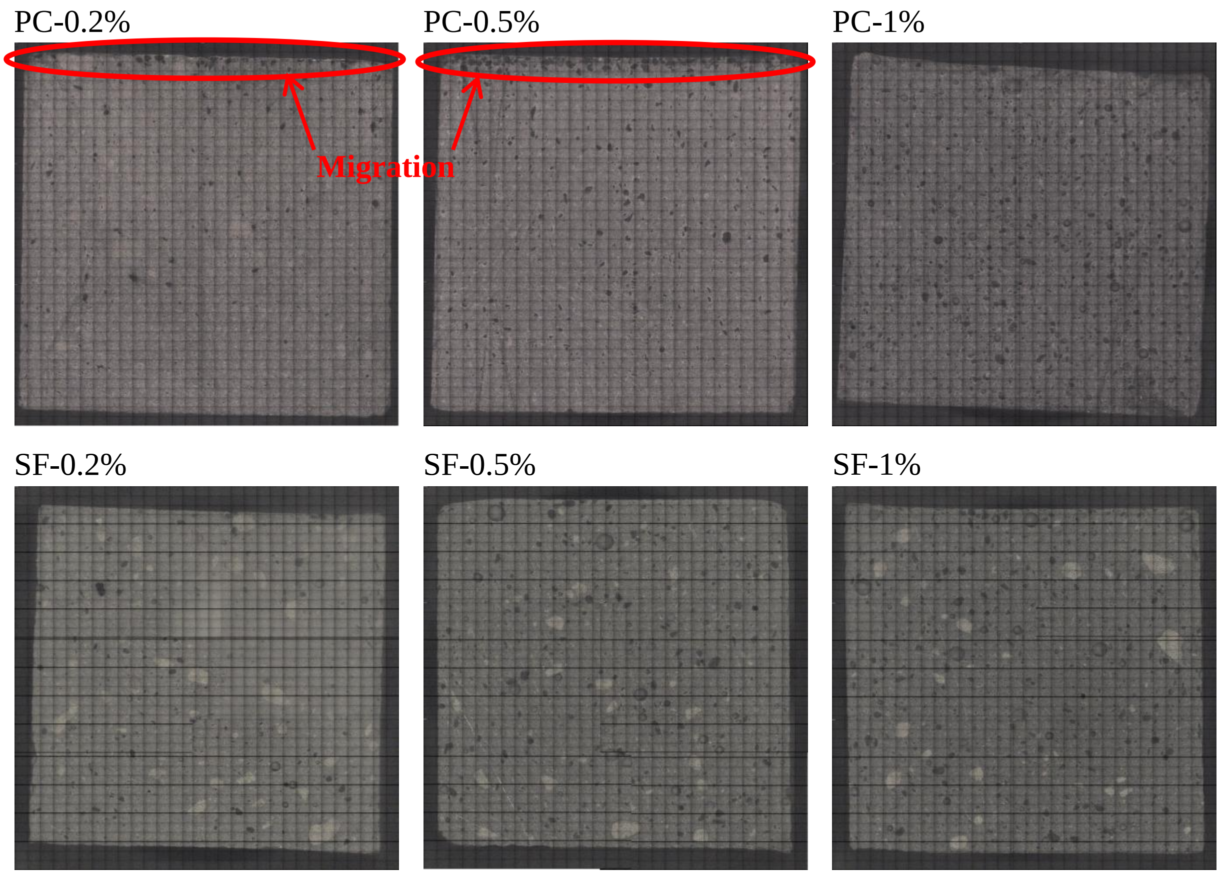

Figure 5.20. Images of cement-based composite cross-sections (PC-0.2%, PC-0.5%, PC-1%, SF-0.2%, SF-0.5% and SF-1%) showing the reduction of CNF migration with the bleed water with the addition of silica fume.

5.4. Conclusions

The macromechanical properties of PC and SF pastes containing CNFs were determined. The effect of the CNF dispersion state and CNF loading on the macromechanical properties were investigated. The following conclusions were made:

- The CNF dispersion state impacted the 7-day flexural strength of PC paste composites with only the composites containing CNFs dispersed with the assistance of P-HRWR showing improvement. Improvements in 7-day flexural strength when surface treatment with HNO_3 in addition to P-HRWR was used to disperse 0.2 wt% CNFs were 21.7%, while the same CNF loading dispersed with P-HRWR alone allowed improvements of 11.1% over the control composite. The surface treatment with HNO_3 allowed an improved interfacial bond between the CNFs and the cement matrix as a result of chemical interactions between the cement matrix and functional groups present at the surface of the CNFs allowing for more strength gain. In contrast, dispersions of CNFs assisted by only surface treatment with HNO_3, N-HRWR, and AE did not improve the 7-day flexural strength of PC paste composites due to the collective weakening behavior of the CNF agglomerates acting as flaws and dominating the strength of the individual CNFs.

- The effects of the addition of various loadings of CNFs dispersed with only P-HRWR on the mechanical properties of PC pastes were mostly revealed in flexure. However, improvements in the structural integrity of the PC pastes after compressive testing were seen with increasing CNF loadings because of the CNFs limiting the propagation of cracks, which allowed the cement matrix to hold together even after failure. Both the 7- and 28-day flexural strength of the PC pastes improved with increasing CNF loadings with increases of over 60% seen for the 1 wt% CNF loading at both 7 and 28 days. Additionally, increases of over 20% in the 7-day flexural modulus were seen for most CNF loadings, and increases related to the increased flexural strength were seen in the 28-day flexural strain capacity and 7- and 28-day flexural toughness. All of the improvements in flexural properties were seen regardless of the presences of poorly distributed and agglomerated CNFs because the weak zones formed in the composites by the poorly distributed and agglomerated CNFs were thought to be partially counterbalanced by the presence of an effective fraction of CNFs.

- The addition of various loadings of CNFs dispersed by only P-HRWR in SF pastes allowed for a similar improvement in structural integrity after compressive testing compared to the CNFs in PC pastes, but the delayed pozzolanic reaction in the SF pastes allowed improvements in the flexural strength to be delayed such that they did not occur at 7 days but were seen at 28 days. The increases in flexural strength were over 40% for both the 0.5 and 1 wt% CNF loading in SF pastes at 28 days. Additionally, the 28-day flexural modulus was improved by over 100% for most CNF loadings while decreases of up to 52% were seen in the 28-day strain capacity and toughness for several CNF loadings in SF pastes.

CHAPTER 6

HYBRID CNF/CF CEMENT-BASED COMPOSITES

6.1. Overview

The use of hybrid fiber reinforcement has the potential to improve cement-based materials beyond the sum of the improvements from each fiber alone [31]. Currently hybrid fiber reinforcement employs mostly micro- and macroscale fiber reinforcement [10, 31, 49, 70-85], but flaws and cracks exist in cement-based materials from the nano- to the macroscale [49, 153]. Therefore, nano- to macrosized fibers may be beneficial for hybrid fiber reinforcement of cement-based materials. The objective of this chapter is to determine the hybrid effect of CNFs and CFs on the microstructure and mechanical properties of cement pastes.

CNFs and CFs were used together as hybrid fiber reinforcement to evaluate the hybrid effect of the fibers on the microstructure and mechanical properties of the cement-based composites. SEM and optical microscopy were used to examine the microstructure of hybrid CNF/CF cement-based composites and the dispersion and distribution of the CNFs in the composites. The mechanical properties were examined on the macro- and microscale. Nanoindentation was used to determine the micromechanical properties of the hybrid CNF/CF cement-based composites, and modified versions of standards for flexural and compressive testing were used to determine the macromechanical properties of the composites.

6.2. Experimental Detail

6.2.1. Materials

The materials discussed in Section 3.2.1 were used in this study, including CNFs, P-HRWR (*Glenium® 7500)*, and type I portland cement. In addition, Product 150 chopped polyacrylonitrile CFs (Toho Tenax America, Inc., Rockwood, TN, USA) were used. As per the manufacturer, the CFs ranged from 6-7 μm in diameter and were 3 mm in length. The manufacturer reported the CFs to have a density of 1.8 g/cm^3, a tensile strength greater than 3.45 GPa, and a tensile modulus greater than 207 GPa. The CNFs and CFs were used "*as received*" in the composites.

6.2.2. Preparation of Hybrid CNF/CF Cement-Based Composites

Cement paste composites were made with 0.5 wt% of CNFs, 0.5 wt% of CFs, and 1 wt% of P-HRWR. A w/c ratio of 0.315, which was selected based on the workability of the fresh pastes, was used. Four different composites were made: (i) a plain cement paste (PC—Control), (ii) a cement paste containing only CNFs (PC-CNF), (iii) a cement paste containing only CFs (PC-CF), and (iv) a cement paste containing both CNFs and CFs (PC-CNF-CF—Hybrid CNF/CF cement-based composite). PC and PC-CNF are also discussed in Section 4.2.2.

All four composites were made in the same manner as in Section 3.2.3.2, but when applicable, the CFs were blended with the dry cement mix before the water-P-HRWR solution or water-P-HRWR-CNF suspension was added. After mixing, the composites were cast in 2.54 cm × 2.54 cm × 68.58 cm (1 in × 1 in × 27 in) beam molds. The beams were cured at room temperature in 100% relative humidity for 3, 7, or 28 days and then cut into 11.43 cm (4.5 in) long specimens before flexural testing. Specimens for compressive testing, sized at 2.54 cm × 2.54 cm × 5.08 cm (1 in × 1 in × 2 in), were prepared from the flexural specimens after testing avoiding the damaged zone.

After macromechanical testing, fracture surfaces were mounted to an aluminum stub using carbon tape for SEM observations. Additionally cross-sections of each composite were cut with a precision saw and prepared for optical microscopy or micromechanical testing. For optical microscopy, the specimens were polished to 35 µm particle size. For micromechanical testing, the specimens were cast in epoxy and polished as described in Section 4.2.2.

6.2.3. Characterization

6.2.3.1. Optical Microscopy

Image mapping of polished cross-sections consisting of 165 images, each 114.3 × 85.6 pixels, was completed at ERDC (Vicksburg, Mississippi, USA) using a Zeiss Axio Imager.Z1 upright motorized microscope (Carl Zeiss MicroImaging, Inc., Thornwood, NY, USA) equipped with digital imaging and Extended Focus and MosiaX software packages (Carl Zeiss MicroImaging, Inc., Thornwood, NY, USA). Image analysis was then completed as described in Section 3.2.4.2.

6.2.3.2. SEM/EDS

The microstructure and morphology of fracture surfaces of the composites was evaluated at ERDC (Vicksburg, Mississippi, USA) using a FEI Nova NanoSEM (FEI Company, Hillsboro, Oregon, USA) equipped with a Schottky field emission gun, high vacuum and low vacuum modes, and digital imaging. An accelerating voltage of 5 kV, a working distance of 7.1 mm, and a spot sized of 5 was used for imaging.

In addition, the FEI Quanta 650 FEG SEM and methods described in Section 4.2.3.2 were used to obtain secondary and backscatter electron images and semi-quantitative chemical data used in the analysis of the micromechanical testing.

6.2.3.3. Nanoindentation

Nanoindentation was completed at ERDC (Vicksburg, Mississippi, USA) using the equipment and methods described in Section 4.2.3.1.

6.2.3.4. Macromechanical Testing

The mechanical performance of the composites was evaluated at 3, 7, and 28 days by uniaxial compressive and three-point bending testing using a Tinius Olsen Super L 60 K (300 kN) universal testing machine (Tinius Olsen, Inc., Horsham, PA, USA). Flexural testing was performed as described in Section 5.2.3.1. Compressive testing was performed in a method similar to the one described in Section 5.2.3.1, but the testing was completed on beam specimens with a test setup as shown in Figure 6.1. A minimum of six (6) specimens of each cement paste type were tested for each loading type, and the ultimate strength, strain capacity, modulus, and toughness values were calculated as discussed in Section 5.2.3.1.

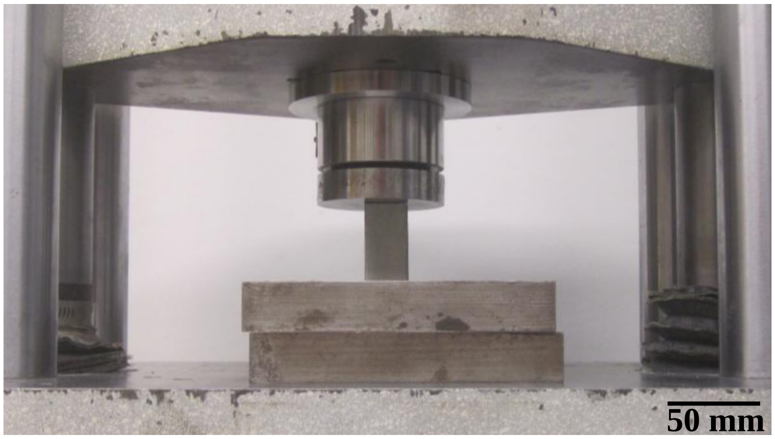

Figure 6.1. Compressive test setup for testing beam specimens of cement-based composites. The beam has a length and width of 25.4 mm (1 in.) and height of 50.8 mm (2 in.).

6.3. Results and Discussion

6.3.1. Microstructure of the Hybrid CNF/CF Cement-Based Composites and CNF Dispersion State

SEM analysis showed CNFs to be present in the cement-based composites as individual fibers and agglomerated, whether or not CFs were present. As in Section 3.3.4, the distribution of individual CNFs was not homogenous throughout the cement-based composites with CNF-rich and CNF-poor regions. In addition, SEM analysis did not show the CNF agglomerates to have a tendency to be located either near or away from CFs (Figure 6.2). Evidence of CF pull-out and cement hydrates on the CF surfaces was present (Figure 6.2).

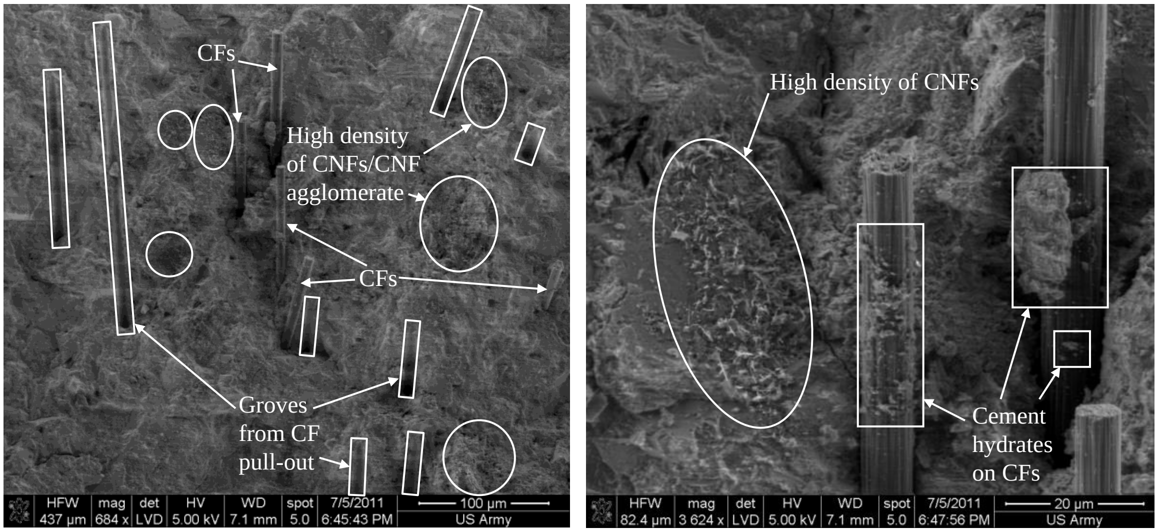

Figure 6.2. Representative SEM images of the hybrid CNF/CF cement-based composites showing the distribution and location of CNFs and CFs within the composites with evidence of CF pull-out and the presence of cement phases on the surface of the CFs.

Image analysis on micrographs from optical microscopy indicated a reduction in the areal coverage of CNF agglomerates sized 0.007 mm^2 and above within the composite cross-sections when CFs were present (i.e., 2.6% for PC-CNF-CF compared to 3.6% for PC-CNF) (Figure 6.3). Visually evident from the binary images in Figure 6.3 was the influence of the CFs on the migration and reagglomeration of the CNFs at the upper surface of the cement-based composite. The CFs reduced the workability of the fresh cement paste, therefore, reducing the migration of the CNFs with the bleed water. The areal coverage of the CNFs within the upper 2 mm of the cement-based composite cross-section was 6.7% for PC-CNF compared to only 2.2% for PC-CNF-CF.

Although the total areal coverage of CNF agglomerates was reduced with the addition of CFs, the distribution of agglomerate sizes was adversely affected by the presence of the CFs. PC-CNF-CF had more agglomerates in all size categories greater than 0.01 mm^2 (i.e., 0.01-0.02 mm^2, 0.02-0.03 mm^2, 0.03-0.04 mm^2, 0.04-0.05 mm^2, and greater than 0.05 mm^2) than PC-CNF, while PC-CNF had more agglomerates less than 0.01 mm^2 indicating a preference for the CNFs to form larger agglomerates (greater than 0.01 mm^2 in size) in the presence of CFs.

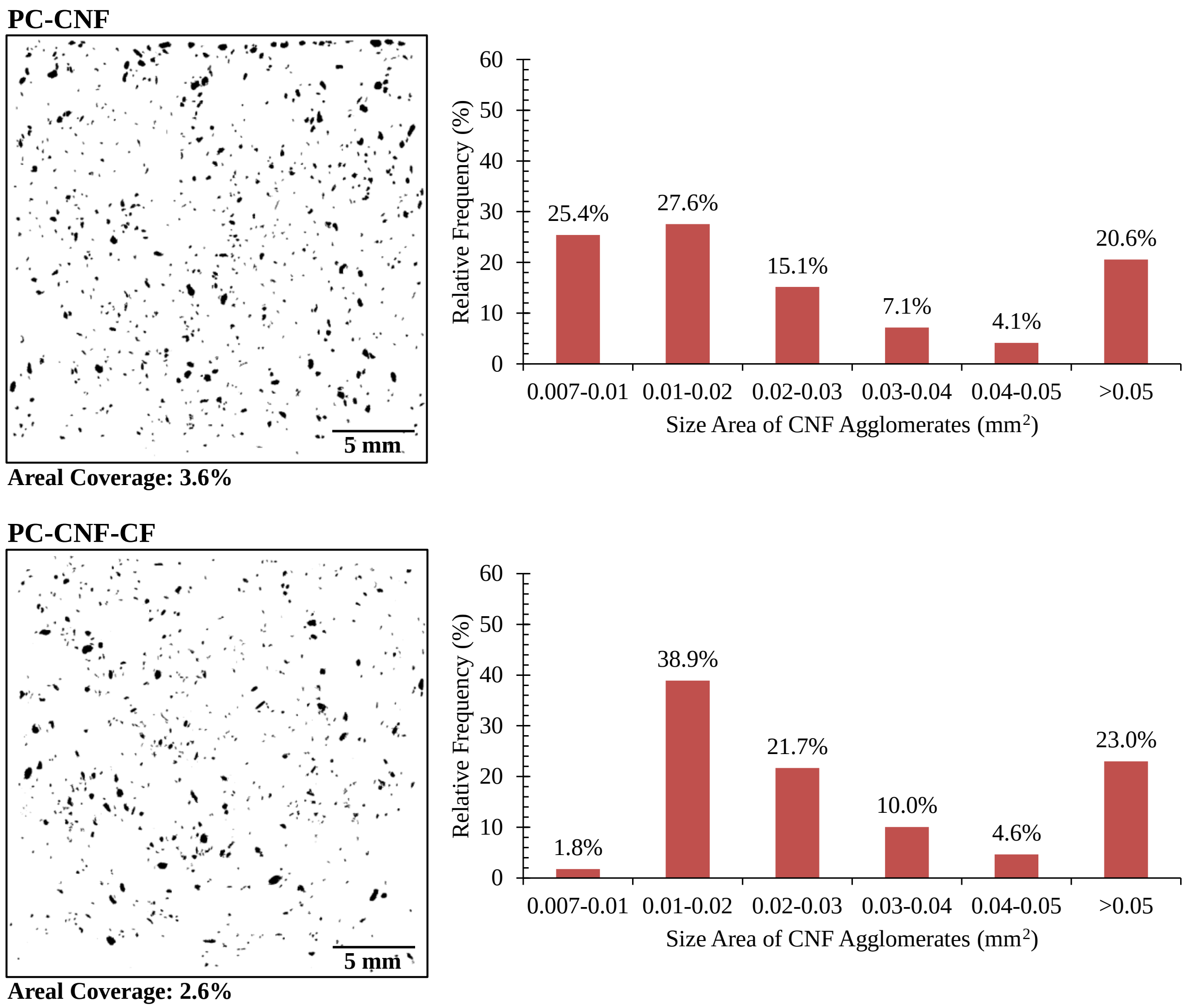

Figure 6.3. Binary images and histograms showing the distribution of CNFs within representative cross-sections of the cement-based composite containing only CNFs and the hybrid CNF/CF cement-based composite (raw data included in Appendix B).

6.3.2. Micromechanical Properties of Hybrid CNF/CF Cement-Based Composites

6.3.2.1. Effects of Hybrid Fiber Reinforcement on the Overall Distribution of Micromechanical Responses from Cement-Based Composite Constituents

As in Section 4.3.1.2, the highest values for the modulus (i.e., greater than 60 GPa) and hardness (greater than 2 GPa) were seen for the unhydrated cement particles; modulus values of *ca*. 15-60 GPa and hardness values of ca. 0.25 GPa-2 GPa were seen for the hydrated cement phases; and the lowest values for the modulus (i.e., less than 15 GPa) and hardness (i.e., less than 0.25 GPa) were observed for flaws (Figures 6.4-6.9). The majority of the CFs seen in the nanoindentation grids showed modulus and hardness values of less than 40 GPa and 1 GPa, respectively, which was thought to be invalid data as a result of the presence of the CFs at the surface of the composite creating a surface roughness that did not allow the required contact area for nanoindentation.

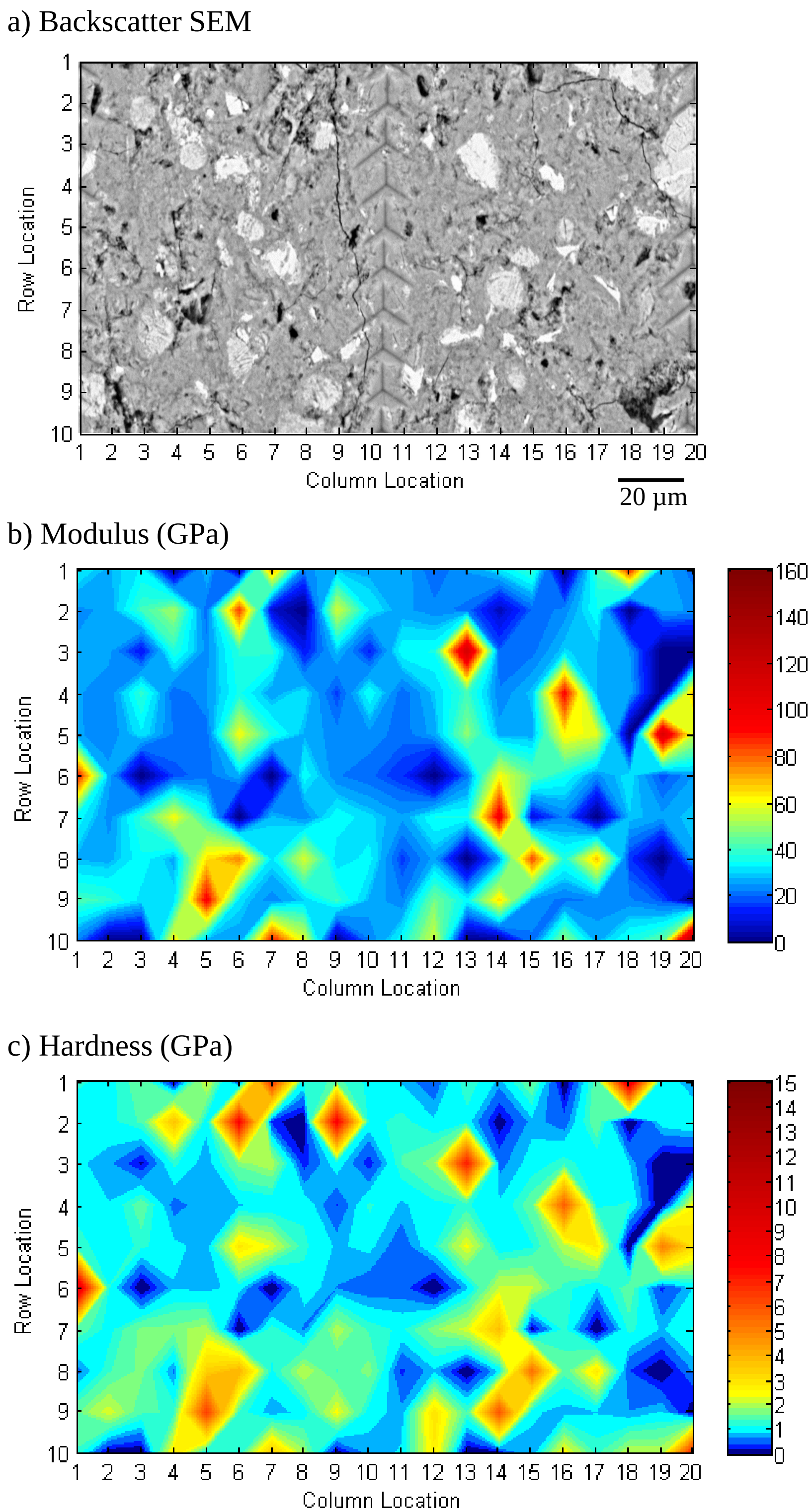

Figure 6.4. Spatial correlation of micromechanical properties of PC-CF A Grid 1 (raw data included in Appendix C). Indents are located in a grid of 200 with 10 rows and 20 columns. a) Backscatter SEM image, b) contour plot of elastic modulus with linear interpolation between indents, c) contour plots of hardness with linear interpolation between indents.

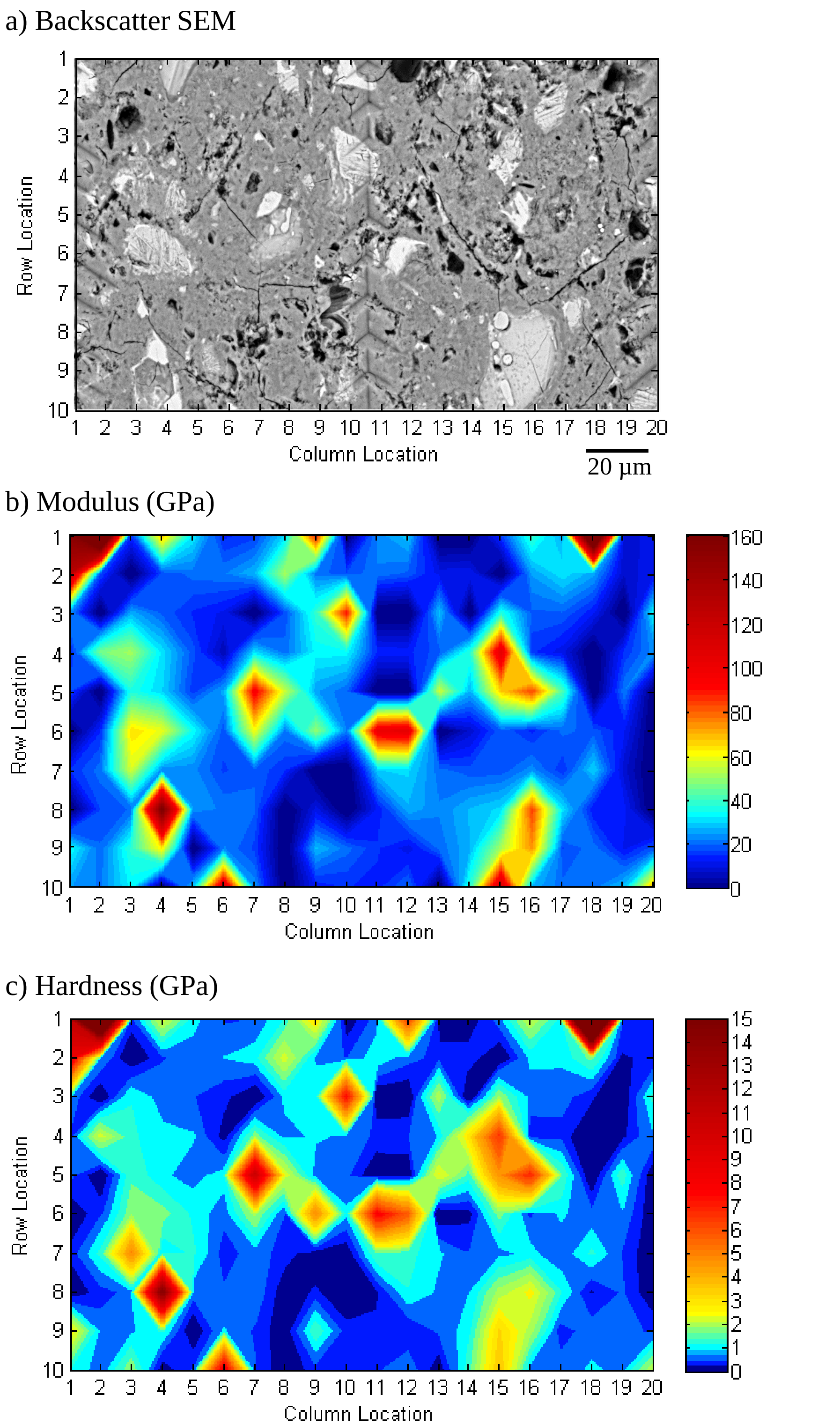

Figure 6.5. Spatial correlation of micromechanical properties of PC-CF A Grid 2 (raw data included in Appendix C). Indents are located in a grid of 200 with 10 rows and 20 columns. a) Backscatter SEM image, b) contour plot of elastic modulus with linear interpolation between indents, c) contour plots of hardness with linear interpolation between indents.

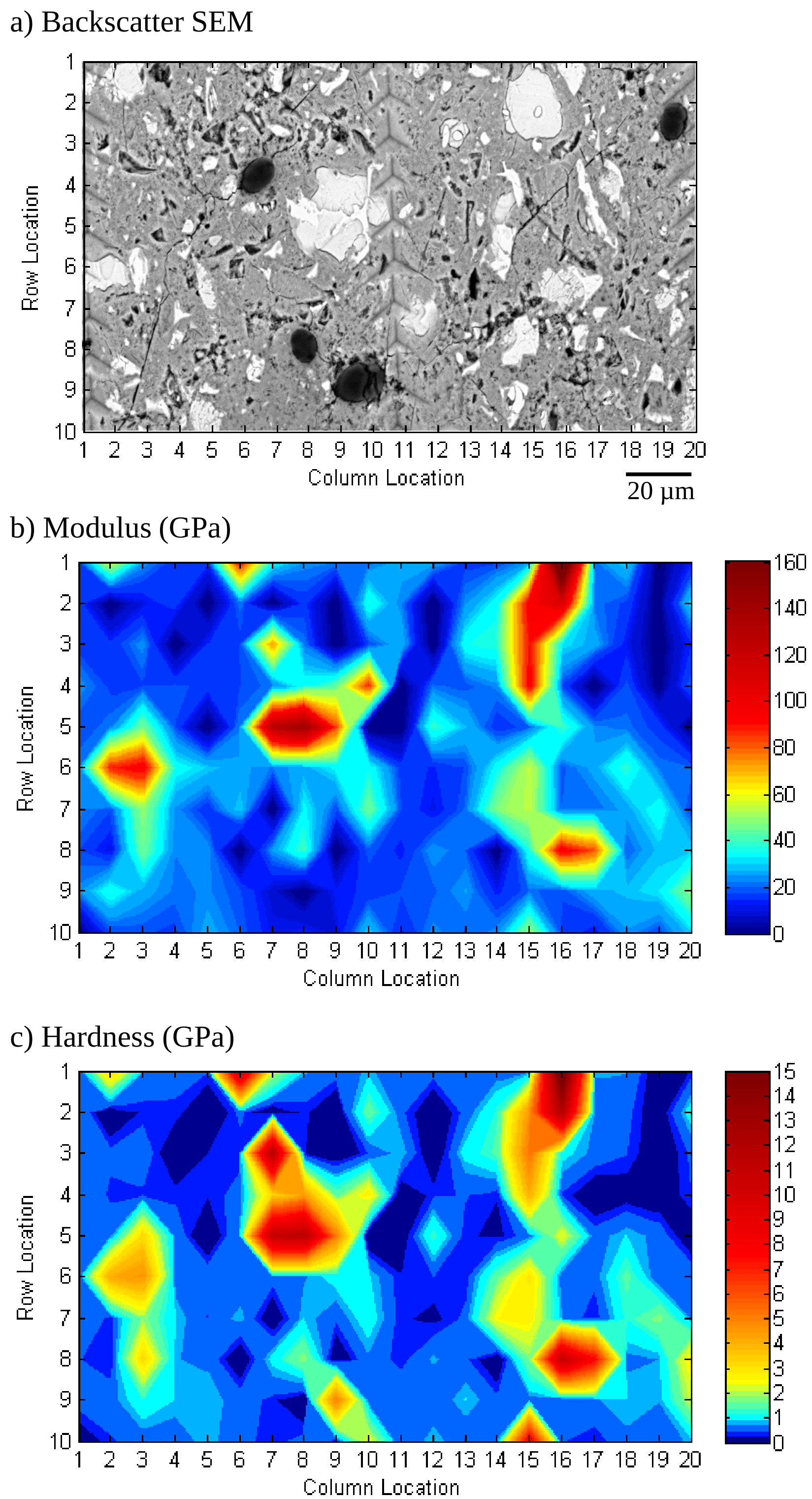

Figure 6.6. Spatial correlation of micromechanical properties of PC-CF B Grid 1 (raw data included in Appendix C). Indents are located in a grid of 200 with 10 rows and 20 columns. a) Backscatter SEM image, b) contour plot of elastic modulus with linear interpolation between indents, c) contour plots of hardness with linear interpolation between indents.

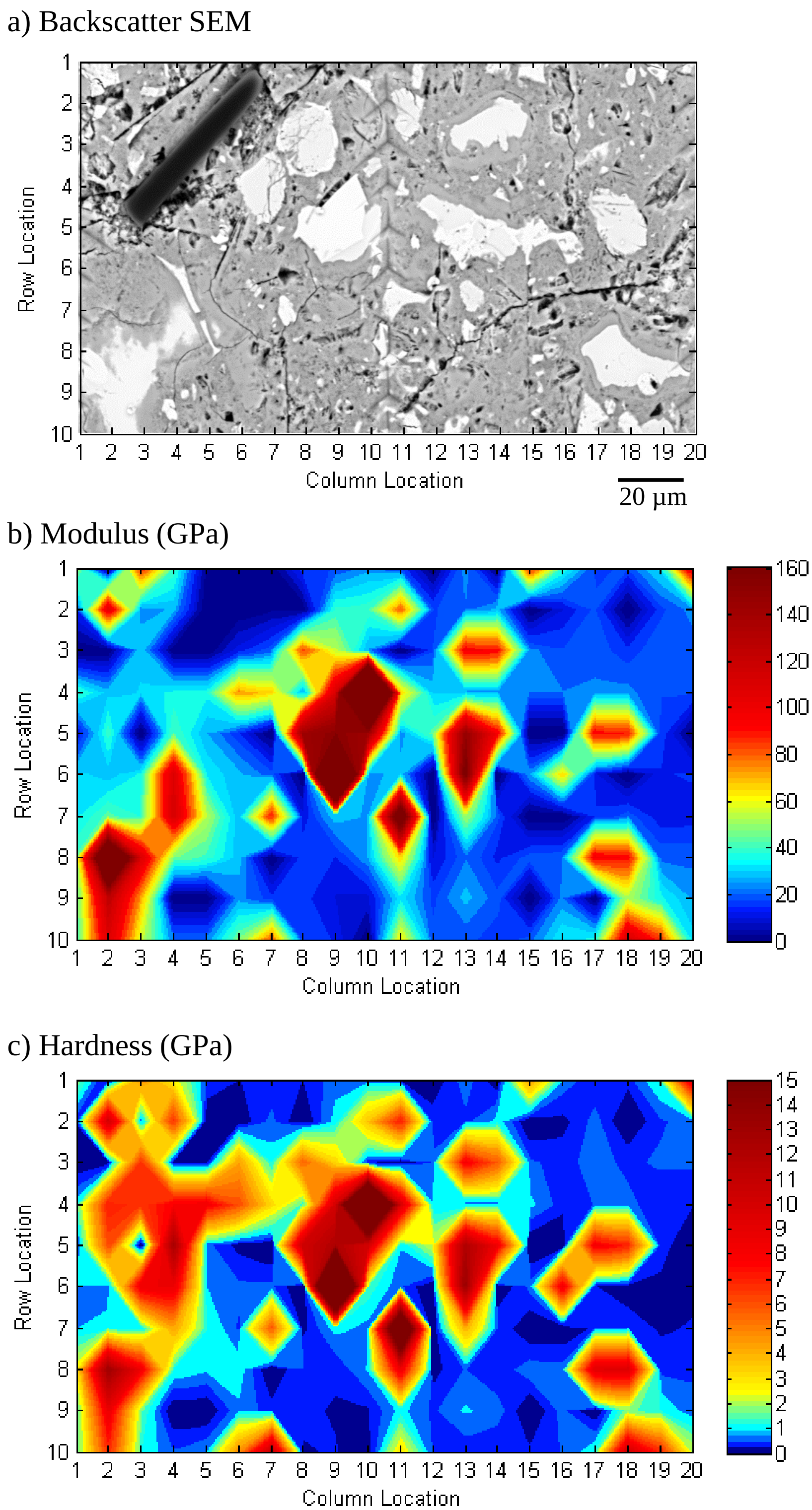

Figure 6.7. Spatial correlation of micromechanical properties of PC-CNF-CF A Grid 1 (raw data included in Appendix C). Indents are located in a grid of 200 with 10 rows and 20 columns. a) Backscatter SEM image, b) contour plot of elastic modulus with linear interpolation between indents, c) contour plots of hardness with linear interpolation between indents.

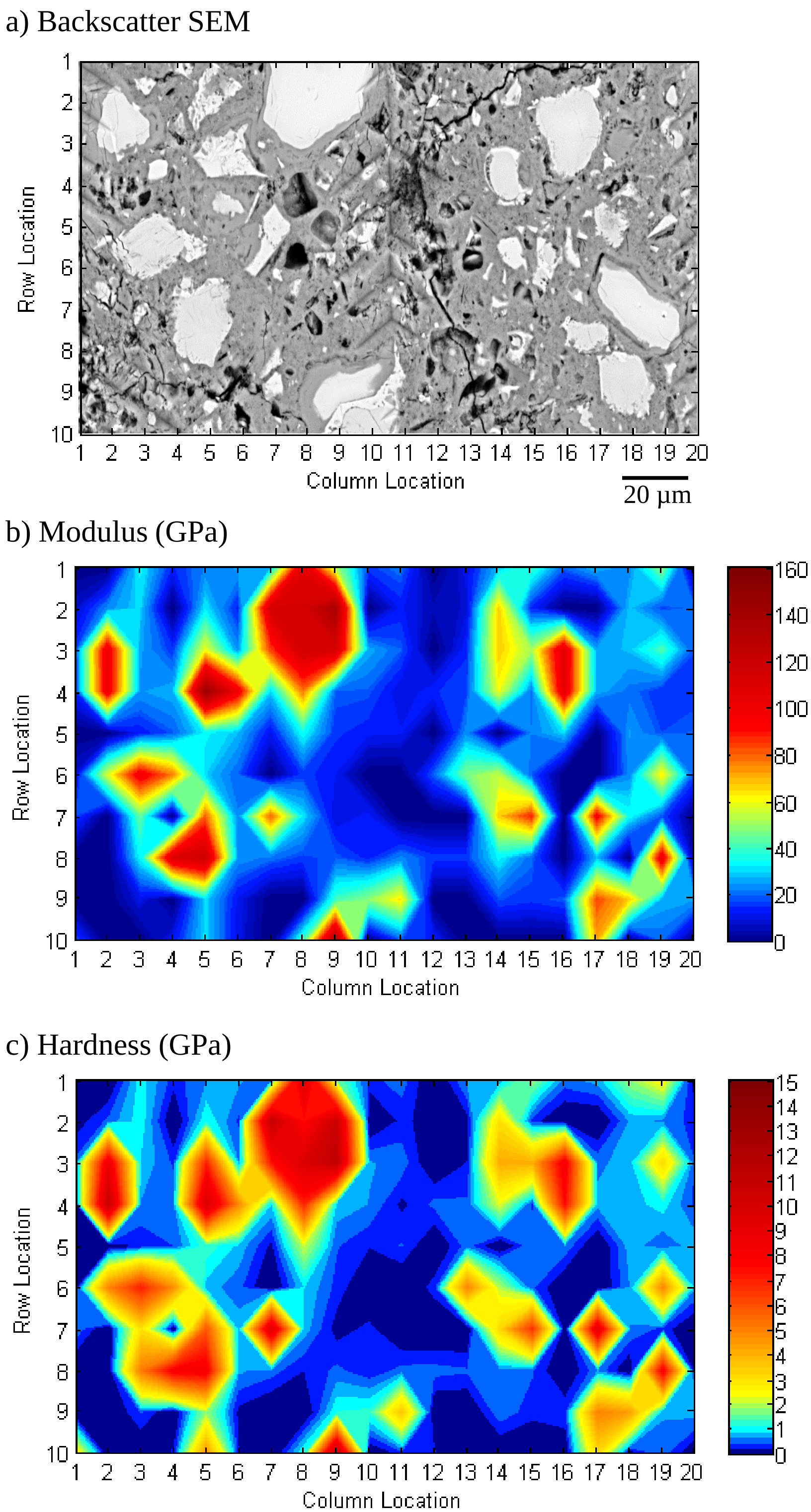

Figure 6.8. Spatial correlation of micromechanical properties of PC-CNF-CF A Grid 2 (raw data included in Appendix C). Indents are located in a grid of 200 with 10 rows and 20 columns. a) Backscatter SEM image, b) contour plot of elastic modulus with linear interpolation between indents, c) contour plots of hardness with linear interpolation between indents.

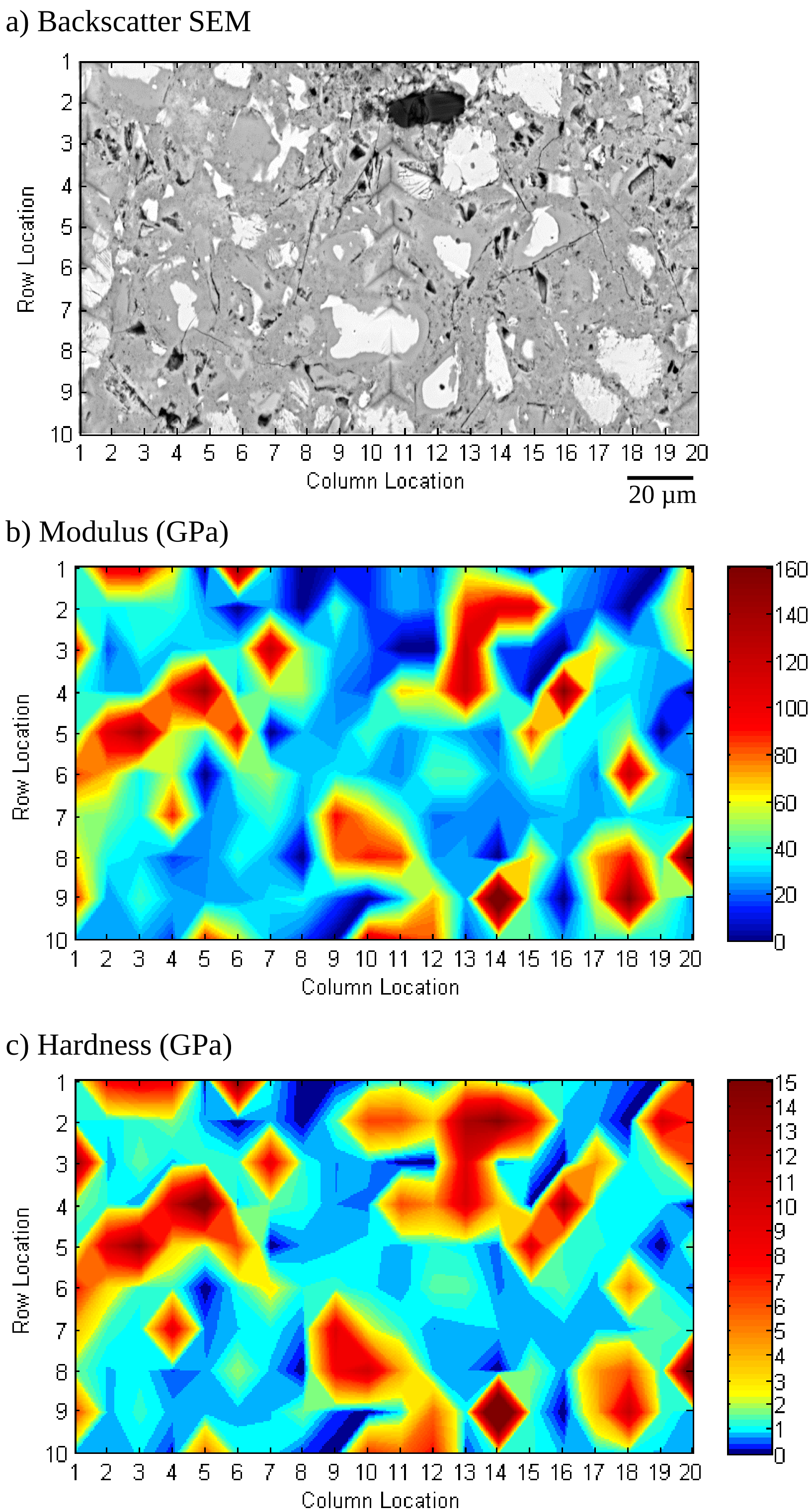

Figure 6.9. Spatial correlation of micromechanical properties of PC-CNF-CF B Grid 1 (raw data included in Appendix C). Indents are located in a grid of 200 with 10 rows and 20 columns. a) Backscatter SEM image, b) contour plot of elastic modulus with linear interpolation between indents, c) contour plots of hardness with linear interpolation between indents.

The shape of the histograms of modulus and hardness values obtained by nanoindentation for both PC-CF and PC-CNF-CF was similar to the shape of the histograms for PC and PC-CNF (Figure 6.10 and Figure 6.11), which were discussed in detail in Section 4.3.1.2. Hybrid CNF/CF reinforcement caused a shift in the main peak of the modulus histogram from the 16-24 GPa range to being almost equally in the 16-24 GPa and 24-32 GPa ranges (Figure 6.10). A shift in the main peak was also seen for PC-CNF and PC-CF with the main peak of both PC-CNF and PC-CF being in the 24-32 GPa range. Decomposition of the histogram of modulus values obtained from nanoindentation coupled with backscatter SEM analysis showed the cement hydrates to be mostly responsible for the shift in the histogram of modulus values for each composite (i.e., PC-CNF, PC-CF, and PC-CNF-CF) suggesting that the CFs, like the CNFs, are influencing the modulus of the cement hydration products. Further examination of the influence of the CNFs and CFs on the modulus of the cement hydrates is included in Section 6.3.2.2. The overall main peak of the hardness histogram (Figure 6.11) was located: (i) in the 0.4-0.8 GPa range for the hybrid CNF/CF cement-based composites and PC-CNF, (ii) equally in the 0.4-0.8 GPa and 0.8-1.2 GPa ranges for PC, and (iii) in the 0.8-1.2 GPa range for PC-CF. In contrast, the main peak of the histogram of hardness values for the cement hydrates as seen from the decomposition of the overall histogram determined by coupling the nanoindentation results with SEM/EDS showed no differences in location for all composites (Figure 6.11).

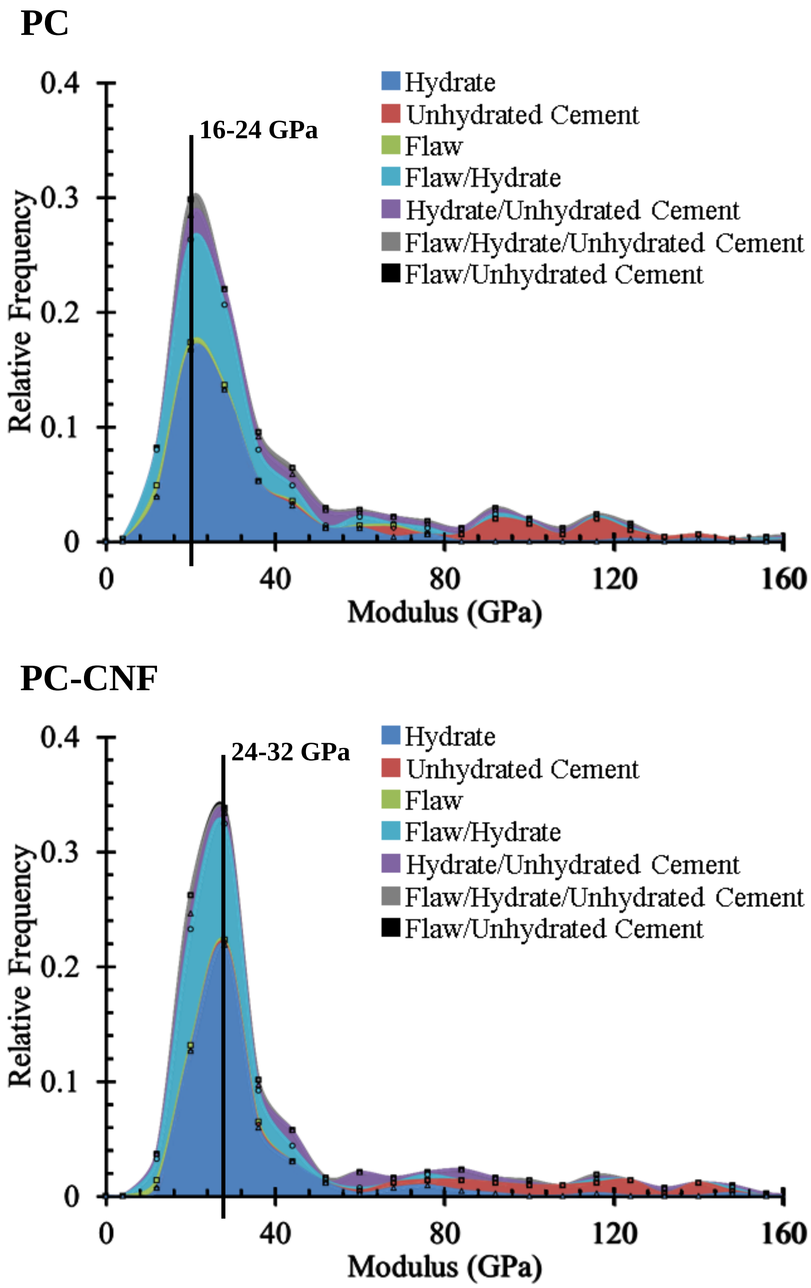

Figure 6.10. Histograms of the modulus values obtained from nanoindentation coupled with backscatter SEM analysis of cement-based composites; including PC, PC-CNF, PC-CF, and PC-CNF-CF; with scaled empirical distributions decomposed into hydrates, unhydrated cement, and flaws (raw data included in Appendix C).

PC-CF

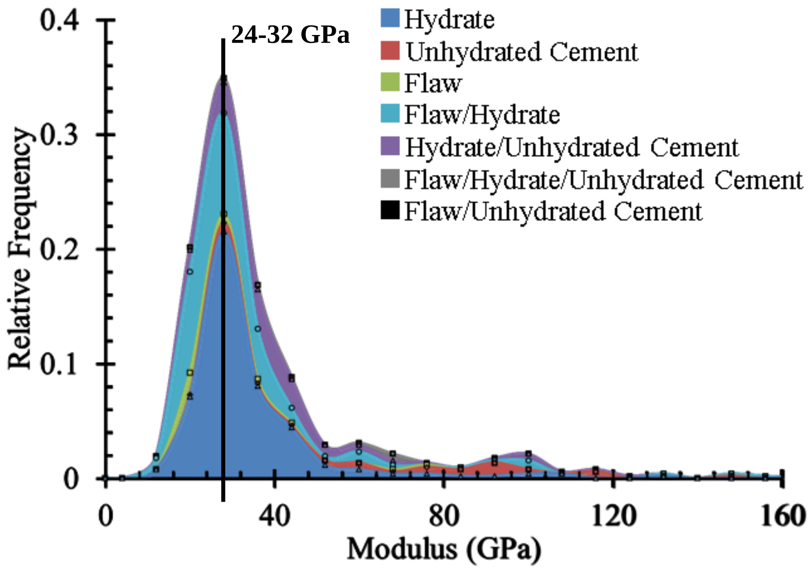

PC-CNF-CF

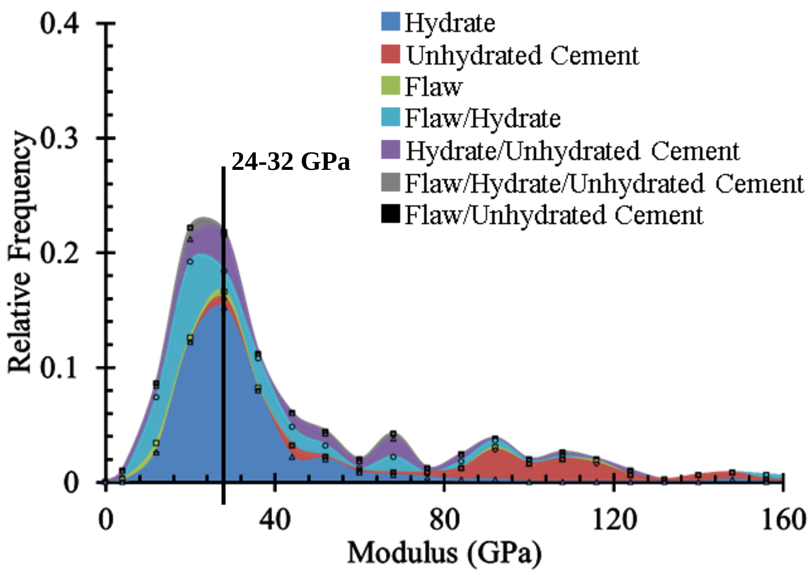

Figure 6.10. Continued

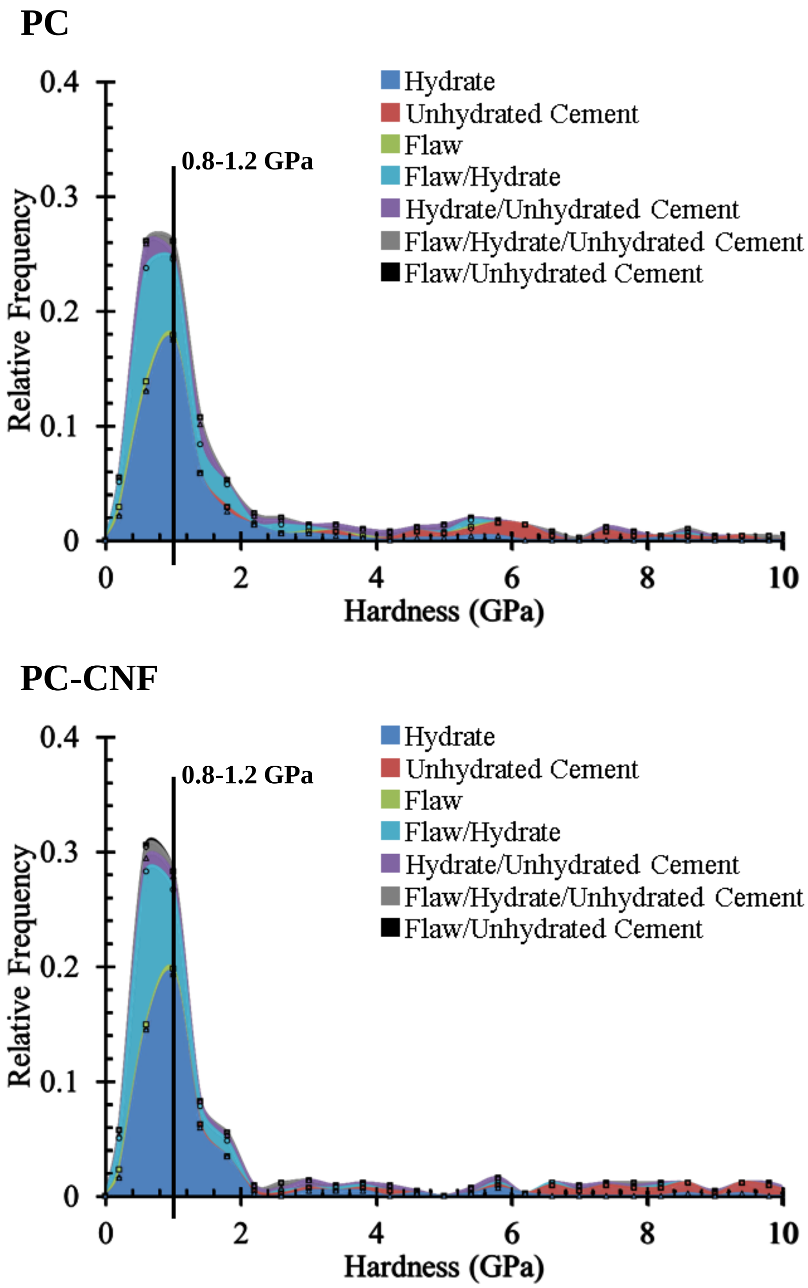

Figure 6.11. Histograms of the hardness values obtained from nanoindentation coupled with backscatter SEM analysis of cement-based composites; including PC, PC-CNF, PC-CF, and PC-CNF-CF; with scaled empirical distributions decomposed into hydrates, unhydrated cement, and flaws (raw data included in Appendix C).

PC-CF

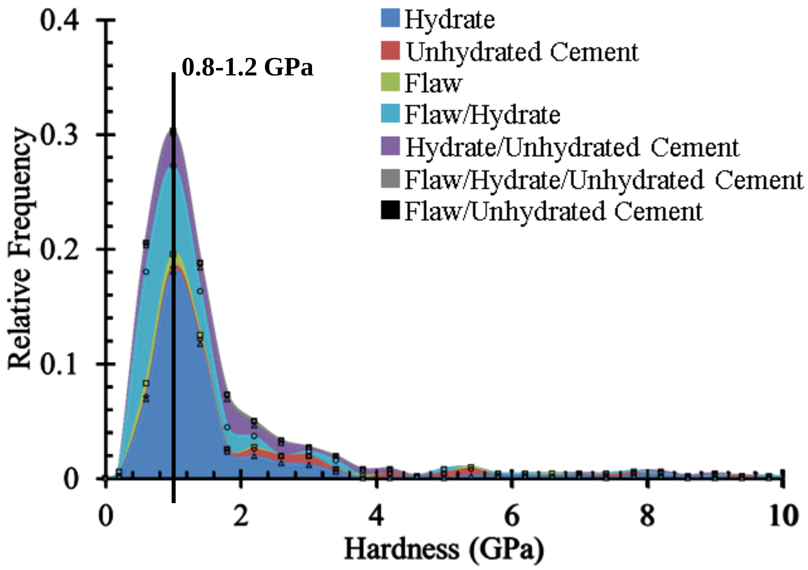

PC-CNF-CF

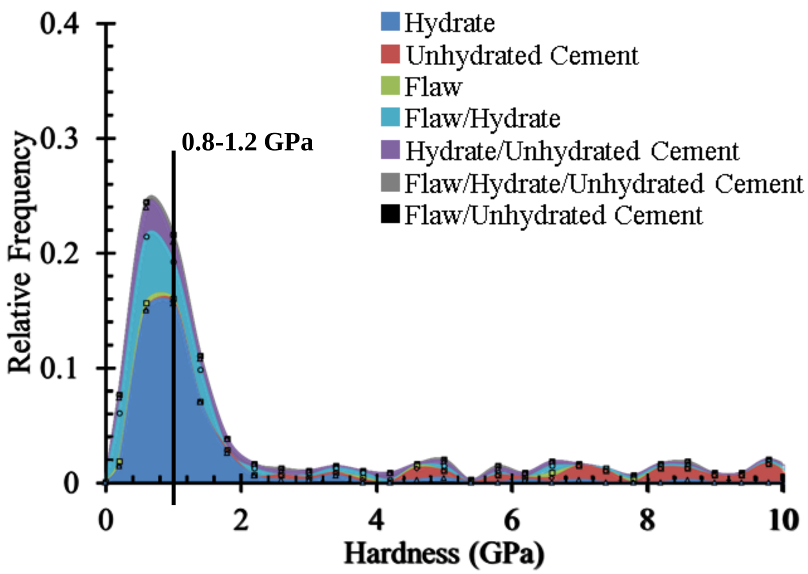

Figure 6.11. Continued

6.3.2.2. Effects of Hybrid CNF/CF Reinforcement on the Micromechanical Properties of Individual Cement Hydrates

Histograms of modulus values that were obtained from indents located solely on cement hydrates as determined by the spatial correlation of backscatter SEM image analysis and nanoindentation showed a shift in the main peak from the 20-25 GPa range, as seen in PC and PC-CF, to the 25-30 GPa range for PC-CNF-CF and PC-CNF (Figure 6.12). The bin sizes of the histograms in Figure 6.12 were refined compared to Figure 6.10, and the shift that was seen in the main peak of the histogram of the modulus values of cement hydrates in PC-CF in Figure 6.10 was no longer seen. Further decomposition of the histogram into the individual representative major cement hydrate phases from spatial correlation of the EDS data with the nanoindentation and SEM analysis showed the shift from the 20-25 GPa to the 25-30 GPa ranges for PC-CNF and PC-CNF-CF to be from the response of the indents located on the C-S-H phase. Though a shift from the 20-25 GPa range to the 25-30 GPa range in the peak of the histogram of modulus values for the C-S-H phase was not seen for PC-CF, the relative frequency of modulus values in the 25-30 GPa range for the C-S-H phase in PC-CF was higher than in PC indicating a likely but less dominant impact of the CFs on the distribution of modulus values compared to the CNFs.

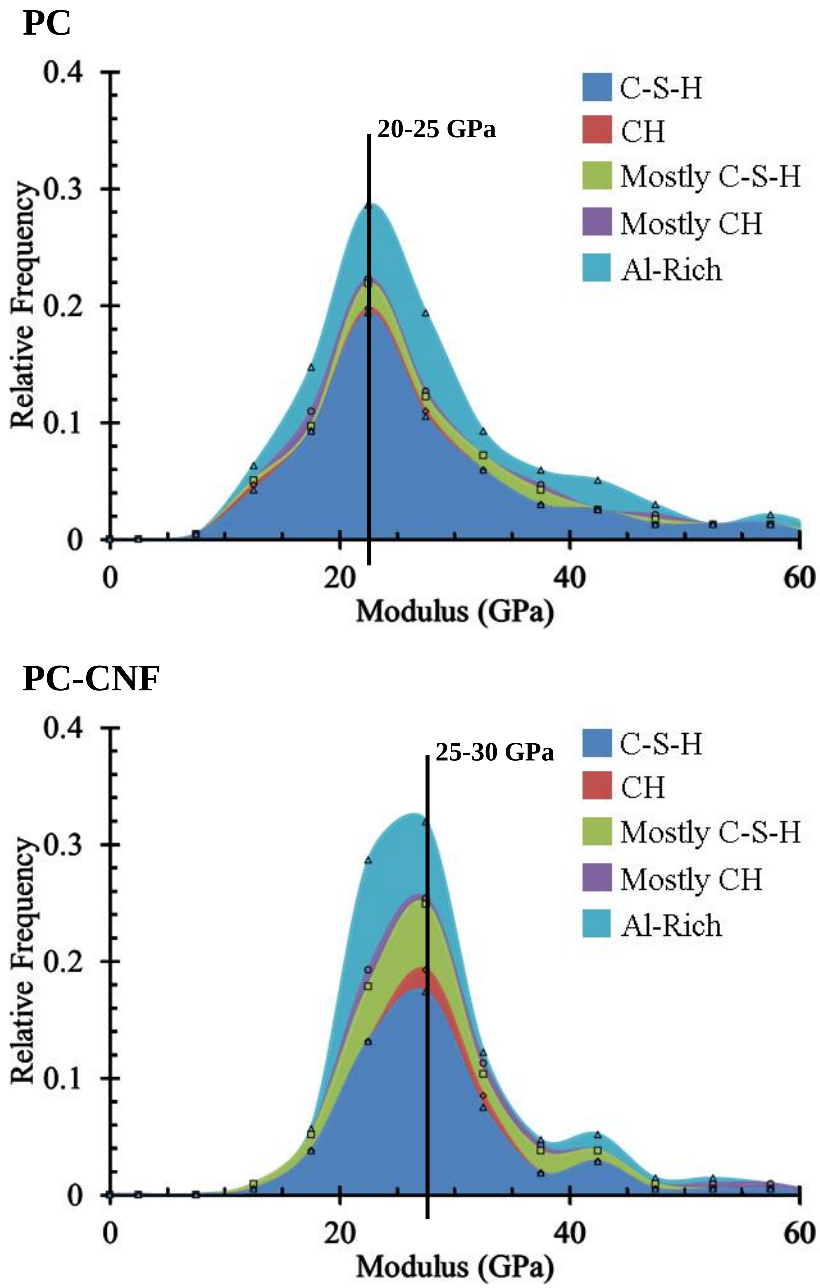

Figure 6.12. Histograms of the modulus values of the cement hydration products with scaled empirical distributions decomposed into the cement hydration phases of C-S-H, CH, a combination of C-S-H and CH but mostly C-S-H, a combination of C-S-H and CH but mostly CH, and Al-rich phases obtained from nanoindentation coupled SEM/EDS on cement-based composites including PC, PC-CNF, PC-CF, and PC-CNF-CF (raw data included in Appendix C).

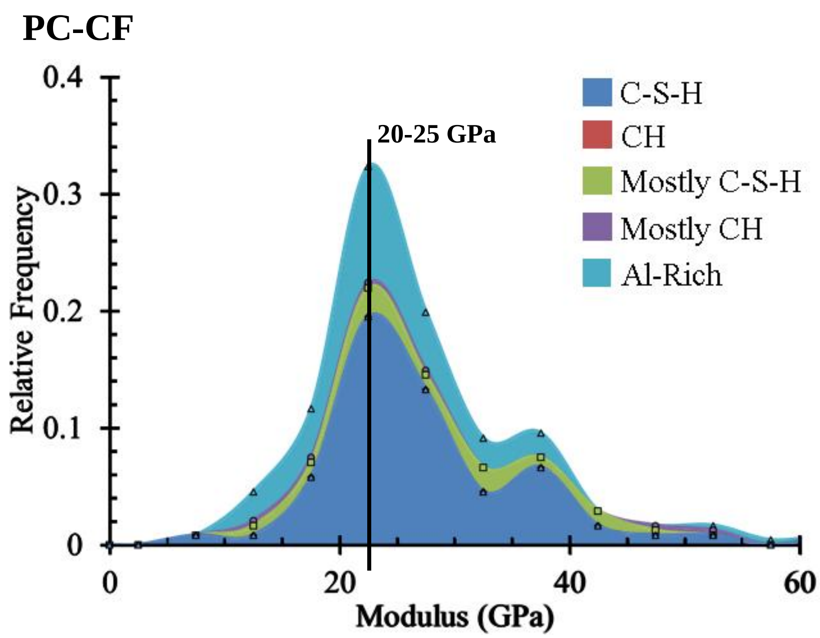

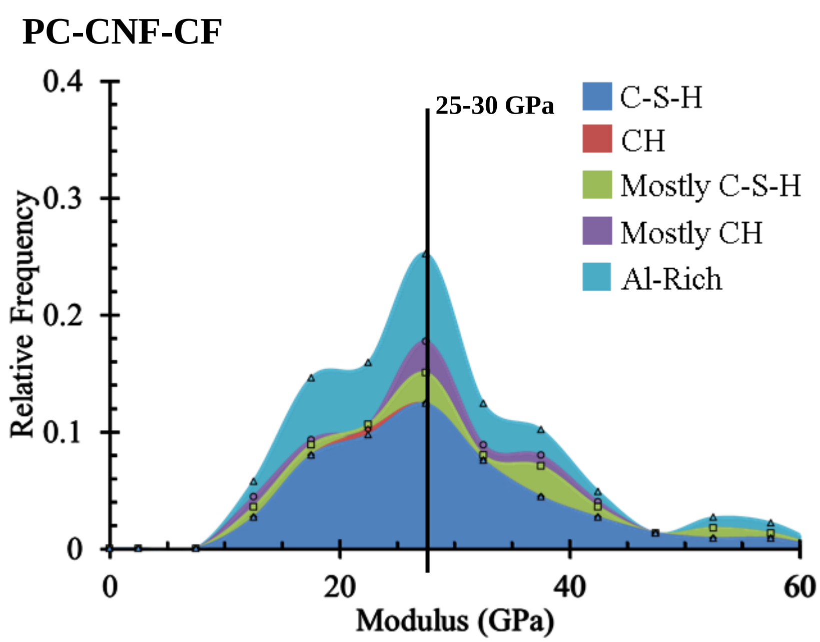

Figure 6.12. Continued

Histograms of the hardness values of indents located on cement hydrates as determined from nanoindentation coupled with SEM showed a shift in the main peak from the 0.8-1 GPa range seen for PC and PC-CNF to the 0.6-0.8 GPa range for the hybrid CNF/CF composite as well as the PC-CF composite (Figure 6.13). Further decomposition of the histograms of hardness values into the individual representative major cement phases using nanoindentation coupled with SEM and EDS showed the main peak of the C-S-H phase to be in the 0.8-1 GPa range for PC and PC-CNF. The histogram of hardness values for the C-S-H phase in PC-CF had two (2) main peaks, one in the 0.6-0.8 GPa range and one in the 1-1.2 GPa range. The histogram of hardness values for the C-S-H phase in hybrid CNF/CF cement-based composites did not, however, have two (2) main peaks, but instead, had one peak in the 0.6-0.8 GPa range.

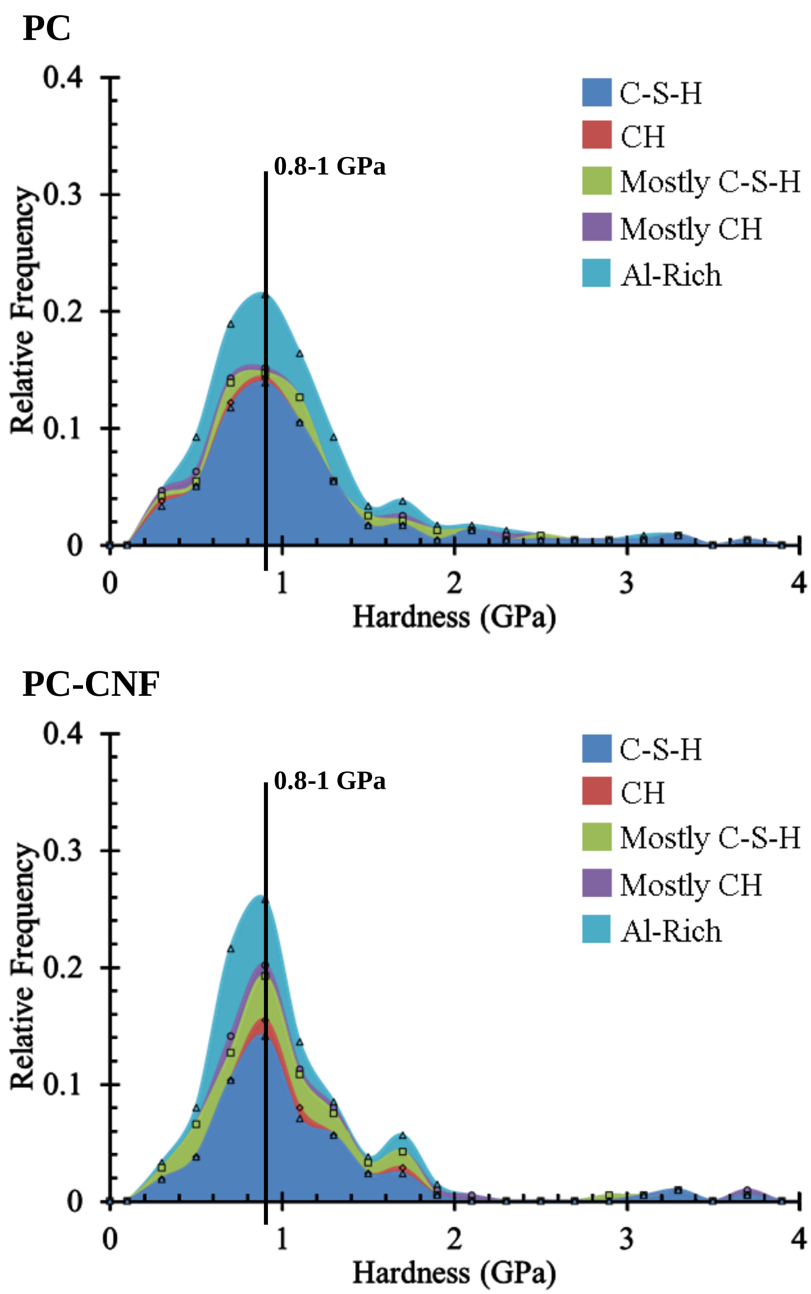

Figure 6.13. Histograms of the hardness values of the cement hydration products with scaled empirical distributions decomposed into the cement hydration phases of C-S-H, CH, a combination of C-S-H and CH but mostly C-S-H, a combination of C-S-H and CH but mostly CH, and Al-rich phases obtained from nanoindentation coupled SEM/EDS on cement-based composites including PC, PC-CNF, PC-CF, and PC-CNF-CF (raw data included in Appendix C).

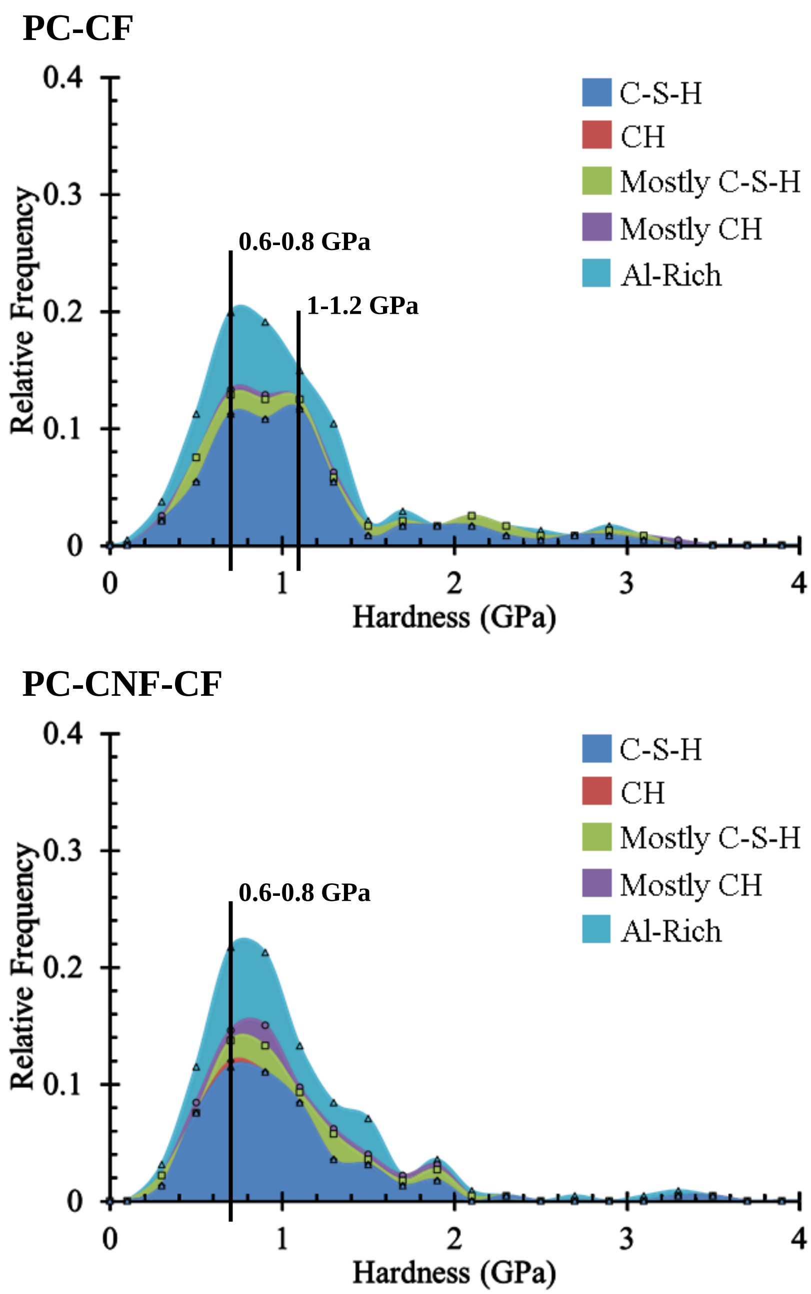

Figure 6.13. Continued

As explained in Section 4.3.2.2, the distributions of the modulus and hardness values were estimated by a Gaussian mixture model (Figure 6.14). The means and standard deviations from the Gaussian mixture model assuming three (3) Gaussian components for both the modulus and hardness along with their respective weight percentages are summarized in Table 6.1.

Although the shift in the main peak of the histogram of modulus values for the C-S-H phase only occurred for PC-CNF and PC-CNF-CF (Figure 6.12), each composite containing fibers (i.e., PC-CNF, PC-CF, and PC-CNF-CF) showed an increased percentage of high stiffness C-S-H at the expense of low stiffness C-S-H. As was discussed in Section 4.3.2.2, it was believed that the CNFs were allowing an increased packing density of the C-S-H causing the increased percentage of high stiffness C-S-H. It was also believed that the CFs had a similar effect upon the C-S-H. The hybrid CNF/CF cement-based composite had the highest reduction in percentage of low stiffness C-S-H (i.e., 14% as determined by the Gaussian mixture model of the modulus values compared to 6% and 10% for PC-CNF and PC-CF, respectively) showing a hybrid effect of the CNFs and CFs on the percentage of high stiffness and low stiffness C-S-H present in the cement-based composite. Though a shift in the main peak of the histogram of modulus values for the C-S-H phase (Figure 6.12) was not seen for PC-CF as it was for PC-CNF and PC-CNF-CF, the CFs actually had more of an impact on the percentages of high stiffness and low stiffness C-S-H compared to the CNFs.

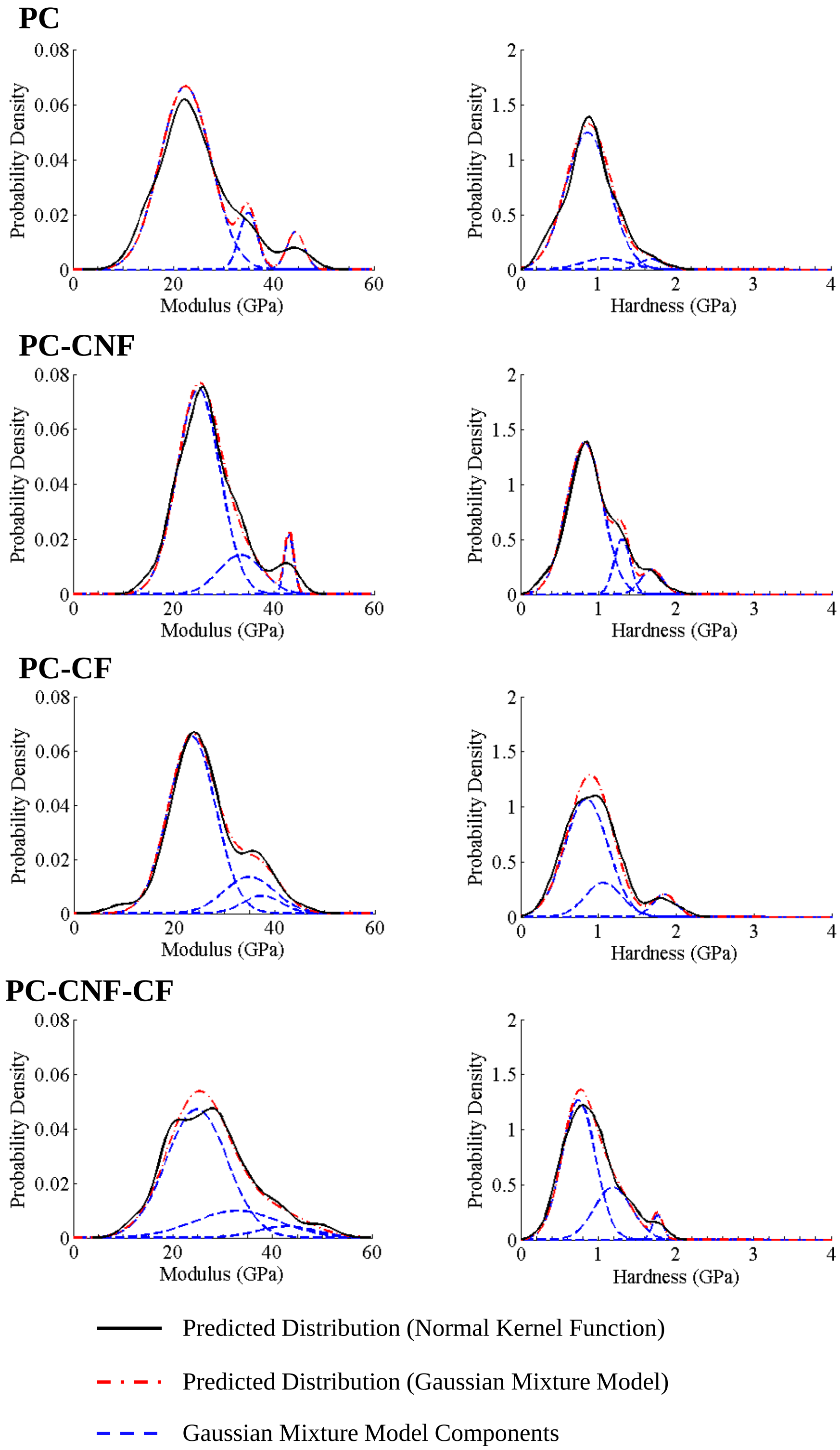

Figure 6.14. Modulus and hardness distributions of the C-S-H phase in cement-based composites as predicted by a Gaussian mixture model and kernel density estimation and the Gaussian components of the Gaussian mixture model for PC, PC-CNF, PC-CF, and PC-CNF-CF (raw data included in Appendix C).

Table 6.1. Summary of mean modulus and hardness values of the C-S-H phases in PC, PC-CNF, PC-CF, and PC-CNF-CF and their weights assuming three Gaussian distributions (raw data included in Appendix C).

		Modulus (GPa)	**Hardness (GPa)**
PC	Ultra-High Stiffness	44.4 ± 1.7 (6.0%)	1.7± 0.2 (3.7%)
	High Stiffness	35.0 ± 1.8 (9.4%)	1.1 ± 0.3 (7.6%)
	Low Stiffness	22.4 ± 5.1 (84.7%)	0.9 ± 0.3 (88.7%)
PC-CNF	Ultra-High Stiffness	43.1 ± 0.9 (5.0%)	1.7 ± 0.1 (7.7%)
	High Stiffness	33.4 ± 4.3 (15.4%)	1.3 ± 0.1 (12.7%)
	Low Stiffness	25.0 ± 4.2 (79.6%)	0.8 ± 0.2 (79.6%)
PC-CF	Ultra-High Stiffness	37.5 ± 3.9 (6.3%)	1.8 ± 0.1 (7.6%)
	High Stiffness	35.0 ± 5.1 (17.1%)	1.1 ± 0.2 (18.0%)
	Low Stiffness	23.5 ± 4.7 (76.6%)	0.8 ± 0.3 (74.4%)
PC-CNF-CF	Ultra-High Stiffness	42.9 ± 5.9 (6.2%)	1.8 ± 0.1 (3.7%)
	High Stiffness	32.9 ± 8.6 (21.2%)	1.2 ± 0.2 (28.5%)
	Low Stiffness	24.8 ± 6.1 (72.6%)	0.7 ± 0.2 (67.8%)

() Indicates % weight of phase in total distribution.

6.3.3. Macromechanical Properties of Hybrid CNF/CF Cement-Based Composites

6.3.3.1. Compressive Properties

The 3-, 7-, and 28-day compressive properties of hybrid CNF/CF cement-based composites compared to composites with only one fiber type and a control composite are summarized in Figure 6.15, Figure 6.16, and Figure 6.17, respectively. In addition, the probability density functions for the 3-, 7-, and 28-day compressive strength results assuming Gaussian distributions are shown in Figure 6.18, Figure 6.19, and Figure 6.20, respectively.

An increase in the median compressive strength of up to *ca*. 44% was seen at 3, 7, and 28 days with the combined addition of CNFs and CFs at or above the 90% confidence level (Welch's t-test, Table 6.2). The hybrid CNF/CF reinforcement did not result, however, in an increase in compressive strength beyond that obtained with the use of CFs alone that was statistically significant at the 95% confidence level. The probability density functions (normal distributions) of the compressive strength of the composites (Figure 6.18, Figure 6.19, and Figure 6.20) clearly showed no influence of the CNFs on the compressive strength of the hybrid CNF/CF composite.

Additionally, the hybrid CNF/CF cement-based composites showed some improvements in the compressive modulus and toughness compared to the control, but the improvements were less than the difference seen for the CF reinforcement alone. The CNFs, therefore, did not positively influence the compressive modulus or toughness in the hybrid CNF/CF cement-based composites and all improvements were the effect of the CFs.

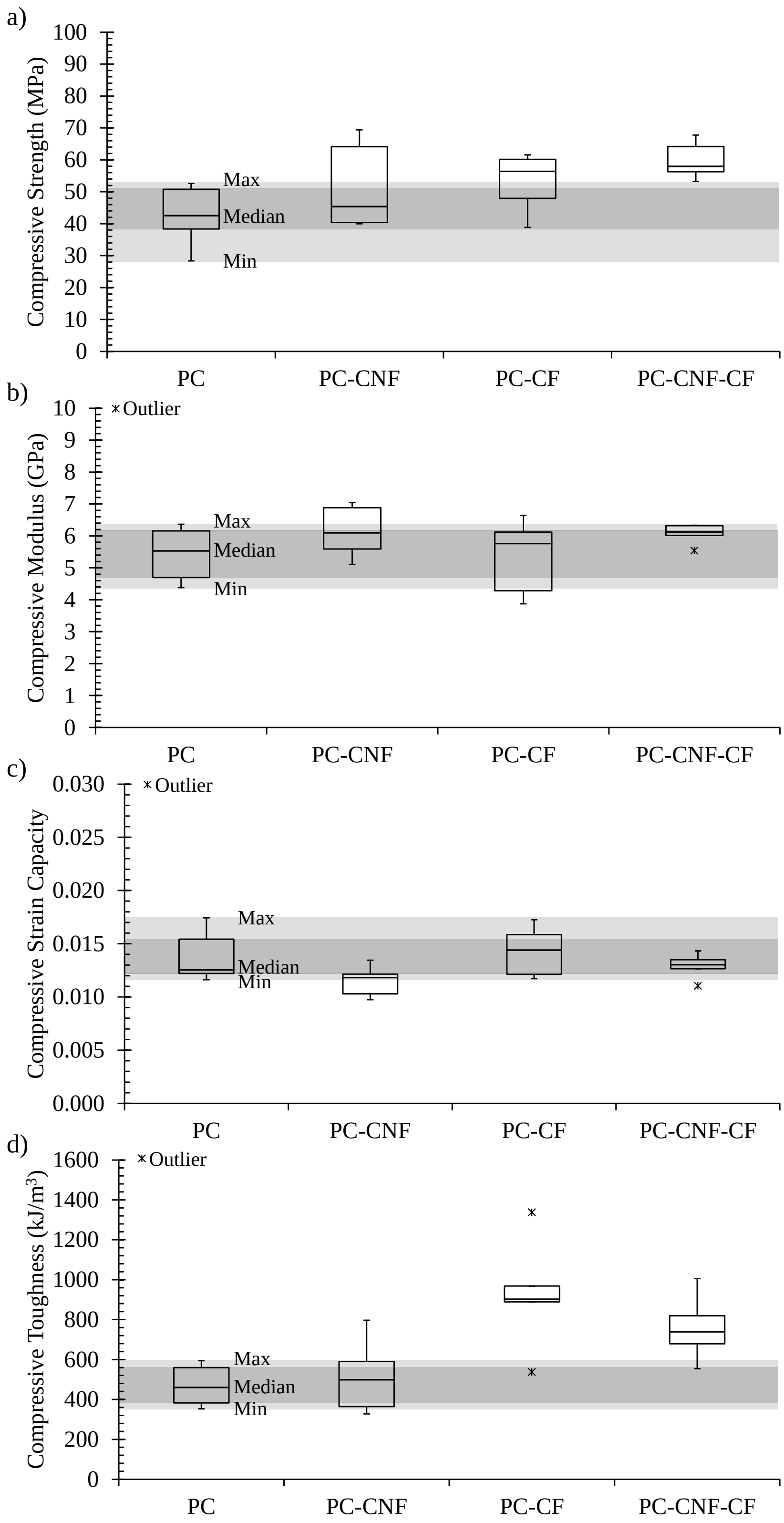

Figure 6.15. 3-day compressive properties of hybrid CNF/CF cement-based composites (raw data included in Appendix D). a) Ultimate strength, b) modulus, c) strain capacity at failure, and d) toughness.

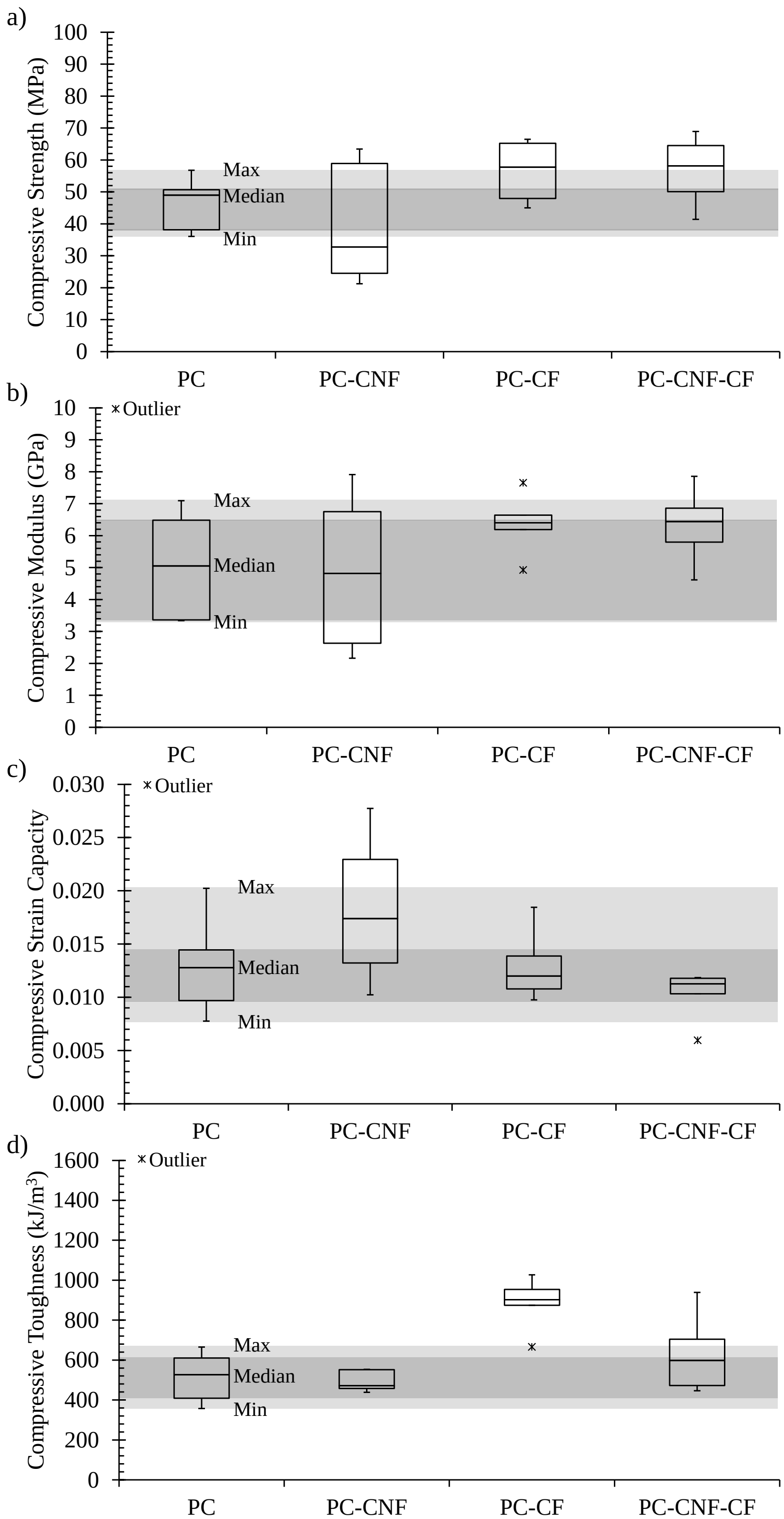

Figure 6.16. 7-day compressive properties of hybrid CNF/CF cement-based composites (raw data included in Appendix D). a) Ultimate strength, b) modulus, c) strain capacity at failure, and d) toughness.

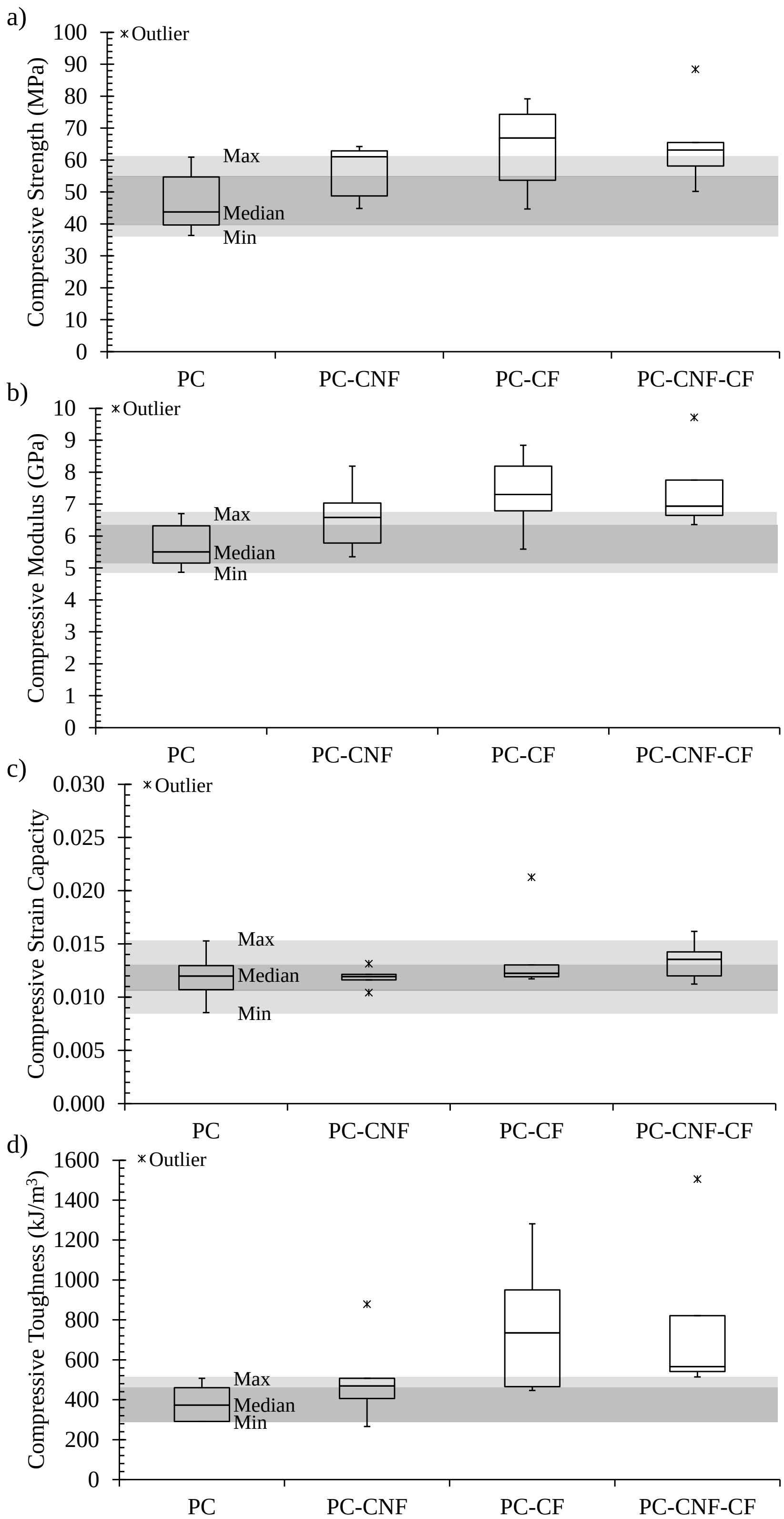

Figure 6.17. 28-day compressive properties of hybrid CNF/CF cement-based composites (raw data included in Appendix D). a) Ultimate strength, b) modulus, c) strain capacity at failure, and d) toughness.

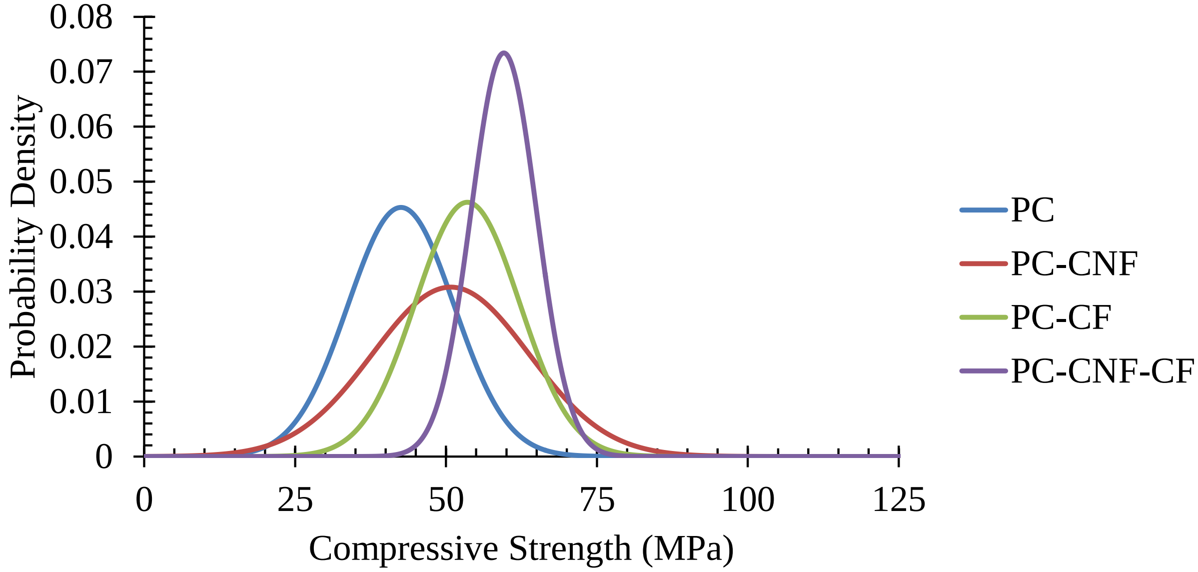

Figure 6.18. Probability density functions of the 3-day compressive strength of the CNF, CF, and hybrid CNF/CF cement-based composites assuming normal distributions (raw data included in Appendix D).

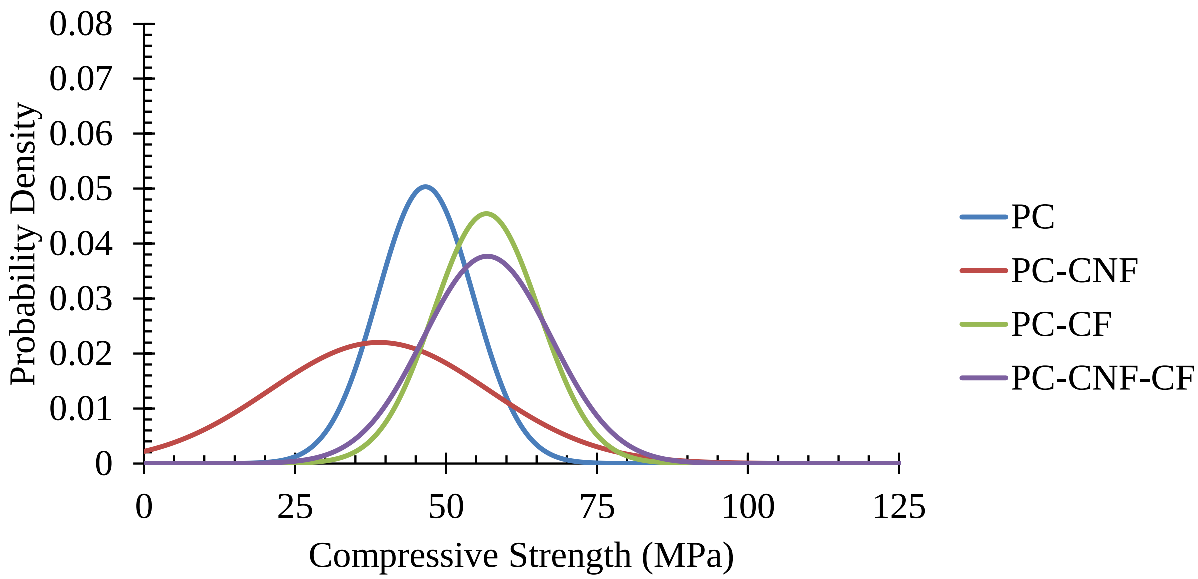

Figure 6.19. Probability density functions of the 7-day compressive strength of the CNF, CF, and hybrid CNF/CF cement-based composites assuming normal distributions (raw data included in Appendix D).

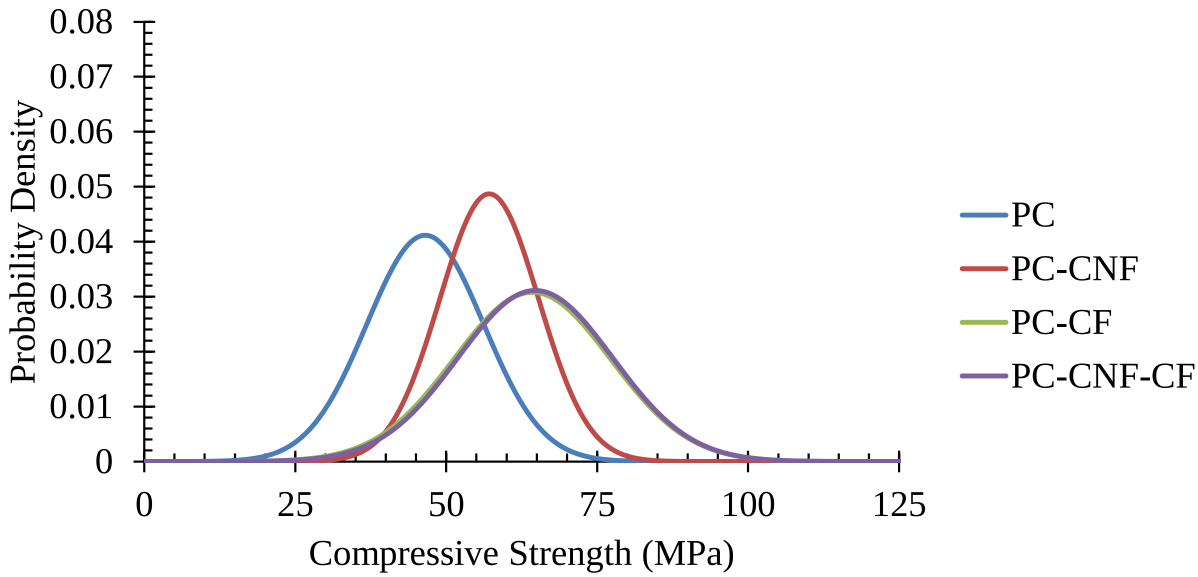

Figure 6.20. Probability density functions of the 28-day compressive strength of the CNF, CF, and hybrid CNF/CF cement-based composites assuming normal distributions (raw data included in Appendix D).

Table 6.2. P-values (Welch's t-test) and conclusions at the 90% and 95% confidence levels for the compressive properties of hybrid CNF/CF cement-based composites compared to the control (raw data included in Appendix D).

	P-value (compared to PC)												**Summary at the 90% and 95% confidence levels**
	Strength			Modulus			Strain Capacity			Toughness			
	3 days	7 days	28 days	3 days	7 days	28 days	3 days	7 days	28 days	3 days	7 days	28 days	
PC-CNF	0.230	0.374	0.069 (39.5%)	0.166	0.867	0.106	0.090 (-5.8%)	0.246	0.964	0.614	0.712	0.248	Increase in 28-day ultimate strength. Decrease in 3-day strain capacity at failure.
PC-CF	0.054 (32.6%)	0.063 (17.9%)	0.024 (52.9%)	0.947	0.149	0.017 (32.7%)	0.617	0.952	0.332	0.005 (96.2%	3.7×10^{-4} (71.4%)	0.031 (96.8%)	Increase in 3-, 7-, and 28-day ultimate strength, 28-day modulus, and 3-, 7-, and 28-day toughness.
PC-CNF-CF	0.003 (36.3%)	0.089 (18.6%)	0.021 (44.4%)	0.120	0.171	0.018 (26.1%)	0.519	0.244	0.213	0.004 (60.8%)	0.260	0.066 (51.5%)	Increase in 3-, 7-, and 28-day ultimate strength, 28-day modulus, and 3- and 28-day toughness.

() Indicates % difference compared to PC.

Indicates P-value less than or equal to 0.100 (significance at the 90% confidence level).

Indicates P-value less than or equal to 0.050 (significance at the 95% confidence level).

6.3.3.2. Flexural Properties

Hybrid CNF/CF cement-based composites had improved 3-, 7-, and 28-day flexural strength, strain capacity, and toughness compared to the control composite (Figure 6.21, Figure 6.22, and Figure 6.23). However, no evidence of fiber "synergy" could be seen from the hybrid CNF/CF cement-based composites as no additional improvements in flexural properties were seen over PC-CF at any curing age.

Ultimate strength. The hybrid CNF/CF cement-based composites showed improvements in 3-, 7-, and 28-day ultimate flexural strength of up to 100% based on the median value at the 95% confidence level (Welch's t-test, Table 6.3). However, the improvements in the flexural strength were not as large as the improvements seen with CFs alone, and therefore, there was no hybrid effect of the CNFs and CFs seen. Probability density functions of the flexural strength of hybrid CNF/CF cement-based composites compared to the control composite and composites with only one fiber type assuming a Gaussian distribution clearly showed the probable strength values of PC-CNF-CF to decrease compared to PC-CF (Figure 6.24, Figure 6.25, and Figure 6.26). The decrease in flexural strength of the hybrid CNF/CF cement-based composites compared to PC-CF was statistically significant at the 95% confidence level with p-values of 0.017, 0.003, and 0.050, for 3, 7, and 28 days, respectively. The decrease was thought to be indicative of the detrimental effect of the CNF agglomerates on the flexural strength of the hybrid CNF/CF cement-based composites.

Modulus. The hybrid fiber reinforcement had no impact on the flexural modulus of cement-based composites at the 95% confidence level compared to the control composite

(Welch's t-test, Table 6.3). However, the CFs when used alone improved the flexural modulus of the cement-based composites by up to 18% at the 95% confidence level (Welch's t-test, Table 6.3).

Strain capacity. Hybrid CF/CNF reinforcement allowed for improvements of the strain capacity at failure of up to 83% based on the median value compared to the control composite at the 95% confidence level (Welch's t-test, Table 6.3). The strain capacity at failure of PC-CF was, however, improved by up to 107% based on the median compared to the control composite at the 95% confidence level (Welch's t-test, Table 6.3).

Toughness. Hybrid CF/CNF reinforcement allowed for increases in flexural toughness of over 2 times the toughness of the control composite at the 95% confidence level (Welch's t-test, Table 6.3), but the flexural toughness of the composite with only CF reinforcement was over 3 times the toughness of the control at the 95% confidence level (Welch's t-test, Table 6.3).

Although CNFs have been shown to improve the flexural properties of cement-based composites (Section 5.3.2.3, Figure 6.22, and Figure 6.23), the hybridization of CNFs with CFs does not further improve the flexural properties of cement-based composites beyond the improvements of composites with CFs alone. It was thought that at the ultimate strengths that the hybrid CNF/CF cement-based composites are failing, crack propagation had advanced beyond the length of the CNFs (i.e., 200 μm) or at least beyond the point at which the embedment length of the CNFs was not sufficient for load transfer such that the reinforcing ability was not realized. It was also believed that the presence of the CNF agglomerates in the hybrid CNF/CF composites lowered the ability of the CNFs to act as reinforcement because a large percentage of the 0.5 wt% of CNFs were located within CNF agglomerates and not individually dispersed throughout the composite for reinforcement of nanoscale cracks.

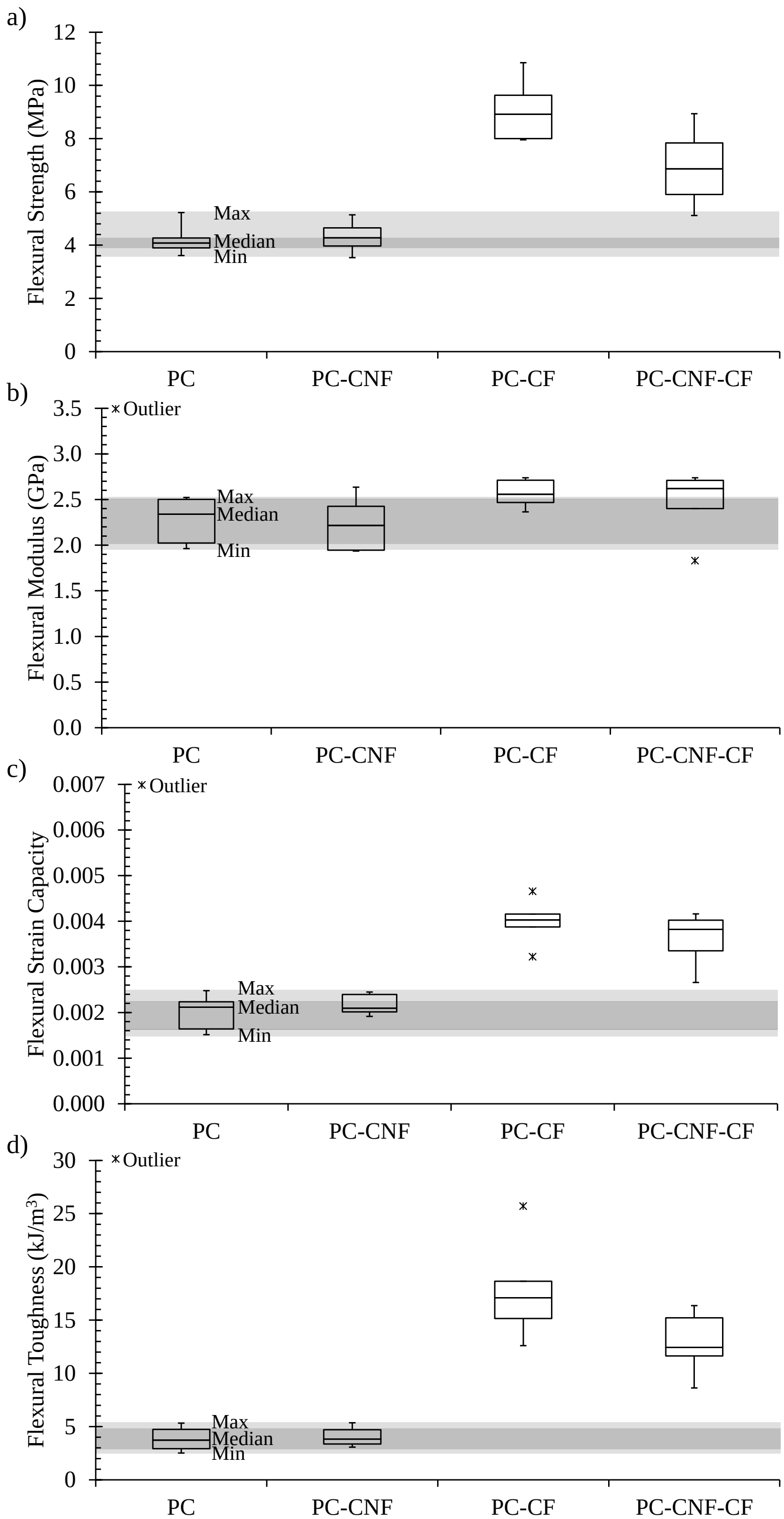

Figure 6.21. 3-day flexural properties of hybrid CNF/CF cement-based composites (raw data included in Appendix D). a) Ultimate strength, b) modulus, c) strain capacity at failure, and d) toughness.

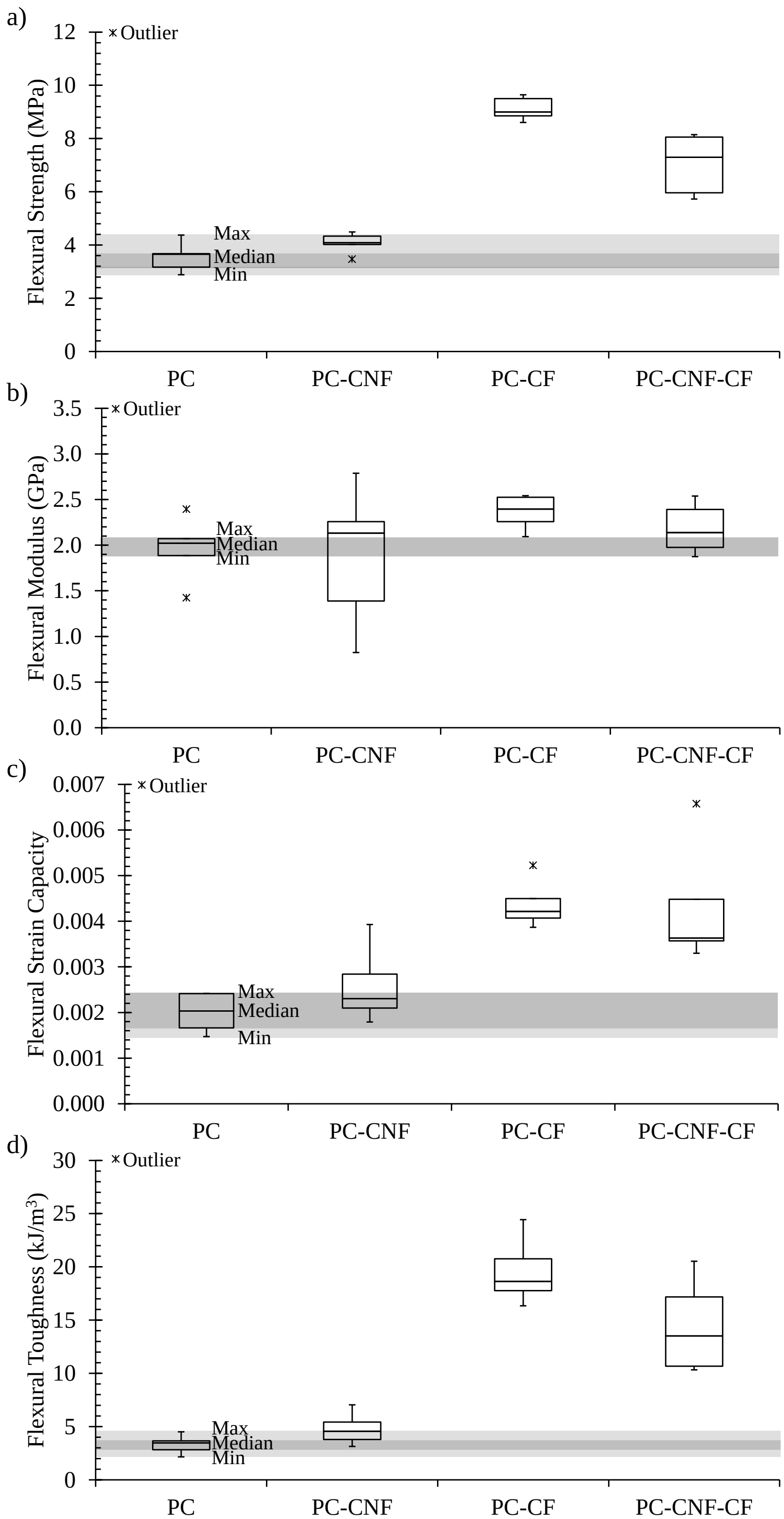

Figure 6.22. 7-day flexural properties of hybrid CNF/CF cement-based composites (raw data included in Appendix D). a) Ultimate strength, b) modulus, c) strain capacity at failure, and d) toughness.

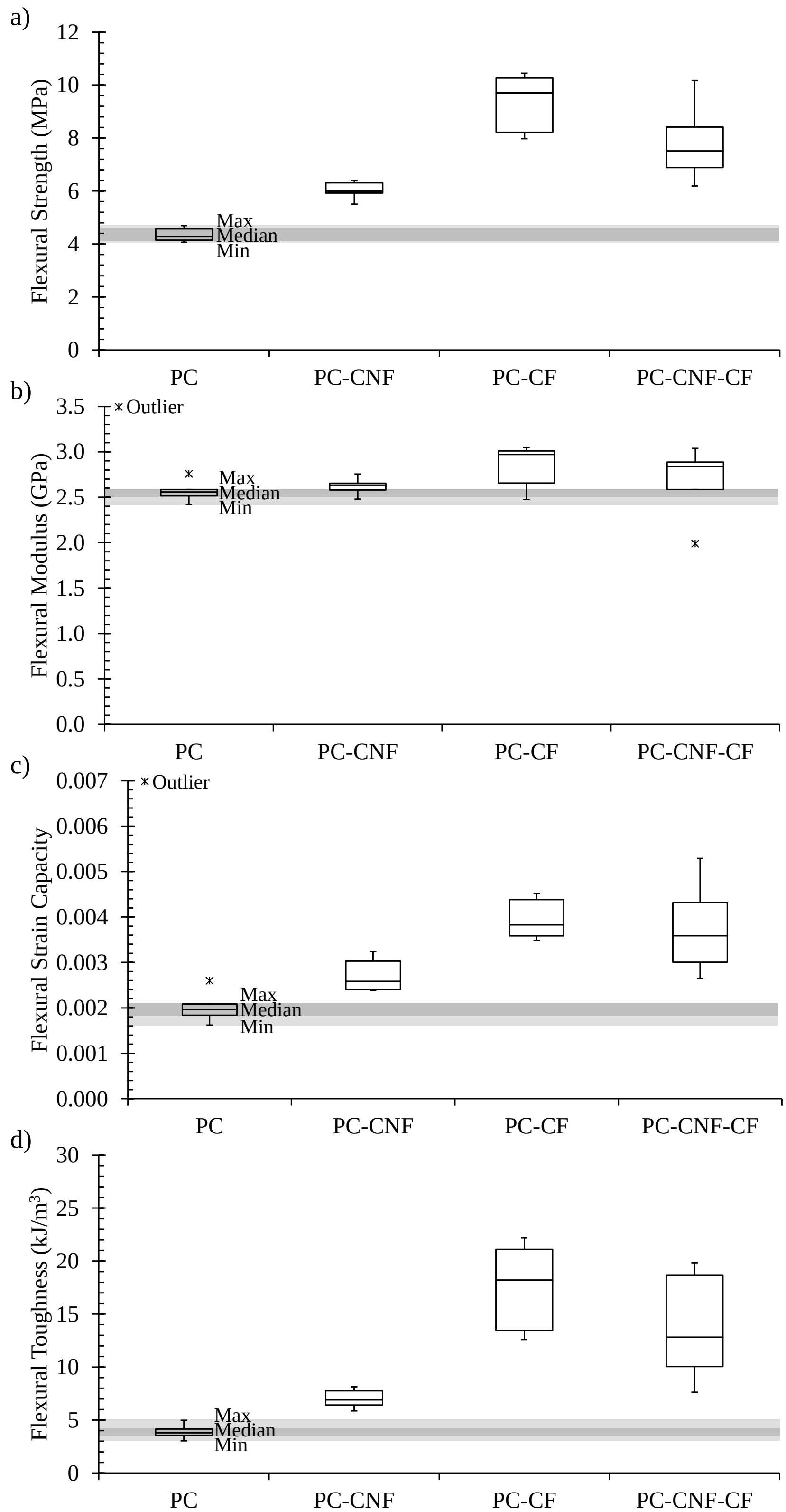

Figure 6.23. 28-day flexural properties of hybrid CNF/CF cement-based composites (raw data included in Appendix D). a) Ultimate strength, b) modulus, c) strain capacity at failure, and d) toughness.

Table 6.3. P-values (Welch's t-test) and conclusions at the 90% and 95% confidence levels for the flexural properties of hybrid CNF/CF cement-based composites compared to the control (raw data included in Appendix D).

	P-value (compared to PC)												**Summary at the 90% and 95% confidence levels**
	Strength			Modulus			Strain Capacity			Toughness			
	3 days	7 days	28 days	3 days	7 days	28 days	3 days	7 days	28 days	3 days	7 days	28 days	
PC-CNF	0.728	0.073 (11.9%)	2.1×10^{-6} (39.8%)	0.732	0.880	0.348	0.438	0.164	0.006 (31.8%)	0.728	0.062 (31.6%)	4.3×10^{-5} (81.2%)	Increase in 7- and 28-day ultimate strength, 28-day strain capacity at failure, and 7- and 28-day toughness.
PC-CF	2.7×10^{-5} (118.6%)	3.1×10^{-9} (146.3%)	4.9×10^{-5} (126.2%)	0.037 (9.3%)	0.028 (18.5%)	0.028 (16.2%)	1.4×10^{-5} (90.4%)	4.2×10^{-6} (107.1%)	7.4×10^{-6} (95.4%)	4.4×10^{-4} (359.5%)	1.5×10^{-5} (437.5%)	3.0×10^{-4} (377.6%)	Increase in 3-, 7-, and 28-day ultimate strength, 3-, 7- and 28-day modulus, 3-, 7- and 28-day strain capacity at failure, and 3-, 7-, and 28-day toughness.
PC-CNF-CF	0.004 (68.2%)	1.1×10^{-4} (99.8%)	0.002 (75.2%)	0.259	0.243	0.446	2.4×10^{-4} (80.6%)	0.006 (78.5%)	0.007 (83.2%)	2.1×10^{-4} (234.3%)	0.001 (289.9%)	0.005 (236.2%)	Increase in 3-, 7-, and 28-day ultimate strength, 3-, 7- and 28-day strain capacity at failure, and 3-, 7-, and 28-day toughness.

() Indicates % difference compared to PC.

Indicates P-value less than or equal to 0.100 (significance at the 90% confidence level).

Indicates P-value less than or equal to 0.050 (significance at the 95% confidence level).

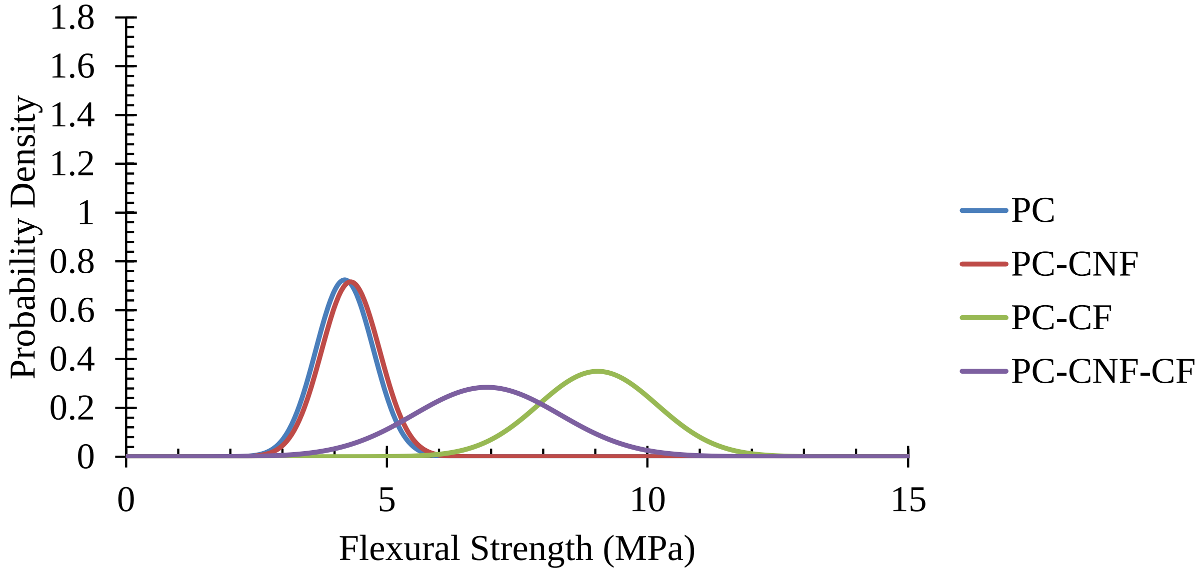

Figure 6.24. Probability density functions of the 3-day flexural strength of the CNF, CF, and hybrid CNF/CF cement-based composites assuming normal distributions (raw data included in Appendix D).

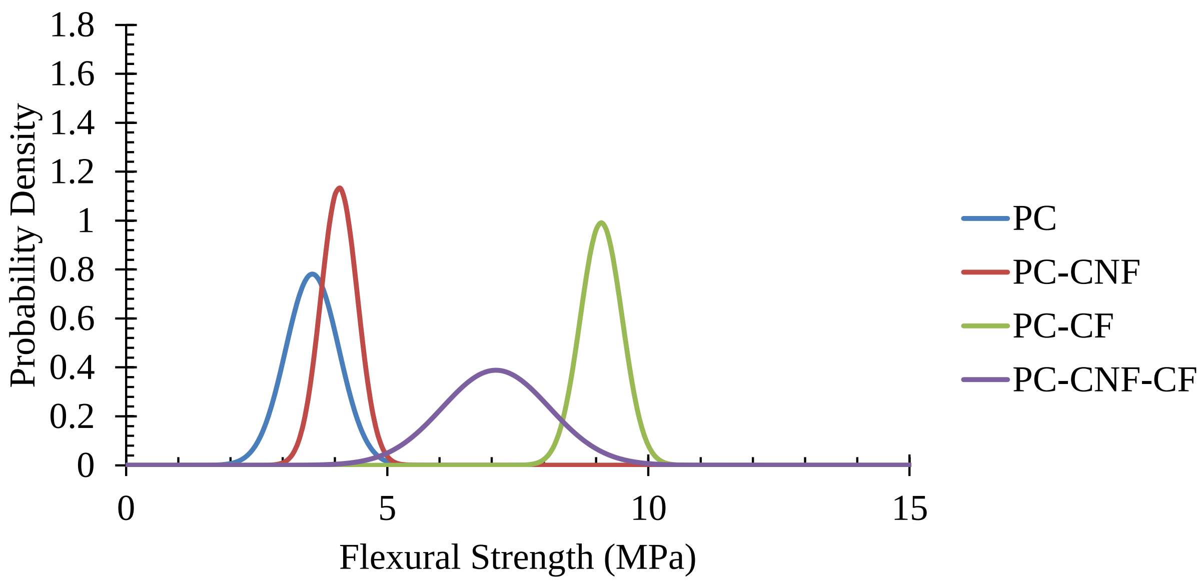

Figure 6.25. Probability density functions of the 7-day flexural strength of the CNF, CF, and hybrid CNF/CF cement-based composites assuming normal distributions (raw data included in Appendix D).

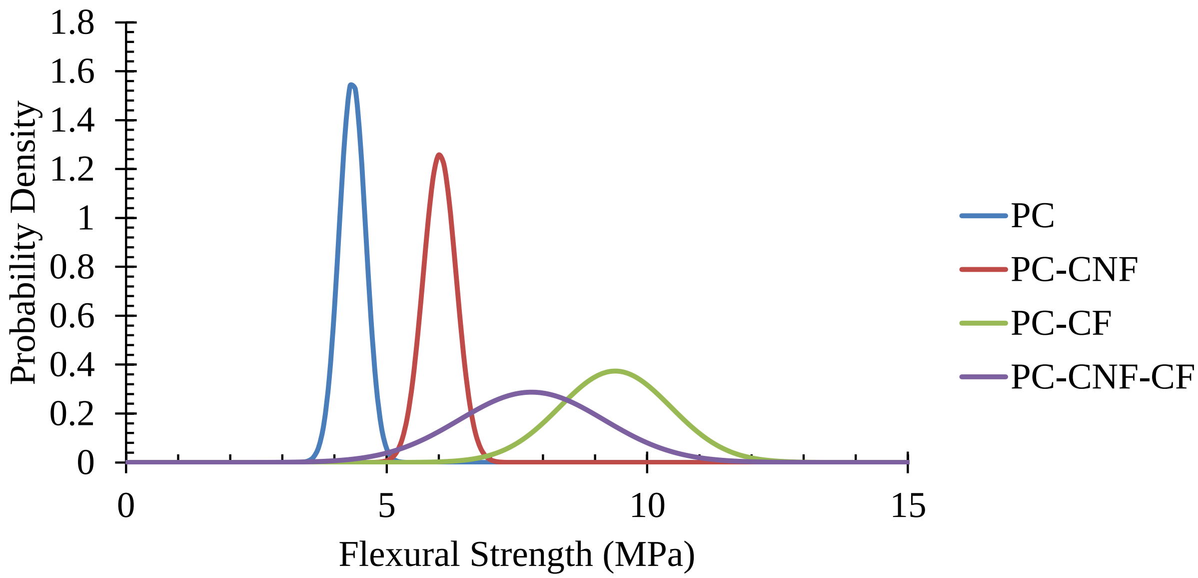

Figure 6.26. Probability density functions of the 28-day flexural strength of the CNF, CF, and hybrid CNF/CF cement-based composites assuming normal distributions (raw data included in Appendix D).

6.4. Conclusions

Hybrid CNF/CF cement-based composites were evaluated to determine the hybrid effects of CNFs and CFs on the microstructure and micro- and macromechanical properties of the composites. The following conclusions could be drawn:

- CNFs were found unequally distributed in the cement paste and as individual fibers and CNF agglomerates no matter if they were used alone or with CFs as hybrid fiber reinforcement.
- The total areal coverage of CNF agglomerates greater than 0.007 mm^2 in size was reduced by nearly 28% in the presence CFs in cement-based composites. The reduction was especially noticed within the upper 2 mm of the cross-section because of a reduction in CNF movement with the bleed water during curing due to a reduced workability of the

fresh cement paste. Although the areal coverage was reduced with CFs, the CNFs had a tendency to form larger agglomerates in the presence of CFs.

- The hybridization of CNFs and CFs allowed a greater percentage of high stiffness C-S-H at the expense of low stiffness C-S-H compared to CNFs and CFs used alone in cement-based composites. A 14% reduction in the percentage of low stiffness C-S-H was seen when CNFs and CFs were used together as determined by the Gaussian mixture model of the modulus values compared to a 6% and 10% reduction when CNFs and CFs were used alone.
- In contrast with the micromechanical properties, no hybrid effect of the CNFs and CFs was found on the compressive or flexural properties of cement-based material. The hybrid CNF/CF reinforcement allowed for increases in the compressive strength and toughness over the control composite of up to 45% and 60%, respectively, but greater increases were seen for the cement paste with CFs alone. Similarly, the flexural strength, strain capacity, and toughness of hybrid CNF/CF cement-based composites increased compared to the control composite by up to 100%, 83%, and 290%, respectively, but greater increases were seen for the cement paste with CFs alone.

CHAPTER 7

SUMMARY AND FUTURE WORK

7.1. Summary

A summary of the findings of this dissertation by chapter is included below.

Chapter 3. CNF dispersing methods including various combinations of covalent, non-covalent, and mechanical methods were investigated in solution using visual inspection and optical microscopy and in cement-based composites using optical microscopy and SEM. It was found that the dispersion of CNFs in an aqueous solution was improved when dispersing agents including P-HRWR, N-HRWR, and AE were used, but was best improved when P-HRWR was used. The use of surface treatment with HNO_3 with P-HRWR further improved the dispersion of CNFs in aqueous solution, but the use of surface treatment with HNO_3 alone was not as efficient at dispersing the CNFs as the dispersing agents. P-HRWR, N-HRWR, and AE were also found to improve the dispersion of CNFs in simulated cement pore water, but the suspension was not stable due to the high pH and ionic strength of the solution with settlement occurring within 30 minutes. CNF reagglomeration occurred in cement pastes during the mixing and curing process regardless of the dispersion method used. Therefore, the dispersion in aqueous solution was not indicative of the subsequent dispersion and distribution of CNFs in cement pastes. The final dispersion state of the CNFs in cement paste was the result of the competition between: (i) the tendency of CNFs to migrate towards each other or existing agglomerates due to Brownian motion and van der Waals interactions during cement mixing, (ii) the influence of the high pH and ionic strength of the cement paste medium on altering the surface properties of the CNFs, resulting in a greater propensity for loss of individual CNFs and rebundling, and (iii) the effect of mechanical mixing, further increasing the probability of CNF agglomerates or individual CNFs to come in contact with each other.

Chapter 4. The micromechanical properties of cement pastes containing CNFs were investigated including the cement phases in and around CNF agglomerates using nanoindentation coupled with SEM/EDS. The main peak of the histogram of modulus values obtained from nanoindentation was shifted toward increased modulus values when CNFs were used in cement paste. The coupling of nanoindentation with SEM/EDS indicated an influence of the CNFs on the C-S-H phase of the cement was responsible for the shift in the main peak of the histogram of modulus values. By estimating the distribution of the modulus values of the C-S-H phase using a Gaussian mixture model with three (3) Gaussian components, it was determined that the CNFs were causing the formation of a higher percentage of high stiffness C-S-H at the expense of low stiffness C-S-H. The percentage of low stiffness C-S-H present in the cement-based composite with CNFs was found to be decreased by 6% as estimated by the Gaussian mixture model of the modulus values. The cement hydration products in and around CNF agglomerates were found to have significantly lower micromechanical properties than the hydration products throughout the paste indicating the CNF agglomerates acted as flaws in the paste. In addition, the edge of the CNF agglomerates had lower micromechanical properties than the cement matrix away from the agglomerate indicating that there was no reinforcing effect around the edge of the CNF agglomerates.

Chapter 5. Traditional testing methods including uniaxial compression, splitting tension, and three-point bending were used to determine the effect of dispersion state of CNFs and CNF loading on the macromechanical properties of cement-based composites including the strength, modulus, strain capacity, and toughness values. The dispersion state of the CNFs was found to impact the 7-day flexural strength of cement pastes with only the CNFs dispersed with P-HRWR showing improvements (increases of over 11% with 0.2 wt% CNFs). Surface treatment of the CNFs with HNO_3 further increased the 7-day flexural strength with 0.2 wt% of CNFs increasing the 7-day flexural strength of cement paste by 22%. The CNFs were found to influence the structural integrity of cement-based composites both with and without the addition of silica fume with increasing CNF loadings showing increased structural integrity. In addition, the 7- and 28-day flexural strength of portland cement pastes showed improvements with increasing CNF loadings including an increase over 60% for the 1 wt% CNF loading at both 7- and 28-days. Portland cement pastes also showed increases of over 20% in the 7-day flexural modulus and increases in the 28-day flexural strain capacity and 7- and 28-day flexural toughness for most CNF loadings. The addition of silica fume to cement pastes with CNFs caused increases in the flexural strength to not be realized at 7 days but be up to 48% at 28 days due to the delayed pozzolanic reaction of the silica fume. In cement pastes both with and without silica fume, the improvements in the flexural properties were seen regardless of the presence of poorly distributed and agglomerated CNFs because the weak zones formed in the composites by the poorly distributed and agglomerated CNFs were thought to be partially counterbalanced by the presence of an effective fraction of CNFs.

Chapter 6. The hybridization of CNFs and CFs in cement pastes was investigated. The dispersion and distribution of the CNFs in the cement paste was evaluated in relation to the CFs using optical microscopy, and the multiscale mechanical properties of the hybrid CNF/CF cement-based composites were determined using nanoindentation coupled with SEM/EDS and traditional macromechanical testing methods including uniaxial compression and three-point bending. The total areal coverage of CNF agglomerates at the surface of a representative cross-section of cement paste was reduced by nearly 28% with the addition of CFs especially in the upper 2 mm of the cross-section because of a reduction in the migration of the CNFs with the bleed water due to a reduced workability of the fresh cement paste when CFs were present. Although the total areal coverage of CNF agglomerates at the surface of a cross-section was reduced in the presence of CFs, the CNFs had a greater tendency to form larger size agglomerates. Estimation of the distribution of modulus values determined by nanoindentation coupled with SEM/EDS for the C-S-H phase in hybrid CNF/CF cement-based composites using a Gaussian mixture model with three (3) Gaussian components indicated that a hybrid effect of the CNFs and CFs were leading to the formation of a higher percentage of high stiffness C-S-H in the hybrid CNF/CF cement-based composite compared to the cement pastes with CNFs and CFs alone. The reduction in the percentage of low stiffness C-S-H present in the hybrid CNF/CF cement-based composites was 14% as determined by the Gaussian mixture model of the modulus values compared to 6% and 10% for the composites with CNFs and CFs alone, respectively. In contrast with results seen on the mechanical properties at the microscale, no evidence of a hybrid effect from the CNFs and CFs was found on the macroscale for the compressive or flexural properties. The hybrid CNF/CF reinforcement allowed for increases in the compressive strength and toughness over the control composite of up to 45% and 60%, respectively, but greater increases were seen for the cement paste with CFs alone. Similarly, the flexural strength, strain capacity, and toughness of hybrid CNF/CF cement-based composites increased compared to the control composite by up to 100%, 83%, and 290%, respectively, but greater increases were seen for the cement paste with CFs alone.

Conclusions. CNFs have been shown to have potential to be excellent nanoscale fiber reinforcement for cement-based composites. However, the dispersion of the CNFs in cement-based composites was found to be influenced by the high pH and ionic strength of the cement paste medium and the tendency of the CNFs to migrate towards each other or existing agglomerates during mixing and curing. Even with the presence of microscale CNF agglomerates, improvements in the mechanical properties of cement-based composites were realized on the micro- and macroscale. On the microscale, a higher percentage of high stiffness C-S-H at the expense of low stiffness C-S-H was seen when CNFs were present, while on the macroscale, the flexural properties and structural integrity after compressive testing of the cement-based composites were improved by CNFs. In hybrid CNF/CF cement-based composites, a hybrid effect of CNFs and CFs was found for the micromechanical properties of cement-based composites with a higher percentage of high stiffness C-S-H being formed at the expense of low stiffness C-S-H compared to composites with CNFs and CFs alone, but no hybrid effect of the CNFs and CFs was found for the macromechanical properties.

7.2. Future Work

Results from this research showed that the use of CNFs as nanoscale fiber reinforcement in cement-based composites is a promising avenue for improving cement-based composites. The use of CNFs as nanoscale fiber reinforcement in cement-based composites could allow for cement-based materials that could be tailored for many applications including damage/strain sensing structural elements, in-motion traffic monitoring roadways, electromagnetic field-shielding structural elements, and self-deicing pavements. However, many scientific questions need to be answered to make these applications possible. Questions that this research has led to include but are not limited to the following:

- How can the reagglomeration of CNFs in cement-based composites due to the mixing process and the high pH and ionic strength of the cement-based medium be mitigated/reduced?
- What is the relationship between the micromechanical properties of the cement phases and the macroscale mechanical properties of the composite? In particular, what is the effect of the percentages of high stiffness C-S-H and low stiffness C-S-H on the composite macromechanical properties?
- Can the percentage of CNFs be tailored to optimize the percentage of high stiffness C-S-H formed and what will the effects of this optimization mean for the macromechanical properties?
- Can mechanical improvements be realized with the hybridization of the CNFs with other fiber reinforcement such that fiber "synergy" is seen?
- Can the reinforcing ability of the CNFs be maintained in cement-based composites for the life of the structural elements (i.e., what is the long-term durability and performance of cement-based composites containing CNFs)?

REFERENCES

[1] Report card for America's infrastructure, in: A.S.o.C. Engineers (Ed.), American Society of Civil Engineers, Reston, Virginia, 2009.

[2] Grand challenges for engineers, in: N.A.o. Engineering (Ed.), National Academy of Sciences, Washington, D.C., 2008.

[3] S. Mindess, J.F. Young, D. Darwin, Concrete, 2nd ed., Pearson Educational, Inc., Upper Saddle River, New Jersey, 2003.

[4] G. Hüsken, M. Hunger, H.J.H. Brouwers, Experimental study of photocatalytic concrete products for air purification, Building and Environment, 44 (2009) 2463-2474.

[5] M. Chen, J.-W. Chu, NOx photocatalytic degradation on active concrete road surface — from experiment to real-scale application, Journal of Cleaner Production, 19 (2011) 1266-1272.

[6] Z. Zhou, G. Ou, Y. Hang, G. Chen, J. Ou, Research and development of plastic optical fiber based smart transparent concrete, Society of Photo-Optical Instrumentation Engineers, Bellingham, WA, ETATS-UNIS, 2009.

[7] B. Chen, J. Liu, Damage in carbon fiber-reinforced concrete, monitored by both electrical resistance measurement and acoustic emission analysis, Construction and Building Materials, 22 (2008) 2196-2201.

[8] D.D.L. Chung, Damage in cement-based materials, studied by electrical resistance measurement, Materials Science and Engineering: R: Reports, 42 (2003) 1-40.

[9] R.F. Zollo, Fiber-reinforced concrete: an overview after 30 years of development, Cement and Concrete Composites, 19 (1997) 107-122.

[10] S. Mindess, Thirty years of fibre reinforced concrete research at the UWM British Colombia, in: T.R.N. Rudolph N. Kraus, Peter Claisse, Sadeghi-Pouya (Ed.) International Conference on sustainable construction materials and technologies, UW Milwaukee CBU, Coventry, 2007, pp. 259-268.

[11] S.P. Shah, K.G. Kuder, B. Mu, Fiber-reinforced cement based composites: a forty year odyssey, in: M.d. Prisco, R. Felicetti, G.A. Plizzari (Eds.) 6th RILEM Symposium on Fibre-Reinforced Concretes (FRC), RILEM Publications SARL, Varenna, Italy, 2004, pp. 28.

[12] D.D.L. Chung, Cement reinforced with short carbon fibers: a multifunctional material, Composites Part B: Engineering, 31 (2000) 511-526.

[13] S. Wansom, N.J. Kidner, L.Y. Woo, T.O. Mason, AC-impedance response of multi-walled carbon nanotube/cement composites, Cement and Concrete Composites, 28 (2006) 509-519.

[14] J. Luo, Z. Duan, The dispersivity of multi-walled carbon nanotubes (NMWTs) and pressure-sensitive property of NMWTs reinforced cement composite, Advanced Materials Research, 60-61 (2009) 475-479.

[15] G.Y. Li, P.M. Wang, X. Zhao, Pressure-sensitive properties and microstructure of carbon nanotube reinforced cement composites, Cement and Concrete Composites, 29 (2007) 377-382.

[16] X. Yu, E. Kwon, A carbon nanotube/cement composite with piezoresistive properties, Smart Materials and Structures, 18 (2009) 055010.

[17] D. Gao, et al., Electrical resistance of carbon-nanofiber concrete, Smart Materials and Structures, 18 (2009) 095039.

[18] X. Fu, D.D.L. Chung, Submicron carbon filament cement-matrix composites for electromagnetic interference shielding, Cement and Concrete Research, 26 (1996) 1467-1472.

[19] X. Fu, D.D.L. Chung, Submicron-diameter-carbon-filament cement-matrix composites, Carbon, 36 (1998) 459-462.

[20] S. Wen, D.D.L. Chung, Carbon fiber-reinforced cement as a strain-sensing coating, Cement and Concrete Research, 31 (2001) 665-667.

[21] X. Fu, D.D.L. Chung, Self-monitoring of fatigue damage in carbon fiber reinforced cement, Cement and Concrete Research, 26 (1996) 15-20.

[22] M. Sun, Q. Liu, Z. Li, Y. Hu, A study of piezoelectric properties of carbon fiber reinforced concrete and plain cement paste during dynamic loading, Cement and Concrete Research, 30 (2000) 1593-1595.

[23] S. Wen, D.D.L. Chung, Self-sensing of flexural damage and strain in carbon fiber reinforced cement and effect of embedded steel reinforcing bars, Carbon, 44 (2006) 1496-1502.

[24] D.-M. Bontea, D.D.L. Chung, G.C. Lee, Damage in carbon fiber-reinforced concrete, monitored by electrical resistance measurement, Cement and Concrete Research, 30 (2000) 651-659.

[25] P.-W. Chen, D.D.L. Chung, Carbon-fiber-reinforced concrete as an intrinsically smart concrete for damage assessment during dynamic loading, Journal of the American Ceramic Society, 78 (1995) 816-818.

[26] B. Han, X. Yu, E. Kwon, A self-sensing carbon nanotube/cement composite for traffic monitoring, Nanotechnology, 20 (2009) 445501.

[27] Z.-Q. Shi, D.D.L. Chung, Carbon fiber-reinforced concrete for traffic monitoring and weighing in motion, Cement and Concrete Research, 29 (1999) 435-439.

[28] L.X. Zheng, Z.Q. Li, X.H. Song, Corrosion monitoring of rebar by compression sensitivity of CFRC, Journal of Experimental Mechnics, 19 (2004) 206–210.

[29] D.D.L. Chung, Electromagnetic interference shielding effectiveness of carbon materials, Carbon, 39 (2001) 279-285.

[30] C.Y. Tuan, Implementation of concductive concrete for deicing (Roca Bridge), in, University of Nebraska-Lincoln, 2008, pp. 154.

[31] N. Banthia, R. Gupta, Hybrid fiber reinforced concrete (HyFRC): fiber synergy in high strength matrices, Materials and Structures, 37 (2004) 707-716.

[32] E.T. Thostenson, Z. Ren, T.-W. Chou, Advances in the science and technology of carbon nanotubes and their composites: a review, Composites Science and Technology, 61 (2001) 1899-1912.

[33] K.P. Chong, E.J. Garboczi, Smart and designer structural material systems, Progress in Structural Engineering and Materials, 4 (2002) 417-430.

[34] P.M. Ajayan, T.W. Ebbesen, Nanometre-size tubes of carbon, Reports on Progress in Physics, 60 (1997) 1025.

[35] J.M. Makar, J.J. Beaudoin, Carbon nanotubes and their application in the construction industry, in: 1st International Symposium on Nanotechnology in Construction, Paisley, Scotland, 2003, pp. 331-341.

[36] A. Cwirzen, K. Habermehl-Cwirzen, V. Penttala, Surface decoration of carbon nanotubes and mechanical properties of cement/carbon nanotube composites, Anglais, 20 (2008) 9.

[37] X. Jiang, T.L. Kowald, T. Staedler, R.H.F. Trettin, Carbon nanotubes as a new reinforcement material for modern cement-based binders, in: Y.d. Miguel, A. Porro, P.J.M. Bartos (Eds.) NICOM 2: 2nd International Symposium on Nanotechnology in Construction, RILEM Publications SARL, Bilbao, Spain, 2006, pp. 209 - 213.

[38] T. Kowald, Influence of surface-modified carbon nanotubes on ultra-high performance concrete, in: M. Schmidt, E. Fehling, C. Geisenhanslueke (Eds.) International Symposium on Ultra-High Performance Concrete, Kassel University Press GmbH, Kassel, Germany, 2004, pp. 868.

[39] G.Y. Li, P.M. Wang, X. Zhao, Mechanical behavior and microstructure of cement composites incorporating surface-treated multi-walled carbon nanotubes, Carbon, 43 (2005) 1239-1245.

[40] S. Musso, J.-M. Tulliani, G. Ferro, A. Tagliaferro, Influence of carbon nanotubes structure on the mechanical behavior of cement composites, Composites Science and Technology, 69 (2009) 1985-1990.

[41] F. Sanchez, Carbon nanofibers/cement composites: challenges and promises as structural materials, [Special issue on Nanotechnology for Structural Materials; Guest Editors: MR Taha and M Al-Haik], 3 (2009) in press.

[42] F. Sanchez, L. Zhang, C. Ince, Multi-scale performance and durability of carbon nanofiber/cement composites, in: P.J.M.B. Zdeněk Bittnar, Jiří Němeček, Vít Šmilauer and Jan Zeman (Ed.) Nanotechnology in Construction 3, Springer Berlin Heidelberg, 2009, pp. 345-350.

[43] J. Luo, Z. Duan, H. Li, The influence of surfactants on the processing of multi-walled carbon nanotubes in reinforced cement matrix composites, physica status solidi (a), 206 (2009) 2783-2790.

[44] G. Yakovlev, J. Keriene, A. Gailius, I. Girniene, Cement based foam concrete reinforced by carbon nanotubes, Materials Science, 12 (2006) 147-151.

[45] A. Cwirzen, K. Habermehl-Cwirzen, A.G. Nasibulin, E.I. Kaupinen, P.R. Mudimela, V. Penttala, SEM/AFM studies of cementitious binder modified by MWCNT and nano-sized Fe needles, Materials Characterization, 60 (2009) 735-740.

[46] C. Gay, F. Sanchez, Performance of carbon nanofibers/cementitious composites with a high-range water-reducer, Transportation Research Record: Journal of the Transportation Research Board, 2 (2010) 109-113.

[47] M.S. Konsta-Gdoutos, Z.S. Metaxa, S.P. Shah, Multi-scale mechanical and fracture characteristics and early-age strain capacity of high performance carbon nanotube/cement nanocomposites, Cement and Concrete Composites, 32 (2010) 110-115.

[48] Z.S. Metaxa, M.S. Konsta-Gdoutos, S.P. Shah, Carbon nanofiber-reinforced cement-based materials, Transportation Research Record: Journal of the Transportation Research Board, 2 (2010) 114-118.

[49] Z.S. Metaxa, M.S. Konsta-Gdoutos, S.P. Shah, Mechanical properties and nanostructure of cement-based materials reinforced with carbon nanofibers and polyvinyl alcohol microfibers, in: ACI Special Publication, 2010, pp. 115-124.

[50] S.P. Shah, M.S. Konsta-Gdoutos, Z.S. Metaxa, P. Mondal, Nanoscale modification of cementitious materials, in: P.J.M.B. Zdeněk Bittnar, Jiří Němeček, Vít Šmilauer and Jan Zeman (Ed.) Nanotechnology in Construction 3, Springer Berlin Heidelberg, 2009, pp. 125-130.

[51] A. Yazdanbakhsh, Z. Grasley, B. Tyson, R. Al-Rub, Distribution of carbon nanofibers and nanotubes in cementitious composites, Transportation Research Record: Journal of the Transportation Research Board, 2 (2010) 89-95.

[52] B.M. Tyson, R.K. Abu Al-Rub, A. Yazdanbakhsh, Z. Grasley, Carbon nanotubes and carbon nanofibers for enhancing the mechanical properties of nanocomposite cementitious materials, J Mater Civ Eng, 23 (2011) 1028-1035.

[53] J.M. Makar, Carbon nanotube/cement composite materials, in: Carbon Nanotubes: Synthesis, Properties and Applications (Book Chapter), 2009.

[54] J. Makar, J. Margeson, J. Luh, Carbon nanotube/cement composites -- early results and potential applications, in: 3rd International Conference on Construction Materials: Performance, Innovations, and Structural Implications, Vancouver, B.C., 2005, pp. 1-10.

[55] I. Campillo, J. Dolado, A. Porro, High-performance nanostructured materials for construction, in: P. Bartos, J. Hughes, P. Trtik, W. Zhu (Eds.) 1st International Symposium on Nanotechnology in Construction, The Royal Society of Chemistry, Paisley, Scotland, 2003, pp. 215-225.

[56] A. Chaipanich, T. Nochaiya, W. Wongkeo, P. Torkittikul, Compressive strength and microstructure of carbon nanotubes-fly ash cement composites, Materials Science and Engineering: A, 527 (2010) 1063-1067.

[57] L.Y. Chan, B. Andrawes, Finite element analysis of carbon nanotube/cement composite with degraded bond strength, Computational Materials Science, 47 (2010) 994-1004.

[58] Z. Duan, J. Luo, Effect of multi-walled carbon nanotubes on the vibration-reduction behavior of cement, in: S. Du, J. Leng, A.K. Asundi (Eds.), SPIE, Harbin, China, 2007, pp. 64230R-64236.

[59] M.S. Konsta-Gdoutos, Z.S. Metaxa, S.P. Shah, Nanoimaging of highly dispersed carbon nanotube reinforced cement based materials, in: R. Gettu (Ed.) BEFIB 2008: 7th RILEM International Symposium on Fibre Reinforced Concrete, RILEM Publications SARL, Chennai, India, 2008, pp. 125-131.

[60] T. Kowald, R. Trettin, Improvement of cementitious binders by multi-walled carbon nanotubes, in: P.J.M.B. Zdeněk Bittnar, Jiří Němeček, Vít Šmilauer and Jan Zeman (Ed.) Nanotechnology in Construction 3, Springer Berlin Heidelberg, 2009, pp. 261-266.

[61] A. Cwirzen, K. Habermehl-Cwirzen, L.I. Nasibulina, S.D. Shandakov, A.G. Nasibulin, E.I. Kauppinen, P.R. Mudimela, V. Penttala, CHH cement composite, in: P.J.M.B. Zdeněk Bittnar, Jiří Němeček, Vít Šmilauer and Jan Zeman (Ed.) Nanotechnology in Construction 3, Springer Berlin Heidelberg, 2009, pp. 181-185.

[62] P.R. Mudimela, L.I. Nasibulina, A.G. Nasibulin, A. Cwirzen, M. Valkeapää, K. Habermehl-Cwirzen, J.E.M. Malm, M.J. Karppinen, V. Penttala, T.S. Koltsova, O.V. Tolochko, E.I. Kauppinen, Synthesis of carbon nanotubes and nanofibers on silica and cement matrix materials, Journal of Nanomaterials, 2009 (2009) 4 pages.

[63] A.G. Nasibulin, et al., A novel cement-based hybrid material, New Journal of Physics, 11 (2009) 023013.

[64] F. Sanchez, C. Ince, Microstructure and macroscopic properties of hybrid carbon nanofiber/silica fume cement composites, Composites Science and Technology, 69 (2009) 1310-1318.

[65] J. Makar, The effect of SWCNT and other nanomaterials on cement hydration and reinforcement in: K. Gopalakrishnan, B. Birgisson, P. Taylor, N.O. Attoh-Okine (Eds.) Nanotechnology in Civil Infrastructure, Springer Berlin Heidelberg, 2011, pp. 103-130.

[66] Y.S.d. Ibarra, J.J. Gaitero, E. Erkizia, I. Campillo, Atomic force microscopy and nanoindentation of cement pastes with nanotube dispersions, physica status solidi (a), 203 (2006) 1076-1081.

[67] J. Vera-Agullo, V. Chozas-Ligero, D. Portillo-Rico, M.J. García-Casas, A. Gutiérrez-Martínez, J.M. Mieres-Royo, J. Grávalos-Moreno, Mortar and concrete reinforced with nanomaterials, in: P.J.M.B. Zdeněk Bittnar, Jiří Němeček, Vít Šmilauer and Jan Zeman (Ed.) Nanotechnology in Construction 3, Springer Berlin Heidelberg, 2009, pp. 383-388.

[68] T.L. Anderson, Fracture Mechanics, CRC Press, Boca Raton, 1991.

[69] G.Y. Wu, Steel fiber reinforced heat resistant pavement, ACI SP 105, 105 (1987) 323-350.

[70] W. Yao, J. Li, K. Wu, Mechanical properties of hybrid fiber-reinforced concrete at low fiber volume fraction, Cement and Concrete Research, 33 (2003) 27-30.

[71] M. Hsie, C. Tu, P.S. Song, Mechanical properties of polypropylene hybrid fiber-reinforced concrete, Materials Science and Engineering: A, 494 (2008) 153-157.

[72] C. Qian, P. Stroeven, Fracture properties of concrete reinforced with steel–polypropylene hybrid fibres, Cement and Concrete Composites, 22 (2000) 343-351.

[73] N. Banthia, N. Nandakumar, Crack growth resistance of hybrid fiber reinforced cement composites, Cement and Concrete Composites, 25 (2003) 3-9.

[74] J.S. Lawler, D. Zampini, S.P. Shah, Microfiber and macrofiber hybrid fiber-reinforced concrete, ASCE, 2005.

[75] P.K. Nelson, V.C. Li, T. Kamada, Fracture toughness of microfiber reinforced cement composites, J Mater Civ Eng, 14 (2002) 384-391.

[76] E.T. Dawood, M. Ramli, High strength characteristics of cement mortar reinforced with hybrid fibres, Construction and Building Materials, 25 (2011) 2240-2247.

[77] J. Lawler, T. Wilhelm, D. Zampini, S. Shah, Fracture processes of hybrid fiber-reinforced mortar, Materials and Structures, 36 (2003) 197-208.

[78] E. Parant, R. Pierre, F.L. Maou, Durability of a multiscale fibre reinforced cement composite in aggressive environment under service load, Cement and Concrete Research, 37 (2007) 1106-1114.

[79] E. Parant, P. Rossi, C. Boulay, Fatigue behavior of a multi-scale cement composite, Cement and Concrete Research, 37 (2007) 264-269.

[80] P. Rossi, Development of new cement composite materials for construction, Proceedings of the Institution of Mechanical Engineers, Part L: Journal of Materials: Design and Applications, 219 (2005) 67-74.

[81] P. Rossi, A. Arca, E. Parant, P. Fakhri, Bending and compressive behaviours of a new cement composite, Cement and Concrete Research, 35 (2005) 27-33.

[82] P. Rossi, High performance multi-modal fiber reinforced cement composite (HPMFRCC); the LCPC experience, ACI Materials Journal, 94 (1997) 478-483.

[83] C. Boulay, P. Rossi, J.L. Tailhan, Uniaxial tensile test on a new cement composite having a hardening behavior, in: Sixth RILEM Symposium on Fiber Reinforced Concrete (FRC) (BEFIB 2004), Varenna-Lecco, Italy, 2004.

[84] P.S. Song, J.C. Wu, S. Hwang, B.C. Sheu, Statistical analysis of impact strength and strength reliability of steel–polypropylene hybrid fiber-reinforced concrete, Construction and Building Materials, 19 (2005) 1-9.

[85] A. Sivakumar, M. Santhanam, Mechanical properties of high strength concrete reinforced with metallic and non-metallic fibres, Cement and Concrete Composites, 29 (2007) 603-608.

[86] I. Kang, Y.Y. Heung, J.H. Kim, J.W. Lee, R. Gollapudi, S. Subramaniam, S. Narasimhadevara, D. Hurd, G.R. Kirikera, V. Shanov, M.J. Schulz, D. Shi, J. Boerio, S. Mall, M. Ruggles-Wren, Introduction to carbon nanotube and nanofiber smart materials, Composites Part B: Engineering, 37 (2006) 382-394.

[87] A comparison of carbon nanotubes and carbon nanofibers, in, Pyrograf Products, Inc.

[88] P.M. Ajayan, Nanotubes from carbon, Chemical Reviews, 99 (1999) 1787-1800.

[89] X. Gong, J. Liu, S. Baskaran, R.D. Voise, J.S. Young, Surfactant-assisted processing of carbon nanotube/polymer composites, Chemistry of Materials, 12 (2000) 1049-1052.

[90] L. Vaisman, H.D. Wagner, G. Marom, The role of surfactants in dispersion of carbon nanotubes, Advances in Colloid and Interface Science, 128-130 (2006) 37-46.

[91] X.-L. Xie, Y.-W. Mai, X.-P. Zhou, Dispersion and alignment of carbon nanotubes in polymer matrix: A review, Materials Science and Engineering: R: Reports, 49 (2005) 89-112.

[92] J.J. Beaudoin, P. Gu, J. Marchand, B. Tamtsia, R.E. Myers, Z. Liu, Solvent replacement studies of hydrated portland cement systems: the role of calcium hydroxide, Advanced Cement Based Materials, 8 (1998) 56-65.

[93] M.S. Dresselhaus, G. Dresselhaus, R. Saito, A. Jorio, Raman spectroscopy of carbon nanotubes, Physics Reports, 409 (2005) 47-99.

[94] D.A. Heller, P.W. Barone, J.P. Swanson, R.M. Mayrhofer, M.S. Strano, Using raman spectroscopy to elucidate the aggregation state of single-walled carbon nanotubes, The Journal of Physical Chemistry B, 108 (2004) 6905-6909.

[95] K. Yurekli, C.A. Mitchell, R. Krishnamoorti, Small-angle neutron scattering from surfactant-assisted aqueous dispersions of carbon nanotubes, Journal of the American Chemical Society, 126 (2004) 9902-9903.

[96] V.C. Moore, M.S. Strano, E.H. Haroz, R.H. Hauge, R.E. Smalley, J. Schmidt, Y. Talmon, Individually suspended single-walled carbon nanotubes in various surfactants, Nano Letters, 3 (2003) 1379-1382.

[97] P. Acker, Micromechanical analysis of creep and shrinkage mechanisms, in: F.-J. Ulm, Bažant, Z.P. and Wittmann F.H. (Ed.) Creep, Shrinkage, and Durability Mechanics of Concrete and Other Quasi-Brittle Materials, Elsevier, London, 2001, pp. 15–25.

[98] P. Acker, Swelling, shrinkage and creep: a mechanical approach to cement hydration, Materials and Structures, 37 (2004) 237-243.

[99] K. Velez, S. Maximilien, D. Damidot, G. Fantozzi, F. Sorrentino, Determination by nanoindentation of elastic modulus and hardness of pure constituents of portland cement clinker, Cement and Concrete Research, 31 (2001) 555-561.

[100] G. Constantinides, F.-J. Ulm, The effect of two types of C-S-H on the elasticity of cement-based materials: results from nanoindentation and micromechanical modeling, Cement and Concrete Research, 34 (2004) 67-80.

[101] G. Constantinides, F. Ulm, K. Van Vliet, On the use of nanoindentation for cementitious materials, Materials and Structures, 36 (2003) 191-196.

[102] J.J. Hughes, P. Trtik, Micro-mechanical properties of cement paste measured by depth-sensing nanoindentation: a preliminary correlation of physical properties with phase type, Materials Characterization, 53 (2004) 223-231.

[103] G. Constantinides, F.-J. Ulm, The nanogranular nature of C-S-H, Journal of the Mechanics and Physics of Solids, 55 (2007) 64-90.

[104] P. Mondal, S.P. Shah, L. Marks, A reliable technique to determine the local mechanical properties at the nanoscale for cementitious materials, Cement and Concrete Research, 37 (2007) 1440-1444.

[105] W. Zhu, J.J. Hughes, N. Bicanic, C.J. Pearce, Nanoindentation mapping of mechanical properties of cement paste and natural rocks, Materials Characterization, 58 (2007) 1189-1198.

[106] H.M. Jennings, J.J. Thomas, J.S. Gevrenov, G. Constantinides, F.-J. Ulm, A multi-technique investigation of the nanoporosity of cement paste, Cement and Concrete Research, 37 (2007) 329-336.

[107] L. Sorelli, G. Constantinides, F.-J. Ulm, F. Toutlemonde, The nano-mechanical signature of Ultra High Performance Concrete by statistical nanoindentation techniques, Cement and Concrete Research, 38 (2008) 1447-1456.

[108] J.J. Chen, L. Sorelli, M. Vandamme, F.-J. Ulm, G. Chanvillard, A coupled nanoindentation/SEM-EDS study on low water/cement ratio portland cement paste: evidence for C–S–H/Ca(OH)2 nanocomposites, Journal of the American Ceramic Society, 93 (2010) 1484-1493.

[109] X.H. Wang, S. Jacobsen, J.Y. He, Z.L. Zhang, S.F. Lee, H.L. Lein, Application of nanoindentation testing to study of the interfacial transition zone in steel fiber reinforced mortar, Cement and Concrete Research, 39 (2009) 701-715.

[110] P. Mondal, Nanomechanical properties of cementitious materials, in: Civil and Environmental Engineering, Northwestern University, Evanston, IL, 2008, pp. 185.

[111] P. Mondal, S.P. Shah, L.D. Marks, Nanomechanical properties of interfacial transition zone, in: Z. Bittnar, P.J.M. Bartos, J. Něměček, V. Šmilauer, J. Zeman (Eds.) Concrete Nanotechnology in Construction 3, Springer Berlin Heidelberg, 2009, pp. 315-320.

[112] S.P. Shah, M.S. Konsta-Gdoutos, Z.S. Metaxa, P. Mondal, Nanoscale modification of cementitious materials, in: Z. Bittnar, P.J.M. Bartos, J. Něměček, V. Šmilauer, J. Zeman (Eds.) Nanotechnology in Construction 3, Springer Berlin Heidelberg, 2009, pp. 125-130.

[113] M.S. Konsta-Gdoutos, Z.S. Metaxa, S.P. Shah, Highly dispersed carbon nanotube reinforced cement based materials, Cement and Concrete Research, 40 (2010) 1052-1059.

[114] T. Kowald, R. Trettin, N. Dorbaum, T. Stadler, X. Jiang, Influence of carbon nanotubes on the micromechanical properties of a model system for ultra-high performance concrete, in: S. Sturwald (Ed.) Second International Symposium on Ultra High Performance Concrete, Kassel University Press GmbH, Kassel, Germany, 2008, pp. 129-134.

[115] A. Bentur, S.T. Wu, N. Banthia, R. Baggott, W. Hansen, A. Katz, C.K.Y. Leung, V.C. Li, B. Mobasher, A.E. Naaman, R. Robertson, P. Soroushian, H. Stang, L.R. Taerwe, Fiber-matrix interfaces in: A.E. Naaman, H.W. Reinhardt (Eds.) Second International Workshop on High Performance Fiber Reinforced Cement Composites, E&FN Spon, University of Michigan and the University of Stuttgart, Ann Arbor, USA, 1995, pp. 149-191.

[116] A. Katz, A. Bentur, Effect of matrix composition on the aging of CFRC, Cement and Concrete Composites, 17 (1995) 87-97.

[117] T.J. Chu, R.E. Robertson, H. Najm, A.E. Naaman, Effects of polyvinyl alcohol on fiber cement interfaces. Part II: Microstructures, Advanced Cement Based Materials, 1 (1994) 122-130.

[118] J.R. Linton, P.L. Berneburg, E.M. Gartner, A. Bentur, Carbon fiber reinforced cement and mortar, in: S. Mindess, J.P. Skalny (Eds.) Fiber Reinforced Cementitious Materials, Materials Research Society, Boston, MA, USA, 1991, pp. 255-264.

[119] T. Ozkan, M. Naraghi, A. Polycarpou, I. Chasiotis, Mechanical strength of pyrolytically stripped and functionalized heat treated vapor grown carbon nanofibers, in: Ith International Congress and Exposition, Society for Experimental Mechanics Inc., Orlando, Florida, 2008.

[120] X. Fu, W. Lu, D.D.L. Chung, Improving the bond strength between carbon fiber and cement by fiber surface treatment and polymer addition to cement mix, Cement and Concrete Research, 26 (1996) 1007-1012.

[121] P. Somasundaran, Encyclopedia of surface and colloid science, in, CRC Press, Boca Raton (FL), 2006, pp. 6675.

[122] R.H. Bogue, The chemistry of portland cement, 2nd ed., Reinhold Pub. Corp., New York, 1955.

[123] B. Lothenbach, F. Winnefeld, Thermodynamic modelling of the hydration of portland cement, Cement and Concrete Research, 36 (2006) 209-226.

[124] K.L. Klein, A.V. Melechko, T.E. McKnight, S.T. Retterer, P.D. Rack, J.D. Fowlkes, D.C. Joy, M.L. Simpson, Surface characterization and functionalization of carbon nanofibers, Journal of Applied Physics, 103 (2008) 061301-061326.

[125] A. Liu, T. Watanabe, I. Honma, J. Wang, H. Zhou, Effect of solution pH and ionic strength on the stability of poly(acrylic acid)-encapsulated multiwalled carbon nanotubes aqueous dispersion and its application for NADH sensor, Biosensors and Bioelectronics, 22 (2006) 694-699.

[126] Y. Marcus, Surface tension of aqueous electrolytes and ions, Journal of Chemical & Engineering Data, 55 (2010) 3641-3644.

[127] F. Hunkeler, The resistivity of pore water solution—a decisive parameter of rebar corrosion and repair methods, Construction and Building Materials, 10 (1996) 381-389.

[128] Y.F. Houst, P. Bowen, F. Perche, A. Kauppi, P. Borget, L. Galmiche, J.-F. Le Meins, F. Lafuma, R.J. Flatt, I. Schober, P.F.G. Banfill, D.S. Swift, B.O. Myrvold, B.G. Petersen, K. Reknes, Design and function of novel superplasticizers for more durable high performance concrete (superplast project), Cement and Concrete Research, 38 (2008) 1197-1209.

[129] F. Sanchez, K. Sobolev, Nanotechnology in concrete–a review, Construction and Building Materials, 24 (2010) 2060-2071.

[130] M. Miller, C. Bobko, M. Vandamme, F.J. Ulm, Surface roughness criteria for cement paste nanoindentation, Cement and Concrete Research, 38 (2008) 467-476.

[131] P. Allison, R. Moser, M. Chandler, T. Rushing, B. Williams, T. Cummins, Nanomechanical structure-property relations of dynamically loaded reactive powder concrete, Surface Effects and Contact Mechanics IX: Computational Methods and Experiments, 62 (2009) 287.

[132] W.C. Oliver, G.M. Pharr, Measurement of hardness and elastic modulus by instrumented indentation: advances in understanding and refinements to methodology, Journal of Materials Research, 19 (2004) 3-20.

[133] P. Trtik, B. Münch, P. Lura, A critical examination of statistical nanoindentation on model materials and hardened cement pastes based on virtual experiments, Cement and Concrete Composites, 31 (2009) 705-714.

[134] F.J. Ulm, M. Vandamme, H.M. Jennings, J. Vanzo, M. Bentivegna, K.J. Krakowiak, G. Constantinides, C.P. Bobko, K.J. Van Vliet, Does microstructure matter for statistical nanoindentation techniques?, Cement and Concrete Composites, 32 (2010) 92-99.

[135] P. Lura, P. Trtik, B. Münch, Validity of recent approaches for statistical nanoindentation of cement pastes, Cement and Concrete Composites, 33 (2011) 457-465.

[136] G. Constantinides, Invariant mechanical properties of calcium-silicate-hydrates (CHS) in cement-based materials: instrumented nanoindentation and microporomechanical modeling, in, Massachusetts Institute of Technology, 2006.

[137] A. Haldar, S. Mahadevan, Probability, reliability, and statistical methods in engineering design, John Wiley, Chichester [England], 2000.

[138] J. Goldstein, D.E. Newbury, D.C. Joy, C.E. Lyman, P. Echlin, E. Lifshin, L. Sawyer, J.R. Michael, Scanning electron microscopy and x-ray microanalysis, 3 ed., Springer, New York, 2003.

[139] J. Pouchou, F. Pichoir, A new model for quantitative x-ray microanalysis. I.--application to the analysis of homogeneous samples, Recherche Aerospatiale, (1984) 167-192.

[140] H.F.W. Taylor, Cement chemistry, Thomas Telford, London, 2004.

[141] D. Davydov, M. Jirásek, L. Kopecký, Critical aspects of nano-indentation technique in application to hardened cement paste, Cement and Concrete Research, 41 (2011) 20-29.

[142] T. Powers, T. Brownyard, Studies of the physical properties of hardened cement paste (nine parts), Journal of the American Concrete Institute, 43 (1946).

[143] Z. Metaxa, M. Konsta-Gdoutos, S. Shah, Carbon nanotubes reinforced concrete, 2009.

[144] Z.S. Metaxa, M.S. Konsta-Gdoutos, S.P. Shah, Crack free concrete made with nanofiber reinforcement, in: Developing a Research Agenda for Transportation Infrastructure Preservation and Renewal Conference, Washington, D.C., 2009.

[145] S. Shah, M. Konsta-Gdoutos, Z. Metaxa, Advanced cement based nanocomposites, in: E.E. Gdoutos, A.N. Kounadis (Eds.) Recent Advances in Mechanics, Springer, 2011, pp. 313-327.

[146] T.K. Moon, The expectation-maximization algorithm, Signal Processing Magazine, IEEE, 13 (1996) 47-60.

[147] B.W. Silverman, Density estimation for statistics and data analysis, Chapman & Hall/CRC, 1986.

[148] L.I. Nasibulina, I.V. Anoshkin, A.G. Nasibulin, A. Cwirzen, V. Penttala, E.I. Kauppinen, Effect of carbon nanotube aqueous dispersion quality on mechanical properties of cement composite, Journal of Nanomaterials, 2012 (2012).

[149] K.L. Lu, R.M. Lago, Y.K. Chen, M.L.H. Green, P.J.F. Harris, S.C. Tsang, Mechanical damage of carbon nanotubes by ultrasound, Carbon, 34 (1996) 814-816.

[150] R. Andrews, D. Jacques, D. Qian, T. Rantell, Multiwall carbon nanotubes: synthesis and application, Accounts of Chemical Research, 35 (2002) 1008-1017.

[151] A. Katz, V.C. Li, A. Kazmer, Bond properties of carbon fibers in cementitious matrix, J Mater Civ Eng, 7 (1995) 125-128.

[152] D.D.L. Chung, Review: improving cement-based materials by using silica fume, Journal of Materials Science, 37 (2002) 673-682.

[153] L. Raki, J. Beaudoin, R. Alizadeh, J. Makar, T. Sato, Cement and concrete nanoscience and nanotechnology, Materials, 3 (2010) 918-942.

APPENDIX A

DISPERSION IN SOLUTION DATA

This appendix contains a summary of the data included in the micrograph analysis of the dispersion of CNFs in solution (Figure 3.2). Ten micrographs were analyzed for 15 drops of each solution. The number of particles (individual CNFs or bundles/agglomerates of CNFs) and the total area of CNFs found in each micrograph are given. In addition a summary for all micrographs for each solution is given.

P-HRWR/T-CNF
Total number of CNF particles: 125211.
Total area covered by CNFs: 1.199 mm^2.
Total number of particles per mm^2 of area covered by CNFs: 104400.

Drop 1

Image	Number of Particles	Total Area of CNFs (mm^2)	Number of Particles Per mm^2 of Area Covered by CNFs
1	853	0.00597	142766
2	558	0.00260	214982
3	890	0.00716	124386
4	840	0.00359	234271
5	808	0.00494	163603
6	973	0.00890	109350
7	587	0.01424	41211
8	801	0.00401	199973
9	906	0.00555	163345
10	955	0.00362	264160

Drop 2

Image	Number of Particles	Total Area of CNFs (mm^2)	Number of Particles Per mm^2 of Area Covered by CNFs
1	996	0.00500	199057
2	1044	0.00932	112024
3	1119	0.01153	97087
4	1151	0.01034	111269
5	1228	0.00852	144057
6	1348	0.01215	110933
7	1186	0.01120	105880
8	1321	0.01157	114127
9	1443	0.01050	137450
10	1357	0.01071	126672

Drop 3

Image	Number of Particles	Total Area of CNFs (mm^2)	Number of Particles Per mm^2 of Area Covered by CNFs
1	961	0.00495	194147
2	806	0.00574	140495
3	927	0.00685	135244
4	1059	0.00480	220689
5	975	0.00540	180481
6	856	0.00641	133588
7	1049	0.00909	115436
8	1052	0.01080	97415
9	750	0.00859	87347
10	953	0.01006	94751

Drop 4

Image	Number of Particles	Total Area of CNFs (mm^2)	Number of Particles Per mm^2 of Area Covered by CNFs
1	821	0.00808	101553
2	995	0.00884	112547
3	682	0.00482	141349
4	858	0.00553	155242
5	1097	0.00896	122394
6	1077	0.00903	119307
7	1030	0.00923	111577
8	1048	0.00919	114078
9	1012	0.00942	107387
10	1079	0.00574	187892

Drop 5

Image	Number of Particles	Total Area of CNFs (mm^2)	Number of Particles Per mm^2 of Area Covered by CNFs
1	646	0.01155	55922
2	413	0.00655	63100
3	662	0.01179	56139
4	570	0.01062	53661
5	556	0.00867	64155
6	550	0.01044	52683
7	412	0.00874	47125
8	495	0.01263	39184
9	513	0.01239	41401
10	529	0.01213	43606

Drop 6

Image	Number of Particles	Total Area of CNFs (mm^2)	Number of Particles Per mm^2 of Area Covered by CNFs
1	552	0.00831	66428
2	661	0.00830	79647
3	695	0.00948	73335
4	640	0.00517	123703
5	739	0.00649	113789
6	553	0.00910	60780
7	611	0.01034	59068
8	713	0.01299	54872
9	661	0.01079	61265
10	520	0.00853	60990

Drop 7

Image	Number of Particles	Total Area of CNFs (mm^2)	Number of Particles Per mm^2 of Area Covered by CNFs
1	532	0.00637	83472
2	323	0.01108	29149
3	492	0.00780	63059
4	492	0.01055	46614
5	465	0.00228	203720
6	597	0.00821	72712
7	560	0.00999	56084
8	567	0.00809	70046
9	474	0.00352	134788
10	583	0.00419	139121

Drop 8

Image	Number of Particles	Total Area of CNFs (mm^2)	Number of Particles Per mm^2 of Area Covered by CNFs
1	494	0.00479	103125
2	496	0.00649	76422
3	527	0.00789	66765
4	537	0.01021	52570
5	482	0.00350	137692
6	558	0.00575	96999
7	546	0.00599	91211
8	392	0.01426	27499
9	564	0.00882	63932
10	560	0.00633	88508

Drop 9

Image	Number of Particles	Total Area of CNFs (mm^2)	Number of Particles Per mm^2 of Area Covered by CNFs
1	999	0.00679	147230
2	885	0.00664	133185
3	939	0.00600	156377
4	823	0.00968	84979
5	942	0.00973	96804
6	946	0.00719	131546
7	798	0.00741	107705
8	852	0.00905	94139
9	1011	0.00793	127528
10	761	0.01156	65831

Drop 10

Image	Number of Particles	Total Area of CNFs (mm^2)	Number of Particles Per mm^2 of Area Covered by CNFs
1	898	0.01192	75357
2	644	0.01542	41753
3	970	0.01105	87762
4	848	0.00649	130668
5	1176	0.00936	125662
6	931	0.00593	156942
7	974	0.00957	101752
8	1217	0.00888	137014
9	1219	0.00837	145599
10	1195	0.00847	141048

Drop 11

Image	Number of Particles	Total Area of CNFs (mm^2)	Number of Particles Per mm^2 of Area Covered by CNFs
1	815	0.00573	142119
2	990	0.00638	155292
3	714	0.00336	212196
4	873	0.00742	117687
5	933	0.01065	87623
6	1109	0.00743	149184
7	985	0.01072	91894
8	1083	0.00972	111420
9	808	0.00627	128775
10	725	0.00917	79102

Drop 12

Image	Number of Particles	Total Area of CNFs (mm^2)	Number of Particles Per mm^2 of Area Covered by CNFs
1	853	0.01654	51577
2	929	0.00624	148907
3	819	0.00520	157483
4	786	0.00836	94046
5	887	0.00677	131077
6	704	0.00804	87548
7	830	0.00390	212881
8	854	0.00519	164661
9	439	0.00786	55836
10	946	0.00765	123676

Drop 13

Image	Number of Particles	Total Area of CNFs (mm^2)	Number of Particles Per mm^2 of Area Covered by CNFs
1	788	0.02044	38544
2	885	0.00478	185155
3	1005	0.00727	138275
4	1267	0.00819	154627
5	1119	0.00673	166252
6	1168	0.01302	89684
7	945	0.01463	64595
8	564	0.00486	116007
9	1180	0.00848	139105
10	1015	0.00673	150925

Drop 14

Image	Number of Particles	Total Area of CNFs (mm^2)	Number of Particles Per mm^2 of Area Covered by CNFs
1	1134	0.00541	209763
2	1222	0.00703	173801
3	804	0.00675	119118
4	806	0.00355	227335
5	941	0.00413	227850
6	725	0.01021	71042
7	783	0.00672	116480
8	698	0.00459	152060
9	990	0.00756	131027
10	788	0.00440	178922

Drop 15

Image	Number of Particles	Total Area of CNFs (mm^2)	Number of Particles Per mm^2 of Area Covered by CNFs
1	726	0.00346	210022
2	868	0.00373	232696
3	814	0.00293	277509
4	832	0.00382	217994
5	1121	0.00728	154076
6	996	0.00733	135835
7	527	0.01105	47699
8	923	0.00659	140137
9	1068	0.00791	134967
10	1016	0.00561	180945

P-HRWR/CNF

Total number of CNF particles: 116929.
Total area covered by CNFs: 1.244 mm^2.
Total number of particles per mm^2 of area covered by CNFs: 94027.

Drop 1

Image	Number of Particles	Total Area of CNFs (mm^2)	Number of Particles Per mm^2 of Area Covered by CNFs
1	565	0.00470	120170
2	660	0.00463	142466
3	712	0.00619	114988
4	674	0.00517	130449
5	698	0.00475	146952
6	589	0.00419	140581
7	614	0.00528	116342
8	600	0.00463	129685
9	528	0.00542	97498
10	574	0.00364	157505

Drop 2

Image	Number of Particles	Total Area of CNFs (mm^2)	Number of Particles Per mm^2 of Area Covered by CNFs
1	831	0.00930	89360
2	719	0.00939	76595
3	673	0.00761	88488
4	655	0.00830	78921
5	497	0.00619	80244
6	798	0.00918	86899
7	793	0.00803	98797
8	722	0.00856	84369
9	784	0.01008	77790
10	760	0.00928	81896

Drop 3

Image	Number of Particles	Total Area of CNFs (mm^2)	Number of Particles Per mm^2 of Area Covered by CNFs
1	828	0.00871	95054
2	682	0.01044	65349
3	984	0.00885	111247
4	901	0.00866	104047
5	976	0.00803	121504
6	1017	0.00809	125706
7	1051	0.00642	163638
8	927	0.00830	111735
9	951	0.00567	167821
10	809	0.00685	118066

Drop 4

Image	Number of Particles	Total Area of CNFs (mm^2)	Number of Particles Per mm^2 of Area Covered by CNFs
1	867	0.00878	98740
2	938	0.00751	124956
3	733	0.00682	107509
4	733	0.00807	90857
5	880	0.00645	136531
6	1110	0.00741	149843
7	819	0.00668	122619
8	610	0.00492	124069
9	539	0.00399	135012
10	705	0.00484	145581

Drop 5

Image	Number of Particles	Total Area of CNFs (mm^2)	Number of Particles Per mm^2 of Area Covered by CNFs
1	1196	0.00685	174715
2	895	0.00810	110535
3	989	0.01083	91300
4	985	0.00988	99713
5	954	0.01298	73499
6	1162	0.01110	104719
7	1122	0.00964	116345
8	951	0.01069	89001
9	901	0.00786	114589
10	1034	0.01373	75308

Drop 6

Image	Number of Particles	Total Area of CNFs (mm^2)	Number of Particles Per mm^2 of Area Covered by CNFs
1	1120	0.01026	109175
2	1152	0.01084	106282
3	1064	0.01206	88219
4	1250	0.01034	120940
5	1231	0.01171	105159
6	1078	0.01081	99718
7	957	0.00571	167707
8	1057	0.00641	164885
9	1003	0.00551	182125
10	1029	0.00772	133224

Drop 7

Image	Number of Particles	Total Area of CNFs (mm^2)	Number of Particles Per mm^2 of Area Covered by CNFs
1	829	0.01088	76212
2	882	0.01113	79246
3	975	0.01023	95327
4	922	0.01070	86157
5	1017	0.01093	93059
6	1038	0.00935	110982
7	902	0.01026	87949
8	932	0.00855	108990
9	917	0.01152	79613
10	1110	0.00842	131882

Drop 8

Image	Number of Particles	Total Area of CNFs (mm^2)	Number of Particles Per mm^2 of Area Covered by CNFs
1	581	0.01238	46946
2	608	0.01136	53511
3	447	0.01504	29717
4	882	0.00892	98892
5	520	0.01264	41125
6	622	0.01297	47970
7	489	0.01197	40868
8	418	0.01405	29742
9	477	0.00929	51335
10	523	0.01077	48563

Drop 9

Image	Number of Particles	Total Area of CNFs (mm^2)	Number of Particles Per mm^2 of Area Covered by CNFs
1	523	0.01022	51165
2	842	0.01413	59569
3	814	0.01023	79588
4	332	0.01175	28249
5	698	0.01085	64356
6	813	0.01403	57956
7	768	0.01551	49526
8	613	0.02026	30250
9	741	0.01631	45432
10	543	0.02015	26945

Drop 10

Image	Number of Particles	Total Area of CNFs (mm^2)	Number of Particles Per ^{mm2} of Area Covered by CNFs
1	361	0.00692	52143
2	395	0.00412	95785
3	230	0.00414	55620
4	268	0.00495	54152
5	368	0.00390	94346
6	362	0.00776	46621
7	460	0.01029	44701
8	380	0.00852	44581
9	513	0.00766	66985
10	397	0.00842	47170

Drop 11

Image	Number of Particles	Total Area of CNFs (mm^2)	Number of Particles Per mm^2 of Area Covered by CNFs
1	570	0.00902	63186
2	611	0.00982	62217
3	546	0.00908	60165
4	505	0.01119	45117
5	612	0.01208	50663
6	622	0.00899	69209
7	670	0.01159	57815
8	517	0.01020	50663
9	618	0.01336	46257
10	804	0.00739	108861

Drop 12

Image	Number of Particles	Total Area of CNFs (mm^2)	Number of Particles Per mm^2 of Area Covered by CNFs
1	852	0.00487	174777
2	994	0.00613	162163
3	944	0.00582	162247
4	557	0.00444	125422
5	862	0.00404	213504
6	1070	0.00449	238497
7	706	0.00460	153524
8	900	0.00534	168447
9	989	0.00599	165230
10	1032	0.00513	201282

Drop 13

Image	Number of Particles	Total Area of CNFs (mm^2)	Number of Particles Per mm^2 of Area Covered by CNFs
1	644	0.00334	192645
2	411	0.00266	154650
3	673	0.00260	258681
4	687	0.00631	108832
5	844	0.00498	169372
6	986	0.00696	141574
7	881	0.00601	146482
8	975	0.00447	217955
9	932	0.00700	133117
10	991	0.00680	145682

Drop 14

Image	Number of Particles	Total Area of CNFs (mm^2)	Number of Particles Per mm^2 of Area Covered by CNFs
1	744	0.00899	82802
2	1080	0.00878	122975
3	863	0.00643	134147
4	853	0.00660	129270
5	800	0.00456	175562
6	941	0.00681	138146
7	539	0.00555	97183
8	879	0.00740	118713
9	819	0.00733	111742
10	933	0.01067	87475

Drop 15

Image	Number of Particles	Total Area of CNFs (mm^2)	Number of Particles Per mm^2 of Area Covered by CNFs
1	637	0.00394	161862
2	933	0.00565	165129
3	857	0.00337	253942
4	1024	0.00714	143320
5	609	0.00336	181453
6	966	0.00522	185128
7	1034	0.00578	178857
8	862	0.00420	205360
9	560	0.01565	35780
10	843	0.00697	120989

N-HRWR/CNF
Total number of CNF particles: 15361.
Total area covered by CNFs: 1.265mm^2.
Total number of particles per mm^2 of area covered by CNFs: 12146.

Drop 1

Image	Number of Particles	Total Area of CNFs (mm^2)	Number of Particles Per mm^2 of Area Covered by CNFs
1	211	0.00723	29197
2	169	0.00698	24196
3	203	0.00320	63410
4	194	0.00384	50490
5	181	0.00648	27943
6	97	0.00939	10325
7	197	0.00867	22729
8	152	0.00713	21306
9	238	0.00628	37909
10	210	0.01229	17091

Drop 2

Image	Number of Particles	Total Area of CNFs (mm^2)	Number of Particles Per mm^2 of Area Covered by CNFs
1	166	0.01028	16147
2	245	0.00802	30543
3	216	0.00659	32792
4	178	0.00914	19482
5	219	0.00877	24980
6	127	0.00905	14026
7	98	0.01227	7988
8	84	0.00749	11219
9	99	0.01251	7915
10	137	0.01094	12523

Drop 3

Image	Number of Particles	Total Area of CNFs (mm^2)	Number of Particles Per mm^2 of Area Covered by CNFs
1	55	0.01474	3732
2	95	0.00863	11005
3	144	0.00888	16217
4	199	0.00591	33691
5	44	0.00753	5842
6	43	0.01707	2518
7	59	0.00608	9701
8	39	0.00970	4021
9	26	0.01374	1892
10	52	0.01136	4578

Drop 4

Image	Number of Particles	Total Area of CNFs (mm^2)	Number of Particles Per mm^2 of Area Covered by CNFs
1	183	0.00335	54584
2	111	0.00941	11799
3	160	0.00465	34387
4	154	0.00427	36067
5	142	0.00243	58319
6	131	0.00508	25808
7	69	0.00860	8021
8	123	0.00513	23981
9	153	0.00418	36644
10	217	0.00426	50928

Drop 5

Image	Number of Particles	Total Area of CNFs (mm^2)	Number of Particles Per mm^2 of Area Covered by CNFs
1	254	0.00758	33515
2	293	0.01069	27421
3	266	0.00898	29620
4	225	0.01205	18669
5	323	0.00916	35250
6	120	0.01038	11557
7	142	0.00955	14873
8	130	0.00697	18662
9	123	0.00634	19390
10	83	0.00387	21424

Drop 6

Image	Number of Particles	Total Area of CNFs (mm^2)	Number of Particles Per mm^2 of Area Covered by CNFs
1	37	0.01675	2209
2	51	0.01490	3423
3	50	0.01646	3038
4	67	0.00345	19427
5	174	0.00119	145875
6	71	0.00086	82975
7	173	0.00266	64988
8	18	0.02589	695
9	14	0.01649	849
10	27	0.00304	8891

Drop 7

Image	Number of Particles	Total Area of CNFs (mm^2)	Number of Particles Per mm^2 of Area Covered by CNFs
1	61	0.00808	7550
2	57	0.00929	6134
3	73	0.00670	10904
4	57	0.00310	18389
5	189	0.00177	106741
6	92	0.01352	6802
7	143	0.00441	32443
8	83	0.01818	4564
9	53	0.00764	6940
10	65	0.00840	7742

Drop 8

Image	Number of Particles	Total Area of CNFs (mm^2)	Number of Particles Per mm^2 of Area Covered by CNFs
1	79	0.01000	7901
2	102	0.01125	9068
3	78	0.00347	22449
4	79	0.00582	13564
5	79	0.00561	14079
6	82	0.00361	22687
7	75	0.00506	14818
8	36	0.00712	5060
9	50	0.01710	2924
10	29	0.00714	4060

Drop 9

Image	Number of Particles	Total Area of CNFs (mm^2)	Number of Particles Per mm^2 of Area Covered by CNFs
1	31	0.00893	3473
2	96	0.01215	7904
3	138	0.00852	16205
4	30	0.00960	3124
5	48	0.00891	5389
6	40	0.02381	1680
7	63	0.00489	12885
8	45	0.01107	4065
9	31	0.00846	3664
10	15	0.00493	3043

Drop 10

Image	Number of Particles	Total Area of CNFs (mm^2)	Number of Particles Per mm^2 of Area Covered by CNFs
1	32	0.00643	4979
2	71	0.00231	30722
3	88	0.00515	17094
4	97	0.00479	20254
5	91	0.00402	22657
6	37	0.00517	7153
7	54	0.00812	6647
8	32	0.00787	4065
9	57	0.00684	8330
10	107	0.00630	16998

Drop 11

Image	Number of Particles	Total Area of CNFs (mm^2)	Number of Particles Per mm^2 of Area Covered by CNFs
1	86	0.00359	23940
2	107	0.00904	11842
3	161	0.01598	10077
4	119	0.01113	10687
5	96	0.00959	10014
6	122	0.01102	11066
7	139	0.00609	22810
8	110	0.01367	8050
9	113	0.00998	11326
10	139	0.00692	20087

Drop 12

Image	Number of Particles	Total Area of CNFs (mm^2)	Number of Particles Per mm^2 of Area Covered by CNFs
1	27	0.00493	5476
2	26	0.00690	3769
3	16	0.00507	3159
4	20	0.00609	3286
5	13	0.01141	1139
6	21	0.01297	1619
7	29	0.01202	2413
8	22	0.00513	4288
9	27	0.01557	1735
10	22	0.01895	1161

Drop 13

Image	Number of Particles	Total Area of CNFs (mm^2)	Number of Particles Per mm^2 of Area Covered by CNFs
1	115	0.00459	25063
2	51	0.00390	13075
3	50	0.00514	9726
4	60	0.00797	7526
5	82	0.00242	33904
6	84	0.01154	7278
7	65	0.00903	7199
8	50	0.01604	3117
9	32	0.01505	2127
10	57	0.01203	4737

Drop 14

Image	Number of Particles	Total Area of CNFs (mm^2)	Number of Particles Per mm^2 of Area Covered by CNFs
1	72	0.00679	10596
2	65	0.00929	6996
3	49	0.00672	7294
4	72	0.01471	4894
5	85	0.00984	8638
6	160	0.00786	20360
7	101	0.00839	12040
8	83	0.00657	12627
9	169	0.00842	20069
10	119	0.00571	20836

Drop 15

Image	Number of Particles	Total Area of CNFs (mm^2)	Number of Particles Per mm^2 of Area Covered by CNFs
1	137	0.00770	17798
2	227	0.01079	21041
3	198	0.00395	50132
4	92	0.00857	10732
5	110	0.01044	10534
6	120	0.00762	15753
7	134	0.00600	22333
8	140	0.00569	24584
9	78	0.00389	20048
10	63	0.00761	8274

AE/CNF

Total number of CNF particles: 60243.
Total area covered by CNFs: 1.160 mm^2.
Total number of particles per mm^2 of area covered by CNFs: 51915.

Drop 1

Image	Number of Particles	Total Area of CNFs (mm^2)	Number of Particles Per mm^2 of Area Covered by CNFs
1	962	0.00904	106368
2	955	0.00589	162207
3	660	0.00461	143142
4	1007	0.00330	304768
5	734	0.00728	100843
6	186	0.00776	23961
7	335	0.00790	42421
8	324	0.00635	51051
9	852	0.00636	134065
10	789	0.00839	94050

Drop 2

Image	Number of Particles	Total Area of CNFs (mm^2)	Number of Particles Per mm^2 of Area Covered by CNFs
1	692	0.00708	97728
2	471	0.00730	64489
3	747	0.00580	128842
4	783	0.00410	191118
5	289	0.00668	43238
6	394	0.00328	120191
7	260	0.00596	43611
8	624	0.00585	106588
9	608	0.01329	45754
10	319	0.00396	80463

Drop 3

Image	Number of Particles	Total Area of CNFs (mm^2)	Number of Particles Per mm^2 of Area Covered by CNFs
1	62	0.00247	25114
2	751	0.00632	118908
3	589	0.00652	90331
4	453	0.00781	58021
5	979	0.00559	174995
6	162	0.00300	53915
7	155	0.00453	34250
8	548	0.00606	90456
9	944	0.01011	93401
10	348	0.00613	56760

Drop 4

Image	Number of Particles	Total Area of CNFs (mm^2)	Number of Particles Per mm^2 of Area Covered by CNFs
1	500	0.00876	57070
2	561	0.00687	81681
3	837	0.01664	50299
4	1274	0.00718	177457
5	1157	0.00993	116465
6	1239	0.00700	177098
7	554	0.00605	91535
8	124	0.00460	26953
9	244	0.01919	12712
10	664	0.01517	43778

Drop 5

Image	Number of Particles	Total Area of CNFs (mm^2)	Number of Particles Per mm^2 of Area Covered by CNFs
1	394	0.00729	54034
2	317	0.00520	60932
3	197	0.00493	39974
4	183	0.00493	37141
5	900	0.01222	73620
6	466	0.01010	46139
7	491	0.00763	64357
8	382	0.00503	75870
9	328	0.00547	59911
10	203	0.00450	45161

Drop 6

Image	Number of Particles	Total Area of CNFs (mm^2)	Number of Particles Per mm^2 of Area Covered by CNFs
1	577	0.01135	50839
2	614	0.01083	56689
3	661	0.01338	49420
4	447	0.00566	78981
5	547	0.00531	102992
6	538	0.00544	98884
7	709	0.01508	47017
8	481	0.01477	32575
9	497	0.01743	28518
10	705	0.01149	61335

Drop 7

Image	Number of Particles	Total Area of CNFs (mm^2)	Number of Particles Per mm^2 of Area Covered by CNFs
1	449	0.00495	90694
2	122	0.01678	7270
3	140	0.00687	20364
4	269	0.00475	56686
5	188	0.00496	37879
6	218	0.00413	52817
7	328	0.01173	27954
8	712	0.00822	86586
9	819	0.01460	56105
10	711	0.01878	37860

Drop 8

Image	Number of Particles	Total Area of CNFs (mm^2)	Number of Particles Per mm^2 of Area Covered by CNFs
1	228	0.00727	31381
2	195	0.00770	25315
3	157	0.00129	121286
4	183	0.00340	53872
5	555	0.00573	96813
6	288	0.00373	77179
7	30	0.02901	1034
8	283	0.00288	98120
9	271	0.00335	80852
10	173	0.00432	40060

Drop 9

Image	Number of Particles	Total Area of CNFs (mm^2)	Number of Particles Per mm^2 of Area Covered by CNFs
1	377	0.00421	89608
2	238	0.00574	41438
3	401	0.00605	66264
4	182	0.01184	15375
5	562	0.00367	153015
6	210	0.00681	30840
7	531	0.00492	107977
8	258	0.00371	69563
9	309	0.00791	39066
10	465	0.00905	51407

Drop 10

Image	Number of Particles	Total Area of CNFs (mm^2)	Number of Particles Per mm^2 of Area Covered by CNFs
1	198	0.00696	28459
2	301	0.00881	34156
3	229	0.00881	25990
4	304	0.01184	25678
5	254	0.01216	20896
6	404	0.01164	34722
7	151	0.02768	5454
8	705	0.00940	75004
9	353	0.00914	38618
10	171	0.00710	24073

Drop 11

Image	Number of Particles	Total Area of CNFs (mm^2)	Number of Particles Per mm^2 of Area Covered by CNFs
1	295	0.00586	50371
2	337	0.01313	25671
3	336	0.00764	43969
4	374	0.01180	31708
5	488	0.00864	56491
6	392	0.01042	37624
7	232	0.01274	18215
8	270	0.00983	27460
9	285	0.01428	19952
10	456	0.01316	34652

Drop 12

Image	Number of Particles	Total Area of CNFs (mm^2)	Number of Particles Per mm^2 of Area Covered by CNFs
1	581	0.00470	123632
2	468	0.00483	96941
3	202	0.02175	9288
4	585	0.00447	130967
5	401	0.00335	119677
6	122	0.01597	7641
7	185	0.00238	77720
8	347	0.00276	125644
9	443	0.00472	93863
10	482	0.00305	158284

Drop 13

Image	Number of Particles	Total Area of CNFs (mm^2)	Number of Particles Per mm^2 of Area Covered by CNFs
1	67	0.01296	5171
2	269	0.00332	81134
3	85	0.00286	29687
4	81	0.00718	11280
5	65	0.00555	11714
6	62	0.00360	17242
7	325	0.00250	129741
8	289	0.00578	50014
9	238	0.00505	47138
10	428	0.00558	76652

Drop 14

Image	Number of Particles	Total Area of CNFs (mm^2)	Number of Particles Per mm^2 of Area Covered by CNFs
1	254	0.00412	61655
2	279	0.00621	44938
3	305	0.00247	123436
4	387	0.00323	119674
5	247	0.01232	20056
6	553	0.00675	81951
7	343	0.00653	52527
8	316	0.00404	78290
9	315	0.00373	84352
10	387	0.00613	63090

Drop 15

Image	Number of Particles	Total Area of CNFs (mm^2)	Number of Particles Per mm^2 of Area Covered by CNFs
1	74	0.00407	18170
2	83	0.00551	15070
3	79	0.00541	14608
4	117	0.00563	20773
5	143	0.00467	30595
6	144	0.00759	18972
7	77	0.00612	12572
8	70	0.00686	10208
9	109	0.01236	8818
10	76	0.00676	11239

APPENDIX B

DISPERSION IN CEMENT DATA

This appendix contains a summary of the data included in the micrograph analysis of the dispersion of CNFs in cement-based composites (Figure 3.9, Figure 3.11, and Figure 6.3). A summary of the composites analyzed is included below. A micrograph of a representative cross-section for each cement-based composite was analyzed to determine the size of each CNF agglomerate greater than 0.007 mm^2 in area. A summary is given for each composite, and the area and maximum Feret's diameter of each agglomerate greater than 0.007 mm^2 in area is given.

Summary of Composites

Composite	Figure(s) Analyzed In	Description
PC-P-HRWR/T-CNF	Figures 3.9 and 3.11	PC paste (w/c=0.28) with 0.2 wt% CNFs surface treated with HNO_3 and dispersed with P-HRWR
PC-P-HRWR/CNF	Figures 3.9 and 3.11	PC paste (w/c=0.28) with 0.2 wt% "*as received*" CNFs and dispersed with P-HRWR
PC-N-HRWR/CNF	Figures 3.9 and 3.11	PC paste (w/c=0.28) with 0.2 wt% "*as received*" CNFs and dispersed with N-HRWR
PC-AE/CNF	Figures 3.9 and 3.11	PC paste (w/c=0.28) with 0.2 wt% "*as received*" CNFs and dispersed with AE
PC-W/T-CNF	Figure 3.11	PC paste (w/c=0.28) with 0.2 wt% CNFs surface treated with HNO_3 and no dispersing agent
PC-W/CNF	Figure 3.11	PC paste (w/c=0.28) with 0.2 wt% "*as received*" CNFs and no dispersing agent
PC-CNF	Figure 6.3	PC paste (w/c=0.315) with 0.5 wt% "*as received*" CNFs and dispersed with P-HRWR
PC-CF-CNF	Figure 6.3	PC paste (w/c=0.315) with 0.5 wt% "*as received*" CNFs, 0.5% CFs, and dispersed with P-HRWR

PC-P-HRWR/T-CNF

Number of CNF agglomerates greater than 0.007 mm^2: 233.
Cumulative area of CNFs agglomerates greater than 0.007 mm^2: 8.143 mm^2.
Area fraction of CNF agglomerates greater than 0.007 mm^2: 1.1%.

Agglomerate	Area (mm^2)	Maximum Feret's Diameter (mm)	Agglomerate	Area (mm^2)	Maximum Feret's Diameter (mm)
1	0.023	0.256	39	0.064	0.387
2	0.033	0.417	40	0.016	0.209
3	0.022	0.362	41	0.016	0.237
4	0.012	0.200	42	0.016	0.248
5	0.018	0.201	43	0.008	0.124
6	0.109	0.937	44	0.020	0.242
7	0.088	0.454	45	0.027	0.268
8	0.067	0.410	46	0.029	0.315
9	0.015	0.181	47	0.012	0.154
10	0.077	0.633	48	0.012	0.162
11	0.204	0.693	49	0.013	0.181
12	0.178	0.802	50	0.115	0.493
13	0.051	0.384	51	0.010	0.196
14	0.019	0.190	52	0.183	0.600
15	0.175	0.603	53	0.049	0.674
16	0.341	0.973	54	0.013	0.196
17	0.035	0.323	55	0.009	0.136
18	0.031	0.266	56	0.067	0.390
19	0.010	0.166	57	0.016	0.181
20	0.023	0.218	58	0.009	0.136
21	0.040	0.424	59	0.008	0.153
22	0.029	0.229	60	0.018	0.182
23	0.104	0.576	61	0.011	0.200
24	0.054	0.441	62	0.014	0.190
25	0.014	0.162	63	0.015	0.181
26	0.048	0.295	64	0.035	0.295
27	0.019	0.196	65	0.022	0.209
28	0.007	0.124	66	0.067	0.389
29	0.219	0.774	67	0.007	0.134
30	0.044	0.306	68	0.029	0.258
31	0.018	0.201	69	0.059	0.423
32	0.120	0.592	70	0.031	0.242
33	0.052	0.356	71	0.049	0.455
34	0.015	0.237	72	0.008	0.181
35	0.027	0.331	73	0.023	0.266
36	0.205	0.659	74	0.013	0.190
37	0.017	0.262	75	0.011	0.153
38	0.051	0.345	76	0.009	0.182

Agglomerate	Area (mm^2)	Maximum Feret's Diameter (mm)	Agglomerate	Area (mm^2)	Maximum Feret's Diameter (mm)
77	0.033	0.315	120	0.011	0.171
78	0.009	0.142	121	0.146	0.608
79	0.011	0.175	122	0.011	0.175
80	0.096	0.576	123	0.020	0.285
81	0.022	0.237	124	0.019	0.288
82	0.018	0.201	125	0.009	0.134
83	0.016	0.266	126	0.014	0.196
84	0.035	0.295	127	0.012	0.201
85	0.011	0.154	128	0.011	0.154
86	0.008	0.124	129	0.069	0.437
87	0.111	0.530	130	0.008	0.136
88	0.196	0.731	131	0.127	0.824
89	0.082	0.429	132	0.134	0.666
90	0.009	0.136	133	0.026	0.237
91	0.013	0.153	134	0.012	0.162
92	0.011	0.153	135	0.008	0.162
93	0.009	0.142	136	0.110	0.703
94	0.008	0.124	137	0.049	0.342
95	0.018	0.362	138	0.094	0.630
96	0.008	0.124	139	0.023	0.242
97	0.058	0.343	140	0.021	0.248
98	0.021	0.304	141	0.074	0.579
99	0.010	0.154	142	0.010	0.190
100	0.016	0.221	143	0.023	0.237
101	0.082	0.390	144	0.066	0.365
102	0.009	0.171	145	0.012	0.196
103	0.011	0.166	146	0.016	0.175
104	0.011	0.153	147	0.018	0.268
105	0.009	0.180	148	0.011	0.150
106	0.008	0.142	149	0.013	0.196
107	0.009	0.153	150	0.010	0.201
108	0.014	0.162	151	0.015	0.213
109	0.008	0.136	152	0.007	0.150
110	0.008	0.154	153	0.086	0.446
111	0.050	0.370	154	0.027	0.248
112	0.007	0.129	155	0.013	0.196
113	0.041	0.429	156	0.016	0.382
114	0.009	0.175	157	0.013	0.212
115	0.007	0.154	158	0.013	0.229
116	0.020	0.229	159	0.008	0.124
117	0.009	0.162	160	0.018	0.221
118	0.009	0.181	161	0.018	0.228
119	0.018	0.209	162	0.033	0.283

Agglomerate	Area (mm^2)	Maximum Feret's Diameter (mm)
163	0.116	0.459
164	0.065	0.387
165	0.008	0.153
166	0.007	0.171
167	0.019	0.283
168	0.012	0.201
169	0.012	0.181
170	0.047	0.324
171	0.019	0.201
172	0.023	0.247
173	0.009	0.153
174	0.090	0.496
175	0.015	0.171
176	0.144	0.679
177	0.015	0.181
178	0.031	0.229
179	0.102	0.547
180	0.015	0.209
181	0.011	0.182
182	0.018	0.190
183	0.018	0.196
184	0.038	0.276
185	0.012	0.162
186	0.009	0.162
187	0.025	0.218
188	0.025	0.237
189	0.059	0.469
190	0.010	0.324
191	0.009	0.166
192	0.009	0.142
193	0.026	0.259
194	0.007	0.124
195	0.017	0.190
196	0.018	0.218
197	0.009	0.162
198	0.012	0.181
199	0.027	0.212
200	0.020	0.212
201	0.012	0.171
202	0.010	0.166
203	0.018	0.228
204	0.010	0.171
205	0.018	0.237
206	0.007	0.142
207	0.076	0.541
208	0.040	0.345
209	0.011	0.142
210	0.008	0.153
211	0.018	0.201
212	0.023	0.218
213	0.026	0.285
214	0.018	0.225
215	0.015	0.196
216	0.014	0.171
217	0.008	0.166
218	0.012	0.171
219	0.013	0.182
220	0.021	0.295
221	0.026	0.268
222	0.045	0.342
223	0.015	0.190
224	0.018	0.221
225	0.017	0.218
226	0.034	0.324
227	0.029	0.242
228	0.013	0.171
229	0.017	0.212
230	0.009	0.142
231	0.010	0.162
232	0.027	0.276
233	0.007	0.153

PC-P-HRWR/CNF

Number of CNF agglomerates greater than 0.007 mm^2: 301.
Cumulative area of CNFs agglomerates greater than 0.007 mm^2: 10.403 mm^2.
Area fraction of CNF agglomerates greater than 0.007 mm^2: 1.4%.

Agglomerate	Area (mm^2)	Maximum Feret's Diameter (mm)	Agglomerate	Area (mm^2)	Maximum Feret's Diameter (mm)
1	0.049	0.376	39	0.022	0.218
2	0.161	0.766	40	0.020	0.201
3	0.111	0.530	41	0.014	0.300
4	0.193	0.636	42	0.027	0.256
5	0.280	0.865	43	0.015	0.201
6	0.013	0.171	44	0.092	0.524
7	0.166	0.573	45	0.121	0.547
8	0.299	1.106	46	0.034	0.268
9	0.018	0.225	47	0.013	0.182
10	0.162	0.603	48	0.022	0.242
11	0.054	0.382	49	0.023	0.237
12	0.016	0.218	50	0.008	0.153
13	0.034	0.306	51	0.016	0.237
14	0.009	0.162	52	0.013	0.182
15	0.016	0.200	53	0.023	0.242
16	0.092	0.424	54	0.033	0.335
17	0.074	0.418	55	0.009	0.154
18	0.047	0.371	56	0.036	0.478
19	0.040	0.306	57	0.020	0.201
20	0.062	0.345	58	0.098	0.446
21	0.092	0.398	59	0.009	0.190
22	0.088	0.628	60	0.121	0.733
23	0.097	0.474	61	0.019	0.382
24	0.081	0.516	62	0.012	0.175
25	0.023	0.283	63	0.019	0.229
26	0.091	0.398	64	0.008	0.142
27	0.053	0.378	65	0.009	0.166
28	0.014	0.171	66	0.009	0.153
29	0.152	0.611	67	0.013	0.201
30	0.062	0.591	68	0.009	0.142
31	0.063	0.391	69	0.035	0.301
32	0.012	0.162	70	0.075	0.497
33	0.009	0.153	71	0.052	0.366
34	0.016	0.209	72	0.015	0.162
35	0.031	0.366	73	0.019	0.228
36	0.018	0.182	74	0.008	0.200
37	0.010	0.162	75	0.063	0.350
38	0.072	0.356	76	0.013	0.154

Agglomerate	Area (mm^2)	Maximum Feret's Diameter (mm)
77	0.026	0.229
78	0.062	0.410
79	0.010	0.154
80	0.044	0.332
81	0.031	0.481
82	0.109	0.624
83	0.045	0.535
84	0.012	0.216
85	0.155	0.645
86	0.018	0.216
87	0.018	0.201
88	0.109	0.513
89	0.031	0.259
90	0.013	0.196
91	0.121	0.477
92	0.016	0.234
93	0.011	0.153
94	0.010	0.209
95	0.008	0.142
96	0.007	0.153
97	0.025	0.229
98	0.063	0.477
99	0.018	0.402
100	0.200	0.893
101	0.141	0.666
102	0.015	0.201
103	0.009	0.181
104	0.013	0.175
105	0.008	0.142
106	0.031	0.329
107	0.017	0.210
108	0.009	0.153
109	0.010	0.153
110	0.016	0.182
111	0.015	0.200
112	0.022	0.255
113	0.013	0.228
114	0.010	0.196
115	0.008	0.124
116	0.007	0.153
117	0.009	0.136
118	0.011	0.196
119	0.031	0.356

Agglomerate	Area (mm^2)	Maximum Feret's Diameter (mm)
120	0.031	0.335
121	0.007	0.171
122	0.013	0.209
123	0.045	0.288
124	0.014	0.182
125	0.015	0.237
126	0.016	0.228
127	0.040	0.272
128	0.143	0.688
129	0.008	0.153
130	0.021	0.196
131	0.040	0.683
132	0.039	0.342
133	0.095	0.513
134	0.045	0.376
135	0.018	0.182
136	0.009	0.142
137	0.009	0.142
138	0.013	0.162
139	0.012	0.229
140	0.032	0.242
141	0.013	0.258
142	0.068	0.350
143	0.035	0.272
144	0.027	0.242
145	0.018	0.190
146	0.008	0.136
147	0.011	0.221
148	0.016	0.212
149	0.009	0.142
150	0.016	0.200
151	0.008	0.142
152	0.024	0.221
153	0.007	0.162
154	0.010	0.171
155	0.011	0.171
156	0.007	0.166
157	0.081	0.496
158	0.196	0.628
159	0.007	0.136
160	0.011	0.153
161	0.053	0.437
162	0.061	0.391

Agglomerate	Area (mm^2)	Maximum Feret's Diameter (mm)	Agglomerate	Area (mm^2)	Maximum Feret's Diameter (mm)
163	0.010	0.171	206	0.016	0.190
164	0.023	0.272	207	0.017	0.196
165	0.030	0.242	208	0.034	0.288
166	0.009	0.142	209	0.102	0.582
167	0.025	0.276	210	0.020	0.196
168	0.012	0.218	211	0.015	0.200
169	0.007	0.124	212	0.008	0.162
170	0.011	0.210	213	0.074	0.474
171	0.023	0.259	214	0.229	0.769
172	0.013	0.209	215	0.015	0.306
173	0.022	0.201	216	0.018	0.248
174	0.033	0.268	217	0.040	0.362
175	0.063	0.329	218	0.109	0.471
176	0.012	0.162	219	0.009	0.136
177	0.022	0.247	220	0.022	0.288
178	0.007	0.124	221	0.008	0.124
179	0.017	0.181	222	0.009	0.142
180	0.018	0.218	223	0.034	0.323
181	0.041	0.309	224	0.019	0.229
182	0.077	0.379	225	0.157	0.653
183	0.019	0.225	226	0.008	0.182
184	0.011	0.200	227	0.014	0.242
185	0.009	0.237	228	0.018	0.276
186	0.059	0.417	229	0.015	0.315
187	0.126	0.645	230	0.030	0.295
188	0.008	0.150	231	0.044	0.371
189	0.014	0.190	232	0.029	0.247
190	0.009	0.162	233	0.028	0.242
191	0.055	0.447	234	0.007	0.136
192	0.020	0.218	235	0.019	0.225
193	0.009	0.134	236	0.008	0.180
194	0.073	0.437	237	0.010	0.192
195	0.010	0.175	238	0.045	0.335
196	0.007	0.142	239	0.021	0.200
197	0.017	0.229	240	0.040	0.370
198	0.013	0.196	241	0.007	0.142
199	0.018	0.181	242	0.031	0.318
200	0.015	0.171	243	0.011	0.201
201	0.021	0.229	244	0.008	0.134
202	0.027	0.335	245	0.008	0.124
203	0.016	0.182	246	0.011	0.175
204	0.098	0.531	247	0.009	0.136
205	0.019	0.196	248	0.075	0.395

Agglomerate	Area (mm^2)	Maximum Feret's Diameter (mm)
249	0.020	0.218
250	0.008	0.134
251	0.011	0.154
252	0.028	0.229
253	0.013	0.209
254	0.026	0.259
255	0.009	0.162
256	0.030	0.301
257	0.007	0.134
258	0.009	0.134
259	0.058	0.324
260	0.011	0.171
261	0.008	0.136
262	0.011	0.150
263	0.020	0.266
264	0.013	0.162
265	0.026	0.242
266	0.007	0.120
267	0.010	0.181
268	0.018	0.229
269	0.014	0.201
270	0.018	0.200
271	0.014	0.190
272	0.070	0.532
273	0.012	0.153
274	0.009	0.196
275	0.013	0.171

Agglomerate	Area (mm^2)	Maximum Feret's Diameter (mm)
276	0.007	0.142
277	0.009	0.175
278	0.013	0.218
279	0.018	0.190
280	0.018	0.266
281	0.033	0.266
282	0.015	0.229
283	0.015	0.209
284	0.014	0.166
285	0.011	0.153
286	0.009	0.142
287	0.025	0.301
288	0.017	0.181
289	0.010	0.142
290	0.015	0.181
291	0.007	0.124
292	0.009	0.136
293	0.008	0.134
294	0.017	0.266
295	0.012	0.181
296	0.012	0.154
297	0.013	0.166
298	0.016	0.247
299	0.012	0.182
300	0.007	0.114
301	0.008	0.150

PC-N-HRWR/CNF
Number of CNF agglomerates greater than 0.007 mm^2: 108.
Cumulative area of CNFs agglomerates greater than 0.007 mm^2: 6.152 mm^2.
Area fraction of CNF agglomerates greater than 0.007 mm^2: 0.9%.

Agglomerate	Area (mm^2)	Maximum Feret's Diameter (mm)
1	0.024	0.266
2	0.044	0.408
3	0.040	0.382
4	0.072	0.455
5	0.019	0.242
6	0.038	0.304

Agglomerate	Area (mm^2)	Maximum Feret's Diameter (mm)
7	0.009	0.154
8	0.052	0.437
9	0.106	0.437
10	0.039	0.407
11	0.040	0.362
12	0.030	0.259

Agglomerate	Area (mm^2)	Maximum Feret's Diameter (mm)	Agglomerate	Area (mm^2)	Maximum Feret's Diameter (mm)
13	0.036	0.272	56	0.013	0.190
14	0.061	0.453	57	0.011	0.154
15	0.097	0.412	58	0.055	0.324
16	0.008	0.209	59	0.019	0.256
17	0.007	0.212	60	0.027	0.242
18	0.009	0.153	61	0.018	0.200
19	0.041	0.315	62	0.007	0.153
20	0.061	0.342	63	0.013	0.166
21	0.111	0.490	64	0.022	0.255
22	0.008	0.134	65	0.010	0.134
23	0.021	0.209	66	0.008	0.171
24	0.034	0.407	67	0.023	0.268
25	0.035	0.391	68	0.017	0.181
26	0.012	0.171	69	0.022	0.379
27	0.011	0.171	70	0.016	0.171
28	0.027	0.304	71	0.050	0.382
29	0.022	0.237	72	0.012	0.162
30	0.046	0.433	73	0.032	0.318
31	0.237	0.676	74	0.008	0.136
32	0.013	0.200	75	0.029	0.229
33	0.017	0.216	76	0.071	0.485
34	0.214	0.808	77	0.026	0.348
35	0.010	0.180	78	0.007	0.154
36	0.018	0.200	79	0.035	0.285
37	0.029	0.350	80	0.016	0.306
38	0.022	0.266	81	0.080	0.537
39	0.014	0.342	82	0.008	0.124
40	0.009	0.229	83	0.013	0.247
41	0.026	0.382	84	0.015	0.365
42	0.010	0.259	85	0.094	0.471
43	0.008	0.166	86	0.040	0.387
44	0.026	0.335	87	0.041	0.288
45	0.009	0.153	88	0.009	0.142
46	0.012	0.162	89	0.020	0.196
47	0.012	0.196	90	0.024	0.242
48	0.028	0.324	91	0.081	0.619
49	0.018	0.255	92	0.007	0.134
50	0.053	0.477	93	0.009	0.134
51	0.008	0.142	94	0.010	0.162
52	0.008	0.142	95	0.021	0.288
53	0.008	0.134	96	0.041	0.405
54	0.008	0.134	97	0.028	0.255
55	0.022	0.427	98	0.234	0.721

Agglomerate	Area (mm^2)	Maximum Feret's Diameter (mm)
99	0.009	0.134
100	0.079	0.391
101	0.025	0.237
102	0.007	0.136
103	0.009	0.142
104	0.014	0.221
105	0.008	0.242
106	0.009	0.153
107	0.013	0.201
108	0.008	0.162
109	0.027	0.454
110	0.013	0.180
111	0.013	0.162
112	0.205	0.577
113	0.021	0.256
114	0.013	0.162
115	0.015	0.182
116	0.023	0.229
117	0.011	0.331
118	0.009	0.136
119	0.018	0.210
120	0.016	0.196
121	0.069	0.343
122	0.013	0.218
123	0.018	0.181
124	0.092	0.511
125	0.016	0.350
126	0.048	0.379
127	0.017	0.196
128	0.024	0.266
129	0.021	0.242
130	0.022	0.228
131	0.079	0.469
132	0.008	0.142
133	0.018	0.182
134	0.011	0.153
135	0.025	0.295
136	0.130	0.641
137	0.128	0.585
138	0.138	0.638
139	0.018	0.221
140	0.028	0.268

Agglomerate	Area (mm^2)	Maximum Feret's Diameter (mm)
141	0.030	0.247
142	0.069	0.370
143	0.131	0.911
144	0.015	0.256
145	0.008	0.134
146	0.014	0.285
147	0.075	0.485
148	0.020	0.221
149	0.021	0.200
150	0.009	0.154
151	0.025	0.237
152	0.033	0.266
153	0.057	0.423
154	0.216	0.918
155	0.014	0.190
156	0.014	0.209
157	0.032	0.276
158	0.007	0.153
159	0.008	0.171
160	0.026	0.435
161	0.020	0.196
162	0.022	0.288
163	0.048	0.335
164	0.036	0.272
165	0.010	0.329
166	0.018	0.248
167	0.058	0.427
168	0.009	0.142
169	0.013	0.181
170	0.021	0.306
171	0.009	0.136
172	0.058	0.315
173	0.008	0.142
174	0.010	0.175
175	0.014	0.268
176	0.090	0.478
177	0.017	0.240
178	0.007	0.114
179	0.017	0.200
180	0.015	0.190

PC-AE/CNF

Number of CNF agglomerates greater than 0.007 mm^2: 200.
Cumulative area of CNFs agglomerates greater than 0.007 mm^2: 8.446 mm^2.
Area fraction of CNF agglomerates greater than 0.007 mm^2: 1.1%.

Agglomerate	Area (mm^2)	Maximum Feret's Diameter (mm)	Agglomerate	Area (mm^2)	Maximum Feret's Diameter (mm)
1	0.007	0.162	39	0.024	0.221
2	0.009	0.134	40	0.009	0.162
3	0.131	0.577	41	0.039	0.412
4	0.045	0.469	42	0.021	0.221
5	0.016	0.228	43	0.048	0.371
6	0.037	0.285	44	0.018	0.285
7	0.052	0.465	45	0.013	0.201
8	0.012	0.171	46	0.007	0.212
9	0.060	0.342	47	0.019	0.200
10	0.047	0.565	48	0.020	0.304
11	0.227	0.806	49	0.008	0.142
12	0.077	0.544	50	0.036	0.288
13	0.011	0.171	51	0.020	0.210
14	0.008	0.166	52	0.093	0.531
15	0.007	0.124	53	0.031	0.279
16	0.020	0.242	54	0.134	0.594
17	0.021	0.221	55	0.018	0.255
18	0.011	0.154	56	0.083	0.711
19	0.010	0.209	57	0.011	0.166
20	0.054	0.412	58	0.018	0.342
21	0.054	0.363	59	0.023	0.449
22	0.016	0.190	60	0.008	0.124
23	0.011	0.162	61	0.045	0.304
24	0.013	0.162	62	0.033	0.321
25	0.010	0.142	63	0.058	0.315
26	0.017	0.272	64	0.011	0.175
27	0.017	0.209	65	0.046	0.295
28	0.013	0.209	66	0.087	0.771
29	0.204	0.729	67	0.020	0.237
30	0.008	0.150	68	0.020	0.259
31	0.015	0.209	69	0.015	0.229
32	0.095	0.617	70	0.116	0.441
33	0.043	0.384	71	0.032	0.304
34	0.104	0.481	72	0.012	0.256
35	0.105	0.449	73	0.099	0.450
36	0.040	0.345	74	0.018	0.295
37	0.028	0.242	75	0.013	0.182
38	0.334	0.831	76	0.013	0.237

Agglomerate	Area (mm^2)	Maximum Feret's Diameter (mm)
77	0.028	0.229
78	0.015	0.212
79	0.009	0.154
80	0.128	0.541
81	0.033	0.285
82	0.017	0.298
83	0.040	0.304
84	0.035	0.350
85	0.034	0.427
86	0.011	0.175
87	0.027	0.266
88	0.008	0.124
89	0.054	0.484
90	0.113	0.474
91	0.027	0.276
92	0.051	0.390
93	0.035	0.285
94	0.091	0.503
95	0.015	0.221
96	0.120	0.501
97	0.017	0.221
98	0.010	0.190
99	0.054	0.504
100	0.017	0.196
101	0.011	0.153
102	0.040	0.449
103	0.027	0.331
104	0.096	0.454
105	0.082	0.454
106	0.075	0.395
107	0.020	0.248
108	0.036	0.295
109	0.115	0.537
110	0.029	0.258
111	0.015	0.196
112	0.010	0.171
113	0.008	0.180
114	0.026	0.247
115	0.088	0.495
116	0.008	0.136
117	0.007	0.136
118	0.011	0.166
119	0.100	0.467

Agglomerate	Area (mm^2)	Maximum Feret's Diameter (mm)
120	0.105	0.435
121	0.226	0.661
122	0.076	0.429
123	0.020	0.212
124	0.041	0.331
125	0.051	0.451
126	0.027	0.255
127	0.039	0.446
128	0.009	0.154
129	0.011	0.166
130	0.034	0.283
131	0.028	0.335
132	0.025	0.268
133	0.008	0.136
134	0.077	0.447
135	0.019	0.182
136	0.027	0.255
137	0.060	0.484
138	0.099	0.459
139	0.015	0.237
140	0.011	0.171
141	0.023	0.242
142	0.011	0.190
143	0.014	0.213
144	0.046	0.370
145	0.016	0.272
146	0.058	0.361
147	0.009	0.166
148	0.178	0.725
149	0.022	0.228
150	0.013	0.212
151	0.013	0.237
152	0.014	0.237
153	0.010	0.166
154	0.020	0.209
155	0.065	0.471
156	0.013	0.182
157	0.013	0.229
158	0.026	0.323
159	0.022	0.228
160	0.008	0.142
161	0.035	0.304
162	0.049	0.343

Agglomerate	Area (mm^2)	Maximum Feret's Diameter (mm)	Agglomerate	Area (mm^2)	Maximum Feret's Diameter (mm)
163	0.068	0.376	182	0.051	0.361
164	0.065	0.365	183	0.011	0.153
165	0.018	0.285	184	0.107	0.459
166	0.042	0.348	185	0.049	0.405
167	0.031	0.288	186	0.031	0.268
168	0.156	0.679	187	0.016	0.182
169	0.071	0.490	188	0.036	0.335
170	0.029	0.309	189	0.034	0.268
171	0.013	0.216	190	0.021	0.259
172	0.021	0.295	191	0.055	0.335
173	0.026	0.242	192	0.021	0.212
174	0.022	0.209	193	0.018	0.229
175	0.057	0.362	194	0.118	0.685
176	0.035	0.285	195	0.013	0.166
177	0.010	0.136	196	0.124	0.744
178	0.030	0.270	197	0.067	0.408
179	0.013	0.216	198	0.026	0.295
180	0.031	0.248	199	0.044	0.295
181	0.051	0.345	200	0.012	0.209

PC-W/T-CNF
Number of CNF agglomerates greater than 0.007 mm^2: 129.
Cumulative area of CNFs agglomerates greater than 0.007 mm^2: 5.664 mm^2.
Area fraction of CNF agglomerates greater than 0.007 mm^2: 0.8%.

Agglomerate	Area (mm^2)	Maximum Feret's Diameter (mm)	Agglomerate	Area (mm^2)	Maximum Feret's Diameter (mm)
1	0.234	0.993	14	0.012	0.162
2	0.010	0.425	15	0.024	0.283
3	0.056	0.324	16	0.030	0.256
4	0.017	0.272	17	0.009	0.153
5	0.012	0.298	18	0.009	0.162
6	0.011	0.142	19	0.007	0.134
7	0.042	0.283	20	0.349	0.758
8	0.048	0.309	21	0.032	0.371
9	0.013	0.216	22	0.011	0.162
10	0.035	0.270	23	0.029	0.256
11	0.025	0.256	24	0.046	0.335
12	0.007	0.216	25	0.017	0.209
13	0.086	0.450	26	0.058	0.427

Agglomerate	Area (mm^2)	Maximum Feret's Diameter (mm)
27	0.057	0.348
28	0.016	0.259
29	0.249	0.671
30	0.023	0.266
31	0.021	0.266
32	0.019	0.228
33	0.010	0.162
34	0.180	0.618
35	0.101	0.724
36	0.011	0.201
37	0.040	0.288
38	0.018	0.321
39	0.012	0.228
40	0.051	0.342
41	0.029	0.342
42	0.047	0.410
43	0.072	0.429
44	0.052	0.402
45	0.022	0.212
46	0.012	0.182
47	0.007	0.142
48	0.020	0.221
49	0.053	0.345
50	0.018	0.259
51	0.020	0.201
52	0.040	0.324
53	0.016	0.225
54	0.014	0.181
55	0.018	0.212
56	0.024	0.272
57	0.024	0.361
58	0.010	0.154
59	0.103	0.495
60	0.009	0.154
61	0.081	0.382
62	0.053	0.405
63	0.008	0.162
64	0.013	0.182
65	0.012	0.196
66	0.018	0.200
67	0.192	0.785
68	0.011	0.212
69	0.012	0.171

Agglomerate	Area (mm^2)	Maximum Feret's Diameter (mm)
70	0.034	0.279
71	0.010	0.182
72	0.138	0.590
73	0.036	0.288
74	0.070	0.437
75	0.098	0.721
76	0.009	0.175
77	0.009	0.153
78	0.117	0.618
79	0.008	0.136
80	0.029	0.279
81	0.014	0.182
82	0.074	0.542
83	0.053	0.469
84	0.037	0.363
85	0.019	0.221
86	0.024	0.229
87	0.098	0.455
88	0.047	0.348
89	0.028	0.313
90	0.022	0.276
91	0.024	0.248
92	0.022	0.259
93	0.018	0.276
94	0.020	0.242
95	0.080	0.496
96	0.054	0.300
97	0.152	0.562
98	0.072	0.488
99	0.059	0.571
100	0.027	0.288
101	0.008	0.154
102	0.018	0.247
103	0.015	0.166
104	0.080	0.433
105	0.009	0.136
106	0.072	0.363
107	0.008	0.124
108	0.072	0.477
109	0.029	0.288
110	0.009	0.162
111	0.027	0.229
112	0.008	0.150

Agglomerate	Area (mm^2)	Maximum Feret's Diameter (mm)
113	0.027	0.247
114	0.024	0.237
115	0.013	0.268
116	0.008	0.162
117	0.087	0.484
118	0.094	0.446
119	0.131	0.582
120	0.054	0.412
121	0.043	0.384

Agglomerate	Area (mm^2)	Maximum Feret's Diameter (mm)
122	0.024	0.209
123	0.105	0.504
124	0.009	0.153
125	0.039	0.288
126	0.036	0.272
127	0.033	0.268
128	0.016	0.277
129	0.015	0.182

PC-W/CNF
Number of CNF agglomerates greater than 0.007 mm^2: 152.
Cumulative area of CNFs agglomerates greater than 0.007 mm^2: 5.403 mm^2.
Area fraction of CNF agglomerates greater than 0.007 mm^2: 0.7%.

Agglomerate	Area (mm^2)	Maximum Feret's Diameter (mm)
1	0.015	0.162
2	0.023	0.423
3	0.031	0.356
4	0.016	0.225
5	0.009	0.142
6	0.607	1.101
7	0.017	0.196
8	0.033	0.268
9	0.011	0.171
10	0.022	0.247
11	0.018	0.200
12	0.012	0.196
13	0.163	0.659
14	0.040	0.324
15	0.018	0.171
16	0.010	0.166
17	0.009	0.229
18	0.013	0.181
19	0.032	0.242
20	0.104	0.441
21	0.033	0.268
22	0.008	0.142
23	0.020	0.216
24	0.021	0.266

Agglomerate	Area (mm^2)	Maximum Feret's Diameter (mm)
25	0.075	0.429
26	0.013	0.162
27	0.022	0.216
28	0.008	0.153
29	0.035	0.304
30	0.031	0.268
31	0.013	0.181
32	0.010	0.153
33	0.031	0.335
34	0.020	0.196
35	0.009	0.196
36	0.009	0.162
37	0.008	0.154
38	0.045	0.329
39	0.008	0.124
40	0.013	0.201
41	0.090	0.402
42	0.008	0.190
43	0.015	0.216
44	0.021	0.200
45	0.022	0.209
46	0.029	0.268
47	0.012	0.162
48	0.010	0.181

Agglomerate	Area (mm^2)	Maximum Feret's Diameter (mm)	Agglomerate	Area (mm^2)	Maximum Feret's Diameter (mm)
49	0.069	0.481	92	0.036	0.348
50	0.007	0.142	93	0.023	0.259
51	0.023	0.417	94	0.049	0.318
52	0.158	0.594	95	0.015	0.181
53	0.008	0.124	96	0.012	0.171
54	0.016	0.190	97	0.049	0.348
55	0.038	0.324	98	0.060	0.417
56	0.010	0.171	99	0.024	0.268
57	0.017	0.200	100	0.016	0.228
58	0.064	0.361	101	0.017	0.192
59	0.018	0.329	102	0.011	0.182
60	0.013	0.196	103	0.153	0.607
61	0.049	0.398	104	0.009	0.221
62	0.013	0.196	105	0.008	0.154
63	0.013	0.182	106	0.008	0.154
64	0.019	0.237	107	0.035	0.342
65	0.042	0.488	108	0.013	0.321
66	0.053	0.353	109	0.011	0.181
67	0.024	0.221	110	0.107	0.571
68	0.011	0.209	111	0.007	0.124
69	0.015	0.180	112	0.022	0.345
70	0.009	0.153	113	0.043	0.345
71	0.012	0.162	114	0.027	0.301
72	0.020	0.209	115	0.009	0.153
73	0.010	0.142	116	0.008	0.166
74	0.050	0.306	117	0.016	0.248
75	0.010	0.182	118	0.027	0.405
76	0.019	0.212	119	0.046	0.315
77	0.018	0.242	120	0.117	0.615
78	0.015	0.256	121	0.015	0.200
79	0.426	0.911	122	0.011	0.181
80	0.017	0.266	123	0.021	0.259
81	0.013	0.212	124	0.020	0.200
82	0.017	0.209	125	0.018	0.324
83	0.011	0.225	126	0.023	0.259
84	0.014	0.200	127	0.008	0.153
85	0.013	0.196	128	0.049	0.331
86	0.130	0.493	129	0.018	0.218
87	0.018	0.229	130	0.013	0.182
88	0.013	0.225	131	0.020	0.242
89	0.128	0.649	132	0.009	0.150
90	0.024	0.283	133	0.020	0.200
91	0.012	0.200	134	0.008	0.154

Agglomerate	Area (mm^2)	Maximum Feret's Diameter (mm)	Agglomerate	Area (mm^2)	Maximum Feret's Diameter (mm)
135	0.008	0.114	144	0.015	0.216
136	0.024	0.256	145	0.027	0.268
137	0.009	0.136	146	0.030	0.387
138	0.009	0.201	147	0.046	0.335
139	0.135	0.541	148	0.054	0.313
140	0.035	0.270	149	0.013	0.221
141	0.018	0.262	150	0.028	0.353
142	0.012	0.182	151	0.038	0.335
143	0.136	0.603	152	0.012	0.216

PC-CNF
Number of CNF agglomerates greater than 0.007 mm^2: 700.
Cumulative area of CNFs agglomerates greater than 0.007 mm^2: 23.917 mm^2.
Area fraction of CNF agglomerates greater than 0.007 mm^2: 3.5%.

Agglomerate	Area (mm^2)	Maximum Feret's Diameter (mm)	Agglomerate	Area (mm^2)	Maximum Feret's Diameter (mm)
1	0.137	0.626	24	0.009	0.146
2	0.255	0.747	25	0.017	0.236
3	0.009	0.171	26	0.010	0.146
4	0.076	0.477	27	0.009	0.188
5	0.088	0.419	28	0.008	0.166
6	0.051	0.473	29	0.023	0.270
7	0.046	0.528	30	0.010	0.166
8	0.033	0.343	31	0.137	0.728
9	0.144	0.564	32	0.061	0.472
10	0.034	0.289	33	0.010	0.146
11	0.079	0.419	34	0.036	0.367
12	0.090	0.501	35	0.011	0.188
13	0.209	0.804	36	0.009	0.171
14	0.092	0.407	37	0.015	0.171
15	0.114	0.477	38	0.047	0.394
16	0.010	0.178	39	0.025	0.316
17	0.051	0.342	40	0.068	0.419
18	0.015	0.197	41	0.081	0.473
19	0.170	0.598	42	0.075	0.447
20	0.040	0.306	43	0.017	0.197
21	0.014	0.171	44	0.017	0.188
22	0.060	0.408	45	0.014	0.197
23	0.129	0.586	46	0.019	0.188

Agglomerate	Area (mm^2)	Maximum Feret's Diameter (mm)
47	0.044	0.416
48	0.014	0.211
49	0.008	0.131
50	0.009	0.158
51	0.024	0.276
52	0.019	0.270
53	0.018	0.334
54	0.068	0.394
55	0.011	0.252
56	0.018	0.294
57	0.130	0.512
58	0.123	0.540
59	0.012	0.171
60	0.275	1.032
61	0.015	0.188
62	0.015	0.236
63	0.022	0.334
64	0.065	0.742
65	0.027	0.252
66	0.091	0.473
67	0.050	0.427
68	0.027	0.262
69	0.014	0.223
70	0.037	0.328
71	0.080	0.463
72	0.027	0.293
73	0.013	0.171
74	0.021	0.223
75	0.121	0.676
76	0.069	0.473
77	0.025	0.262
78	0.009	0.158
79	0.049	0.531
80	0.009	0.146
81	0.009	0.131
82	0.185	0.715
83	0.118	0.545
84	0.025	0.270
85	0.027	0.236
86	0.076	0.416
87	0.219	0.691
88	0.121	0.604
89	0.190	0.564

Agglomerate	Area (mm^2)	Maximum Feret's Diameter (mm)
90	0.010	0.158
91	0.022	0.229
92	0.014	0.197
93	0.024	0.316
94	0.015	0.188
95	0.084	0.408
96	0.009	0.185
97	0.010	0.242
98	0.098	0.512
99	0.020	0.276
100	0.054	0.373
101	0.025	0.278
102	0.028	0.299
103	0.051	0.356
104	0.011	0.197
105	0.033	0.252
106	0.060	0.382
107	0.053	0.553
108	0.015	0.328
109	0.027	0.270
110	0.012	0.158
111	0.009	0.171
112	0.015	0.223
113	0.077	0.560
114	0.018	0.171
115	0.023	0.252
116	0.053	0.334
117	0.015	0.270
118	0.009	0.158
119	0.009	0.146
120	0.009	0.131
121	0.174	0.593
122	0.014	0.242
123	0.011	0.188
124	0.016	0.185
125	0.012	0.171
126	0.009	0.223
127	0.084	0.463
128	0.175	0.735
129	0.027	0.328
130	0.036	0.302
131	0.008	0.146
132	0.012	0.223

Agglomerate	Area (mm^2)	Maximum Feret's Diameter (mm)	Agglomerate	Area (mm^2)	Maximum Feret's Diameter (mm)
133	0.025	0.270	176	0.009	0.185
134	0.048	0.463	177	0.101	0.483
135	0.112	0.463	178	0.009	0.213
136	0.008	0.131	179	0.009	0.158
137	0.021	0.276	180	0.008	0.188
138	0.065	0.398	181	0.015	0.229
139	0.071	0.524	182	0.013	0.185
140	0.013	0.197	183	0.010	0.211
141	0.009	0.166	184	0.015	0.270
142	0.009	0.158	185	0.045	0.316
143	0.009	0.171	186	0.012	0.249
144	0.023	0.293	187	0.021	0.223
145	0.019	0.278	188	0.020	0.229
146	0.015	0.250	189	0.008	0.131
147	0.009	0.197	190	0.020	0.278
148	0.009	0.158	191	0.110	0.610
149	0.017	0.188	192	0.035	0.270
150	0.185	0.827	193	0.018	0.270
151	0.076	0.485	194	0.009	0.213
152	0.008	0.188	195	0.074	0.427
153	0.041	0.302	196	0.015	0.249
154	0.051	0.302	197	0.018	0.242
155	0.032	0.252	198	0.010	0.146
156	0.009	0.131	199	0.021	0.265
157	0.012	0.171	200	0.020	0.289
158	0.009	0.146	201	0.038	0.443
159	0.009	0.158	202	0.021	0.278
160	0.057	0.398	203	0.014	0.188
161	0.011	0.146	204	0.008	0.185
162	0.024	0.294	205	0.032	0.252
163	0.121	0.593	206	0.010	0.171
164	0.010	0.158	207	0.028	0.252
165	0.016	0.211	208	0.041	0.306
166	0.009	0.211	209	0.009	0.158
167	0.032	0.334	210	0.013	0.270
168	0.009	0.197	211	0.009	0.146
169	0.089	0.483	212	0.029	0.270
170	0.025	0.334	213	0.021	0.213
171	0.123	0.501	214	0.065	0.398
172	0.012	0.242	215	0.008	0.131
173	0.088	0.564	216	0.009	0.131
174	0.033	0.473	217	0.042	0.353
175	0.008	0.131	218	0.011	0.197

Agglomerate	Area (mm^2)	Maximum Feret's Diameter (mm)	Agglomerate	Area (mm^2)	Maximum Feret's Diameter (mm)
219	0.009	0.166	262	0.015	0.185
220	0.009	0.171	263	0.038	0.317
221	0.013	0.207	264	0.015	0.213
222	0.046	0.382	265	0.060	0.455
223	0.026	0.270	266	0.023	0.229
224	0.062	0.353	267	0.009	0.188
225	0.028	0.236	268	0.016	0.207
226	0.023	0.250	269	0.015	0.188
227	0.058	0.535	270	0.019	0.270
228	0.111	0.480	271	0.031	0.353
229	0.025	0.223	272	0.029	0.411
230	0.009	0.146	273	0.020	0.188
231	0.017	0.293	274	0.038	0.290
232	0.032	0.407	275	0.009	0.146
233	0.020	0.270	276	0.011	0.211
234	0.056	0.375	277	0.017	0.188
235	0.042	0.528	278	0.010	0.171
236	0.009	0.146	279	0.072	0.472
237	0.066	0.419	280	0.071	0.446
238	0.034	0.316	281	0.009	0.171
239	0.014	0.185	282	0.024	0.270
240	0.070	0.398	283	0.071	0.414
241	0.022	0.197	284	0.025	0.262
242	0.010	0.197	285	0.017	0.343
243	0.056	0.358	286	0.078	0.483
244	0.027	0.252	287	0.008	0.131
245	0.053	0.328	288	0.028	0.642
246	0.018	0.213	289	0.011	0.171
247	0.022	0.229	290	0.010	0.229
248	0.019	0.211	291	0.012	0.242
249	0.071	0.419	292	0.082	0.547
250	0.066	0.371	293	0.008	0.131
251	0.049	0.343	294	0.023	0.276
252	0.009	0.146	295	0.052	0.398
253	0.022	0.229	296	0.026	0.299
254	0.022	0.276	297	0.016	0.317
255	0.023	0.213	298	0.014	0.223
256	0.015	0.211	299	0.009	0.171
257	0.013	0.188	300	0.010	0.158
258	0.055	0.472	301	0.009	0.146
259	0.017	0.197	302	0.008	0.146
260	0.011	0.158	303	0.012	0.207
261	0.015	0.185	304	0.027	0.293

Agglomerate	Area (mm^2)	Maximum Feret's Diameter (mm)	Agglomerate	Area (mm^2)	Maximum Feret's Diameter (mm)
305	0.015	0.188	348	0.009	0.158
306	0.058	0.382	349	0.029	0.278
307	0.041	0.362	350	0.093	0.621
308	0.009	0.185	351	0.017	0.197
309	0.037	0.276	352	0.012	0.185
310	0.014	0.207	353	0.020	0.242
311	0.102	0.491	354	0.012	0.166
312	0.014	0.197	355	0.036	0.276
313	0.009	0.146	356	0.011	0.236
314	0.027	0.252	357	0.009	0.149
315	0.022	0.311	358	0.014	0.185
316	0.027	0.293	359	0.009	0.197
317	0.038	0.328	360	0.153	0.556
318	0.016	0.213	361	0.034	0.306
319	0.011	0.171	362	0.010	0.171
320	0.088	0.447	363	0.008	0.131
321	0.035	0.262	364	0.009	0.131
322	0.008	0.146	365	0.009	0.166
323	0.021	0.223	366	0.025	0.250
324	0.008	0.158	367	0.009	0.149
325	0.010	0.166	368	0.012	0.211
326	0.053	0.362	369	0.027	0.294
327	0.008	0.131	370	0.015	0.229
328	0.039	0.342	371	0.015	0.262
329	0.071	0.433	372	0.021	0.262
330	0.011	0.188	373	0.013	0.185
331	0.058	0.414	374	0.009	0.131
332	0.088	0.480	375	0.021	0.229
333	0.028	0.276	376	0.008	0.131
334	0.100	0.528	377	0.033	0.265
335	0.018	0.229	378	0.009	0.146
336	0.009	0.158	379	0.010	0.197
337	0.057	0.436	380	0.015	0.213
338	0.008	0.197	381	0.112	0.621
339	0.025	0.293	382	0.015	0.211
340	0.027	0.252	383	0.027	0.236
341	0.041	0.317	384	0.008	0.158
342	0.009	0.171	385	0.082	0.446
343	0.010	0.146	386	0.015	0.171
344	0.020	0.278	387	0.017	0.207
345	0.035	0.306	388	0.085	0.569
346	0.015	0.171	389	0.020	0.211
347	0.015	0.252	390	0.018	0.252

Agglomerate	Area (mm^2)	Maximum Feret's Diameter (mm)
391	0.021	0.270
392	0.044	0.311
393	0.020	0.302
394	0.009	0.146
395	0.025	0.250
396	0.011	0.158
397	0.016	0.211
398	0.010	0.146
399	0.010	0.185
400	0.023	0.236
401	0.037	0.278
402	0.022	0.252
403	0.013	0.171
404	0.039	0.317
405	0.022	0.229
406	0.009	0.185
407	0.016	0.223
408	0.016	0.197
409	0.015	0.171
410	0.157	0.715
411	0.011	0.188
412	0.009	0.185
413	0.021	0.316
414	0.015	0.188
415	0.032	0.276
416	0.009	0.185
417	0.010	0.213
418	0.014	0.188
419	0.009	0.166
420	0.012	0.158
421	0.016	0.236
422	0.009	0.146
423	0.030	0.293
424	0.025	0.211
425	0.072	0.499
426	0.103	0.439
427	0.051	0.398
428	0.015	0.171
429	0.010	0.188
430	0.009	0.211
431	0.009	0.131
432	0.038	0.398
433	0.036	0.270

Agglomerate	Area (mm^2)	Maximum Feret's Diameter (mm)
434	0.070	0.391
435	0.092	0.642
436	0.010	0.146
437	0.033	0.381
438	0.010	0.131
439	0.010	0.146
440	0.027	0.252
441	0.025	0.289
442	0.051	0.356
443	0.015	0.213
444	0.022	0.262
445	0.237	0.910
446	0.015	0.270
447	0.014	0.223
448	0.018	0.197
449	0.030	0.306
450	0.012	0.171
451	0.015	0.211
452	0.009	0.171
453	0.013	0.197
454	0.022	0.262
455	0.018	0.211
456	0.009	0.146
457	0.078	0.535
458	0.042	0.472
459	0.009	0.146
460	0.008	0.149
461	0.008	0.171
462	0.008	0.158
463	0.022	0.447
464	0.197	0.741
465	0.014	0.302
466	0.015	0.250
467	0.012	0.262
468	0.013	0.188
469	0.008	0.188
470	0.123	0.576
471	0.022	0.211
472	0.010	0.166
473	0.009	0.146
474	0.012	0.158
475	0.010	0.158
476	0.016	0.211

Agglomerate	Area (mm^2)	Maximum Feret’s Diameter (mm)	Agglomerate	Area (mm^2)	Maximum Feret’s Diameter (mm)
477	0.056	0.540	520	0.017	0.213
478	0.009	0.188	521	0.008	0.131
479	0.028	0.262	522	0.032	0.328
480	0.018	0.185	523	0.016	0.207
481	0.008	0.236	524	0.077	0.381
482	0.058	0.512	525	0.018	0.211
483	0.017	0.213	526	0.012	0.171
484	0.017	0.207	527	0.034	0.407
485	0.008	0.131	528	0.029	0.293
486	0.047	0.316	529	0.009	0.146
487	0.008	0.171	530	0.011	0.188
488	0.024	0.317	531	0.015	0.171
489	0.019	0.223	532	0.095	0.512
490	0.010	0.211	533	0.039	0.448
491	0.009	0.185	534	0.008	0.188
492	0.083	0.501	535	0.027	0.252
493	0.045	0.317	536	0.032	0.375
494	0.021	0.252	537	0.010	0.149
495	0.036	0.316	538	0.024	0.242
496	0.020	0.270	539	0.008	0.171
497	0.032	0.299	540	0.032	0.270
498	0.021	0.229	541	0.010	0.171
499	0.066	0.423	542	0.008	0.124
500	0.014	0.185	543	0.010	0.211
501	0.010	0.171	544	0.012	0.158
502	0.012	0.171	545	0.012	0.213
503	0.009	0.149	546	0.013	0.166
504	0.015	0.250	547	0.011	0.166
505	0.017	0.197	548	0.055	0.331
506	0.009	0.211	549	0.008	0.211
507	0.066	0.512	550	0.009	0.131
508	0.012	0.185	551	0.031	0.236
509	0.011	0.171	552	0.154	0.696
510	0.008	0.124	553	0.010	0.242
511	0.021	0.242	554	0.017	0.236
512	0.027	0.262	555	0.029	0.375
513	0.011	0.171	556	0.013	0.158
514	0.021	0.223	557	0.021	0.302
515	0.049	0.342	558	0.043	0.302
516	0.008	0.131	559	0.013	0.158
517	0.013	0.211	560	0.077	0.499
518	0.012	0.197	561	0.043	0.317
519	0.068	0.446	562	0.009	0.158

Agglomerate	Area (mm^2)	Maximum Feret's Diameter (mm)	Agglomerate	Area (mm^2)	Maximum Feret's Diameter (mm)
563	0.009	0.171	606	0.018	0.316
564	0.009	0.197	607	0.010	0.213
565	0.066	0.393	608	0.014	0.188
566	0.009	0.158	609	0.051	0.391
567	0.167	0.632	610	0.021	0.236
568	0.015	0.252	611	0.032	0.276
569	0.017	0.278	612	0.051	0.477
570	0.033	0.398	613	0.009	0.131
571	0.021	0.229	614	0.008	0.131
572	0.011	0.171	615	0.008	0.171
573	0.109	0.498	616	0.021	0.293
574	0.028	0.538	617	0.152	0.610
575	0.144	0.725	618	0.008	0.171
576	0.054	0.448	619	0.018	0.197
577	0.190	0.610	620	0.009	0.197
578	0.008	0.171	621	0.010	0.166
579	0.046	0.427	622	0.011	0.211
580	0.013	0.207	623	0.015	0.188
581	0.041	0.391	624	0.017	0.223
582	0.017	0.207	625	0.092	0.433
583	0.045	0.381	626	0.076	0.436
584	0.079	0.423	627	0.051	0.317
585	0.009	0.158	628	0.040	0.293
586	0.148	0.539	629	0.076	0.566
587	0.099	0.483	630	0.056	0.455
588	0.070	0.373	631	0.011	0.146
589	0.044	0.289	632	0.009	0.146
590	0.155	0.676	633	0.009	0.171
591	0.010	0.197	634	0.011	0.276
592	0.022	0.250	635	0.009	0.236
593	0.028	0.306	636	0.009	0.131
594	0.012	0.166	637	0.032	0.382
595	0.148	0.540	638	0.027	0.236
596	0.014	0.188	639	0.108	0.512
597	0.009	0.211	640	0.014	0.213
598	0.014	0.188	641	0.030	0.250
599	0.070	0.354	642	0.009	0.158
600	0.008	0.211	643	0.033	0.328
601	0.011	0.171	644	0.021	0.211
602	0.118	0.556	645	0.021	0.242
603	0.022	0.223	646	0.020	0.213
604	0.173	0.696	647	0.008	0.149
605	0.009	0.188	648	0.063	0.408

Agglomerate	Area (mm^2)	Maximum Feret's Diameter (mm)
649	0.008	0.131
650	0.019	0.262
651	0.008	0.131
652	0.112	0.621
653	0.008	0.158
654	0.016	0.211
655	0.027	0.242
656	0.014	0.188
657	0.047	0.391
658	0.009	0.158
659	0.071	0.447
660	0.058	0.604
661	0.040	0.278
662	0.008	0.131
663	0.021	0.242
664	0.067	0.408
665	0.026	0.299
666	0.009	0.146
667	0.036	0.306
668	0.009	0.171
669	0.014	0.185
670	0.040	0.416
671	0.027	0.249
672	0.017	0.250
673	0.015	0.229
674	0.039	0.317
675	0.008	0.131
676	0.035	0.311
677	0.009	0.146
678	0.027	0.242
679	0.015	0.207
680	0.021	0.229
681	0.009	0.146
682	0.017	0.207
683	0.018	0.236
684	0.015	0.197
685	0.017	0.236
686	0.013	0.249
687	0.047	0.342
688	0.024	0.229
689	0.043	0.354
690	0.009	0.166
691	0.009	0.171
692	0.009	0.146
693	0.012	0.185
694	0.021	0.236
695	0.015	0.356
696	0.009	0.146
697	0.014	0.197
698	0.008	0.131
699	0.010	0.211
700	0.010	0.188

PC-CNF-CF

Number of CNF agglomerates greater than 0.007 mm^2: 627.
Cumulative area of CNFs agglomerates greater than 0.007 mm^2: 29.805 mm^2.
Area fraction of CNF agglomerates greater than 0.007 mm^2: 2.6%.

Agglomerate	Area (mm^2)	Maximum Feret's Diameter (mm)
1	0.023	0.302
2	0.013	0.252
3	0.016	0.278
4	0.016	0.213
5	0.015	0.197
6	0.019	0.197
7	0.013	0.211
8	0.026	0.289
9	0.015	0.188
10	0.027	0.278

Agglomerate	Area (mm^2)	Maximum Feret's Diameter (mm)	Agglomerate	Area (mm^2)	Maximum Feret's Diameter (mm)
11	0.033	0.252	54	0.017	0.276
12	0.020	0.293	55	0.021	0.211
13	0.021	0.236	56	0.033	0.289
14	0.106	0.713	57	0.050	0.334
15	0.019	0.276	58	0.026	0.289
16	0.017	0.223	59	0.041	0.342
17	0.022	0.252	60	0.118	0.566
18	0.031	0.289	61	0.026	0.262
19	0.035	0.316	62	0.015	0.185
20	0.021	0.262	63	0.017	0.262
21	0.028	0.328	64	0.014	0.207
22	0.028	0.328	65	0.014	0.213
23	0.081	0.433	66	0.086	0.398
24	0.015	0.276	67	0.015	0.171
25	0.013	0.197	68	0.057	0.394
26	0.100	0.512	69	0.034	0.328
27	0.012	0.229	70	0.010	0.188
28	0.024	0.270	71	0.019	0.229
29	0.078	0.480	72	0.033	0.398
30	0.030	0.334	73	0.045	0.408
31	0.027	0.236	74	0.045	0.419
32	0.033	0.353	75	0.109	0.473
33	0.024	0.223	76	0.021	0.299
34	0.077	0.353	77	0.040	0.289
35	0.051	0.382	78	0.015	0.211
36	0.030	0.306	79	0.045	0.343
37	0.020	0.316	80	0.058	0.447
38	0.030	0.302	81	0.014	0.229
39	0.023	0.294	82	0.088	0.463
40	0.021	0.262	83	0.013	0.252
41	0.023	0.250	84	0.077	0.448
42	0.154	0.621	85	0.014	0.223
43	0.092	0.504	86	0.030	0.342
44	0.027	0.252	87	0.102	0.545
45	0.064	0.407	88	0.021	0.197
46	0.026	0.236	89	0.015	0.211
47	0.025	0.531	90	0.022	0.342
48	0.013	0.211	91	0.027	0.276
49	0.023	0.262	92	0.059	0.358
50	0.070	0.408	93	0.031	0.311
51	0.070	0.407	94	0.025	0.317
52	0.181	0.676	95	0.126	0.563
53	0.033	0.252	96	0.036	0.485

Agglomerate	Area (mm^2)	Maximum Feret's Diameter (mm)	Agglomerate	Area (mm^2)	Maximum Feret's Diameter (mm)
97	0.018	0.213	140	0.032	0.328
98	0.017	0.270	141	0.444	0.970
99	0.065	0.458	142	0.044	0.342
100	0.293	0.817	143	0.014	0.207
101	0.031	0.262	144	0.015	0.185
102	0.025	0.236	145	0.022	0.252
103	0.013	0.188	146	0.055	0.539
104	0.014	0.185	147	0.032	0.448
105	0.019	0.316	148	0.009	0.146
106	0.015	0.250	149	0.015	0.236
107	0.023	0.381	150	0.015	0.354
108	0.027	0.229	151	0.026	0.262
109	0.030	0.362	152	0.036	0.316
110	0.015	0.188	153	0.016	0.276
111	0.015	0.229	154	0.064	0.393
112	0.302	0.966	155	0.042	0.463
113	0.058	0.531	156	0.024	0.270
114	0.039	0.331	157	0.033	0.306
115	0.050	0.358	158	0.024	0.382
116	0.145	0.522	159	0.019	0.265
117	0.015	0.242	160	0.014	0.316
118	0.014	0.236	161	0.036	0.317
119	0.021	0.252	162	0.039	0.358
120	0.013	0.197	163	0.014	0.185
121	0.013	0.213	164	0.030	0.427
122	0.021	0.306	165	0.147	0.569
123	0.016	0.229	166	0.065	0.473
124	0.142	0.566	167	0.033	0.334
125	0.070	0.398	168	0.073	0.491
126	0.017	0.306	169	0.017	0.262
127	0.040	0.375	170	0.047	0.385
128	0.038	0.342	171	0.015	0.316
129	0.016	0.207	172	0.027	0.236
130	0.015	0.197	173	0.016	0.276
131	0.020	0.270	174	0.021	0.252
132	0.010	0.229	175	0.008	0.158
133	0.038	0.334	176	0.177	0.623
134	0.027	0.408	177	0.012	0.236
135	0.146	0.504	178	0.030	0.343
136	0.031	0.367	179	0.202	0.778
137	0.013	0.302	180	0.298	0.834
138	0.019	0.278	181	0.022	0.289
139	0.039	0.316	182	0.110	0.626

Agglomerate	Area (mm^2)	Maximum Feret's Diameter (mm)
183	0.028	0.236
184	0.013	0.188
185	0.028	0.250
186	0.014	0.278
187	0.016	0.252
188	0.016	0.294
189	0.027	0.477
190	0.015	0.316
191	0.013	0.211
192	0.041	0.519
193	0.020	0.223
194	0.022	0.236
195	0.013	0.236
196	0.025	0.289
197	0.015	0.223
198	0.016	0.223
199	0.020	0.317
200	0.288	0.945
201	0.034	0.393
202	0.063	0.463
203	0.125	0.684
204	0.078	0.569
205	0.021	0.328
206	0.146	0.603
207	0.130	0.627
208	0.026	0.391
209	0.026	0.242
210	0.031	0.381
211	0.015	0.276
212	0.042	0.531
213	0.180	0.725
214	0.013	0.223
215	0.017	0.262
216	0.015	0.270
217	0.051	0.419
218	0.013	0.197
219	0.031	0.306
220	0.012	0.229
221	0.015	0.207
222	0.015	0.236
223	0.013	0.213
224	0.039	0.302
225	0.060	0.463

Agglomerate	Area (mm^2)	Maximum Feret's Diameter (mm)
226	0.042	0.408
227	0.102	0.528
228	0.015	0.211
229	0.185	1.008
230	0.041	0.531
231	0.014	0.197
232	0.015	0.185
233	0.335	0.936
234	0.039	0.358
235	0.013	0.171
236	0.014	0.188
237	0.021	0.252
238	0.008	0.131
239	0.101	0.564
240	0.019	0.197
241	0.023	0.276
242	0.023	0.250
243	0.027	0.328
244	0.041	0.276
245	0.015	0.213
246	0.014	0.197
247	0.177	0.742
248	0.061	0.874
249	0.015	0.249
250	0.016	0.236
251	0.014	0.171
252	0.019	0.252
253	0.021	0.252
254	0.017	0.213
255	0.016	0.270
256	0.027	0.328
257	0.015	0.185
258	0.030	0.311
259	0.122	0.556
260	0.154	0.681
261	0.030	0.353
262	0.019	0.276
263	0.014	0.270
264	0.028	0.398
265	0.013	0.250
266	0.043	0.311
267	0.028	0.316
268	0.037	0.436

Agglomerate	Area (mm^2)	Maximum Feret's Diameter (mm)
269	0.284	0.810
270	0.021	0.252
271	0.023	0.394
272	0.031	0.488
273	0.015	0.213
274	0.023	0.512
275	0.014	0.197
276	0.191	0.834
277	0.014	0.197
278	0.045	0.414
279	0.015	0.262
280	0.013	0.229
281	0.021	0.331
282	0.061	0.408
283	0.014	0.262
284	0.023	0.375
285	0.108	0.604
286	0.247	0.915
287	0.013	0.211
288	0.022	0.278
289	0.038	0.356
290	0.023	0.367
291	0.015	0.270
292	0.018	0.223
293	0.045	0.423
294	0.028	0.302
295	0.027	0.385
296	0.013	0.213
297	0.048	0.358
298	0.029	0.331
299	0.037	0.334
300	0.121	0.621
301	0.027	0.334
302	0.013	0.236
303	0.044	0.375
304	0.016	0.171
305	0.044	0.342
306	0.013	0.242
307	0.023	0.278
308	0.014	0.343
309	0.110	0.501
310	0.013	0.223
311	0.015	0.250

Agglomerate	Area (mm^2)	Maximum Feret's Diameter (mm)
312	0.009	0.146
313	0.015	0.250
314	0.017	0.252
315	0.015	0.197
316	0.095	0.604
317	0.027	0.433
318	0.051	0.501
319	0.017	0.229
320	0.109	0.708
321	0.016	0.242
322	0.020	0.236
323	0.015	0.211
324	0.016	0.171
325	0.117	0.497
326	0.021	0.223
327	0.028	0.276
328	0.015	0.188
329	0.044	0.306
330	0.045	0.334
331	0.013	0.207
332	0.052	0.328
333	0.014	0.158
334	0.078	0.480
335	0.056	0.371
336	0.206	0.709
337	0.038	0.317
338	0.023	0.293
339	0.015	0.207
340	0.106	0.681
341	0.435	1.090
342	0.013	0.188
343	0.023	0.236
344	0.015	0.223
345	0.139	0.843
346	0.034	0.334
347	0.112	0.473
348	0.014	0.197
349	0.128	0.540
350	0.020	0.197
351	0.028	0.353
352	0.151	0.713
353	0.020	0.211
354	0.020	0.328

Agglomerate	Area (mm^2)	Maximum Feret's Diameter (mm)	Agglomerate	Area (mm^2)	Maximum Feret's Diameter (mm)
355	0.135	0.715	398	0.199	0.881
356	0.016	0.223	399	0.033	0.447
357	0.017	0.306	400	0.015	0.213
358	0.045	0.362	401	0.021	0.229
359	0.016	0.213	402	0.013	0.213
360	0.137	0.788	403	0.019	0.185
361	0.023	0.367	404	0.024	0.213
362	0.019	0.276	405	0.038	0.381
363	0.013	0.188	406	0.014	0.197
364	0.022	0.262	407	0.062	0.382
365	0.029	0.358	408	0.035	0.334
366	0.076	0.566	409	0.018	0.252
367	0.015	0.242	410	0.016	0.362
368	0.014	0.250	411	0.015	0.171
369	0.020	0.236	412	0.235	0.866
370	0.027	0.371	413	0.017	0.252
371	0.031	0.270	414	0.014	0.188
372	0.017	0.223	415	0.155	0.564
373	0.016	0.229	416	0.159	0.694
374	0.070	0.658	417	0.035	0.262
375	0.019	0.223	418	0.017	0.289
376	0.021	0.236	419	0.056	0.473
377	0.013	0.223	420	0.022	0.328
378	0.092	0.436	421	0.013	0.211
379	0.021	0.289	422	0.033	0.407
380	0.019	0.270	423	0.097	0.724
381	0.035	0.354	424	0.020	0.250
382	0.013	0.171	425	0.008	0.146
383	0.039	0.354	426	0.013	0.223
384	0.021	0.316	427	0.029	0.249
385	0.275	0.741	428	0.089	0.414
386	0.157	0.686	429	0.031	0.317
387	0.249	1.167	430	0.049	0.391
388	0.027	0.436	431	0.021	0.276
389	0.028	0.317	432	0.055	0.334
390	0.018	0.250	433	0.088	0.416
391	0.014	0.185	434	0.061	0.414
392	0.146	0.512	435	0.038	0.416
393	0.059	0.436	436	0.088	0.488
394	0.015	0.188	437	0.031	0.293
395	0.021	0.250	438	0.027	0.328
396	0.029	0.353	439	0.053	0.398
397	0.013	0.207	440	0.017	0.188

Agglomerate	Area (mm^2)	Maximum Feret's Diameter (mm)	Agglomerate	Area (mm^2)	Maximum Feret's Diameter (mm)
441	0.028	0.317	484	0.013	0.223
442	0.013	0.197	485	0.031	0.299
443	0.015	0.223	486	0.021	0.289
444	0.021	0.270	487	0.070	0.618
445	0.014	0.252	488	0.232	0.984
446	0.013	0.171	489	0.033	0.343
447	0.015	0.252	490	0.072	0.560
448	0.130	0.488	491	0.021	0.252
449	0.080	0.463	492	0.019	0.236
450	0.082	0.560	493	0.019	0.316
451	0.017	0.252	494	0.182	0.708
452	0.013	0.306	495	0.020	0.223
453	0.037	0.306	496	0.023	0.302
454	0.020	0.270	497	0.044	0.382
455	0.015	0.171	498	0.012	0.242
456	0.082	0.463	499	0.104	0.545
457	0.010	0.197	500	0.020	0.306
458	0.013	0.171	501	0.027	0.276
459	0.120	0.610	502	0.090	0.540
460	0.024	0.289	503	0.100	0.427
461	0.024	0.250	504	0.015	0.213
462	0.052	0.342	505	0.021	0.328
463	0.033	0.302	506	0.017	0.299
464	0.020	0.265	507	0.018	0.236
465	0.015	0.302	508	0.013	0.252
466	0.023	0.306	509	0.328	0.868
467	0.087	0.459	510	0.013	0.242
468	0.015	0.223	511	0.021	0.211
469	0.051	0.375	512	0.015	0.276
470	0.361	0.904	513	0.016	0.185
471	0.112	0.623	514	0.027	0.229
472	0.021	0.289	515	0.015	0.197
473	0.015	0.250	516	0.016	0.223
474	0.019	0.302	517	0.045	0.293
475	0.096	0.459	518	0.048	0.302
476	0.021	0.393	519	0.013	0.207
477	0.021	0.328	520	0.013	0.197
478	0.016	0.223	521	0.519	1.342
479	0.027	0.316	522	0.015	0.211
480	0.100	0.709	523	0.018	0.236
481	0.087	0.463	524	0.016	0.252
482	0.016	0.185	525	0.017	0.236
483	0.022	0.270	526	0.039	0.382

Agglomerate	Area (mm^2)	Maximum Feret's Diameter (mm)	Agglomerate	Area (mm^2)	Maximum Feret's Diameter (mm)
527	0.023	0.276	570	0.018	0.223
528	0.020	0.316	571	0.016	0.250
529	0.011	0.211	572	0.040	0.299
530	0.015	0.229	573	0.017	0.229
531	0.009	0.158	574	0.082	0.569
532	0.208	0.761	575	0.078	0.664
533	0.141	0.563	576	0.014	0.236
534	0.027	0.353	577	0.019	0.278
535	0.218	0.814	578	0.029	0.252
536	0.038	0.294	579	0.014	0.250
537	0.037	0.443	580	0.027	0.276
538	0.025	0.358	581	0.021	0.223
539	0.015	0.223	582	0.016	0.242
540	0.384	1.131	583	0.014	0.213
541	0.084	0.553	584	0.084	0.512
542	0.095	0.463	585	0.013	0.252
543	0.156	0.540	586	0.013	0.171
544	0.221	0.871	587	0.015	0.236
545	0.013	0.278	588	0.014	0.289
546	0.018	0.311	589	0.035	0.328
547	0.027	0.289	590	0.020	0.242
548	0.021	0.250	591	0.017	0.211
549	0.014	0.250	592	0.016	0.270
550	0.040	0.289	593	0.014	0.197
551	0.019	0.252	594	0.049	0.334
552	0.021	0.278	595	0.058	0.535
553	0.009	0.149	596	0.022	0.290
554	0.037	0.302	597	0.013	0.211
555	0.014	0.211	598	0.013	0.265
556	0.021	0.276	599	0.009	0.146
557	0.027	0.270	600	0.030	0.278
558	0.021	0.223	601	0.013	0.188
559	0.084	0.528	602	0.015	0.223
560	0.022	0.276	603	0.362	0.839
561	0.069	0.436	604	0.020	0.197
562	0.014	0.265	605	0.014	0.229
563	0.022	0.270	606	0.021	0.207
564	0.038	0.270	607	0.026	0.223
565	0.014	0.242	608	0.210	1.029
566	0.039	0.317	609	0.035	0.316
567	0.065	0.528	610	0.018	0.185
568	0.058	0.382	611	0.013	0.213
569	0.044	0.362	612	0.015	0.211

Agglomerate	Area (mm^2)	Maximum Feret's Diameter (mm)
613	0.036	0.334
614	0.026	0.371
615	0.019	0.270
616	0.015	0.213
617	0.112	0.535
618	0.132	0.725
619	0.015	0.213
620	0.033	0.328
621	0.017	0.185
622	0.015	0.188
623	0.017	0.185
624	0.020	0.299
625	0.053	0.373
626	0.020	0.270
627	0.028	0.250

APPENDIX C

MICROMECHANICAL DATA

This appendix contains the SEM images and a summary of the data used in the study of the micromechanical properties of cement-based composites with CNFs (Chapter 4 and Section 6.3.2). A backscatter and secondary SEM image; a backscatter SEM image with false color and indentation locations imposed; the location of each indent (i.e., flaw, hydrate, unhydrated particle, etc.) as determined using the false color image; the modulus, hardness, and contact displacement values obtained by nanoindentation; and the Si/Ca and Al/Ca ratios obtained from EDS are included for each nanoindentation grid. Calibrations for the Si/Ca and Al/Ca ratios were made with calcium carbonate, silicon dioxide, albite, magnesium oxide, aluminum oxide, gallium phosphide, iron sulphide, MAD-10 feldspar, wollastonite, manganese, and iron, and the XPP scheme, a Phi-Rho-Z method, was used for matrix corrections as analyzed by INCA Energy Software (Oxford Instruments, Abingdon, Oxfordshire, England) [139].

PC-A Grid 1

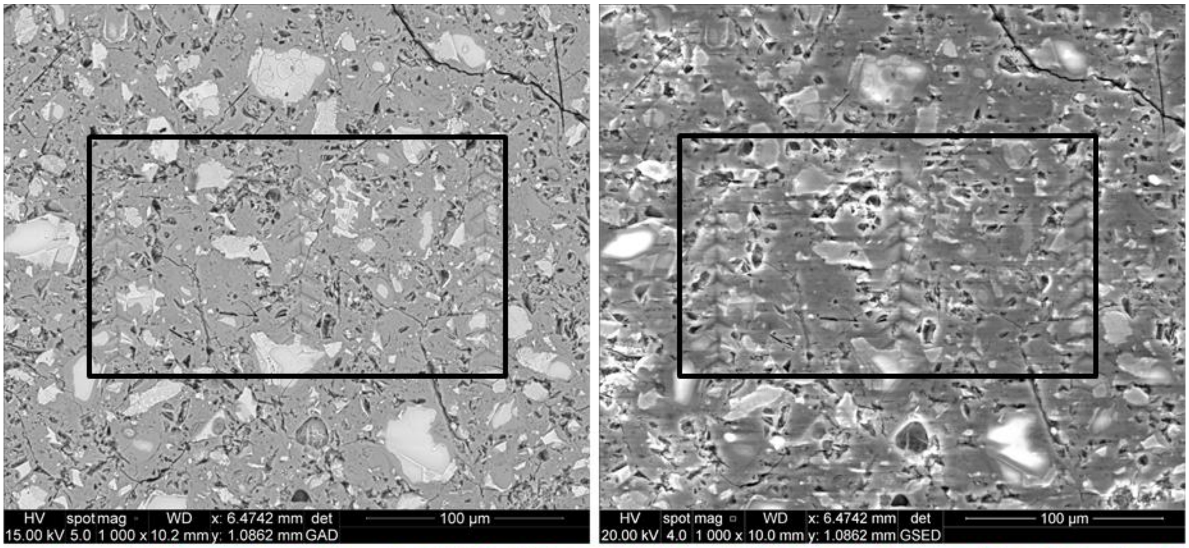

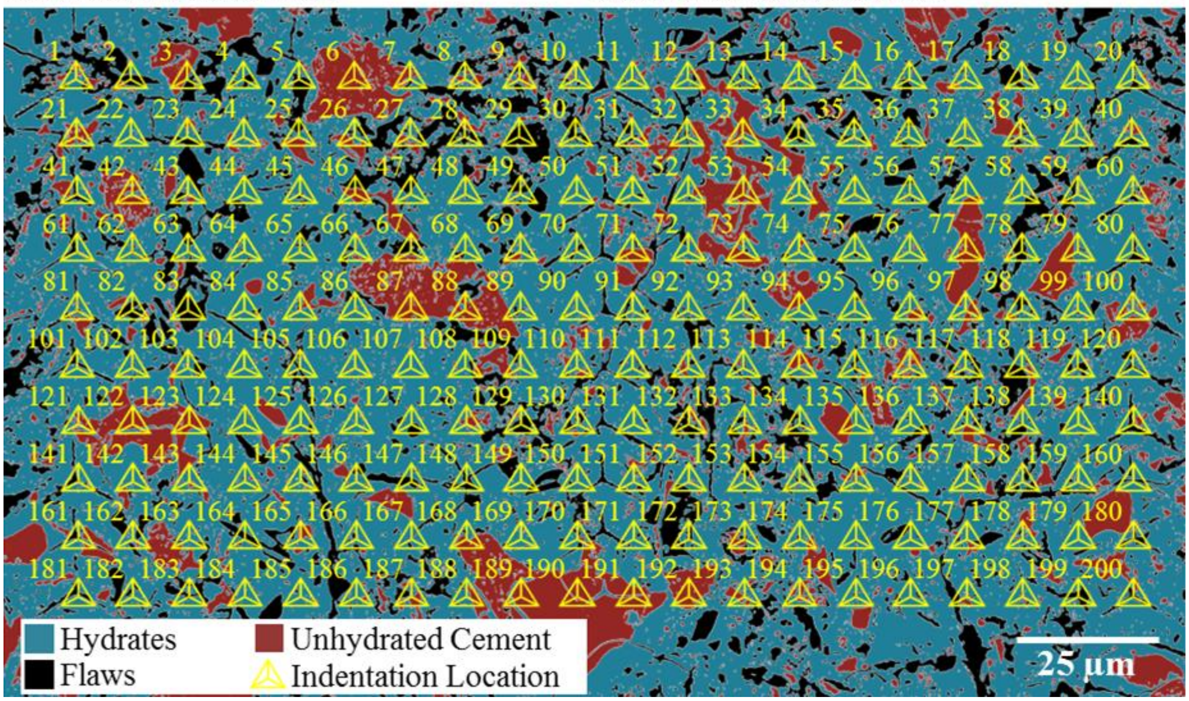

Indent	Type*	Modulus (GPa)	Hardness (GPa)	Maximum Displacement (nm)	Si/Ca Ratio	Al/Ca Ratio
1	h	10.765	0.275	544.088	0.275	0.051
2	f	21.974	0.818	313.738	0.228	0.106
3	h/u	100.021	14.151	71.95	0.056	1.190
4	f/h	11.583	0.259	561.308	0.512	0.104
5	f/h	error	error	error	0.600	0.078
6	u	105.235	7.485	100.679	0.578	0.033
7	h/u	“invalid”	“invalid”	“invalid”	0.536	0.086

Indent	Type*	Modulus (GPa)	Hardness (GPa)	Maximum Displacement (nm)	Si/Ca Ratio	Al/Ca Ratio
8	h/u	“invalid”	“invalid”	“invalid”	0.493	0.172
9	h/u	“invalid”	“invalid”	“invalid”	0.056	0.014
10	f/h	error	error	error	0.334	0.137
11	h	17.756	0.740	329.723	0.450	0.092
12	h	“invalid”	“invalid”	“invalid”	0.546	0.125
13	f/h	127.784	13.012	75.308	0.284	0.443
14	h	21.126	0.718	334.843	0.583	0.104
15	h	19.420	0.798	317.342	0.601	0.082
16	f/h	15.531	0.538	387.772	0.406	0.195
17	h	26.954	1.131	266	0.483	0.199
18	f/h	90.052	5.380	119.517	0.355	0.298
19	h	14.069	0.476	412.299	0.623	0.095
20	f/h	“invalid”	“invalid”	“invalid”	0.583	0.079
21	h/u	88.522	7.251	102.36	0.366	0.226
22	h	21.007	0.644	353.964	0.460	0.212
23	f/h	“invalid”	“invalid”	“invalid”	0.506	0.136
24	h	22.045	0.742	329.597	0.409	0.314
25	h	error	error	error	0.374	0.229
26	h	23.465	1.215	256.372	0.536	0.072
27	h	error	error	error	0.506	0.153
28	f	“invalid”	“invalid”	“invalid”	0.196	0.036
29	f	“invalid”	“invalid”	“invalid”	0.255	0.036
30	f/h	“invalid”	“invalid”	“invalid”	0.528	0.146
31	f/h	“invalid”	“invalid”	“invalid”	0.327	0.123
32	f/h	31.303	0.832	310.915	0.170	0.440
33	f/h/u	45.024	1.383	240.091	0.358	0.142
34	f	“invalid”	“invalid”	“invalid”	0.506	0.396
35	f/h/u	21.901	0.850	307.387	0.499	0.217
36	h	13.909	0.619	361.351	0.454	0.229
37	h	21.783	0.988	284.94	0.602	0.108
38	f/h/u	20.741	1.011	281.643	0.428	0.203
39	h	“invalid”	“invalid”	“invalid”	0.685	0.107
40	h/u	45.814	4.195	136.067	0.459	0.162
41	h	27.568	0.750	327.928	0.565	0.046
42	h/u	“invalid”	“invalid”	“invalid”	0.540	0.056
43	f/h	“invalid”	“invalid”	“invalid”	0.397	0.253
44	h	21.503	0.791	318.912	0.583	0.095
45	f/h	26.773	0.994	284.129	0.567	0.131
46	u	80.093	7.319	101.818	0.547	0.108
47	f/h	“invalid”	“invalid”	“invalid”	0.333	0.412

Indent	Type*	Modulus (GPa)	Hardness (GPa)	Maximum Displacement (nm)	Si/Ca Ratio	Al/Ca Ratio
48	h	17.189	0.514	396.495	0.623	0.083
49	h	“invalid”	“invalid”	“invalid”	0.583	0.134
50	h	22.137	0.705	338.21	0.630	0.095
51	h	16.264	0.536	388.254	0.498	0.091
52	h	29.317	1.441	235.195	0.586	0.099
53	u	“invalid”	“invalid”	“invalid”	0.152	0.523
54	h	24.010	0.982	285.813	0.448	0.217
55	h	18.915	0.789	319.554	0.576	0.140
56	h/u	19.923	0.701	339.275	0.393	0.287
57	h	76.771	5.614	116.939	0.606	0.099
58	h	17.928	0.651	351.816	0.560	0.178
59	f/h	22.624	0.651	352	0.417	0.055
60	h	29.458	1.473	232.416	0.642	0.073
61	h	35.610	5.574	117.334	0.634	0.111
62	f/h	15.617	0.429	435.088	0.545	0.107
63	f/h	9.288	0.300	520.456	0.501	0.202
64	f/h	20.960	0.757	326.099	0.403	0.092
65	f/h	23.682	0.767	324.106	0.634	0.075
66	f/h	25.504	0.836	310.22	0.645	0.076
67	f	59.602	3.693	145.179	0.496	0.087
68	f/h	“invalid”	“invalid”	“invalid”	0.642	0.096
69	h/u	“invalid”	“invalid”	“invalid”	0.582	0.241
70	f/h	“invalid”	“invalid”	“invalid”	0.578	0.203
71	u	90.702	9.237	90.122	0.210	0.326
72	f	25.541	0.972	287.343	0.537	0.137
73	f/h/u	89.383	9.869	87.043	0.154	0.539
74	f/h	27.590	1.091	270.943	0.493	0.177
75	f/h	17.673	0.645	353.653	0.669	0.085
76	h	23.932	0.832	310.919	0.460	0.221
77	u	88.377	6.790	105.87	0.450	0.079
78	f	“invalid”	“invalid”	“invalid”	0.522	0.255
79	f/h	56.941	1.474	232.372	0.143	0.575
80	h	14.939	0.450	424.572	0.608	0.083
81	h	33.637	2.605	173.73	0.497	0.074
82	f/h	“invalid”	“invalid”	“invalid”	0.436	0.143
83	f	“invalid”	“invalid”	“invalid”	0.475	0.200
84	h	29.281	1.263	251.543	0.590	0.088
85	f/h/u	33.522	1.401	238.422	0.565	0.078
86	f/h	21.634	0.758	325.899	0.532	0.115
87	u	error	error	error	0.152	0.456

Indent	Type*	Modulus (GPa)	Hardness (GPa)	Maximum Displacement (nm)	Si/Ca Ratio	Al/Ca Ratio
88	h/u	82.302	8.563	93.83	0.177	0.448
89	f/h	73.633	5.315	120.33	0.212	0.494
90	h	21.760	0.724	333.497	0.592	0.099
91	h	13.772	0.679	344.564	0.490	0.067
92	h	21.699	0.801	316.798	0.492	0.187
93	h	19.561	0.759	325.695	0.660	0.079
94	h/u	41.184	1.385	240.02	0.374	0.257
95	f/h	21.630	0.716	335.447	0.541	0.118
96	f/h	"invalid"	"invalid"	"invalid"	0.556	0.088
97	h	64.908	5.874	114.206	0.218	0.376
98	f/h	15.912	0.496	404.171	0.354	0.240
99	h	28.485	1.04	277.415	0.546	0.110
100	h	41.261	3.169	157.073	0.427	0.200
101	h	15.358	0.367	470.083	0.633	0.121
102	f/h	17.582	0.623	359.999	0.510	0.120
103	f/h	32.549	0.929	294.089	0.248	0.413
104	h	27.139	1.027	279.339	0.603	0.099
105	f/h	19.681	0.636	356.146	0.650	0.152
106	h	19.561	0.625	359.177	0.506	0.070
107	h	24.716	1.004	282.39	0.563	0.073
108	h	13.420	0.480	410.637	0.613	0.066
109	f/h	13.735	0.518	395.243	0.334	0.308
110	h	21.197	0.735	331.104	0.529	0.105
111	h	15.767	0.493	404.874	0.496	0.101
112	h	47.299	2.451	179.189	0.372	0.150
113	f/h	24.174	0.828	311.525	0.567	0.123
114	h/u	49.277	2.999	161.543	0.469	0.185
115	f/h	21.461	0.903	298.158	0.575	0.144
116	h/u	38.764	2.652	172.022	0.506	0.108
117	h	"invalid"	"invalid"	"invalid"	0.468	0.252
118	f/h	24.511	1.454	233.952	0.243	0.226
119	f	15.460	0.316	507.404	0.626	0.108
120	f	14.210	0.626	359.011	0.573	0.072
121	u	119.724	11.214	81.367	0.501	0.141
122	u	133.276	11.753	79.434	0.261	0.196
123	u	145.433	13.237	74.601	0.401	0.046
124	f/h	22.696	0.843	308.816	0.295	0.363
125	h	27.446	1.312	246.661	0.609	0.081
126	h	22.142	0.955	289.848	0.495	0.155
127	f/h	21.031	0.817	313.919	0.599	0.091

Indent	Type*	Modulus (GPa)	Hardness (GPa)	Maximum Displacement (nm)	Si/Ca Ratio	Al/Ca Ratio
128	h/u	"invalid"	"invalid"	"invalid"	0.664	0.076
129	f	10.898	0.358	476.2	0.475	0.119
130	f/h	"invalid"	"invalid"	"invalid"	0.565	0.136
131	h	16.523	0.441	428.537	0.554	0.096
132	f	"invalid"	"invalid"	"invalid"	0.530	0.128
133	f/h/u	"invalid"	"invalid"	"invalid"	0.194	0.154
134	f/h	32.086	1.473	232.595	0.372	0.074
135	h	34.763	1.162	262.237	0.406	0.038
136	h	20.271	0.739	329.821	0.516	0.113
137	h	32.275	2.070	195.472	0.428	0.223
138	f/h	23.906	0.814	314.407	0.404	0.088
139	f/h	18.102	0.582	372.772	0.668	0.078
140	f/h	19.246	1.122	267.042	0.683	0.094
141	f/h	19.054	0.602	366.377	0.547	0.172
142	h	30.833	1.336	244.469	0.534	0.092
143	h/u	"invalid"	"invalid"	"invalid"	0.533	0.131
144	f/h	18.128	0.648	352.658	0.441	0.101
145	h	17.788	0.569	377.051	0.349	0.324
146	h	19.784	0.943	291.721	0.623	0.079
147	f	19.117	0.482	409.812	0.432	0.043
148	f	10.717	0.298	522.596	0.628	0.092
149	h	15.497	0.48	410.623	0.592	0.081
150	h	13.635	0.367	470.282	0.553	0.099
151	h	22.953	0.743	329.244	0.615	0.084
152	h/u	18.720	0.665	348.112	0.252	0.758
153	h	"invalid"	"invalid"	"invalid"	0.659	0.079
154	f/h	"invalid"	"invalid"	"invalid"	0.563	0.136
155	h	21.308	0.874	303.312	0.600	0.063
156	f/h	18.083	0.653	351.445	0.676	0.086
157	f/h	16.727	0.624	359.646	0.546	0.126
158	h	"invalid"	"invalid"	"invalid"	0.495	0.187
159	f/h	"invalid"	"invalid"	"invalid"	0.599	0.099
160	f/h	18.106	0.673	346.099	0.420	0.033
161	f/h	45.908	1.506	229.862	0.589	0.065
162	h	"invalid"	"invalid"	"invalid"	0.187	0.503
163	h	28.866	0.879	302.293	0.551	0.052
164	f/h	20.191	0.570	376.59	0.515	0.066
165	h/u	31.213	2.023	197.782	0.280	0.450
166	f/h	6.857	0.252	568.97	0.298	0.075
167	f/h	22.002	0.900	298.767	0.640	0.094

Indent	Type*	Modulus (GPa)	Hardness (GPa)	Maximum Displacement (nm)	Si/Ca Ratio	Al/Ca Ratio
168	h/u	71.440	6.509	108.273	0.484	0.117
169	h	44.514	1.361	242.084	0.192	0.586
170	f/h/u	41.159	2.292	185.55	0.569	0.057
171	h	18.243	0.558	380.665	0.661	0.100
172	f/h	11.246	0.308	513.472	0.570	0.420
173	f/h/u	“invalid”	“invalid”	“invalid”	0.458	0.192
174	f/h	“invalid”	“invalid”	“invalid”	0.456	0.165
175	f/h	28.521	1.159	262.615	0.619	0.101
176	h	17.639	0.507	399.077	0.609	0.077
177	h/u	20.090	0.438	430.216	0.613	0.162
178	h	16.980	0.537	388.05	0.515	0.194
179	h	24.237	1.170	261.344	0.568	0.103
180	f/h	“invalid”	“invalid”	“invalid”	0.195	0.569
181	f/h	“invalid”	“invalid”	“invalid”	0.387	0.141
182	f/h	“invalid”	“invalid”	“invalid”	0.511	0.124
183	f	“invalid”	“invalid”	“invalid”	0.602	0.140
184	h	“invalid”	“invalid”	“invalid”	0.209	0.552
185	h	13.131	0.716	335.341	0.467	0.702
186	h	9.544	0.356	477.611	0.596	0.150
187	h/u	20.295	1.155	263.165	0.414	0.120
188	h	43.606	1.022	279.916	0.420	0.074
189	u	102.681	5.098	122.928	0.190	0.496
190	u	94.100	5.712	115.851	0.417	0.040
191	u	90.803	8.056	96.795	0.401	0.033
192	u	93.438	8.671	93.209	0.588	0.076
193	h/u	39.212	3.910	141.056	0.560	0.119
194	h/u	22.540	1.257	251.963	0.555	0.228
195	f/h	24.732	0.661	349.462	0.487	0.073
196	h	20.802	1.106	269.123	0.645	0.074
197	f/h	12.977	0.378	463.319	0.647	0.084
198	f/h	16.458	0.575	374.812	0.567	0.154
199	f	12.653	0.326	499.669	0.377	0.079
200	f/h	43.541	1.654	219.148	0.622	0.101

*Type: f=flaw, h=hydrate, u=unhydrated particle, f/h=flaw and hydrate combination, f/u=flaw and unhydrated particle combination, f/h/u=flaw, hydrate, and unhydrated particle combination, and h/u=hydrate and unhydrated particle combination.

PC-B **Grid 1**

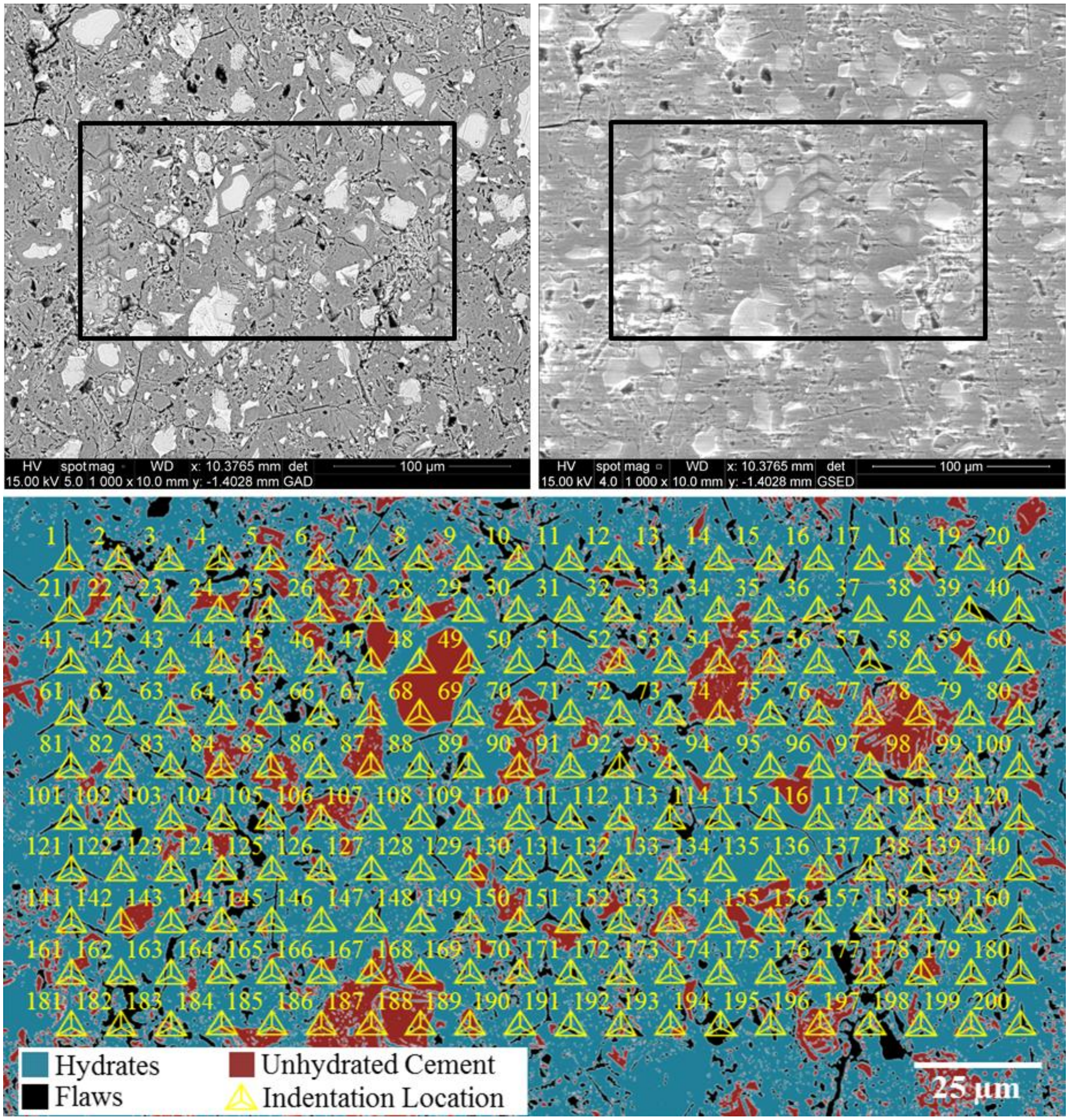

Indent	Type*	Modulus (GPa)	Hardness (GPa)	Maximum Displacement (nm)	Si/Ca Ratio	Al/Ca Ratio
1	h	26.168	0.964	288.431	0.623	0.107
2	h/u	20.015	0.798	317.248	0.186	0.492
3	f/h	10.690	0.214	616.897	0.475	0.141
4	f/h	“invalid”	“invalid”	“invalid”	0.492	0.217
5	f/h	error	error	error	0.191	0.401
6	h/u	30.189	1.482	231.673	0.199	0.430
7	h	40.098	1.158	263.003	0.463	0.164
8	h/u	13.350	0.401	449.221	0.490	0.245

Indent	Type*	Modulus (GPa)	Hardness (GPa)	Maximum Displacement (nm)	Si/Ca Ratio	Al/Ca Ratio
9	h	19.737	0.842	308.84	0.523	0.115
10	h	15.330	0.522	393.516	0.300	0.295
11	h	22.376	0.886	300.91	0.550	0.088
12	f/h	16.180	0.247	573.629	0.492	0.073
13	f/h	23.130	0.655	350.727	0.348	0.073
14	h/u	32.480	0.669	347.084	0.106	0.335
15	f/h/u	"invalid"	"invalid"	"invalid"	0.543	0.102
16	h	22.182	0.786	319.584	0.550	0.154
17	h	36.134	1.178	260.351	0.497	0.094
18	h/u	49.213	2.084	194.557	0.446	0.151
19	h	30.175	1.013	281.037	0.530	0.052
20	h	31.835	1.200	257.924	0.557	0.067
21	f/h	17.282	0.511	397.849	0.434	0.042
22	f/h	24.037	0.574	375.052	0.332	0.311
23	h	18.169	0.548	383.857	0.567	0.062
24	f/h	"invalid"	"invalid"	"invalid"	0.502	0.074
25	f/h	21.795	0.517	395.759	0.583	0.116
26	f/h/u	37.260	0.900	298.853	0.403	0.143
27	f	66.746	5.250	120.966	0.419	0.192
28	f/h	79.760	5.462	118.461	0.305	0.083
29	h	26.158	1.013	281.102	0.477	0.131
30	h	17.569	0.764	324.479	0.399	0.038
31	f/h	14.521	0.432	432.839	0.307	0.029
32	h	24.043	0.617	361.796	0.549	0.099
33	h	"invalid"	"invalid"	"invalid"	0.525	0.055
34	h	70.845	3.362	152.411	0.551	0.078
35	h	21.249	0.637	355.814	0.503	0.076
36	f/h	25.019	0.735	330.747	0.568	0.029
37	h	27.227	0.799	317.205	0.506	0.220
38	h	35.875	1.298	247.963	0.512	0.180
39	f/h	29.512	1.183	259.979	0.580	0.098
40	f/h	23.361	0.766	324.066	0.592	0.078
41	f	27.789	0.757	325.909	0.362	0.269
42	h	21.732	0.648	352.627	0.410	0.031
43	f/h	25.922	0.978	286.515	0.625	0.068
44	h	19.188	0.273	546.119	0.547	0.094
45	h	14.814	0.235	588.089	0.514	0.097
46	h	59.168	3.641	146.195	0.496	0.096
47	h	59.772	5.582	117.176	0.382	0.172
48	h/u	106.077	4.449	131.83	0.577	0.079

Indent	Type*	Modulus (GPa)	Hardness (GPa)	Maximum Displacement (nm)	Si/Ca Ratio	Al/Ca Ratio
49	u	105.594	5.795	114.943	0.426	0.148
50	f/h	26.555	0.725	333.083	0.526	0.062
51	h	13.464	0.371	467.831	0.569	0.102
52	h/u	59.239	3.244	155.182	0.468	0.133
53	f/h	21.237	0.804	316.03	0.295	0.483
54	u	123.004	9.114	90.774	0.345	0.258
55	h/u	38.384	1.489	231.225	0.544	0.127
56	h	21.187	0.914	296.195	0.623	0.072
57	h	26.017	0.811	314.809	0.436	0.254
58	h	29.362	1.013	281.086	0.353	0.084
59	u	47.684	1.850	207.125	0.236	0.364
60	f/h	31.129	0.816	313.784	0.545	0.018
61	f/h	22.654	0.616	361.699	0.313	0.219
62	h	24.335	0.823	312.528	0.116	0.430
63	f/h	20.377	0.683	343.377	0.533	0.066
64	h	23.730	0.945	291.382	0.137	0.023
65	f/h	15.442	0.778	321.401	0.306	0.046
66	h	25.643	0.916	295.731	0.318	0.249
67	u	113.008	7.725	98.899	0.491	0.096
68	u	135.922	6.229	110.715	0.115	0.119
69	h	30.440	0.950	290.563	0.143	0.587
70	u	160.060	12.407	77.17	0.478	0.212
71	f/h	21.414	0.823	312.35	0.536	0.072
72	f/h	15.651	0.601	366.358	0.300	0.259
73	f/h	17.635	0.387	457.531	0.502	0.136
74	f/h/u	169.267	11.534	80.199	0.526	0.059
75	h	26.574	0.790	319.151	0.631	0.074
76	f/h	58.453	3.120	158.332	0.630	0.085
77	u	102.606	7.306	101.905	0.276	0.035
78	u	121.304	10.459	84.4	0.580	0.156
79	f/h	24.815	0.753	326.711	0.535	0.072
80	f/h	57.550	1.692	216.537	0.440	0.083
81	h	21.889	0.794	317.949	0.130	0.518
82	h	25.299	0.894	299.897	0.561	0.067
83	h	12.995	0.284	535.103	0.537	0.051
84	u	66.763	4.409	132.509	0.524	0.064
85	u	71.536	10.168	85.727	0.522	0.071
86	h	16.009	0.267	551.801	0.566	0.083
87	u	141.607	12.941	75.42	0.426	0.121
88	h	26.728	0.916	295.852	0.483	0.169

Indent	Type*	Modulus (GPa)	Hardness (GPa)	Maximum Displacement (nm)	Si/Ca Ratio	Al/Ca Ratio
89	f/h	17.845	0.489	406.703	0.409	0.050
90	u	99.244	4.545	130.444	0.550	0.093
91	f/h	31.094	1.036	277.927	0.319	0.052
92	f/h	10.250	0.224	602.909	0.515	0.113
93	f/h/u	72.799	6.728	106.387	0.455	0.196
94	f/h	23.535	0.733	331.303	0.618	0.088
95	h	36.107	0.912	296.491	0.553	0.110
96	h	39.425	1.553	226.358	0.389	0.158
97	f/h	“invalid”	“invalid”	“invalid”	0.553	0.066
98	u	“invalid”	“invalid”	“invalid”	0.573	0.080
99	h	24.717	0.537	388.093	0.288	0.415
100	f/h	22.761	0.731	331.716	0.350	0.064
101	f/h	33.943	1.445	234.595	0.487	0.157
102	h	33.980	1.336	244.368	0.461	0.075
103	h	16.758	0.572	375.519	0.153	0.034
104	h	11.935	0.383	459.827	0.060	0.014
105	h	“invalid”	“invalid”	“invalid”	0.436	0.064
106	f/h	“invalid”	“invalid”	“invalid”	0.397	0.042
107	h	193.278	13.198	74.649	0.173	0.026
108	h	20.946	0.643	354.026	0.495	0.243
109	h	43.744	1.337	244.209	0.388	0.204
110	h	26.527	0.825	312.05	0.484	0.167
111	h/u	18.839	0.577	374.216	0.461	0.148
112	h/u	“invalid”	“invalid”	“invalid”	0.512	0.058
113	f	22.088	0.745	328.53	0.574	0.060
114	f/h	23.467	0.767	323.864	0.447	0.134
115	f/h	25.947	0.788	319.424	0.408	0.205
116	h	27.779	1.044	276.794	0.269	0.089
117	f/h/u	20.625	0.641	354.818	0.471	0.149
118	f/h	30.573	0.543	385.754	0.477	0.111
119	f/h	29.818	0.423	437.763	0.395	0.050
120	f/h	34.602	2.644	172.319	0.424	0.149
121	h	24.148	0.708	337.176	0.502	0.170
122	f/h	24.413	1.008	282.027	0.521	0.082
123	h	34.172	1.704	215.706	0.271	0.083
124	h/u	74.798	7.222	102.468	0.042	0.008
125	h	19.245	0.508	398.879	0.170	0.070
126	f/h	21.386	0.702	338.707	0.157	0.085
127	f/h	25.130	0.888	300.787	0.525	0.071
128	h	26.972	1.145	264.288	0.583	0.061

Indent	Type*	Modulus (GPa)	Hardness (GPa)	Maximum Displacement (nm)	Si/Ca Ratio	Al/Ca Ratio
129	h/u	127.140	5.875	114.146	0.520	0.085
130	f/h/u	22.689	0.957	289.548	0.517	0.117
131	h	19.489	0.935	292.78	0.173	0.526
132	h/u	25.707	0.731	331.669	0.373	0.073
133	h	41.215	1.368	241.345	0.478	0.206
134	h/u	16.729	0.537	387.912	0.468	0.112
135	h	38.062	1.936	202.289	0.436	0.110
136	h/u	54.711	3.266	154.662	0.161	0.036
137	f/h	“invalid”	“invalid”	“invalid”	0.457	0.095
138	f/h	16.581	0.682	343.288	0.516	0.066
139	h/u	17.989	0.247	574.86	0.233	0.050
140	f/h	25.336	1.030	278.812	0.496	0.147
141	h	23.800	0.944	291.509	0.496	0.078
142	h/u	70.683	4.515	130.711	0.290	0.328
143	h	29.871	1.287	248.849	0.478	0.172
144	h	20.712	0.573	374.977	0.115	0.124
145	f/h	24.641	0.819	313.306	0.093	0.076
146	h	25.638	0.807	315.373	0.531	0.145
147	h	21.865	0.713	336.114	0.522	0.114
148	h	44.723	1.460	233.599	0.499	0.101
149	f/h	20.942	0.842	308.996	0.347	0.221
150	h/u	106.570	7.975	97.299	0.111	0.539
151	h	17.440	0.814	314.228	0.114	0.596
152	h	“invalid”	“invalid”	“invalid”	0.427	0.231
153	h/u	64.110	4.305	134.021	0.487	0.225
154	h	48.599	2.270	186.44	0.439	0.171
155	h	74.412	2.003	198.633	0.428	0.074
156	h	18.823	0.592	369.277	0.167	0.438
157	f/h/u	23.180	0.397	451.968	0.566	0.071
158	f/h	31.157	0.752	327.273	0.518	0.228
159	f/h	11.980	0.309	513.301	0.499	0.079
160	f/h	22.714	0.663	348.479	0.437	0.140
161	h	“invalid”	“invalid”	“invalid”	0.440	0.161
162	h	20.344	0.674	345.887	0.557	0.107
163	h	“invalid”	“invalid”	“invalid”	0.514	0.189
164	h	23.968	0.674	345.83	0.094	0.016
165	h	22.273	0.662	348.755	0.557	0.070
166	f/h	72.759	5.099	122.756	0.553	0.069
167	u	124.847	6.470	108.665	0.532	0.039
168	u	“invalid”	“invalid”	“invalid”	0.419	0.199

Indent	Type*	Modulus (GPa)	Hardness (GPa)	Maximum Displacement (nm)	Si/Ca Ratio	Al/Ca Ratio
169	h	35.399	1.377	240.711	0.408	0.140
170	f/h	32.268	1.454	233.909	0.274	0.178
171	f/h	"invalid"	"invalid"	"invalid"	0.286	0.129
172	f/h	25.675	0.757	325.754	0.232	0.337
173	h	25.437	0.783	320.489	0.321	0.142
174	h	19.517	0.788	319.373	0.429	0.129
175	h	22.698	0.814	314.136	0.563	0.081
176	f/h	101.364	8.634	93.323	0.252	0.033
177	h/u	41.850	1.097	269.802	0.563	0.057
178	u	80.036	9.377	89.4	0.448	0.104
179	h	28.478	1.289	248.894	0.540	0.051
180	f/h	16.744	0.658	349.996	0.213	0.032
181	h	16.138	0.307	514.331	0.188	0.049
182	f/h	24.235	0.699	339.182	0.175	0.026
183	h/u	16.692	0.546	384.906	0.217	0.480
184	h/u	44.099	1.539	227.253	0.538	0.122
185	h	234.620	15.575	68.433	0.389	0.028
186	u	error	error	error	0.402	0.049
187	u	error	error	error	0.400	0.156
188	u	192.055	8.639	93.356	0.471	0.134
189	h/u	88.614	9.092	90.93	0.621	0.077
190	h	33.920	1.389	239.514	0.413	0.216
191	h	24.417	1.009	281.614	0.517	0.062
192	h	38.353	0.677	345.21	0.290	0.075
193	h	23.856	0.723	333.65	0.246	0.502
194	f/h	26.761	0.984	285.494	0.432	0.070
195	h	28.343	0.671	346.755	0.224	0.030
196	u	error	error	error	0.375	0.221
197	f/h	"invalid"	"invalid"	"invalid"	0.496	0.089
198	f/h	23.938	0.835	310.26	0.487	0.168
199	h	49.391	2.323	184.071	0.511	0.090
200	f/h	25.071	0.841	309.174	0.392	0.072

*Type: f=flaw, h=hydrate, u=unhydrated particle, f/h=flaw and hydrate combination, f/u=flaw and unhydrated particle combination, f/h/u=flaw, hydrate, and unhydrated particle combination, and h/u=hydrate and unhydrated particle combination.

PC-B **Grid 2**

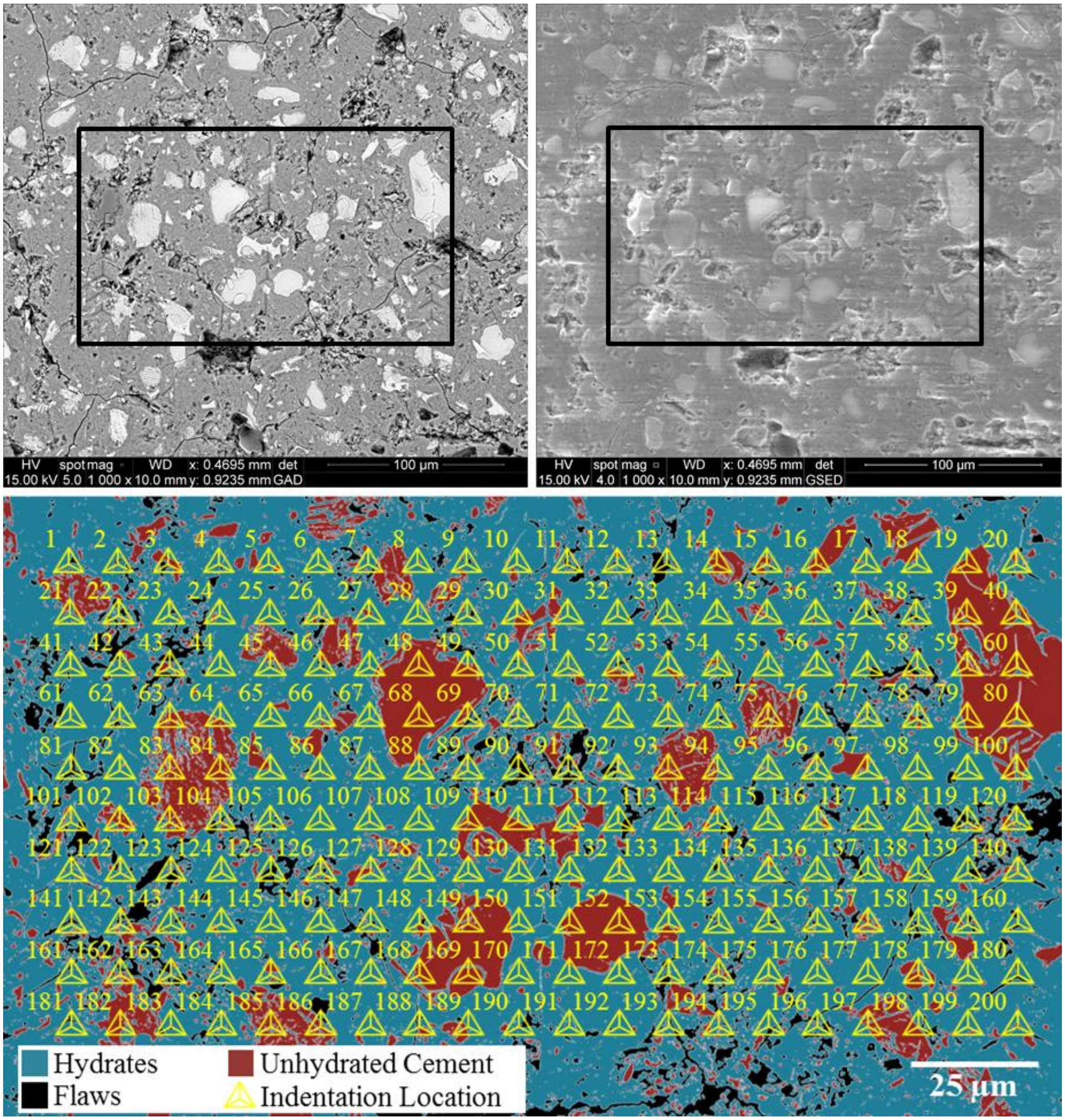

Indent	Type*	Modulus (GPa)	Hardness (GPa)	Maximum Displacement (nm)	Si/Ca Ratio	Al/Ca Ratio
1	f/h	23.220	1.137	265.179	0.442	0.170
2	f/h	47.147	2.545	175.667	0.333	0.112
3	h/u	73.199	7.899	97.802	0.158	0.587
4	h	26.827	0.911	296.624	0.493	0.136
5	h	38.236	1.271	250.691	0.276	0.426
6	h	21.365	1.010	281.726	0.665	0.122
7	h	78.551	8.110	96.455	0.407	0.148
8	h/u	30.207	1.789	210.525	0.623	0.122

Indent	Type*	Modulus (GPa)	Hardness (GPa)	Maximum Displacement (nm)	Si/Ca Ratio	Al/Ca Ratio
9	h	21.808	0.882	301.345	0.415	0.144
10	h	29.556	1.066	273.981	0.494	0.171
11	f	43.634	2.949	162.862	0.359	0.153
12	f/h	25.995	1.360	242.155	0.573	0.093
13	f	“invalid”	“invalid”	“invalid”	0.268	0.087
14	u	error	error	error	0.509	0.050
15	h/u	“invalid”	“invalid”	“invalid”	0.490	0.078
16	u	186.293	19.135	61.264	0.426	0.109
17	h	25.820	1.243	253.385	0.552	0.088
18	h	43.843	1.745	213.346	0.564	0.096
19	u	96.743	5.604	117.025	0.412	0.029
20	h/u	30.875	2.343	183.289	0.498	0.081
21	h	error	error	error	0.489	0.053
22	h	52.142	1.377	240.501	0.413	0.112
23	h	“invalid”	“invalid”	“invalid”	0.549	0.166
24	h	32.506	1.664	218.419	0.521	0.079
25	h	25.645	1.148	263.761	0.534	0.116
26	h	47.350	2.138	192.263	0.545	0.093
27	h/u	38.869	3.365	152.22	0.538	0.094
28	h	22.061	0.916	295.773	0.407	0.106
29	h	19.425	0.804	316.279	0.538	0.084
30	h/u	166.308	10.535	84.124	0.496	0.144
31	h	41.398	1.533	227.823	0.563	0.108
32	h	24.422	1.020	280.087	0.552	0.123
33	h	14.929	0.828	311.776	0.575	0.085
34	h	25.811	0.952	290.148	0.507	0.131
35	h/u	35.993	1.210	256.866	0.403	0.152
36	h	19.437	1.090	270.756	0.245	0.326
37	h	29.595	1.614	221.723	0.515	0.173
38	f/h	47.900	1.696	216.348	0.553	0.060
39	u	112.977	5.344	119.906	0.402	0.033
40	u	115.103	5.761	115.257	0.424	0.067
41	h	138.883	18.046	63.239	1.153	0.118
42	h	122.982	21.508	57.578	0.580	0.110
43	h/u	“invalid”	“invalid”	“invalid”	0.371	0.155
44	h	error	error	error	0.386	0.098
45	f/h	40.641	1.212	256.639	0.374	0.248
46	h	32.479	2.478	178.22	0.449	0.081
47	h	36.839	1.249	252.652	0.416	0.029
48	u	125.474	6.291	110.084	0.415	0.040

Indent	Type*	Modulus (GPa)	Hardness (GPa)	Maximum Displacement (nm)	Si/Ca Ratio	Al/Ca Ratio
49	u	64.466	1.845	207.187	0.605	0.076
50	h	48.162	1.790	210.301	0.283	0.242
51	f/h	28.153	0.947	290.838	0.541	0.123
52	f/h	35.776	2.442	179.416	0.465	0.143
53	h/u	21.710	1.359	242.352	0.554	0.114
54	h	26.179	1.272	250.443	0.338	0.357
55	h	24.640	0.849	307.381	0.312	0.291
56	h	23.952	1.037	277.835	0.504	0.148
57	h/u	50.507	4.100	137.502	0.210	0.439
58	f/h/u	22.014	1.161	262.154	0.581	0.065
59	u	error	error	error	0.421	0.039
60	u	116.023	5.560	117.482	0.405	0.045
61	h	error	error	error	20.746	0.484
62	f/h	112.086	12.518	76.845	0.552	0.051
63	u	84.873	3.585	147.394	0.561	0.068
64	h/u	84.056	4.939	124.943	0.505	0.099
65	h	24.494	1.006	282.211	0.418	0.111
66	f/h	44.547	1.980	199.962	0.641	0.142
67	h	30.400	0.688	342.441	0.427	0.058
68	u	error	error	error	0.421	0.164
69	f/h/u	59.018	2.637	172.677	0.330	0.081
70	h	22.165	1.135	265.377	0.354	0.057
71	h	21.101	0.830	311.076	0.518	0.067
72	h	21.242	0.884	301.265	0.601	0.075
73	f/h	23.947	0.812	314.693	0.432	0.222
74	h	51.290	4.635	128.913	0.560	0.078
75	u	98.414	6.085	112.028	0.597	0.155
76	h	error	error	error	0.625	0.119
77	h	26.574	1.454	233.759	0.442	0.381
78	f/h/u	48.162	1.932	202.303	0.407	0.185
79	u	103.355	4.574	129.984	0.409	0.086
80	u	117.382	4.856	126.086	0.535	0.367
81	f/h	95.957	14.161	71.929	0.573	0.074
82	h	20.723	0.945	291.274	0.573	0.041
83	u	91.818	5.590	117.123	0.540	0.049
84	u	113.719	7.873	98.042	0.424	0.185
85	h/u	49.031	3.941	140.243	0.543	0.135
86	h	46.491	2.072	195.304	0.571	0.080
87	h	37.004	1.619	221.541	0.530	0.067
88	h	33.933	1.322	245.539	0.555	0.118

Indent	Type*	Modulus (GPa)	Hardness (GPa)	Maximum Displacement (nm)	Si/Ca Ratio	Al/Ca Ratio
89	h	13.359	0.529	390.727	0.173	0.223
90	h	19.171	0.951	290.238	0.329	0.170
91	f/h	17.357	0.599	366.939	0.411	0.130
92	f/h	13.180	0.699	339.387	0.534	0.067
93	u	99.949	5.795	114.912	0.580	0.088
94	h/u	63.954	5.082	123.07	0.494	0.138
95	h	34.239	1.686	216.968	0.419	0.126
96	f/h	28.380	1.467	232.87	0.581	0.107
97	f/h/u	43.427	1.204	257.649	0.613	0.074
98	h	21.355	1.064	274.394	0.585	0.075
99	h	27.326	0.883	301.543	0.190	0.536
100	h/u	164.118	5.212	121.563	0.325	0.109
101	f/h	156.191	23.507	54.845	0.167	0.555
102	u	110.319	13.620	73.438	0.541	0.074
103	u	“invalid”	“invalid”	“invalid”	0.584	0.194
104	f/h/u	156.913	7.079	103.641	0.340	0.274
105	h	22.358	0.768	323.635	0.467	0.122
106	h	23.528	0.928	293.806	0.431	0.152
107	h	27.415	0.970	287.423	0.461	0.103
108	h	25.186	1.052	275.774	0.331	0.187
109	u	139.368	11.605	79.911	0.161	0.603
110	h/u	210.241	16.384	66.595	0.079	0.142
111	h	57.510	1.705	215.749	0.361	0.311
112	h	41.483	1.858	206.327	0.357	0.237
113	h	60.416	1.894	204.507	0.315	0.084
114	h	59.721	4.867	125.799	0.503	0.082
115	h	22.839	0.919	295.428	0.580	0.130
116	h	25.343	1.003	282.592	0.361	0.194
117	h	16.587	0.898	298.813	0.576	0.138
118	h	error	error	error	0.295	0.142
119	f/h	39.110	1.909	203.582	0.426	0.133
120	f/h	70.324	3.130	158.006	0.256	0.052
121	h	13.974	0.544	385.209	0.492	0.143
122	h	“invalid”	“invalid”	“invalid”	0.407	0.148
123	f/h/u	108.362	13.833	72.807	0.507	0.099
124	h/u	28.946	1.218	255.944	0.238	0.062
125	f/h	29.548	2.475	178.35	0.305	0.137
126	f/h	48.300	1.882	205.124	0.420	0.093
127	h/u	error	error	error	0.425	0.241
128	h	21.842	0.830	311.08	0.474	0.113

Indent	Type*	Modulus (GPa)	Hardness (GPa)	Maximum Displacement (nm)	Si/Ca Ratio	Al/Ca Ratio
129	h	43.472	1.160	262.505	0.516	0.075
130	h	30.931	1.090	270.896	0.454	0.074
131	h	26.629	0.919	295.301	0.443	0.079
132	h	35.001	1.616	221.643	0.209	0.100
133	h	25.947	0.931	293.329	0.076	0.098
134	h	21.228	0.757	325.853	0.337	0.108
135	h	25.766	0.895	299.38	0.440	0.222
136	f/h	“invalid”	“invalid”	“invalid”	0.221	0.064
137	h	32.862	1.197	258.28	0.504	0.093
138	h	27.175	1.237	253.93	0.552	0.103
139	f/h	37.342	2.071	195.366	0.352	0.167
140	f/h	31.274	1.089	270.941	0.540	0.318
141	f/h	30.479	1.729	214.325	0.291	0.096
142	f/h	9.019	0.272	547.133	0.502	0.171
143	h	23.910	1.054	275.423	0.258	0.108
144	h	30.381	1.095	270.329	0.476	0.161
145	h	31.237	1.246	253.112	0.406	0.145
146	h	21.186	0.960	289.012	0.493	0.062
147	f/h	19.095	0.716	335.229	0.118	0.031
148	h/u	25.130	0.787	319.516	0.174	0.038
149	u	88.456	3.310	153.464	0.383	0.054
150	h	36.371	1.560	225.593	0.258	0.031
151	u	101.532	6.139	111.493	0.449	0.337
152	u	116.226	6.057	112.292	0.568	0.196
153	h/u	48.155	1.297	248.001	0.516	0.084
154	f/h	32.898	1.162	262.277	0.523	0.123
155	f/h	28.449	0.898	298.853	0.607	0.034
156	f/h	35.511	1.886	204.834	0.386	0.124
157	h/u	43.622	2.455	179.022	0.262	0.445
158	f/h	32.516	1.229	254.93	0.572	0.134
159	f/h	56.789	1.650	219.461	0.176	0.457
160	f/h	38.314	1.340	243.873	0.639	0.119
161	h	45.967	2.271	186.256	0.207	0.069
162	h/u	“invalid”	“invalid”	“invalid”	0.529	0.173
163	f/h/u	120.695	8.510	94.103	0.440	0.038
164	h	error	error	error	0.672	0.113
165	h/u	86.762	4.907	125.328	0.543	0.088
166	h	34.550	1.803	209.572	0.385	0.039
167	h	24.498	0.839	309.446	0.542	0.048
168	u	95.182	4.229	135.24	0.535	0.087

Indent	Type*	Modulus (GPa)	Hardness (GPa)	Maximum Displacement (nm)	Si/Ca Ratio	Al/Ca Ratio
169	u	95.389	6.073	112.225	0.520	0.059
170	h	28.306	1.186	259.551	0.577	0.059
171	h	29.643	1.081	271.916	0.269	0.323
172	h	35.572	1.467	232.937	0.367	0.100
173	f/h	42.333	1.302	247.371	0.529	0.051
174	f/h/u	117.517	9.695	87.887	0.496	0.089
175	h	26.644	0.895	299.301	0.491	0.088
176	h	26.414	0.792	318.613	0.544	0.061
177	h	16.855	0.796	317.707	0.514	0.079
178	u	67.936	6.376	109.331	0.493	0.073
179	h	24.437	0.843	308.802	0.559	0.093
180	f/h	24.745	1.080	272.148	0.586	0.138
181	h	23.515	0.629	357.78	0.515	0.113
182	u	118.778	5.746	115.44	0.476	0.116
183	f/h	37.200	1.480	231.814	0.544	0.049
184	h	21.580	0.672	346.084	0.309	0.290
185	u	92.429	7.327	101.794	0.483	0.122
186	u	114.835	17.763	63.773	0.557	0.088
187	h	23.832	1.010	281.523	0.535	0.080
188	f/h/u	20.373	0.894	299.65	0.395	0.181
189	h	44.240	2.832	166.303	0.523	0.081
190	f/h	"invalid"	"invalid"	"invalid"	0.515	0.139
191	h	20.659	0.573	375.134	0.298	0.116
192	h	32.718	1.132	265.783	0.330	0.085
193	h	56.400	3.050	160.182	0.521	0.130
194	h	22.222	0.923	294.873	0.307	0.067
195	h	20.511	1.020	280.086	0.517	0.044
196	h	21.664	1.280	249.684	0.219	0.267
197	h/u	48.562	3.633	146.269	0.290	0.355
198	h	51.004	3.395	151.503	0.506	0.070
199	h	31.471	1.029	278.942	0.349	0.236
200	f/h	35.803	1.748	213.007	0.508	0.105

*Type: f=flaw, h=hydrate, u=unhydrated particle, f/h=flaw and hydrate combination, f/u=flaw and unhydrated particle combination, f/h/u=flaw, hydrate, and unhydrated particle combination, and h/u=hydrate and unhydrated particle combination.

PC-CNF-A Grid 1

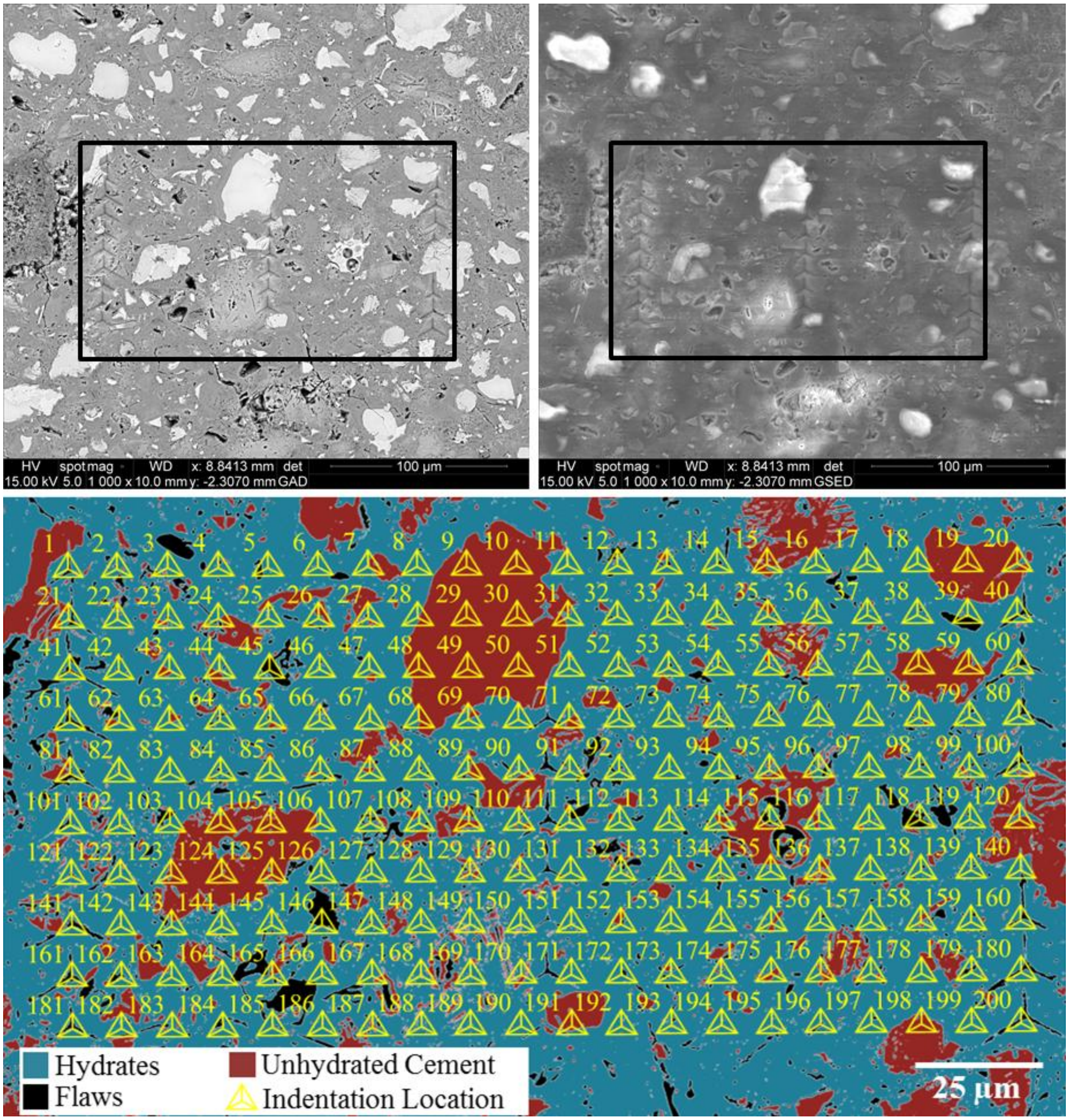

Indent	Type*	Modulus (GPa)	Hardness (GPa)	Maximum Displacement (nm)	Si/Ca Ratio	Al/Ca Ratio
1	h	46.616	1.737	214.224	0.483	0.197
2	f/h	30.008	0.856	306.815	0.368	0.110
3	h	26.176	1.274	250.993	0.345	0.114
4	h	20.869	0.918	295.882	0.415	0.065
5	h	28.943	0.898	299.418	0.460	0.072
6	h	26.165	0.861	305.771	0.451	0.099
7	h	79.140	5.687	116.614	0.522	0.070
8	h	35.318	1.441	235.442	0.371	0.043

Indent	Type*	Modulus (GPa)	Hardness (GPa)	Maximum Displacement (nm)	Si/Ca Ratio	Al/Ca Ratio
9	u	124.437	9.406	89.79	0.400	0.033
10	u	142.227	9.754	88.144	0.430	0.038
11	f/h	30.444	1.265	251.775	0.566	0.072
12	h	21.268	0.850	308.015	0.437	0.064
13	f/h	26.726	0.621	360.999	0.204	0.039
14	f/h	29.779	0.779	321.865	0.329	0.292
15	u	95.114	4.312	134.523	0.557	0.081
16	h	81.352	3.362	152.932	0.510	0.092
17	h	32.230	1.023	280.38	0.438	0.050
18	h	38.892	1.447	235.13	0.360	0.028
19	u	126.459	8.368	95.467	0.492	0.038
20	u	122.729	9.765	88.097	0.499	0.066
21	h	47.060	1.467	233.512	0.498	0.073
22	f/h	26.745	0.815	314.459	0.460	0.048
23	f/h	29.326	1.093	271.146	0.322	0.063
24	h	“invalid”	“invalid”	“invalid”	0.507	0.092
25	f/h	30.491	0.906	298.146	0.491	0.057
26	h	“invalid”	“invalid”	“invalid”	0.375	0.039
27	f/h	42.966	1.501	230.8	0.371	0.023
28	h	149.040	9.202	90.788	0.398	0.026
29	u	125.801	8.139	96.809	0.416	0.026
30	u	122.658	9.412	89.74	0.568	0.057
31	h	70.699	5.412	119.683	0.606	0.070
32	h	25.232	0.797	318.19	0.517	0.056
33	h	21.722	0.699	339.842	0.569	0.063
34	f/h	25.414	0.789	319.734	0.552	0.043
35	f/h/u	error	error	error	0.376	0.063
36	h	29.592	0.999	283.653	0.510	0.045
37	h	28.178	0.992	284.949	0.401	0.027
38	h	25.353	0.776	322.49	0.410	0.164
39	h	66.845	2.020	198.347	0.157	0.026
40	h	33.928	1.086	272.006	0.554	0.101
41	f	14.043	0.909	297.875	0.478	0.092
42	f/h	26.661	0.846	308.675	0.471	0.141
43	h/u	65.864	7.233	102.974	0.296	0.139
44	f/h	75.638	5.962	113.793	0.418	0.049
45	f	36.044	1.031	279.541	0.513	0.099
46	f/h	27.290	0.623	360.365	0.308	0.029
47	h	28.561	0.886	301.49	0.372	0.028
48	u	error	error	error	0.479	0.033

Indent	Type*	Modulus (GPa)	Hardness (GPa)	Maximum Displacement (nm)	Si/Ca Ratio	Al/Ca Ratio
49	u	111.706	9.423	89.666	0.472	0.041
50	u	116.885	8.516	94.557	0.234	0.258
51	h	35.996	1.432	236.461	0.478	0.056
52	f/h	20.400	0.705	338.646	0.519	0.206
53	f/h	22.565	0.676	345.83	0.449	0.057
54	f/h	21.906	0.641	355.112	0.095	0.059
55	f/h/u	49.098	2.408	181.34	0.509	0.063
56	f/h	32.855	0.999	283.941	0.481	0.045
57	h	39.599	1.668	218.696	0.403	0.129
58	u	103.607	8.762	93.162	0.548	0.070
59	u	90.939	5.778	115.676	0.397	0.165
60	f/h	24.720	0.728	332.952	0.498	0.068
61	f/h	“invalid”	“invalid”	“invalid”	0.554	0.063
62	h/u	“invalid”	“invalid”	“invalid”	0.611	0.073
63	u	35.331	2.033	197.654	0.158	0.301
64	f/h	24.976	0.512	397.649	0.605	0.079
65	f/h	33.426	0.904	298.558	0.532	0.049
66	h	25.361	0.869	304.638	0.515	0.063
67	f/h	30.258	0.885	301.801	0.242	0.053
68	h/u	81.603	5.458	119.074	0.545	0.068
69	h/u	65.456	4.587	130.375	0.397	0.068
70	h	53.287	1.658	219.413	0.403	0.161
71	h/u	31.548	1.596	223.683	0.481	0.044
72	h	29.936	1.654	219.548	0.309	0.110
73	h	28.722	1.049	276.832	0.030	0.013
74	h	30.105	0.849	308.087	0.087	0.021
75	h	20.175	0.728	332.992	0.374	0.090
76	h	41.357	1.712	215.799	0.361	0.058
77	h	34.963	1.294	248.803	0.303	0.052
78	h	31.861	1.345	244.015	0.518	0.073
79	h	25.206	0.731	332.488	0.526	0.098
80	h	23.783	0.718	335.356	0.536	0.092
81	f/h/u	118.857	11.842	79.629	0.383	0.048
82	f/h	33.500	0.992	284.926	0.542	0.078
83	h	“invalid”	“invalid”	“invalid”	0.578	0.091
84	f/h	error	error	error	0.538	0.056
85	h	26.317	0.876	303.331	0.527	0.079
86	h	“invalid”	“invalid”	“invalid”	0.234	0.032
87	h/u	60.697	5.474	118.873	0.157	0.447
88	f/h	22.453	0.579	373.898	0.144	0.547

Indent	Type*	Modulus (GPa)	Hardness (GPa)	Maximum Displacement (nm)	Si/Ca Ratio	Al/Ca Ratio
89	h/u	97.676	8.342	95.604	0.423	0.149
90	h	43.355	1.282	249.917	0.411	0.100
91	f/h	26.114	1.055	275.906	0.168	0.042
92	h	24.645	0.791	319.4	0.066	0.461
93	h	21.170	0.949	291.34	0.074	0.494
94	h	42.930	1.927	203.285	0.349	0.205
95	h	72.165	3.306	154.27	0.503	0.122
96	h	174.057	15.446	69.203	0.179	0.381
97	h	24.292	0.900	299.191	0.487	0.108
98	h	23.587	0.733	332.039	0.552	0.043
99	h	21.397	0.851	307.707	0.530	0.049
100	h	“invalid”	“invalid”	“invalid”	0.408	0.148
101	h	36.522	1.235	254.93	0.548	0.051
102	h	“invalid”	“invalid”	“invalid”	0.509	0.068
103	h	208.876	15.623	68.849	0.115	0.560
104	u	144.027	12.064	78.835	0.094	0.066
105	u	109.291	7.436	101.466	0.368	0.094
106	h	“invalid”	“invalid”	“invalid”	0.206	0.258
107	f/h	22.690	0.833	311.322	0.274	0.290
108	h	33.922	1.340	244.46	0.118	0.024
109	u	64.360	2.794	168.04	0.493	0.052
110	h/u	131.157	13.666	73.792	0.496	0.086
111	h	16.575	0.351	481.371	0.382	0.160
112	h	“invalid”	“invalid”	“invalid”	0.359	0.048
113	h	22.988	0.933	293.803	0.314	0.247
114	u	88.332	7.816	98.855	0.437	0.072
115	f/h	119.008	8.320	95.726	0.238	0.067
116	h/u	“invalid”	“invalid”	“invalid”	0.233	0.307
117	u	26.484	1.244	253.771	0.533	0.049
118	f	“invalid”	“invalid”	“invalid”	0.494	0.066
119	h	194.063	12.226	78.331	0.577	0.053
120	u	error	error	error	0.400	0.136
121	f/h	23.586	0.914	296.97	0.305	0.318
122	f/h	22.672	0.711	337.151	0.514	0.052
123	h/u	146.957	10.547	84.558	0.525	0.078
124	h/u	93.263	6.839	106.022	0.495	0.127
125	u	132.239	6.734	106.854	0.437	0.038
126	h	28.038	1.030	279.268	0.058	0.015
127	h	23.039	1.001	283.517	0.368	0.079
128	h	40.936	1.662	219.026	0.432	0.050

Indent	Type*	Modulus (GPa)	Hardness (GPa)	Maximum Displacement (nm)	Si/Ca Ratio	Al/Ca Ratio
129	h/u	42.725	2.121	193.476	0.289	0.068
130	h	33.416	1.594	223.692	0.499	0.066
131	h	28.213	0.793	319.008	0.155	0.031
132	h	32.555	1.422	237.241	0.408	0.140
133	h	24.716	0.765	324.93	0.553	0.050
134	h	94.046	4.570	130.678	0.103	0.018
135	h	81.582	6.026	113.149	0.344	0.189
136	h/u	80.315	5.627	117.299	0.402	0.093
137	h	42.306	1.778	211.641	0.490	0.048
138	h	34.767	0.899	299.445	0.396	0.030
139	h	25.631	0.799	317.711	0.509	0.170
140	h	error	error	error	0.447	0.069
141	f/h	“invalid”	“invalid”	“invalid”	0.432	0.146
142	h	28.008	0.814	314.842	0.396	0.156
143	h	113.425	8.452	94.889	0.157	0.116
144	f/h	151.495	17.079	65.674	0.390	0.062
145	h	30.797	0.924	295.42	0.119	0.021
146	f	11.417	0.313	510.17	0.033	0.006
147	f/h	23.073	0.560	380.497	0.159	0.025
148	h	55.411	1.874	206.14	0.176	0.029
149	h	“invalid”	“invalid”	“invalid”	0.387	0.129
150	h	42.438	1.951	201.986	0.559	0.091
151	h	33.462	1.265	251.759	0.476	0.070
152	f/h/u	“invalid”	“invalid”	“invalid”	0.323	0.233
153	h	28.754	1.156	263.726	0.399	0.103
154	h	25.168	0.904	298.424	0.478	0.071
155	h	59.904	3.095	159.52	0.402	0.056
156	h	22.064	0.651	352.284	0.170	0.046
157	h	29.677	1.271	251.079	0.420	0.046
158	h/u	“invalid”	“invalid”	“invalid”	0.380	0.027
159	h	23.488	0.676	345.765	0.539	0.068
160	h	32.295	1.100	270.256	0.118	0.166
161	f/h	“invalid”	“invalid”	“invalid”	0.377	0.290
162	f/h	21.671	0.528	391.799	0.420	0.211
163	h	27.782	1.120	267.826	0.398	0.234
164	h	41.441	1.565	225.807	0.339	0.154
165	h/u	“invalid”	“invalid”	“invalid”	0.037	0.009
166	h	33.865	1.685	217.585	0.030	0.007
167	h	“invalid”	“invalid”	“invalid”	0.251	0.040
168	h/u	“invalid”	“invalid”	“invalid”	0.336	0.053

Indent	Type*	Modulus (GPa)	Hardness (GPa)	Maximum Displacement (nm)	Si/Ca Ratio	Al/Ca Ratio
169	h	“invalid”	“invalid”	“invalid”	0.562	0.087
170	h/u	“invalid”	“invalid”	“invalid”	0.412	0.052
171	h	28.069	1.014	281.56	0.463	0.072
172	f/h	24.510	0.687	343.226	0.527	0.090
173	h	26.084	0.971	287.932	0.516	0.074
174	h	28.737	1.166	262.432	0.372	0.182
175	h/u	“invalid”	“invalid”	“invalid”	0.433	0.108
176	h/u	63.037	4.348	133.958	0.364	0.041
177	h	31.066	0.715	336.174	0.426	0.091
178	h	49.253	1.679	218.011	0.252	0.038
179	f/h	25.722	0.539	387.479	0.514	0.106
180	f/h	17.306	0.456	421.657	0.509	0.134
181	f/h	24.541	0.766	324.735	0.420	0.200
182	h	74.647	5.774	115.715	0.485	0.156
183	h	24.042	1.182	260.458	0.475	0.075
184	f/h	23.830	0.596	368.777	0.038	0.011
185	f/h	24.260	0.828	311.996	0.036	0.008
186	h	28.088	0.819	313.595	0.033	0.008
187	h/u	“invalid”	“invalid”	“invalid”	0.269	0.030
188	h	“invalid”	“invalid”	“invalid”	0.496	0.101
189	h	“invalid”	“invalid”	“invalid”	0.229	0.040
190	h	32.111	0.965	288.617	0.482	0.079
191	u	error	error	error	0.522	0.084
192	h	27.259	1.185	260.151	0.482	0.098
193	f/h	12.948	0.351	480.845	0.519	0.063
194	h	20.505	0.831	311.531	0.473	0.122
195	h	25.983	0.946	291.832	0.284	0.317
196	f/h	27.647	0.939	292.834	0.496	0.092
197	h	26.073	0.719	335.212	0.443	0.056
198	u	97.293	7.409	101.661	0.506	0.143
199	h	24.447	0.832	311.195	0.338	0.106
200	h	26.662	0.879	302.696	0.454	0.078

*Type: f=flaw, h=hydrate, u=unhydrated particle, f/h=flaw and hydrate combination, f/u=flaw and unhydrated particle combination, f/h/u=flaw, hydrate, and unhydrated particle combination, and h/u=hydrate and unhydrated particle combination.

PC-CNF-A Grid 2

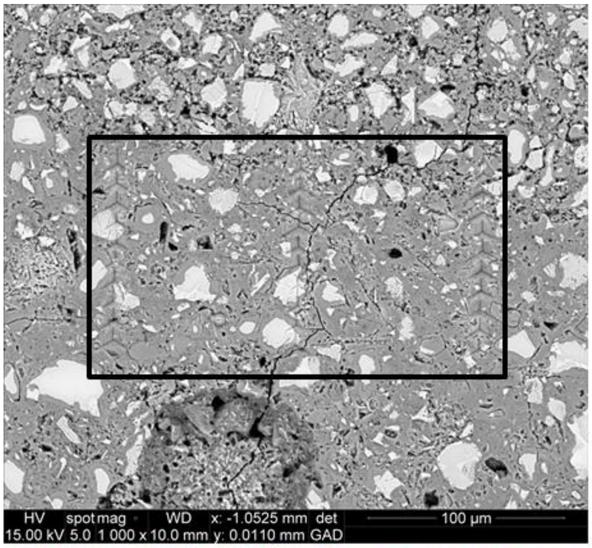

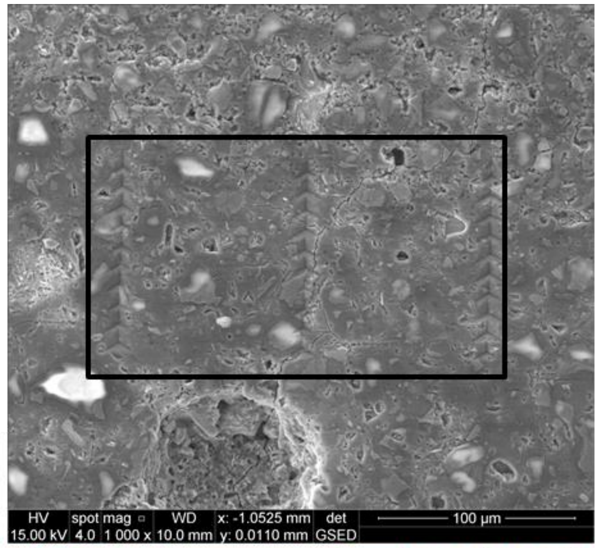

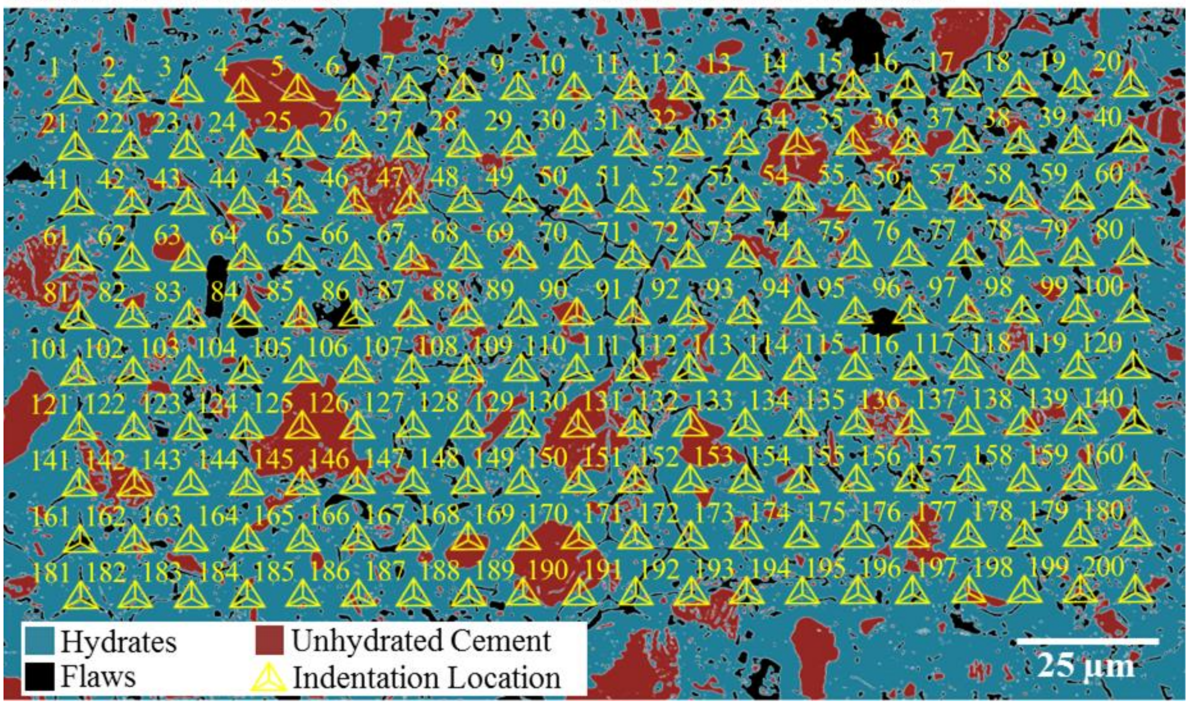

Indent	Type*	Modulus (GPa)	Hardness (GPa)	Maximum Displacement (nm)	Si/Ca Ratio	Al/Ca Ratio
1	h	23.606	0.709	337.787	0.322	0.115
2	h	19.491	0.458	421.186	0.405	0.087
3	h	29.267	0.844	308.93	0.507	0.055
4	u	111.119	8.983	91.978	0.381	0.024
5	u	72.484	7.464	101.318	0.395	0.028
6	h	24.727	0.917	296.527	0.418	0.172
7	h/u	14.022	0.508	399.843	0.140	0.238
8	f/h/u	32.233	1.062	274.866	0.426	0.149

Indent	Type*	Modulus (GPa)	Hardness (GPa)	Maximum Displacement (nm)	Si/Ca Ratio	Al/Ca Ratio
9	h	28.190	1.102	270.02	0.393	0.088
10	u	58.792	3.166	157.679	0.364	0.137
11	f/h	34.996	1.136	265.826	0.353	0.055
12	h/u	27.839	0.860	306.198	0.238	0.169
13	f/h	18.905	0.638	356.075	0.442	0.087
14	f/h	13.071	0.219	612.166	0.409	0.205
15	h	10.718	0.213	619.218	0.343	0.116
16	f	9.762	0.206	629.117	0.423	0.125
17	f/h	16.008	0.456	421.719	0.394	0.186
18	f/h/u	26.268	1.779	211.738	0.374	0.090
19	h	26.809	1.273	250.915	0.548	0.072
20	f/h	43.187	1.405	238.707	0.366	0.195
21	h	24.632	0.888	301.314	0.355	0.065
22	f/h	17.897	0.380	462.724	0.399	0.113
23	h	22.519	0.688	342.887	0.408	0.165
24	f/h	32.858	1.443	235.52	0.466	0.068
25	h	35.920	1.290	249.359	0.367	0.036
26	f/h	23.437	0.619	361.93	0.427	0.109
27	f/h	19.810	0.517	396.167	0.417	0.160
28	h	26.670	1.065	274.752	0.400	0.099
29	h	24.764	0.925	295.21	0.487	0.098
30	h	28.023	0.665	348.859	0.504	0.098
31	f/h	23.400	0.411	444.584	0.210	0.076
32	h/u	22.854	0.810	315.617	0.249	0.266
33	f	16.960	0.393	454.75	0.465	0.096
34	u	71.200	6.463	109.185	0.411	0.201
35	u	119.793	10.638	84.214	0.261	0.336
36	f/h	27.944	0.731	332.54	0.456	0.108
37	h	19.425	0.481	410.437	0.432	0.148
38	f/h	31.872	0.564	379.359	0.333	0.067
39	f/h	14.379	0.370	468.716	0.168	0.038
40	h	28.454	1.107	269.348	0.252	0.450
41	f/h	24.772	0.957	290.021	0.075	0.024
42	h	21.987	0.957	290.035	0.263	0.236
43	f/h	21.036	0.569	377.299	0.459	0.078
44	f/h	38.812	0.935	293.643	0.501	0.068
45	f/h	41.597	1.933	202.892	0.463	0.068
46	u	121.344	9.289	90.397	0.543	0.075
47	h	72.393	5.708	116.404	0.360	0.243
48	f/h	12.294	0.205	632.205	0.425	0.188

Indent	Type*	Modulus (GPa)	Hardness (GPa)	Maximum Displacement (nm)	Si/Ca Ratio	Al/Ca Ratio
49	h	21.242	0.821	313.592	0.321	0.243
50	h	“invalid”	“invalid”	“invalid”	0.432	0.330
51	h	22.773	0.677	345.643	0.320	0.256
52	h/u	31.413	1.041	278.043	0.379	0.168
53	f/u	24.604	0.671	347.436	0.449	0.154
54	h	31.632	0.671	347.28	0.427	0.182
55	f/h	38.699	0.750	328.045	0.526	0.057
56	h	22.707	0.590	370.441	0.276	0.259
57	h/u	“invalid”	“invalid”	“invalid”	0.510	0.111
58	f/h/u	17.566	0.341	488.771	0.408	0.136
59	f/h	24.838	0.452	423.941	0.407	0.118
60	f/h	40.134	2.484	178.536	0.292	0.193
61	f/h	36.842	1.842	208.048	0.498	0.077
62	f/h	30.132	1.214	257.023	0.223	0.403
63	h	29.468	1.178	261.026	0.284	0.182
64	f/h/u	36.461	2.548	176.214	0.361	0.061
65	h	43.477	1.368	241.985	0.453	0.095
66	h	22.702	0.540	387.11	0.512	0.053
67	f/h/u	“invalid”	“invalid”	“invalid”	0.531	0.045
68	h	26.410	0.812	315.17	0.487	0.123
69	h/u	23.977	0.967	288.759	0.553	0.057
70	h	24.840	0.719	335.281	0.439	0.113
71	h	15.123	0.478	412.141	0.424	0.100
72	h	21.241	0.576	374.889	0.314	0.071
73	f/h	63.104	3.542	148.841	0.420	0.086
74	h	24.284	0.701	339.62	0.233	0.362
75	h	27.212	0.887	301.286	0.306	0.106
76	h	20.832	0.638	356.092	0.332	0.271
77	h	26.231	0.620	362.009	0.288	0.102
78	h	14.422	0.288	531.794	0.499	0.103
79	h	24.200	0.765	324.973	0.456	0.077
80	f/h	30.441	1.114	268.554	0.283	0.093
81	f/h	45.294	1.902	204.717	0.440	0.059
82	h	38.069	1.711	216.068	0.493	0.128
83	h	18.866	0.647	353.642	0.566	0.049
84	f/h	31.763	1.734	214.393	0.521	0.271
85	h/u	39.124	2.532	176.701	0.237	0.177
86	f/h	26.479	1.015	281.276	0.293	0.120
87	h	33.417	1.357	242.811	0.415	0.111
88	h	30.136	1.658	219.349	0.426	0.073

Indent	Type*	Modulus (GPa)	Hardness (GPa)	Maximum Displacement (nm)	Si/Ca Ratio	Al/Ca Ratio
89	f/h	22.883	0.654	351.759	0.728	0.105
90	h/u	92.046	10.352	85.461	0.735	0.052
91	f/h/u	17.112	0.704	338.867	0.500	0.227
92	h	24.167	0.510	398.869	0.479	0.034
93	h	16.420	0.264	556.058	0.380	0.079
94	h	22.431	0.629	358.522	0.479	0.391
95	f/h	13.827	0.508	399.442	0.355	0.097
96	h	24.408	0.513	397.507	0.375	0.073
97	h	51.429	3.753	144.442	0.239	0.094
98	f/h	25.662	0.444	427.95	0.198	0.011
99	h	27.985	0.968	288.371	0.317	0.184
100	f/h	19.114	0.599	367.823	0.296	0.061
101	f/h	49.811	3.741	144.747	0.364	0.049
102	f/h	19.369	0.804	316.791	0.438	0.059
103	h	22.088	0.782	321.143	0.293	0.055
104	f/h	19.114	0.482	410.277	0.461	0.408
105	h	35.782	1.026	279.856	0.368	0.054
106	f/h	23.721	0.593	369.301	0.590	0.084
107	h	26.338	0.661	349.577	0.269	0.239
108	h	“invalid”	“invalid”	“invalid”	0.328	0.070
109	h	26.871	0.865	305.266	0.366	0.168
110	h	21.793	0.675	346.184	0.567	0.060
111	f/h/u	23.569	1.092	271.349	0.426	0.123
112	f/h	25.569	0.561	379.884	0.403	0.134
113	h	25.892	0.808	315.974	0.240	0.222
114	h	21.857	0.487	408.715	0.485	0.161
115	h	26.354	0.834	311.034	0.513	0.070
116	f/h	20.300	0.367	470.551	0.508	0.083
117	h	27.008	0.909	297.86	0.464	0.163
118	h	27.888	0.840	310.093	0.037	0.014
119	h	31.347	1.212	257.278	0.463	0.104
120	f/h	14.977	0.311	511.987	0.461	0.058
121	f/h	20.622	0.712	336.923	0.150	0.536
122	h	21.100	0.602	366.823	0.238	0.387
123	f/h	16.610	0.567	378.188	0.509	0.069
124	h/u	28.077	1.343	244.397	0.329	0.106
125	u	110.937	8.683	93.604	0.534	0.081
126	h/u	47.494	1.807	210	0.355	0.201
127	h	20.166	0.667	348.557	0.463	0.072
128	h	37.665	1.075	273.627	0.132	0.086

Indent	Type*	Modulus (GPa)	Hardness (GPa)	Maximum Displacement (nm)	Si/Ca Ratio	Al/Ca Ratio
129	h	26.970	1.027	279.772	0.504	0.072
130	u	137.710	9.906	87.366	0.429	0.211
131	h/u	158.736	15.199	69.825	0.457	0.125
132	h/u	73.116	6.835	106.028	0.469	0.081
133	h	23.269	0.640	355.489	0.124	0.027
134	f/h	26.615	0.727	333.655	0.426	0.141
135	f/h	35.552	0.590	370.45	0.463	0.130
136	h/u	45.540	1.057	275.909	0.191	0.033
137	h	21.223	0.882	302.224	0.532	0.105
138	h/u	44.072	4.321	134.382	0.436	0.071
139	f	23.577	0.659	350.356	0.123	0.076
140	f/h	28.080	0.928	294.743	0.338	0.304
141	f/h	37.492	0.924	295.434	0.495	0.077
142	u	85.092	7.190	103.244	0.471	0.107
143	h	27.717	0.842	309.476	0.257	0.388
144	h	19.930	0.615	363.206	0.512	0.142
145	f/h	79.242	6.496	108.912	0.418	0.068
146	h/u	59.760	5.962	113.873	0.168	0.442
147	h	24.062	0.751	327.93	0.342	0.251
148	h	20.022	0.763	325.41	0.461	0.095
149	h	23.329	0.579	374.008	0.365	0.059
150	h/u	40.134	1.925	203.241	0.179	0.476
151	f/h/u	17.519	0.392	455.465	0.518	0.120
152	h	31.614	1.193	259.247	0.483	0.112
153	f/h	22.014	0.752	327.777	0.503	0.064
154	f/h	28.203	0.593	370.051	0.441	0.110
155	h	42.226	1.776	211.901	0.478	0.160
156	f	25.683	0.475	413.2	0.169	0.186
157	h	21.109	0.602	366.517	0.442	0.104
158	h	25.081	1.033	278.873	0.550	0.042
159	h	26.314	1.069	273.998	0.423	0.131
160	f/h	30.701	1.490	231.527	0.487	0.105
161	f/h	“invalid”	“invalid”	“invalid”	0.480	0.080
162	h	27.516	0.995	284.459	0.303	0.100
163	h	25.979	1.092	271.226	0.555	0.081
164	f/h	24.575	0.736	331.166	0.503	0.091
165	h	27.908	0.848	308.231	0.514	0.061
166	f/h/u	22.829	0.777	322.367	0.299	0.049
167	f/h	22.037	0.663	348.977	0.497	0.068
168	u	84.105	10.343	85.443	0.404	0.131

Indent	Type*	Modulus (GPa)	Hardness (GPa)	Maximum Displacement (nm)	Si/Ca Ratio	Al/Ca Ratio
169	h/u	44.397	2.314	185.188	0.564	0.071
170	u	89.040	7.434	101.575	0.307	0.060
171	h	25.613	0.501	402.431	0.399	0.107
172	h	22.266	0.669	348.184	0.357	0.158
173	f/h	26.468	0.850	308.095	0.441	0.180
174	f/h	18.828	0.574	375.439	0.121	0.029
175	h	26.401	0.886	301.696	0.300	0.279
176	h/u	83.499	2.893	165.173	0.333	0.070
177	f/h	25.715	0.715	336.167	0.326	0.047
178	h	16.775	0.419	440.393	0.290	0.044
179	h	22.381	0.818	314.187	0.438	0.069
180	f/h	21.308	0.463	418.661	0.491	0.111
181	f/h	“invalid”	“invalid”	“invalid”	0.498	0.085
182	h	24.222	0.788	319.851	0.370	0.155
183	f/h	26.251	0.848	308.386	0.494	0.131
184	f/h	37.333	1.124	267.158	0.485	0.105
185	h	33.052	1.262	252.158	0.438	0.055
186	h	41.846	2.879	165.512	0.384	0.034
187	h	32.032	1.327	245.559	0.392	0.142
188	f/h	22.681	0.689	342.711	0.518	0.070
189	f/h	25.586	1.911	204.096	0.368	0.253
190	h/u	58.739	3.069	160.275	0.278	0.297
191	f/h	19.074	0.725	333.632	0.163	0.240
192	f/h	32.227	0.857	306.826	0.300	0.053
193	f/h	23.817	0.390	456.813	0.340	0.053
194	h	24.948	0.707	337.95	0.383	0.081
195	h	29.208	0.935	293.365	0.325	0.059
196	h	20.642	0.551	384.002	0.528	0.057
197	h/u	61.649	3.412	151.746	0.446	0.164
198	h	30.959	1.167	262.209	0.504	0.061
199	u	“invalid”	“invalid”	“invalid”	0.465	0.105
200	f/h	29.157	1.452	234.592	0.516	0.087

*Type: f=flaw, h=hydrate, u=unhydrated particle, f/h=flaw and hydrate combination, f/u=flaw and unhydrated particle combination, f/h/u=flaw, hydrate, and unhydrated particle combination, and h/u=hydrate and unhydrated particle combination.

PC-CNF-B Grid 1

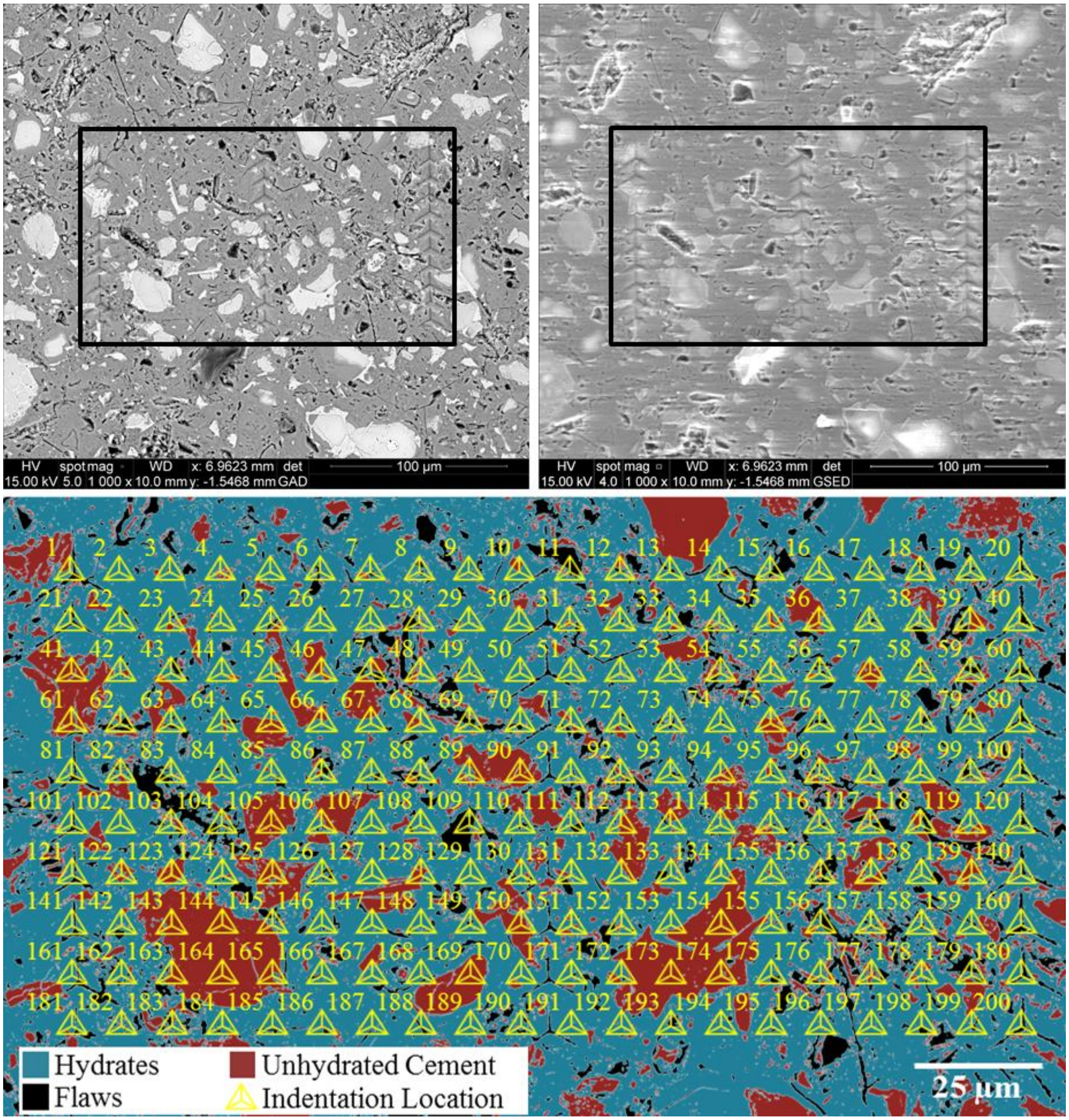

Indent	Type*	Modulus (GPa)	Hardness (GPa)	Maximum Displacement (nm)	Si/Ca Ratio	Al/Ca Ratio
1	h	“invalid”	“invalid”	“invalid”	0.486	0.201
2	h	27.127	0.908	297.87	0.454	0.113
3	f/h	27.842	0.930	294.298	0.525	0.055
4	h/u	“invalid”	“invalid”	“invalid”	0.525	0.073
5	h	23.904	0.842	309.43	0.421	0.058
6	f/h	20.035	0.450	425.05	0.560	0.046
7	f/h	“invalid”	“invalid”	“invalid”	0.478	0.066
8	h	“invalid”	“invalid”	“invalid”	0.463	0.078

Indent	Type*	Modulus (GPa)	Hardness (GPa)	Maximum Displacement (nm)	Si/Ca Ratio	Al/Ca Ratio
9	h	22.913	0.755	326.915	0.329	0.342
10	h/u	“invalid”	“invalid”	“invalid”	0.644	0.082
11	f	“invalid”	“invalid”	“invalid”	0.435	0.222
12	f/h	18.897	0.461	419.412	0.118	0.386
13	f/h	“invalid”	“invalid”	“invalid”	0.476	0.065
14	h	“invalid”	“invalid”	“invalid”	0.427	0.039
15	f/h	“invalid”	“invalid”	“invalid”	0.403	0.125
16	f/h	“invalid”	“invalid”	“invalid”	0.212	0.103
17	f/h	23.060	0.793	319.112	0.494	0.068
18	f/h	“invalid”	“invalid”	“invalid”	0.412	0.095
19	f/h	18.175	0.557	381.812	0.542	0.117
20	f/h	“invalid”	“invalid”	“invalid”	0.387	0.325
21	f/h	“invalid”	“invalid”	“invalid”	0.494	0.123
22	h	23.213	0.623	360.66	0.584	0.087
23	h/u	59.303	3.052	160.677	0.428	0.208
24	h	26.347	0.819	313.799	0.443	0.118
25	f/h	“invalid”	“invalid”	“invalid”	0.381	0.062
26	h	28.815	1.075	273.467	0.298	0.054
27	h	24.082	0.911	297.503	0.239	0.060
28	f/h/u	16.873	0.496	404.847	0.528	0.089
29	h	“invalid”	“invalid”	“invalid”	0.604	0.061
30	h	37.878	1.340	244.499	0.428	0.196
31	u	“invalid”	“invalid”	“invalid”	0.495	0.126
32	f/h	“invalid”	“invalid”	“invalid”	0.295	0.369
33	h	18.380	0.572	376.314	0.256	0.046
34	h	“invalid”	“invalid”	“invalid”	0.159	0.051
35	u	“invalid”	“invalid”	“invalid”	0.333	0.246
36	u	82.179	6.851	105.938	0.587	0.082
37	h	“invalid”	“invalid”	“invalid”	0.273	0.091
38	f/h/u	“invalid”	“invalid”	“invalid”	0.400	0.129
39	f/h/u	96.954	7.944	98.086	0.528	0.220
40	f/h	“invalid”	“invalid”	“invalid”	0.302	0.106
41	u	“invalid”	“invalid”	“invalid”	0.532	0.095
42	h	“invalid”	“invalid”	“invalid”	0.463	0.101
43	h	“invalid”	“invalid”	“invalid”	0.559	0.096
44	h	“invalid”	“invalid”	“invalid”	0.463	0.060
45	h	29.590	1.338	244.835	0.501	0.089
46	u	“invalid”	“invalid”	“invalid”	0.579	0.084
47	f/h	“invalid”	“invalid”	“invalid”	0.371	0.052
48	h	22.971	0.744	329.895	0.481	0.171

Indent	Type*	Modulus (GPa)	Hardness (GPa)	Maximum Displacement (nm)	Si/Ca Ratio	Al/Ca Ratio
49	h	“invalid”	“invalid”	“invalid”	0.163	0.506
50	h	28.426	0.857	306.913	0.614	0.094
51	h	21.002	0.587	371.336	0.428	0.082
52	f/h	“invalid”	“invalid”	“invalid”	0.465	0.269
53	h	“invalid”	“invalid”	“invalid”	0.320	0.109
54	f/h/u	“invalid”	“invalid”	“invalid”	0.367	0.273
55	h/u	17.559	0.696	340.756	0.443	0.073
56	h	“invalid”	“invalid”	“invalid”	0.526	0.090
57	h/u	37.803	3.818	143.263	0.399	0.173
58	f/h	“invalid”	“invalid”	“invalid”	0.554	0.082
59	f/h	“invalid”	“invalid”	“invalid”	0.533	0.184
60	f/h	“invalid”	“invalid”	“invalid”	0.286	0.132
61	u	error	error	“invalid”	0.117	0.027
62	f/h/u	21.024	0.474	414.329	0.551	0.064
63	f/h	“invalid”	“invalid”	“invalid”	0.544	0.088
64	h/u	“invalid”	“invalid”	“invalid”	0.576	0.082
65	u	85.918	4.228	135.918	0.560	0.089
66	h	34.930	1.214	257.126	0.654	0.076
67	h	“invalid”	“invalid”	“invalid”	0.526	0.062
68	h/u	“invalid”	“invalid”	“invalid”	0.585	0.019
69	f	“invalid”	“invalid”	“invalid”	0.403	0.109
70	f/h	22.717	0.543	386.586	0.340	0.089
71	h/u	22.743	0.576	375.189	0.591	0.081
72	h	“invalid”	“invalid”	“invalid”	0.550	0.078
73	f/h	18.080	0.396	453.587	0.517	0.098
74	f/h	“invalid”	“invalid”	“invalid”	0.276	0.073
75	u	“invalid”	“invalid”	“invalid”	0.463	0.124
76	f/h	“invalid”	“invalid”	“invalid”	0.401	0.234
77	h	21.726	0.699	340.04	0.511	0.094
78	f/h	13.217	0.672	346.828	0.451	0.118
79	h	“invalid”	“invalid”	“invalid”	0.402	0.070
80	f/h	“invalid”	“invalid”	“invalid”	0.386	0.049
81	f/h	“invalid”	“invalid”	“invalid”	0.562	0.095
82	h/u	“invalid”	“invalid”	“invalid”	0.072	0.021
83	h/u	“invalid”	“invalid”	“invalid”	0.557	0.030
84	f/h	29.654	0.873	304.001	0.348	0.193
85	h	16.044	0.236	588.127	0.505	0.109
86	h/u	22.202	0.597	368.519	0.325	0.129
87	f/h	46.927	1.898	204.785	0.123	0.173
88	f/h	“invalid”	“invalid”	“invalid”	0.245	0.333

Indent	Type*	Modulus (GPa)	Hardness (GPa)	Maximum Displacement (nm)	Si/Ca Ratio	Al/Ca Ratio
89	h/u	87.139	7.971	97.892	0.489	0.288
90	u	“invalid”	“invalid”	“invalid”	0.320	0.274
91	h	18.113	0.339	489.979	0.553	0.052
92	h/u	15.765	0.254	567.513	0.510	0.048
93	f/h	“invalid”	“invalid”	“invalid”	0.478	0.091
94	h/u	“invalid”	“invalid”	“invalid”	0.283	0.102
95	h/u	“invalid”	“invalid”	“invalid”	0.121	0.538
96	f/h	“invalid”	“invalid”	“invalid”	0.373	0.143
97	f/h	“invalid”	“invalid”	“invalid”	0.573	0.119
98	f/h	“invalid”	“invalid”	“invalid”	0.238	0.044
99	f/h	“invalid”	“invalid”	“invalid”	0.502	0.074
100	f/h	“invalid”	“invalid”	“invalid”	0.472	0.081
101	f/h	24.978	0.855	307.371	0.138	0.481
102	h	“invalid”	“invalid”	“invalid”	0.481	0.127
103	h/u	16.215	0.462	419.223	0.582	0.040
104	f/h	“invalid”	“invalid”	“invalid”	0.317	0.073
105	u	112.515	6.800	106.372	0.584	0.075
106	h	33.520	1.094	271.034	0.469	0.137
107	h	29.757	1.050	276.656	0.558	0.123
108	h	26.109	0.589	370.935	0.536	0.103
109	f/h	8.639	0.132	789.424	0.594	0.069
110	f/h	17.968	0.458	421.045	0.165	0.543
111	f/h	“invalid”	“invalid”	“invalid”	0.131	0.090
112	u	“invalid”	“invalid”	“invalid”	0.492	0.075
113	f/h	“invalid”	“invalid”	“invalid”	0.538	0.128
114	h	“invalid”	“invalid”	“invalid”	0.346	0.074
115	f/h	“invalid”	“invalid”	“invalid”	0.351	0.339
116	f/h	“invalid”	“invalid”	“invalid”	0.229	0.417
117	f/h	“invalid”	“invalid”	“invalid”	0.203	0.428
118	h/u	“invalid”	“invalid”	“invalid”	0.392	0.064
119	h	“invalid”	“invalid”	“invalid”	0.345	0.136
120	f/h	“invalid”	“invalid”	“invalid”	0.387	0.032
121	h	“invalid”	“invalid”	“invalid”	0.580	0.035
122	h/u	“invalid”	“invalid”	“invalid”	0.601	0.055
123	u	“invalid”	“invalid”	“invalid”	0.318	0.132
124	h	“invalid”	“invalid”	“invalid”	0.471	0.074
125	u	74.617	3.873	142.136	0.489	0.045
126	f/h	“invalid”	“invalid”	“invalid”	0.486	0.081
127	h	30.880	1.114	268.466	0.370	0.045
128	u	“invalid”	“invalid”	“invalid”	0.472	0.163

Indent	Type*	Modulus (GPa)	Hardness (GPa)	Maximum Displacement (nm)	Si/Ca Ratio	Al/Ca Ratio
129	h	27.296	0.886	301.728	0.484	0.087
130	h	“invalid”	“invalid”	“invalid”	0.577	0.073
131	h	“invalid”	“invalid”	“invalid”	0.486	0.062
132	h	52.950	1.478	232.695	0.405	0.047
133	h	“invalid”	“invalid”	“invalid”	0.416	0.260
134	h	“invalid”	“invalid”	“invalid”	0.376	0.154
135	h/u	“invalid”	“invalid”	“invalid”	0.408	0.236
136	h/u	“invalid”	“invalid”	“invalid”	0.276	0.234
137	h	error	error	error	0.368	0.146
138	f/h	16.357	0.620	361.26	0.527	0.099
139	h/u	“invalid”	“invalid”	“invalid”	0.355	0.047
140	f/h	“invalid”	“invalid”	“invalid”	0.386	0.028
141	h	25.941	0.777	322.59	0.569	0.030
142	h	19.154	0.362	474.445	0.539	0.043
143	u	“invalid”	“invalid”	“invalid”	0.521	0.104
144	u	141.489	7.999	97.762	0.546	0.079
145	h/u	“invalid”	“invalid”	“invalid”	0.510	0.113
146	h	“invalid”	“invalid”	“invalid”	0.510	0.210
147	h	28.317	0.919	296.08	0.557	0.063
148	h	“invalid”	“invalid”	“invalid”	0.434	0.087
149	f/h	27.030	0.783	320.941	0.198	0.299
150	u	99.272	8.090	97.203	0.154	0.558
151	h	“invalid”	“invalid”	“invalid”	0.330	0.190
152	h/u	“invalid”	“invalid”	“invalid”	0.382	0.090
153	h	“invalid”	“invalid”	“invalid”	0.358	0.053
154	u	102.066	6.623	107.807	0.286	0.074
155	h	“invalid”	“invalid”	“invalid”	0.249	0.059
156	f/h	“invalid”	“invalid”	“invalid”	0.125	0.025
157	f/h	21.645	0.397	452.437	0.498	0.084
158	f/h	18.151	0.358	477.311	0.463	0.062
159	f/h	“invalid”	“invalid”	“invalid”	0.134	0.473
160	f/h	“invalid”	“invalid”	“invalid”	0.381	0.083
161	h	“invalid”	“invalid”	“invalid”	0.350	0.085
162	h	error	error	error	0.516	0.097
163	u	113.663	8.766	93.245	0.578	0.095
164	u	138.566	7.950	98.051	0.577	0.071
165	h/u	130.661	9.684	88.463	0.412	0.068
166	f/h	23.305	0.896	300.182	0.402	0.030
167	h	25.853	0.951	291.195	0.445	0.147
168	h	“invalid”	“invalid”	“invalid”	0.566	0.058

Indent	Type*	Modulus (GPa)	Hardness (GPa)	Maximum Displacement (nm)	Si/Ca Ratio	Al/Ca Ratio
169	u	“invalid”	“invalid”	“invalid”	0.513	0.060
170	h	“invalid”	“invalid”	“invalid”	0.170	0.527
171	f/h	“invalid”	“invalid”	“invalid”	0.236	0.407
172	h	“invalid”	“invalid”	“invalid”	0.482	0.158
173	u	138.172	9.883	87.498	0.462	0.092
174	h/u	116.441	8.943	92.266	0.303	0.297
175	f/h	“invalid”	“invalid”	“invalid”	0.312	0.320
176	h	“invalid”	“invalid”	“invalid”	0.444	0.137
177	h/u	“invalid”	“invalid”	“invalid”	0.417	0.254
178	h	“invalid”	“invalid”	“invalid”	0.409	0.121
179	h	69.904	3.627	147.168	0.589	0.014
180	f/h	“invalid”	“invalid”	“invalid”	0.350	0.290
181	h	“invalid”	“invalid”	“invalid”	0.144	0.458
182	h	“invalid”	“invalid”	“invalid”	0.536	0.115
183	f/h	“invalid”	“invalid”	“invalid”	0.436	0.160
184	h	44.277	1.131	266.611	0.582	0.080
185	h	“invalid”	“invalid”	“invalid”	0.547	0.092
186	f/h	25.054	0.566	378.151	0.497	0.111
187	h	“invalid”	“invalid”	“invalid”	0.422	0.105
188	f/h	“invalid”	“invalid”	“invalid”	0.490	0.056
189	h	“invalid”	“invalid”	“invalid”	0.534	0.132
190	h	“invalid”	“invalid”	“invalid”	0.503	0.045
191	h	“invalid”	“invalid”	“invalid”	0.486	0.061
192	h	“invalid”	“invalid”	“invalid”	0.418	0.189
193	f/h	“invalid”	“invalid”	“invalid”	0.135	0.074
194	h	23.003	0.852	307.815	0.457	0.106
195	h	25.312	0.651	352.794	0.488	0.073
196	h	“invalid”	“invalid”	“invalid”	0.477	0.077
197	h	22.209	0.580	373.835	0.369	0.234
198	f/h	“invalid”	“invalid”	“invalid”	0.492	0.089
199	h	“invalid”	“invalid”	“invalid”	0.564	0.029
200	f/h	“invalid”	“invalid”	“invalid”	0.350	0.234

*Type: f=flaw, h=hydrate, u=unhydrated particle, f/h=flaw and hydrate combination, f/u=flaw and unhydrated particle combination, f/h/u=flaw, hydrate, and unhydrated particle combination, and h/u=hydrate and unhydrated particle combination.

PC-CF-A Grid 1

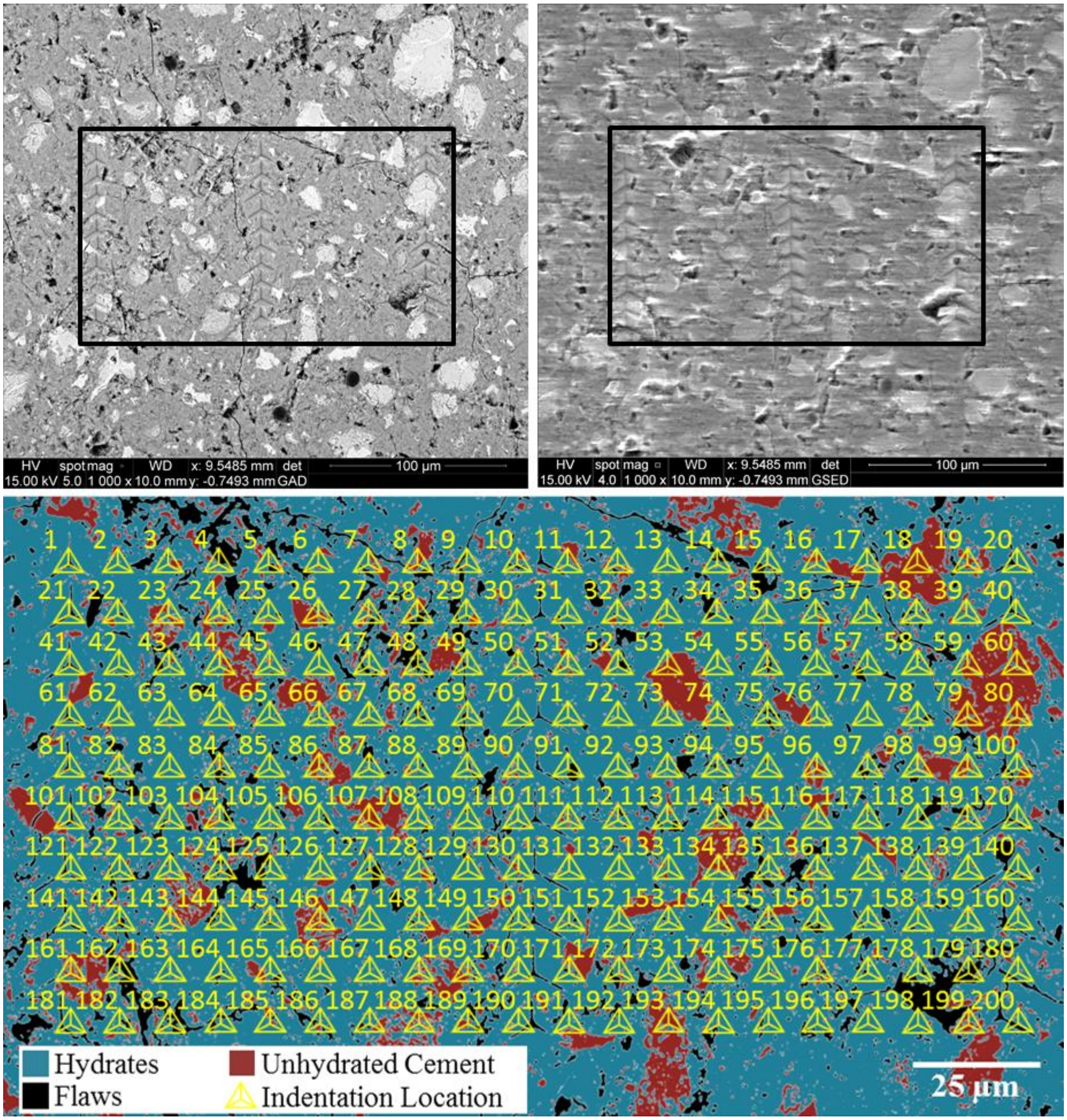

Indent	Type*	Modulus (GPa)	Hardness (GPa)	Maximum Displacement (nm)	Si/Ca Ratio	Al/Ca Ratio
1	h	33.368	1.313	247.423	0.503	0.068
2	h	28.250	1.126	267.326	0.460	0.194
3	h	33.487	1.619	222.475	0.355	0.182
4	f/h	“invalid”	“invalid”	“invalid”	0.231	0.038
5	h	31.049	2.400	181.996	0.300	0.137
6	h	error	error	error	0.307	0.127
7	h	75.267	6.970	105.368	0.349	0.244
8	u	24.622	1.235	255.119	0.397	0.149

Indent	Type*	Modulus (GPa)	Hardness (GPa)	Maximum Displacement (nm)	Si/Ca Ratio	Al/Ca Ratio
9	h/u	28.423	1.488	232.058	0.554	0.130
10	f/h	27.539	1.172	261.938	0.443	0.148
11	f/h	28.738	0.904	298.619	0.515	0.109
12	h	19.962	0.526	392.94	0.589	0.101
13	h	26.364	1.456	234.645	0.455	0.071
14	h	33.595	0.897	299.958	0.409	0.047
15	h/u	41.433	1.753	213.582	0.572	0.111
16	f/h	error	error	error	0.593	0.119
17	h/u	41.594	1.616	222.545	0.214	0.265
18	u	90.958	9.239	90.968	0.195	0.235
19	u	27.896	1.189	259.992	0.558	0.109
20	h	20.693	0.702	339.786	0.447	0.099
21	h	25.315	0.993	285.025	0.560	0.097
22	f/h	26.500	1.143	265.408	0.512	0.120
23	h/u	41.006	1.466	234.021	0.416	0.152
24	h/u	51.327	3.735	145.229	0.377	0.119
25	h	20.261	1.023	280.641	0.548	0.117
26	h/u	85.500	7.860	98.987	0.517	0.197
27	h/u	9.496	0.428	435.035	0.555	0.079
28	f/h	“invalid”	“invalid”	“invalid”	0.397	0.099
29	f/h	57.467	8.016	97.971	0.296	0.343
30	f/h	33.057	1.123	267.691	0.120	0.513
31	h	26.896	1.339	244.657	0.525	0.142
32	f/h	24.106	0.994	284.55	0.365	0.118
33	h	22.177	1.103	270.083	0.372	0.159
34	f/h	6.941	0.127	803.289	0.453	0.116
35	h	20.836	0.864	305.565	0.431	0.151
36	h/u	24.170	0.601	367.139	0.498	0.124
37	h	36.061	1.675	218.774	0.571	0.029
38	h/u	“invalid”	“invalid”	“invalid”	0.416	0.182
39	h	26.810	1.101	270.418	0.555	0.127
40	h	25.508	1.249	253.748	0.127	0.036
41	h	26.344	1.009	282.583	0.430	0.066
42	h	27.138	0.821	313.987	0.402	0.110
43	h	12.785	0.220	609.758	0.324	0.296
44	h	38.720	1.296	249.121	0.499	0.099
45	h	24.853	0.809	315.97	0.587	0.143
46	h	39.231	1.777	212.072	0.446	0.143
47	h	39.966	2.106	194.652	0.351	0.149
48	f	13.198	0.343	487.95	0.410	0.260

Indent	Type*	Modulus (GPa)	Hardness (GPa)	Maximum Displacement (nm)	Si/Ca Ratio	Al/Ca Ratio
49	f/h	30.075	1.149	264.966	0.441	0.125
50	h	14.700	0.324	501.856	0.234	0.108
51	f/h	35.519	1.442	235.861	0.559	0.094
52	f/h	36.312	1.858	207.479	0.504	0.104
53	u	115.378	7.265	103.077	0.476	0.164
54	h	20.412	0.662	349.831	0.467	0.100
55	f	21.860	1.069	274.47	0.170	0.366
56	h	30.604	1.347	244.245	0.457	0.131
57	h	28.838	1.032	279.436	0.506	0.113
58	h	26.097	0.950	291.334	0.448	0.222
59	u	“invalid”	“invalid”	“invalid”	0.550	0.136
60	u	“invalid”	“invalid”	“invalid”	0.306	0.098
61	h	26.487	1.126	267.426	0.553	0.062
62	h	23.505	0.961	289.727	0.525	0.147
63	h	40.053	1.607	223.119	0.353	0.125
64	h	20.569	0.646	353.985	0.223	0.336
65	h	25.865	0.922	295.632	0.550	0.126
66	f/h	36.751	0.932	294.466	0.358	0.166
67	f/h	26.770	0.960	289.814	0.219	0.131
68	f/h	32.330	1.181	260.982	0.310	0.203
69	f/h	17.795	0.455	422.839	0.331	0.129
70	h	36.221	1.286	249.865	0.372	0.256
71	h	20.948	0.898	299.716	0.490	0.162
72	h	30.049	1.152	264.333	0.378	0.090
73	h	41.086	1.278	250.919	0.495	0.104
74	h	23.477	0.986	285.994	0.366	0.164
75	f/h	29.910	1.604	223.342	0.487	0.121
76	h	93.459	5.784	116.023	0.346	0.144
77	h	26.752	1.127	267.039	0.537	0.133
78	h	28.262	1.272	251.321	0.511	0.091
79	u	“invalid”	“invalid”	“invalid”	0.368	0.186
80	u	75.872	2.623	173.881	0.503	0.129
81	h	26.836	1.373	241.892	0.456	0.099
82	h	23.003	1.046	277.761	0.502	0.128
83	h	32.565	1.294	249.233	0.227	0.202
84	f/h	22.752	1.018	281.201	0.525	0.113
85	h	21.174	0.845	309.182	0.455	0.186
86	h/u	61.268	2.932	164.253	0.371	0.143
87	h/u	38.253	2.348	184.099	0.457	0.133
88	h	28.464	1.281	250.575	0.401	0.108

Indent	Type*	Modulus (GPa)	Hardness (GPa)	Maximum Displacement (nm)	Si/Ca Ratio	Al/Ca Ratio
89	h	24.156	0.908	298.377	0.563	0.141
90	h	25.151	1.027	280.214	0.414	0.144
91	h	21.380	0.570	377.288	0.134	0.589
92	h	27.201	1.221	256.437	0.481	0.097
93	h	49.566	2.479	179.122	0.374	0.110
94	f/h	27.553	1.040	278.498	0.433	0.159
95	h	27.576	1.199	259.046	0.580	0.066
96	u	63.297	2.046	197.54	0.383	0.143
97	f/h	58.390	2.918	164.639	0.578	0.029
98	h	“invalid”	“invalid”	“invalid”	0.541	0.064
99	u	110.984	5.125	123.401	0.516	0.158
100	h	54.692	3.095	159.968	0.488	0.096
101	f/h	93.425	9.579	89.317	0.594	0.074
102	h	27.556	1.243	254.307	0.404	0.220
103	f/h	“invalid”	“invalid”	“invalid”	0.266	0.291
104	h/u	18.851	0.933	293.977	0.460	0.108
105	h	21.654	0.844	309.12	0.367	0.267
106	h	28.475	1.081	272.927	0.287	0.293
107	u	“invalid”	“invalid”	“invalid”	0.573	0.067
108	h/u	35.384	1.152	264.372	0.473	0.084
109	h	23.376	0.750	328.405	0.416	0.064
110	h/u	20.767	0.584	372.733	0.538	0.101
111	h	16.707	0.612	363.748	0.130	0.537
112	h	“invalid”	“invalid”	“invalid”	0.321	0.079
113	h	22.240	0.907	298.313	0.116	0.557
114	f/h/u	61.178	2.225	189.178	0.442	0.173
115	h	44.724	2.231	188.878	0.565	0.118
116	h	36.395	1.326	246.11	0.492	0.108
117	f/h	24.769	0.974	287.759	0.258	0.413
118	f/h	32.350	1.611	223.038	0.403	0.220
119	h/u	18.503	0.413	443.839	0.386	0.232
120	h	26.356	0.971	288.283	0.339	0.165
121	h	35.753	1.638	221.161	0.601	0.111
122	h	24.413	1.127	267.156	0.465	0.140
123	h	40.000	1.794	211.046	0.170	0.376
124	f/h/u	60.966	1.798	211.019	0.389	0.172
125	h	38.199	2.043	197.504	0.557	0.114
126	h	error	error	error	0.526	0.104
127	f/h	29.848	1.387	240.562	0.462	0.114
128	h	23.414	0.706	339.005	0.414	0.144

Indent	Type*	Modulus (GPa)	Hardness (GPa)	Maximum Displacement (nm)	Si/Ca Ratio	Al/Ca Ratio
129	h	35.842	2.068	196.425	0.384	0.071
130	h/u	31.035	1.371	241.922	0.356	0.071
131	h	26.638	1.170	262.23	0.419	0.161
132	h	36.312	1.843	208.162	0.455	0.063
133	h	36.419	2.290	186.366	0.556	0.074
134	h/u	98.155	3.819	143.559	0.566	0.088
135	h	10.677	0.179	676.719	0.474	0.190
136	h	23.501	1.343	244.583	0.433	0.236
137	h/u	error	error	error	0.505	0.103
138	h	30.084	1.317	247.046	0.398	0.188
139	h	26.842	0.909	297.994	0.310	0.359
140	h	30.362	1.280	250.704	0.240	0.465
141	h	28.503	0.616	362.88	0.598	0.089
142	f	27.520	1.390	240.379	0.531	0.125
143	h/u	35.350	1.792	211.065	0.606	0.082
144	h	27.670	0.705	338.836	0.331	0.270
145	f	64.978	3.425	151.719	0.482	0.188
146	u	77.460	4.071	138.903	0.585	0.080
147	h	31.887	1.186	260.232	0.383	0.086
148	f/h	58.075	2.138	193.24	0.479	0.184
149	h/u	30.523	1.384	240.916	0.521	0.102
150	h	34.521	1.835	208.644	0.512	0.093
151	f/h	17.586	0.417	441.868	0.360	0.169
152	h	27.179	0.915	297.025	0.599	0.043
153	f/h	“invalid”	“invalid”	“invalid”	0.151	0.505
154	h/u	26.058	1.019	281.371	0.369	0.184
155	f/h	83.302	5.403	120.111	0.540	0.081
156	f/h	37.828	1.498	231.457	0.472	0.143
157	h	69.799	2.899	165.262	0.353	0.102
158	h	16.707	0.478	412.4	0.276	0.116
159	h	error	error	error	0.265	0.326
160	h	28.118	0.809	316.063	0.382	0.097
161	h/u	41.695	1.659	219.709	0.430	0.204
162	h/u	39.671	2.347	184.234	0.255	0.076
163	f/h	31.911	1.470	233.304	0.530	0.151
164	f/h	31.764	1.384	240.864	0.386	0.085
165	h	95.274	6.449	109.642	0.310	0.266
166	h	31.640	1.392	240.157	0.295	0.081
167	h	24.047	0.799	318.116	0.484	0.168
168	h/u	30.339	1.062	275.205	0.575	0.081

Indent	Type*	Modulus (GPa)	Hardness (GPa)	Maximum Displacement (nm)	Si/Ca Ratio	Al/Ca Ratio
169	h/u	40.928	2.502	178.256	0.485	0.122
170	h	28.432	1.072	274.272	0.497	0.113
171	f/h	23.162	0.837	310.392	0.537	0.057
172	h/u	47.116	3.032	161.485	0.409	0.112
173	h	34.595	1.465	233.974	0.377	0.129
174	f/h	65.728	6.081	112.975	0.480	0.119
175	f/h	25.411	1.019	281.136	0.534	0.080
176	f	21.956	0.812	315.559	0.550	0.077
177	f/h	23.775	0.933	293.921	0.435	0.098
178	h	23.808	0.772	323.5	0.409	0.090
179	f	19.123	0.986	286.069	0.478	0.188
180	h	error	error	error	0.470	0.103
181	h	22.676	1.383	241.051	0.477	0.195
182	h	"invalid"	"invalid"	"invalid"	0.257	0.324
183	f/h	"invalid"	"invalid"	"invalid"	0.261	0.348
184	h	64.558	2.827	167.378	0.506	0.133
185	h/u	25.323	0.884	302.05	0.474	0.154
186	h/u	26.541	1.322	246.529	0.489	0.125
187	h/u	92.743	3.633	147.226	0.440	0.169
188	h/u	59.933	2.025	198.442	0.500	0.134
189	h/u	"invalid"	"invalid"	"invalid"	0.190	0.438
190	h	22.619	0.820	313.956	0.314	0.301
191	h	35.995	0.989	285.585	0.146	0.563
192	h	57.739	2.818	167.631	0.285	0.348
193	h/u	"invalid"	"invalid"	"invalid"	0.564	0.077
194	h/u	"invalid"	"invalid"	"invalid"	0.511	0.084
195	h	22.267	0.815	314.906	0.476	0.068
196	h	50.792	2.674	172.222	0.542	0.088
197	h	28.102	1.417	237.953	0.466	0.090
198	h	37.999	2.181	191.207	0.459	0.117
199	u	45.662	2.145	192.694	0.482	0.185
200	f/h	145.460	7.603	100.768	0.432	0.135

*Type: f=flaw, h=hydrate, u=unhydrated particle, f/h=flaw and hydrate combination, f/u=flaw and unhydrated particle combination, f/h/u=flaw, hydrate, and unhydrated particle combination, and h/u=hydrate and unhydrated particle combination.

PC-CF-A Grid 2

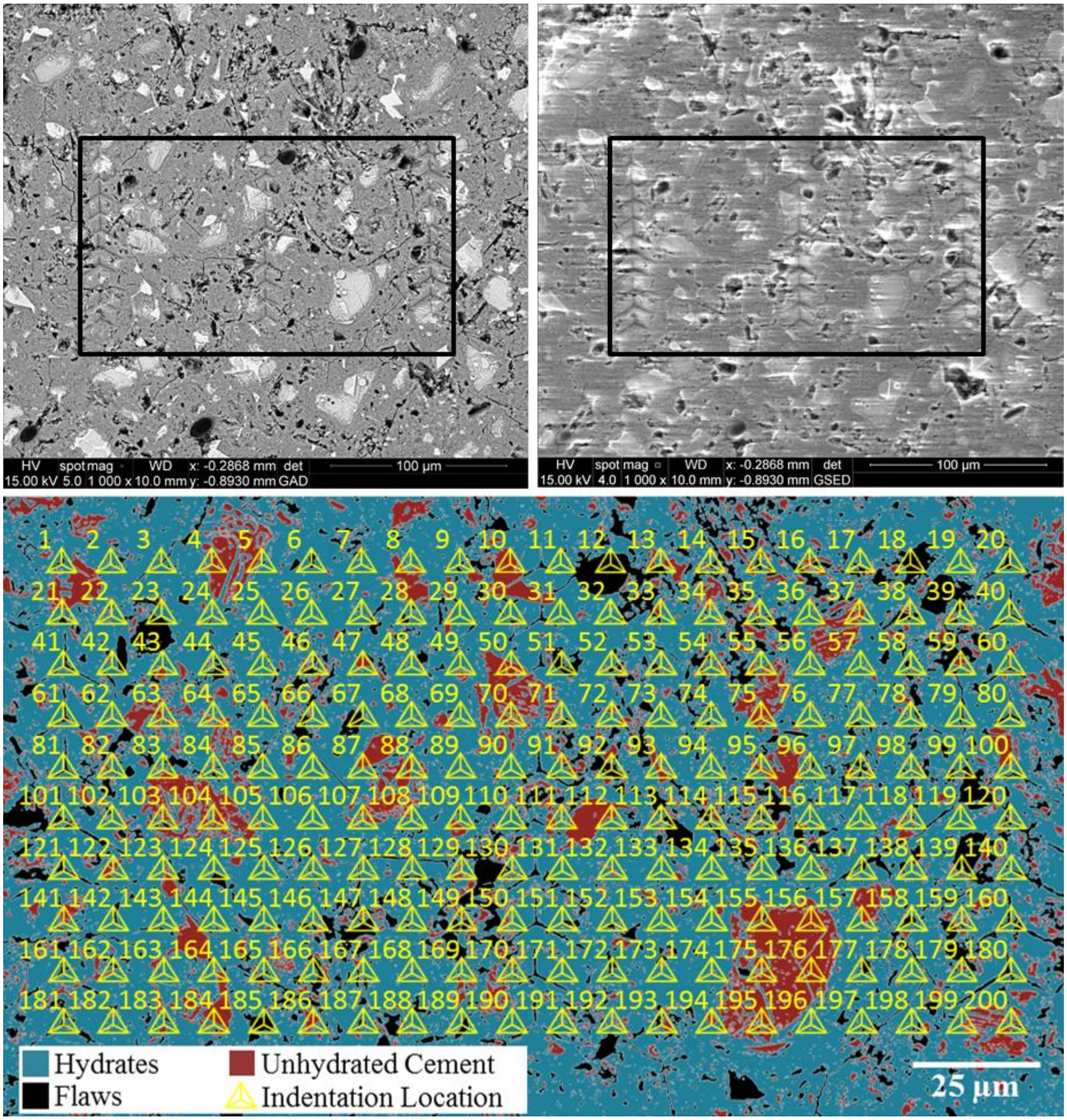

Indent	Type*	Modulus (GPa)	Hardness (GPa)	Maximum Displacement (nm)	Si/Ca Ratio	Al/Ca Ratio
1	f/h	155.739	11.305	81.918	0.451	0.320
2	h	250.272	24.864	54.087	0.527	0.120
3	f/h	18.798	0.546	385.644	0.521	0.070
4	u	72.344	2.472	179.358	0.403	0.051
5	f/h	35.290	1.144	265.313	0.664	0.075
6	f	16.268	0.609	364.716	0.563	0.096
7	h	18.431	0.689	342.697	0.586	0.078
8	h	32.981	1.333	245.461	0.245	0.459

Indent	Type*	Modulus (GPa)	Hardness (GPa)	Maximum Displacement (nm)	Si/Ca Ratio	Al/Ca Ratio
9	f/h	93.777	3.146	158.448	0.292	0.349
10	h	error	error	error	0.139	0.599
11	u	26.220	0.818	314.451	0.657	0.088
12	f	31.721	6.569	108.528	0.384	0.193
13	f/h	“invalid”	“invalid”	“invalid”	0.182	0.168
14	f/h	“invalid”	“invalid”	“invalid”	0.374	0.202
15	f/h	19.412	0.853	307.811	0.302	0.092
16	u	41.839	2.349	184.001	0.361	0.216
17	f/h	27.647	1.218	257.019	0.341	0.181
18	f	233.925	33.539	46.126	0.365	0.142
19	h	11.689	0.488	407.725	0.627	0.108
20	f/h	13.065	0.435	432.029	0.394	0.114
21	f/h	131.678	8.951	92.55	0.623	0.210
22	f/h	20.629	0.971	288.217	0.595	0.113
23	h	“invalid”	“invalid”	“invalid”	0.179	0.086
24	h	20.152	0.637	356.459	0.377	0.068
25	h	23.430	0.800	317.861	0.661	0.076
26	h	24.438	1.008	282.685	0.453	0.172
27	h	29.788	1.199	259.054	0.504	0.078
28	h	53.914	2.473	179.309	0.485	0.175
29	h	23.812	0.931	294.178	0.538	0.080
30	h	20.187	0.639	356.092	0.646	0.084
31	h	24.284	1.255	252.991	0.506	0.125
32	h	21.612	0.783	321.432	0.586	0.088
33	f/h/u	13.830	0.554	382.765	0.440	0.103
34	h	14.673	0.530	391.509	0.337	0.138
35	f/h	“invalid”	“invalid”	“invalid”	0.260	0.285
36	h	27.634	1.058	275.876	0.580	0.050
37	h/u	34.086	1.049	277.3	0.662	0.067
38	f/h	28.186	1.769	212.485	0.496	0.074
39	f/h	10.218	0.313	510.343	0.361	0.259
40	f/h	15.013	0.377	464.508	0.520	0.220
41	h	27.258	0.931	294.336	0.657	0.103
42	h	“invalid”	“invalid”	“invalid”	0.604	0.099
43	h/u	28.896	1.314	247.28	0.286	0.429
44	h	21.801	0.829	311.963	0.491	0.240
45	h	16.940	0.689	342.694	0.418	0.131
46	f/h	14.282	0.440	429.877	0.416	0.172
47	f/h/u	error	error	error	0.634	0.077
48	h	20.655	1.091	271.617	0.499	0.091

Indent	Type*	Modulus (GPa)	Hardness (GPa)	Maximum Displacement (nm)	Si/Ca Ratio	Al/Ca Ratio
49	h	41.073	1.225	256.001	0.515	0.046
50	u	90.760	7.710	99.956	0.572	0.057
51	f	“invalid”	“invalid”	“invalid”	0.571	0.174
52	f/h	“invalid”	“invalid”	“invalid”	0.503	0.198
53	h	31.120	2.174	191.428	0.519	0.147
54	h	“invalid”	“invalid”	“invalid”	0.296	0.067
55	h	39.441	1.942	202.685	0.543	0.045
56	h	21.780	0.855	307.594	0.631	0.118
57	h	22.161	0.838	310.358	0.571	0.094
58	f/h	15.418	0.407	447.055	0.276	0.158
59	h/u	“invalid”	“invalid”	“invalid”	0.523	0.126
60	h	38.243	1.407	238.834	0.428	0.194
61	f/h	15.567	0.568	378.035	0.570	0.092
62	h/u	48.715	2.474	179.263	0.324	0.254
63	h/u	53.366	1.378	241.316	0.580	0.077
64	h/u	33.946	1.104	269.928	0.597	0.044
65	h	20.890	1.031	279.698	0.503	0.081
66	h	7.805	0.205	630.169	0.493	0.089
67	f/h	33.603	1.808	210.21	0.296	0.317
68	h	23.344	0.879	303.041	0.553	0.071
69	h	35.793	1.050	277.078	0.557	0.054
70	h/u	36.220	0.925	295.565	0.460	0.189
71	h/u	16.983	0.571	376.943	0.304	0.237
72	h	16.601	0.648	353.706	0.358	0.249
73	h	21.466	1.005	283.182	0.420	0.109
74	h	40.371	3.061	160.811	0.346	0.080
75	h/u	107.537	6.714	107.414	0.266	0.125
76	h	17.949	0.462	419.291	0.522	0.075
77	h	13.323	0.530	391.177	0.396	0.143
78	h	“invalid”	“invalid”	“invalid”	0.440	0.156
79	f/h	17.834	0.232	593.015	0.646	0.122
80	h	26.327	0.968	288.489	0.261	0.325
81	h	20.288	0.776	322.967	0.341	0.100
82	h	“invalid”	“invalid”	“invalid”	0.435	0.092
83	h/u	38.931	1.593	224.423	0.605	0.055
84	f/h	32.536	1.058	276.003	0.324	0.074
85	h	18.574	0.854	307.368	0.332	0.145
86	h	28.395	1.157	263.738	0.710	0.103
87	f/h	97.087	10.809	83.88	0.501	0.033
88	h/u	57.243	2.517	177.726	0.304	0.037

Indent	Type*	Modulus (GPa)	Hardness (GPa)	Maximum Displacement (nm)	Si/Ca Ratio	Al/Ca Ratio
89	h	27.698	0.784	321.196	0.487	0.087
90	h	22.662	0.749	328.497	0.276	0.161
91	h	“invalid”	“invalid”	“invalid”	0.671	0.176
92	f	“invalid”	“invalid”	“invalid”	0.747	0.328
93	u	58.053	2.684	172.023	0.432	0.103
94	h	29.385	1.482	232.636	0.298	0.114
95	u	68.884	4.792	127.825	0.493	0.078
96	f/h	85.554	7.115	104.209	0.460	0.100
97	f/h	43.992	1.687	217.837	0.336	0.082
98	f/h	error	error	error	0.308	0.247
99	f/h	24.798	1.516	229.797	0.659	0.309
100	h	“invalid”	“invalid”	“invalid”	0.407	0.090
101	f/h	“invalid”	“invalid”	“invalid”	0.461	0.081
102	h	17.037	0.590	370.73	0.645	0.097
103	f/h/u	66.771	1.852	207.671	0.269	0.176
104	h/u	61.076	1.804	210.42	0.307	0.078
105	h	36.565	1.240	254.432	0.421	0.187
106	h	20.997	0.761	326.173	0.820	0.150
107	h	62.715	2.107	194.571	0.498	0.060
108	h	24.149	0.602	367.233	0.521	0.082
109	h	52.162	5.033	124.625	0.145	0.084
110	h	24.653	1.055	276.356	0.312	0.368
111	h	103.434	8.090	97.469	0.619	0.086
112	h	106.100	5.937	114.414	0.563	0.120
113	f/h	“invalid”	“invalid”	“invalid”	0.479	0.142
114	f/h	10.908	0.242	580.386	0.490	0.125
115	f/h/u	21.947	1.818	209.676	0.493	0.188
116	f/h	16.720	0.611	363.817	0.364	0.328
117	h	23.104	1.075	273.564	0.431	0.115
118	h/u	21.165	0.724	334.453	0.290	0.135
119	h	15.241	0.954	290.796	0.111	0.075
120	f/h	“invalid”	“invalid”	“invalid”	0.223	0.085
121	f/h	17.296	0.456	422.335	0.118	0.438
122	h/u	23.718	1.427	237.121	0.587	0.113
123	f/h	59.096	4.983	125.23	0.508	0.086
124	f/h	25.725	0.986	286.139	0.641	0.098
125	f/h	25.690	1.384	240.751	0.379	0.088
126	f/h	19.412	0.553	382.986	0.511	0.195
127	h	21.900	0.794	319.081	0.389	0.149
128	f/h	17.550	0.538	388.409	0.547	0.072

Indent	Type*	Modulus (GPa)	Hardness (GPa)	Maximum Displacement (nm)	Si/Ca Ratio	Al/Ca Ratio
129	h	"invalid"	"invalid"	"invalid"	0.225	0.071
130	f/h	"invalid"	"invalid"	"invalid"	0.473	0.079
131	h	32.142	1.695	217.095	0.494	0.094
132	h/u	32.827	1.449	235.108	0.606	0.081
133	h	23.196	1.053	276.565	0.573	0.066
134	f/h	20.645	0.667	348.319	0.556	0.056
135	f/h	20.740	0.867	305.243	0.403	0.048
136	f/h	26.107	1.127	267.256	0.402	0.045
137	f/h	17.776	0.701	339.874	0.552	0.052
138	h	32.476	1.394	240.017	0.295	0.213
139	f/h	10.869	0.624	359.993	0.427	0.098
140	f/h	"invalid"	"invalid"	"invalid"	0.344	0.116
141	h/u	"invalid"	"invalid"	"invalid"	0.355	0.147
142	f/h	19.736	0.511	398.763	0.455	0.153
143	h	22.732	0.791	319.707	0.572	0.080
144	h	165.838	14.771	71.207	0.244	0.372
145	h	27.407	0.790	319.965	0.496	0.161
146	h/u	24.023	0.702	339.414	0.406	0.092
147	f/h	22.787	0.988	285.477	0.631	0.079
148	h	"invalid"	"invalid"	"invalid"	0.609	0.070
149	f/h	13.412	0.390	456.645	0.564	0.161
150	h	"invalid"	"invalid"	"invalid"	0.604	0.124
151	f/h	15.446	0.298	523.842	0.643	0.076
152	f/h	29.324	1.311	247.576	0.517	0.103
153	h	25.190	0.919	296.341	0.421	0.162
154	f/h	30.073	0.971	288.397	0.612	0.064
155	f/h	33.014	2.111	194.26	0.420	0.059
156	u	85.998	2.771	169.16	0.403	0.042
157	h/u	33.816	1.339	244.824	0.390	0.110
158	f	15.191	0.315	508.763	0.400	0.110
159	h	15.939	0.717	335.823	0.297	0.213
160	f/h	error	error	error	0.321	0.252
161	f/h	37.278	2.873	165.995	0.453	0.082
162	h/u	22.764	0.856	307.288	0.644	0.089
163	h	40.472	0.940	293.017	0.491	0.142
164	f/h	65.397	1.375	241.661	0.314	0.067
165	f/h	"invalid"	"invalid"	"invalid"	0.294	0.083
166	f/h	25.079	1.025	280.422	0.492	0.102
167	h	19.175	0.606	365.73	0.400	0.273
168	f/h	"invalid"	"invalid"	"invalid"	0.547	0.084

Indent	Type*	Modulus (GPa)	Hardness (GPa)	Maximum Displacement (nm)	Si/Ca Ratio	Al/Ca Ratio
169	f/h	30.223	1.626	222.125	0.471	0.139
170	f/h	23.352	0.472	414.809	0.254	0.320
171	h	17.735	0.373	467.36	0.503	0.102
172	f/h	13.450	0.325	501.011	0.528	0.050
173	h	23.078	0.714	336.537	0.149	0.652
174	f/h/u	29.758	1.180	261.238	0.567	0.066
175	f/h/u	54.038	3.374	152.925	0.400	0.060
176	u	76.016	2.159	192.123	0.630	0.092
177	f/h	19.716	0.519	395.321	0.513	0.112
178	h	23.873	0.854	307.539	0.311	0.154
179	h	14.336	0.801	317.588	0.558	0.056
180	f/h	21.677	0.603	366.598	0.401	0.125
181	f/h	27.554	1.233	255.358	0.360	0.236
182	h	24.303	0.810	315.804	0.606	0.111
183	h/u	35.711	1.949	202.34	0.352	0.287
184	h/u	error	error	error	0.484	0.236
185	f	32.181	0.697	340.859	0.495	0.180
186	h/u	113.216	8.811	93.23	0.490	0.087
187	f/h	26.959	0.697	341.083	0.346	0.384
188	h	“invalid”	“invalid”	“invalid”	0.420	0.118
189	f/h	15.155	0.487	408.391	0.291	0.343
190	h	17.463	0.615	362.887	0.516	0.150
191	h	16.573	0.624	360.5	0.531	0.106
192	h	23.393	0.979	286.75	0.448	0.085
193	f/h	“invalid”	“invalid”	“invalid”	0.514	0.106
194	h/u	41.236	1.527	229.28	0.496	0.086
195	h/u	116.114	3.700	145.966	0.440	0.078
196	f/h	29.204	0.812	315.326	0.526	0.116
197	h	23.136	0.830	312.172	0.438	0.181
198	h	23.972	1.047	277.424	0.532	0.122
199	h/u	31.521	0.928	294.975	0.603	0.089
200	h/u	75.794	2.307	185.853	0.629	0.125

*Type: f=flaw, h=hydrate, u=unhydrated particle, f/h=flaw and hydrate combination, f/u=flaw and unhydrated particle combination, f/h/u=flaw, hydrate, and unhydrated particle combination, and h/u=hydrate and unhydrated particle combination.

PC-CF-B Grid 1

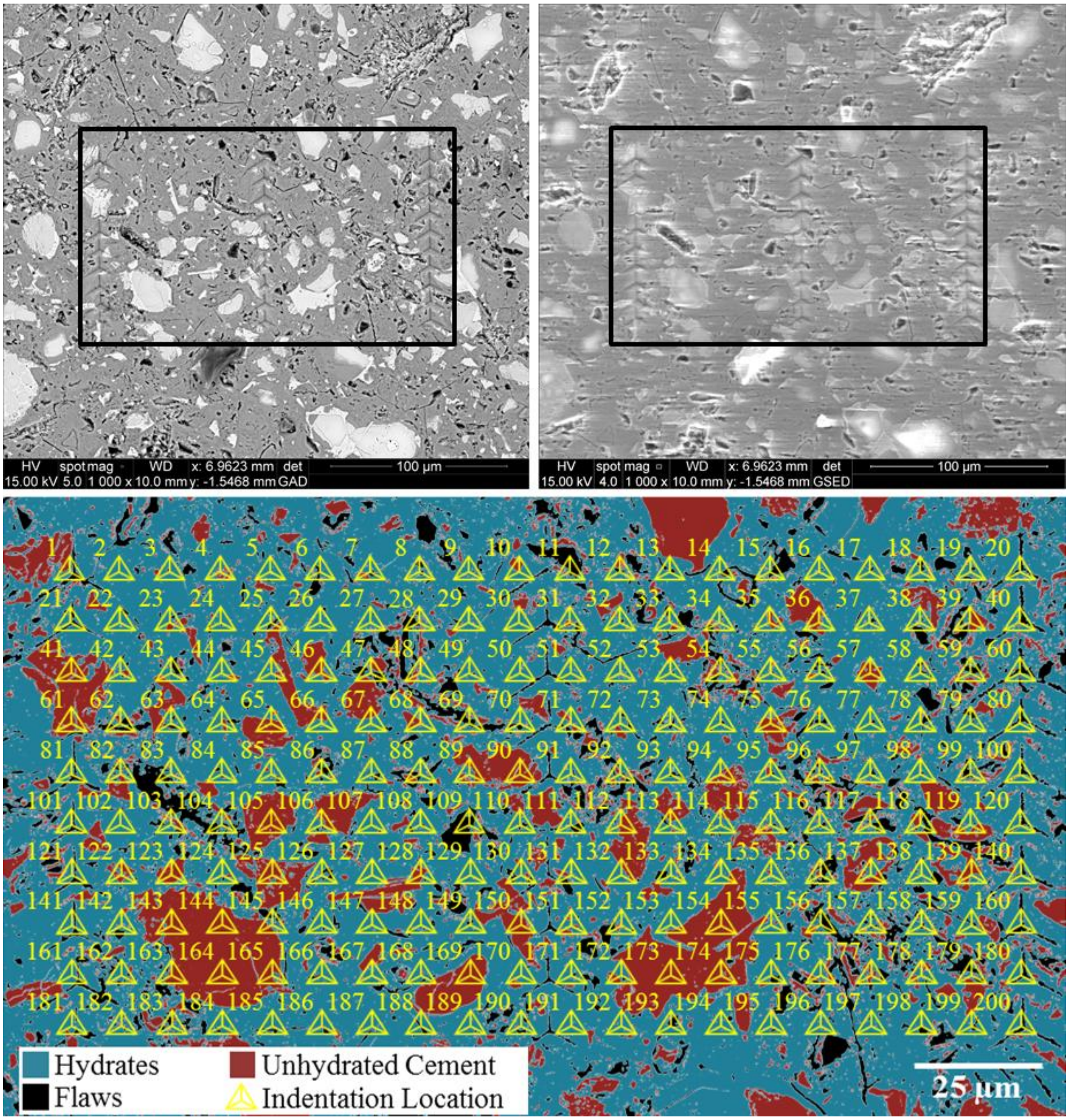

Indent	Type*	Modulus (GPa)	Hardness (GPa)	Maximum Displacement (nm)	Si/Ca Ratio	Al/Ca Ratio
1	f/h	16.752	0.441	429.461	0.524	0.100
2	u	56.280	3.331	154.098	0.175	0.509
3	h	24.943	0.790	320.272	0.603	0.150
4	h/u	16.717	0.569	377.47	0.344	0.331
5	f/h	16.918	0.491	407.379	0.612	0.107
6	u	91.864	10.448	85.351	0.297	0.326
7	u	35.334	2.207	189.942	0.441	0.110
8	h	24.429	0.855	307.431	0.361	0.126

Indent	Type*	Modulus (GPa)	Hardness (GPa)	Maximum Displacement (nm)	Si/Ca Ratio	Al/Ca Ratio
9	f/h	22.761	0.589	371.352	0.417	0.292
10	h	21.945	0.878	303.2	0.567	0.127
11	f/h	26.830	0.607	365.577	0.593	0.103
12	h	26.848	0.621	361.766	0.486	0.071
13	f/h	17.808	0.496	405.072	0.277	0.411
14	h	19.010	0.609	364.705	0.438	0.202
15	h	25.590	0.726	334.135	0.530	0.089
16	h/u	195.364	16.531	67.195	0.293	0.356
17	h/u	21.846	0.866	305.348	0.563	0.121
18	h	31.296	0.832	311.712	0.553	0.085
19	h	“invalid”	“invalid”	“invalid”	0.571	0.195
20	f/h	14.377	0.328	498.587	0.449	0.129
21	h	19.156	0.726	334.057	0.505	0.161
22	h	“invalid”	“invalid”	“invalid”	0.448	0.168
23	h	12.670	0.387	458.725	0.594	0.603
24	h/u	18.377	0.449	425.507	0.498	0.160
25	h/u	“invalid”	“invalid”	“invalid”	0.564	0.122
26	f/h	22.207	0.549	384.473	0.378	0.102
27	f/h	“invalid”	“invalid”	“invalid”	0.446	0.172
28	h/u	17.422	0.393	454.98	0.425	0.150
29	f/h	error	error	error	0.499	0.205
30	h/u	37.586	1.698	217.143	0.245	0.236
31	h	23.380	0.591	370.592	0.614	0.029
32	h	“invalid”	“invalid”	“invalid”	0.615	0.100
33	f/h	24.411	0.593	370.149	0.583	0.137
34	h	35.294	1.386	240.604	0.585	0.082
35	u	94.862	4.651	129.776	0.383	0.189
36	u	111.297	11.992	79.474	0.440	0.191
37	h	22.456	0.596	369.609	0.418	0.095
38	h	18.238	0.598	368.188	0.538	0.304
39	h	“invalid”	“invalid”	“invalid”	0.246	0.610
40	h	31.951	1.163	263.438	0.520	0.141
41	f/h	17.519	0.518	395.921	0.529	0.101
42	f/h	16.838	0.560	380.99	0.525	0.112
43	h	24.694	0.692	342.155	0.570	0.134
44	f/h	“invalid”	“invalid”	“invalid”	0.377	0.191
45	f/h	15.850	0.330	497.532	0.393	0.078
46	f/h	17.937	0.395	454.386	0.210	0.073
47	f	73.389	11.718	80.393	0.498	0.223
48	f/h	22.651	0.357	477.561	0.292	0.253

Indent	Type*	Modulus (GPa)	Hardness (GPa)	Maximum Displacement (nm)	Si/Ca Ratio	Al/Ca Ratio
49	f	“invalid”	“invalid”	“invalid”	0.439	0.092
50	f/h	18.613	0.463	419.281	0.493	0.078
51	h	28.488	0.965	289.351	0.441	0.155
52	f/h/u	“invalid”	“invalid”	“invalid”	0.446	0.113
53	h	36.312	1.099	270.793	0.617	0.074
54	f/h/u	38.816	1.561	226.581	0.216	0.304
55	u	90.746	5.334	120.87	0.138	0.579
56	h	32.506	1.115	268.875	0.572	0.132
57	h	26.920	0.716	336.864	0.580	0.097
58	h	13.289	0.506	400.737	0.423	0.608
59	f	error	error	error	0.251	0.776
60	f/h	15.144	0.546	385.713	0.330	0.266
61	h	24.784	0.740	331.307	0.595	0.098
62	h	18.189	0.437	431.521	0.538	0.142
63	f/h	18.753	0.442	429.28	0.145	0.082
64	f/h	19.724	0.425	437.487	0.508	0.233
65	f/h	18.745	0.357	477.527	0.103	0.187
66	f	19.198	0.606	366.124	0.575	0.241
67	f/h	22.317	3.218	156.784	0.450	0.098
68	h	35.797	4.425	133.074	0.542	0.113
69	u	44.414	1.654	219.952	0.587	0.118
70	h	87.024	2.843	166.911	0.482	0.066
71	h	“invalid”	“invalid”	“invalid”	0.184	0.445
72	h	21.981	0.440	430.673	0.522	0.058
73	f	19.946	0.518	396.208	0.459	0.044
74	u	23.984	0.350	483.023	0.406	0.033
75	h/u	94.887	4.112	138.262	0.156	0.593
76	f/h	19.289	0.465	418.277	0.403	0.116
77	f/h/u	“invalid”	“invalid”	“invalid”	0.448	0.144
78	f/h	20.040	0.126	813.867	0.550	0.236
79	f/h	error	error	error	0.339	0.150
80	h	21.184	0.487	409.042	0.417	0.350
81	f	18.938	0.485	409.737	0.606	0.098
82	f/h	22.781	0.677	345.858	0.591	0.170
83	h	46.459	3.264	155.529	0.161	0.096
84	u	19.272	0.681	345.029	0.482	0.146
85	h	“invalid”	“invalid”	“invalid”	0.164	0.097
86	h	22.720	0.805	316.828	0.362	0.140
87	h	127.530	10.860	83.667	0.294	0.123
88	u	143.865	11.645	80.713	0.538	0.086

Indent	Type*	Modulus (GPa)	Hardness (GPa)	Maximum Displacement (nm)	Si/Ca Ratio	Al/Ca Ratio
89	u	83.291	5.082	123.995	0.557	0.080
90	u	“invalid”	“invalid”	“invalid”	0.552	0.083
91	f/h	“invalid”	“invalid”	“invalid”	0.510	0.068
92	h/u	40.158	1.424	237.487	0.529	0.084
93	h/u	29.003	0.397	453.062	0.421	0.032
94	h/u	16.961	0.241	582.29	0.448	0.048
95	f/h	21.343	0.707	338.577	0.467	0.067
96	h	40.795	2.392	182.427	0.364	0.107
97	h	24.063	0.635	357.692	0.559	0.126
98	f/h	21.849	0.991	285.409	0.542	0.165
99	h	17.793	0.692	342.194	0.360	0.116
100	f/h	“invalid”	“invalid”	“invalid”	0.370	0.270
101	h/u	23.126	0.572	377.19	0.620	0.096
102	u	88.213	4.172	137.295	0.592	0.130
103	f/h	96.881	4.729	128.647	0.308	0.246
104	f/h	35.361	0.630	359.239	0.489	0.142
105	f/h	30.561	0.678	345.972	0.369	0.207
106	h	26.133	0.495	405.388	0.279	0.081
107	h	22.909	0.664	349.546	0.238	0.146
108	h	27.369	0.761	326.075	0.485	0.162
109	h	34.148	1.146	265.086	0.417	0.085
110	h	36.203	1.019	281.41	0.571	0.064
111	h	17.392	0.354	479.974	0.584	0.064
112	f	15.195	0.495	405.6	0.571	0.071
113	h	19.492	0.394	454.633	0.422	0.039
114	h/u	35.155	1.663	219.359	0.560	0.065
115	f/h	56.269	3.006	162.334	0.523	0.102
116	h	20.712	0.567	378.559	0.431	0.211
117	h	26.791	0.602	367.094	0.571	0.127
118	f/h	39.836	1.582	225.123	0.622	0.127
119	h	22.437	0.506	400.808	0.535	0.090
120	h	21.465	0.706	338.501	0.176	0.066
121	h	24.011	0.699	340.809	0.312	0.162
122	h	19.318	0.443	428.676	0.536	0.175
123	f/h	49.904	1.911	204.531	0.418	0.282
124	f/h	24.282	0.971	288.296	0.469	0.099
125	h	16.787	0.481	411.465	0.249	0.176
126	f/h	30.717	0.922	295.997	0.043	0.017
127	h	“invalid”	“invalid”	“invalid”	0.204	0.098
128	f/h/u	34.158	0.947	292.17	0.595	0.128

Indent	Type*	Modulus (GPa)	Hardness (GPa)	Maximum Displacement (nm)	Si/Ca Ratio	Al/Ca Ratio
129	f/h	18.927	0.557	381.983	0.550	0.064
130	h	45.800	1.200	258.896	0.484	0.063
131	h/u	19.303	0.379	463.902	0.509	0.057
132	f/h	12.920	0.244	579.291	0.430	0.048
133	h	21.383	0.572	377.001	0.451	0.040
134	h	48.232	2.603	174.672	0.604	0.077
135	u	55.322	2.771	169.235	0.570	0.110
136	h/u	21.359	0.766	324.798	0.638	0.107
137	h	21.532	0.329	497.581	0.599	0.157
138	f/h/u	26.819	1.326	246.032	0.549	0.041
139	h/u	36.700	1.944	202.742	0.598	0.084
140	h/u	18.083	0.814	315.42	0.437	0.125
141	h	19.270	0.509	399.439	0.455	0.139
142	h/u	12.420	0.331	496.153	0.581	0.091
143	f/h	46.172	3.253	155.77	0.187	0.122
144	f/h	23.281	0.829	312.402	0.427	0.118
145	f/h	24.804	0.768	324.776	0.464	0.114
146	h	“invalid”	“invalid”	“invalid”	0.491	0.114
147	h	25.080	1.089	271.92	0.623	0.128
148	f	41.053	1.948	202.431	0.575	0.083
149	f/h	error	error	error	0.384	0.056
150	h	20.840	0.746	329.398	0.326	0.243
151	h	14.247	0.380	462.962	0.364	0.242
152	f/h	25.045	0.865	305.762	0.464	0.049
153	f/h	21.285	0.570	377.523	0.405	0.034
154	h/u	“invalid”	“invalid”	“invalid”	0.469	0.101
155	h	37.954	1.851	207.852	0.605	0.091
156	u	97.315	10.986	83.166	0.569	0.085
157	h	82.270	7.727	99.833	0.416	0.256
158	f/h	21.187	0.739	331.361	0.482	0.077
159	h/u	29.749	0.822	313.521	0.391	0.058
160	h/u	30.381	2.775	169.094	0.408	0.039
161	h	24.297	0.644	355.078	0.630	0.107
162	f/h	37.148	0.665	348.903	0.375	0.126
163	f/h	27.044	1.270	251.588	0.475	0.162
164	h/u	22.431	0.959	289.996	0.397	0.161
165	h	23.585	0.930	294.786	1.295	0.152
166	h	19.466	0.679	345.566	0.514	0.068
167	h	9.653	0.408	446.156	0.559	0.074
168	h/u	error	error	error	0.454	0.189

Indent	Type*	Modulus (GPa)	Hardness (GPa)	Maximum Displacement (nm)	Si/Ca Ratio	Al/Ca Ratio
169	f	14.426	5.111	123.596	0.625	0.078
170	f	15.998	0.591	370.604	0.346	0.089
171	h	19.472	0.807	316.639	0.539	0.088
172	h	20.416	0.525	393.535	0.569	0.082
173	f	25.399	0.995	284.958	0.387	0.116
174	f/h	14.381	0.581	373.463	0.536	0.103
175	f/h	21.688	0.685	344.273	0.374	0.165
176	f/h	19.859	0.537	389	0.670	0.289
177	f/h	27.583	0.775	323.402	0.629	0.101
178	h	29.753	0.984	286.341	0.601	0.126
179	f/h	32.809	0.836	310.915	0.377	0.058
180	h/u	48.927	2.191	190.694	0.034	0.036
181	f/h	"invalid"	"invalid"	"invalid"	0.447	0.171
182	f/h	18.704	0.450	425.461	0.542	0.188
183	f/h	19.659	0.628	359.628	0.725	0.252
184	f/h	18.306	0.593	369.637	0.570	0.117
185	f/h	26.826	0.946	292.244	0.359	0.213
186	f/h	21.203	0.562	380.569	0.266	0.044
187	f/h	12.889	0.415	442.825	0.031	0.044
188	f/h	15.159	0.608	365.657	0.771	0.053
189	f/h	10.891	0.291	529.261	0.609	0.091
190	h	30.849	2.461	179.867	0.497	0.070
191	h	14.478	0.461	420.049	0.472	0.210
192	h	24.044	0.958	290.233	0.602	0.085
193	h	20.920	0.554	382.972	0.347	0.065
194	h/u	24.691	0.828	312.421	0.447	0.074
195	h/u	51.120	8.489	95.138	0.542	0.128
196	f/h	17.780	0.497	404.473	0.468	0.159
197	f/h	12.991	0.323	502.174	0.529	0.094
198	f/h	24.664	0.713	337.055	0.367	0.158
199	h	18.806	0.479	412.204	0.451	0.284
200	h/u	30.741	0.904	298.946	0.556	0.079

*Type: f=flaw, h=hydrate, u=unhydrated particle, f/h=flaw and hydrate combination, f/u=flaw and unhydrated particle combination, f/h/u=flaw, hydrate, and unhydrated particle combination, and h/u=hydrate and unhydrated particle combination.

PC-CNF-CF-A Grid 1

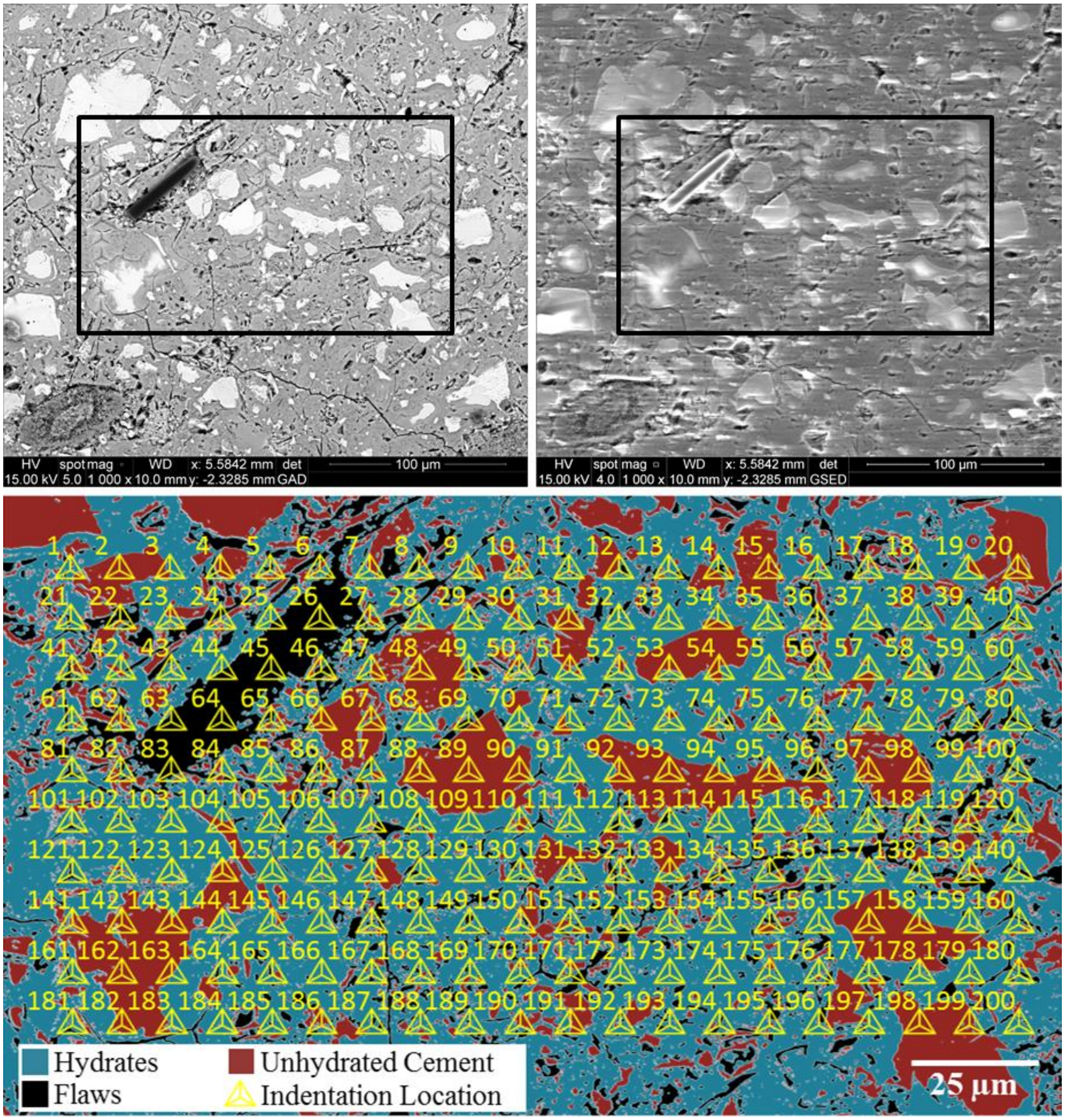

Indent	Type*	Modulus (GPa)	Hardness (GPa)	Maximum Displacement (nm)	Si/Ca Ratio	Al/Ca Ratio
1	h	52.474	1.983	200.892	0.439	0.064
2	u	“invalid”	“invalid”	“invalid”	0.182	0.497
3	h	89.986	4.871	126.921	0.399	0.043
4	u	42.303	2.810	168.2	0.494	0.078
5	f/h	1.547	0.618	362.593	0.558	0.067
6	h/u	0.980	0.337	492.435	0.139	0.034
7	h/u	1.166	0.432	434.306	0.544	0.112
8	f/h	17.899	0.372	468.052	0.416	0.140

Indent	Type*	Modulus (GPa)	Hardness (GPa)	Maximum Displacement (nm)	Si/Ca Ratio	Al/Ca Ratio
9	h	20.206	0.879	303.454	0.492	0.228
10	h/u	26.211	0.821	314.108	0.563	0.072
11	h/u	18.377	0.351	482.416	0.353	0.045
12	h/u	“invalid”	“invalid”	“invalid”	0.182	0.496
13	f/h	25.889	0.895	300.502	0.583	0.068
14	f/h	“invalid”	“invalid”	“invalid”	0.499	0.072
15	u	89.960	4.585	130.903	0.559	0.046
16	f/h	39.016	0.951	291.59	0.388	0.160
17	h/u	18.485	0.396	453.566	0.564	0.113
18	f/h	20.691	0.462	419.561	0.481	0.073
19	h/u	32.825	1.454	235.257	0.482	0.107
20	u	107.149	8.993	92.583	0.403	0.036
21	f/h	15.407	0.381	462.314	0.267	0.063
22	f/h/u	106.179	10.219	86.534	0.134	0.508
23	f/h	25.756	0.966	288.99	0.489	0.082
24	h/u	28.662	6.718	107.637	0.504	0.085
25	h	error	error	error	0.467	0.103
26	f	error	error	error	0.467	0.111
27	h/u	3.201	0.802	317.785	0.263	0.122
28	f/h	“invalid”	“invalid”	“invalid”	0.314	0.309
29	f/h	40.693	1.205	258.711	0.126	0.059
30	u	41.850	3.815	143.769	0.457	0.064
31	u	81.933	7.265	103.377	0.587	0.067
32	h	19.274	0.554	382.89	0.254	0.170
33	h	23.161	0.583	373.325	0.451	0.097
34	h/u	28.731	1.188	260.356	0.405	0.085
35	h	“invalid”	“invalid”	“invalid”	0.532	0.048
36	h/u	12.220	0.228	598.842	0.564	0.068
37	h	21.075	0.829	312.386	0.161	0.473
38	h	“invalid”	“invalid”	“invalid”	0.317	0.162
39	h	18.637	0.635	357.363	0.629	0.102
40	h	25.324	0.851	308.316	0.390	0.037
41	f/h	“invalid”	“invalid”	“invalid”	0.614	0.085
42	h/u	“invalid”	“invalid”	“invalid”	0.069	0.043
43	h/u	31.002	6.695	107.755	0.384	0.110
44	f/h	error	error	error	0.094	0.025
45	f	error	error	error	0.586	0.097
46	f	13.807	4.495	132.218	0.574	0.193
47	f/h/u	22.311	1.255	253.259	0.181	0.089
48	u	84.426	5.758	116.485	0.189	0.048

Indent	Type*	Modulus (GPa)	Hardness (GPa)	Maximum Displacement (nm)	Si/Ca Ratio	Al/Ca Ratio
49	h	55.938	3.419	152.184	0.585	0.126
50	h/u	26.918	0.509	399.764	0.350	0.059
51	h/u	“invalid”	“invalid”	“invalid”	0.525	0.094
52	h/u	19.400	0.755	327.894	0.569	0.108
53	h/u	98.338	8.113	97.608	0.309	0.259
54	u	92.088	5.969	114.393	0.610	0.066
55	h	24.996	0.749	329.017	0.493	0.099
56	h	20.155	0.560	380.873	0.425	0.110
57	h	22.221	0.829	312.521	0.518	0.159
58	h	17.527	0.604	366.669	0.253	0.372
59	h	23.142	0.754	327.97	0.419	0.163
60	h	21.814	0.754	327.792	0.610	0.091
61	h	41.090	1.217	257.364	0.604	0.090
62	u	29.991	7.300	103.07	0.202	0.256
63	f	31.917	6.663	108.072	0.515	0.123
64	f	36.889	7.994	98.349	0.545	0.115
65	f/h	37.014	8.336	96.267	0.513	0.179
66	h	76.033	6.175	112.343	0.468	0.217
67	h/u	68.123	3.357	153.619	0.077	0.035
68	h	29.193	1.472	233.698	0.576	0.053
69	f	112.548	10.082	87.171	0.530	0.045
70	h	386.517	28.852	50.204	0.591	0.103
71	f/h	67.899	9.785	88.531	0.340	0.267
72	h	30.727	1.049	277.438	0.515	0.180
73	h	27.384	0.804	317.421	0.561	0.073
74	h/u	26.510	0.959	290.265	0.374	0.031
75	h/u	24.063	1.147	265.009	0.372	0.032
76	f/h/u	23.787	0.474	414.666	0.556	0.077
77	h	24.513	0.704	339.241	0.589	0.081
78	h	25.110	0.786	321.128	0.598	0.091
79	h	19.981	0.470	416.067	0.481	0.091
80	f/h	19.923	0.358	477.502	0.485	0.165
81	f/h	10.860	0.237	587.185	0.277	0.272
82	h/u	41.152	6.315	111.071	0.321	0.070
83	f	error	error	error	0.382	0.223
84	h/u	43.511	12.618	77.586	0.338	0.121
85	h	27.999	0.840	310.517	0.186	0.044
86	f/h	17.357	0.239	585.217	0.391	0.060
87	h/u	“invalid”	“invalid”	“invalid”	0.584	0.010
88	u	143.881	10.452	85.58	0.532	0.083

Indent	Type*	Modulus (GPa)	Hardness (GPa)	Maximum Displacement (nm)	Si/Ca Ratio	Al/Ca Ratio
89	u	153.982	12.357	78.483	0.475	0.148
90	u	142.139	10.071	87.286	0.137	0.562
91	h	25.602	1.074	274.112	0.532	0.089
92	u	45.374	2.446	180.556	0.547	0.119
93	u	148.198	12.291	78.651	0.512	0.074
94	u	95.356	8.387	96.037	0.537	0.145
95	u	“invalid”	“invalid”	“invalid”	0.449	0.174
96	f	“invalid”	“invalid”	“invalid”	0.641	0.082
97	u	95.888	8.293	96.529	0.219	0.361
98	u	90.517	7.081	104.734	0.553	0.142
99	h	18.742	0.516	397.044	0.561	0.106
100	f/h	“invalid”	“invalid”	“invalid”	0.419	0.174
101	h	33.157	1.048	277.667	0.559	0.151
102	h	29.067	0.697	341.249	0.471	0.126
103	h	36.569	8.576	94.791	0.162	0.036
104	h/u	112.474	8.791	93.617	0.253	0.072
105	h	35.049	1.048	277.469	0.575	0.093
106	h	28.654	0.774	323.265	0.568	0.076
107	h/u	21.605	0.747	329.477	0.484	0.067
108	h	“invalid”	“invalid”	“invalid”	0.511	0.075
109	h	400.261	35.114	45.191	0.093	0.495
110	u	25.417	1.626	222.107	0.110	0.479
111	h	29.946	0.728	333.983	0.406	0.170
112	f/h	“invalid”	“invalid”	“invalid”	0.453	0.060
113	f/h	164.527	13.313	75.447	0.373	0.056
114	h	“invalid”	“invalid”	“invalid”	0.379	0.070
115	h	26.836	0.808	316.816	0.384	0.238
116	f/h	67.267	8.513	95.213	0.484	0.171
117	h	13.459	0.370	469.018	0.359	0.091
118	f/h	“invalid”	“invalid”	“invalid”	0.511	0.169
119	h/u	15.402	0.246	576.882	0.449	0.290
120	f/h	16.317	0.226	601.688	0.338	0.280
121	h	34.615	1.033	279.781	0.536	0.065
122	f/h	45.150	1.324	246.575	0.543	0.065
123	h	39.521	1.050	277.2	0.516	0.060
124	u	113.849	4.484	132.393	0.508	0.050
125	h	54.959	1.410	238.857	0.505	0.217
126	h	27.789	0.668	348.258	0.452	0.063
127	f/h	90.390	5.924	114.862	0.605	0.074
128	f/h	13.368	0.255	567.075	0.321	0.099

Indent	Type*	Modulus (GPa)	Hardness (GPa)	Maximum Displacement (nm)	Si/Ca Ratio	Al/Ca Ratio
129	h	30.649	1.197	259.651	0.488	0.077
130	h	26.828	0.893	300.948	0.545	0.072
131	f/h	192.320	22.554	57.22	0.403	0.238
132	h/u	"invalid"	"invalid"	"invalid"	0.433	0.053
133	h/u	52.565	4.182	137.402	0.343	0.141
134	f/h	20.912	0.677	346.131	0.528	0.085
135	f/h	"invalid"	"invalid"	"invalid"	0.541	0.074
136	h	"invalid"	"invalid"	"invalid"	0.503	0.105
137	h	16.468	0.465	418.676	0.502	0.207
138	f/h	22.100	0.694	341.923	0.395	0.192
139	h/u	13.189	0.270	550.246	0.541	0.123
140	f/h	14.081	0.394	455.108	0.372	0.161
141	u	44.285	2.646	173.459	0.536	0.058
142	u	234.388	13.219	75.749	0.473	0.048
143	u	111.153	8.416	95.728	0.411	0.049
144	h	48.173	1.345	244.586	0.470	0.038
145	h	41.997	1.085	272.813	0.400	0.024
146	h	29.516	1.231	255.681	0.465	0.041
147	f/h	"invalid"	"invalid"	"invalid"	0.523	0.067
148	h	19.212	0.700	340.386	0.513	0.079
149	f/h	15.535	0.401	450.489	0.566	0.068
150	h/u	27.121	1.066	275.161	0.472	0.125
151	f/h/u	66.978	8.696	94.152	0.319	0.225
152	h	11.562	0.221	609.148	0.495	0.090
153	h/u	23.161	0.705	339.256	0.490	0.141
154	h	14.953	0.470	416.196	0.106	0.041
155	f/h/u	21.767	0.898	299.979	0.239	0.055
156	h	23.171	0.823	313.76	0.395	0.175
157	u	99.206	9.289	90.982	0.461	0.200
158	u	93.941	9.617	89.399	0.441	0.073
159	h	22.823	0.612	364.54	0.289	0.066
160	h	22.458	0.641	355.877	0.067	0.019
161	h	39.587	1.183	261.047	0.532	0.073
162	u	126.260	8.754	93.785	0.205	0.425
163	h/u	71.956	1.768	213.019	0.404	0.025
164	h	"invalid"	"invalid"	"invalid"	0.447	0.046
165	f/h	"invalid"	"invalid"	"invalid"	0.530	0.071
166	h	25.641	0.962	289.833	0.408	0.198
167	f/h	17.276	0.491	407.277	0.457	0.070
168	f/h/u	17.079	0.406	448.095	0.417	0.150

Indent	Type*	Modulus (GPa)	Hardness (GPa)	Maximum Displacement (nm)	Si/Ca Ratio	Al/Ca Ratio
169	h	11.577	0.315	509.146	0.420	0.203
170	h	10.534	0.287	533.676	0.366	0.133
171	f/h	33.769	1.160	263.739	0.121	0.050
172	h	18.937	0.611	364.491	0.429	0.125
173	h	29.116	1.097	271.292	0.467	0.076
174	h	20.942	0.833	311.904	0.541	0.086
175	h	"invalid"	"invalid"	"invalid"	0.502	0.107
176	h/u	25.109	0.804	317.386	0.474	0.195
177	h	"invalid"	"invalid"	"invalid"	0.525	0.067
178	h	54.149	1.886	206.099	0.380	0.039
179	h	36.578	1.380	241.557	0.379	0.038
180	h	27.066	0.801	318.126	0.475	0.120
181	h	40.188	1.242	254.603	0.521	0.055
182	u	109.880	6.872	106.334	0.483	0.039
183	h	56.569	1.340	245.084	0.397	0.025
184	h	23.236	0.751	328.571	0.463	0.060
185	f/h	24.256	1.026	280.453	0.492	0.071
186	u	48.699	4.967	125.668	0.502	0.150
187	f/h	84.016	11.172	82.667	0.492	0.120
188	h	19.292	0.320	505.531	0.474	0.125
189	f/h	15.133	0.367	471.442	0.348	0.209
190	h/u	"invalid"	"invalid"	"invalid"	0.373	0.210
191	h/u	64.116	3.120	159.386	0.335	0.185
192	h	20.904	0.605	366.295	0.553	0.130
193	h	20.532	0.449	426.299	0.120	0.568
194	f/h	18.323	0.457	422.205	0.480	0.120
195	h/u	22.304	0.429	435.851	0.425	0.202
196	h/u	35.595	0.706	339.129	0.434	0.112
197	h	37.804	1.394	240.366	0.130	0.505
198	u	115.929	10.474	85.492	0.152	0.510
199	u	88.898	7.111	104.503	0.598	0.033
200	h	33.008	2.352	184.245	0.540	0.102

*Type: f=flaw, h=hydrate, u=unhydrated particle, f/h=flaw and hydrate combination, f/u=flaw and unhydrated particle combination, f/h/u=flaw, hydrate, and unhydrated particle combination, and h/u=hydrate and unhydrated particle combination.

PC-CNF-CF-A Grid 2

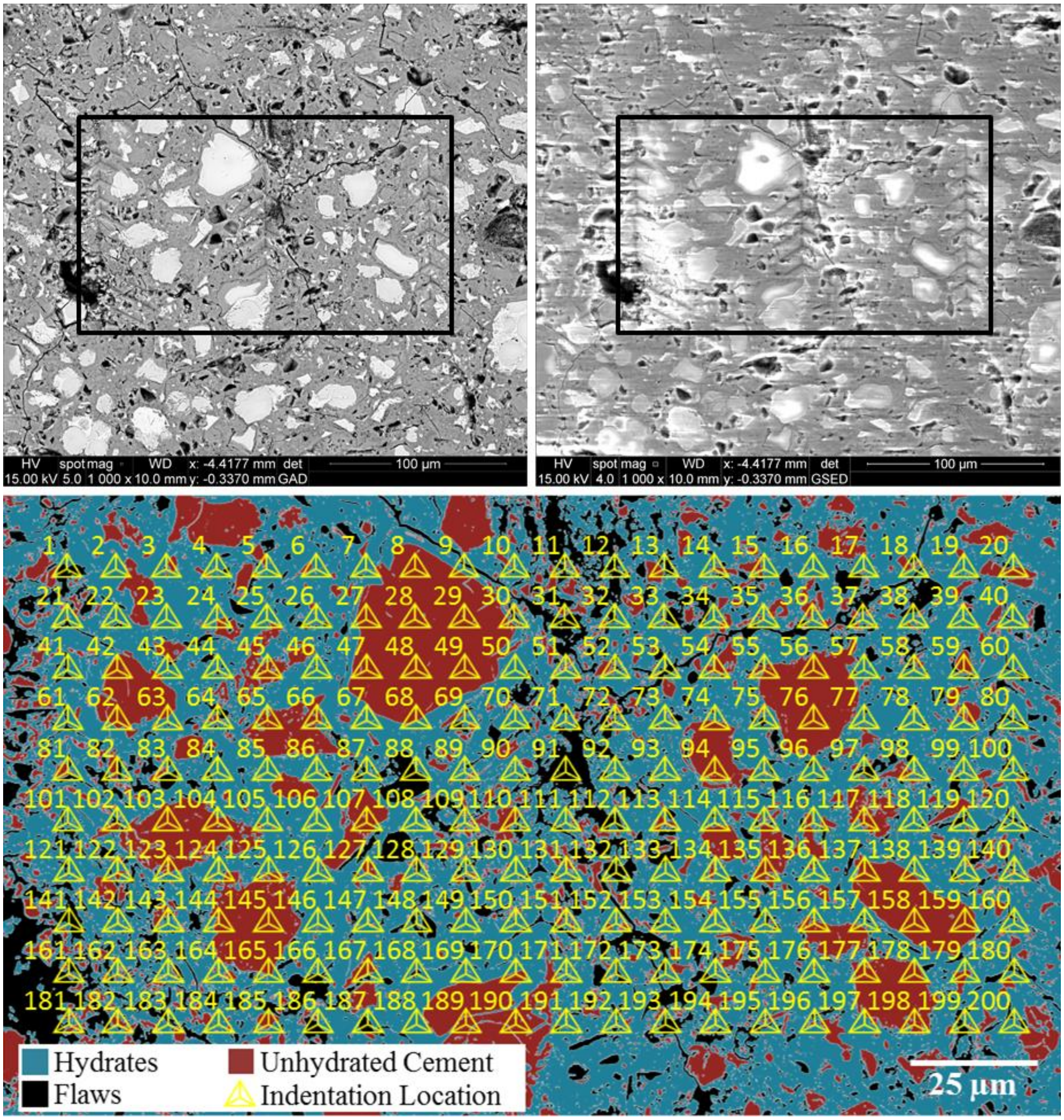

Indent	Type*	Modulus (GPa)	Hardness (GPa)	Maximum Displacement (nm)	Si/Ca Ratio	Al/Ca Ratio
1	f	“invalid”	“invalid”	“invalid”	0.079	0.047
2	h	error	error	error	0.370	0.185
3	f/h	34.291	1.136	266.421	0.518	0.074
4	f/h	15.340	0.448	426.364	0.555	0.082
5	h	23.437	0.779	322.512	0.489	0.140
6	h	27.044	0.838	310.73	0.509	0.111
7	h	27.347	0.623	360.897	0.515	0.073
8	u	105.623	9.985	87.673	0.396	0.031

Indent	Type*	Modulus (GPa)	Hardness (GPa)	Maximum Displacement (nm)	Si/Ca Ratio	Al/Ca Ratio
9	h	52.242	1.685	218.22	0.394	0.031
10	f/h	17.870	0.475	414.059	0.518	0.111
11	f/h	22.179	0.698	340.959	0.116	0.052
12	f	error	error	error	0.189	0.044
13	f/h	11.248	0.861	306.764	0.486	0.223
14	h/u	28.551	0.798	318.791	0.534	0.096
15	h	41.582	1.904	205.195	0.323	0.276
16	h	21.466	0.714	337.121	0.419	0.236
17	h	30.346	0.909	298.415	0.228	0.035
18	h/u	23.802	1.940	203.212	0.378	0.093
19	h	50.113	2.716	171.199	0.427	0.169
20	h/u	“invalid”	“invalid”	“invalid”	0.307	0.192
21	f/h	8.062	0.180	674.967	0.572	0.085
22	h	24.101	0.620	362.317	0.477	0.095
23	h	31.084	1.167	263.055	0.422	0.230
24	h/u	error	error	error	0.359	0.110
25	h	32.630	1.237	255.336	0.469	0.128
26	h	14.720	0.509	399.865	0.506	0.155
27	u	113.806	10.945	83.618	0.382	0.029
28	u	114.493	7.493	101.802	0.400	0.038
29	u	137.096	10.638	84.812	0.410	0.034
30	f/h	error	error	error	0.560	0.068
31	f	13.611	0.406	448.582	0.133	0.140
32	f	6.265	0.195	647.587	0.485	0.264
33	f/h	9.183	0.245	577.495	0.516	0.155
34	h	67.761	3.152	158.676	0.330	0.156
35	h/u	15.315	0.455	422.708	0.334	0.102
36	f/h	“invalid”	“invalid”	“invalid”	0.571	0.085
37	h	“invalid”	“invalid”	“invalid”	0.538	0.128
38	h	29.659	0.838	310.965	0.380	0.138
39	h	18.250	0.763	326.006	0.534	0.117
40	h	20.884	0.445	427.69	0.552	0.150
41	f/h	16.741	0.634	357.805	0.529	0.076
42	u	102.608	8.758	93.802	0.370	0.062
43	h	26.698	0.991	285.528	0.400	0.037
44	f/h	16.831	0.520	395.405	0.238	0.361
45	u	60.898	7.069	104.772	0.454	0.159
46	h	24.521	0.784	321.455	0.466	0.075
47	u	85.007	7.366	102.622	0.382	0.027
48	u	116.090	9.796	88.492	0.407	0.038

Indent	Type*	Modulus (GPa)	Hardness (GPa)	Maximum Displacement (nm)	Si/Ca Ratio	Al/Ca Ratio
49	u	113.390	11.126	82.85	0.503	0.069
50	h	27.611	0.809	316.433	0.388	0.624
51	h/u	20.186	0.713	337.385	0.512	0.169
52	f/h	error	error	error	0.381	0.176
53	f/h	15.163	0.344	487.311	0.348	0.201
54	h/u	68.531	4.182	137.322	0.500	0.093
55	h/u	52.659	4.158	137.769	0.511	0.033
56	u	107.120	8.171	97.248	0.554	0.027
57	h	26.913	0.724	334.724	0.545	0.099
58	h	29.226	0.913	297.785	0.383	0.233
59	u	42.219	3.295	155.22	0.581	0.095
60	h	18.758	0.526	393.393	0.563	0.094
61	f/h	15.195	0.268	552.405	0.355	0.157
62	u	101.681	10.898	83.746	0.367	0.120
63	h	25.447	0.769	324.616	0.133	0.433
64	h/u	28.116	0.780	322.235	0.570	0.081
65	u	144.768	9.856	88.276	0.220	0.290
66	u	99.720	4.857	127.098	0.341	0.157
67	h	30.737	1.028	280.337	0.455	0.111
68	h/u	78.690	7.061	104.898	0.487	0.233
69	f/h	20.081	0.941	293.164	0.533	0.149
70	h	19.624	0.779	322.681	0.456	0.237
71	f/h	10.034	0.273	546.808	0.264	0.876
72	f/h	15.338	0.641	355.871	0.469	0.115
73	h	17.782	0.606	366.302	0.471	0.125
74	h/u	60.723	2.341	184.736	0.581	0.023
75	f	22.276	0.522	394.755	0.492	0.127
76	u	105.830	7.531	101.464	0.527	0.112
77	f/h	28.011	0.864	305.944	0.525	0.132
78	h	21.732	0.894	300.95	0.439	0.162
79	h/u	16.272	1.138	266.232	0.556	0.085
80	f/h	17.205	0.482	411.248	0.504	0.082
81	h/u	“invalid”	“invalid”	“invalid”	0.399	0.049
82	f/h/u	“invalid”	“invalid”	“invalid”	0.497	0.134
83	f/h/u	13.770	0.368	470.764	0.516	0.049
84	h	19.491	0.564	379.495	0.552	0.102
85	h	33.841	1.407	239.041	0.493	0.058
86	h	28.774	0.953	291.181	0.536	0.078
87	f/h	12.458	0.269	551.039	0.156	0.615
88	f/h	35.615	2.207	190.205	0.534	0.509

Indent	Type*	Modulus (GPa)	Hardness (GPa)	Maximum Displacement (nm)	Si/Ca Ratio	Al/Ca Ratio
89	h	16.527	0.588	372.013	0.370	0.236
90	h	13.904	0.358	477.877	0.360	0.268
91	f	13.222	0.584	373.125	0.244	0.134
92	h	error	error	error	0.592	0.364
93	h	24.561	0.694	342.076	0.162	0.433
94	u	error	error	error	0.301	0.312
95	h/u	23.012	0.781	322.143	0.590	0.068
96	h	31.053	0.743	330.301	0.425	0.142
97	f	“invalid”	“invalid”	“invalid”	0.506	0.366
98	f/h/u	26.160	0.922	296.624	0.406	0.193
99	h	18.683	0.593	370.079	0.488	0.090
100	h	20.425	0.945	292.45	0.498	0.129
101	f/h	9.333	0.217	614.02	0.340	0.096
102	f/h/u	57.754	4.969	125.685	0.339	0.121
103	u	99.277	7.127	104.333	0.462	0.211
104	u	77.420	4.771	128.351	0.564	0.058
105	h	30.485	0.915	297.591	0.509	0.120
106	h	20.286	0.638	357.265	0.284	0.300
107	u	error	error	error	0.604	0.151
108	h	17.321	1.023	280.911	0.441	0.211
109	h	12.859	0.481	411.352	0.597	0.120
110	h/u	error	error	error	0.712	0.135
111	h	“invalid”	“invalid”	“invalid”	0.591	0.166
112	f/h	20.429	0.459	422.166	0.196	0.036
113	h/u	47.747	4.986	125.449	0.416	0.208
114	f/h	55.356	2.091	195.631	0.413	0.132
115	h	19.934	0.617	362.747	0.156	0.512
116	h	“invalid”	“invalid”	“invalid”	0.478	0.151
117	u	error	error	error	0.393	0.035
118	h	24.153	0.798	318.666	0.427	0.186
119	f/h	63.993	4.953	125.845	0.555	0.116
120	f/h	18.901	0.828	312.836	0.354	0.189
121	h	18.973	0.740	330.842	0.354	0.132
122	h/u	error	error	error	0.364	0.136
123	h/u	45.108	3.137	159.085	0.347	0.289
124	h	“invalid”	“invalid”	“invalid”	0.571	0.012
125	h/u	81.126	5.985	114.167	0.571	0.026
126	h	23.553	0.932	294.382	0.519	0.052
127	h/u	80.939	9.639	89.234	0.533	0.101
128	f/h	32.164	0.927	295.409	0.394	0.372

Indent	Type*	Modulus (GPa)	Hardness (GPa)	Maximum Displacement (nm)	Si/Ca Ratio	Al/Ca Ratio
129	h/u	10.130	0.216	615.44	0.584	0.178
130	h	14.081	0.416	443.253	0.564	0.113
131	h	“invalid”	“invalid”	“invalid”	0.530	0.167
132	f	“invalid”	“invalid”	“invalid”	0.482	0.222
133	h	error	error	Error	0.553	0.074
134	f/h	67.751	3.315	154.652	0.564	0.110
135	u	88.388	6.700	107.679	0.387	0.093
136	h	“invalid”	“invalid”	“invalid”	0.561	0.079
137	u	96.471	9.101	91.997	0.421	0.040
138	h	35.302	0.786	321.114	0.393	0.037
139	h	19.224	0.477	413.293	0.533	0.086
140	h/u	“invalid”	“invalid”	“invalid”	0.506	0.067
141	f/h	“invalid”	“invalid”	“invalid”	0.294	0.082
142	f/h	“invalid”	“invalid”	“invalid”	0.448	0.212
143	f/h	34.425	5.165	123.142	0.529	0.074
144	u	109.533	8.011	98.215	0.518	0.101
145	u	119.044	8.231	96.883	0.267	0.117
146	h	25.378	0.838	310.904	0.337	0.256
147	f/h	21.735	0.672	347.372	0.384	0.079
148	f/h	17.639	0.338	492.163	0.540	0.064
149	h	19.950	0.630	359.128	0.443	0.051
150	f/h	14.724	0.392	456.566	0.435	0.161
151	f/h	23.817	0.653	352.86	0.574	0.205
152	h	17.078	0.661	350.24	0.574	0.108
153	h	17.136	0.599	368.124	0.485	0.170
154	h	33.915	0.693	342.315	0.218	0.445
155	f/h	21.063	0.594	370.075	0.446	0.160
156	u	“invalid”	“invalid”	“invalid”	0.494	0.080
157	h	28.666	0.754	327.861	0.558	0.029
158	u	“invalid”	“invalid”	“invalid”	0.519	0.106
159	u	103.915	8.134	97.455	0.156	0.073
160	h	“invalid”	“invalid”	“invalid”	0.360	0.170
161	f/h/u	“invalid”	“invalid”	“invalid”	0.390	0.206
162	h/u	error	error	error	0.387	0.165
163	h	11.199	0.587	371.753	0.405	0.105
164	f/h/u	“invalid”	“invalid”	“invalid”	0.478	0.178
165	h/u	31.320	1.946	202.889	0.570	0.125
166	f/h	12.088	0.243	579.937	0.488	0.160
167	h/u	error	error	error	0.556	0.082
168	f/h	“invalid”	“invalid”	“invalid”	0.391	0.082

Indent	Type*	Modulus (GPa)	Hardness (GPa)	Maximum Displacement (nm)	Si/Ca Ratio	Al/Ca Ratio
169	f/h	41.128	1.253	253.601	0.514	0.051
170	h/u	49.395	1.331	246.034	0.452	0.181
171	f/h	64.407	3.701	146.319	0.471	0.176
172	f/h	“invalid”	“invalid”	“invalid”	0.492	0.129
173	f/h	“invalid”	“invalid”	“invalid”	0.450	0.130
174	h	18.993	0.739	331.594	0.402	0.209
175	h	16.988	0.423	438.919	0.379	0.348
176	h	20.000	0.543	386.705	0.520	0.058
177	u	83.678	5.005	125.217	0.479	0.079
178	u	68.148	4.430	133.371	0.548	0.083
179	u	28.029	0.811	315.847	0.518	0.146
180	h	26.486	0.907	298.53	0.125	0.454
181	f/h	19.749	2.964	163.679	0.617	0.266
182	h/u	“invalid”	“invalid”	“invalid”	0.408	0.269
183	f/h	“invalid”	“invalid”	“invalid”	0.519	0.142
184	f/h	12.662	0.404	449.27	0.557	0.084
185	u	31.185	4.698	129.363	0.544	0.083
186	f/h	11.087	0.363	474.298	0.518	0.113
187	f	“invalid”	“invalid”	“invalid”	0.539	0.090
188	h	42.667	1.309	248.053	0.498	0.054
189	u	133.598	11.360	82.005	0.143	0.510
190	u	error	error	error	0.576	0.095
191	h	18.899	0.435	433.096	0.508	0.113
192	h	14.626	0.374	467.157	0.548	0.112
193	f	“invalid”	“invalid”	“invalid”	0.264	0.076
194	f/h	“invalid”	“invalid”	“invalid”	0.462	0.129
195	h/u	“invalid”	“invalid”	“invalid”	0.471	0.152
196	h/u	“invalid”	“invalid”	“invalid”	0.540	0.110
197	h	71.792	3.263	155.888	0.446	0.095
198	u	error	error	error	0.536	0.104
199	f/h	20.643	0.691	342.922	0.471	0.158
200	h	“invalid”	“invalid”	“invalid”	0.480	0.124

*Type: f=flaw, h=hydrate, u=unhydrated particle, f/h=flaw and hydrate combination, f/u=flaw and unhydrated particle combination, f/h/u=flaw, hydrate, and unhydrated particle combination, and h/u=hydrate and unhydrated particle combination.

PC-CNF-CF-B Grid 1

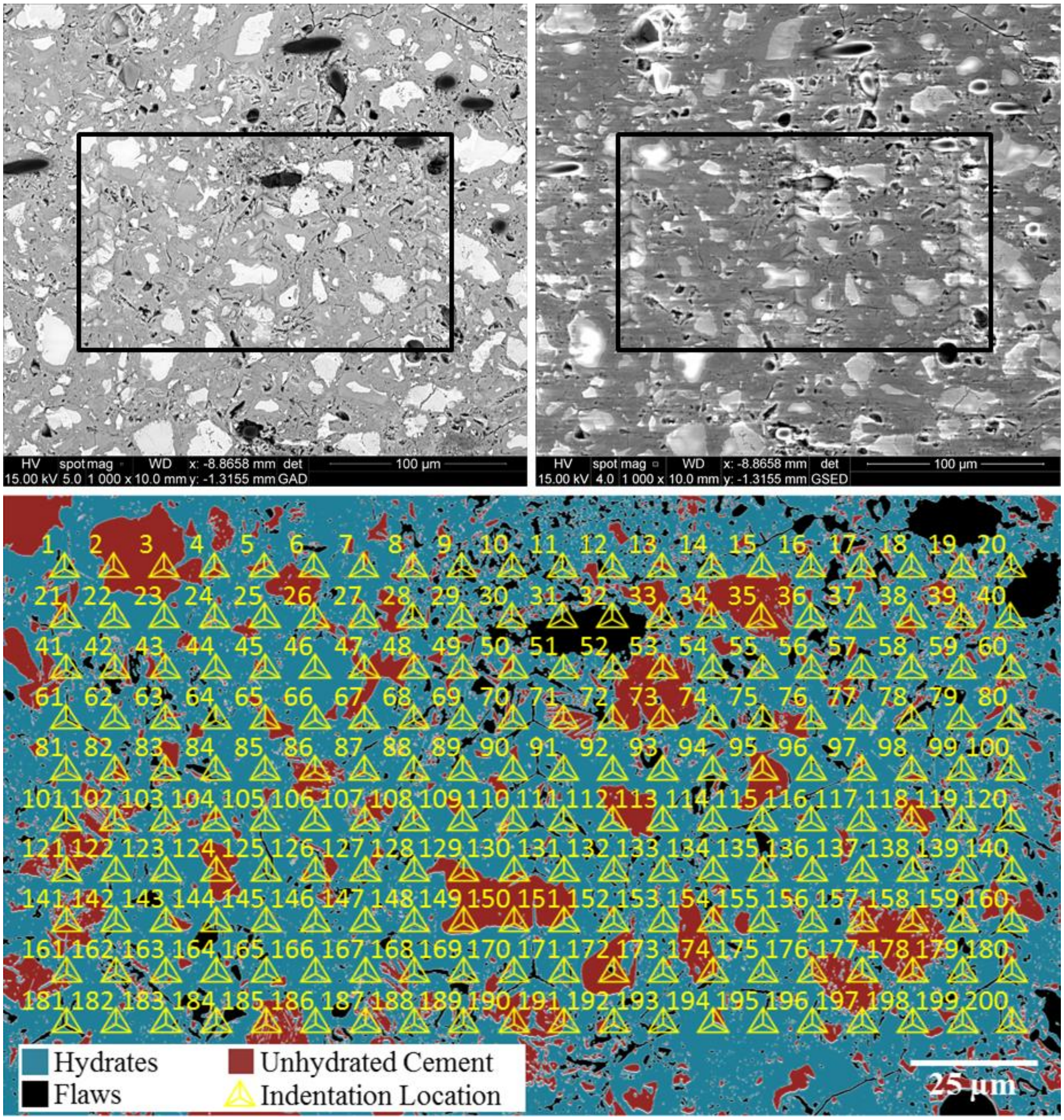

Indent	Type*	Modulus (GPa)	Hardness (GPa)	Maximum Displacement (nm)	Si/Ca Ratio	Al/Ca Ratio
1	h	32.376	1.099	271.046	0.306	0.090
2	u	104.940	8.502	95.354	0.378	0.024
3	u	105.503	9.563	89.678	0.375	0.030
4	h/u	66.341	8.848	93.285	0.457	0.116
5	h/u	“invalid”	“invalid”	“invalid”	0.152	0.102
6	f/h	159.360	15.936	68.75	0.297	0.209
7	f/h	32.288	1.209	258.238	0.419	0.142
8	f/h	“invalid”	“invalid”	“invalid”	0.063	0.019

Indent	Type*	Modulus (GPa)	Hardness (GPa)	Maximum Displacement (nm)	Si/Ca Ratio	Al/Ca Ratio
9	f	8.907	0.232	593.319	0.288	0.066
10	h	14.749	0.695	341.692	0.167	0.041
11	f/h	30.402	1.428	237.397	0.170	0.050
12	h	19.839	0.608	365.22	0.314	0.090
13	f/h/u	52.366	2.481	179.273	0.325	0.189
14	h	30.604	0.978	287.501	0.388	0.192
15	h	“invalid”	“invalid”	“invalid”	0.452	0.129
16	f/h	35.555	1.321	246.913	0.522	0.236
17	h	22.311	0.912	297.846	0.537	0.094
18	h	14.521	0.669	348.161	0.427	0.162
19	h	error	error	error	0.144	0.028
20	f/h	80.293	7.524	101.514	0.258	0.079
21	h	37.839	1.317	247.243	0.391	0.029
22	h	35.196	1.161	263.544	0.510	0.046
23	h	36.126	1.434	236.864	0.432	0.044
24	h	39.450	1.998	200.101	0.359	0.096
25	h	28.622	0.857	307.141	0.273	0.037
26	h	“invalid”	“invalid”	“invalid”	0.140	0.482
27	h	28.810	0.939	293.424	0.244	0.330
28	f/h	“invalid”	“invalid”	“invalid”	0.384	0.231
29	h/u	43.396	1.579	225.503	0.195	0.046
30	f/h	16.332	6.545	109.004	0.313	0.093
31	f	27.872	6.475	109.634	0.087	0.030
32	f	23.297	3.831	143.571	0.061	0.026
33	f/h	89.260	12.502	77.983	0.132	0.531
34	f/h	107.447	14.883	71.175	0.504	0.068
35	u	107.380	8.878	93.134	0.530	0.060
36	h	25.692	0.925	295.615	0.442	0.124
37	f/h	20.435	0.837	310.895	0.361	0.152
38	u	“invalid”	“invalid”	“invalid”	0.355	0.090
39	f/h	47.285	10.334	86.1	0.188	0.494
40	h	75.667	7.004	105.301	0.212	0.092
41	f/h	97.386	14.762	71.465	0.195	0.032
42	f/h	18.701	0.757	327.273	0.368	0.083
43	h	36.523	1.824	209.608	0.506	0.103
44	h	29.722	0.944	292.536	0.535	0.048
45	h	32.542	1.550	227.604	0.151	0.038
46	h	37.856	1.462	234.513	0.462	0.135
47	h/u	125.262	9.217	91.367	0.141	0.528
48	h/u	48.750	1.368	242.511	0.399	0.189

Indent	Type*	Modulus (GPa)	Hardness (GPa)	Maximum Displacement (nm)	Si/Ca Ratio	Al/Ca Ratio
49	f/h	29.667	0.772	324.021	0.222	0.107
50	f/h/u	23.434	0.905	299.071	0.355	0.413
51	h	error	error	error	0.341	0.136
52	f/h	“invalid”	“invalid”	“invalid”	0.352	0.156
53	u	123.321	9.653	89.141	0.091	0.027
54	h	18.995	0.741	330.81	0.408	0.147
55	h	17.004	1.241	254.789	0.430	0.291
56	h	“invalid”	“invalid”	“invalid”	0.329	0.096
57	h	65.467	4.901	126.541	0.330	0.126
58	h	34.986	1.134	266.687	0.404	0.048
59	h	29.064	1.672	219.101	0.215	0.043
60	f/h	68.300	6.635	108.336	0.284	0.056
61	h	38.239	2.015	199.192	0.144	0.576
62	h	28.568	1.336	245.469	0.433	0.465
63	h/u	25.109	0.754	327.814	0.142	0.238
64	f	94.658	11.101	82.974	0.370	0.185
65	u	151.633	17.405	65.576	0.216	0.032
66	h	29.218	0.989	285.759	0.486	0.053
67	h	54.641	1.840	208.623	0.431	0.122
68	f/h	52.986	1.385	241.058	0.372	0.102
69	h	23.705	0.785	321.364	0.249	0.191
70	f/h	18.537	0.698	340.838	0.331	0.203
71	h/u	67.522	6.359	110.715	0.571	0.142
72	h/u	61.317	4.840	127.354	0.384	0.193
73	u	121.964	9.815	88.392	0.368	0.231
74	f/h	49.919	4.101	138.678	0.480	0.162
75	f/h	“invalid”	“invalid”	“invalid”	0.367	0.130
76	f/h	158.752	13.770	74.15	0.442	0.081
77	h/u	31.265	1.245	254.275	0.308	0.260
78	f/h	33.169	1.251	253.874	0.120	0.237
79	f/h	27.587	1.207	258.368	0.290	0.169
80	f/h/u	“invalid”	“invalid”	“invalid”	0.560	0.087
81	h	38.900	1.238	255.232	0.263	0.096
82	h/u	106.923	10.082	87.234	0.442	0.090
83	h	144.856	14.556	72.018	0.233	0.397
84	h	58.272	3.305	154.81	0.125	0.489
85	h/u	42.095	2.023	198.798	0.423	0.055
86	u	103.876	6.626	108.307	0.166	0.444
87	h/u	“invalid”	“invalid”	“invalid”	0.427	0.128
88	f	30.401	0.850	308.806	0.146	0.029

Indent	Type*	Modulus (GPa)	Hardness (GPa)	Maximum Displacement (nm)	Si/Ca Ratio	Al/Ca Ratio
89	h	25.514	0.984	286.523	0.226	0.071
90	f/h	42.192	1.175	262.094	0.363	0.440
91	h	24.612	0.884	302.309	0.533	0.093
92	h	32.820	1.339	245.27	0.508	0.158
93	h	25.610	1.165	263.158	0.248	0.248
94	h	20.205	0.600	368.154	0.494	0.072
95	u	87.200	9.923	87.875	0.478	0.115
96	h	33.343	1.317	247.244	0.249	0.262
97	h	35.102	1.406	239.033	0.138	0.127
98	h	49.954	1.077	273.759	0.425	0.077
99	f/h	“invalid”	“invalid”	“invalid”	0.406	0.109
100	h	33.507	1.962	202.085	0.467	0.087
101	f/h	87.290	7.856	99.246	0.506	0.108
102	f/h	71.263	3.202	157.425	0.536	0.049
103	h	33.897	1.445	235.945	0.415	0.161
104	h	57.246	1.555	227.402	0.550	0.085
105	h	error	error	error	0.417	0.057
106	h	43.088	1.365	242.727	0.145	0.049
107	h/u	51.990	2.796	168.621	0.533	0.150
108	h	30.094	1.309	248.099	0.400	0.058
109	h	34.554	1.423	237.688	0.460	0.164
110	h	29.303	1.134	266.579	0.263	0.366
111	h	22.970	0.801	318.073	0.485	0.069
112	h	43.985	1.684	218.25	0.486	0.060
113	h	43.290	1.695	217.464	0.528	0.058
114	h	25.462	0.716	336.644	0.463	0.121
115	h	41.986	1.105	270.282	0.307	0.248
116	h	36.933	1.748	214.23	0.427	0.053
117	f/h	21.776	0.781	322.27	0.470	0.148
118	h/u	123.928	5.379	120.63	0.485	0.110
119	f/h	41.972	1.299	249.094	0.363	0.097
120	h	19.706	0.592	370.215	0.214	0.080
121	f/h	51.025	3.913	142.08	0.372	0.066
122	h	48.289	1.511	230.602	0.524	0.047
123	h	34.918	1.103	270.478	0.330	0.271
124	u	90.446	9.429	90.284	0.538	0.045
125	f/h	23.997	0.656	351.782	0.422	0.065
126	h	29.033	1.019	281.716	0.521	0.057
127	f/h	41.609	1.280	250.877	0.330	0.044
128	f/h	25.033	0.668	348.5	0.158	0.032

Indent	Type*	Modulus (GPa)	Hardness (GPa)	Maximum Displacement (nm)	Si/Ca Ratio	Al/Ca Ratio
129	u	93.218	9.671	89.111	0.538	0.057
130	h/u	69.781	2.590	175.371	0.450	0.057
131	h	43.314	1.495	231.795	0.379	0.110
132	f/h	22.572	0.771	324.15	0.433	0.092
133	h	23.285	0.957	290.72	0.333	0.148
134	h	23.171	1.050	277.286	0.559	0.075
135	h	25.286	0.797	318.63	0.382	0.277
136	h	30.270	0.915	297.191	0.483	0.070
137	h	28.355	0.950	291.668	0.529	0.082
138	h	32.158	0.844	309.757	0.415	0.151
139	h/u	31.652	1.781	212.128	0.489	0.093
140	h	26.118	1.440	236.193	0.346	0.306
141	h/u	65.848	1.880	206.359	0.520	0.130
142	f/h	35.854	0.985	286.487	0.334	0.289
143	f/h	32.707	1.242	254.898	0.330	0.161
144	f/h	17.403	0.493	406.134	0.499	0.049
145	h	23.415	0.815	315.279	0.536	0.077
146	h	37.680	2.138	193.231	0.314	0.063
147	h	28.627	0.955	290.902	0.478	0.130
148	h	error	error	error	0.497	0.086
149	u	78.844	8.474	95.39	0.262	0.218
150	u	90.565	10.505	85.316	0.513	0.047
151	h	87.058	4.528	131.843	0.522	0.052
152	h	24.052	0.975	287.795	0.560	0.089
153	h	27.478	0.832	311.929	0.490	0.075
154	h	error	error	error	0.420	0.158
155	f/h	66.277	2.017	199.149	0.557	0.072
156	h	25.580	0.760	326.46	0.469	0.099
157	h/u	73.152	4.587	130.923	0.513	0.089
158	u	93.276	6.315	111.061	0.502	0.098
159	f/h	39.741	1.219	257.118	0.226	0.063
160	h	212.151	21.275	58.962	0.496	0.097
161	f/h	92.343	6.559	108.891	0.509	0.150
162	f/h	25.098	0.937	293.72	0.536	0.057
163	h	39.695	1.412	238.718	0.531	0.066
164	h	29.422	0.920	296.567	0.514	0.092
165	h	25.229	0.873	304.578	0.564	0.069
166	h	25.574	0.878	303.388	0.157	0.023
167	h	33.167	1.011	282.676	0.492	0.091
168	h	37.137	1.860	207.478	0.198	0.058

Indent	Type*	Modulus (GPa)	Hardness (GPa)	Maximum Displacement (nm)	Si/Ca Ratio	Al/Ca Ratio
169	f/h	20.039	0.514	397.945	0.457	0.041
170	h	“invalid”	“invalid”	“invalid”	0.372	0.046
171	h	28.968	1.147	265.246	0.371	0.036
172	f/h/u	71.284	5.707	117.02	0.380	0.133
173	h	28.254	1.114	269.115	0.409	0.210
174	h/u	210.782	26.387	52.649	0.294	0.395
175	h	38.161	1.420	237.833	0.314	0.377
176	h/u	“invalid”	“invalid”	“invalid”	0.553	0.104
177	h/u	59.307	3.923	141.858	0.221	0.310
178	u	161.927	11.140	82.78	0.537	0.090
179	f/h	51.232	1.540	228.418	0.317	0.064
180	h	25.657	0.782	321.725	0.151	0.371
181	h	26.816	0.921	296.428	0.375	0.121
182	h	27.137	0.800	318.231	0.203	0.054
183	h	28.718	1.086	272.563	0.175	0.028
184	f/h	16.937	0.354	479.657	0.462	0.054
185	u	91.017	5.669	117.396	0.465	0.105
186	h	59.507	1.345	244.678	0.302	0.201
187	h	28.773	1.185	261.044	0.503	0.074
188	h	18.480	0.442	429.244	0.583	0.108
189	f/h	error	error	error	0.517	0.059
190	u	112.995	7.021	105.204	0.356	0.114
191	h/u	92.451	5.628	117.882	0.521	0.079
192	h/u	83.239	7.626	100.768	0.382	0.032
193	h	17.191	0.476	413.68	0.388	0.188
194	h	37.046	1.477	233.393	0.162	0.493
195	h	44.578	1.358	243.441	0.288	0.042
196	h	26.857	0.982	286.779	0.387	0.192
197	f/h	40.664	1.034	279.42	0.435	0.067
198	h	31.761	1.040	278.651	0.538	0.036
199	h	36.616	1.002	283.834	0.524	0.089
200	h/u	28.775	0.965	289.526	0.178	0.305

*Type: f=flaw, h=hydrate, u=unhydrated particle, f/h=flaw and hydrate combination, f/u=flaw and unhydrated particle combination, f/h/u=flaw, hydrate, and unhydrated particle combination, and h/u=hydrate and unhydrated particle combination.

PC-1% Grid 1

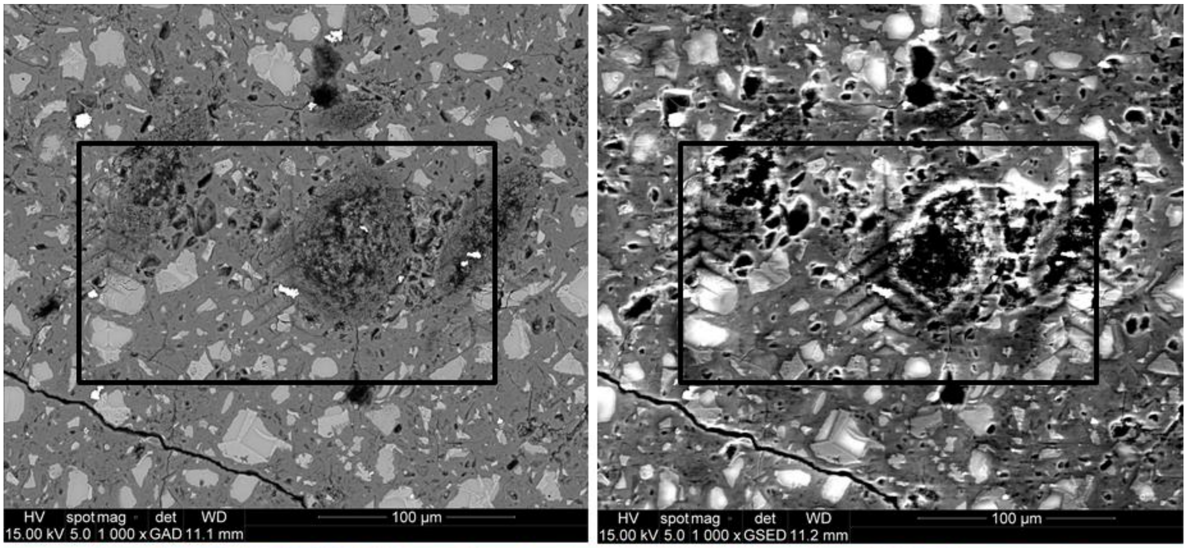

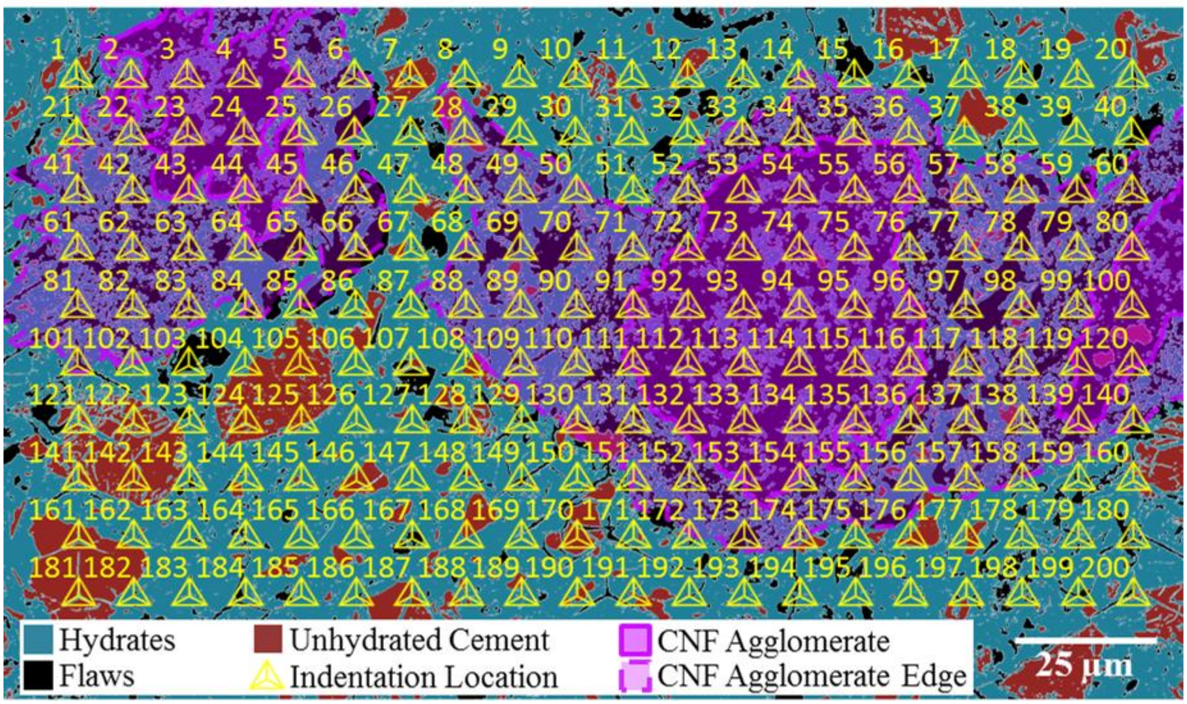

Indent	Type*	Location**	Modulus (GPa)	Hardness (GPa)	Maximum Displacement (nm)	Si/Ca Ratio	Al/Ca Ratio
1	f/h	n	22.112	0.982	286.946	0.206	0.450
2	h/u	o	“invalid”	“invalid”	“invalid”	0.365	0.182
3	f/h	i	“invalid”	“invalid”	“invalid”	0.624	0.196
4	f/h	i	“invalid”	“invalid”	“invalid”	0.829	0.208
5	f/h	i	error	error	error	0.268	0.407
6	f/h	o	13.386	1.024	280.689	0.413	0.247
7	h/u	n	error	error	error	0.438	0.137
8	h/u	n	26.519	1.159	263.922	0.586	0.170

Indent	Type*	Location**	Modulus (GPa)	Hardness (GPa)	Maximum Displacement (nm)	Si/Ca Ratio	Al/Ca Ratio
9	h	n	32.192	1.722	215.762	0.507	0.129
10	h	n	29.985	1.132	266.961	0.573	0.152
11	h	n	“invalid”	“invalid”	“invalid”	0.601	0.279
12	h/u	n	16.489	0.538	388.604	0.446	0.278
13	h	n	12.300	0.816	315.011	0.386	0.200
14	f/h	n	7.452	0.313	510.723	0.363	0.186
15	f	n	9.517	0.425	437.624	0.509	0.181
16	f/h	n	“invalid”	“invalid”	“invalid”	0.395	0.121
17	h	n	51.125	1.943	202.946	0.548	0.107
18	h	n	27.392	1.178	261.645	0.476	0.087
19	h	n	22.858	1.125	267.923	0.625	0.093
20	f/h	n	18.882	0.549	385.119	0.546	0.121
21	h	n	62.664	4.064	139.306	0.543	0.059
22	h	o	error	error	error	0.357	0.129
23	f	i	5.926	0.168	698.631	0.464	0.109
24	f	i	“invalid”	“invalid”	“invalid”	0.418	0.117
25	f/h	o	5.712	0.205	630.587	0.427	0.181
26	f	o	11.440	0.618	362.346	0.581	0.254
27	h	n	19.249	1.042	278.355	0.643	0.104
28	h	o	113.901	13.201	75.773	0.371	0.195
29	h	n	30.356	2.256	188.023	0.182	0.058
30	f/h	n	39.633	1.849	208.124	0.378	0.215
31	h	n	25.860	2.033	198.332	0.584	0.087
32	h	n	13.320	0.799	318.374	0.273	0.158
33	f/h	o	“invalid”	“invalid”	“invalid”	0.690	0.236
34	f/h	o	4.574	0.130	794.739	0.566	0.163
35	f/h	o	“invalid”	“invalid”	“invalid”	0.296	0.100
36	f/h	o	8.859	0.493	406.286	0.567	0.139
37	h	n	“invalid”	“invalid”	“invalid”	0.395	0.153
38	h	n	33.998	1.900	205.335	0.417	0.052
39	h	n	error	error	error	0.332	0.098
40	f/h	n	29.125	2.105	194.834	0.526	0.116
41	f/h	o	9.492	0.399	452.262	0.442	0.424
42	h	o	8.431	0.419	440.88	0.433	0.209
43	f	i	“invalid”	“invalid”	“invalid”	0.607	0.145
44	h	o	2.640	0.092	946.43	0.504	0.208
45	h	i	“invalid”	“invalid”	“invalid”	0.411	0.210
46	f	o	29.910	1.942	202.955	0.555	0.217
47	h	n	error	error	error	0.568	0.147
48	f/h	o	16.174	1.129	267.284	0.567	0.139

Indent	Type*	Location**	Modulus (GPa)	Hardness (GPa)	Maximum Displacement (nm)	Si/Ca Ratio	Al/Ca Ratio
49	h	o	“invalid”	“invalid”	“invalid”	0.582	0.172
50	h	o	24.160	2.409	181.97	0.476	0.159
51	f/h	n	8.259	0.439	431.004	0.401	0.093
52	f/h	o	3.151	0.084	987.111	0.525	0.160
53	f	i	6.261	0.390	457.556	0.506	0.264
54	f	i	5.304	0.204	633.784	0.393	0.184
55	f/h	i	“invalid”	“invalid”	“invalid”	0.283	0.067
56	f	i	error	error	error	0.455	0.334
57	h	o	43.237	2.787	168.829	0.198	0.291
58	h	o	42.683	2.866	166.44	0.544	0.120
59	f	o	35.023	3.122	159.424	0.400	0.125
60	f	o	“invalid”	“invalid”	“invalid”	0.340	0.271
61	f/h	o	7.140	0.235	590.135	0.373	0.253
62	f/h	o	“invalid”	“invalid”	“invalid”	0.347	0.193
63	f/h	o	“invalid”	“invalid”	“invalid”	0.500	0.182
64	h	o	“invalid”	“invalid”	“invalid”	0.637	0.152
65	f	o	12.901	0.936	293.852	0.394	0.217
66	f/h	o	18.042	1.618	222.7	0.436	0.133
67	h	n	error	error	error	0.382	0.270
68	h	o	30.652	1.407	239.221	0.445	0.144
69	f/h	o	“invalid”	“invalid”	“invalid”	0.398	0.229
70	f/h	o	7.150	0.383	461.458	0.409	0.088
71	f/h	o	7.871	0.438	431.364	0.478	0.096
72	f	i	error	error	error	0.567	0.123
73	f	i	“invalid”	“invalid”	“invalid”	0.634	0.164
74	f/h	i	“invalid”	“invalid”	“invalid”	0.607	0.275
75	f	i	“invalid”	“invalid”	“invalid”	0.433	0.527
76	f/h	o	3.097	0.061	1160.07	0.324	0.106
77	h	o	22.493	0.841	310.125	0.438	0.164
78	f/h	o	45.436	2.836	167.49	0.483	0.126
79	f/h	o	error	error	error	0.521	0.053
80	f	i	“invalid”	“invalid”	“invalid”	0.463	0.155
81	f/h	o	5.408	0.223	605.51	0.430	0.169
82	f/h	o	5.963	0.276	544.29	0.492	0.220
83	f/h	o	“invalid”	“invalid”	“invalid”	0.556	0.273
84	h	o	13.036	0.706	338.95	0.571	0.139
85	f/h	n	“invalid”	“invalid”	“invalid”	0.196	0.069
86	h	n	“invalid”	“invalid”	“invalid”	0.502	0.197
87	h	n	25.616	1.677	218.73	0.355	0.173
88	h	o	“invalid”	“invalid”	“invalid”	0.412	0.238

Indent	Type*	Location**	Modulus (GPa)	Hardness (GPa)	Maximum Displacement (nm)	Si/Ca Ratio	Al/Ca Ratio
89	f/h	o	7.510	0.345	486.352	0.517	0.131
90	f/h	o	7.318	0.387	459.329	0.431	0.259
91	f/h	i	3.982	0.196	645.76	0.544	0.115
92	f/h	i	4.362	0.167	700.389	0.503	0.348
93	f	i	3.201	0.077	1035.13	0.493	0.407
94	f/h	i	2.788	0.047	1326.38	0.447	0.391
95	f	i	error	error	error	0.506	0.210
96	f/h	i	error	error	error	0.457	0.178
97	f/h	o	“invalid”	“invalid”	“invalid”	0.456	0.075
98	f/h	o	error	error	error	0.405	0.036
99	f/h	o	5.058	0.197	644.08	0.545	0.132
100	f	i	“invalid”	“invalid”	“invalid”	0.482	0.146
101	f/h	o	8.049	0.361	475.715	0.379	0.135
102	h	n	9.324	0.357	477.934	0.317	0.102
103	f	n	“invalid”	“invalid”	“invalid”	0.536	0.143
104	h	n	143.094	10.453	85.589	0.527	0.265
105	u	n	100.732	8.431	95.629	0.138	0.526
106	h	n	“invalid”	“invalid”	“invalid”	0.649	0.144
107	h/u	n	30.782	5.388	120.476	0.221	0.428
108	h/u	n	96.902	10.050	87.297	0.482	0.190
109	f/h	o	“invalid”	“invalid”	“invalid”	0.438	0.143
110	f/h	o	6.616	0.269	551.418	0.619	0.194
111	f/h	i	“invalid”	“invalid”	“invalid”	0.660	0.098
112	f/h	i	error	error	error	0.301	0.160
113	f/h	i	5.867	0.348	484.495	0.544	0.328
114	f	i	3.637	0.128	799.707	0.425	0.275
115	f	i	2.874	0.072	1071.04	0.395	0.271
116	f/h	i	4.445	0.144	756.532	0.599	0.154
117	f/h	o	“invalid”	“invalid”	“invalid”	0.623	0.088
118	f/h	o	10.791	0.507	400.749	0.298	0.263
119	f/h	i	2.106	0.085	983.676	0.534	0.127
120	f	i	error	error	error	0.496	0.092
121	h/u	n	63.909	4.689	129.357	0.492	0.186
122	h/u	n	63.284	4.599	130.761	0.453	0.040
123	h	n	25.226	0.947	292.101	0.542	0.033
124	u	n	83.175	6.377	110.525	0.521	0.087
125	u	n	38.872	1.604	223.743	0.511	0.042
126	h	n	28.553	1.166	262.962	0.544	0.101
127	h	n	29.424	1.322	246.801	0.395	0.224
128	h	n	48.831	2.919	165.066	0.408	0.185

Indent	Type*	Location**	Modulus (GPa)	Hardness (GPa)	Maximum Displacement (nm)	Si/Ca Ratio	Al/Ca Ratio
129	f/h	n	15.628	0.699	340.621	0.532	0.062
130	f/h/u	o	“invalid”	“invalid”	“invalid”	0.372	0.202
131	f/h	o	5.597	0.278	542.088	0.504	0.098
132	f	i	5.626	0.212	620.815	0.546	0.144
133	f	i	4.939	0.172	689.946	0.497	0.234
134	f	i	“invalid”	“invalid”	“invalid”	0.479	0.109
135	f/h	i	error	error	error	0.387	0.159
136	f	o	7.544	0.708	338.243	0.564	0.131
137	f/h	o	“invalid”	“invalid”	“invalid”	0.123	0.469
138	f/h	o	error	error	error	0.402	0.209
139	f	i	“invalid”	“invalid”	“invalid”	0.481	0.090
140	f/h	o	error	error	error	0.263	0.091
141	h/u	n	74.182	5.383	120.617	0.455	0.121
142	u	n	82.980	7.860	99.169	0.440	0.043
143	f/h	n	17.731	0.360	475.821	0.493	0.042
144	h	n	25.821	1.337	245.325	0.471	0.176
145	h/u	n	32.879	1.502	231.328	0.595	0.078
146	u	n	102.125	8.713	94.013	0.601	0.065
147	h	n	23.904	1.229	256.051	0.376	0.038
148	h	n	38.034	1.257	253.149	0.615	0.063
149	f/h	n	“invalid”	“invalid”	“invalid”	0.366	0.121
150	h	n	error	error	error	0.437	0.175
151	f/h	o	“invalid”	“invalid”	“invalid”	0.498	0.188
152	f/h	o	4.459	0.165	703.669	0.468	0.124
153	f/h	i	“invalid”	“invalid”	“invalid”	0.313	0.197
154	h	o	“invalid”	“invalid”	“invalid”	0.302	0.196
155	h	o	“invalid”	“invalid”	“invalid”	0.314	0.088
156	h	o	23.192	1.441	236.297	0.447	0.229
157	f/h	o	35.260	2.409	181.906	0.560	0.220
158	h	n	6.995	0.408	447.694	0.493	0.212
159	f/h	n	9.815	0.876	303.864	0.464	0.092
160	h	n	43.526	2.592	175.284	0.483	0.110
161	u	n	113.914	8.782	93.636	0.370	0.031
162	h	n	35.814	1.335	245.464	0.364	0.029
163	h	n	“invalid”	“invalid”	“invalid”	0.346	0.157
164	f/h	n	42.550	2.055	197.343	0.476	0.074
165	h	n	28.566	1.310	247.833	0.472	0.087
166	h	n	24.143	1.315	247.446	0.552	0.096
167	f	n	53.368	2.855	166.812	0.648	0.103
168	h/u	n	32.658	1.346	244.623	0.435	0.148

Indent	Type*	Location**	Modulus (GPa)	Hardness (GPa)	Maximum Displacement (nm)	Si/Ca Ratio	Al/Ca Ratio
169	h	n	29.010	1.541	228.362	0.615	0.095
170	u	n	84.101	9.292	90.993	0.500	0.055
171	h	n	32.525	2.089	195.572	0.440	0.042
172	h/u	n	“invalid”	“invalid”	“invalid”	0.463	0.171
173	f/h	o	14.577	0.578	375.186	0.460	0.128
174	h	o	“invalid”	“invalid”	“invalid”	0.481	0.255
175	h	n	29.569	1.732	215.197	0.519	0.086
176	h/u	n	68.680	3.475	150.977	0.480	0.161
177	h/u	n	72.620	8.610	94.629	0.488	0.063
178	h	n	18.660	1.056	276.433	0.371	0.109
179	h	n	13.492	0.513	397.886	0.325	0.236
180	f/h	n	“invalid”	“invalid”	“invalid”	0.464	0.174
181	u	n	120.452	9.135	91.818	0.265	0.263
182	f/h	n	20.502	0.625	360.741	0.324	0.143
183	h	n	12.555	0.601	367.542	0.588	0.089
184	f/h	n	10.343	0.481	411.305	0.654	0.085
185	h	n	“invalid”	“invalid”	“invalid”	0.284	0.172
186	h	n	29.890	0.925	295.742	0.434	0.090
187	h/u	n	57.817	3.247	156.249	0.380	0.028
188	h	n	“invalid”	“invalid”	“invalid”	0.481	0.184
189	h	n	15.458	0.680	345.318	0.593	0.078
190	h/u	n	87.843	9.123	91.946	0.542	0.083
191	h/u	n	65.443	3.443	151.669	0.614	0.105
192	f/h	n	12.611	0.362	474.701	0.227	0.381
193	h	n	25.091	1.519	230.06	0.533	0.084
194	f/h	n	“invalid”	“invalid”	“invalid”	0.468	0.124
195	h	n	21.979	0.849	308.768	0.522	0.104
196	h	n	27.878	1.290	250.05	0.572	0.094
197	h	n	19.398	0.987	286.13	0.453	0.094
198	h	n	17.629	1.256	253.253	0.535	0.089
199	f/h	n	21.817	0.955	290.831	0.448	0.178
200	f/h	n	error	error	error	0.508	0.076

*Type: f=flaw, h=hydrate, u=unhydrated particle, f/h=flaw and hydrate combination, f/u=flaw and unhydrated particle combination, f/h/u=flaw, hydrate, and unhydrated particle combination, and h/u=hydrate and unhydrated particle combination.

**Location in relation to CNF agglomerate: i=inner CNF agglomerate, n=not in CNF agglomerate, and o=outer CNF agglomerate (around CNF agglomerate edge).

PC-1% Grid 2

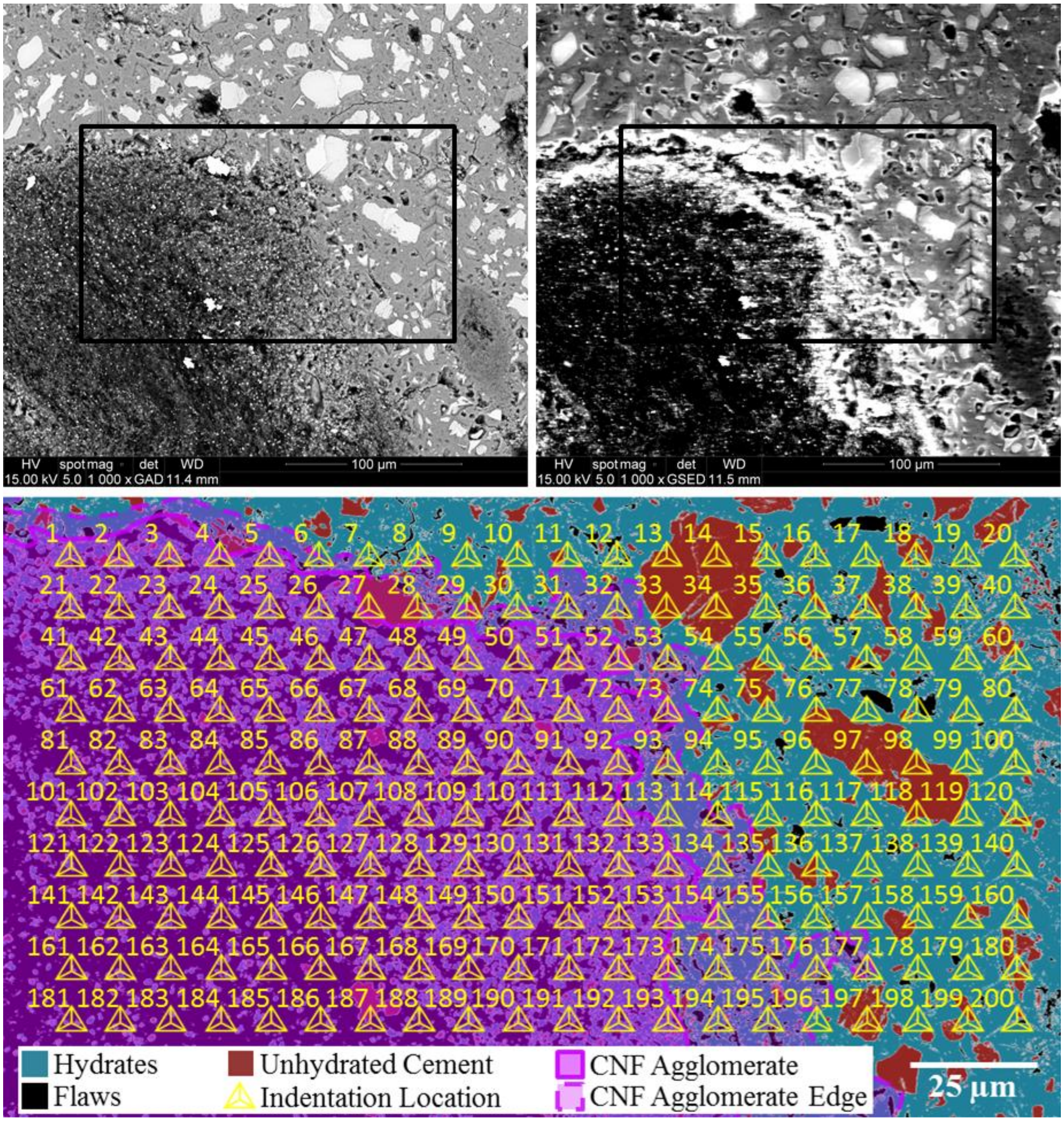

Indent	Type*	Location**	Modulus (GPa)	Hardness (GPa)	Maximum Displacement (nm)	Si/Ca Ratio	Al/Ca Ratio
1	h	i	36.269	0.928	295.686	0.349	0.217
2	f/h	i	60.418	6.147	112.625	0.430	0.324
3	h/u	i	“invalid”	“invalid”	1072.85	0.368	0.255
4	f/h	i	“invalid”	“invalid”	250.601	0.268	0.228
5	f/h	i	error	error	error	0.259	0.169
6	h	o	88.548	7.820	99.47	0.339	0.127
7	h	n	47.488	4.841	127.364	0.460	0.179
8	h	n	error	error	error	0.442	0.132

Indent	Type*	Location**	Modulus (GPa)	Hardness (GPa)	Maximum Displacement (nm)	Si/Ca Ratio	Al/Ca Ratio
9	h	n	22.055	1.589	224.648	0.489	0.127
10	h	n	54.101	3.867	142.926	0.443	0.205
11	h	n	31.017	1.099	271.143	0.390	0.041
12	h	n	“invalid”	“invalid”	“invalid”	0.384	0.204
13	u	n	error	error	error	0.089	0.449
14	u	n	138.101	10.876	83.789	0.371	0.030
15	h	n	22.281	1.019	281.51	0.468	0.065
16	f/h	n	14.375	0.638	356.613	0.406	0.119
17	h	n	18.164	0.846	309.272	0.437	0.246
18	h	n	“invalid”	“invalid”	“invalid”	0.183	0.258
19	h	n	“invalid”	“invalid”	“invalid”	0.464	0.111
20	h	n	43.199	2.467	179.719	0.438	0.147
21	h	i	21.403	1.207	258.42	0.410	0.208
22	f	i	“invalid”	“invalid”	“invalid”	0.441	0.165
23	f/h	i	14.973	0.365	473.277	0.775	0.306
24	f/h	i	17.399	1.140	266.429	0.392	0.465
25	f/h	i	“invalid”	“invalid”	“invalid”	0.602	0.499
26	h	i	error	error	error	0.550	0.306
27	u	o	“invalid”	“invalid”	“invalid”	0.250	0.159
28	u	o	7.734	0.135	780.355	0.318	0.187
29	u	o	“invalid”	“invalid”	“invalid”	0.251	0.153
30	h/u	o	“invalid”	“invalid”	“invalid”	0.252	0.203
31	h	o	“invalid”	“invalid”	“invalid”	0.376	0.227
32	u	o	“invalid”	“invalid”	“invalid”	0.321	0.292
33	u	n	228.266	20.275	60.518	0.084	0.413
34	u	n	187.639	13.871	73.832	0.360	0.029
35	h	n	22.695	0.876	303.836	0.540	0.087
36	h	n	148.033	13.627	74.494	0.234	0.234
37	f/h	n	17.635	0.502	402.339	0.284	0.112
38	h/u	n	34.083	2.221	189.637	0.892	0.038
39	h	n	18.393	0.840	310.367	0.407	0.311
40	f/h	n	“invalid”	“invalid”	“invalid”	0.436	0.080
41	f/h	i	“invalid”	“invalid”	“invalid”	0.477	0.453
42	f	i	10.444	0.422	439.443	0.351	0.302
43	f	i	“invalid”	“invalid”	“invalid”	0.314	0.403
44	f/h	i	“invalid”	“invalid”	“invalid”	0.297	0.350
45	f	i	18.530	1.395	240.332	0.458	0.237
46	f	i	22.813	2.157	192.331	0.423	0.277
47	f/h	i	14.090	0.468	417.216	0.612	0.331
48	f/h	i	21.401	1.155	264.304	0.436	0.199

Indent	Type*	Location**	Modulus (GPa)	Hardness (GPa)	Maximum Displacement (nm)	Si/Ca Ratio	Al/Ca Ratio
49	f/h	i	11.843	0.525	393.639	0.327	0.256
50	f/h	i	error	error	error	0.349	0.290
51	h/u	i	error	error	error	0.223	0.291
52	f/h	i	“invalid”	“invalid”	“invalid”	0.181	0.151
53	f/h	o	386.635	19.604	61.586	0.261	0.120
54	h	n	34.922	1.546	227.947	0.659	0.091
55	h	n	error	error	error	0.431	0.141
56	h	n	55.326	1.948	202.736	0.259	0.342
57	f/h	n	19.949	1.115	268.957	0.312	0.282
58	h	n	30.378	1.809	210.543	0.462	0.162
59	h	n	14.869	0.710	338.127	0.477	0.155
60	h	n	21.785	1.001	283.934	0.519	0.066
61	f	i	“invalid”	“invalid”	“invalid”	0.408	0.547
62	f	i	32.287	2.665	172.847	0.380	0.445
63	f	i	“invalid”	“invalid”	“invalid”	0.392	0.623
64	f/h	i	“invalid”	“invalid”	“invalid”	0.278	0.422
65	f	i	7.663	0.152	735.279	0.263	0.347
66	f/h	i	61.260	3.320	154.563	0.336	0.366
67	f/h	i	152.542	19.252	62.189	0.229	0.276
68	f	i	“invalid”	“invalid”	“invalid”	0.345	0.358
69	f/h	i	“invalid”	“invalid”	“invalid”	0.379	0.246
70	f	i	“invalid”	“invalid”	“invalid”	0.616	0.260
71	h	i	“invalid”	“invalid”	“invalid”	0.640	0.261
72	h/u	i	“invalid”	“invalid”	“invalid”	0.518	0.298
73	f/h	i	“invalid”	“invalid”	“invalid”	0.258	0.158
74	h	n	“invalid”	“invalid”	“invalid”	0.351	0.148
75	h	n	44.065	2.158	192.405	0.388	0.204
76	u	n	111.895	6.745	107.334	0.372	0.041
77	h	n	26.899	1.278	251.053	0.575	0.096
78	h	n	26.030	1.115	269.04	0.503	0.205
79	h	n	20.909	1.026	280.584	0.408	0.138
80	h	n	“invalid”	“invalid”	“invalid”	0.291	0.222
81	f	i	26.035	2.686	172.122	0.481	0.886
82	f	i	33.662	2.542	176.959	0.486	0.902
83	f	i	“invalid”	“invalid”	“invalid”	0.405	0.859
84	f	i	54.067	3.499	150.422	0.384	0.906
85	f/h	i	“invalid”	“invalid”	“invalid”	0.352	0.647
86	f	i	“invalid”	“invalid”	“invalid”	0.333	0.480
87	f/h	i	178.401	21.289	58.974	0.278	0.302
88	f	i	20.323	1.350	244.221	0.202	0.189

Indent	Type*	Location**	Modulus (GPa)	Hardness (GPa)	Maximum Displacement (nm)	Si/Ca Ratio	Al/Ca Ratio
89	f/h	i	error	error	error	0.248	0.218
90	f/h	i	"invalid"	"invalid"	"invalid"	0.307	0.165
91	f/h	i	error	error	error	0.470	0.228
92	h	i	"invalid"	"invalid"	"invalid"	0.504	0.234
93	h/u	o	error	error	error	0.553	0.095
94	h	n	error	error	error	0.436	0.124
95	h	n	20.941	0.969	288.852	0.485	0.137
96	h	n	27.865	1.530	229.177	0.544	0.083
97	u	n	140.097	9.942	87.786	0.336	0.067
98	u	n	117.955	9.844	88.246	0.363	0.033
99	h	n	27.304	1.121	268.181	0.534	0.091
100	f/h	n	10.454	0.334	494.55	0.357	0.094
101	f	i	29.474	3.596	148.334	0.296	0.841
102	f	i	29.948	2.776	169.244	0.250	0.715
103	f	i	"invalid"	"invalid"	"invalid"	0.221	0.601
104	f/h	i	32.563	2.653	173.235	0.413	1.249
105	f	i	20.564	0.976	287.661	0.367	0.814
106	f/h	i	52.319	3.048	161.277	0.340	0.656
107	f/h	i	154.945	16.793	66.82	0.325	0.610
108	f/h	i	"invalid"	"invalid"	"invalid"	0.246	0.368
109	f	i	"invalid"	"invalid"	"invalid"	0.247	0.294
110	f	i	"invalid"	"invalid"	"invalid"	0.182	0.117
111	f	i	4.166	0.104	887.885	0.248	0.124
112	h	i	"invalid"	"invalid"	"invalid"	0.527	0.219
113	h	o	18.971	1.261	252.849	0.384	0.232
114	f/h	o	19.611	0.991	285.611	0.153	0.110
115	h	n	31.442	1.831	209.239	0.449	0.145
116	h	n	14.028	0.684	344.556	0.511	0.111
117	h	n	"invalid"	"invalid"	"invalid"	0.478	0.098
118	u	n	121.385	8.731	93.951	0.366	0.037
119	h	n	31.455	1.122	268.117	0.581	0.085
120	h/u	n	63.900	3.365	153.399	0.175	0.275
121	f/h	i	34.602	5.558	118.543	0.446	1.274
122	f	i	31.077	3.071	160.775	0.419	1.193
123	f	i	"invalid"	"invalid"	"invalid"	0.315	1.036
124	f/h	i	33.130	2.573	175.868	0.208	0.729
125	f	i	error	error	error	0.334	1.000
126	f/h	i	52.189	3.384	152.922	0.336	0.840
127	f/h	i	"invalid"	"invalid"	"invalid"	0.364	0.719
128	f	i	33.212	2.753	170.048	0.358	0.570

Indent	Type*	Location**	Modulus (GPa)	Hardness (GPa)	Maximum Displacement (nm)	Si/Ca Ratio	Al/Ca Ratio
129	f/h	i	error	error	error	0.376	0.484
130	f/h	i	“invalid”	“invalid”	“invalid”	0.246	0.214
131	f	i	error	error	error	0.183	0.113
132	h	i	3.558	0.095	931.708	0.360	0.145
133	f/h	i	error	error	error	0.304	0.220
134	h	o	error	error	error	0.290	0.147
135	h	n	42.352	5.197	122.827	0.401	0.134
136	h/u	n	95.863	7.890	99.024	0.194	0.420
137	h	n	“invalid”	“invalid”	“invalid”	0.510	0.097
138	h	n	29.022	1.656	220.047	0.560	0.075
139	h	n	23.093	0.963	289.799	0.484	0.125
140	h	n	20.103	1.261	252.653	0.496	0.079
141	f	i	36.699	5.042	124.662	0.164	0.477
142	f/h	i	37.422	3.720	145.685	0.395	1.487
143	f/h	i	13.334	0.511	399.349	0.427	1.946
144	f/h	i	26.813	1.796	211.343	0.375	1.322
145	f/h	i	22.341	1.114	269.208	0.316	0.994
146	f	i	46.484	2.603	175.058	0.400	1.173
147	f/h	i	“invalid”	“invalid”	“invalid”	0.337	0.766
148	f/h	i	“invalid”	“invalid”	“invalid”	0.395	0.673
149	f/h	i	18.173	0.560	381.547	0.372	0.432
150	f/h	i	“invalid”	“invalid”	“invalid”	0.393	0.397
151	f/h	i	“invalid”	“invalid”	“invalid”	0.168	0.127
152	f/h	i	6.682	0.366	471.701	0.368	0.152
153	f/h	i	19.009	1.348	244.473	0.424	0.164
154	h	o	“invalid”	“invalid”	“invalid”	0.407	0.224
155	f/h	o	“invalid”	“invalid”	“invalid”	0.280	0.167
156	h	n	26.721	1.615	222.962	0.538	0.109
157	h	n	28.489	1.609	223.467	0.503	0.109
158	h	n	32.300	0.853	308.198	0.443	0.047
159	h	n	38.174	2.360	183.799	0.364	0.142
160	h	n	29.217	1.396	240.17	0.251	0.146
161	f/h	i	“invalid”	“invalid”	“invalid”	0.379	1.122
162	f/h	i	“invalid”	“invalid”	“invalid”	0.350	1.234
163	f/h	i	17.076	0.835	311.502	0.319	1.438
164	f/h	i	28.373	1.994	200.317	0.326	1.167
165	f/h	i	error	error	error	0.402	1.599
166	f	i	28.162	1.319	247.055	0.238	0.693
167	f/h	i	“invalid”	“invalid”	“invalid”	0.304	0.733
168	f	i	“invalid”	“invalid”	“invalid”	0.356	0.752

Indent	Type*	Location**	Modulus (GPa)	Hardness (GPa)	Maximum Displacement (nm)	Si/Ca Ratio	Al/Ca Ratio
169	f	i	error	error	error	0.333	0.352
170	f/h	i	“invalid”	“invalid”	“invalid”	0.319	0.339
171	f/h	i	error	error	error	0.275	0.284
172	f	i	error	error	error	0.454	0.295
173	f/h	i	error	error	error	0.296	0.200
174	f/h	o	error	error	error	0.451	0.142
175	f/h	o	error	error	error	0.448	0.211
176	f/h	o	“invalid”	“invalid”	“invalid”	0.409	0.310
177	f/h	o	“invalid”	“invalid”	“invalid”	0.264	0.198
178	h	n	21.500	1.015	282.017	0.433	0.198
179	h	n	17.391	0.650	353.419	0.519	0.097
180	h/u	n	86.350	6.424	110.079	0.372	0.059
181	f	i	error	error	error	0.395	1.674
182	f	i	“invalid”	“invalid”	“invalid”	0.358	1.487
183	f	i	“invalid”	“invalid”	“invalid”	0.392	1.747
184	f	i	“invalid”	“invalid”	“invalid”	0.405	1.807
185	f/h	i	“invalid”	“invalid”	“invalid”	0.416	1.688
186	f	i	29.891	1.144	265.826	0.325	1.080
187	f/u	i	“invalid”	“invalid”	“invalid”	0.333	0.976
188	f/h	i	“invalid”	“invalid”	“invalid”	0.325	0.730
189	f/h	i	“invalid”	“invalid”	“invalid”	0.263	0.458
190	h/u	i	4.506	0.150	739.41	0.319	0.415
191	f/h	i	6.791	0.220	610.777	0.372	0.430
192	f/h	i	“invalid”	“invalid”	“invalid”	0.464	0.338
193	f/h	i	9.313	0.482	410.876	0.409	0.410
194	f/h	o	“invalid”	“invalid”	“invalid”	0.413	0.219
195	f/h	o	“invalid”	“invalid”	“invalid”	0.348	0.181
196	h	n	“invalid”	“invalid”	“invalid”	0.476	0.083
197	u	n	77.302	4.023	140.126	0.464	0.047
198	h	n	26.376	1.445	235.855	0.620	0.089
199	h	n	“invalid”	“invalid”	“invalid”	0.480	0.097
200	h	n	39.347	4.818	127.703	0.768	0.121

*Type: f=flaw, h=hydrate, u=unhydrated particle, f/h=flaw and hydrate combination, f/u=flaw and unhydrated particle combination, f/h/u=flaw, hydrate, and unhydrated particle combination, and h/u=hydrate and unhydrated particle combination.

**Location in relation to CNF agglomerate: i=inner CNF agglomerate, n=not in CNF agglomerate, and o=outer CNF agglomerate (around CNF agglomerate edge).

APPENDIX D

MACROMECHANICAL DATA

This appendix contains the data used to study the macromechanical properties of cement-based materials containing CNFs (Chapter 5 and Section 0). Three different sets of macromechanical data are included: dispersion method (Section 5.3.1), CNF loading (Section 5.3.2 and Section 5.3.3), and hybrid composites (Section 0). The force displacement curves for each specimen are given as well as the specimen mass and size.

<u>Dispersion Method</u>
Testing method: flexural (three-point bending).
Beam length: *ca.* 114.3 mm.
Beam span: 76.2 mm.

PC-W/Control (7 days)

Sample	Mass (g)	Average Height (mm)	Average Width (mm)
A	154.3	25.9	24.3
B	148.4	25.5	24.3
C	146.6	25.2	24.3
D	146.8	25.2	24.4
E	144.9	25.1	24.4
F	148.1	25.1	24.6

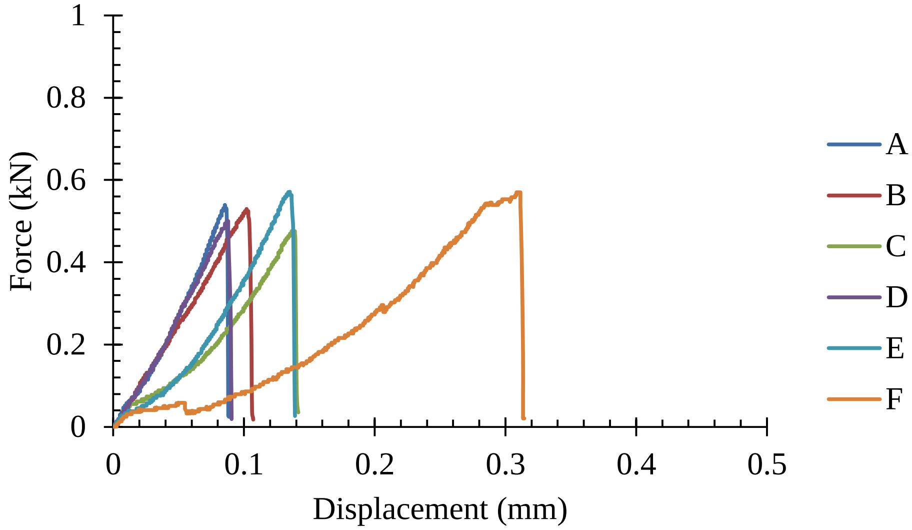

PC-W/CNF (7 days)

Sample	Mass (g)	Average Height (mm)	Average Width (mm)
A	144.1	24.9	24.2
B	140.0	24.7	24.2
C	140.3	24.4	24.5
D	141.4	24.2	24.7
E	141.0	24.1	24.7
F	143.6	24.3	24.8

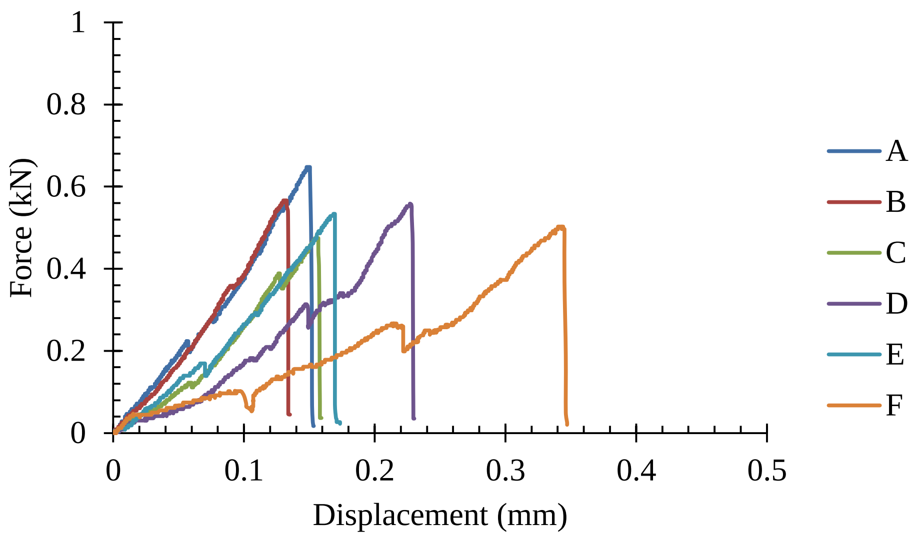

PC-W/T-CNF (7 days)

Sample	Mass (g)	Average Height (mm)	Average Width (mm)
A	157.8	26.8	25.0
B	149.4	25.5	24.8
C	148.8	25.1	24.9
D	144.7	24.4	25.0
E	144.5	24.5	25.0
F	155.3	24.9	24.8

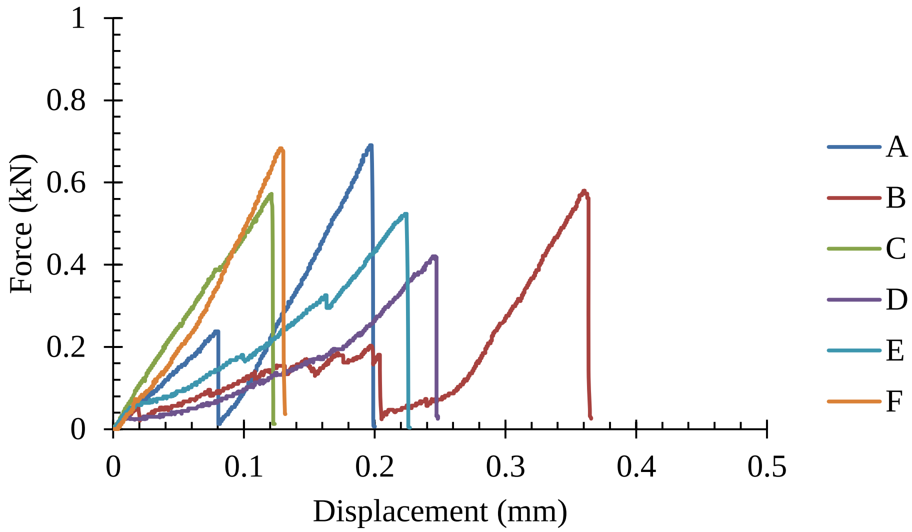

PC-N-HRWR/Control (7 days)

Sample	Mass (g)	Average Height (mm)	Average Width (mm)
A	155.6	27.1	25.8
B	111.2	26.7	25.8
C	153.1	27.2	26.3
D	154.7	27.5	26.6
E	157.1	28.0	27.3
F	162.5	28.1	27.5

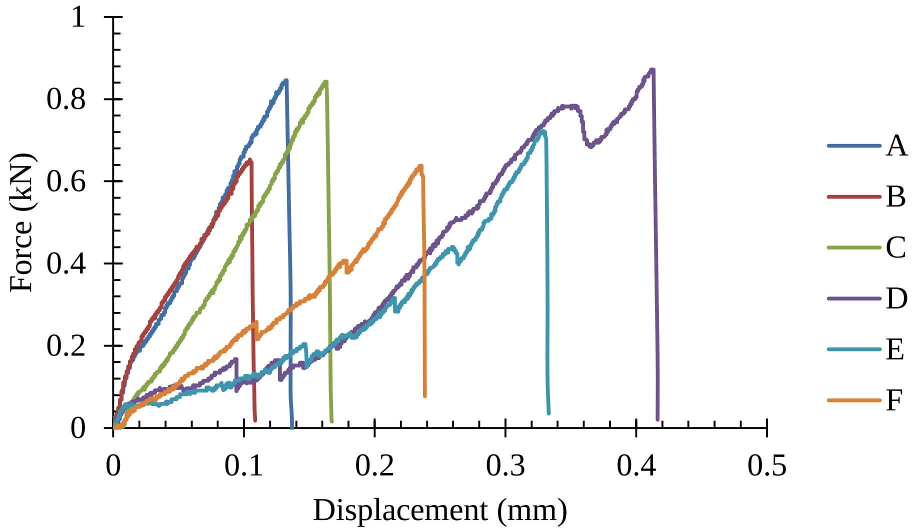

PC-N-HRWR/CNF (7 days)

Sample	Mass (g)	Average Height (mm)	Average Width (mm)
A	Discarded	Discarded	Discarded
B	155.1	26.4	25.8
C	154.5	26.3	25.6
D	155.0	26.3	26.2
E	158.0	26.7	27.4
F	161.1	27.3	26.2

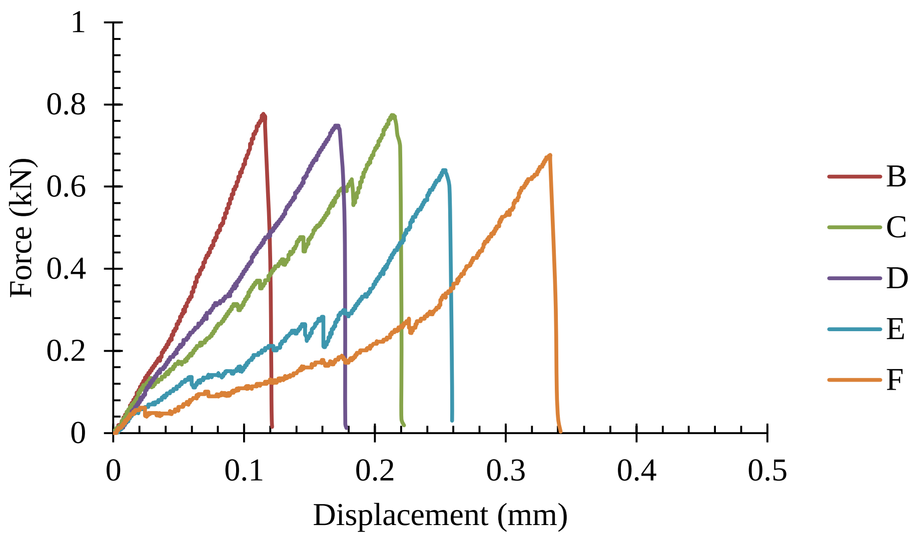

PC-AE/Control (7 days)

Sample	Mass (g)	Average Height (mm)	Average Width (mm)
A	156.0	26.7	26.3
B	156.8	26.9	26.6
C	154.2	27.1	26.8
D	158.4	26.8	26.4
E	152.5	26.3	26.3
F	161.4	26.1	26.1

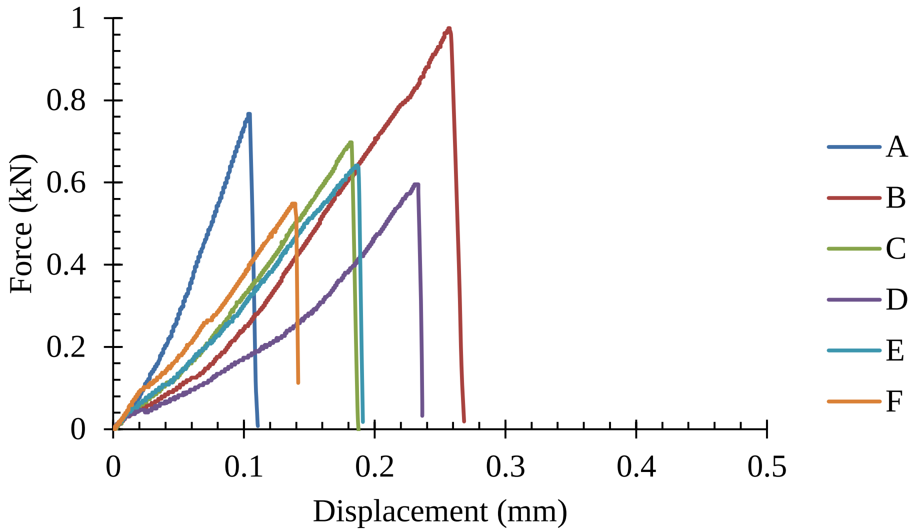

PC-AE/CNF (7 days)

Sample	Mass (g)	Average Height (mm)	Average Width (mm)
A	137.9	24.5	24.4
B	136.3	24.7	24.3
C	135.5	24.7	24.6
D	136.4	24.2	24.8
E	137.1	24.4	24.8
F	138.7	24.5	24.9

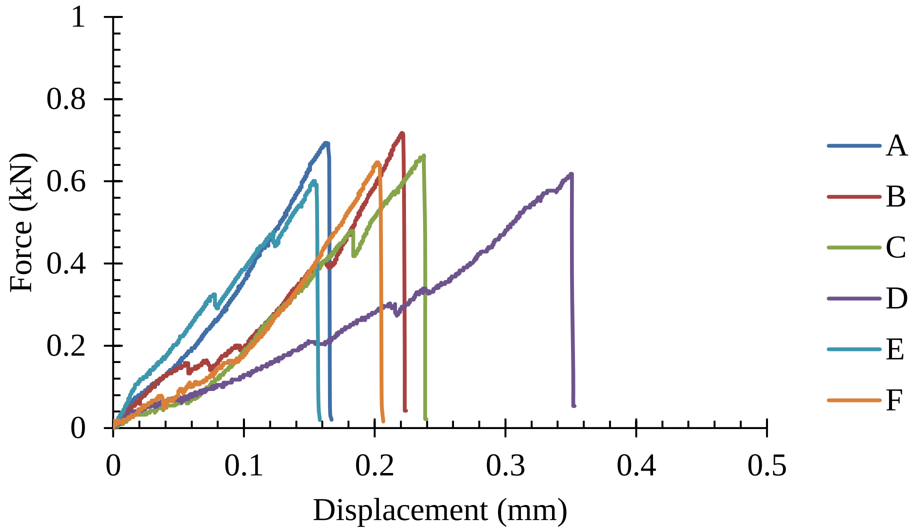

PC-P-HRWR/Control (7 days)

Sample	Mass (g)	Average Height (mm)	Average Width (mm)
A	138.9	23.6	24.1
B	133.4	23.4	24.0
C	136.3	23.3	24.2
D	135.9	23.1	24.4
E	135.9	23.0	24.5
F	139.1	22.9	24.8

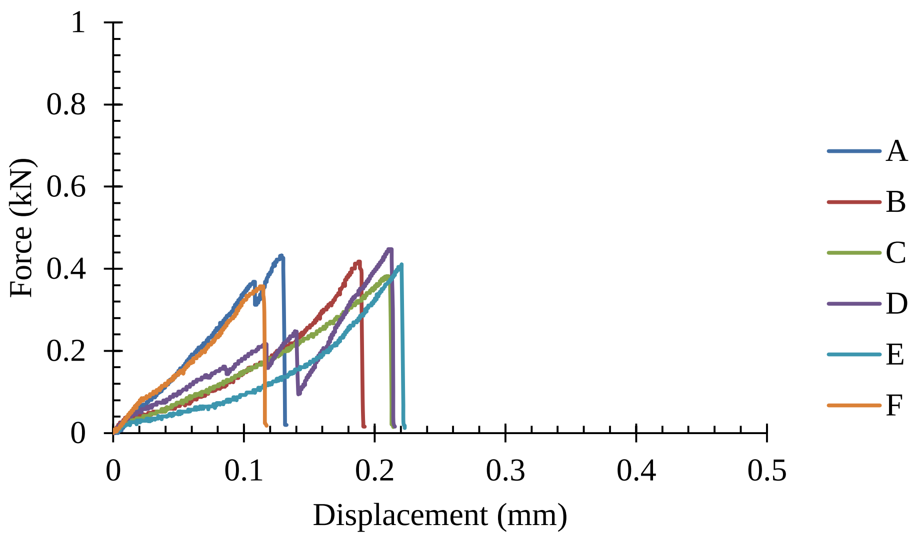

PC-P-HRWR/CNF (7 days)

Sample	Mass (g)	Average Height (mm)	Average Width (mm)
A	145.7	25.1	24.7
B	148.0	25.1	24.7
C	146.8	25.1	24.6
D	148.7	25.3	24.6
E	148.0	25.3	24.5
F	153.7	25.5	24.5

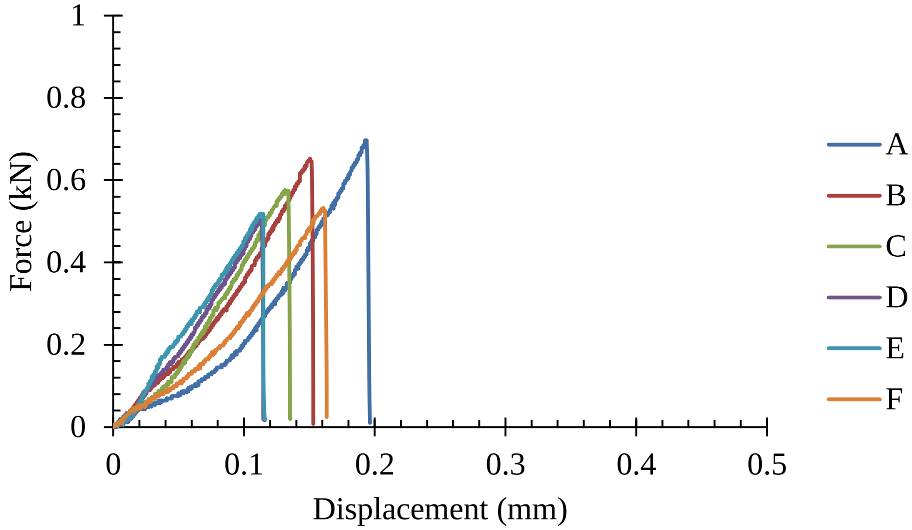

PC-P-HRWR/T-CNF (7 days)

Sample	Mass (g)	Average Height (mm)	Average Width (mm)
A	145.2	25.1	24.3
B	141.6	24.7	24.3
C	140.9	24.3	24.5
D	142.1	24.0	24.7
E	140.0	23.8	24.8
F	148.2	23.8	24.9

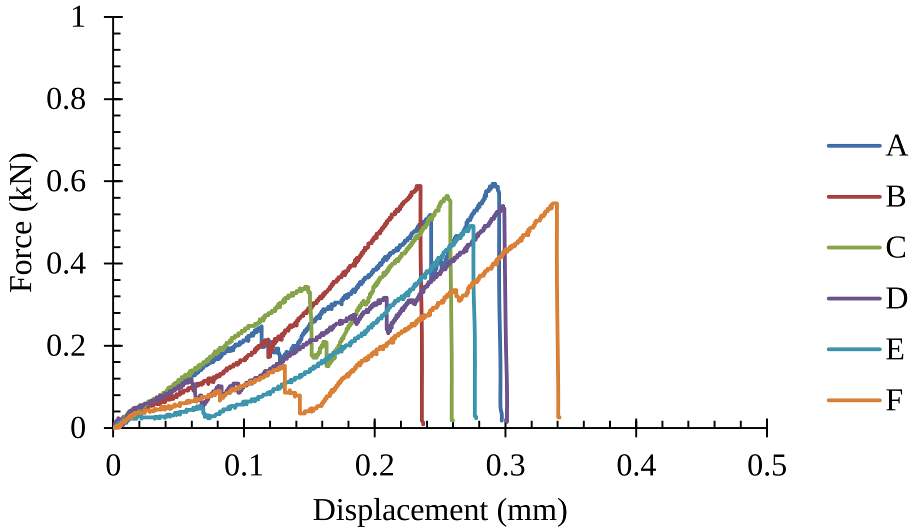

CNF Loading

Testing method: compression (uniaxial on cylinders), splitting tensile, and flexural (three-point bending).

Compression

PC-0% (7 days)

Sample	Mass (g)	Diameter (mm)	Average Height (mm)
A	396.2	50.6	93.5
B	395.8	50.4	92.8
C	396.4	50.5	93.8
D	397.4	50.6	93.8
E	399.6	50.6	93.6

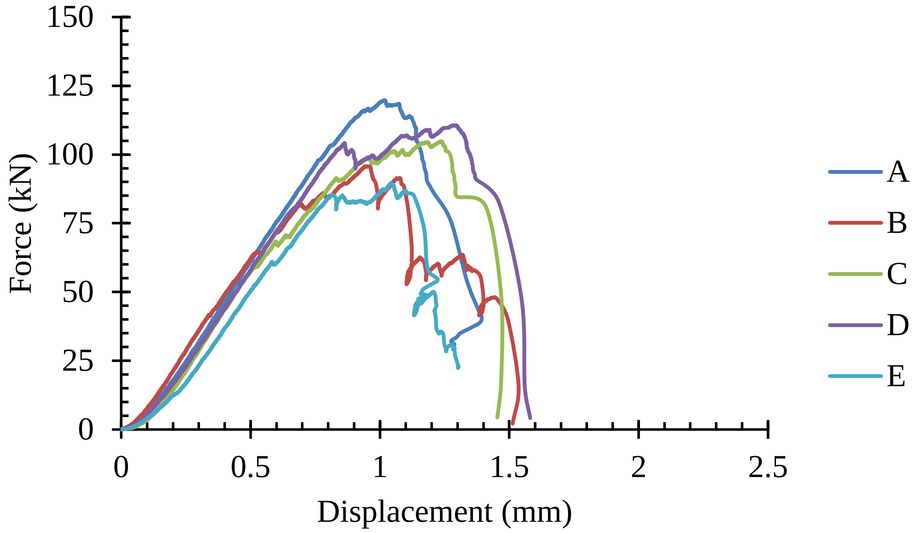

PC-0% (28 days)

Sample	Mass (g)	Diameter (mm)	Average Height (mm)
A	397.2	50.5	93.3
B	393.4	50.6	92.9
C	402.7	50.5	94.3
D	402.6	50.5	94.2
E	397.6	50.4	93.9

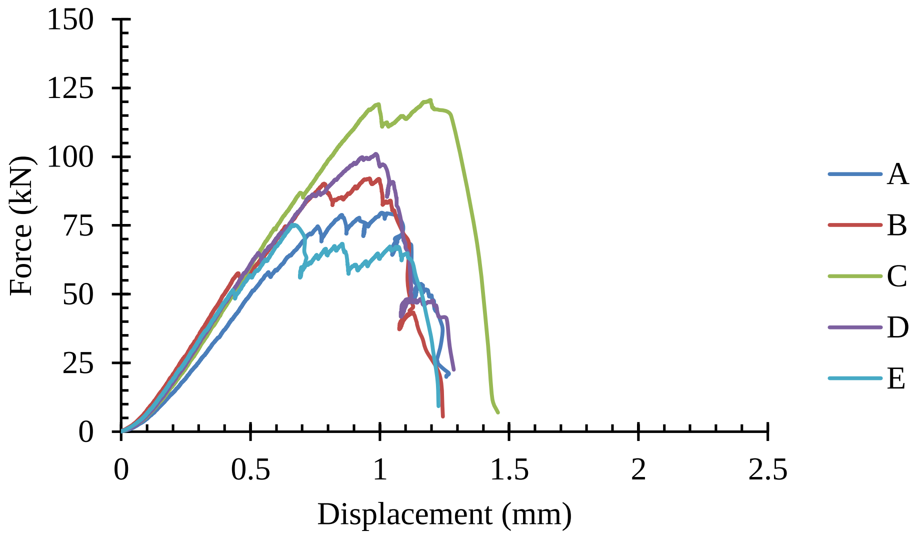

PC-0.02% (7 days)

Sample	Mass (g)	Diameter (mm)	Average Height (mm)
A	400.7	50.5	93.7
B	400.9	50.6	93.8
C	396.1	50.5	92.4
D	399.5	50.7	93.5
E	399.0	50.5	93.6

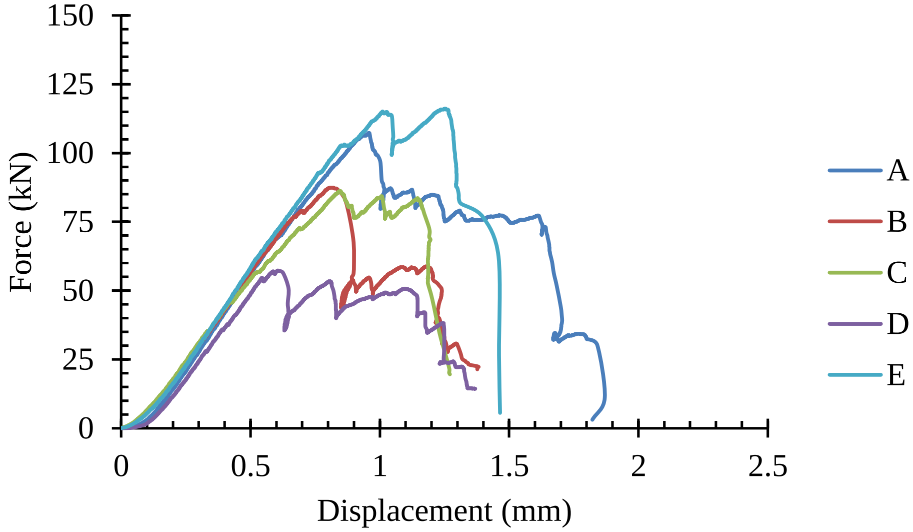

PC-0.02% (28 days)

Sample	Mass (g)	Diameter (mm)	Average Height (mm)
A	405.7	50.4	94.4
B	406.1	50.6	94.9
C	400.5	50.6	93.3
D	399.9	50.6	94.1
E	400.2	50.5	93.5

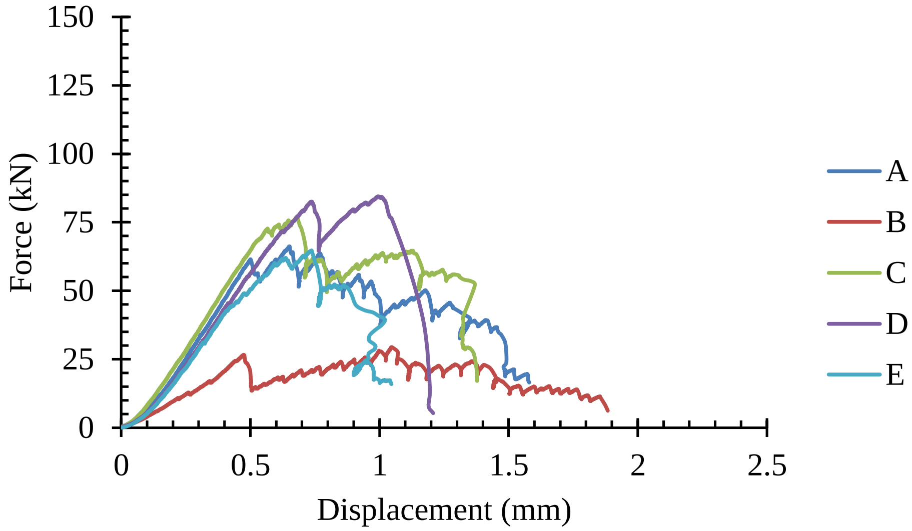

PC-0.08% (7 days)

Sample	Mass (g)	Diameter (mm)	Average Height (mm)
A	397.0	50.6	92.4
B	401.5	50.5	93.0
C	399.8	50.6	93.3
D	388.9	50.7	90.7
E	401.5	50.6	93.7

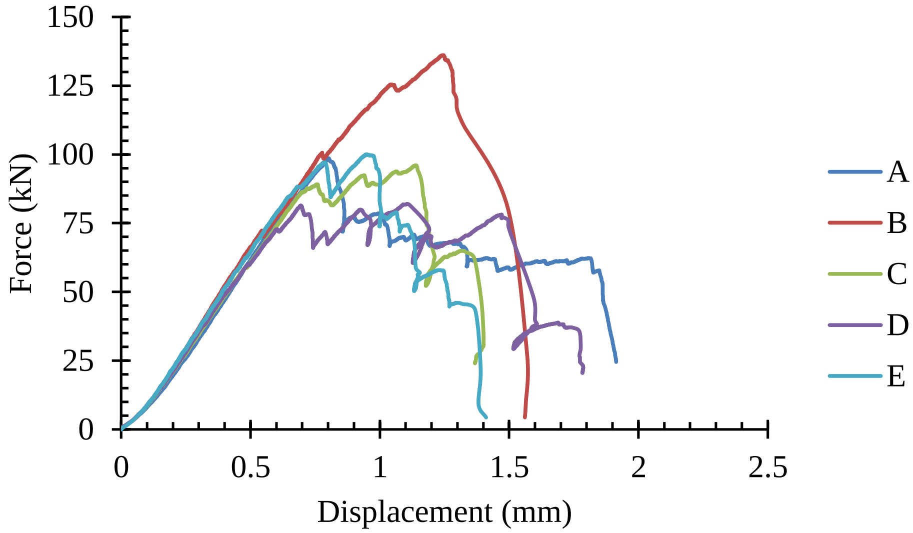

PC-0.08% (28 days)

Sample	Mass (g)	Diameter (mm)	Average Height (mm)
A	405.7	50.5	94.3
B	404.6	50.7	94.5
C	406.2	50.5	94.3
D	411.3	50.5	95.2
E	402.0	50.6	93.3

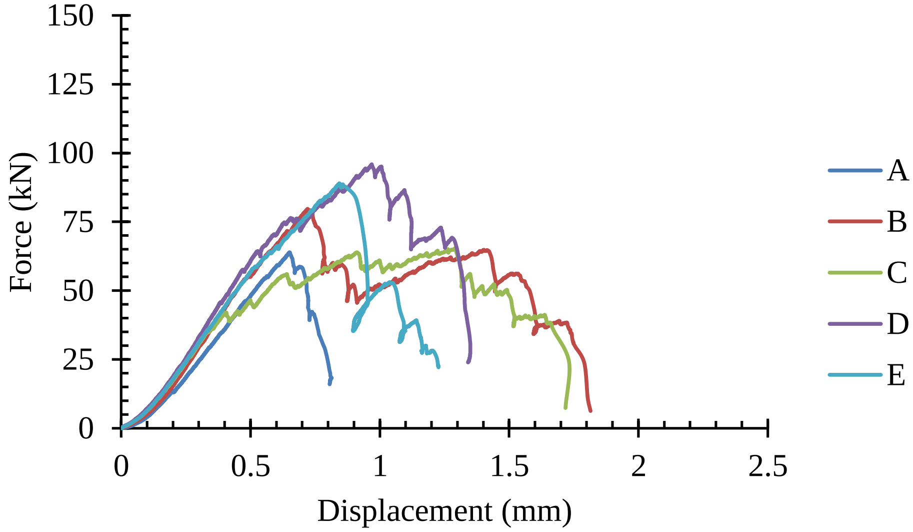

PC-0.2% (7 days)

Sample	Mass (g)	Diameter (mm)	Average Height (mm)
A	400.2	50.7	92.9
B	399.7	50.7	92.4
C	408.4	50.6	93.9
D	404.7	50.6	93.6
E	400.6	50.6	92.6

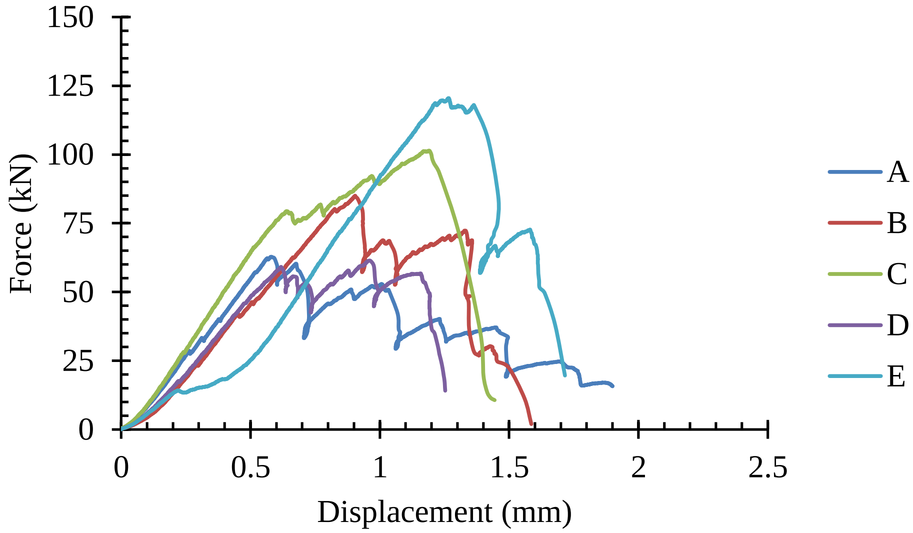

PC-0.2% (28 days)

Sample	Mass (g)	Diameter (mm)	Average Height (mm)
A	400.2	50.5	92.4
B	396.9	50.6	91.6
C	409.9	50.5	93.9
D	400.7	50.6	93.1
E	403.8	50.5	93.2

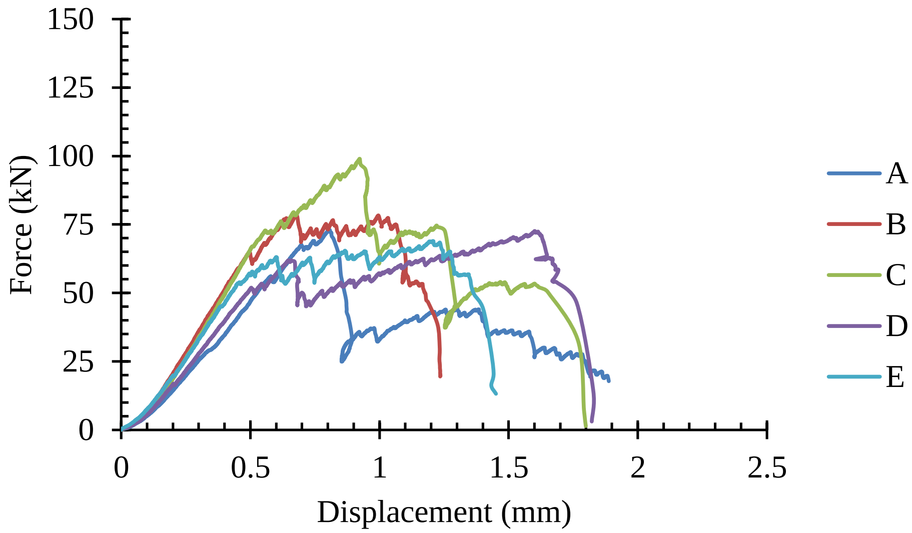

PC-0.5% (7 days)

Sample	Mass (g)	Diameter (mm)	Average Height (mm)
A	400.9	50.5	94.4
B	396.9	50.5	92.6
C	410.8	50.5	94.8
D	402.9	50.3	93.6
E	403.2	50.6	93.3

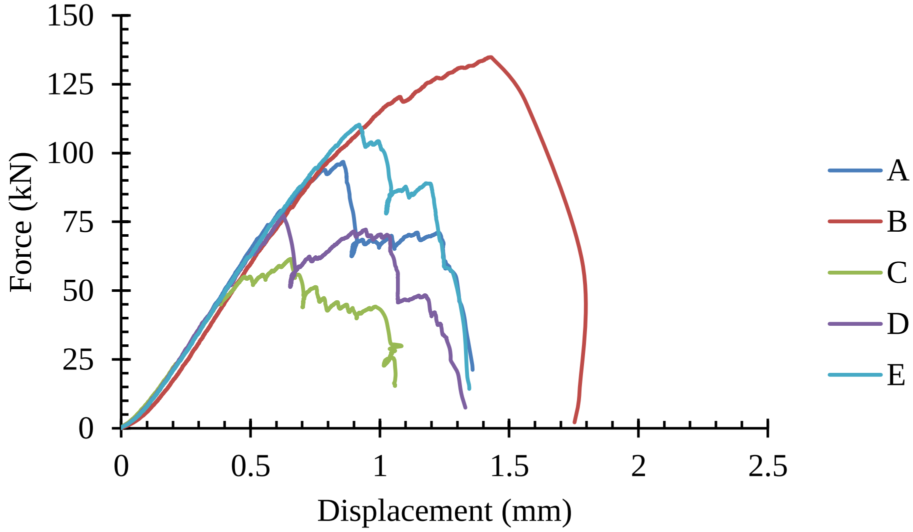

PC-0.5% (28 days)

Sample	Mass (g)	Diameter (mm)	Average Height (mm)
A	409.6	50.5	93.6
B	396.2	50.3	93.6
C	398.9	50.5	93.9
D	399.4	50.3	94.1
E	396.8	50.4	93.3

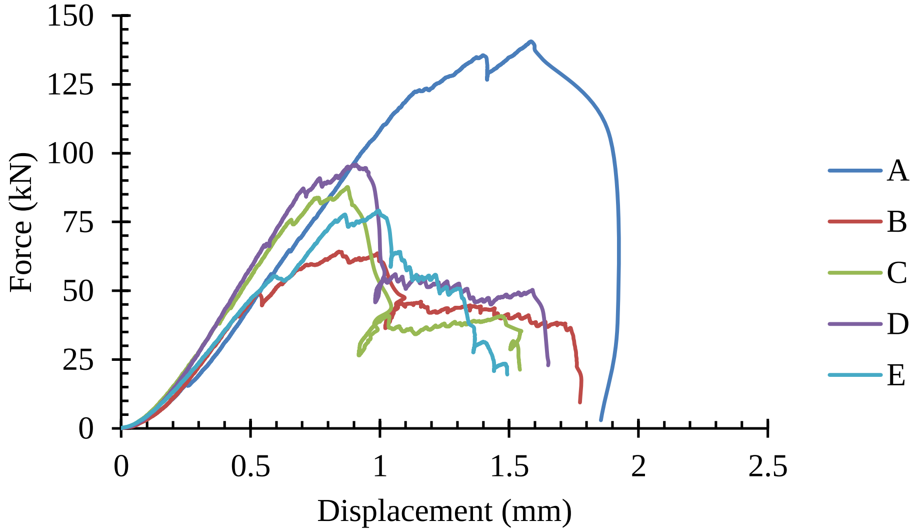

PC-1% (7 days)

Sample	Mass (g)	Diameter (mm)	Average Height (mm)
A	384.7	50.5	94.2
B	370.5	50.3	92.3
C	377.0	50.4	93.5
D	382.2	50.4	93.5
E	375.1	50.5	93.2

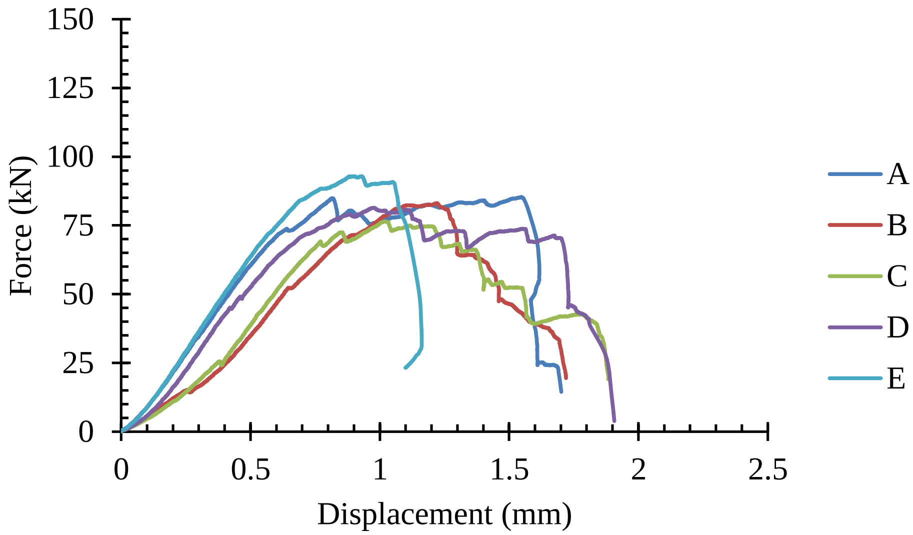

PC-1% (28 days)

Sample	Mass (g)	Diameter (mm)	Average Height (mm)
A	377.0	50.5	92.7
B	Discarded	Discarded	Discarded
C	376.8	50.5	93.9
D	369.5	50.5	90.8
E	371.1	50.4	92.0

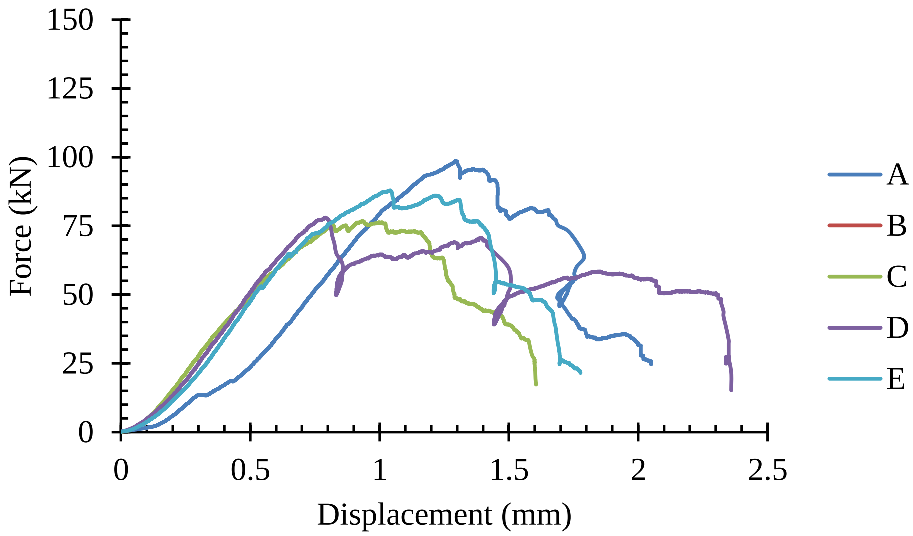

SF-0% (7 days)

Sample	Mass (g)	Diameter (mm)	Average Height (mm)
A	387.3	50.2	93.6
B	385.8	50.4	94.3
C	370.5	50.3	90.3
D	384.6	50.2	94.0
E	386.3	50.2	94.1

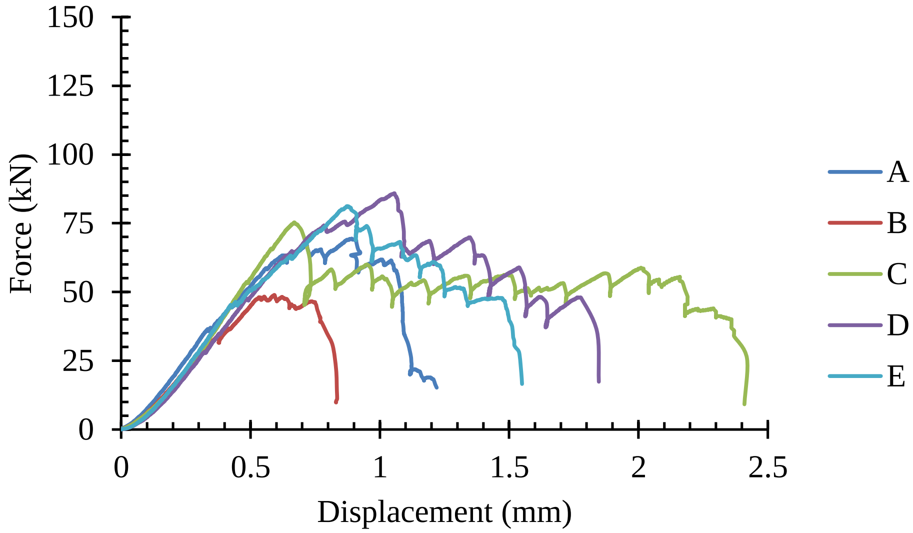

SF-0% (28 days)

Sample	Mass (g)	Diameter (mm)	Average Height (mm)
A	381.4	50.2	92.8
B	386.0	50.4	93.8
C	379.8	50.6	91.9
D	385.7	50.5	93.9
E	381.3	50.6	93.3

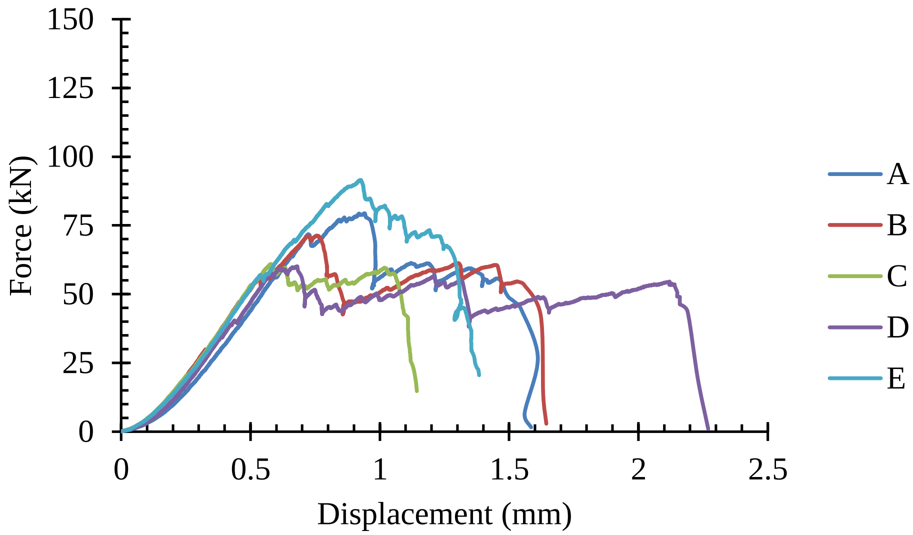

SF-0.02% (7 days)

Sample	Mass (g)	Diameter (mm)	Average Height (mm)
A	383.9	50.3	93.2
B	373.4	50.4	90.8
C	389.4	50.4	94.5
D	386.4	50.1	94.0
E	387.0	50.4	93.5

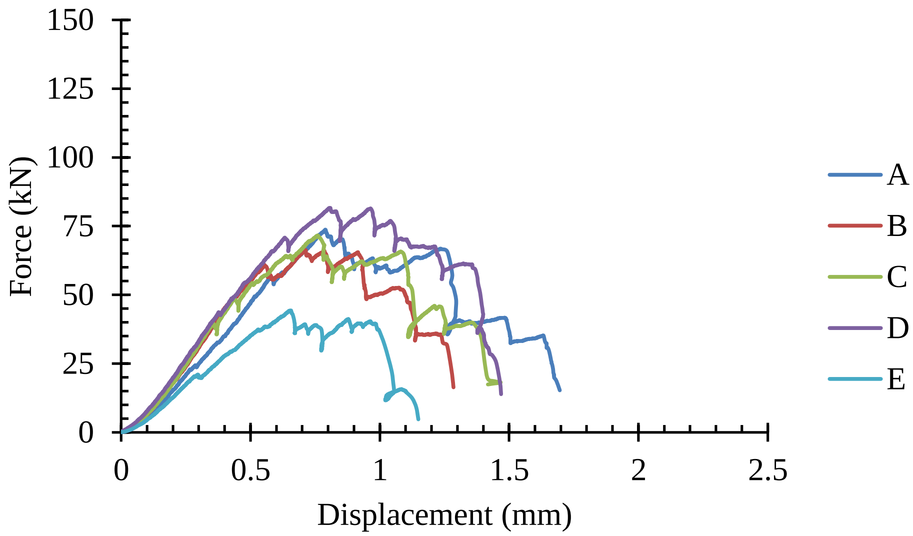

SF-0.02% (28 days)

Sample	Mass (g)	Diameter (mm)	Average Height (mm)
A	374.2	50.5	90.3
B	385.2	50.6	93.6
C	382.8	50.4	93.2
D	384.7	50.7	93.6
E	387.1	50.5	94.0

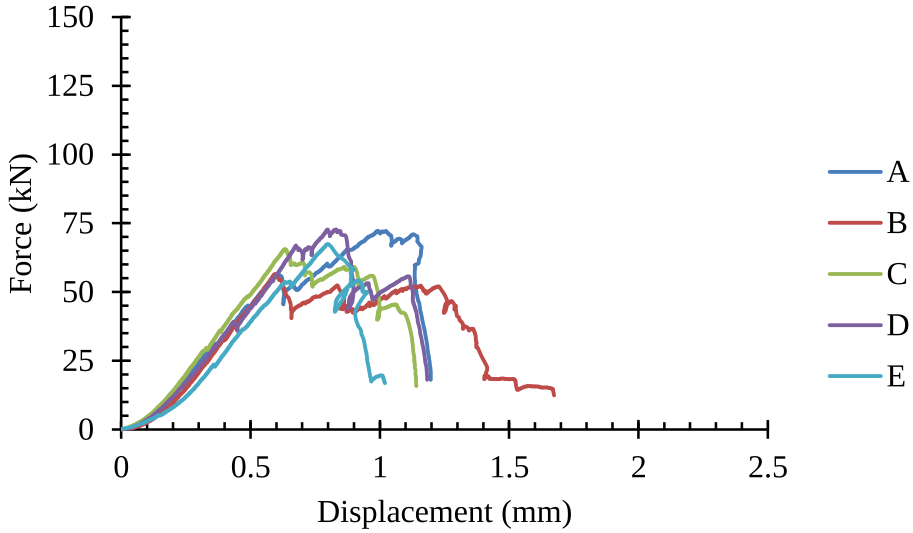

SF-0.08% (7 days)

Sample	Mass (g)	Diameter (mm)	Average Height (mm)
A	378.0	50.4	92.9
B	377.5	50.4	92.6
C	395.5	50.4	95.1
D	382.0	50.4	93.5
E	388.9	50.3	94.1

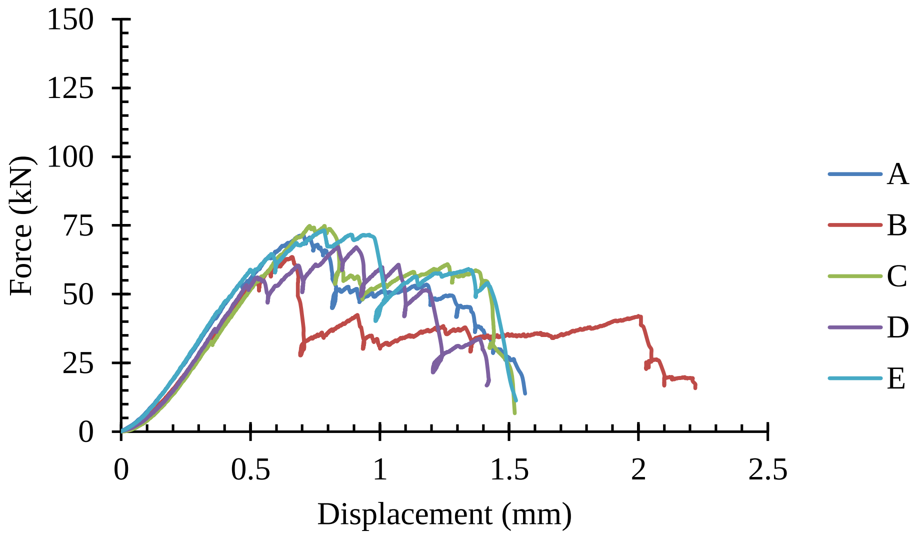

SF-0.08% (28 days)

Sample	Mass (g)	Diameter (mm)	Average Height (mm)
A	393.0	50.6	94.4
B	384.1	50.5	92.0
C	384.7	50.3	93.1
D	386.4	50.5	94.5
E	390.9	50.7	93.2

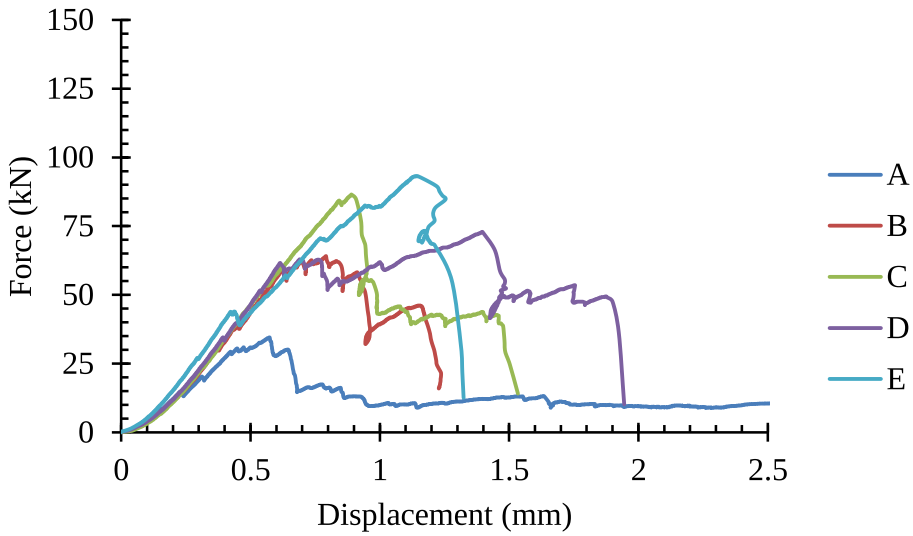

SF-0.2% (7 days)

Sample	Mass (g)	Diameter (mm)	Average Height (mm)
A	383.0	50.3	93.1
B	385.4	50.2	93.4
C	386.6	50.3	93.4
D	385.6	50.4	93.3
E	385.5	50.4	92.9

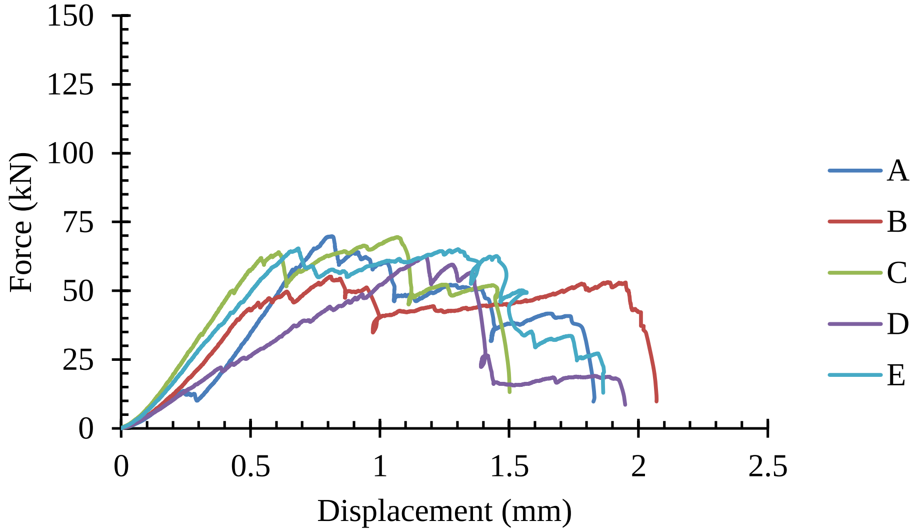

SF-0.2% (28 days)

Sample	Mass (g)	Diameter (mm)	Average Height (mm)
A	381.5	50.2	92.6
B	385.4	50.3	92.6
C	381.7	50.2	92.9
D	379.0	50.3	92.4
E	382.8	50.4	93.1

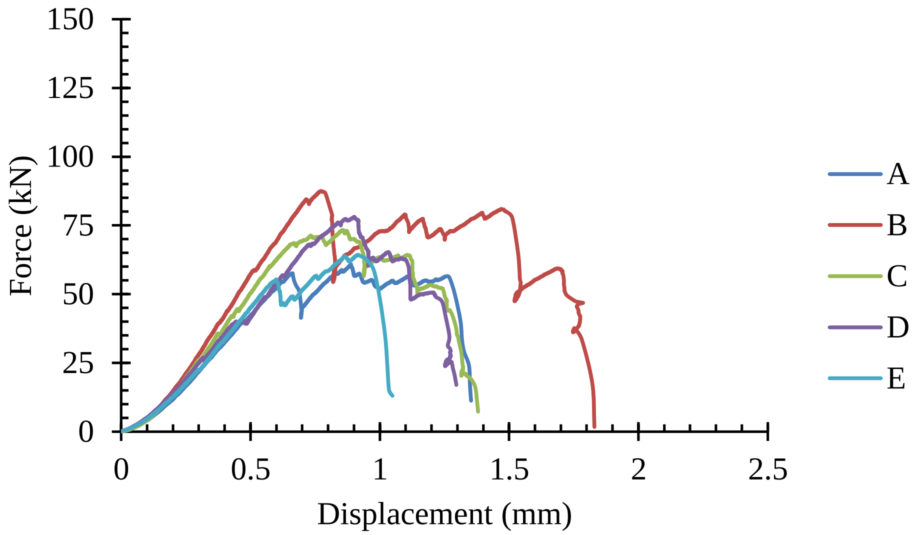

SF-0.5% (7 days)

Sample	Mass (g)	Diameter (mm)	Average Height (mm)
A	377.6	50.2	92.7
B	388.7	50.4	95.0
C	381.0	50.3	93.3
D	381.9	50.1	92.1
E	382.5	50.3	93.7

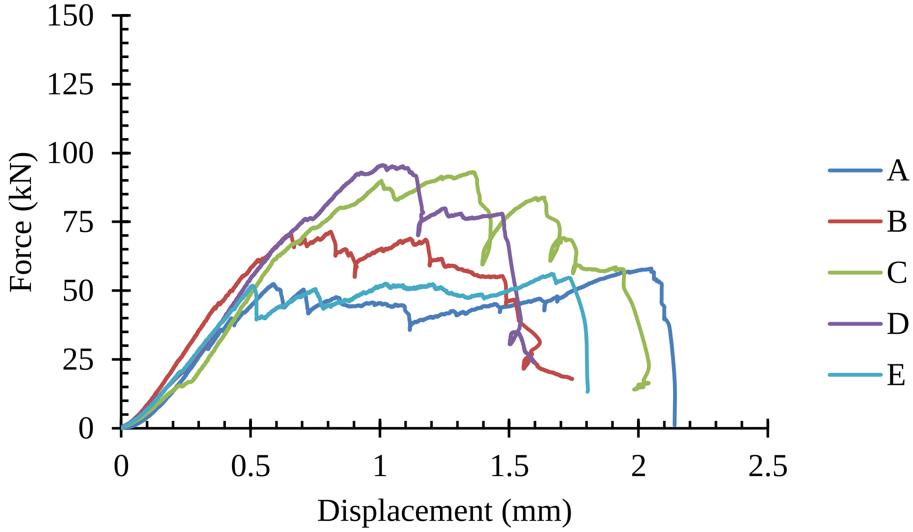

SF-0.5% (28 days)

Sample	Mass (g)	Diameter (mm)	Average Height (mm)
A	376.0	50.5	92.3
B	382.7	50.3	93.2
C	377.2	50.4	92.6
D	379.8	50.6	92.4
E	384.7	50.4	92.9

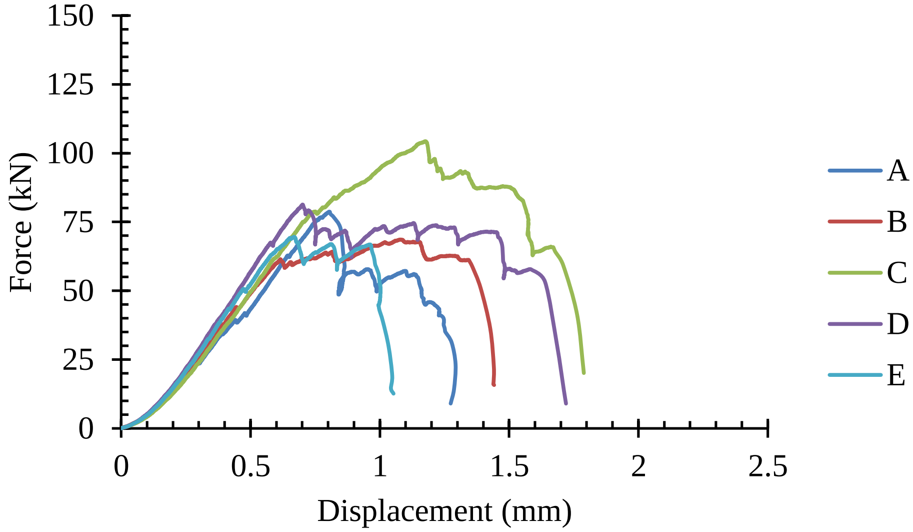

SF-1% (7 days)

Sample	Mass (g)	Diameter (mm)	Average Height (mm)
A	371.8	50.3	92.4
B	369.8	50.2	92.7
C	375.9	50.3	92.7
D	368.3	50.4	91.5
E	379.9	50.3	94.0

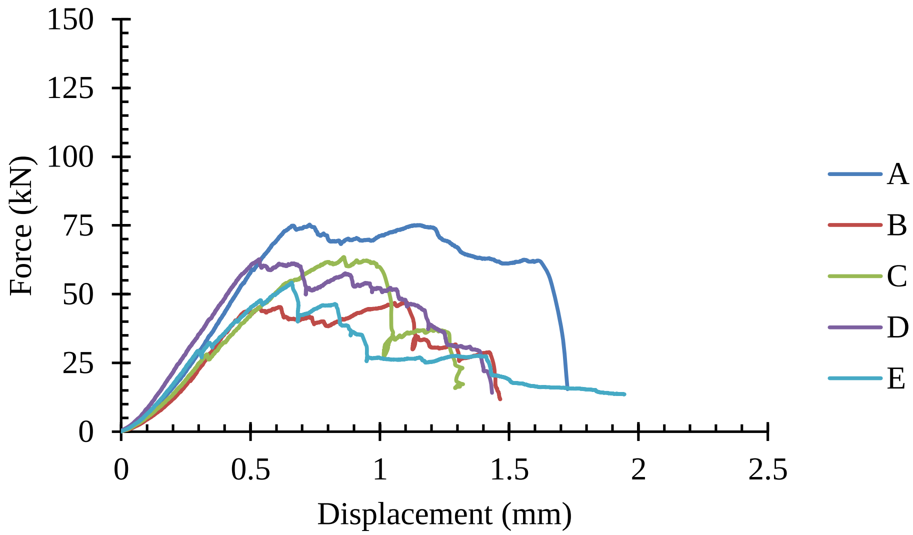

SF-1% (28 days)

Sample	Mass (g)	Diameter (mm)	Average Height (mm)
A	378.8	50.4	93.0
B	373.2	50.5	92.4
C	374.6	50.6	93.1
D	380.3	50.4	95.0
E	375.3	50.5	91.3

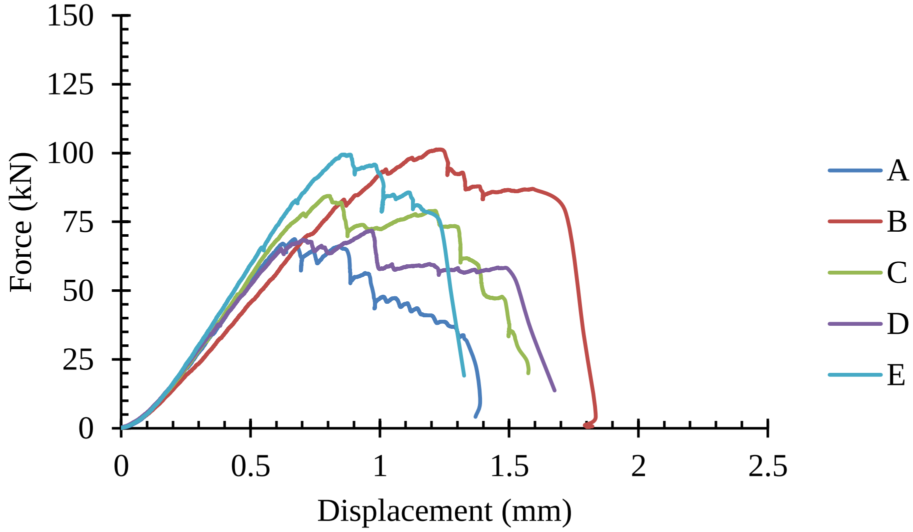

Splitting Tensile

PC-0% (7 days)

Sample	Mass (g)	Diameter (mm)	Average Height (mm)
A	420.4	50.6	99.4
B	416.1	50.6	98.8
C	403.1	50.6	96.2
D	416.2	50.5	98.8
E	406.1	50.6	103.0

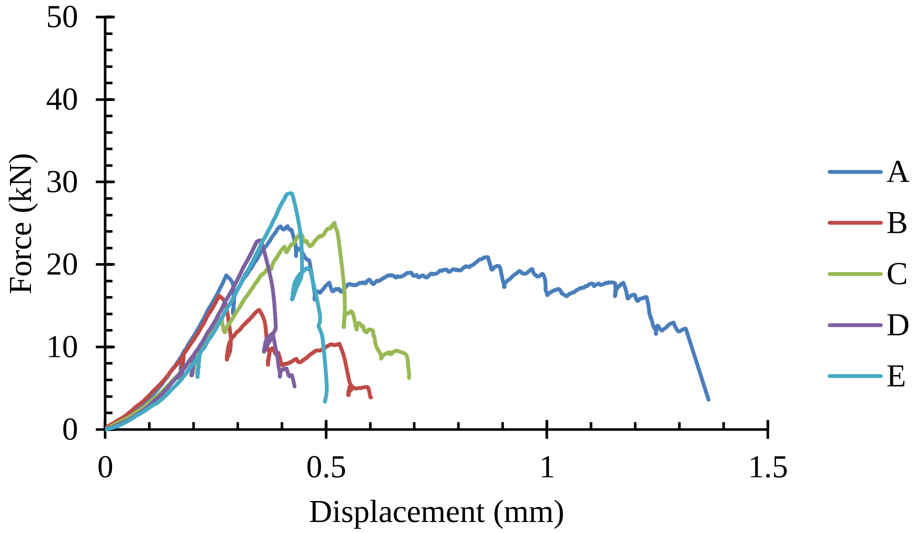

PC-0% (28 days)

Sample	Mass (g)	Diameter (mm)	Average Height (mm)
A	395.0	50.5	92.6
B	413.7	50.6	97.7
C	405.3	50.5	95.5
D	388.0	50.5	91.8
E	415.3	50.6	98.8

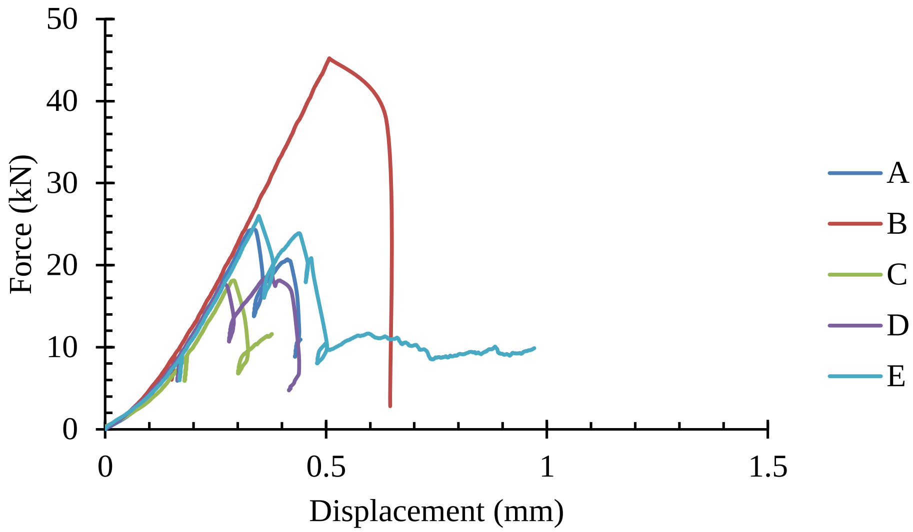

PC-0.02% (7 days)

Sample	Mass (g)	Diameter (mm)	Average Height (mm)
A	399.4	50.7	94.1
B	419.9	50.7	99.1
C	411.4	50.7	98.0
D	403.0	50.6	94.9
E	410.4	50.7	96.9

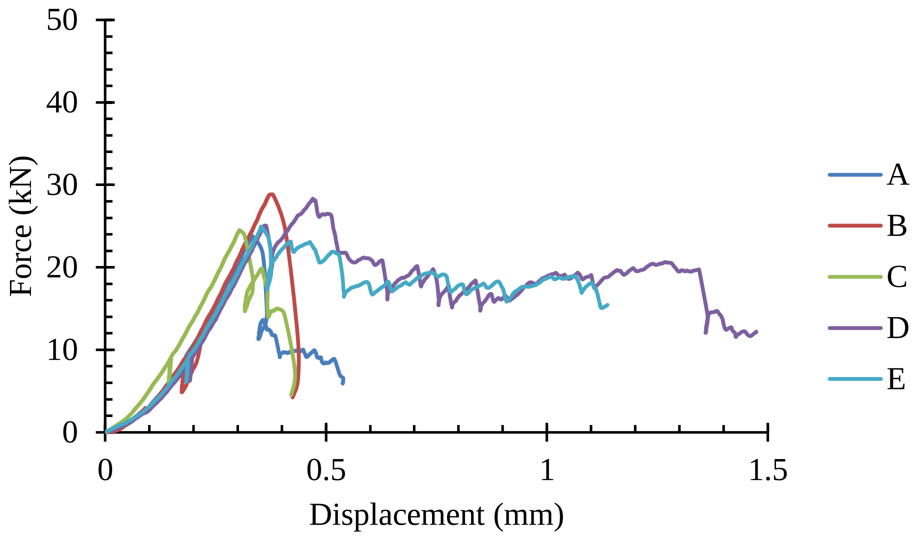

PC-0.02% (28 days)

Sample	Mass (g)	Diameter (mm)	Average Height (mm)
A	407.4	50.7	96.2
B	415.2	50.5	97.9
C	399.4	50.6	93.8
D	402.9	50.5	95.7
E	396.6	50.5	93.8

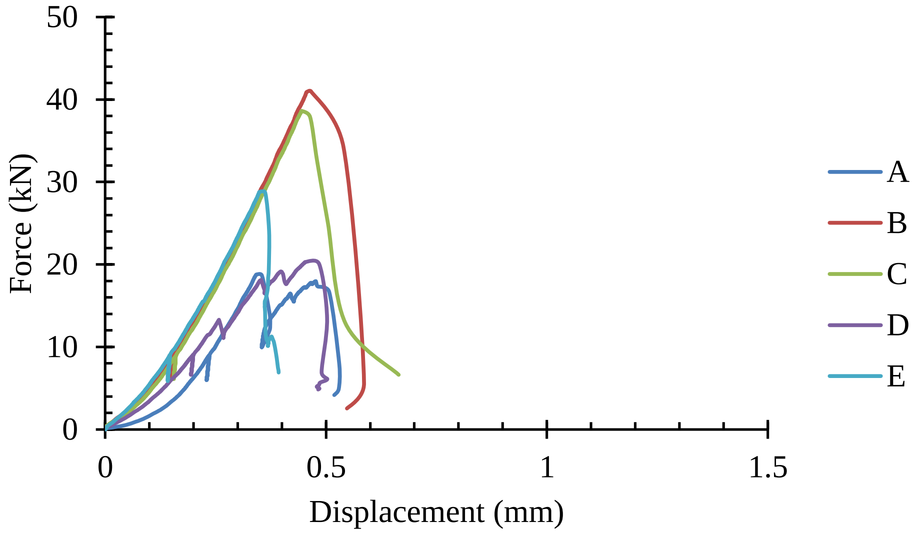

PC-0.08% (7 days)

Sample	Mass (g)	Diameter (mm)	Average Height (mm)
A	418.2	50.7	98.0
B	418.8	50.7	98.4
C	402.3	50.7	94.8
D	427.5	50.5	100.8
E	407.8	50.7	96.0

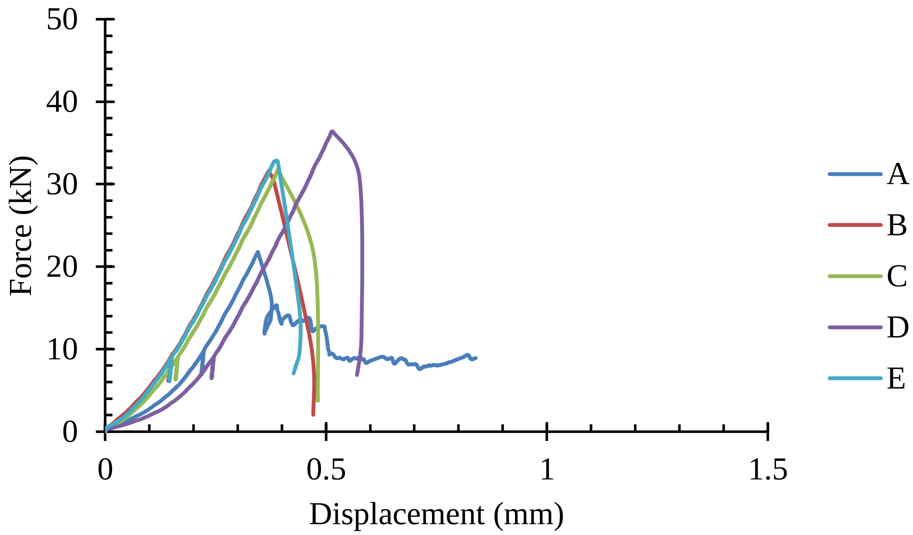

PC-0.08% (28 days)

Sample	Mass (g)	Diameter (mm)	Average Height (mm)
A	413.8	50.6	97.5
B	424.9	50.6	99.6
C	403.7	50.6	95.3
D	419.8	50.6	98.8
E	414.2	50.5	97.5

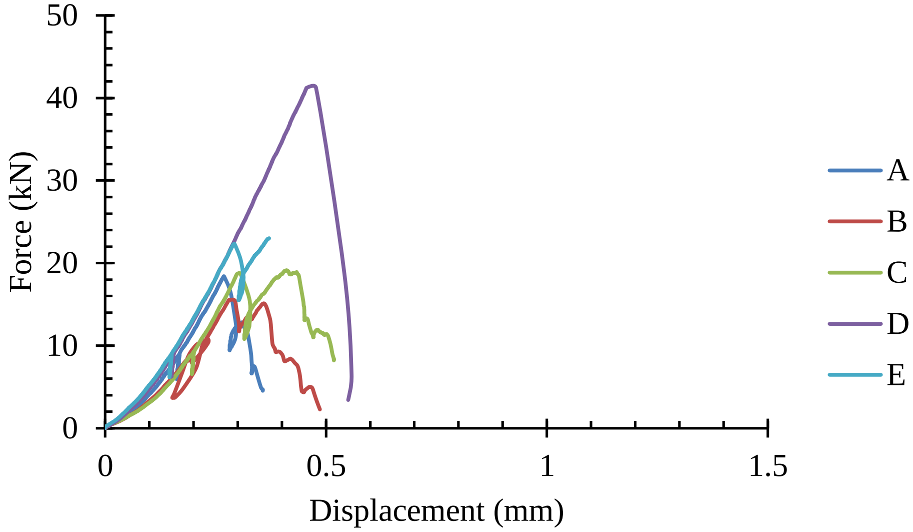

PC-0.2% (7 days)

Sample	Mass (g)	Diameter (mm)	Average Height (mm)
A	403.6	50.7	93.8
B	412.9	50.7	96.9
C	413.6	50.5	96.9
D	404.4	50.8	95.4
E	423.4	50.7	98.9

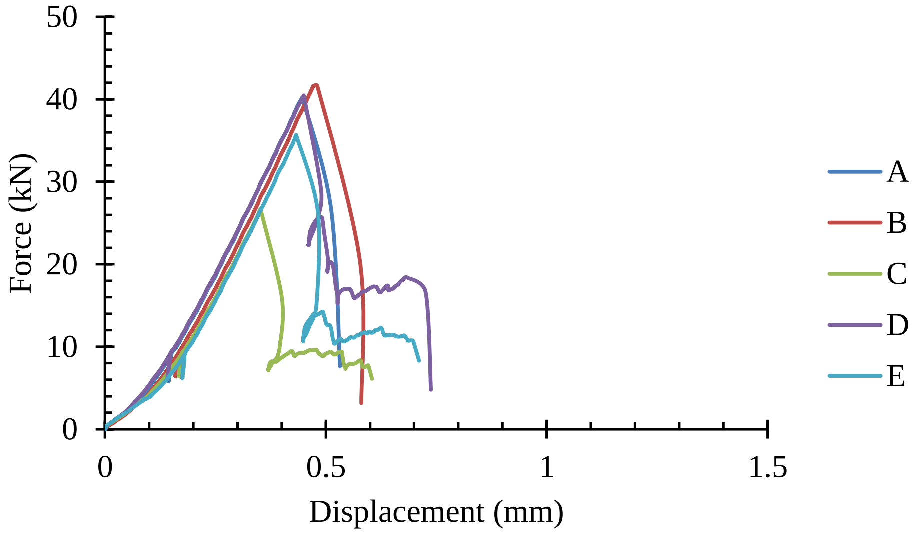

PC-0.2% (28 days)

Sample	Mass (g)	Diameter (mm)	Average Height (mm)
A	416.5	50.6	98.9
B	422.0	50.7	99.5
C	418.3	50.6	98.3
D	407.8	50.6	96.8
E	410.5	50.6	96.6

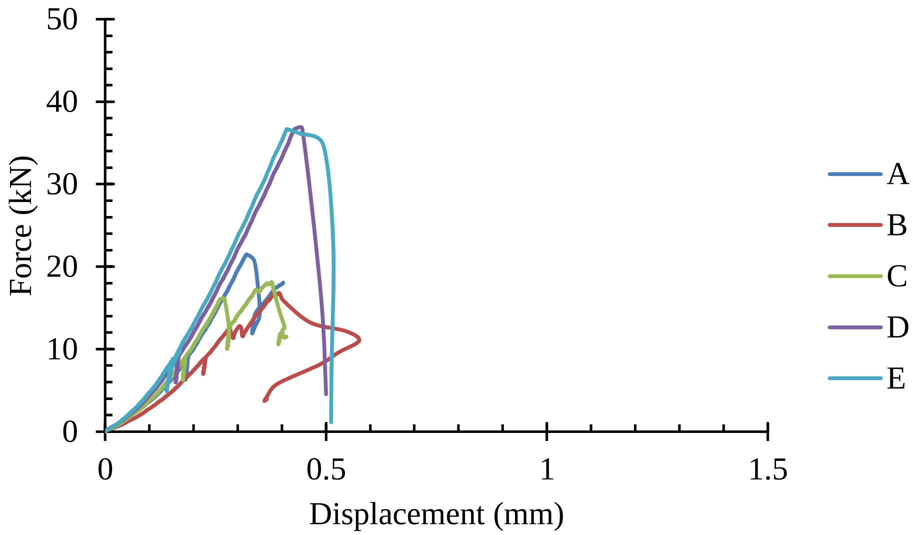

PC-0.5% (7 days)

Sample	Mass (g)	Diameter (mm)	Average Height (mm)
A	414.1	50.6	98.1
B	423.0	50.5	99.5
C	415.7	50.5	98.5
D	412.0	50.6	97.8
E	409.3	50.6	96.6

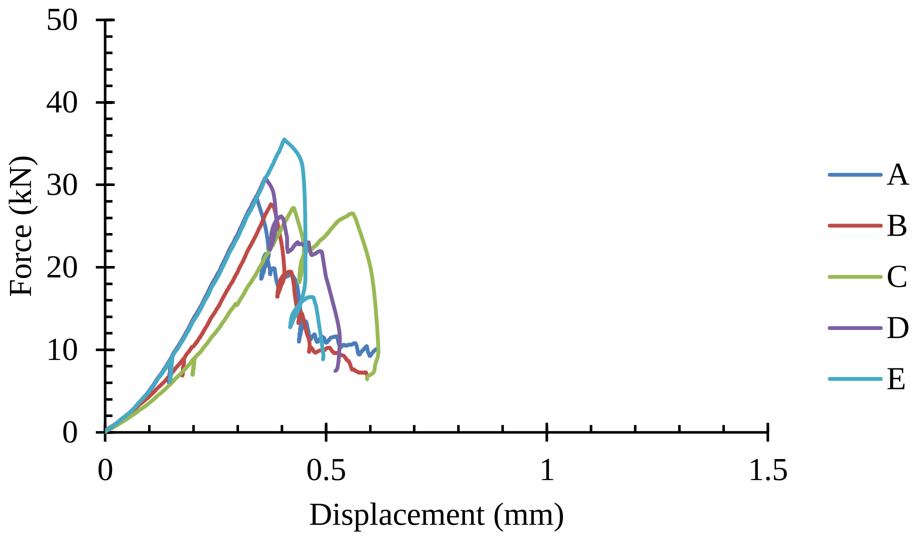

PC-0.5% (28 days)

Sample	Mass (g)	Diameter (mm)	Average Height (mm)
A	410.5	50.5	97.9
B	410.9	50.6	96.0
C	420.3	50.4	99.9
D	413.5	50.6	99.2
E	408.7	50.4	98.6

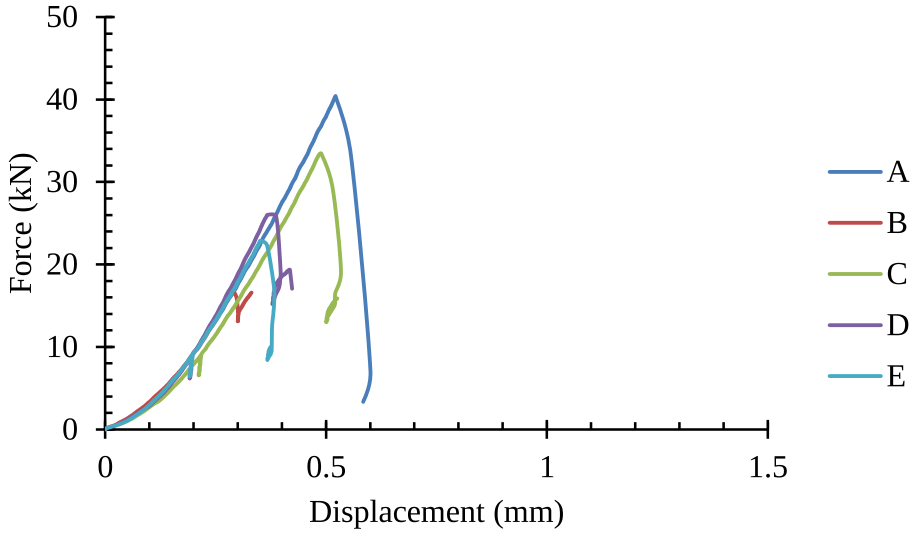

PC-1% (7 days)

Sample	Mass (g)	Diameter (mm)	Average Height (mm)
A	394.3	50.4	99.5
B	394.0	50.3	97.3
C	397.2	50.4	99.3
D	403.5	50.4	100.3
E	394.7	50.5	98.7

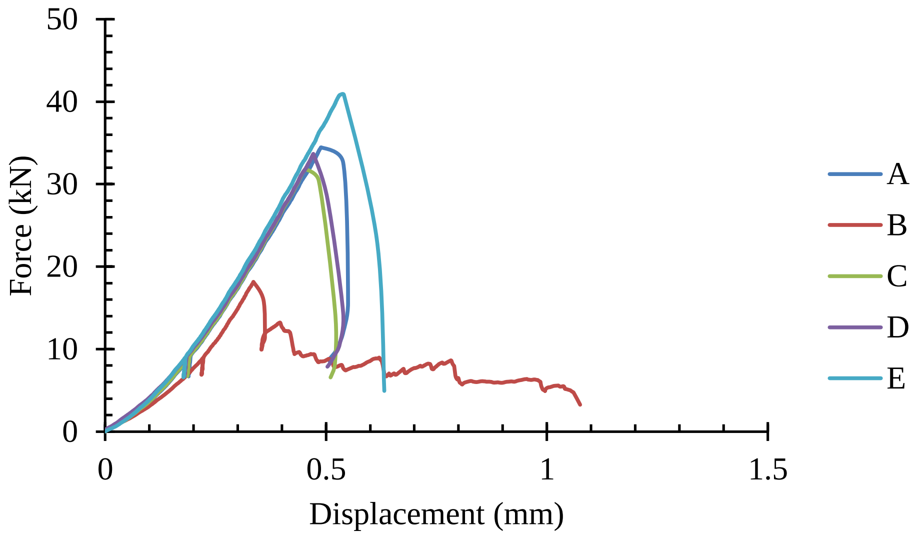

PC-1% (28 days)

Sample	Mass (g)	Diameter (mm)	Average Height (mm)
A	402.1	50.5	99.8
B	406.6	50.6	101.0
C	392.1	50.4	97.9
D	399.6	50.5	98.6
E	396.5	50.6	97.6

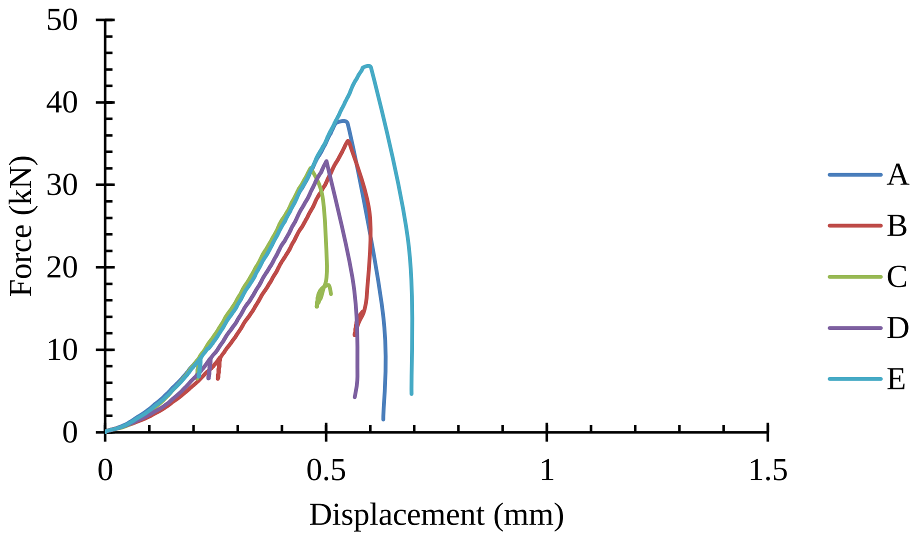

SF-0% (7 days)

Sample	Mass (g)	Diameter (mm)	Average Height (mm)
A	397.2	50.4	97.2
B	415.0	50.4	100.9
C	400.3	50.2	98.8
D	379.6	50.4	92.4
E	400.7	50.3	99.2

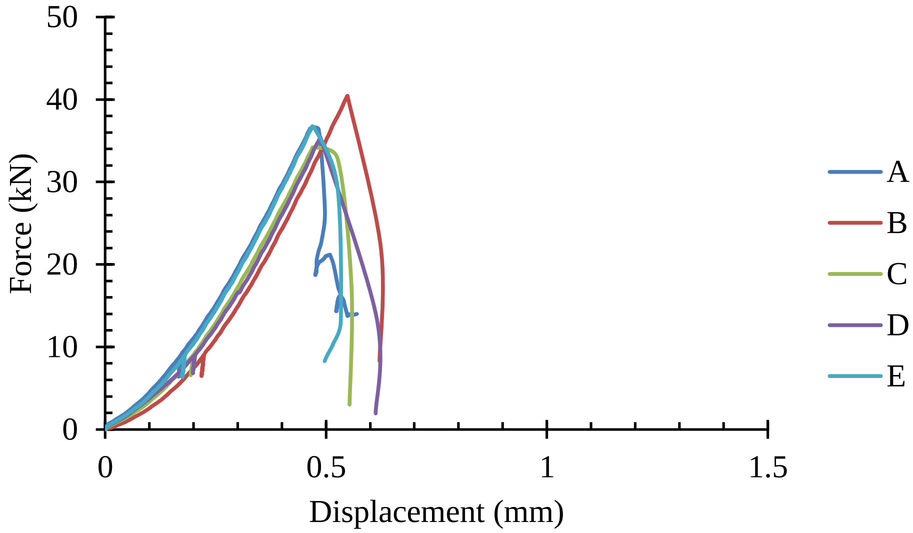

SF-0% (28 days)

Sample	Mass (g)	Diameter (mm)	Average Height (mm)
A	393.8	50.3	96.5
B	400.4	50.4	98.5
C	392.7	50.6	97.7
D	401.7	50.4	98.5
E	395.4	50.4	97.1

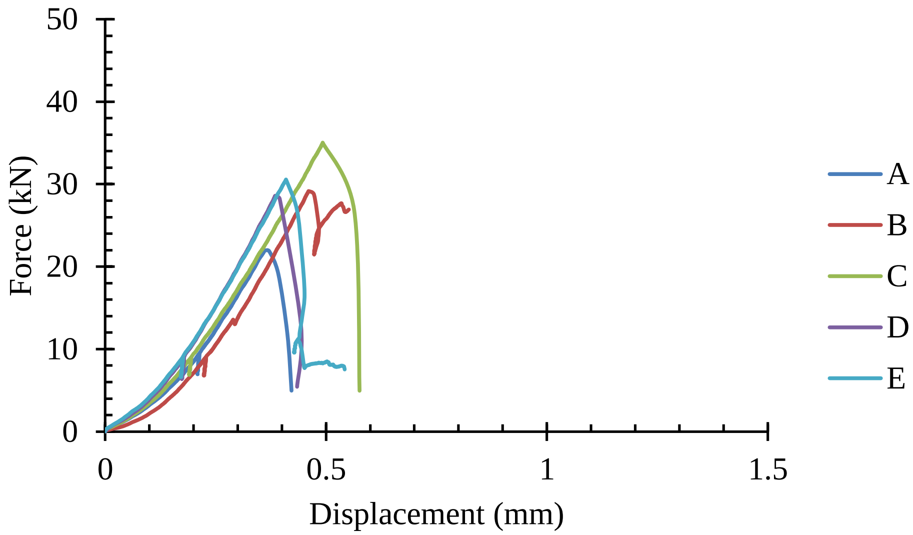

SF-0.02% (7 days)

Sample	Mass (g)	Diameter (mm)	Average Height (mm)
A	387.7	50.5	95.5
B	390.2	50.6	96.1
C	395.3	50.2	96.9
D	390.6	50.4	96.3
E	402.2	50.3	98.7

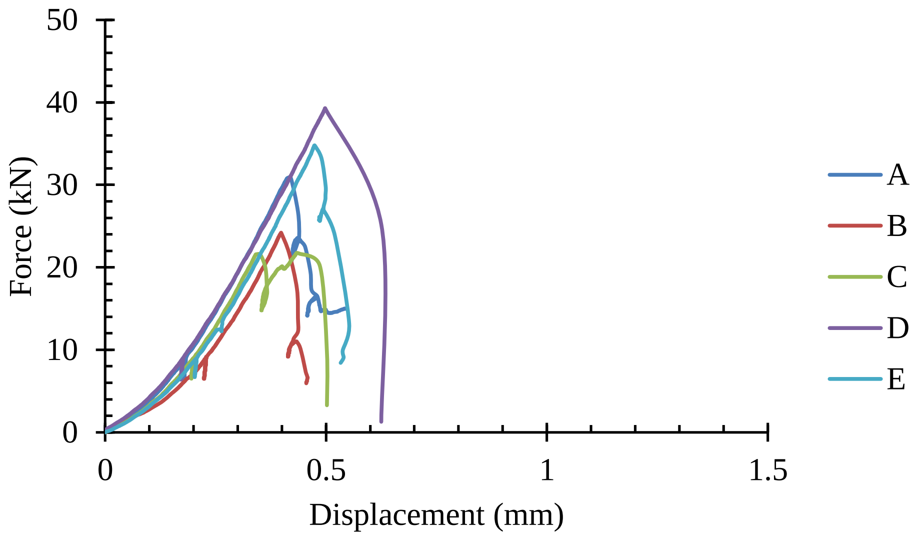

SF-0.02% (28 days)

Sample	Mass (g)	Diameter (mm)	Average Height (mm)
A	386.3	50.4	95.3
B	395.1	50.5	97.3
C	398.8	50.5	97.2
D	390.3	50.5	96.1
E	398.8	50.4	97.3

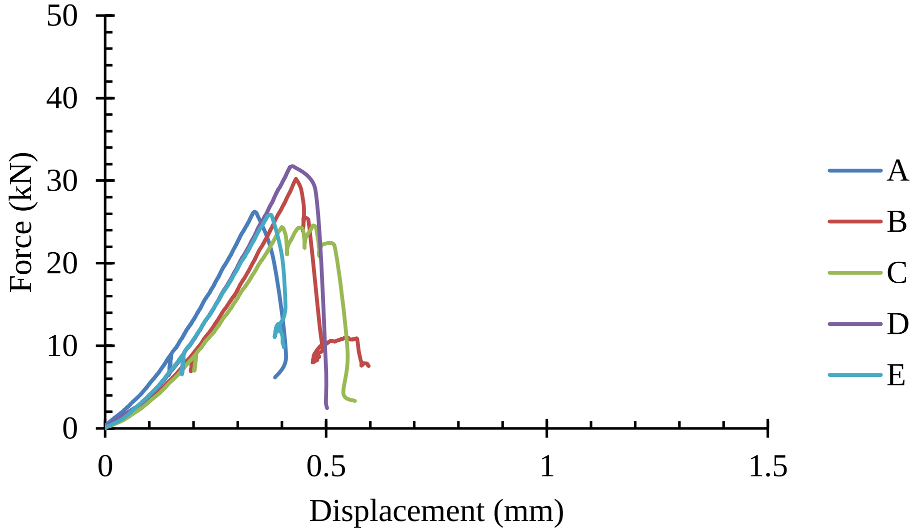

SF-0.08% (7 days)

Sample	Mass (g)	Diameter (mm)	Average Height (mm)
A	401.3	50.3	99.1
B	399.1	50.3	97.4
C	392.0	50.4	97.9
D	406.6	50.3	101.1
E	393.2	50.4	95.8

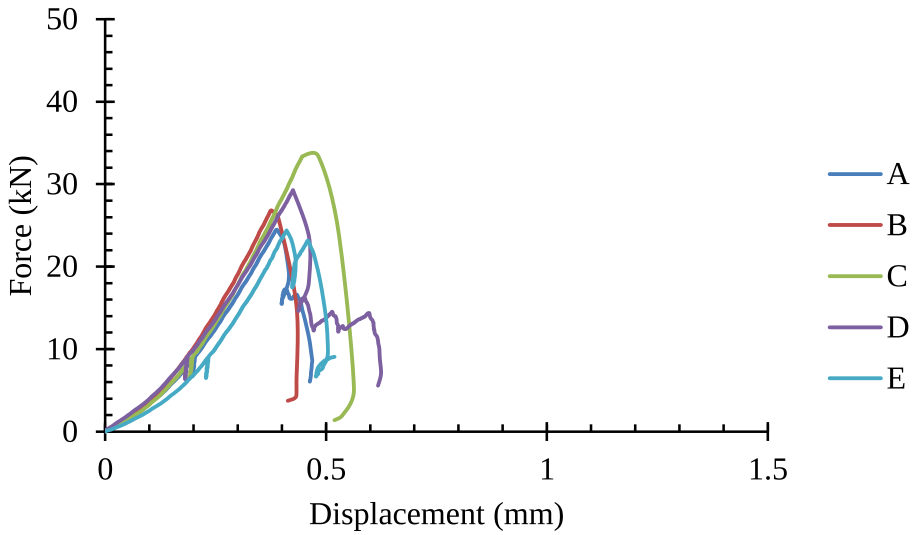

SF-0.08% (28 days)

Sample	Mass (g)	Diameter (mm)	Average Height (mm)
A	392.2	50.6	96.5
B	392.6	50.1	96.2
C	401.7	50.5	99.5
D	384.0	50.4	96.1
E	389.9	50.5	97.2

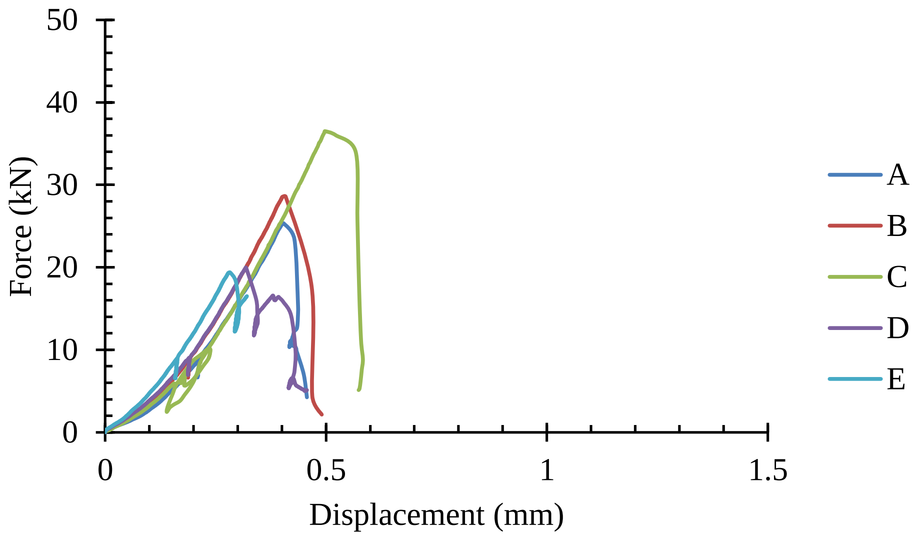

SF-0.2% (7 days)

Sample	Mass (g)	Diameter (mm)	Average Height (mm)
A	399.9	50.6	97.9
B	401.6	50.2	98.0
C	411.4	50.5	98.8
D	400.1	50.4	98.2
E	400.1	50.5	97.6

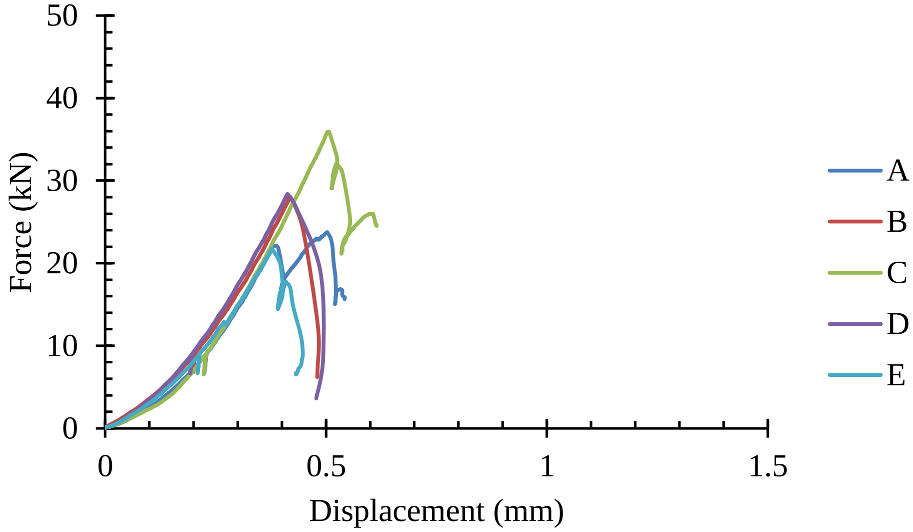

SF-0.2% (28 days)

Sample	Mass (g)	Diameter (mm)	Average Height (mm)
A	417.5	50.4	102.2
B	396.7	50.4	97.3
C	410.6	50.5	99.5
D	410.7	50.4	99.9
E	404.0	50.5	98.8

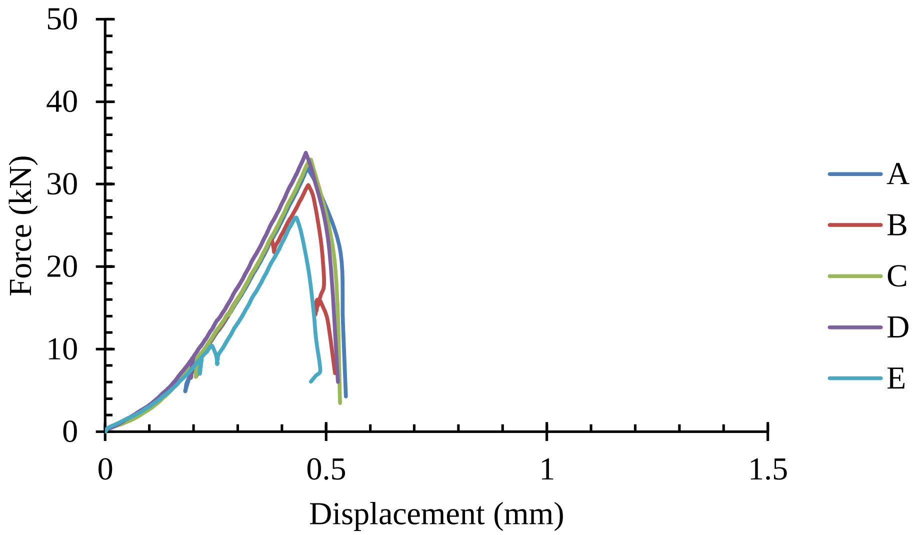

SF-0.5% (7 days)

Sample	Mass (g)	Diameter (mm)	Average Height (mm)
A	397.3	50.6	99.0
B	409.8	50.3	99.8
C	407.6	50.2	100.2
D	404.6	50.5	100.0
E	400.3	50.5	98.0

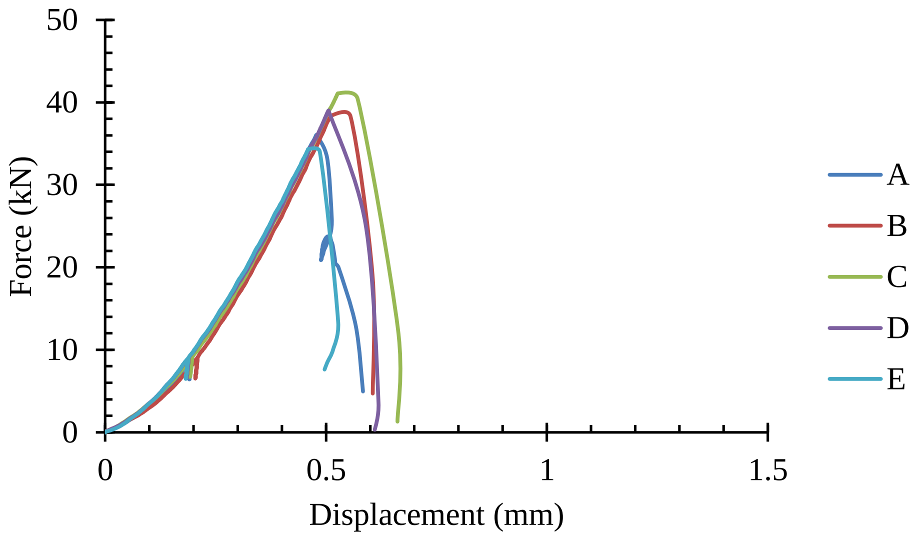

SF-0.5% (28 days)

Sample	Mass (g)	Diameter (mm)	Average Height (mm)
A	403.0	50.5	99.2
B	411.6	50.5	100.2
C	397.0	50.5	98.7
D	400.2	50.7	98.8
E	399.3	50.5	98.3

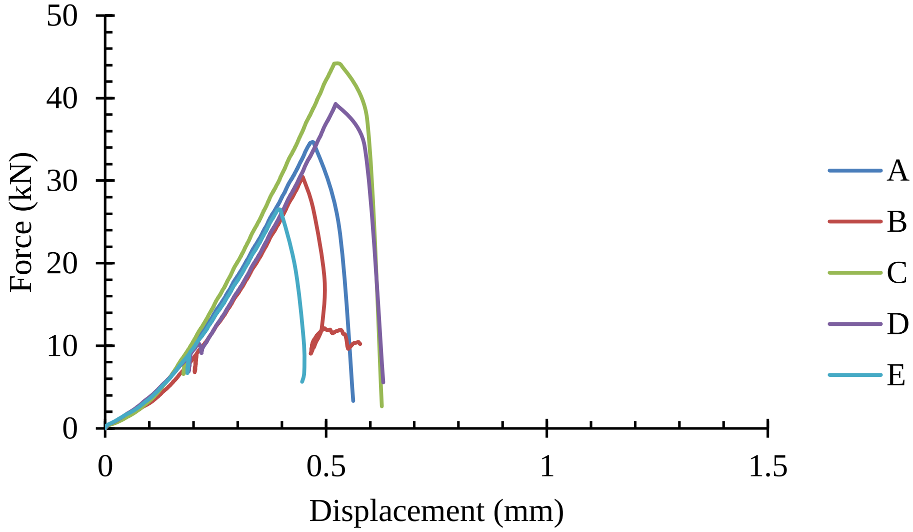

SF-1% (7 days)

Sample	Mass (g)	Diameter (mm)	Average Height (mm)
A	393.4	50.4	98.4
B	397.6	50.5	97.2
C	392.2	50.3	97.8
D	387.1	50.4	97.4
E	401.0	50.6	99.5

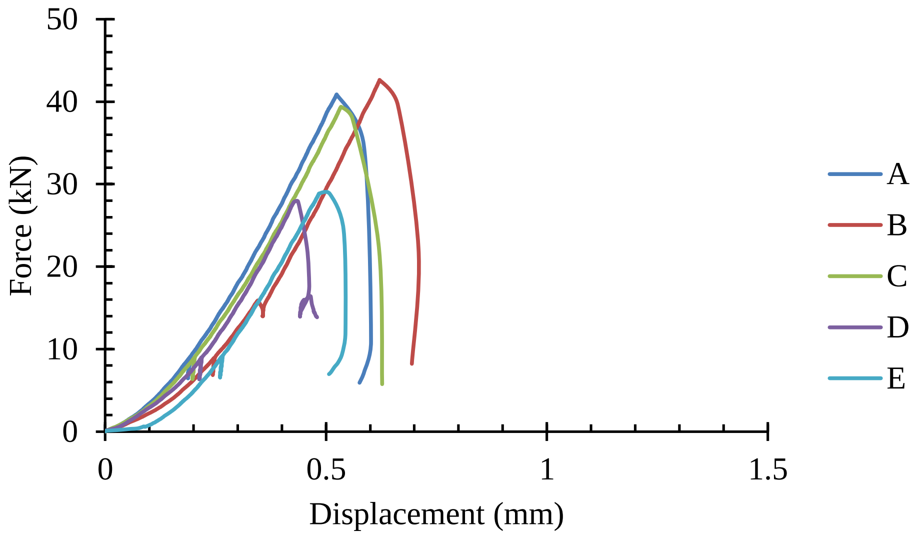

SF-1% (28 days)

Sample	Mass (g)	Diameter (mm)	Average Height (mm)
A	382.8	50.5	95.0
B	397.2	50.4	97.5
C	404.0	50.5	100.3
D	389.3	50.5	97.7
E	390.6	50.5	97.9

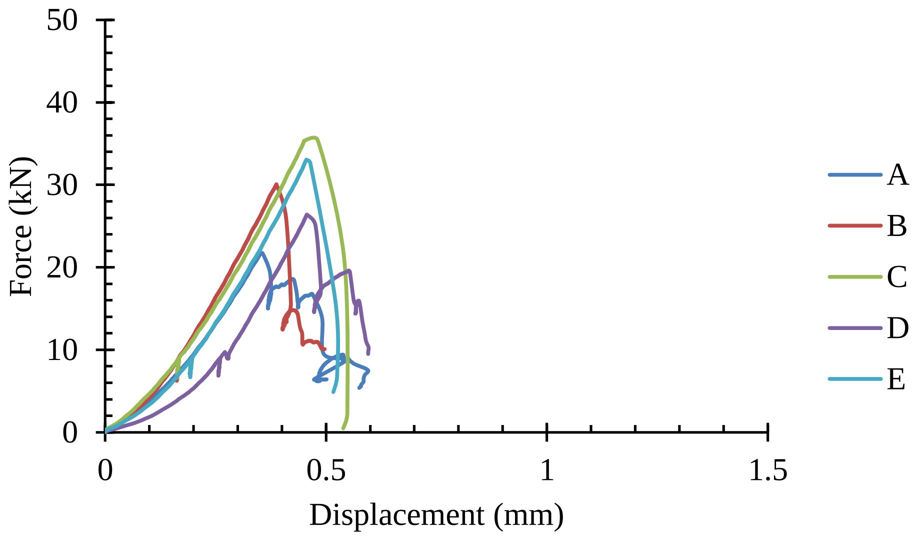

Flexural
Beam length: *ca.* 114.3 mm.
Beam span: 76.2 mm.

PC-0% (7 days)

Sample	Mass (g)	Average Height (mm)	Average Width (mm)
A	138.9	23.6	24.1
B	133.4	23.4	24.0
C	136.3	23.3	24.2
D	135.9	23.1	24.4
E	135.9	23.0	24.5
F	139.1	22.9	24.8

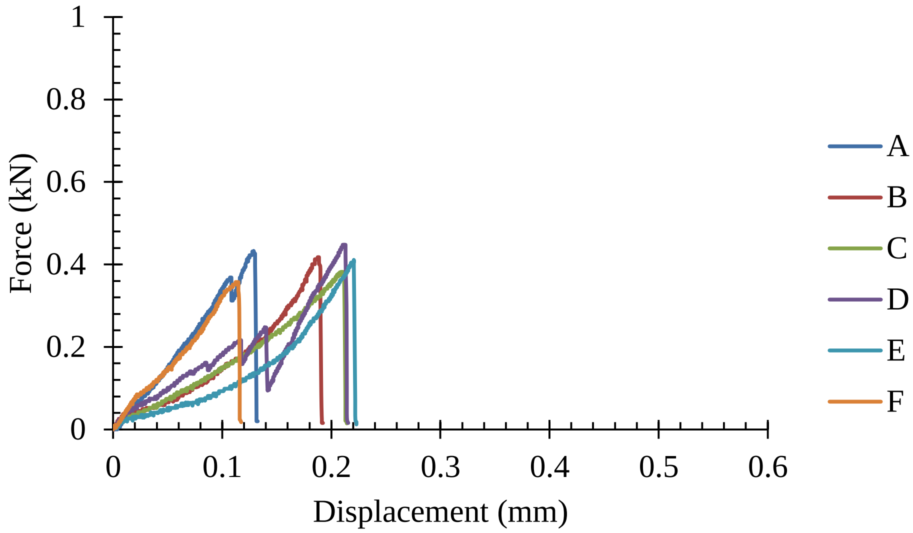

PC-0% (28 days)

Sample	Mass (g)	Average Height (mm)	Average Width (mm)
A	144.3	24.9	24.5
B	145.0	24.9	24.5
C	145.3	25.1	24.4
D	145.6	25.3	24.3
E	147.3	25.4	24.3
F	152.5	25.5	24.5

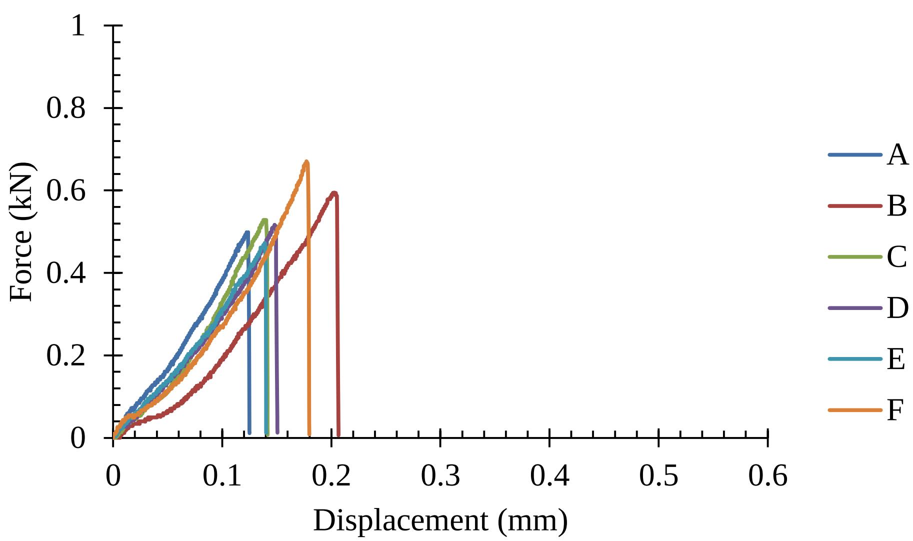

PC-0.02% (7 days)

Sample	Mass (g)	Average Height (mm)	Average Width (mm)
A	147.4	25.1	24.6
B	145.7	25.1	24.6
C	148.9	25.1	24.5
D	148.6	25.1	24.4
E	149.9	25.3	24.4
F	155.8	25.4	24.4

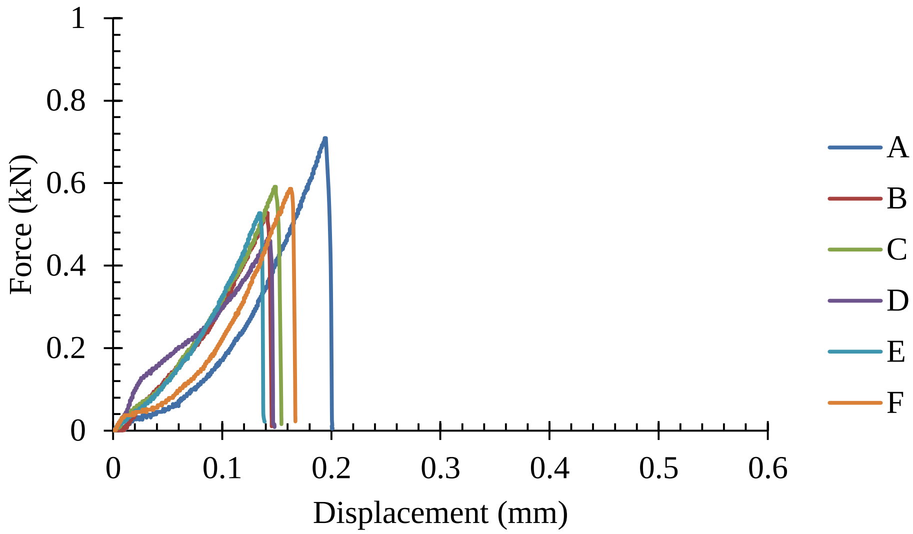

PC-0.02% (28 days)

Sample	Mass (g)	Average Height (mm)	Average Width (mm)
A	145.6	25.0	24.4
B	145.8	25.1	24.6
C	147.2	25.0	24.8
D	144.8	24.6	25.0
E	144.2	24.7	25.0
F	151.7	24.7	25.1

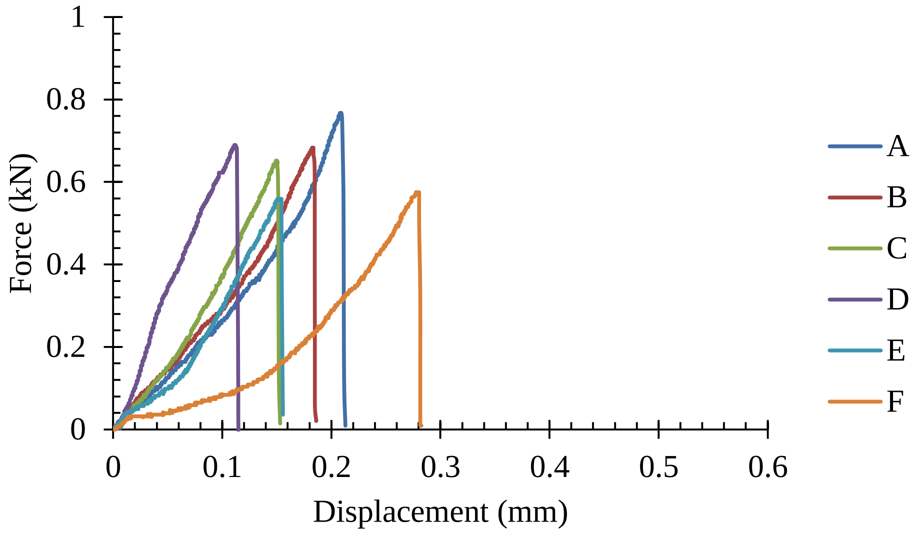

PC-0.08% (7 days)

Sample	Mass (g)	Average Height (mm)	Average Width (mm)
A	143.6	24.9	24.7
B	145.2	24.9	24.6
C	146.6	25.0	24.6
D	146.1	25.1	24.5
E	146.3	25.2	24.4
F	152.3	25.4	24.4

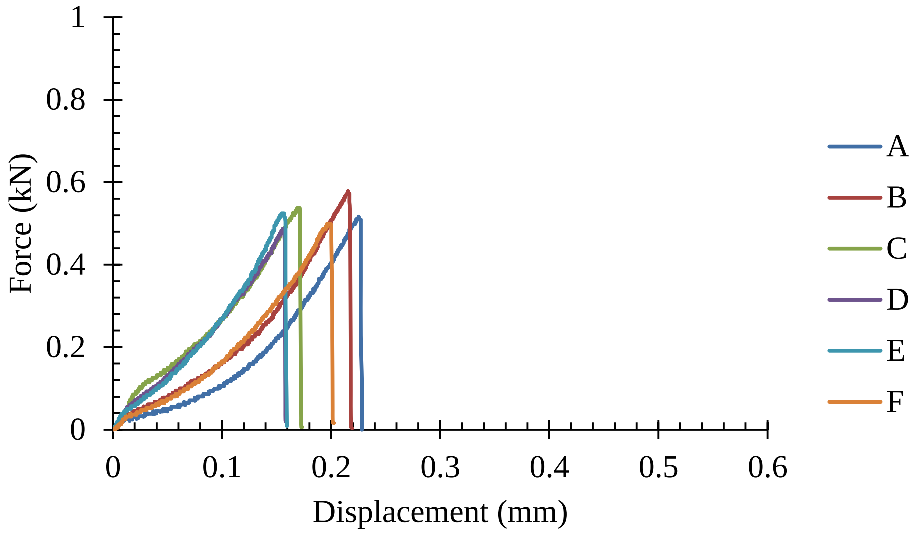

PC-0.08% (28 days)

Sample	Mass (g)	Average Height (mm)	Average Width (mm)
A	142.7	24.6	24.4
B	144.6	24.5	24.5
C	147.4	24.6	24.8
D	147.7	24.5	25.0
E	145.7	24.4	25.0
F	150.8	24.3	25.0

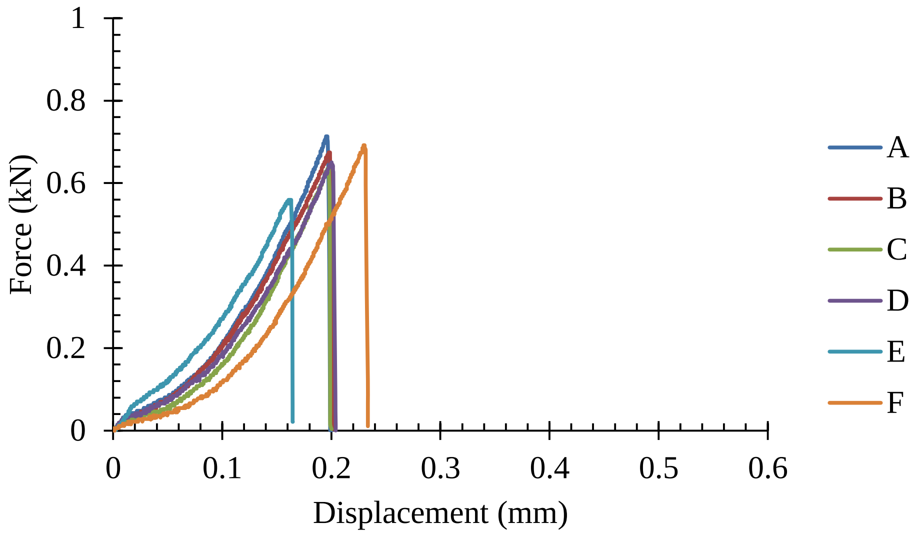

PC-0.2% (7 days)

Sample	Mass (g)	Average Height (mm)	Average Width (mm)
A	145.7	24.7	25.1
B	148.0	24.7	25.1
C	146.8	24.6	25.1
D	148.7	24.6	25.3
E	148.0	24.5	25.3
F	153.7	24.5	25.5

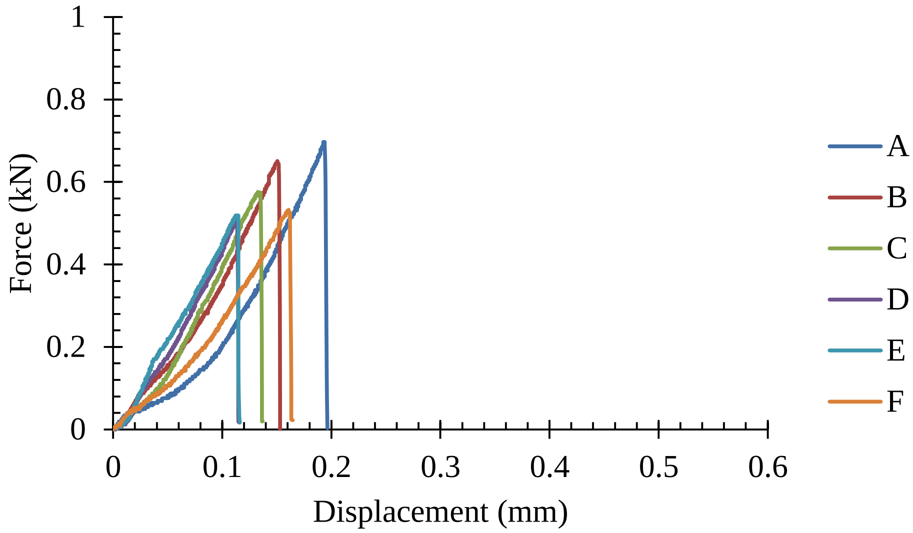

PC-0.2% (28 days)

Sample	Mass (g)	Average Height (mm)	Average Width (mm)
A	142.6	24.7	24.3
B	142.3	24.8	24.6
C	144.6	24.6	24.8
D	143.1	24.4	25.0
E	146.0	24.3	25.1
F	148.8	24.2	25.1

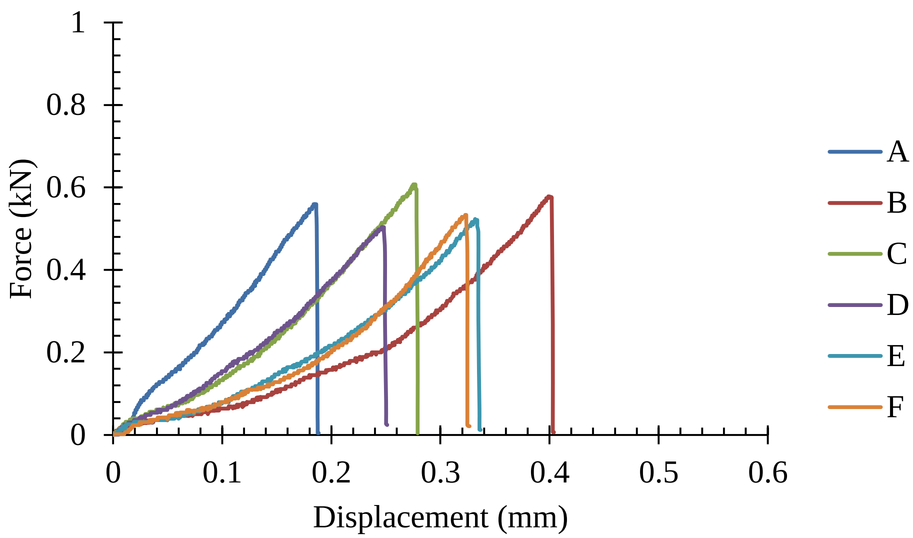

PC-0.5% (7 days)

Sample	Mass (g)	Average Height (mm)	Average Width (mm)
A	149.5	25.6	24.3
B	148.9	25.5	24.4
C	148.5	25.3	24.7
D	149.5	25.0	25.0
E	149.6	25.0	25.1
F	152.7	25.3	25.1

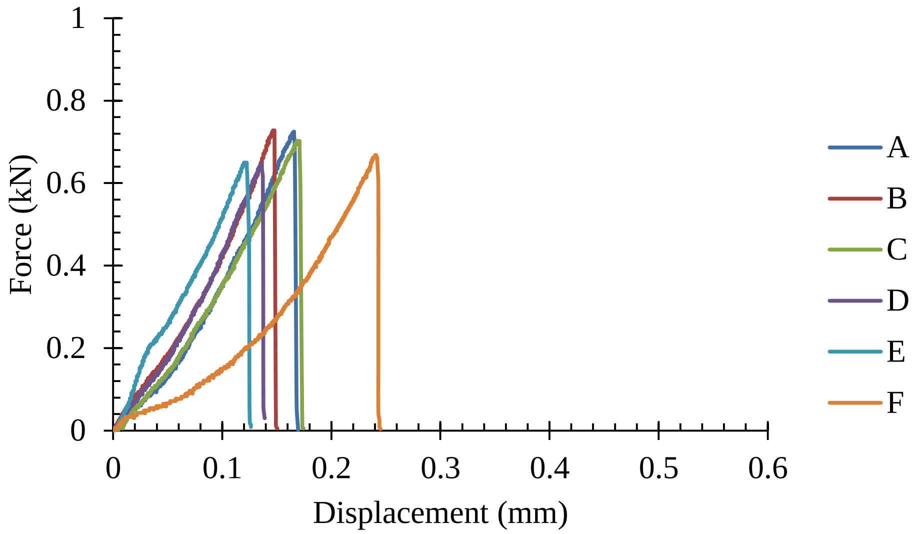

PC-0.5% (28 days)

Sample	Mass (g)	Average Height (mm)	Average Width (mm)
A	149.9	25.3	25.0
B	150.1	25.3	24.7
C	151.5	25.7	24.6
D	151.0	25.6	24.5
E	151.5	26.0	24.5
F	154.8	26.4	24.6

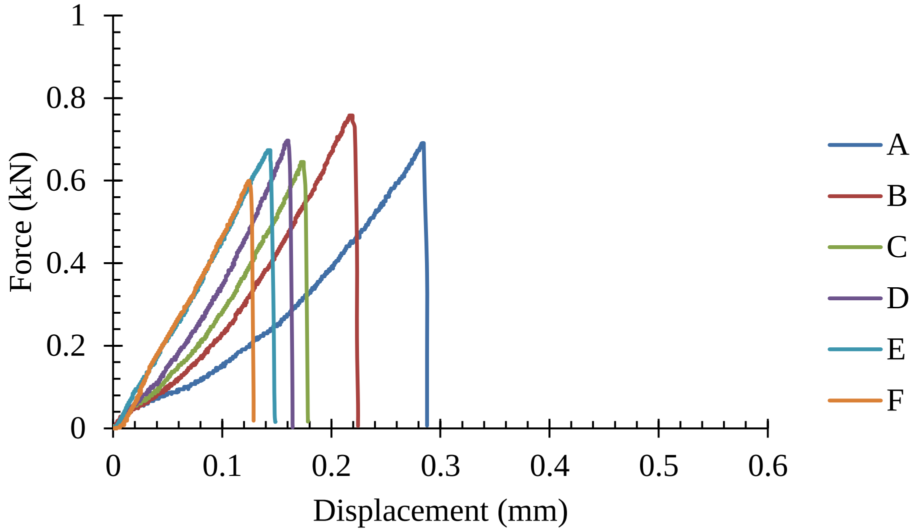

PC-1% (7 days)

Sample	Mass (g)	Average Height (mm)	Average Width (mm)
A	145.4	25.2	24.5
B	142.0	24.8	24.3
C	141.1	24.6	24.3
D	141.9	24.3	24.5
E	141.3	24.3	24.7
F	153.1	24.4	24.7

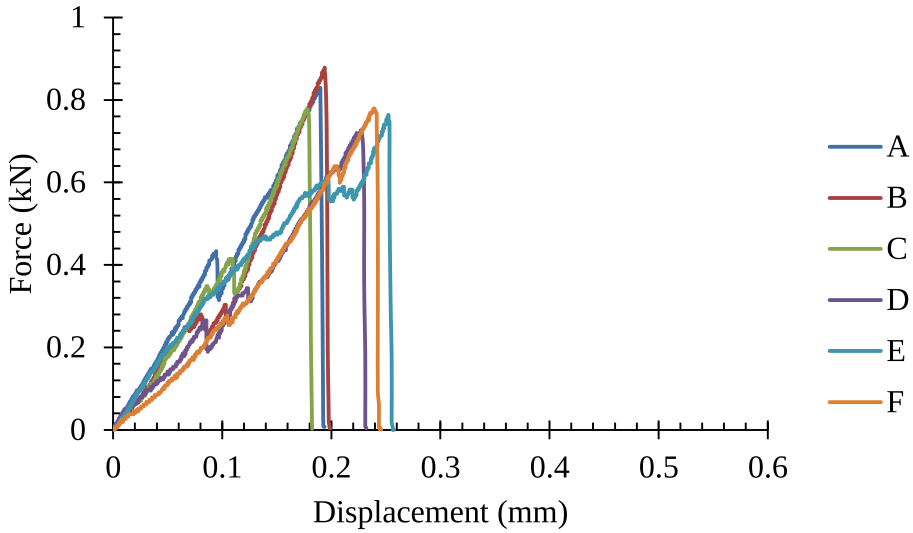

PC-1% (28 days)

Sample	Mass (g)	Average Height (mm)	Average Width (mm)
A	148.0	25.2	24.7
B	147.2	25.0	24.8
C	148.3	25.4	24.8
D	148.2	25.3	24.7
E	150.2	25.5	24.6
F	155.1	25.8	24.5

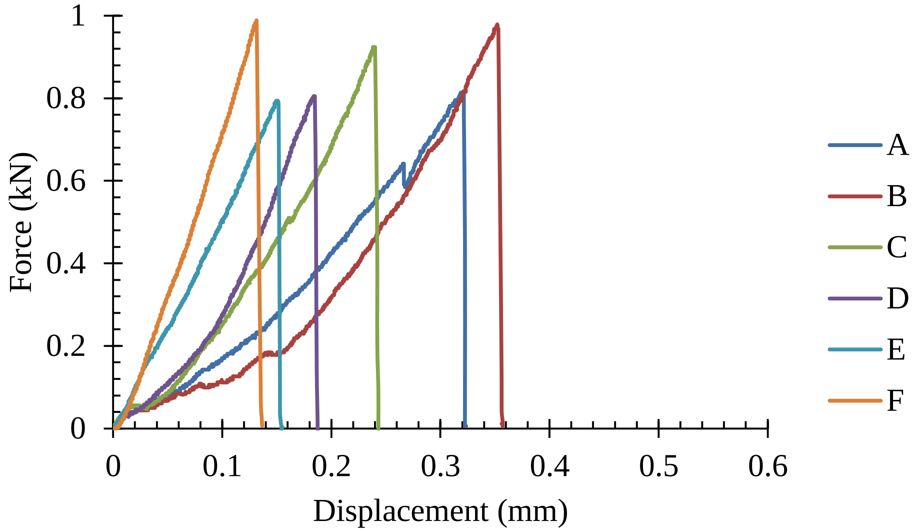

SF-0% (7 days)

Sample	Mass (g)	Average Height (mm)	Average Width (mm)
A	139.8	25.5	24.2
B	133.5	25.0	23.9
C	130.4	24.8	24.0
D	135.2	24.6	24.2
E	137.6	24.8	24.4
F	146.1	25.1	24.7

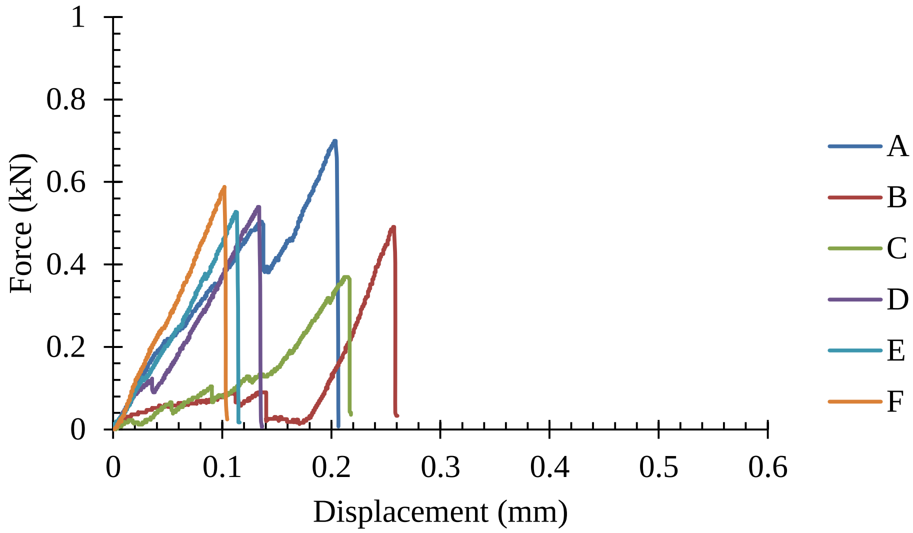

SF-0% (28 days)

Sample	Mass (g)	Average Height (mm)	Average Width (mm)
A	132.3	24.3	24.2
B	127.3	24.2	24.3
C	131.1	24.0	24.4
D	132.9	23.9	24.6
E	132.3	23.9	24.7
F	136.3	23.7	24.8

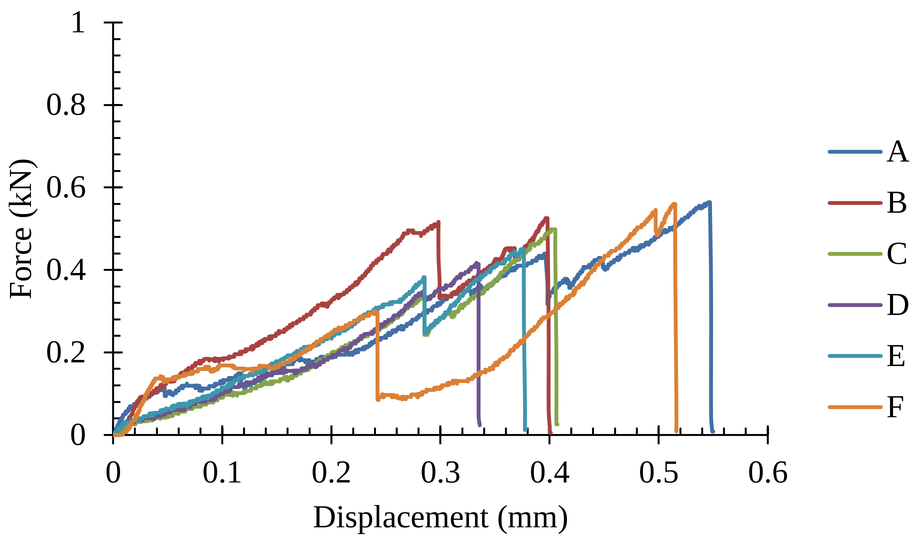

SF-0.02% (7 days)

Sample	Mass (g)	Average Height (mm)	Average Width (mm)
A	144.8	26.2	24.4
B	139.9	26.1	24.4
C	144.2	25.9	24.3
D	144.8	25.6	24.6
E	139.9	25.4	24.7
F	149.7	25.3	24.7

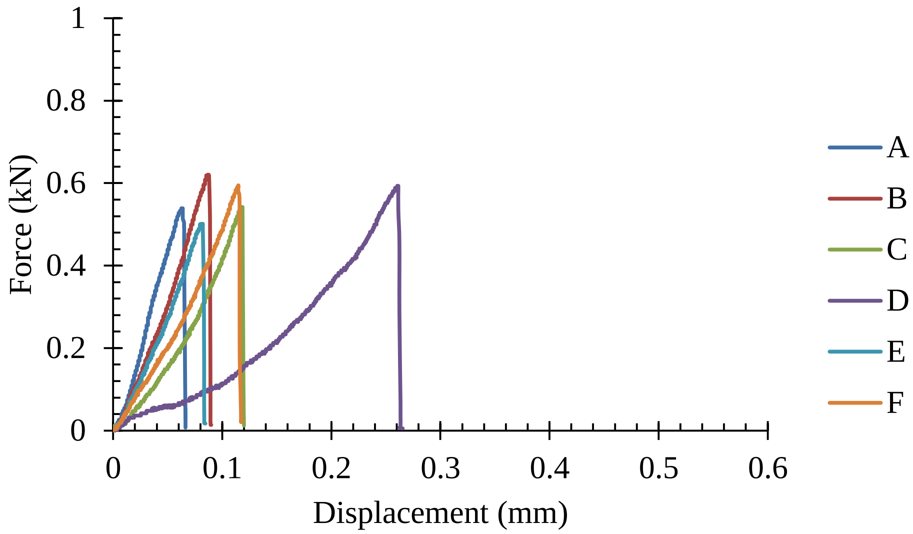

SF-0.02% (28 days)

Sample	Mass (g)	Average Height (mm)	Average Width (mm)
A	138.0	24.7	24.2
B	135.2	24.6	24.1
C	137.8	24.4	24.2
D	135.5	24.2	24.4
E	135.6	24.3	24.5
F	142.9	24.4	24.7

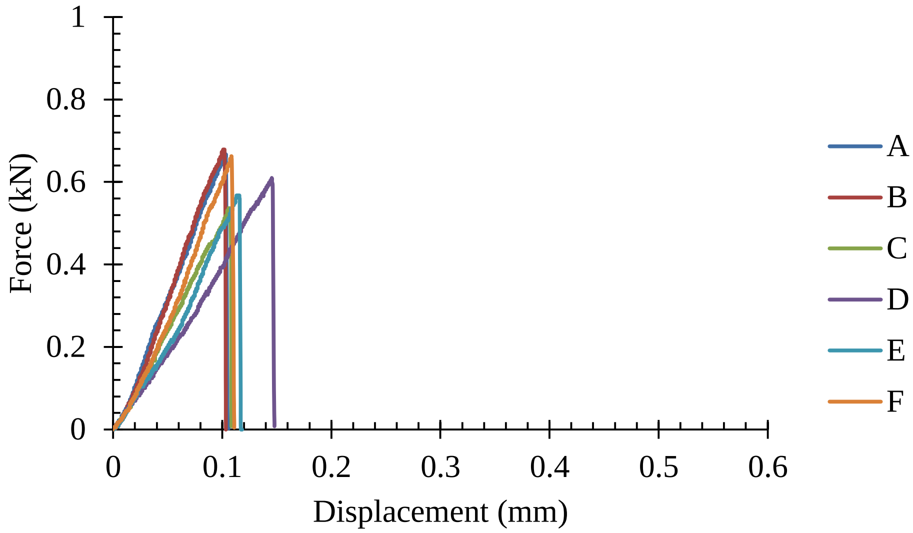

SF-0.08% (7 days)

Sample	Mass (g)	Average Height (mm)	Average Width (mm)
A	141.3	25.3	24.4
B	140.1	25.2	24.3
C	137.8	25.5	24.2
D	139.9	25.5	24.1
E	140.2	25.6	24.1
F	146.5	25.7	24.1

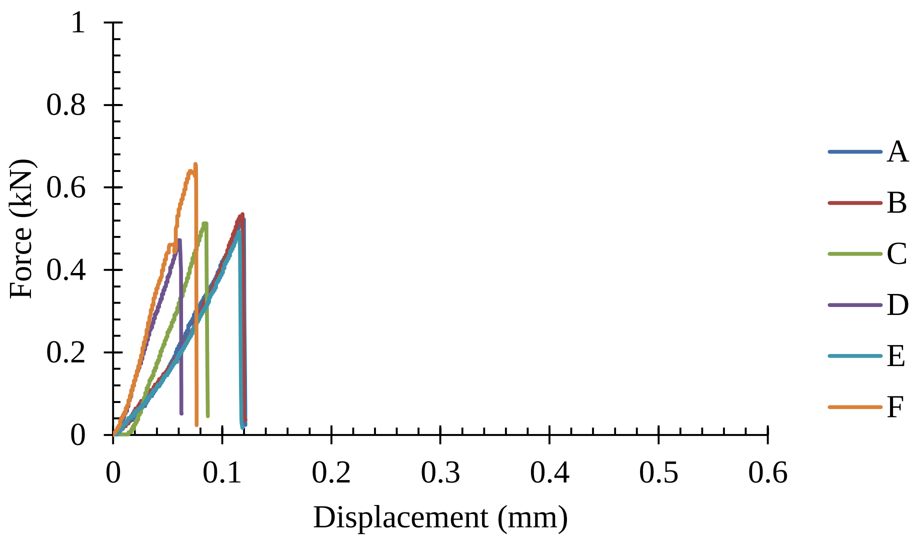

SF-0.08% (28 days)

Sample	Mass (g)	Average Height (mm)	Average Width (mm)
A	136.5	24.4	24.1
B	134.8	24.2	24.1
C	133.1	24.0	24.3
D	131.3	23.6	24.5
E	133.0	23.5	24.6
F	135.1	23.7	24.8

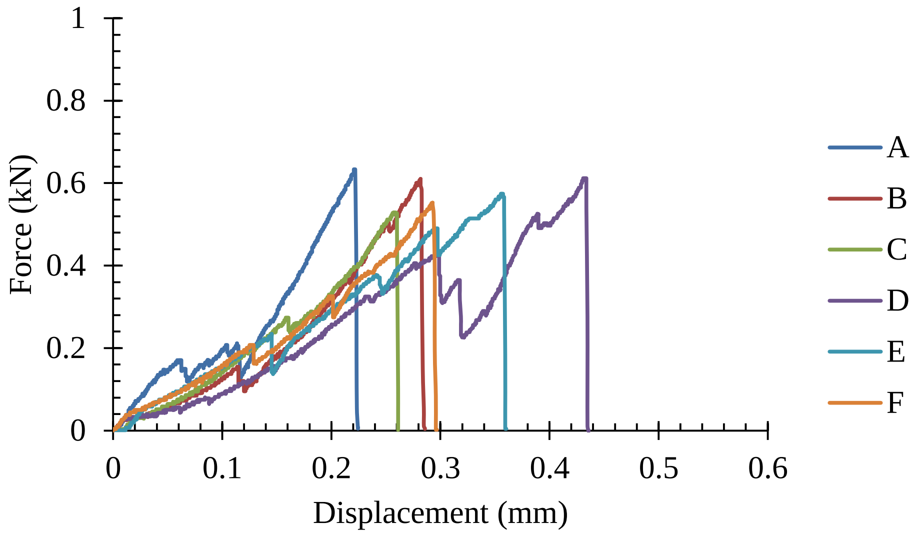

SF-0.2% (7 days)

Sample	Mass (g)	Average Height (mm)	Average Width (mm)
A	142.2	25.5	24.3
B	144.5	25.3	24.3
C	144.1	25.2	24.5
D	142.8	24.9	24.6
E	141.4	24.7	24.7
F	147.1	24.8	24.7

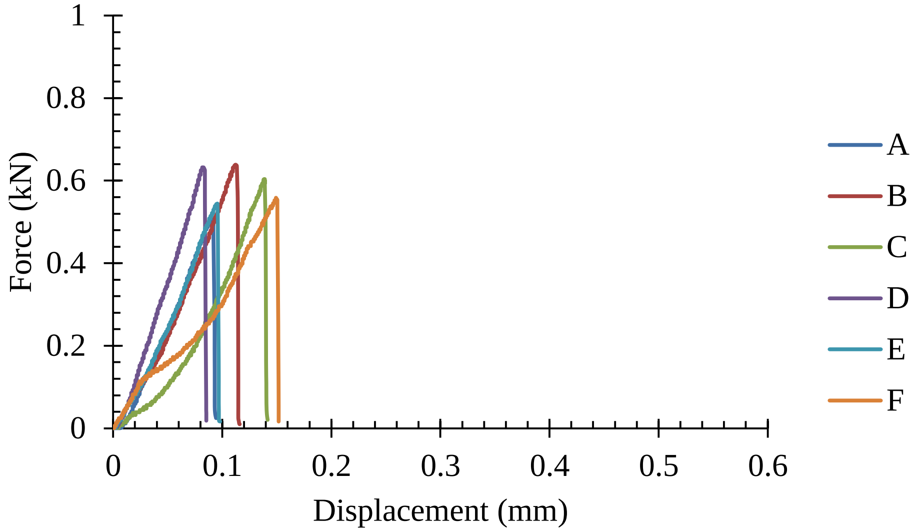

SF-0.2% (28 days)

Sample	Mass (g)	Average Height (mm)	Average Width (mm)
A	142.7	24.3	24.8
B	136.5	24.1	24.7
C	135.5	24.1	24.6
D	136.4	24.1	24.4
E	136.1	24.2	24.1
F	137.8	24.4	24.2

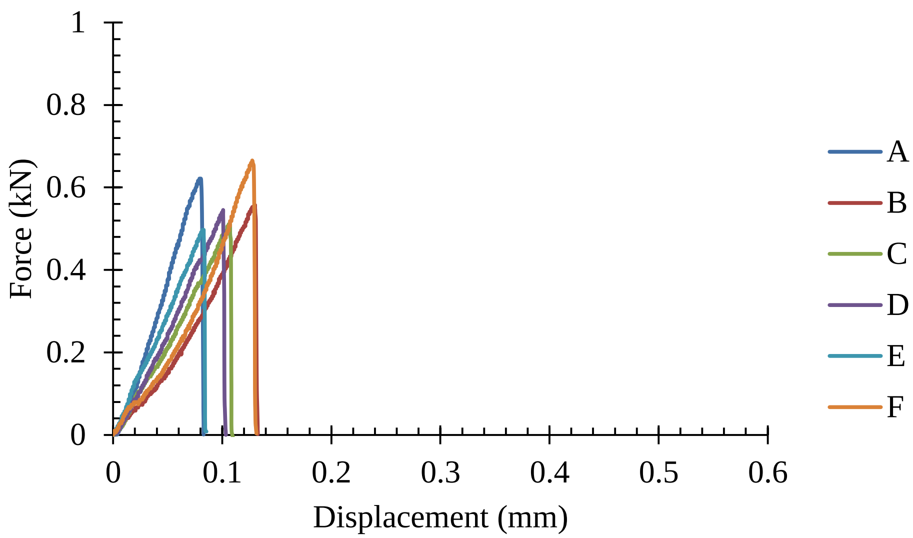

SF-0.5% (7 days)

Sample	Mass (g)	Average Height (mm)	Average Width (mm)
A	141.5	24.7	24.1
B	134.6	24.3	23.9
C	135.8	24.2	24.0
D	136.3	23.9	24.3
E	138.0	24.0	24.5
F	139.9	24.1	24.6

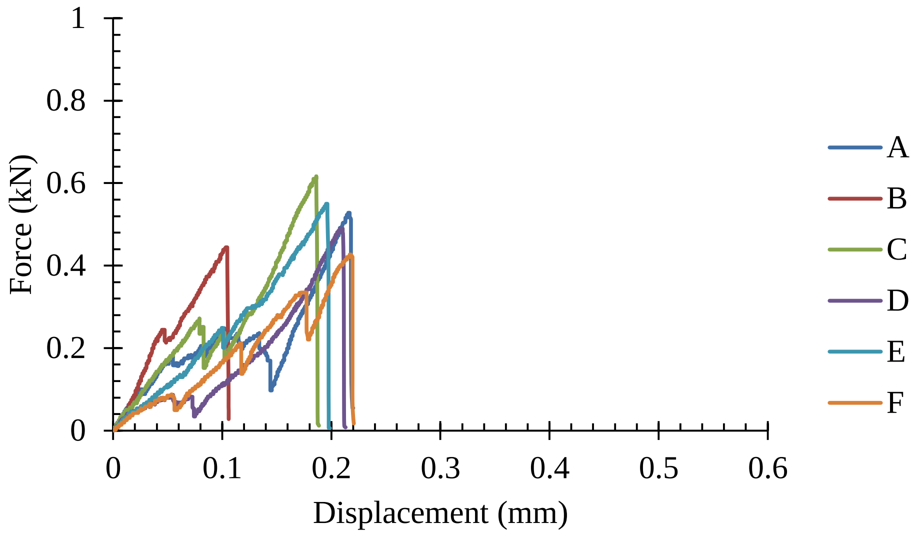

SF-0.5% (28 days)

Sample	Mass (g)	Average Height (mm)	Average Width (mm)
A	143.8	25.5	24.2
B	140.8	25.4	24.0
C	140.7	25.2	24.3
D	143.4	25.1	24.5
E	141.8	25.1	25.0
F	147.5	25.3	25.8

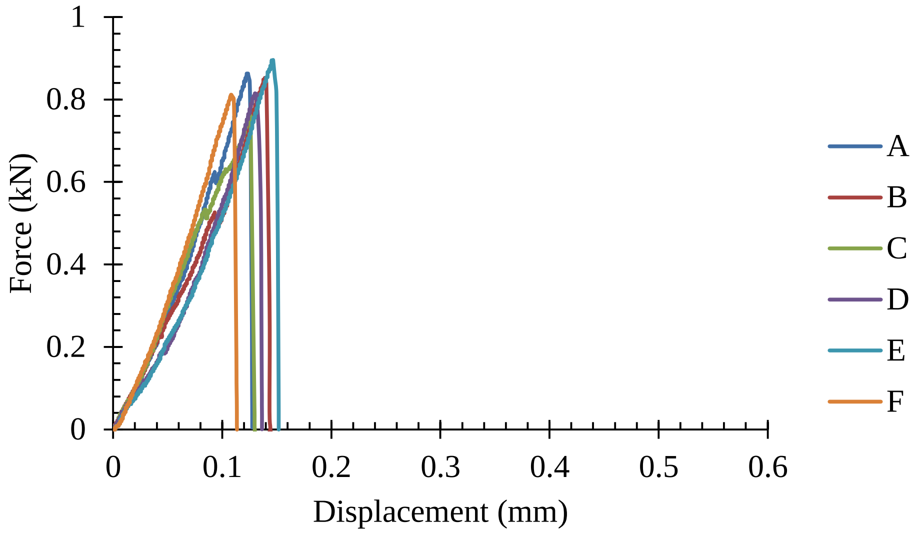

SF-1% (7 days)

Sample	Mass (g)	Average Height (mm)	Average Width (mm)
A	136.8	25.0	24.5
B	133.9	24.6	24.4
C	136.4	24.7	24.4
D	136.6	24.4	24.4
E	135.8	24.8	24.3
F	143.8	25.1	24.3

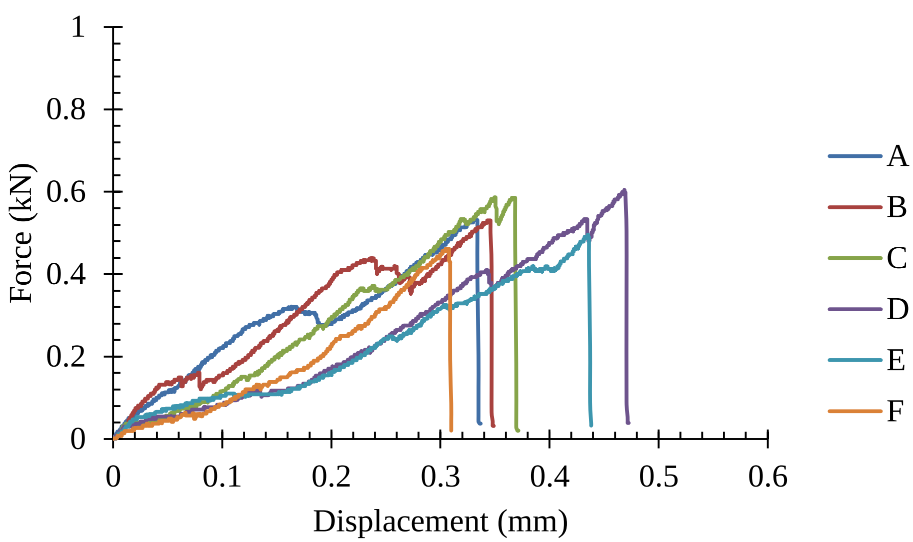

SF-1% (28 days)

Sample	Mass (g)	Average Height (mm)	Average Width (mm)
A	144.3	25.5	24.5
B	141.7	25.3	24.5
C	143.8	25.2	24.9
D	143.2	25.1	25.0
E	144.8	25.0	25.1
F	145.8	25.0	25.0

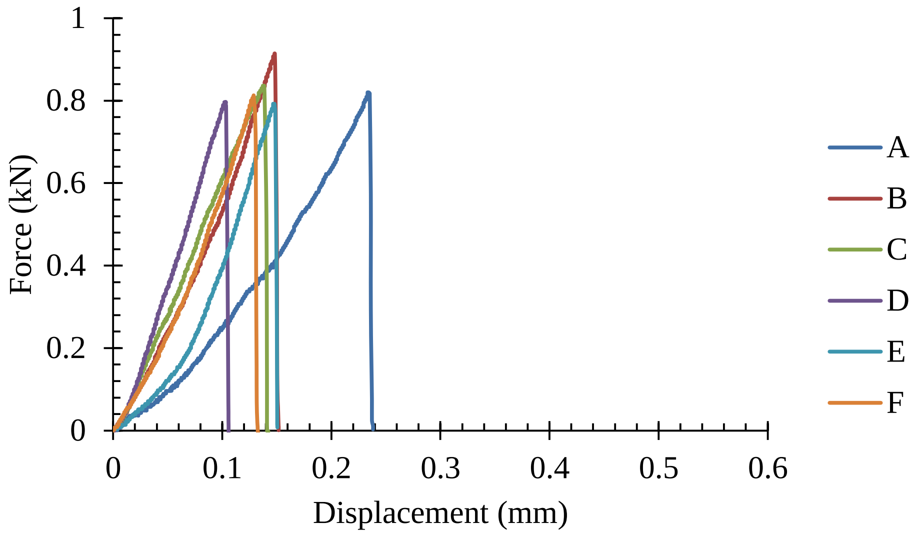

Hybrid Composites

Testing method: compression (uniaxial on prisms) and flexural (three-point bending).

Compression

Prism Height: 50.8 mm.

PC (3 days)

Sample	Mass (g)	Average Width (mm)	Average Depth (mm)
A	63.6	25.0	25.0
B	63.7	25.3	24.6
C	61.6	25.5	24.5
D	61.5	25.4	24.4
E	62.3	25.3	24.3
F	60.8	25.2	24.5

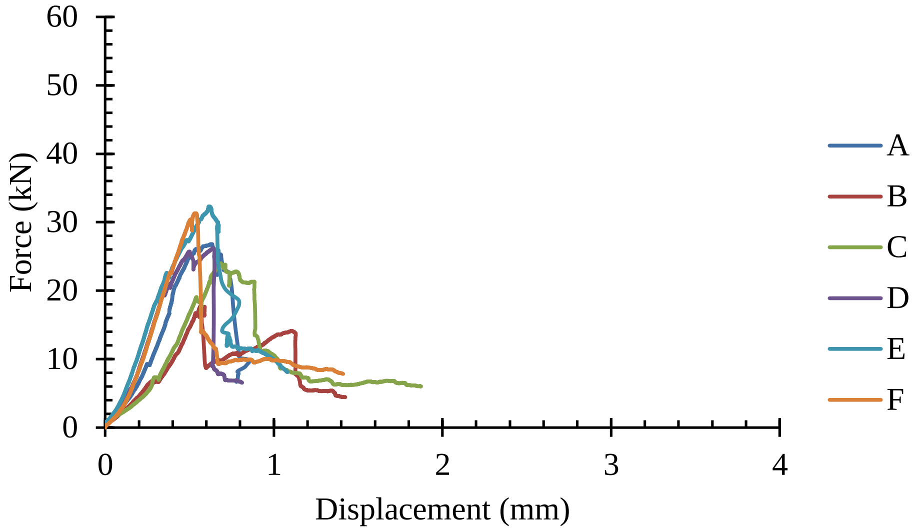

PC (7 days)

Sample	Mass (g)	Average Width (mm)	Average Depth (mm)
A	69.0	26.0	26.3
B	69.0	26.0	25.9
C	68.4	26.0	25.9
D	68.4	26.2	25.8
E	69.6	26.1	25.8
F	69.5	26.1	25.8

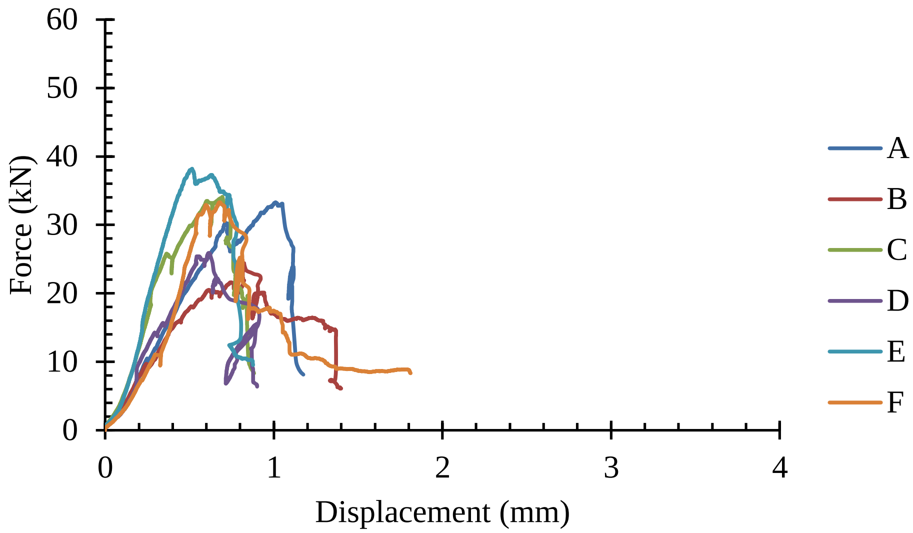

PC (28 days)

Sample	Mass (g)	Average Width (mm)	Average Depth (mm)
A	68.2	25.8	25.4
B	68.1	25.7	25.4
C	69.0	25.5	25.4
D	67.7	25.4	25.2
E	67.9	25.4	25.1
F	67.3	25.4	25.1

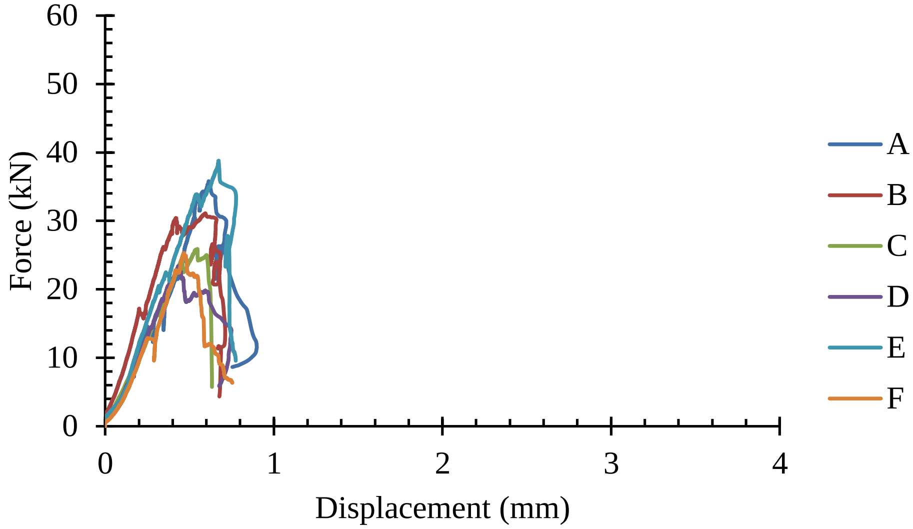

PC-CNF (3 days)

Sample	Mass (g)	Average Width (mm)	Average Depth (mm)
A	68.6	25.5	25.3
B	67.9	25.6	25.5
C	68.0	25.5	25.5
D	67.6	25.6	25.8
E	70.9	25.8	26.0
F	69.3	25.8	26.1

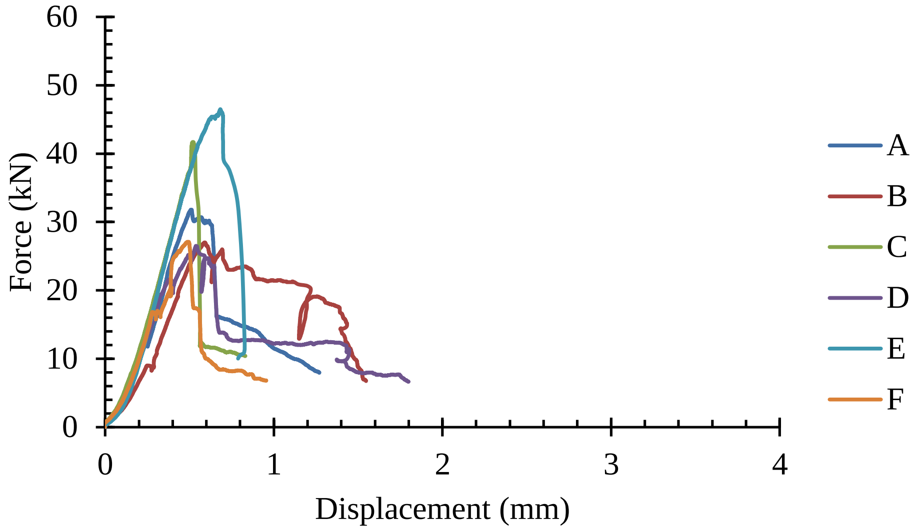

PC-CNF (7 days)

Sample	Mass (g)	Average Width (mm)	Average Depth (mm)
A	64.7	24.6	25.4
B	64.7	24.6	25.0
C	62.9	24.7	25.0
D	62.8	24.6	24.6
E*	62.5	24.7	24.2
F	63.0	25.0	24.3

*Software froze while saving data.

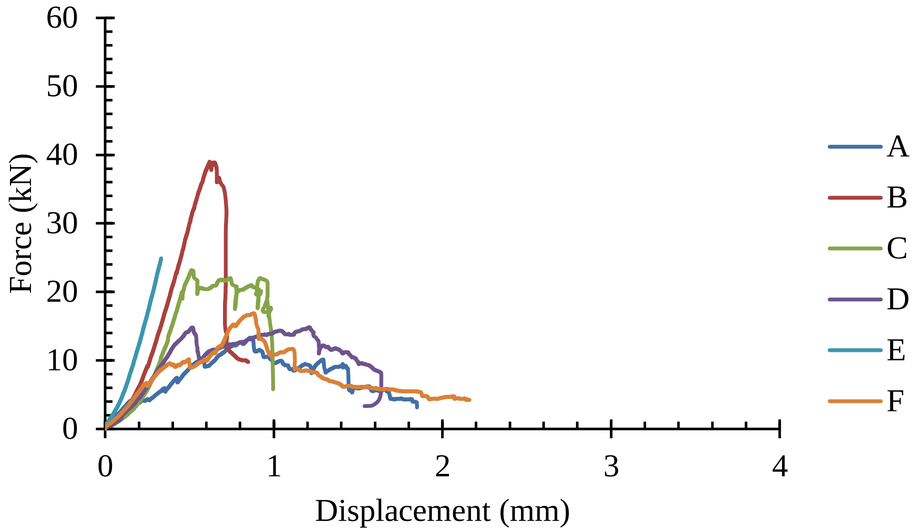

PC-CNF (28 days)

Sample	Mass (g)	Average Width (mm)	Average Depth (mm)
A	71.2	25.5	25.8
B	71.8	25.4	25.7
C	71.0	25.2	25.7
D	69.9	25.0	25.7
E	70.6	25.0	25.6
F	69.0	25.3	25.5

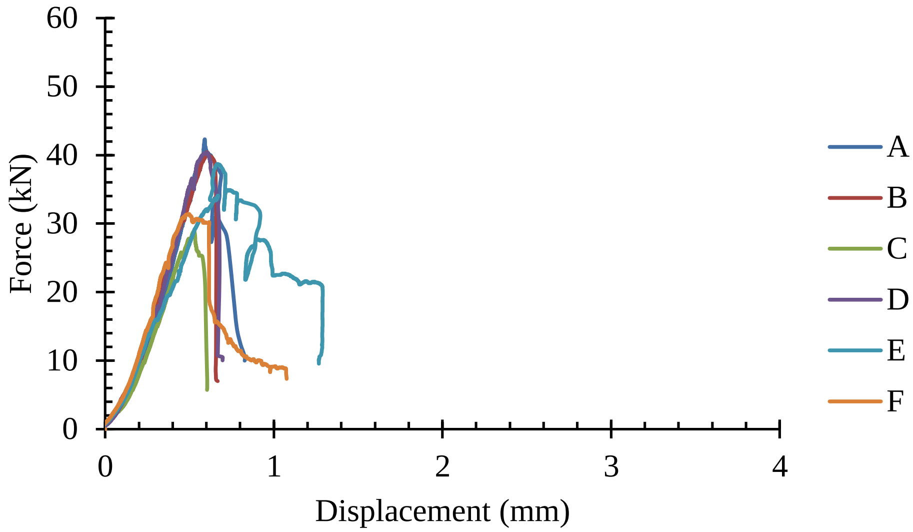

PC-CF (3 days)

Sample	Mass (g)	Average Width (mm)	Average Depth (mm)
A	58.8	24.5	24.7
B	59.4	24.6	24.6
C	59.8	24.6	24.4
D	59.8	24.6	24.6
E	59.3	24.6	24.6
F	61.0	24.6	24.6

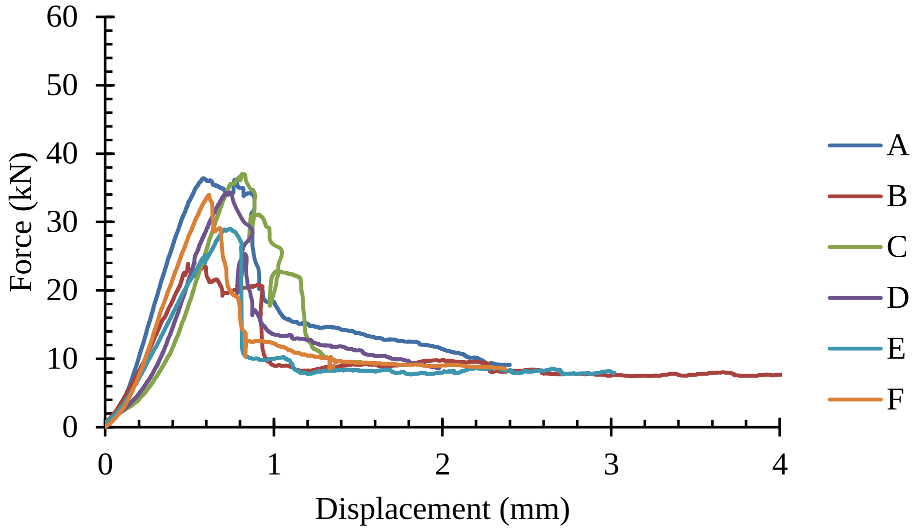

PC-CF (7 days)

Sample	Mass (g)	Average Width (mm)	Average Depth (mm)
A	68.2	26.4	26.3
B	68.3	26.1	26.4
C	67.3	26.3	26.2
D	69.0	26.1	26.2
E	68.1	26.1	26.2
F	68.6	26.1	26.4

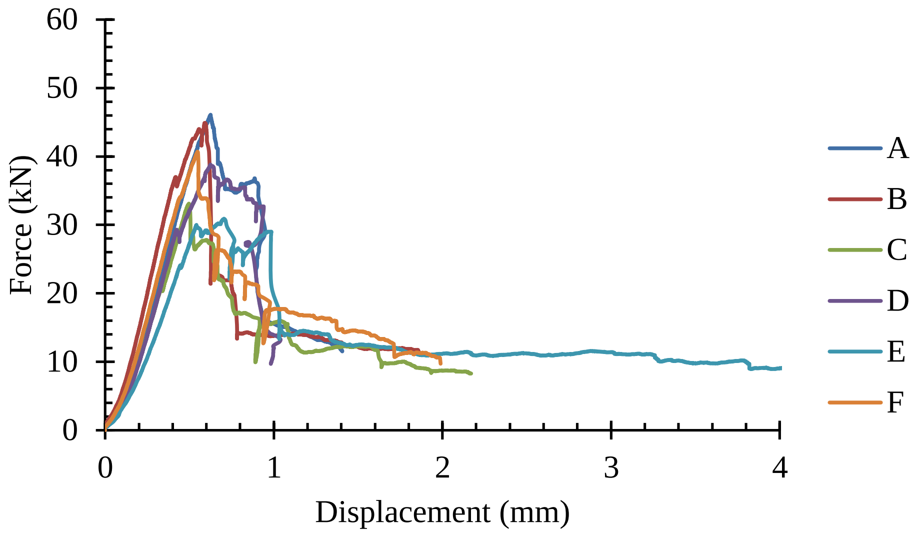

PC-CF (28 days)

Sample	Mass (g)	Average Width (mm)	Average Depth (mm)
A	61.6	24.4	24.8
B	62.1	24.3	24.6
C	61.7	24.2	24.7
D	61.6	24.2	24.8
E	62.0	24.2	24.9
F	63.8	24.4	25.0

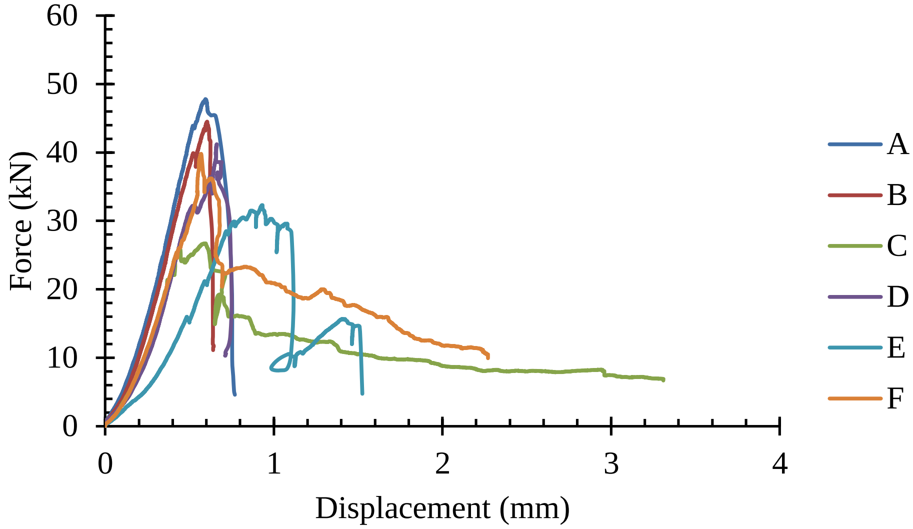

PC-CNF-CF (3 days)

Sample	Mass (g)	Average Width (mm)	Average Depth (mm)
A	65.1	25.9	24.8
B	65.5	25.9	24.9
C	67.0	25.7	25.1
D	68.0	25.7	25.3
E	66.6	25.5	25.2
F	68.1	25.8	25.4

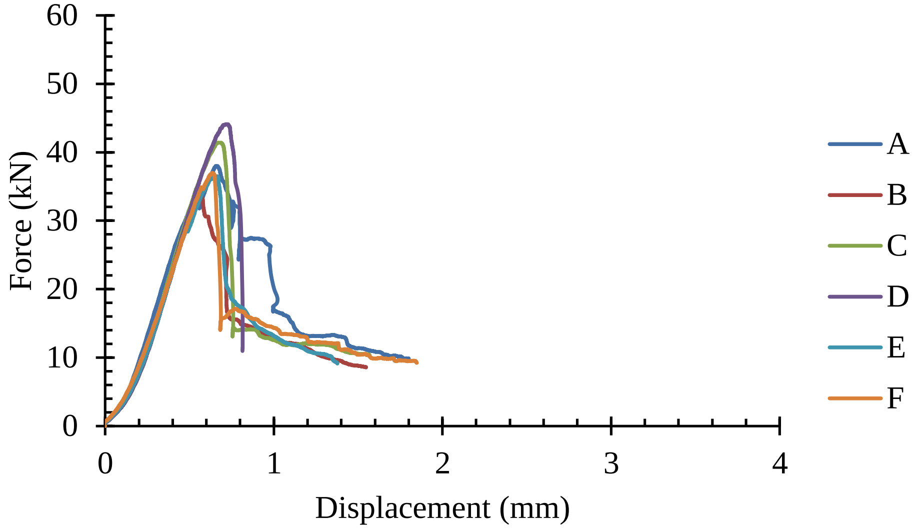

PC-CNF-CF (7 days)

Sample	Mass (g)	Average Width (mm)	Average Depth (mm)
A	69.2	25.5	26.9
B	68.2	25.5	26.5
C	68.8	25.6	26.0
D	67.3	25.6	25.6
E	67.5	25.6	25.2
F	67.3	25.7	24.9

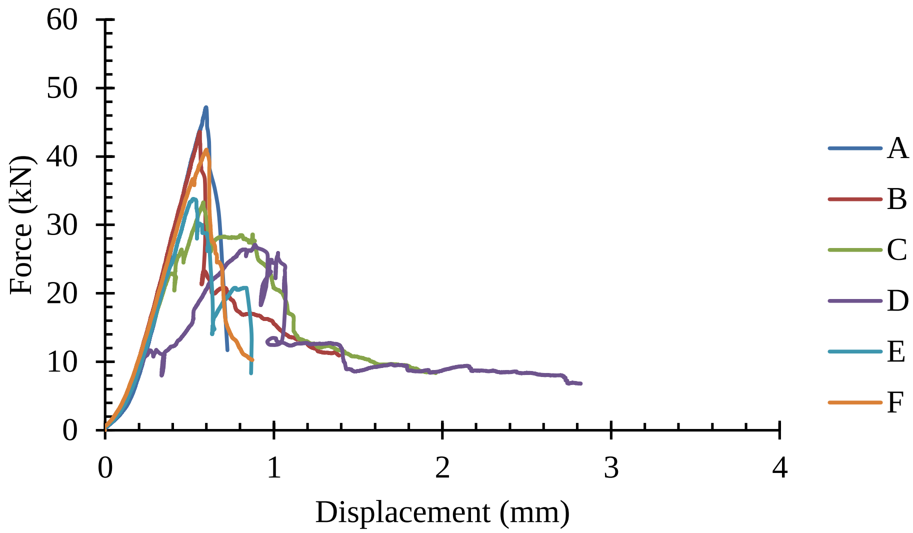

PC-CNF-CF (28 days)

Sample	Mass (g)	Average Width (mm)	Average Depth (mm)
A	71.3	25.6	26.5
B	69.1	25.3	26.3
C	69.1	25.3	26.1
D	68.8	25.4	25.9
E	68.7	25.6	25.7
F	69.6	25.6	25.7

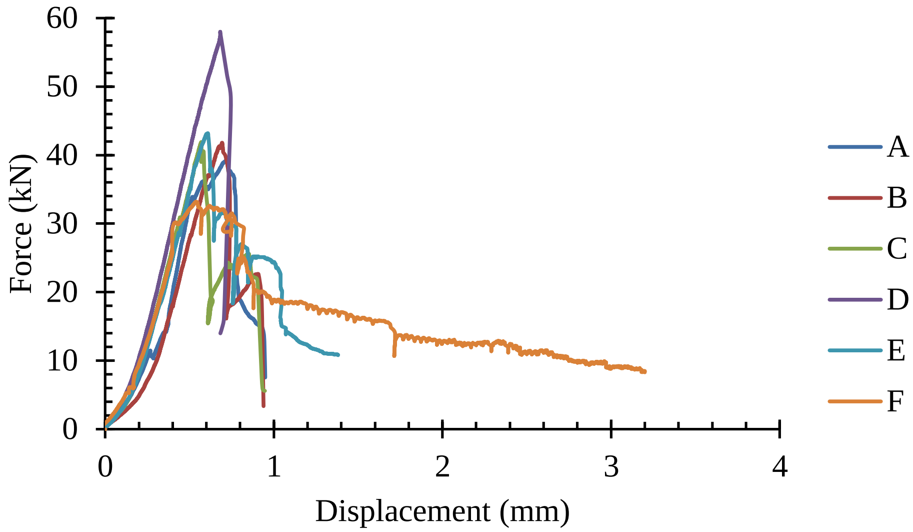

Flexural
Beam length: *ca.* 114.3 mm.
Beam span: 76.2 mm.

PC (3 days)

Sample	Mass (g)	Average Height (mm)	Average Width (mm)
A	139.4	25.1	25.2
B	139.6	24.8	25.2
C	137.9	24.6	25.4
D	137.2	24.4	25.4
E	136.9	24.3	25.3
F	144.5	24.4	25.2

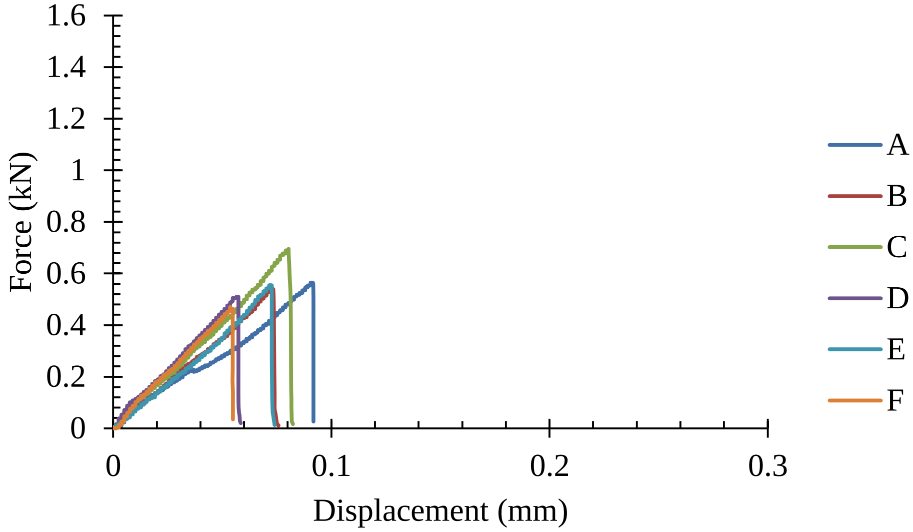

PC (7 days)

Sample	Mass (g)	Average Height (mm)	Average Width (mm)
A	156.8	26.1	26.0
B	152.1	26.0	26.0
C	153.8	25.8	26.0
D	152.6	25.8	26.0
E	152.0	25.7	26.0
F	153.2	25.7	26.0

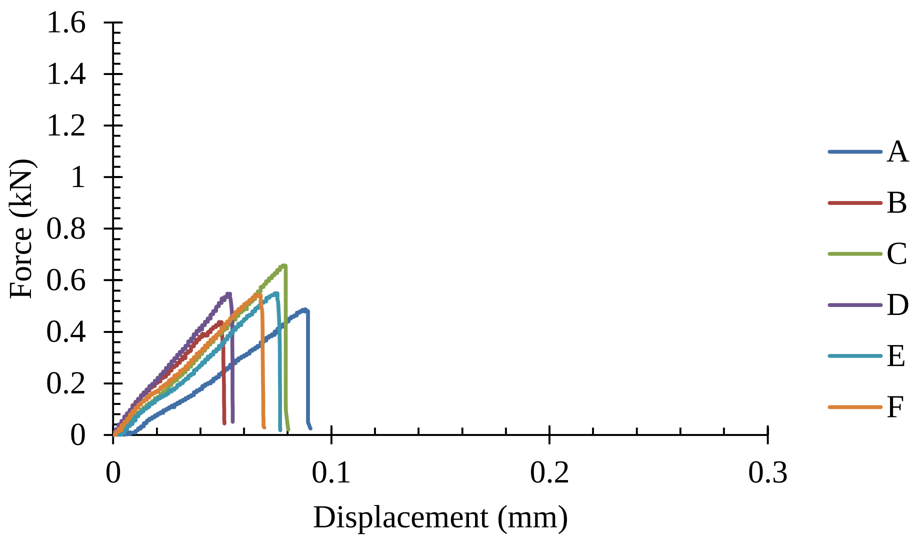

PC (28 days)

Sample	Mass (g)	Average Height (mm)	Average Width (mm)
A	154.0	25.6	25.9
B	152.0	25.5	25.7
C	151.2	25.3	25.6
D	147.9	25.2	25.5
E	149.0	25.1	25.5
F	147.8	25.2	25.4

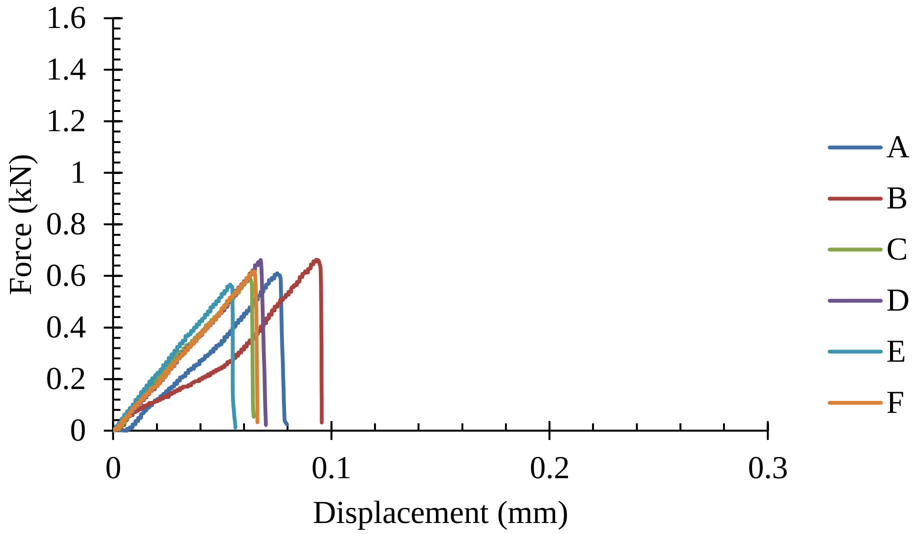

PC-CNF (3 days)

Sample	Mass (g)	Average Height (mm)	Average Width (mm)
A	152.2	25.4	25.4
B	150.9	25.5	25.5
C	150.4	25.5	25.5
D	151.4	25.8	25.6
E	154.7	25.9	25.7
F	154.8	26.1	25.8

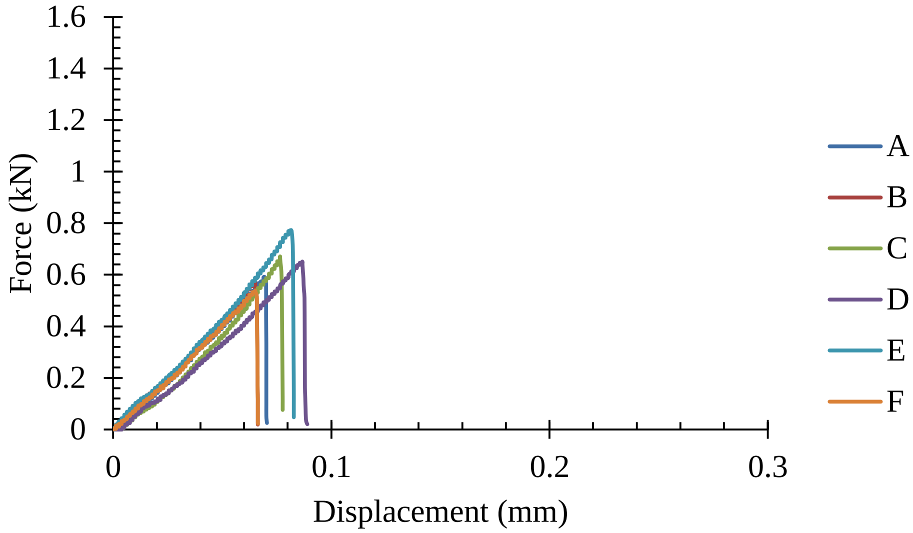

PC-CNF (7 days)

Sample	Mass (g)	Average Height (mm)	Average Width (mm)
A	146.8	25.5	24.7
B	140.7	25.1	24.5
C	139.8	24.8	24.6
D	139.4	24.5	24.6
E	137.8	24.2	24.7
F	142.2	24.3	24.9

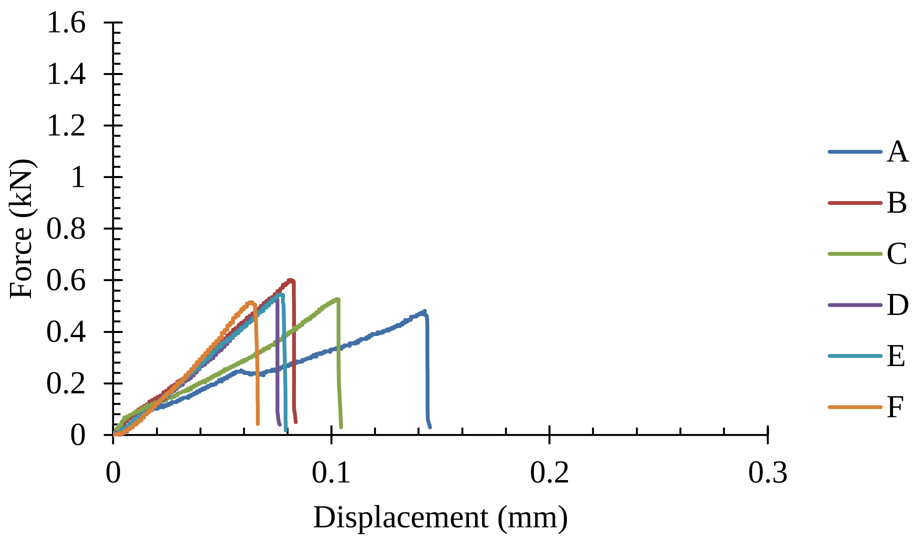

PC-CNF (28 days)

Sample	Mass (g)	Average Height (mm)	Average Width (mm)
A	162.4	26.0	25.6
B	158.6	25.8	25.4
C	155.0	25.8	25.2
D	153.6	25.9	24.9
E	155.3	25.7	25.3
F	153.3	25.6	25.4

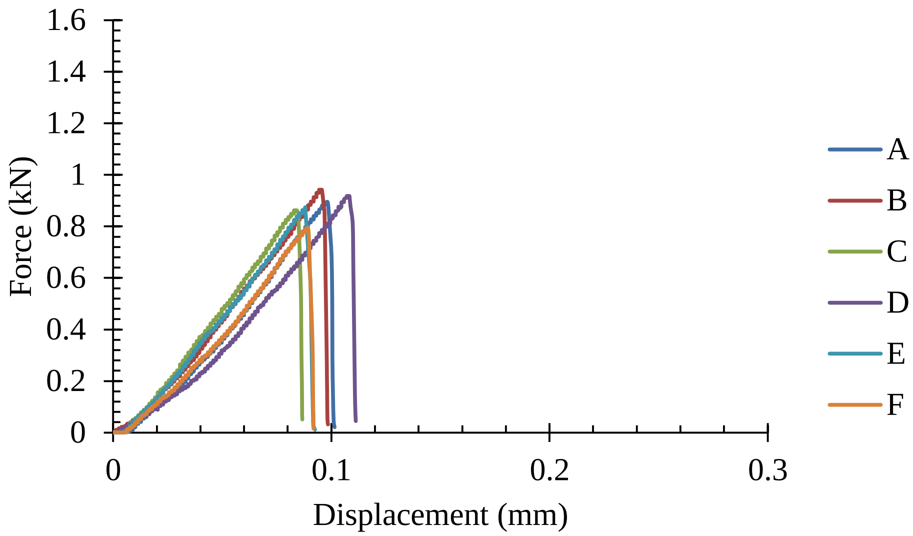

PC-CF (3 days)

Sample	Mass (g)	Average Height (mm)	Average Width (mm)
A	134.2	24.6	24.5
B	129.9	24.5	24.6
C	131.4	24.5	24.6
D	133.4	24.5	24.6
E	131.3	24.5	24.5
F	140.6	24.7	24.6

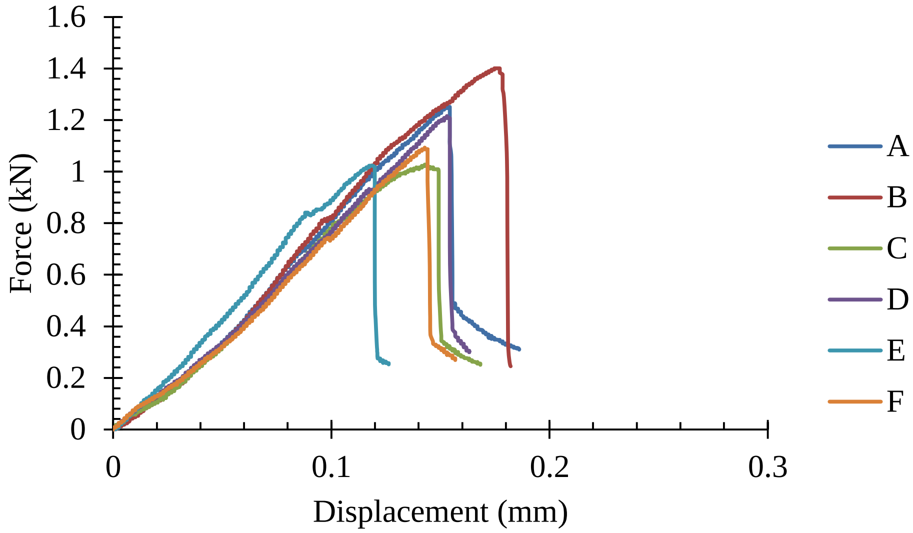

PC-CF (7 days)

Sample	Mass (g)	Average Height (mm)	Average Width (mm)
A	157.0	26.2	26.2
B	150.5	26.2	26.0
C	151.0	26.2	26.2
D	151.0	26.1	26.0
E	152.7	26.2	25.9
F	154.7	26.4	26.1

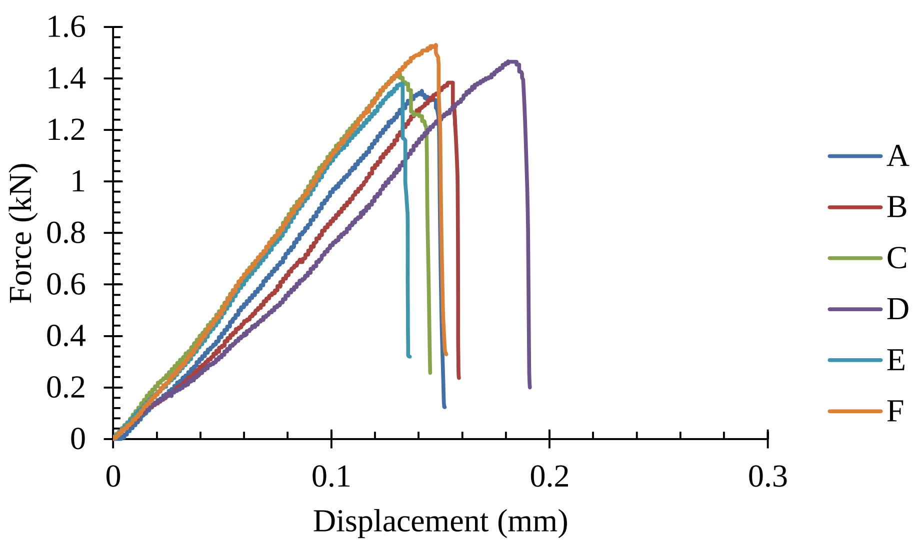

PC-CF (28 days)

Sample	Mass (g)	Average Height (mm)	Average Width (mm)
A	137.6	24.7	24.5
B	135.7	24.7	24.4
C	136.0	24.7	24.3
D	136.4	24.8	24.3
E	138.2	24.9	24.4
F	142.2	25.0	24.5

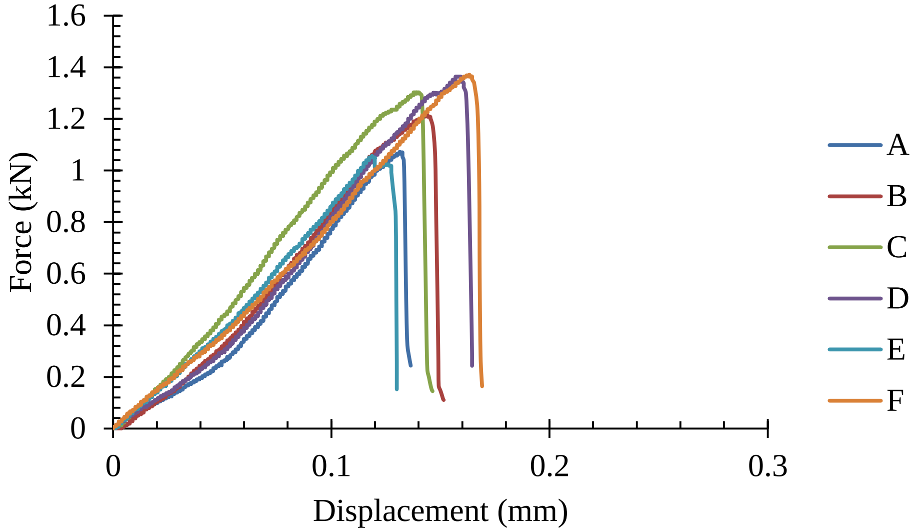

PC-CNF-CF (3 days)

Sample	Mass (g)	Average Height (mm)	Average Width (mm)
A	148.2	25.0	25.9
B	144.1	25.0	25.8
C	146.3	25.2	25.7
D	147.5	25.5	25.7
E	144.9	25.4	25.5
F	155.2	25.5	25.8

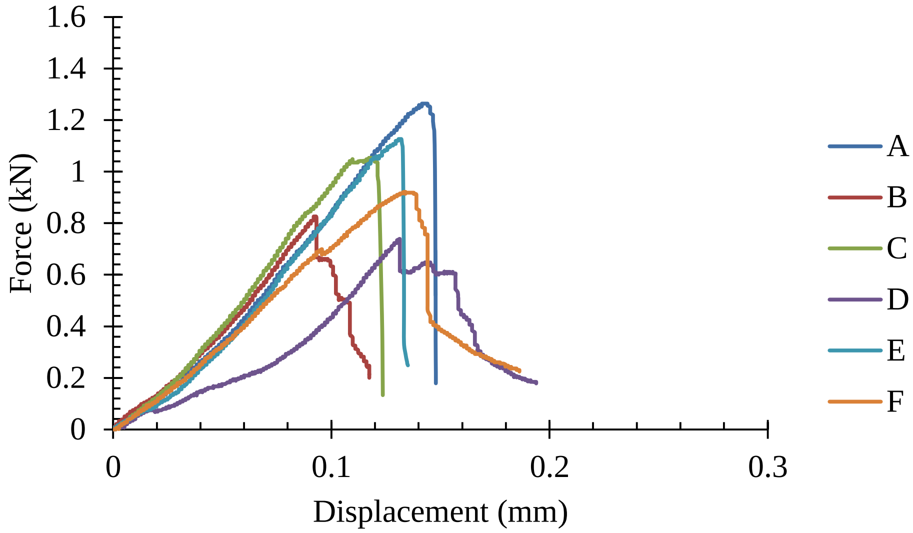

PC-CNF-CF (7 days)

Sample	Mass (g)	Average Height (mm)	Average Width (mm)
A	157.6	26.9	25.5
B	153.5	26.4	25.5
C	150.8	25.8	25.7
D	146.2	25.5	25.6
E	146.7	25.1	25.6
F	147.9	24.9	25.8

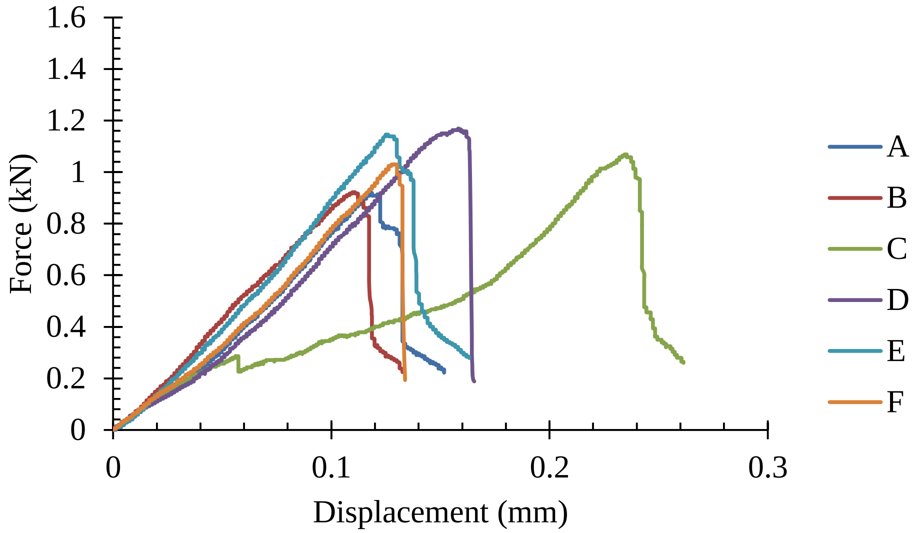

PC-CNF-CF (28 days)

Sample	Mass (g)	Average Height (mm)	Average Width (mm)
A	159.5	26.6	25.9
B	153.4	26.4	25.5
C	153.3	26.2	25.3
D	152.5	25.9	25.4
E	152.4	25.8	25.7
F	152.8	25.6	25.7